Universidade de Aveiro Departamento de Ambiente e Ordenamento
2013

Daniel dos Santos Félix das Neves

Evaluation of thermochemical biomass conversion in fluidized bed

Avaliação da conversão termoquímica de biomassa em leito fluidizado

Universidade de Aveiro
2013

Departamento de Ambiente e Ordenamento

Daniel dos Santos Félix das Neves

Evaluation of thermochemical biomass conversion in fluidized bed

Avaliação da conversão termoquímica de biomassa em leito fluidizado

Tese apresentada à Universidade de Aveiro para cumprimento dos requisitos necessários à obtenção do grau de Doutor em Ciências e Engenharia do Ambiente, realizada sob a orientação científica do Doutor Manuel Arlindo Amador de Matos, Professor Auxiliar do Departamento de Ambiente e Ordenamento da Universidade de Aveiro e co-orientação do Doutor Karl Henrik Stensson Thunman, Professor, Department of Energy and Environment, Chalmers University of Technology.

Este trabalho teve apoio financeiro da FCT, Portugal, através da bolsa de doutoramento SFRH/BD/39567/2007 e dos projetos de investigação PTDC/AAC-AMB/098112/2008 e PTDC/AAC-AMB/116568/2010, tendo sido realizado em cooperação com a Chalmers University of Technology, com financiamento da Swedish Energy Agency, Swedish Gasification Centre (SFC), e o apoio de Akademiska Hus, Chalmers, Göteborg Energi e Metso.

This work was funded by FCT, Portugal, through PhD grant SFRH/BD/39567/2007 and research projects PTDC/AAC-AMB/098112/2008 and PTDC/AAC-AMB/116568/2010, in co-operation with the work conducted at Chalmers University of Technology funded by the Swedish Energy Agency, the Swedish Gasification Centre (SFC), and the industrial co-operation between Akademiska Hus, Chalmers, Göteborg Energi and Metso.

Dedico este trabalho aos meus pais, Josué e Maria, irmã Cristina, avós Carlos e Carolina, e Joaquim e Celeste, e também à Carmen.

"Valeu a pena? Tudo vale a pena se a alma não é pequena."
Fernando Pessoa – Mar Português

o júri

presidente

Doutor António Manuel Melo de Sousa Pereira
Professor Catedrático da Universidade de Aveiro

Doutor Casimiro Adrião Pio
Professor Catedrático da Universidade de Aveiro

Doutor Karl Henrik Stensson Thunman
Professor, Chalmers University of Technology (Coorientador)

Doutora Maria Filomena Jesus Pinto
Investigadora Principal do LNEG – Laboratório Nacional de Energia e Geologia

Doutor Manuel Arlindo Amador de Matos
Professor Auxiliar da Universidade de Aveiro (Orientador)

Doutor Luís António da Cruz Tarelho
Professor Auxiliar da Universidade de Aveiro

Doutor Martin Christoph Seemann
Assistant Professor, Chalmers University of Technology

acknowledgements

I would like to thank my supervisor Professor Arlindo Matos for his skilful guidance and also his best efforts in developing the experimental facilities used in this work. His ability to fix almost any technical problem encountered during the experiments with a minimum of resources was crucial to keep this work on the track.

I also express my gratitude to my co-supervisor Professor Henrik Thunman, first of all, for the kind way he has received me at Gothenburg and his confidence on this work. Then, for the excellent working conditions provided to me at the Division of Energy Technology, Chalmers. As well, I would like to thank him for sharing his wide knowledge in the field of biomass conversion during many fruitful discussions.

My gratitude is extended to Professor Luís Tarelho who has always supported me and this is clearly beyond the scope of this thesis work. It has been really a pleasure to work with him during the last decade.

Special thanks to German Maldonado for the help, friendship and the never ending evenings. He really managed to make Gothenburg feel like home to me.

Ulf Stenman is thanked for his valuable help in developing the experimental setup at Chalmers, sometimes working overnight!

I also would like to thank to all co-authors at Chalmers, Anton Larsson and Martin Seemann, and University of Seville, Alberto Gómez-Barea, and yet Pedro Ideias.

I've much appreciated the friendly atmosphere provided by all the colleagues and staff that are or have been working at the Department of Environment and Planning, Aveiro, and Division of Energy Technology, Chalmers.

Not to forget my love and best friend, Carmen, who has been amazing.

palavras-chave

Biomassa, madeira, celulose, lenhina, voláteis, carbonizado, pirólise, gasificação, combustão, leito fluidizado, medição, modelação, revisão.

resumo

Dado o aumento acelerado dos preços dos combustíveis fósseis e as incertezas quanto à sua disponibilidade futura, tem surgido um novo interesse nas tecnologias da biomassa aplicadas à produção de calor, eletricidade ou combustíveis sintéticos. Não obstante, para a conversão termoquímica de uma partícula de biomassa sólida concorrem fenómenos bastante complexos que levam, em primeiro lugar, à secagem do combustível, depois à pirólise e finalmente à combustão ou gasificação propriamente ditas. Uma descrição relativamente incompleta de alguns desses estágios de conversão constitui ainda um obstáculo ao desenvolvimento das tecnologias que importa ultrapassar. Em particular, a presença de elevados conteúdos de matéria volátil na biomassa põe em evidência o interesse prático do estudo da pirólise. A importância da pirólise durante a combustão de biomassa foi evidenciada neste trabalho através de ensaios realizados num reator piloto de leito fluidizado borbulhante. Verificou-se que o processo ocorre em grande parte à superfície do leito com chamas de difusão devido à libertação de voláteis, o que dificulta o controlo da temperatura do reator acima do leito. No caso da gasificação de biomassa a pirólise pode inclusivamente determinar a eficiência química do processo. Isso foi mostrado neste trabalho durante ensaios de gasificação num reator de leito fluidizado de $2MW_{th}$, onde um novo método de medição permitiu fechar o balanço de massa ao gasificador e monitorizar o grau de conversão da biomassa. A partir destes resultados tornou-se clara a necessidade de descrever adequadamente a pirólise de biomassa com vista ao projeto e controlo dos processos. Em aplicações de engenharia há particular interesse na estequiometria e propriedades dos principais produtos pirolíticos. Neste trabalho procurou-se responder a esta necessidade, inicialmente através da estruturação de dados bibliográficos sobre rendimentos de carbonizado, líquidos pirolíticos e gases, assim como composições elementares e poderes caloríficos. O resultado traduziu-se num conjunto de parâmetros empíricos de interesse prático que permitiram elucidar o comportamento geral da pirólise de biomassa numa gama ampla de condições operatórias. Para além disso, propôs-se um modelo empírico para a composição dos voláteis que pode ser integrado em modelos compreensivos de reatores desde que os parâmetros usados sejam adequados ao combustível ensaiado. Esta abordagem despoletou um conjunto de ensaios de pirólise com várias biomassas, lenhina e celulose, e temperaturas entre os 600 e 975ºC. Elevadas taxas de aquecimento do combustível foram alcançadas em

reatores laboratoriais de leito fluidizado borbulhante e leito fixo, ao passo que um sistema termo-gravimétrico permitiu estudar o efeito de taxas de aquecimento mais baixas. Os resultados mostram que, em condições típicas de processos de combustão e gasificação, a quantidade de voláteis libertada da biomassa é pouco influenciada pela temperatura do reator mas varia bastante entre combustíveis. Uma análise mais aprofundada deste assunto permitiu mostrar que o rendimento de carbonizado está intimamente relacionado com o rácio O/C do combustível original, sendo proposto um modelo simples para descrever esta relação. Embora a quantidade total de voláteis libertada seja estabelecida pela composição da biomassa, a respetiva composição química depende bastante da temperatura do reator. Rendimentos de espécies condensáveis (água e espécies orgânicas), CO_2 e hidrocarbonetos leves descrevem um máximo relativamente à temperatura para dar lugar a CO e H_2 às temperaturas mais altas. Não obstante, em certas gamas de temperatura, os rendimentos de algumas das principais espécies gasosas (e.g. CO, H_2, CH_4) estão bem correlacionados entre si, o que permitiu desenvolver modelos empíricos que minimizam o efeito das condições operatórias e, ao mesmo tempo, realçam o efeito do combustível na composição do gás. Em suma, os ensaios de pirólise realizados neste trabalho permitiram constatar que a estequiometria da pirólise de biomassa se relaciona de várias formas com a composição elementar do combustível original o que levanta várias possibilidades para a avaliação e projeto de processos de combustão e gasificação de biomassa.

keywords

Biomass, wood, cellulose, lignin, volatiles, char, pyrolysis, gasification, combustion, fluidized bed, measurement, modeling, review.

abstract

With ever increasing fossil fuel prices and concern over supply, there is a renewed interest on biomass technology for heat, electricity and synthetic fuels. Yet, the conversion behavior of a solid biomass particle is due to complex thermochemical phenomena leading to fuel drying first, then pyrolysis, and then combustion and/or gasification. The relative lack of knowledge within some of these conversion stages is still a major obstacle for further technology development. In particular, the description of the kinetics and stoichiometry of the pyrolytic stage is of high interest given the high volatile matter content of biomass fuels. The role of the pyrolytic degradation during biomass combustion was investigated in this work by experiments conducted in a pilot-scale fluidized bed reactor showing that the release of the volatiles in the vicinity of the fuel feed port leads to extensive flaming and can make it difficult to control the operating temperature in the freeboard. Under gasification conditions the pyrolytic degradation is even more important and can dictate the chemical efficiency of the process. This was also shown in this work by experiments in a $2MW_{th}$ dual fluidized bed steam gasifier, where a new online measurement method for the composition of the raw gasification gas made it possible to close the mass balance across the gasifier and monitor the extent of fuel conversion. These results show that a good understanding of the pyrolysis behavior of biomass is demanded for designing and controlling efficient combustion and gasification processes. With this in regard, it is often sufficient for engineers to describe the ultimate yields and the properties of the pyrolytic products. This can be done, firstly, by examining the huge set of literature data that was structured in this work, including the yields of the most relevant pyrolytic products (char, condensable organics, water and permanent gases) and the respective elemental compositions and heating values. The outcome from the analysis of the literature data is a number of empirical parameters that can be used to close the mass and energy balances describing the pyrolytic stage; by doing so the general trends for the composition of the pyrolytic volatiles could be elucidated in this work over a wide range of operating conditions. Moreover, this empirical-based approach can be used to predict the stoichiometry of biomass pyrolysis in comprehensive reactor modeling if the parameters are conveniently modified by measurements specialized for the fuel under concern. This has motivated a set of pyrolysis experiments conducted in this work with a number of biomasses, lignin and cellulose, and peak temperatures in range of 600-975ºC. Pyrolysis under slow heating was investigated in a thermobalance

analyzer while the more severe thermal conditions were achieved in laboratory-scale fluidized bed and fixed bed quartz tube reactors. The results showed that, under thermal conditions typical of combustion and gasification processes, the extent of fuel volatilization is weakly dependent of the reactor temperature but, in turns, varies widely among different fuel types. A more detailed analysis of this issue revealed a very approximated relationship between the yield of char and the O/C ratio of parent fuel, with a simple model being proposed in this work to describe this behavior. Whereas the total amount of pyrolytic volatiles released from solid fuel is governed by the composition of fuel, its chemical composition changes continuously as a function of the reactor temperature. Yields of condensable species (organics + water), CO_2 and light hydrocarbons go through maxima with respect to temperature to give rise to CO and H_2 at the higher temperatures tested. Nevertheless, the yields of major gas species (e.g. CO, H_2, CH_4) were found well correlated over a wide temperature range, which suggested one to cross plot the respective yields in an attempt to eliminate the effect of the temperature while highlighting the effect of the parent fuel. The resulting relationships are surprisingly good and complement the trends derived from the literature data structured in this work. On the whole, the experiments conducted in the laboratory facilities show that the stoichiometry of the pyrolytic stage can be related to the composition of fuel feed in many ways which provide a good deal of usefulness for evaluating and predicting the operation of biomass combustors and gasifiers.

Table of contents

List of Figures

List of Tables

List of Publications

This thesis is based on the following papers, referred to by Roman numerals in the text:

I. Tarelho LAC, Neves DSF, Matos MAA. Forest biomass waste combustion in a pilot-scale bubbling fluidized bed combustor, Biomass and Bioenergy, 2011, 35, 1511-23.

II. Neves D, Thunman H, Tarelho L, Larsson A, Seemann M, Matos A. Elemental composition of raw gas from dual fluidised bed biomass gasifier: measurement and application in operational monitoring., Applied Energy 2014, 113, 932-45.

III. Neves D, Thunman H, Matos A, Tarelho L, Gómez-Barea A. Characterization and prediction of biomass pyrolysis products, Progress in Energy and Combustion Science, 2011, 37, 611-30.

IV. Neves D, Matos A, Tarelho L, Thunman H, Larsson A, Seemann M. Dependence of char yield on the elemental composition of biomass. Submitted for publication in Biomass & Bioenergy.

V. Neves D, Matos A, Tarelho L, Thunman H, Larsson A, Seemann M. Volatile gases from biomass pyrolysis under conditions relevant for fluidized bed gasifiers and combustors. Submitted for publication in Fuel.

Conference papers published during the course of the work and partially overlapping with the papers I to V are (see Appendixes):

VI. Larsson A, Thunman H, Neves D, Pallarés D, Seemann M. Zero-dimensional modeling of indirect fluidized bed gasification. In: Proceedings of the XIII Fluidization Conference, 2010, Gyeong-ju, Korea.

VII. Neves D, Thunman H, Tarelho L, Larsson A, Seemann M, Matos A. Online measurement of raw gas elemental composition in fluidized bed biomass steam gasification. In: Proceedings of the World Bioenergy 2012, Conference & Exhibition on Biomass for Energy, 2012, Jönköping, Sweden.

VIII. Neves D, Thunman H, Seeman M, Ideias P, Matos A, Tarelho L et al. A database on biomass pyrolysis for gasification applications. In: Proceedings of the 17th European Biomass Conference & Exhibition, 2009, Hamburg, Germany.

IX. Neves D, Thunman H, Matos A, Tarelho L, Gómez-Barea A. Empirical correlations for biomass pyrolysis predictions. In: Proceedings of the 18th European Biomass Conference & Exhibition, 2010, Lyon, France.

Other conference papers published during the course of the work but out of the scope of this thesis are:

X. Matos A, Neves D, Tarelho L, Loureiro J. Rate limitations during NO reduction over biomass char in a bubbling fluidized bed reactor. In: Proceedings of the 17th European Biomass Conference & Exhibition, 2009, Hamburg, Germany.

XI. Tarelho LAC, Gordaliza AIC, Neves DSF, Alves CA, Matos MAA. Characteristics of wood combustion in a Portuguese fireplace and stove. In: Proceedings of the 19th European Biomass Conference & Exhibition, 2011, Berlin, Germany.

Chapter 1 - Introduction

1.1 *Biomass as a renewable energy source*

The solar flux reaching the Earth's surface corresponds to about 20MW/person [1] which means that the total energy incoming for a few persons would be enough to cover the current electricity demand of a small town like Aveiro, Portugal. On the Earth's surface, this virtually inexhaustible incoming power spreads among various renewable energy flows. Less than 0.1% is continuously converted into carbohydrates (e.g., plants) by photosynthesis [1,2], and part of it is used in an assort of ways for providing roughly one-tenth of the current world's primary energy demand [1,2]. In comparison, the "new" forms of renewable energy, like hydro and wind power, provide an estimated 3% of the primary energy worldwide, while fossil fuels and nuclear energy accounts for the remainder, with oil providing ≈32%, natural gas ≈21% and coal ≈28% [2-4]. Nevertheless, the situation changes slowly with time and varies notably from one region of the world to another. For instance, the utilization of gas, coal and renewable energy has been increasing at faster rates over the last 10-15 years [3], especially due to China, as a major coal producer and consumer, and the European Union (EU), as a major impeller towards natural gas and renewables. Indeed, China, US and EU-27, together, are responsible for one half of current world's primary energy consumption; the share of the Union is ≈14% (1760Mtoe in 2010 [3]), of which coal represents 16%, oil 35%, gas 25%, nuclear 13% and renewables 10%. The contribution of biomass to the total renewable energy usage in Europe is just below 70% (118Mtoe in 2010 [3]), being mainly used for heating purposes and electricity. It is unfortunate that the renewables still make such a modest contribution to the primary energy balance of the Union. However, rather large variations exist among the member states regarding the share of the renewables, from above 30% in the Nordic economies to less than 5% in e.g. the UK [3]; the respective share of the renewables to the primary energy mix in Portugal is about 24% (5.65Mtoe in 2010 [3, 5]), as illustrated in Figure 1.1.

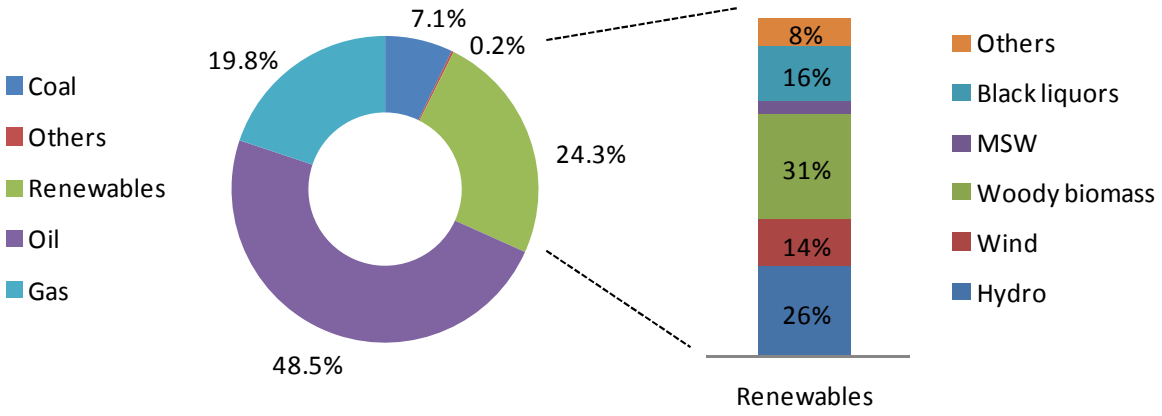

Figure 1.1 - Portuguese primary energy consumption by source, 2010 [5]. On the right, other sources refer to solar, geothermal, biogas and biodiesel.

Like other member states, wood-based biomass (e.g. agricultural byproducts, forest residues) is estimated as the major contributor to the primary renewable energy supply in Portugal (≈30% or 1.68Mtoe in 2010), followed by hydro (26%), renewable wastes (e.g. municipal solid wastes (MSW), biogas, black liquors) (20%), wind power (14%) and biodiesel (6%) [5]. Although the major part of this wood-based fuels is used as a source of heat in the industrial (e.g. in ceramic kilns) and domestic sectors, its use for electricity production is rising relatively fast, from less than 0.03Mtoe in 2005 to ≈0.24Mtoe in 2010 [5,6], whereas conversion into alternative energy carriers (e.g. charcoal) is comparably small. However, the conversion of biomass into electricity is unacceptably inefficient (say, <30% efficiency) which means that, unless the process also features heating or cooling applications, the major part of the biomass energy is lost into the environment. In 2010, an overall ≈2200GWh of electricity was produced in Portugal from biomass (excluding MSW and biogas) [7], which gives about 4% of the gross electricity generation. Of this, about 1580GWh corresponds to electricity produced in combined heat and power (CHP) plants in the industrial sector, mainly using black liquors (>80% of fuel feed [8]) and eucalyptus barks; the remainder 610GWh were generated in dedicated power plants without waste heat recovery, running mostly on forest residues from eucalyptus and pine plantations (tops, barks, branches) and to less extent on agricultural byproducts.

Figure 1.2 shows the major Portuguese biomass power plants for dedicated electricity generation from forest residues, representing a total of ≈105MW_e installed capacity [8-11], of which more than 50% is owned by EDP Bioeléctrica [8]. It is worth noting that only the Mortágua power plant was under operation in 2005. Three of these biomass power plans are equipped with grate furnaces (total capacity just above 23MW_e) and the remainder use

fluidized beds. The Portuguese Government objective for 2020 is an overall 250MW_e of electricity generation from forest biomass residues, in which the new dedicated plants will have capacities typically below 20MW_e [10,12]. A rough estimate based on operational data for the current dedicated plants is that an average of 1.9kton of forest residues are needed for producing 1GWh of electricity [8]. Thus, considering the aforementioned value for the electricity produced in these plants, an estimated 1.2-1.4Mton/year of forest residues are currently used in Portugal for electricity production. This value is expected to rise to close to 3Mton/year when the new power plants get into operation. The current knowledge on the amount of biomass residues that can be taken from the Portuguese forest in a sustainable way is rather uncertain. An optimist figure based on estimates by [9,12-14] is that this availability is no more than a few Mton/year. Thus, producing 250MW_e from forest residues means that the resources will be used at a rate in the order or exceeding its re-growth. However, the situation can become striking on the short term if other activities also start using large quantities of forest biomass residues; for example, it is surprisingly noting that more than a dozen of pellets mills are currently operating in Portugal with an overall capacity of roughly 1Mton/year [8,15]. Even though producing pellets from forest residues might be often difficult due to e.g. soil incorporated in the residues, its utilization for drying the fuel entering the pelletizer is likely. In the same vein, there are many other small boilers around the country which most likely runs on forest residues [9]. Also the highly frequent forest fires which consume typically 1-5% of the Portuguese forest every year (mostly pine forest) [16], might have a negative impact on the future availability of forest biomass residues.

In summary, there is a need for ascertaining whether producing 250MW_e of electric power in dedicated power plants is compatible with a sustainable management of the long rotation forest typical of Portugal. It is likely that agricultural as well as industrial byproducts might be increasingly used as substitute for forest residues in existing and/or planned power plants. Residues from pruning activities in Portugal are estimated at about 0.2Mtoe/year [14], but the potential from the agriculture sector including e.g. residues from olives, vineyards, wine industries (e.g. bagasses), fruit shells (e.g. almond, pine nuts), cork industry (e.g. cork powder, ≈0.04Mton/year [17]) might be relatively higher. Other fuels like refuse-derive fuels and biological sludge from certain industries might be also of interest, especially for co-firing applications with forest residues. Moreover, to keep up with the even-rising demand for forest biomass, it is of utmost importance to find out the more efficient ways for using biomass in dedicated power plants. Apart from electricity production, all technical options for using the waste heat for producing alternative energy carriers from biomass (e.g., gaseous fuels, charcoal) shall be exploited in the short term.

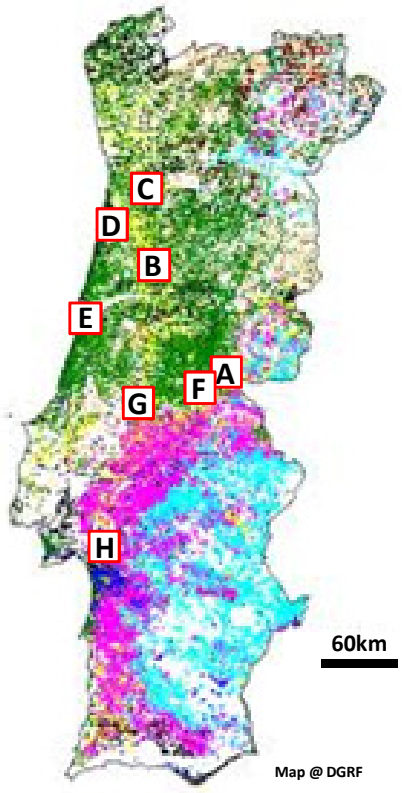

Figure 1.2 - Major biomass power plants for dedicated electricity generation (6 to 30 MW_e; A to C – grate technology; D to H – fluidized bed technology) and distribution of forest stands in Portugal (green and dark blue- pine, pink and light blue – corks, yellow – eucalyptus). Adapted from [8-11].

1.2 *Biomass in the context of the present work*

Unless stated, in this work biomass refers to naturally occurring materials of plants, thus excluding e.g. animal biomass, MSW, sewage sludge and refuse-derived fuels. In turns, wood-based forest biomass (e.g. chips, barks, branches), herbaceous biomass (e.g. straw), agricultural residues (e.g. fruit shells, husks, pruning residues), industrial biomass residues (e.g. sawdust), as well as commercial wood-based fuels (e.g. pellets) are within the scope of this work. These types of biomass are largely composed of organic structures but also include water (i.e. moisture), inorganics (i.e. ash) and, perhaps, extraneous materials such as soil depending on the harvesting techniques. The organic structures composing the cells are mainly lignin, cellulose and hemicellulose, and minor amount of extractives such as resins, to which corresponds an overall elemental composition of typically 45-55 %C, 35-50 %O, 5-7 %H, <3 %N and negligible amount of sulfur (mass% of dry ash-free fuel) [18,19]. Cellulose and hemicellulose are made of long chains of glucose monomers while lignin is mostly of an

aromatic nature and its composition varies somewhat from plant to plant. Softwoods such as conifers typically have higher content of lignin than hardwoods [20]. Note however that, when harvested, as much as 60% by mass of the just fallen biomass is moisture, the value of which decreases to about 10-15% after an air-drying stage. The ash content of biomass varies widely and is typically higher for herbaceous varieties. Materials like straw might have ash contents above 5%, while for wood this value is often below 1% (mass % of dry fuel) [18]. The heating value of biomass is intimately linked to the respective CHONS composition [21,22], in which fuels having higher oxygen contents exhibit lower heating values. The lower heating value of lignins is in the order of 25MJ/kg dry fuel [23,24] while for cellulose it is about two-thirds of the heating value of lignin; the heating value of dry biomass fuels is typically within those of lignin and cellulose. However, for as-received fuels (i.e. immediately after harvesting), the heating value can easily decrease to <10MJ/kg due to the large amount of energy needed to evaporate out the moisture. This compares to values of e.g. 25-35MJ/kg for coals (dry ash-free), and 42-45MJ/kg for oil-derived liquid fuels (see overview in e.g. [24]). The bulk density of biomass fuels depends on a number of factors such as the moisture content, particle size and loading technique. A very rough estimate is about 250 to >600kg/m^3 for loose beds of wood chips and wood pellets, respectively [25]. Such a low density of as-received biomass fuels often makes its transport unacceptably expensive which limits the size of the biomass-fueled processes.

1.3 *Thermochemical biomass conversion*

In thermochemical processes, the solid biomass converts as a result of heat flux and chemical reactions, thus distinguishing from processes involving biological reactions (e.g. anaerobic digestion) or mechanical operations such as those employed for extracting vegetable oils from seeds (see e.g. [26,27] for a survey of conversion routes). Depending on the wanted final products, the thermochemical processes can be structured according to combustion, gasification and pyrolysis processes. Combustion is used when the aim is to fully convert the fuel into thermal energy (i.e. sensible and latent heat) while gasification and pyrolysis permits to recover part of the chemical energy of the parent fuel into the products; gaseous fuels are the preferred products during gasification whereas solid and liquid fuels are favored via pyrolysis. The solid product from pyrolysis is usually referred to as “char” or, sometimes, “charcoal”. The liquid products are operationally defined as a lump of species condensing at ambient conditions, including water and organics (e.g. tars). The optimum operating condition varies widely among the thermochemical processes as discussed latter on in this section.

1.3.1 *Conversion of a fuel particle*

Figure 1.3 illustrates the conversion of a biomass particle in a thermochemical reactor. The major stages are drawn as function of the temperature and include drying, pyrolysis and combustion or gasification; in the open literature the pyrolysis stage is often referred to as devolatilization. It shall be stressed that in this context, pyrolysis, gasification and combustion stages are to be understood as reactions or groups of reactions to distinguish from the aforementioned thermochemical processes (i.e. applications). The basic aspects of the conversion of thermally-tick biomass particles are drawn below as these are of practical interest for most thermochemical processes, as well as it permits a better understanding of the contents of this thesis work.

When the biomass particle is exposed to the hot surrounding gas, the fuel heats by convection and radiation and, as the temperature of the surface layer increases, water (i.e. moisture) starts to evolve; the temperature remains constant during evaporation but depends somewhat on the pressure. As the water escapes from the particle, the drying front goes deeper into the wet fuel while the dry surface layer behind it continues heating up; this will cause the organic structures of biomass to thermal decompose. The cellulose and hemicellulose decompose first, mainly at temperatures below 350ºC, while lignin needs slightly higher temperatures [28]. Anyway, the bulk of the pyrolytic degradation is complete at temperature of about 500ºC [28,29]. Studies on the mechanisms of cellulose pyrolysis (e.g. [30-32]) indicate that the process is initiated by a dehydration stage up to a temperature of ≈250ºC with the liberation of additional water; further heating of the anhydrocellulose leads to a depolymerization stage, yielding a large set of volatile fragments. The detailed mechanism describing the temperature-dependent conversion of the remainder solid are beyond this work but, the degradation proceeds on the basis of the stability of the atomic and/or molecular bonds in the solid matrix. A series of thermal scissions including e.g. decarbonylations, decarboxylations, demethanations along with further dehydrations is expected [30]. It appears likely that the decomposition of the hemicellulose and lignin also proceeds through an early dehydration stage followed by depolymerization/cleavage [33]. The outcome is a vast set of volatile species being released from the pyrolysis front, including water, tarry vapors (e.g., PAHs, levoglucosan, acids, acetone, alcohols), and permanent gases (e.g. CO, CO_2, CH_4), even though the present knowledge on its composition and yields is rather uncertain. Since the pyrolysis reaction is faster near the surface than within the converting particle, after a certain time the outer layer of the particle will be exhausted of volatile matter; this new product layer formed after the passage of the pyrolysis front is the char layer and consists mainly of solid carbon. At intermediate conversion three layers might appear within the fuel particle: an outer layer consisting of char, an intermediate layer of dry

fuel undergoing pyrolysis, and an inner layer of wet (i.e. virgin) fuel undergoing drying. The newly formed species (i.e. moisture + volatiles) always follow in the direction of the external particle surface and, past the outer char layer, escape the particle. It is worth noting that, during transport through the solid matrix, the volatiles experience ever increasing temperatures and decreasing pressures, as well as they can react among each other. The outflow of volatiles is though sufficiently rapid to prevent the bulk gas to diffuse into the particle [34]; accordingly, the nature of the bulk gas is likely of limited importance on the course of the drying and pyrolysis stages. The time required to drive all the volatile matter out of the fuel particle is highly dependent on the operating conditions. It can vary from several tens of minutes in case of carbonization processes to less than 1 minute in case of combustion and gasification in fluidized beds. In combustion processes, the escaping volatiles mix with oxygen at some distance from the particle yielding a highly exothermic reaction with flaming; CO_2, H_2O and N_2 are the final products if conditions are right. In gasification processes, depending on the heat available, the oxidizer is oxygen (or air) at low equivalence ratio and/or steam to secure as much chemical energy in the product gas as possible; here the major reactions involving the escaping volatiles include oxidations, reforming (with H_2O or CO_2), hydrogenations, thermal cracking and water-gas shift reaction. By the end of the pyrolysis stage, the particle is simply char and represents only a fraction of both the volume (say, 50%) and mass (<30%) of the parent fuel particle. In practice, comminution of the char might occur to some extent owing to fragmentation and attrition phenomena [35,36]. The char is then subjected to gasification by the oxygen and/or steam diffusing from the bulk gas, leading mainly to CO_2, or CO and H_2 as major products, respectively. Note that the reactions of oxygen or steam with the char (i.e. carbon) are both types of gasification reactions as the char is converted into gases; the detailed mechanisms of the heterogeneous reactions leading to the conversion of the char are out of the scope of this work (see e.g. Paper X for an evaluation of the char gasification in a fluidized bed reactor). Under combustion like conditions, the time required for char gasification is typically one order of magnitude longer than that need for drying and pyrolysis [37]. Off course that, in the case of pyrolysis processes, the utilization of an extraneous oxidizer is kept at a minimum or not used at all. As a result, the conversion of the fuel particle is quenched once all the volatile matter has been released as the oxygen available in the parent fuel is insufficient to gasify the char; in this case the volatiles are simply discarded or recovered for further processing.

From the description above, it can be stated that: (1) pyrolysis and gasification are both aspects of biomass conversion in combustors; (2) an initial pyrolytic stage is always involved in biomass gasification processes; and (3) combustion and gasification are both undesirable stages in biomass pyrolysis processes.

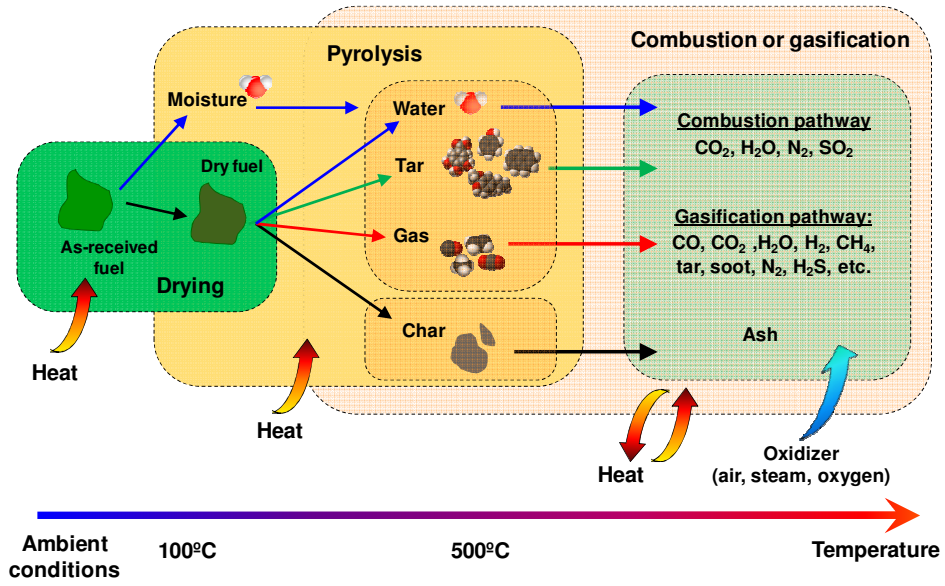

Figure 1.3 - Illustration of the conversion of a biomass particle in a thermochemical reactor. Drying, pyrolysis and combustion/gasification processes are drawn with respect to the temperature of the fuel particle.

1.3.2 *Technologies and applications*

This section provides a brief overview of the most important biomass technologies and applications, as well as it highlights some typical energy carriers obtainable from biomass. Figure 1.4 shows approximated ranges of operating temperatures for a wide range of technologies, including examples of combustion, pyrolysis and gasification processes. This overview is also useful to better understand the possible fields of application for this thesis work.

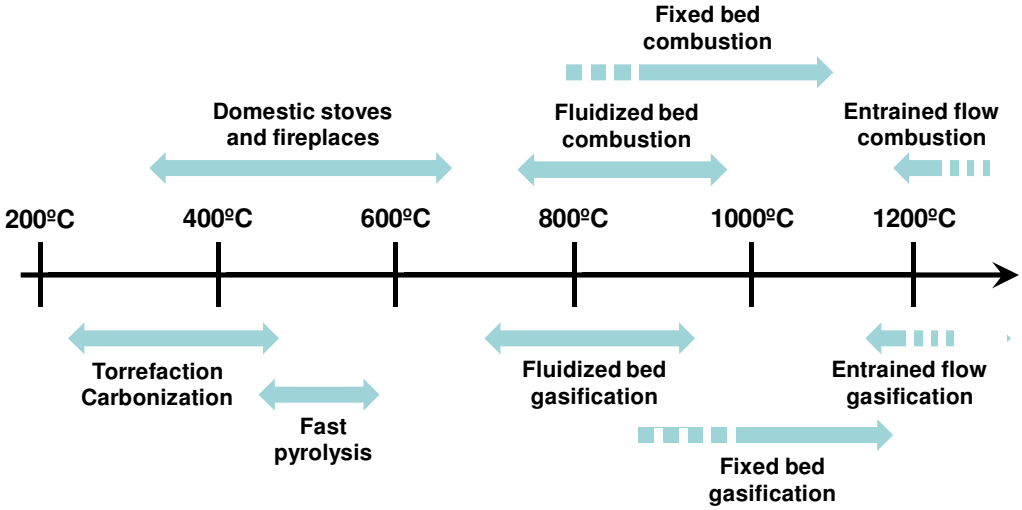

Figure 1.4 - Common technologies for biomass pyrolysis, combustion and gasification and approximated ranges of operating temperatures.

1.3.2.1 *Combustion*

Biomass combustion technologies are widely employed nowadays with capacities ranging from less than 10kW$_{th}$ in domestic systems to above, say, 100MW$_{th}$ in industrial boilers. Apart from cooking, biomass is used in households mainly for space heating through fireplaces, stoves and boilers with over-bed combustion, running mostly on wood logs or pellets. Thermal efficiencies varies from 10-20% in traditional fireplaces to above 80-90% in modern pellet-fuelled systems (see e.g. [27,38]) with built-in fuel feeding system and air-staging features for an efficient burnout of the volatiles. Variants includes e.g. reverse combustion systems in which the primary air is fed above the fuel bed and moves downwards across the fuel; this makes combustion to occur upwards against the air flow in the direction of the fuel surface. The combustion temperatures in domestic appliances are typically within 300-650ºC even though large variations can occur during batch operations (see e.g. Paper XI for a log-fired fireplace and stove). At industrial scale the available combustion methods often evolved from technologies designed for coal combustion with temperatures ranging from about 750ºC to well above 1000ºC. The widely used technologies for large-scale biomass combustion are stationary grates (up to 5MW$_{th}$), moving/vibrating grates (many in range of 20-50MW$_{th}$) and fluidized beds (typically within 10-100MW$_{th}$) [39-41], both of which are relatively simple to operate and can fire a wide range of fuels of varying moisture and particle sizes. These systems are commonly used as boilers to produce steam for different purposes. For example, in cogeneration power plants high quality steam is produced to drive a back-pressure steam turbine for combined electricity generation and steam extraction for processes or district heating systems; this permits to rise the overall efficiency of the cogeneration plant to, say, >85% [25,27]. Grate systems are a kind of fixed bed combustion which allows the fuel bed to travel slowly along the grate while feeding the primary air under the bed (see Figure 1.5 and [40] for an overview). Due to limited mixing of the fuel bed, both the temperature and fuel conversion varies along the grate. Drying and pyrolysis stages occurs in the vicinity of the fuel feed port while the combustion of the char occurs closer to the grate outlet. As a result, local fuel-rich zones are formed above the fuel bed which demands for secondary air supply in the freeboard for mixing and burnout of the volatile matter. In turns, in fluidized beds the relatively rapid mixing of the fuel with the bed solids (e.g. sand) lead to nearly isothermal conditions and better distribution of the volatiles and char across the bed. For the same reasons, fluidized beds resists better to operating instabilities which make it rather flexible with respect to fuel feed even during co-firing applications. Figure 1.5 shows typical designs of fluidized beds operating under bubbling and fast-fluidization regimes; transition between the two operating modes is accomplished by adjusting the fluidizing air velocities from 0.5-2m/s in bubbling beds up to, say, 5m/s in

circulating beds [36]. The latter type greatly enhances the gas-solid contact along the freeboard which also permits a more uniform temperature along the boiler; the entrainment of char and bed solids with the gas is compensated by a recirculation leg (i.e. cyclone and siphon). Further details on fluidized beds can be found in standard text books (e.g. [42,43]) and an evaluation of a bubbling bed combustor with biomass feeding is done in Paper I. Co-firing of biomass with coal in entrained flow boilers is also being considered [44,45] in an attempt to use existing large utility coal-fired boilers (say, >100MW_{th}). In this technology the fuel is ground to fine powder (<400μm for coal [46]) and mixed with the combustion air in a burner before entering the boiler. The resulting combustion rates are very high and boiler temperatures typically exceeds, say, 1200ºC. Nevertheless, the need for fine fuel particles can make it costly to use biomass blends in entrained flow boilers as grinding equipment is needed to be able to pulverize biomass (recommended particle sizes for biomass are below about 5mm [45,47]); also, the boiler responds fast to changes in operating conditions which makes it more suited for high grade fuels and limits the share of biomass. Anyway, co-firing of biomass with coal has the advantage of reducing the emissions of CO_2, SO_2 and NO_x in comparison to coal combustion. Apart from the low S content of typical biomass fuels, it has been argued that the alkaline ash and the volatiles released from biomass in co-firing systems are beneficial in capturing SO_2 while providing an in-situ deNO_x source, respectively [45]. Other technologies used or under consideration for biomass combustion spans from regular kilns to internal combustion engines. Kilns are used in many industrial processes, such as in the manufacturing of ceramics during the high temperature thermal treatment of e.g. bricks; in this case both continuous (e.g. tunnel kilns) and batch operations are possible. Solid fueled internal combustion engines were tested for coal dust and recent developments suggest that it might work also for biomass as its high volatile matter content is likely to promote ignition in the combustion chamber [48].

1.3.2.2 *Pyrolysis*

Carbonization, torrefaction and fast pyrolysis are common branches of pyrolysis processes that use specific operating conditions to increase the selectivity of the process towards a given pyrolytic product. Carbonization technologies have been used since a long time and are directed to the production of chars with high carbon contents. Torrefaction is related to carbonization but recent developments are mainly focused on its use for upgrading of biomass fuels. In turns, fast pyrolysis is aimed at maximizing the recovery of the condensable volatiles released from biomass. All these pyrolysis technologies ensure a reducing atmosphere but the temperatures, residence times and heating rates of fuel vary widely among the processes.

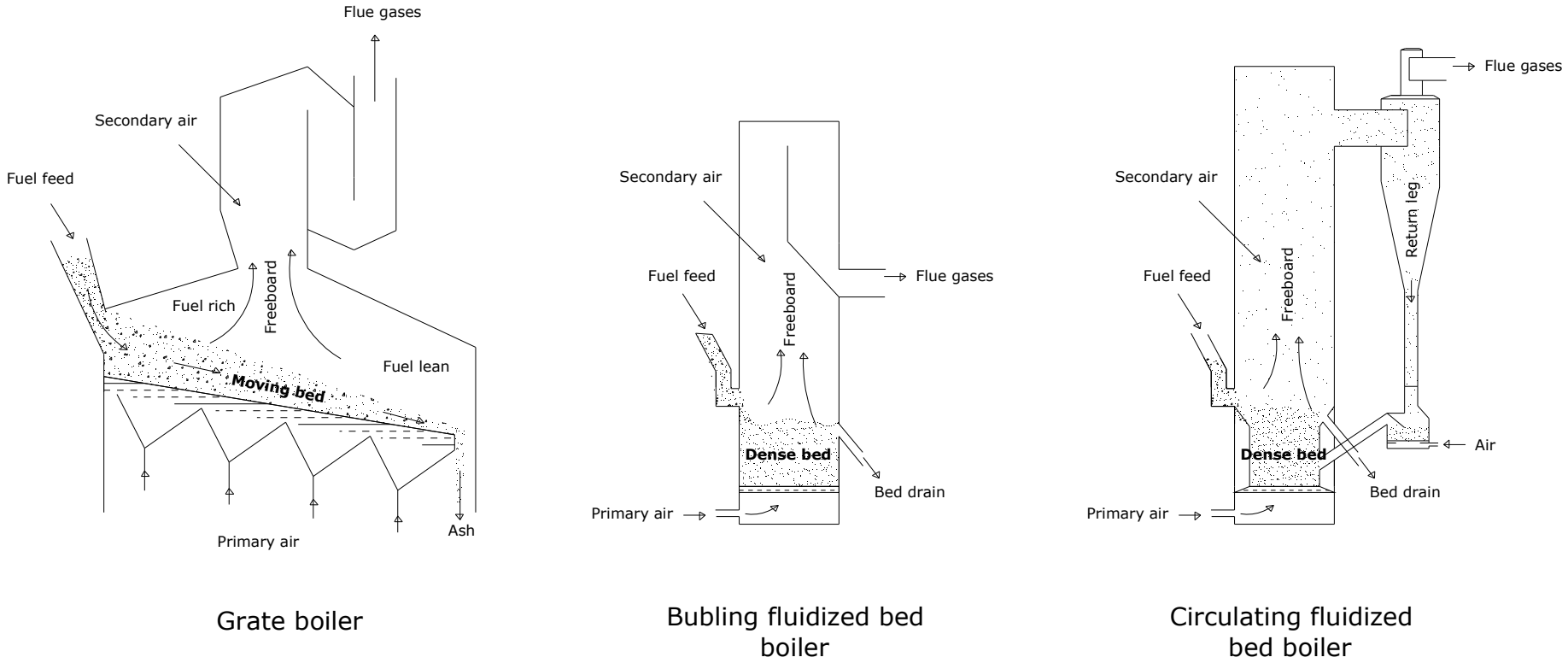

Figure 1.5 - Typical boiler (or combustor) designs for large-scale biomass combustion.

Chars produced from the carbonization of biomass find a wide range of applications in the industry owing to a unique combination of properties like, 1) high carbon content, 2) high heating value, 3) low sulfur, nitrogen and ash contents, 4) high surface areas, 5) high reactivity and catalytic activity, and 6) low electric resistance. The straightforward application of chars is as a low-volatile-matter fuel to support glowing combustion. Apart from cooking fuel, char is commonly used as a reducing fuel in the metallurgical industry to produce iron, steel, ferrosilicon, etc., and has replaced coke to some extent due to its lower amounts of impurities and higher reactivity. As a catalyst, chars have been widely investigated for conditioning the raw gases from gasifiers through primary methods (e.g. [49-51]); in comparison to other catalysts (e.g. dolomites, nickel), the char also offer a good catalytic activity for tars but has the advantage of being continuously formed within the gasifier thus reducing the need for catalyst regeneration/make-up. Chars can be also used as activated carbons in both water and air purification/filtration operations after thermal treatment with H_2O or CO_2 to further increase its surface areas. For essentially the same reasons chars can be useful in separation processes (e.g. chromatographic columns, nickel-plated carbons). Other applications of the char include e.g. the fabrication of electrodes and arts material. Chars resulting from mild thermal treatments of biomass, such as during torrefaction, greatly improve handling while increasing the quality/uniformity of the fuel. Torrefied biomass is hydrophobic, easy to grind to fine particles such as those demanded in pulverized coal burners, and the slight loss of mass due to the release of the pyrolytic volatiles is closely counteracted by the higher heating value of the char (see e.g. [52]). It is also worth noting the renewed interest on the use of biomass chars as a soil amendment which also acts as sequester for CO_2.

The knowledge on the fundamentals and technology of the carbonization process were summarized by Antal et. al. [53]. The highest temperature at which biomass is heated has a great impact on the properties (e.g. carbon content) of the char product. Typical temperatures in torrefaction processes are 250-300ºC but somewhat higher values of, say, 400-500ºC, are desirable to produce high quality chars. The most popular route to increase the selectivity of the pyrolysis process towards the formation of char consists in heating large pieces of biomass slowly, at pressures close to atmospheric pressure. Kilns employing internal heating (i.e. controlled partial combustion of the fuel pile) and retorts employing external heating (e.g. by burning the escaping volatiles to deliver heat back to the retort) are the most common carbonization technologies. These technologies are operated batchwise with reaction times ranging from several hours to several days *per* batch cycle, and volume of the vessel from less than $5m^3$ to above $100m^3$ [53,54]. Nevertheless, there are also examples of continuous processes such as those of Lambiotte and Lurgi [54]. To be able to realize high yields of char while reducing the reaction time in batch operations, pressurized technologies

were proposed (say, 1MPa) in which the tar fragments released from the converting fuel are allowed to re-polymerize into coke [53,55,56].

For the production of pyrolytic liquids (commonly referred to as "bio-oil"), the fast pyrolysis processes are operated in a reversed manner to that of carbonization processes. The essential features of this type of pyrolysis are very high heating rates of finely ground fuel particles (say, mm-sized), peak temperatures within about 450-550ºC, and limited residence time of the volatiles in the hot region. Moreover, the fuel feed must be dry to avoid dilution of the liquid products with water. This means that the range of suitable technologies is limited, as outlined in a book series by Bridgwater et. al. [57-59]: fluidized beds, entrained flow reactors, and ablative reactors. The basics of fluidized beds and entrained flow reactors were already outlined above. Ablative pyrolysis was tested in an attempt to handle larger fuel particles than the reminder technologies; in this case heat is transported to the fuel by pressing the fuel particles against the hot reactor walls by means of centrifugal forces (e.g. Vortex cone reactor [60]) or a rotating blade. Only the fluidized beds (bubbling and circulating types) have reached sizes above 1ton/h fuel [61]. An important feature of the processes scheme is that the pyrolytic volatiles might be immediately cooled down; this can be complemented by operations under vacuum to help in sucking the volatiles out of the converting fuel. By proper manipulation of the process, up to ≈75% of the dry fuel feed can be recovered as bio-oil [29]. However, the bio-oil is a complex soup of water and organics, and its composition and yields cannot be predicted based on current knowledge. It typically consists of a dark-brown viscous liquid, with high water content and mixed solids. Even though there are many potential uses for the bio-oil, such as energy production in boilers and engines, or as transportation fuels, actually mainly the recovery of chemicals (e.g. food flavorings, tars, specialities) is profitable due to handling difficulties and the need for extensive upgrading of the bio-oil.

1.3.2.3 *Gasification*

Unlike pyrolysis processes, gasification of biomass is aimed at converting both the char and the volatiles into useful combustible gases. Accordingly, in gasification processes the pyrolytic volatiles are held captive during longer residence times at temperatures above, say, 750ºC, to convert the heavy organics (i.e. bio-oil) into light gases, whereas the utilization of an oxidizing agent permits to also convert the char into gases. As a practical matter, the quality of the product gas leaving the gasifier becomes a strong function of the temperature as the margin to increase the gas residence time is relatively small. When the heat required for the process is added indirectly by heat transfer, the oxidizer of interest is steam as it permits to increase the heating value of the product gas (say, 13-15MJ/kg); otherwise, heat can be provided directly by partial combustion of the fuel, at an expense of the heating value

of the product gas (say, 5-7MJ/kg). A state of the art review on the biomass gasification processes and technologies can be found in e.g. [62]. The widely investigated reactor designs are fixed (or moving) beds, fluidized beds and entrained flow reactors. Proper selection of a contacting mode is done on the basis of the quality required for the gas and, principally, on the size-scale of the application. Fixed-bed designs are basically updraft (countercurrent) and downdraft (concurrent) being usually operated with air (i.e. direct gasifiers) and at temperatures within typically 900-1200ºC [62]. In an updraft gasifier the fuel is fed on top of the reactor while the air intake is at the bottom. Heat is generated by oxidation of the bottom fuel bed and is convected up across the unconverted fuel with the product gases released from the oxidation zone. As a result, the temperature decreases upwards along the reactor height which means that drying occurs on top while pyrolysis occurs at middle-height of the bed. Thus, the pyrolytic volatiles formed inside the fuel bed are rapidly cooled as they are allowed to pass through the cold fuel before leaving the gasifier. The outcome is a product gas with high content of tars. While this is a minor problem if the gas is to be used hot in e.g. gas burners, some gas cleaning is needed if the gas is to be delivered into e.g. an engine thereby producing electricity. To overcome this problem, in a downdraft gasifier the air intake is closer to the top of the fuel bed while the product gas leaves together with the ashes at the bottom. In practice, this permits to shift the oxidation zone to middle-height of the fuel bed while keeping the drying/pyrolysis front in a confined region close to the top of the bed. Considering that the pyrolytic volatiles have to pass through the oxidation zone before leaving at the bottom of the gasifier, a drastic reduction in the tar content of the raw gas is achieved in down draft gasifiers. This was a motivation for new designs of two-stage fixed-bed gasifiers (e.g. Viking gasifier [63]), in which pyrolysis and gasification occurs in separated vessels; the process is conducted in such a way that allows the volatiles formed in the pyrolytic reactor to pass through a hot char bed for breaking down the longer organics. The principle weakness of the fixed bed gasifiers is that it is difficult to secure a uniform temperature in the oxidation zone when using wide gasifiers which, in practice, limits the size of these units to a few MW_{th} [27,36,62]. For larger sizes, fluidized bed and entrained flow designs are preferred as advantage is taken from the high heating rates of solid fuel that are needed to realize low yields of char during the pyrolysis stage; though, they operate with rather different temperatures thus matching to different applications. In fluidized bed gasifiers the temperatures are usually controlled to within 700-900ºC which permits relatively high contents of hydrocarbon species (e.g. CH_4) and tars in the product gas. Tars are unwanted components but the hydrocarbons are desirable when the aim is to e.g. obtain a substitute for natural gas. Nevertheless, fluidized beds were mainly demonstrated for direct gasification with air [62], which dilutes the product gas with N_2 (typically >50%v N_2). To improve the gas, pure oxygen can be used as fluidizing medium instead of air but an oxygen

plant is costly. Otherwise, a dual fluidized bed design permits to drive an autothermal gasification process without the need for pure oxygen. In this design part of the biomass is burned in one reactor while the remainder fuel is gasified in a second reactor fluidized with steam. As the bed material is circulated between the two interconnected reactors, heat is continuously transferred from the combustor to the gasifier without mixing the respective flue gases. In the same vein, some char is likely to be transported back to the combustor as pyrolysis is able to produce more char than what the gasifier can consume. Examples of this dual-bed technology are found in a $8MW_{th}$ plant in Güssing (Austria) [64] and $2+12MW_{th}$ plant at Chalmers University of Technology (Sweden) [41,65], both of which yield a product gas with less than 5-10%v nitrogen and heating value above 13MJ/kg. For applications requiring lower amounts of hydrocarbons in the raw gas (e.g. synthesis), entrained flow gasifiers might be interesting as the inherently high temperatures (say, >1200ºC) enables the gas to approach thermodynamic equilibrium. Also pressurized operations are easier with entrained flow gasifier if the biomass particle size is small enough for slurry feeding. Some drawbacks of this technology are related to aggressive nature of biomass ash during slagging operation.

1.3.2.4 *Integrated technologies*

The most well know example of integrated technologies is the so-called Integrated Gasification Combined Cycle (IGCC) in which biomass is converted in a gasifier and the so obtained raw gas is combusted in a gas turbine whereby producing electricity; the hot exhaust gases from the turbine are in turn used to produce high quality steam to drive a Rankine cycle. However, Figure 1.6 shows many other ways for using biomass combustion in combination with pyrolysis and/or gasification technologies. Note the possible routes through which dedicated power plants (i.e. electricity only) can be retrofitted to be able to attain a more reversible biomass conversion process. The basic improvement is to deliver part of the unused heat into e.g. a district heating system (i.e. cogeneration plant). Other possibility is to drive an integrated drying or pyrolysis process by means of low enthalpy heat (see e.g. [66]). When high enthalpy heat is available in large amounts the aforesaid dual fluidized bed technology can be used to provide heat to an indirect biomass gasifier which greatly increases the possibilities for using biomass, from e.g. reburning applications to Fisher-Tropsh synthesis [41,67].

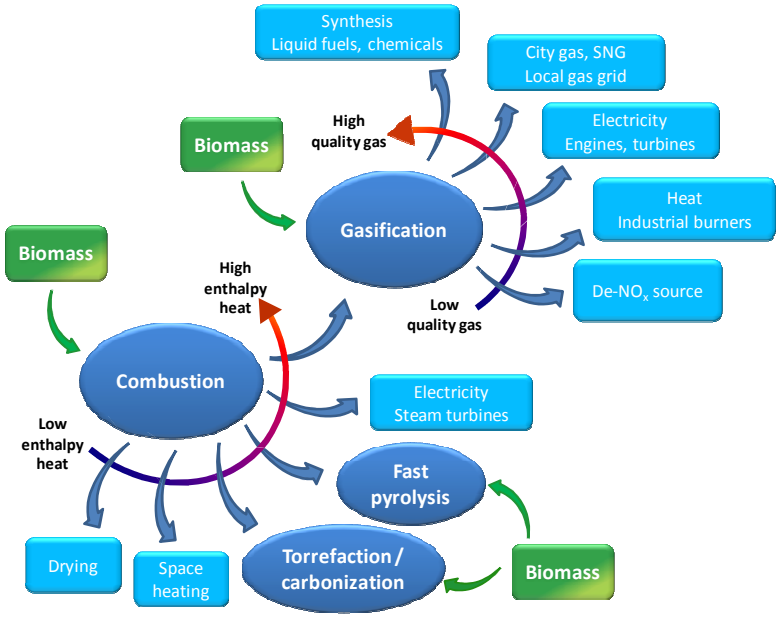

Figure 1.6 - Synergies between the combustion, pyrolysis and gasification processes for poly-generation of various energy carries from biomass.

1.4 *Aim of the present work*

This thesis work is intended to contribute to the deployment of low-carbon growing economies with ever decreasing emissions of pollutants into the environment. In this regard, renewable energy and energy efficiency will play major roles in displacing fossil fuels. High interest in biomass exists nowadays as it is a renewable source of carbon and hydrogen and, thus, biomass-derived energy suits to a wide range of end-users. In what ways the biomass resources shall be used in the future can be discussed, but considering the high dependence of the technological societies on fossil energy, solutions have to be found in the short term for an efficient use of biomass in the energy systems. The present work focuses on the thermochemical conversion of solid biomass, covering combustion and, especially, gasification processes; however, it was felt that the practical design of biomass combustors and gasifiers should more closely rely in basic investigations on the pyrolysis stage, which is why pyrolysis plays the large part in this work. It also intends at assisting in the development of integrated processes to simultaneously produce various energy carriers from biomass. The previous section showed that the fluidized bed is the reactor of choice for most thermochemical processes which was the motivation for using this type of reactor in this work.

For the understanding of the fundamentals of biomass thermochemical conversion in fluidized beds, guidance from dedicated experiments is needed. Indeed, the intricate gas-solid

contacting pattern of fluidized beds, the high volatile matter content of biomass fuels, and the plausible kinetic, mass and heat transfer limitations, greatly increase the complexity of the conversion process which means that mechanistic models to describe a converting fuel particle tend to be too sophisticated. At the present state, unless the process is largely governed by thermodynamics, models for predicting the stoichiometry (and kinetics) of the overall reaction are often of limited practical usefulness and demands for empirical information. This is especially the case of biomass gasification (and pyrolysis) in fluidized beds as the yields and properties of the pyrolytic products are required to evaluate and predict the operation of the reactor; existing particle models clearly have limited predictive capabilities with respect to biomass pyrolysis. Also for combustion applications a description of the pyrolytic stage might be necessary if the fuel conversion along the reactor and the pollutant formation are to be treated. Otherwise, when only the overall heat release and an estimate of the composition of the exit flue gases are needed, the assumption of infinitely fast reaction might be enough. A similar treatment for the case of biomass gasification (and pyrolysis) in fluidized beds is still not possible and one really hopes that this thesis work can contribute to bridge this gap.

Considering the aim of this work, there was early consensus that experimentation was the first option to get the wanted information. The investigation that was carried out can be divided into two main parts. The first part intends at clarifying the operation of a fluidized bed combustor and a fluidized bed steam gasifier. The second part intends at summarizing and complementing the current knowledge on the pyrolytic decomposition of biomass. In both cases the conversion process is investigated with respect to the characteristics of fuel feed and the operating conditions. One of the prime motivations for the experiments was also to help in defining sensible problems through which essential progress in modeling work could also be achieved.

The part of this work related to biomass gasification is highlighted. In this regard the aim was at developing critical design parameters related to the conversion behavior of biomass for a new process of highly efficient poly-generation of electricity, heat and transportation fuel. This innovative process was demonstrated at industrial scale in a project at Chalmers University of Technology (hereinafter referred to as Chalmers), into which this work was incorporated. The intent was to perform dedicated pyrolysis measurements in laboratorial scale at the University of Aveiro (hereinafter referred to as UA) to support the evaluation and optimize the operation of the Chalmers gasifier. During the evaluation of the gasifier a measurement method for the composition the raw gasification gas turned necessary, which has motivated one to also work in this field. This shows how this work is intended at providing data useful for practitioners, which is why the word “engineering” is used throughout this thesis work.

1.5 *Experimental facilities*

Various experimental facilities were used during the course of this work, from laboratorial scale (gasification gas combustion apparatus, fluidized bed and fixed bed biomass pyrolysis reactors, thermogravimetric analyzer), pilot scale (fluidized bed biomass combustor), to industrial scale (dual fluidized bed biomass gasifier), as listed in Table 1.1.

For addressing the combustion behavior of biomass in fluidized bed, the pilot-scale bubbling fluidized bed facility at the UA was used. This facility has been developed in [68,69]. An evaluation of the effect of the initial thermal degradation of biomass into volatiles and char on the progress of fuel conversion along the reactor height was made thanks to multiple sampling probes for gases and a set of measuring systems, namely for gas composition, pressures, temperatures and mass flow rates of gases and solid fuel.

The $2MW_{th}$ Chalmers gasifier provided the opportunity of working with a kind of dual fluidized bed process at industrial scale. The gasifier has been designed for research purposes thus offering suitable conditions to accomplish a great deal of measurements. A set of gasification experiments were conducted in this work aiming at developing suitable monitoring tools for the process. The analysis of the composition of the raw gas leaving the gasifier was done with the help of the gas combustion apparatus developed in this work. Through this apparatus, a "one step" analysis of the CHON contents of the raw gas is possible which means that gasification process can be monitored with a high time resolution. This new method consists in burning a slipstream of the raw gasification gas in a small gas combustor at first and, then, retrieving its CHON composition by mass balance across the small gas combustor. Figure 1.7 shows the principle of the proposed new measurement method.

The laboratory fluidized bed facility was used for studying the pyrolysis behavior of biomass under operating conditions relevant for industrial fluidized bed combustors and, especially, gasifiers. All the major pyrolytic products (char, permanent gas, condensables and soot) can be collected for subsequent analysis. Experiments were done with the fuels used in the pilot scale fluidized bed combustor and the Chalmers $2MW_{th}$ gasifier thus supporting the evaluation of these units. The laboratorial fluidized bed facility, including the reactor, analysis systems and control systems, was developed to a large extent during this work.

To complement and verify the measurements carried out in the laboratory fluidized bed, additional experiments were done in the small fixed bed apparatus offering similar thermal conditions to those in the fluidized bed. However, here the focus was only on the recovery of the char fraction for subsequent gravimetric analysis. A large set of biomass fuels were used in the experiments to investigate how the composition of parent fuel influences the yield of char. Some improvements to this fixed bed apparatus were also done in this work. The

analysis of the charring process was also supported by a set of pyrolysis experiments conducted with slow heating of biomass in a thermogravimetric analyzer.

The intent of this section is to provide an overview of the experimental facilities listed in Table 1.1, including details not given in the papers supporting this thesis. Nevertheless, a partial overlap of the contents given in the papers could not be avoided. The facilities developed during the course of this work are, of course, described in a more detailed manner and some results are given for a better understanding of the respective operation modes. Table 1.1 also shows the papers in which the facilities were used. The fuels and ancillary equipments used for fuel preparation are also covered in this section.

Table 1.1 - Experimental facilities used in this work for evaluating the conversion characteristics of biomass upon pyrolysis, gasification and combustion in fluidized bed.

Laboratorial scale	Pilot scale	Demonstration scale
Gasification gas combustion apparatus (Paper II)*,†	$30kW_{th}$ bubbling fluidized bed combustor (Paper I) ‡	$2MW_{th}$ bubbling fluidized bed gasifier (Paper II) †
Bubbling fluidized bed reactor (Papers IV and V)*,‡		
Fixed-bed pyrolysis apparatus (Paper IV)*,‡		
Thermogravimetric analyzer (Paper IV)†		

* Developed or improved during the course of this work; † Located at Chalmers; ‡ Located at UA.

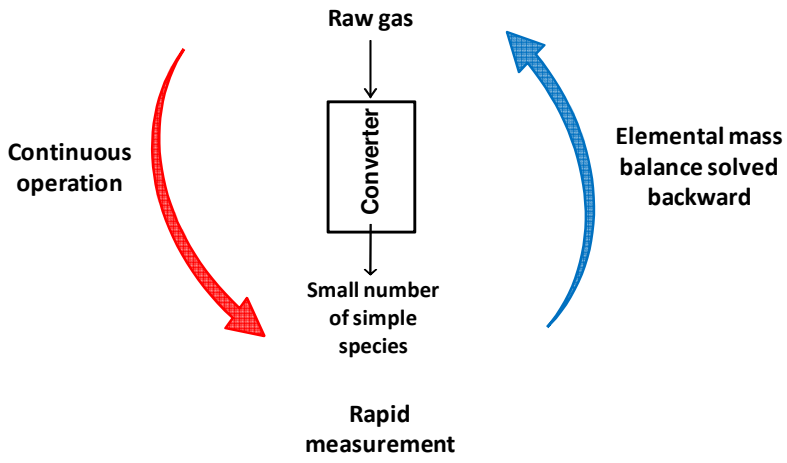

Figure 1.7 – Operating principle of the proposed measurement method for the CHON composition of the raw gas leaving a biomass gasifier.

1.5.1 *30kW$_{th}$ fluidized bed combustion facility*

Figure 1.8 shows a photograph of the pilot scale fluidized bed combustion facility. A detailed description of this facility is beyond this thesis work because this can be found in several publications (e.g. [68-71]). This facility can be divided into three main sections: fluidized bed combustion section, gas sampling and analysis section, and data acquisition and control section for a remote control and monitoring the whole facility via computer.

The core of the combustion section is a thermally insulated bubbling fluidized bed reactor (AISI 310 SS) with overall dimensions of 0.25m ID and 3m height. This reactor features bed of silica sand (500-710μm particles) with ≈0.23m in height, a nozzle-type distributor for the primary combustion air used as fluidizing medium, nine water-cooled ports for sampling gases, and monitoring pressures and temperatures along the reactor height (three of which inside the bed), ports for charging/discharging of bed solids, as well as specific ports accommodating various devices: (1) an auxiliary gas burner, (2) a zirconia O_2 cell, (3) a connection for the fuel feeding system, (4) a connection for the secondary combustion air supply line, and (5) various water-cooled heat-exchangers. The biomass fuel is fed to the reactor by a screw-feeder located on top of the freeboard and, then, falls down through a vertical SS tube over the surface of the bed. This vertical tube also permits to inject and transport the secondary air together with the fuel, from the air inlet port at the reactor top flange to close to 20cm above the surface of the bed. The freeboard temperature is controlled by a water-cooled tube also wound around the fuel feeding tube. In turns, the bed temperature is controlled by eight radial water-cooled probes inserted into the bed. The fuel feeding system is calibrated manually by means of a scale and timer or automatically through a load cell. The mass flow rates of the primary and secondary combustion air are measured by separated rotameters (0-300LPM), together with suitable manometers and thermocouples; calibration of the rotameters is done by a dynamic volumetric method described in [68]. Also integrated in the bottom part of the reactor tube is an electrically heated oven for heating the primary combustion air during the start-up procedure of the reator. The pneumatic circuits for controlling the various gas streams entering the fluidized bed reactor (e.g. combustion air, N_2 purging gas, propane for the start-up gas burner) make use of solenoid valves to be able to operate the system either in an automatic or manual manner.

The gas sampling and analysis section comprises a series of water-cooled probes, suitable pneumatic systems integrating gas conditioning devices and PTFE diaphragm pump, a set of online gas analyzers, as well as pressure sensors and thermocouples. The water-cooled gas sampling probes are inserted into the aforesaid sampling ports along the reactor tube, each one with built-in K-type thermocouple, a plug filter for removing particles, and a

backup condenser for removing water and heavy organics. The exception is one probe inserted into the freeboard through the reactor top flange for sampling gases by a 180ºC heated line. The pneumatic circuits are integrated into automatic gas control and distribution units which permits to selected a specific probe for sampling gases and turn the online gas analyzers into service in a controlled way (see [68] for a detailed description of this units). The set of online gas analyzers used in this work includes O_2 (paramagnetic, ADC 700), CO_2 (NDIR, ADC 1450 Luft), CO (NDIR, ADC RF558), NO (chemiluminescent, ThermoElectron 10A), N_2O (NDIR, ADC RF558) analyzers for measuring the dry gas composition, and a total hydrocarbon analyzer (flame ionization detection, Dyna-Fid, SE-310) for measuring hydrocarbon species in the wet gas. Calibration of the gas analyzers was done regularly against standard gases. All the sensor signals are read by the automatic data acquisition system referred above (see [68] for details).

The set of operating conditions as well as the specific experimental procedures used during the course of the combustion experiments that were carried are described in Paper I.

1.5.2 *2MW$_{th}$ dual fluidized bed gasifier*

At Chalmers University of Technology, a bubbling fluidized bed biomass gasifier has been integrated onto an existing 12MW$_{th}$ circulating fluidized bed boiler. The gasification concept at Chalmers use the thermal flywheel of the circulating bed material as a mean of providing heat to the pyrolysis and char gasification taking place in the gasifier. Details of the Chalmers gasification process are available elsewhere [41,65] and only an overview is provided here. Figure 1.9-a shows how the Chalmers gasifier is connected to the boiler. With a high fluidizing velocity, the hot bed material is carried out of the boiler with the combustion flue gases and separated from the flue gas in a cyclone. The separated material fall down into a particle distributor that is fluidized with air or dry flue gas. Here the bed material is allowed to return to the boiler directly, via an external heat exchanger, or pass into the gasifier to realize the sensible heat for the endothermal reactions. To put the gasifier into service, two loop seals located upstream and downstream the gasifier and fluidized with steam are used to allow the circulation of bed material across the gasifier and to prevent bypassing of gas (especially N_2) from the boiler. Steam is also used as fluidizing medium in the gasifier where the flow rate is adjusted to the requested steam-fuel ratio (usually, 0.7-1.1 kg/kg). Silica sand with an average particle diameter of 270μm is used as bed material and the circulating rates can be varied between 14 and 25ton/h [72-74]. Fresh biomass is fed by a screw feeder and two rotary valves placed in series to the surface of the bubbling bed gasifier (typical bed temperatures of 750-850ºC); about 2MW$_{th}$ of fuel are fed, causing the temperature of the bed material to drop in 20-40ºC across the gasifier. Any char that might leave the gasifier

Figure 1.8 - Pilot-scale bubbling fluidized bed combustion facility at UA.

unconverted is transported to the boiler with the circulating bed material. At the present state, the produced raw gasification gas is also sucked into the boiler to produce additional heat, which leads to a slight under-pressure in gasifier (≈-1 kPa).

To be able to evaluate the process and how the fuel converts, the Chalmers gasifier is provided with a great deal of ports for sampling gas and bed material as well as probes for measuring temperatures and pressures. As an example, Figure 1.9-b shows a set of ports for collecting samples from inside the bed up to the freeboard of the gasifier; additional ports are located close to the bed material inlet and outlet ports and along the raw gas standpipe. Temperatures are also measured within the dense bed as well as at the aforesaid ports by PT100 probes or thermocouples. Venturi type meters are used for measuring the flow rate of steam (≈140ºC, 25MPa) entering the loop seals, as well as, the distributor of the gasifier. In order to monitor the fuel feed rate into the gasifier a scale is used to continuously weighting the fuel silo.

Under the evaluation of the operation of the gasifier carried out in this work, a small flow rate of the raw gas was taken from a sampling port located at about 2m downstream the raw gas outlet of the gasifier. After passage through an in-situ ceramic filter, the slipstream of the raw gas was transported by heated line (≈360-400ºC) into systems for measuring its chemical and elemental compositions (see section 1.5.3); details on the operating condition of the Chalmers gasifier during the course of the experiments are given in Papers II and VII.

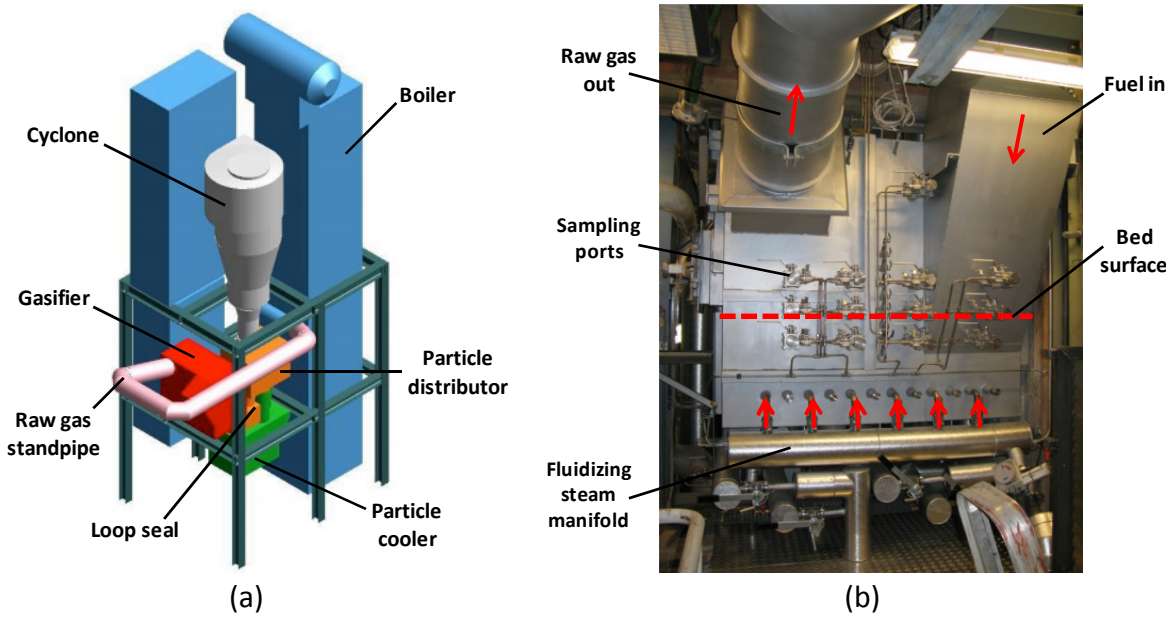

Figure 1.9 – Chalmers (2+12)MW_{th} dual fluidized bed biomass gasification process. Coupling of the 2MW_{th} bubbling fluidized bed gasifier onto the infrastructure of the 12MW_{th} circulating fluidized bed boiler (a) and front view of the gasifier (b). Figures adapted from [41,65].

1.5.3 *Gasification gas monitoring facility*

The gasification gas monitoring facility was designed for obtaining a "real-time" analysis of the CHON composition and condensables content of the raw gas leaving the Chalmers gasifier. Figure 1.10 provides the process schematic for this facility, including an online gas combustion apparatus and ancillary systems for (1) injecting a know flow rate of a tracer gas (He) into the gasifier, (2) drying and cleaning a slipstream of the raw gas leaving the gasifier and (3) analyzing the chemical composition of a permanent gas sample. The system for injecting helium into the gasifier was needed to be able to close the overall mass balance across the gasifier. In combination with the system for conditioning the raw gas, helium injection also provided an estimate of the amount of condensables (water + organics) in the raw gas. The gas analysis system serve to multiple purposes around the experiments, including the analysis of the flue gases leaving the combustion apparatus and the raw gas leaving the Chalmers gasifier. The facility, experimental methods as well as examples of operation are described in considerable detail in Papers II and VII; some aspects specific for the online combustion apparatus are given hereinafter.

1.5.3.1 *Online gas combustion apparatus*

Figure 1.11 shows a photograph of the online gas combustion apparatus developed in this work; the overall dimensions of the apparatus were limited to 2×0.9×0.6m to be able to transport it to close to the Chalmers gasifier. The combustion apparatus can be divided into four main sections: (1) gas combustion section, (2) flow control and measurement section, (3) flue gas conditioning and measurement section, and (4) electronic control section.

Gas combustion section

The gas combustion section includes a gas burner, reactor tube and an electrically heated oven. Apart from the raw gas, the burner also permits to handle standard gases from cylinders in a controlled manner which is useful during the calibration procedures of the method. In this case, the reactants enter the burner through separated ports and mix only in the tip of the burner; a perforated nozzle attached to the burner helps in spreading the flame while enabling to insert a 1.5mm OD thermocouple (K-type) down into the combustion chamber (see Figure 1.12). Though, in case of burning the raw gas, the oxidizer and raw gas mix in a small venturi placed upstream the burner (Figure 1.110), which is used for sucking the raw gas from the outlet port of the gasifier. A hole bored through the reactor top flange accommodates the burner in a vertical position. The reactor tube is made of 253MA SS with dimensions of 33.4mm OD and 770mm length (Figure 1.13); the tube dimensions were selected to fit the size of an existing 2.8kW$_e$ electrically heated oven. The purpose of the

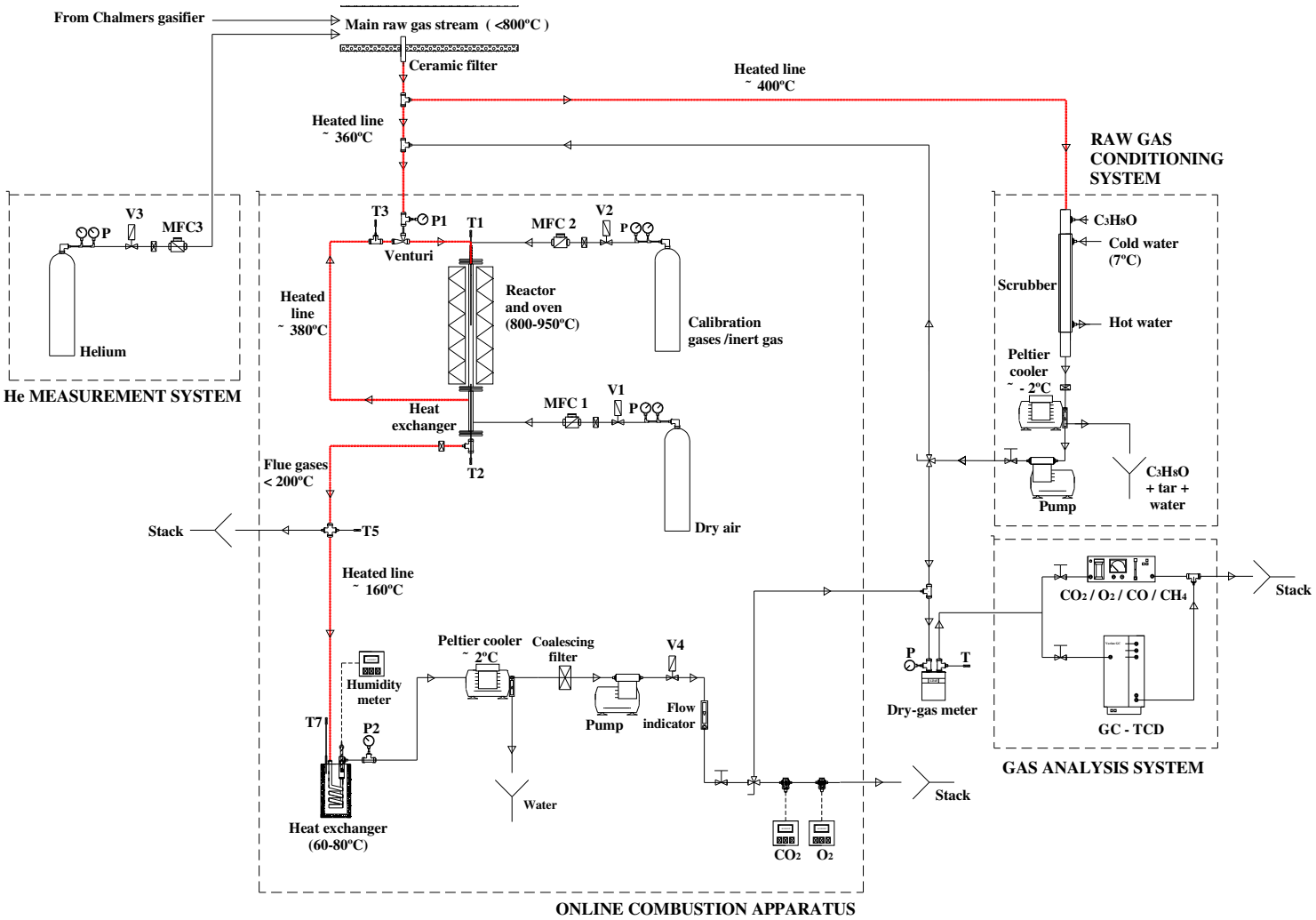

Figure 1.10 - Illustration of the gasification gas monitoring facility, including the online gas combustion apparatus and ancillary systems. Red lines indicate heated sampling lines. T – temperature measurement, P – pressure measurement, MFC – mass flow controller, V – solenoid valves.

reactor was to convert the slipstream of the raw gasification gas into CO_2, H_2O and N_2 and the practice showed that this was feasible over a wide range of combustion conditions, including temperatures within 800-950ºC, atmospheric pressure, excess-air above 10% and gas residence time below 0.5s, with no need for a combustion catalyst.

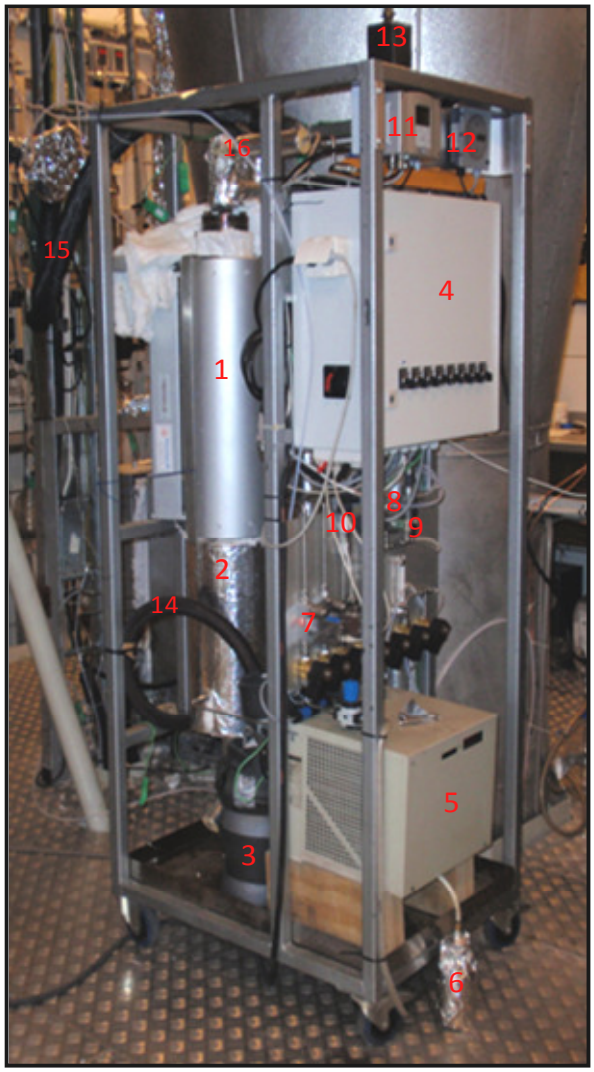

Figure 1.11 - Online gas combustion apparatus. 1- reactor & oven; 2 – counter-flow heat exchanger; 3 – online moisture measurement; 4 – electronic control section; 5 – Peltier cooler; 6 - condensate; 7 – mass-flow controllers; 8 - O_2 cell; 9 - CO_2 cell; 10 - pressure transducers; 11 - humidity transmitter; 12 - CO_2 transmitter; 13 -stack; 14 – 160ºC heated hose (flue gases); 15 – 360ºC heated hose (raw gas); 16 - heated venturi & burner.

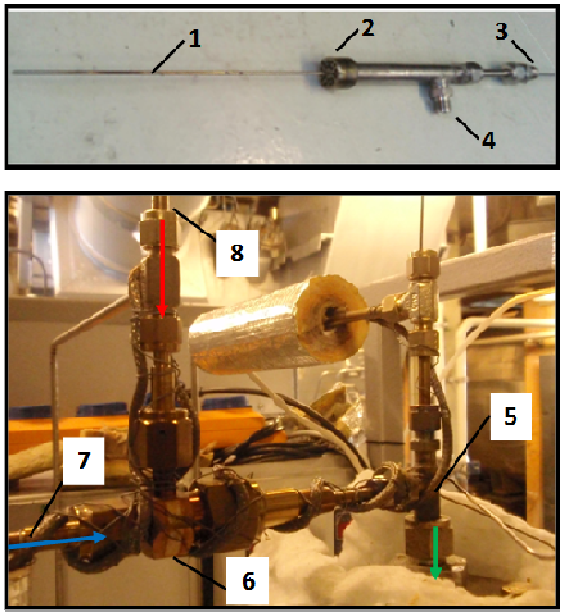

Figure 1.12 - Gas burner (top) and respective connections to the venturi and combustion reactor (down). 1 – thermocouple; 2 – nozzle; 3 –calibration gas or inert gas inlets; 4 and 7 – combustion air inlet; 5 – gas burner mounted on the reactor top flange; 6 - venturi; 8 – raw gas inlet. Arrows indicate flow directions.

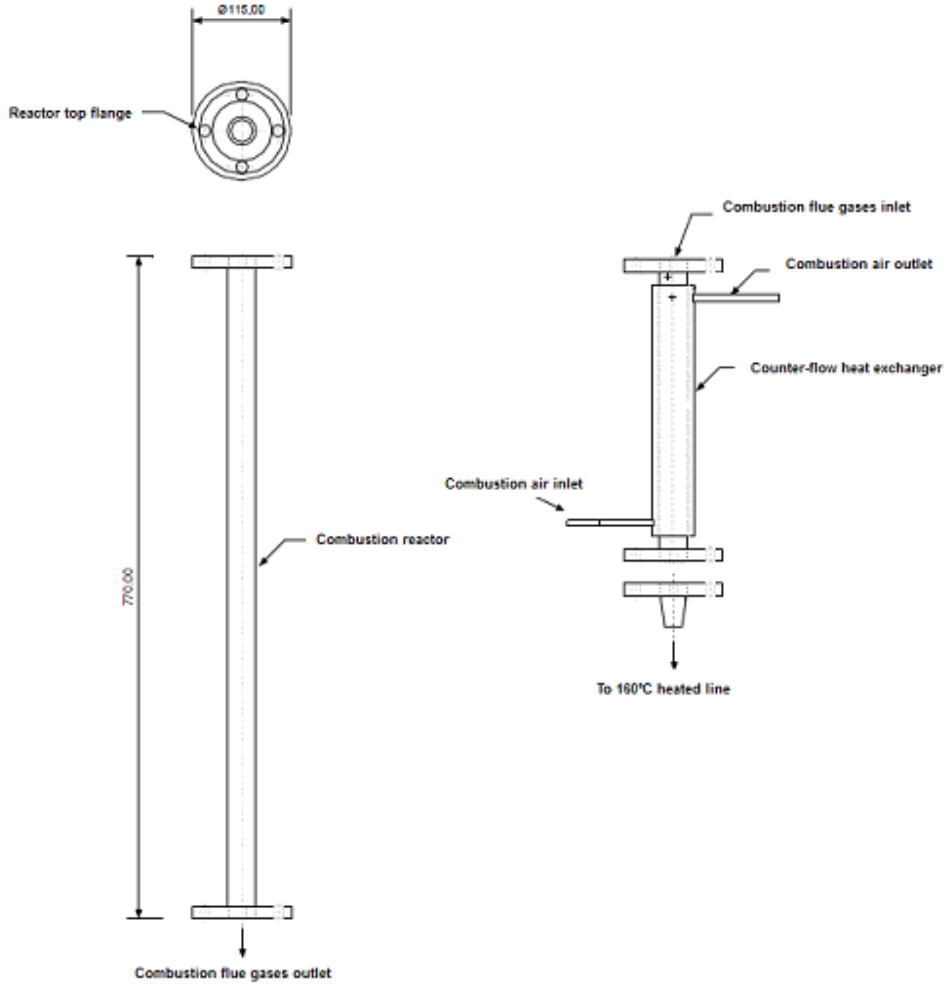

Figure 1.13 – Combustion reactor and counter-flow heat exchanger with respective flanged connections.

Flow control and measurement section

The flow control and measurement section comprises a suitable SS pneumatic circuit operated by solenoid valves, two thermal mass flow controllers (Bronkhorst EL-FLOW, 0-29 and 0-5NLPM), two absolute pressure sensors (WIKA S10, 0-1.6bar) and an all-welded SS venturi (ApTech, AP70), as outlined in Figure 1.14. The pneumatic circuit enabled to open or close the gas supply to the burner in an automatic way; apart from the combustion air and the calibration gases, also an inert gas (He or N_2) could be supplied for measurement reasons or security reasons. The gas flow rates are adjusted and measured by the mass-flow controllers, with ranges of 0-20NLPM for the combustion air and 0-5NLPM for the other gases. These controllers were factory calibrated and were tested in our laboratory within certain ranges by means of a 1L bubble meter and timer. The pneumatic circuit also includes a multiplexing feature for reading pressures in various points through one single pressure sensor (P1). The

combustion air pass through the venturi positioned immediately before the burner, where constriction of the air flow causes the raw gas to flow into the vacuum port of the venturi (see photograph of the venturi setup in Figure 1.12). The ratio of vacuum to pressurized flow rates entering the venturi is a function of the gas flow rate through the pressurized side which made it possible to adjust the air/fuel ratio during the experiments (see Paper VII); the generated vacuum could also be monitored by one of the pressure sensors. A high temperature heating hose (0.28kW/m, 8mm OD SS tubing) is used to keep the slipstream of the raw gas at a temperature above 350ºC all the way between the outlet of the Chalmers gasifier and the vacuum port of the venturi. The venturi itself and the gas burner are also heated to ≈380ºC by trace heating (0.25kW/m) and are well insulated by ceramic wool.

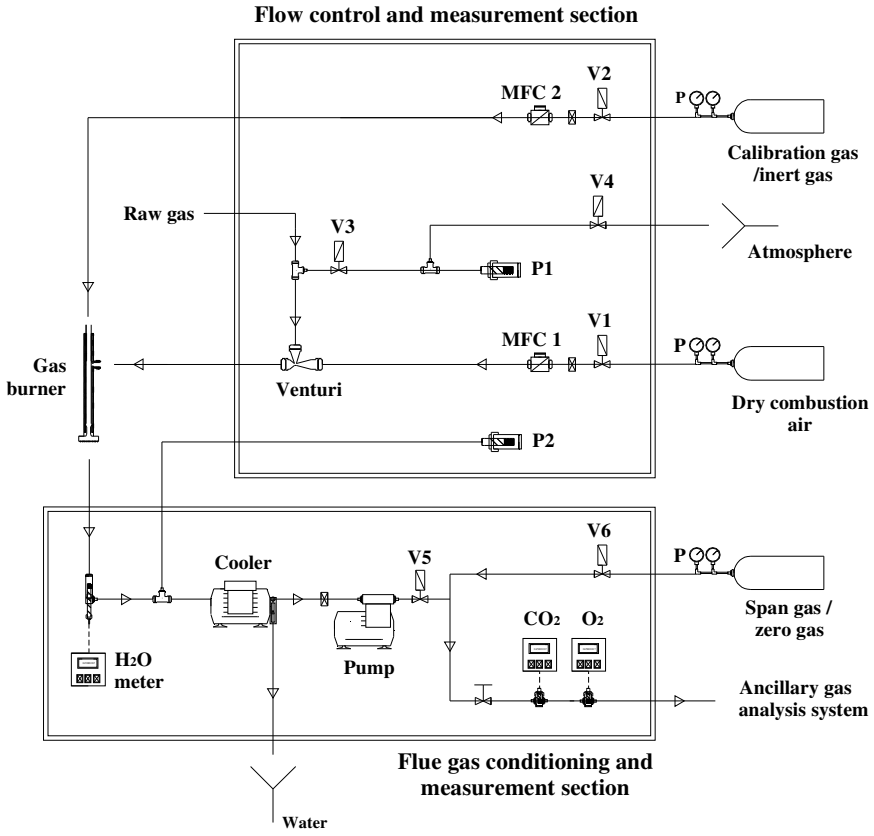

Figure 1.14 – Simplified sketch of the pneumatic circuits of the gas combustion apparatus. With the exception of the solenoid valves V1 to V6, the abbreviations are according to Figure 1.10.

Flue gas conditioning and measurement section

The flue gas conditioning and measurement section allows to cool, dry and clean the gas exiting the small combustion reactor as well as to analyze the respective composition (H_2O, O_2 and CO_2). A counter-flow heat exchanger was designed to rapidly cool the flue gases to below 200ºC (see Figure 1.13), being connected to the reactor bottom flange. Construction

was also made with 253MA SS and the insulation consists of rock wool. The coolant is the dry combustion air which flows up through the outer tube of the heat exchanger. Air preheating is beneficial for increasing the volumetric flow rate across the venturi as well as to avoid condensation of certain components of the raw gas in the venturi (mainly tars). A thermocouple (1.5mm OD) is placed close to the pressure port of the venturi to ascertain that the temperature of the incoming air is above that of the heating hose transporting the raw gas. A small flow rate of the flue gases (2-4LPM) is sampled downstream the heat exchanger by a diaphragm pump and the remainder gas is discarded. A sampling line has been setup for measuring the concentration of H_2O in the gas-phase. This is done by a another heating hose (0.14kW/m, 6mm OD PTFE tubing) transporting the flue gases at ≈160ºC to an online moisture measurement system [75], incorporating a relative humidity probe (Vaisala HMT338, 0-100%), PT100 temperature sensor and a connection to an absolute pressure sensor (P2 in Figure 1.14); to improve the accuracy of the measurements, the flue gases are further cooled to below 80ºC in oil-bath heat exchanger so that the relative humidity increases to within 50-80%. The humidity probe was also factory calibrated and tested against the conventional gravimetric method for measuring the moisture content of gases (see results in Paper II). After the moisture measurement system, the flue gases pass through a Peltier cooler and coalescing filter for separating out the water and aerosols. The dry and clean flue gases are finally passed through built-in O_2 (Figaro KE-25, electrochemical cell, 0-100%v) and CO_2 (Vaisala GMT 220, NDIR, 0-10%v) gas sensors for monitoring the operation of the combustion reactor within a short time. However, for the evaluation of the proposed method for the CHON composition (and condensables content) of the raw gas, the ancillary gas analysis system shown in Figure 1.10 was used instead. This system combines an online gas analyzer (Rosemount NGA2000, NDIR) for measuring CO_2, O_2, CO and CH_4 and a gas chromatograph (Varian GC4900) with a pre-configured channel for measuring both He and N_2 (see Paper II for details); the ancillary gas analysis system is part of the research infrastructure at the Chalmers power central and is regularly calibrated against standards.

Electronic control section

The core of the electronic control section is a real-time control and data acquisition system (National Instruments, CompactRIO) with embedded controller and data-logging features, being programmed with LabView graphical language. The system also features RS232-connection for the mass flow controllers and configurable chassis with up to eight I/O modules for application development. The setup used in the present work included the following modules: NI9205 (16 channel, ±10V analog input), NI9211 (4+4 channel, ±80mV thermocouple input, cold junction compensated), NI9485 (8 channel, SSR 60VDC switching) and NI9401 (8channel, 5V/TTL digital I/O). The first two modules were used for reading the

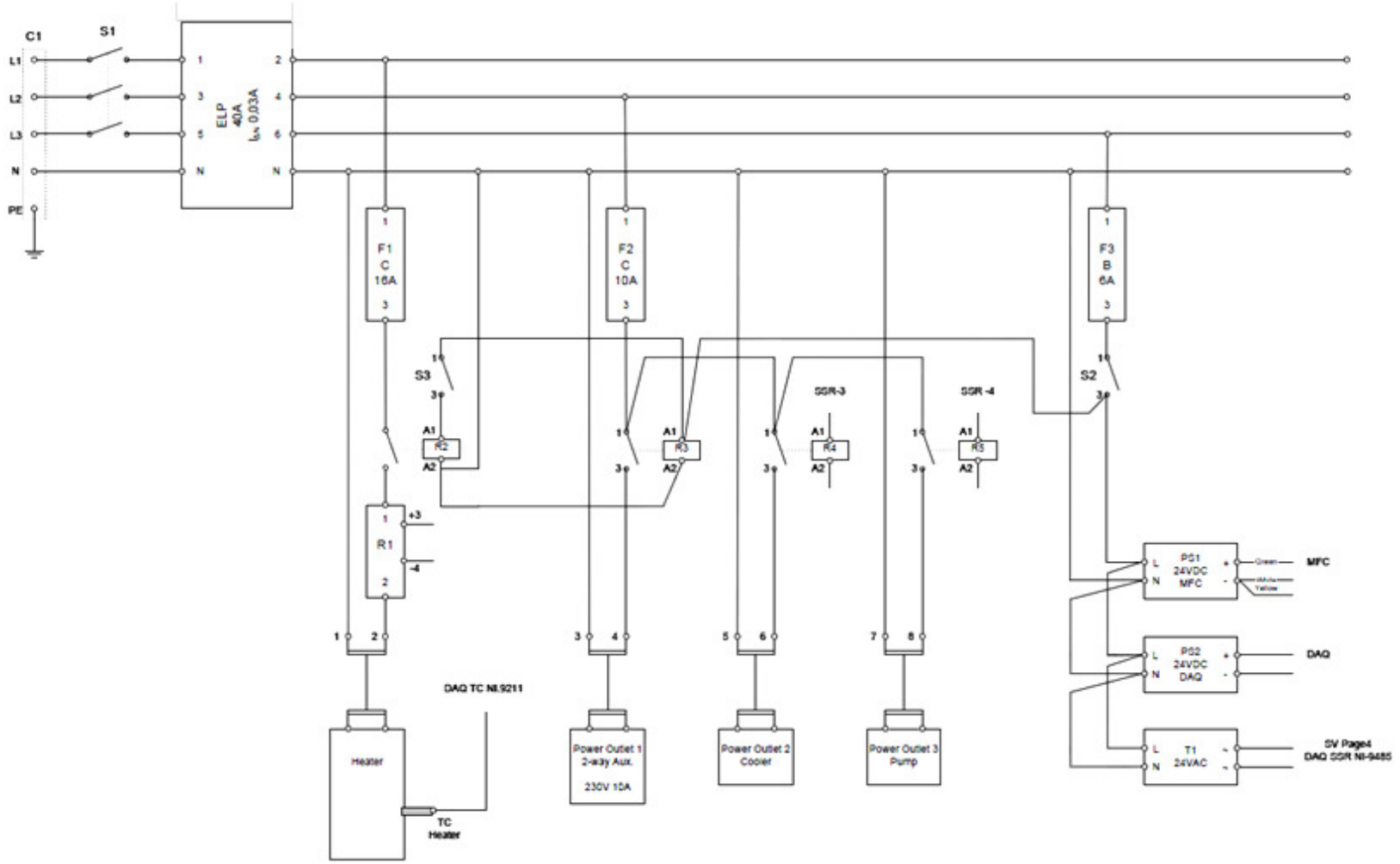

Figure 1.15 – Main electric circuit of the online combustion apparatus. ELP – 3-phase monitoring relay; S1 to S3 – manual switches; F1 to F3 – fuse switches, R1 – solid state contactor; R2 to R5 – electromechanical relays; SSR 3 and SSR4 – solid state relays.

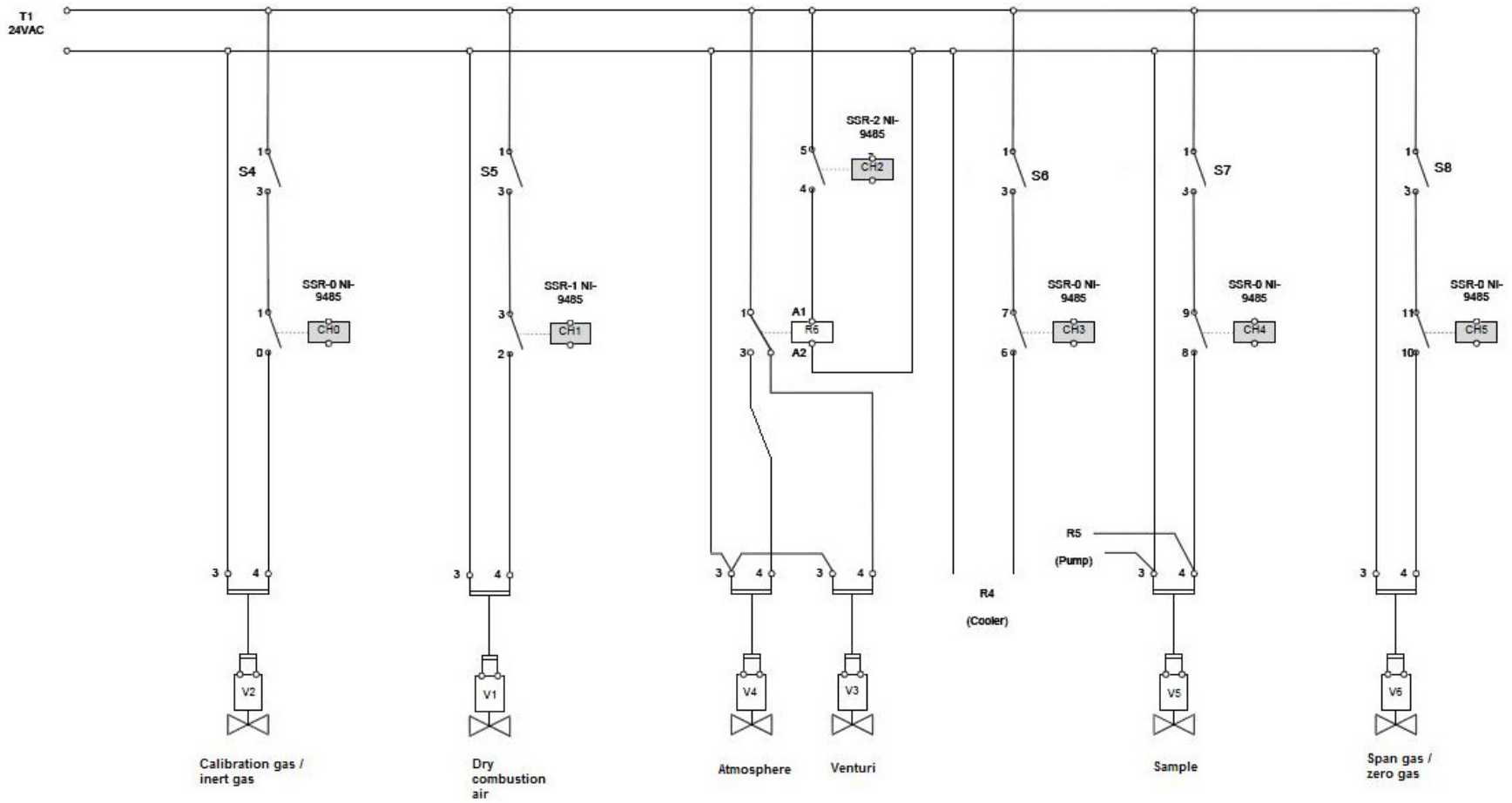

Figure 1.16 - Electric circuit driving the pneumatic circuit of the online combustion apparatus. V1 to V6 – solenoid valves; S4 to S8 – manual switches; R6 – electromechanical relays; SSR 0 and SSR5 – solid state relays.

sensor signals among the gas combustion apparatus (humidity sensor, pressure sensors, O_2 and CO_2 gas sensors, thermocouples and PT100); the SSR module enables to control the solenoid valves and various electromechanical relays; the digital I/O module was need for driving the power circuit of the reactor oven via solid state contactor. Figure 1.15 shows the main electric circuit of the combustion apparatus, where it can be seen the separated phases for powering the reactor oven, various 220VAC loads (e.g. Peltier cooler, diaphragm pump), the CompactRIO system and mass flow controllers (24VDC), and the solenoid valves (24VAC). In turns, Figure 1.16 shows the details of the electric circuit for an automated operation of the solenoid valves shown in Figure 1.14 as well as the pump and cooler. A suitable Labview application was developed to control and monitor the operation of the combustion reactor via a laptop computer, which included an embedded routine for controlling the temperature of the reactor oven. Figure 1.17 shows the graphical interface enabling to carry out any individual task among the experimental rig.

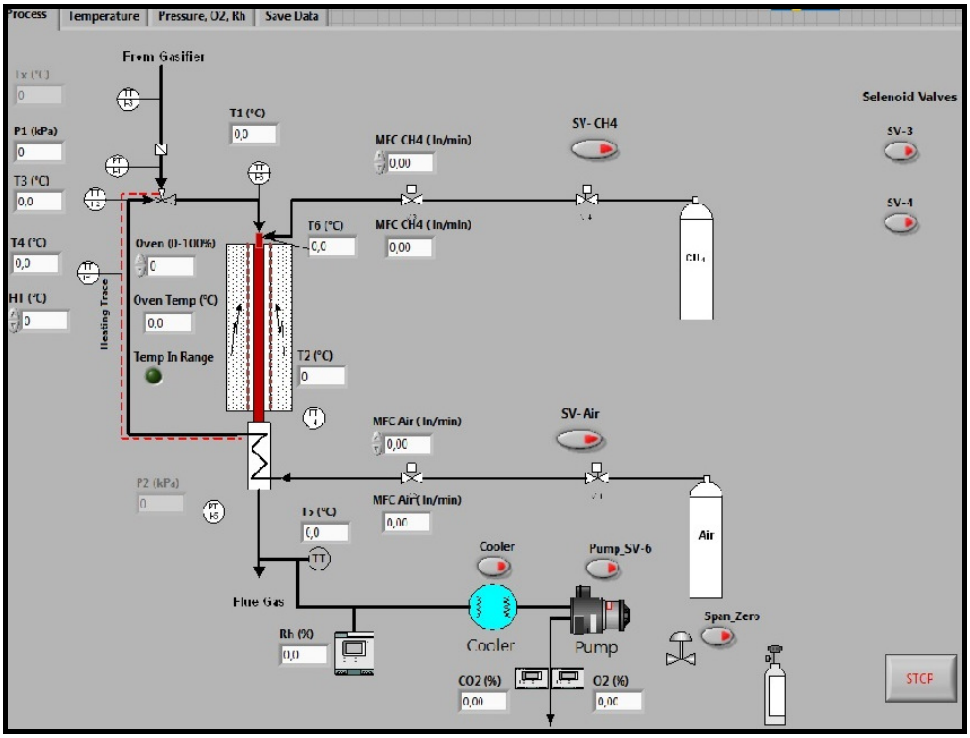

Figure 1.17 - Labview graphical interface for controlling and monitoring of the online gas combustion apparatus.

1.5.4 *Laboratorial fluidized bed pyrolysis facility*

This facility is composed of a small bubbling fluidized bed reactor and ancillaries for biomass fuel feeding, fluidizing gas measurement and control, and flue gas conditioning and

analysis, as outlined in Figure 1.18. It was used in experiments described in Papers IV and V, where it is investigated the yields and properties of the major pyrolytic species released from biomass under operating conditions relevant for large-scale fluidized bed combustors and gasifiers.

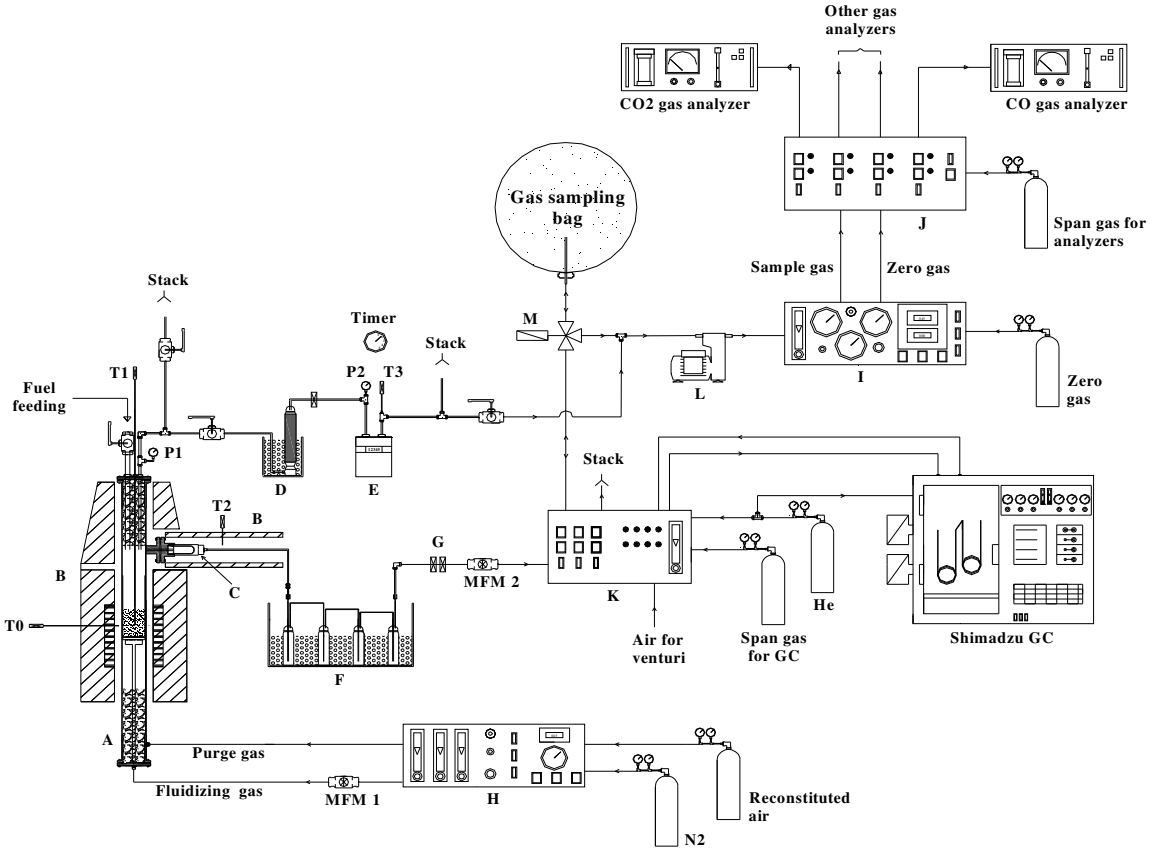

Figure 1.18 - Outline of the laboratorial fluidized bed pyrolysis facility at UA. A – bubbling fluidized bed reactor, B – electrically heated ovens, C – heated quartz thimble filter, D – ice bath with silica gel tower, E – bellows-type volume meter, F – ice bath with impinger bottles, G – quartz backup filters, H – fluidizing gas control and measurement unit, I – gas sampling and conditioning unit, J – gas distribution unit, K – volatile gas control and measurement unit, L – diaphragm pump, M – 3-way solenoid valve, P1 and P2 – pressure measurement, T0 to T3 – thermocouples, MFM1 and MFM2 – mass flow meters.

1.5.4.1 *Fluidized bed reactor*

The fluidized bed reactor has been though to accomplish two types of experiments: pyrolysis of solid biomass under inert atmosphere, with fast-heating to peak temperature within ≈600-1000ºC, and combustion of the char formed during the pyrolysis stage. Some issues taken into account for the reactor design were: possibility of feeding of cm-sized fuel particles; interface with various gas sampling lines (including heat line); recovery of the char formed in-bed; integration into existing control and monitoring system (e.g. electrically

heated furnace). A detailed sketch of the fluidized bed reactor is shown in Figure 1.19. The reactor main body consists of an AISI 310 SS tube with dimensions of 700mm ID and 920mm length. The top and bottom connections are of a flange type and sealed with suitable gaskets. A hole bored through the bottom flange enables to insert a SS tube along the axial line of the reactor which transports the fluidizing gas through the preheating zone and then into the bed. The bed is held in another 62mm ID SS tube (note the inner concentric tube in Figure 1.19) incorporating suitable distributor plate and winbox. The bed together with the freeboard extends over ≈270mm up to the thermal insulation material (ceramic wool) placed in the upper part of the reactor tube. On top of the freeboard the escaping gases are allowed to enter into alternative sampling lines: (a) the volatiles formed during the initial pyrolysis stage enter the side port and are lead by heated line, while (b) the flue gases formed during the subsequent burnout of the char enter the upper port and are cooled in the other line. This upper port is also used as (a) a pressure tap during the pyrolysis stage or (b) gas exhaust. Also on top of the freeboard is the fuel feeding tube which is connected to a ½ in. ball valve placed outside the reactor. To help in feeding various fuel particles in simultaneous, an accessory is used to guide the particles across the ball valve. A third hole bored through the top flange accommodates a K-type thermocouple (3mm OD) to ascertain the temperature from inside the dense bed up to the top of the freeboard. Also worth to mention is the side port in the bottom part of the reactor tube which is used for purging the whole vessel with inert gas.

Distributor

The distributor consists of an AISI 310 SS perforated plate. This kind of distributors can be designed from orifice theory following procedures given in e.g. [42,43]. The critical point is that the pressure drop across the distributor (ΔP_d) might be high enough for an even distribution of the fluidizing gas over the entire cross sectional area of the bed. The practice shows that ΔP_d shall be preferably within 0.2-0.4 times the pressure drop across the bed (ΔP_b) [42,43], as given by Eq. 1.1. Due to technical reasons, the orifice diameter (d_{or}) is taken as 0.6mm and the number of orifices (N_{or}) is then determined by Eq. 1.2, where u_{or} is the gas velocity through one orifice (Eq. 1.3). The results obtained following this procedure are summarized in Table 1.2 for a wide range of operating conditions. It is seen that N_{or} varies considerably and, one possibility followed here, was to take N_{or} as the mean value over the conditions of interest (N_{or}=30). Though, during the construction phase the layout shown in Figure 1.19 was adopted where the number of orifices is 29. The initial result with this distributor showed that stagnant zones could be avoided even at low fluidizing velocities and, therefore, it was used throughout this work.

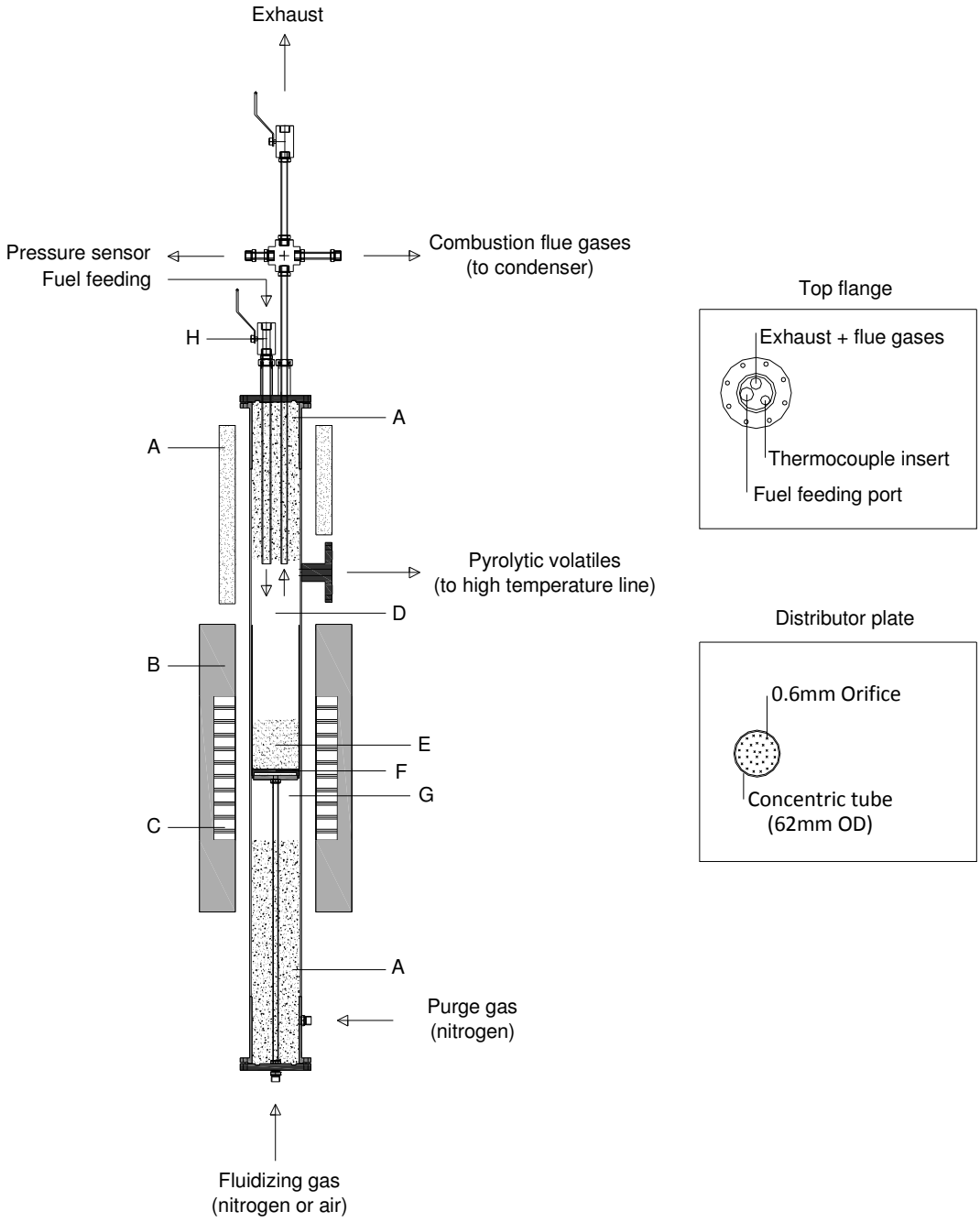

Figure 1.19 - Sketch of the laboratorial bubbling fluidized bed reactor. A – thermal insulation, B – 2.5kW$_e$ oven, C – heating element, D – freeboard, E – dense bed, F – distributor plate, G – fluidizing gas preheater, H – ball valve.

$$\frac{\Delta P_b}{H_{mf}} = \left(1-\varepsilon_{mf}\right)\left(\rho_p - \rho_g\right)g \qquad \text{Eq. 1.1}$$

$$N_{or} = \frac{4u}{\pi d_{or}^2 u_{or}} \qquad \text{Eq. 1.2}$$

$$u_{or} = C_{d,or}\left(\frac{2\Delta P_b}{\rho_g}\right)^{1/2} \qquad C_{d,or} \approx 0.8 \qquad \text{Eq. 1.3}$$

Table 1.2 - Design of the distributor plate of the small fluidized bed reactor. Effect of bed temperature (T_b), gas fluidizing velocity relative to minimum fluidizing velocity (u/u_{mf}), and pressure drop across the distributor (ΔP_d), on the number of orifices of the plate.

	$\Delta P_d=0.2\Delta P_b$		$\Delta P_d=0.3\Delta P_b$		$\Delta P_d=0.4\Delta P_b$	
T (ºC)	$u/u_{mf}=3$	$u/u_{mf}=4$	$u/u_{mf}=3$	$u/u_{mf}=4$	$u/u_{mf}=3$	$u/u_{mf}=4$
600	31	41	25	34	22	29
700	27	37	22	30	19	26
800	25	33	20	27	17	23
900	22	30	18	24	16	21
1000	20	27	17	22	14	19

Bed material and fluidization parameters

The bed material is silica sand supplied by a commercial company. The particle size distribution of the raw sand was measured by means of test sieves (Retsch) with mesh sizes of 125, 180, 250, 355 and 500μm. According to a method given in [68,76], the particles resting within the 125-500μm sieves can be represented by a mean Sauter diameter of 170μm. However, to avoid the very smallest and largest sand particles, only the particles resting within the 180-250μm sieves were used as bed material. Table 1.3 summarizes the properties for this class of particles which correspond to group B solids according to the Geldart classification [42,43]. The minimum fluidizing velocity (u_{mf}) for this bed material can be estimated from the Ergun equation (Eq. 1.4), where the bed voidage at minimum fluidization condition (ε_{mf}) is taken from literature. For round particles with sizes within 200-300μm, ε_{mf} has been measured within 0.42-0.44 [43] and, thus, a value of 0.43 can be used in this work. Conversely, the maximum fluidizing velocity at which the bed shall be operated corresponds to the free-fall velocity of the sand particles (u_t) given that the entrainment of bed material might be avoided. Figure 1.20-a provides u_{mf} as well as various values of u/u_{mf} for the bed particles as a function of bed temperature and flow rate of fluidizing gas. During the pyrolysis experiments in Papers IV and V the bed was operated with flow rates of nitrogen of about 2.5NLPM which leads to fluidizing velocities (u) within typically 2.5 to 4 times the values of u_{mf} (i.e. bubbling regime, $u_{mf}<u<u_t$). the predicted values of u_{mf} agreed fairly well with the minimum bubbling velocities observed during the experiments (visualization through the fuel feeding port). Figure 1.20-b shows the operating condition of the small fluidized bed reactor in the general regime map.

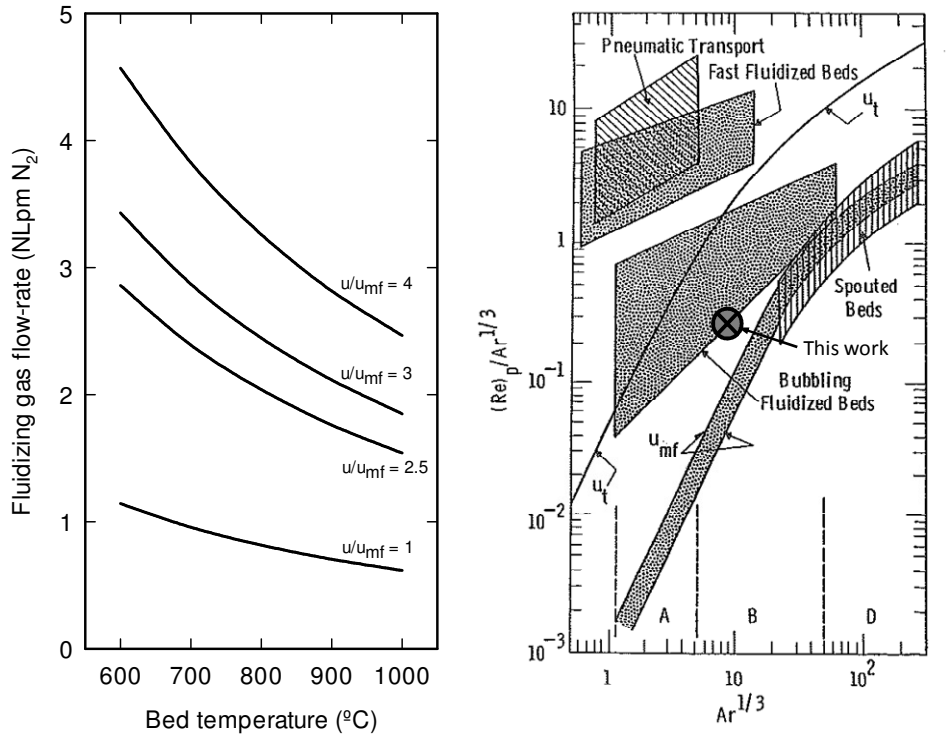

Figure 1.20 - Fluidization characteristics of the laboratorial fluidized bed reactor. Fluidizing velocities with pure N_2 as a function of bed temperature (left) and general regime map(right).

Table 1.3 - Properties of the bed material used in the laboratorial fluidized bed reactor.

Parameter	Units	Value	Reference
Min. and Max. diameters	μm	180-250	This work
Mean Sauter diameter	μm	208	This work
Bulk density	kg/m^3	1530	This work
True density (ρ_p)	kg/m^3	2600	[43]
Sphericity (φ_s)	--	0.86	[43]
Voidage at u_{mf} (ε_{mf})	--	0.43	[43]

The amount of bed material used in the reactor depends upon a number of issues. First, the design of the electrically heated furnace which is provided with one heating coil at middle height of the furnace (see Figure 1.19) which might furnish heat mainly to the bed and to the fluidizing gas preheater. Thus, the distributor is positioned at half height of the heating zone and the bed height is adjusted to minimize heat losses in the upper part of the bed. Also, the bed has to provide good thermal inertia so that the fresh fuel particles decompose under nearly isothermal conditions. Finally, it is useful to keep the bed aspect ratio close to unity. After an exploratory study, it was found suitable to use 250g of silica sand which leads to 55mm static bed height. The bed height at incipient fluidization is given by Eq. 1.5 while the bed expansion factor (H/H_{mf}) depends upon the fluidizing velocity. Bed expansion due to bubbles can be estimated e.g. by the two phase theory of fluidization as given by Eq. 1.6

[43,77], where u_b is the bubble rise velocity given as a function of the bubble size, or by suitable correlations from the literature (see e.g. [36]). For the conditions used in the experiments the outcome is that $H/H_{mf} \approx 1.25$ which corresponds to a bubbling bed height of ≈70mm. One possibility to check out this value is to measure the temperature profile along the fluidized bed reactor, as shown in Figure 1.21. It can be seen nearly isothermal conditions from the distributor plate up to a height of 60mm and a slight temperature decrease from the 60 to 80mm. These results indicate that the bed surface is somewhere within 60-80mm height which is in agreement with the theoretical values of H/H_{mf} and also shows that the fluidizing gas preheater works properly. Also, major temperature variations could also be avoided during the course of pyrolysis of one fuel batch with this bed. For example, Figure 1.22 shows the time-dependent bed temperature (T1) during pyrolysis of typical fuel batches (2-5 dry particles). The bed temperature decreases rapidly once the fuel particles reach the bed surface, with minimum values somewhat dependent on the mass dry fuel fed. However, in general, the bed temperature doesn't decrease below -2% of the initial value.

$$u_{mf} = \frac{d_p^2 (\rho_p - \rho_g) g}{150\mu} \frac{\varepsilon_{mf}^3 \varphi_s^2}{1-\varepsilon_{mf}} \qquad Re_{p,mf} < 20 \qquad \text{Eq. 1.4}$$

$$H_{mf} = \frac{m_p}{\rho_p A_r (1-\varepsilon_{mf})} \qquad \text{Eq. 1.5}$$

$$\frac{H - H_{mf}}{H_{mf}} = \frac{u - u_{mf}}{u_b} \qquad \text{Eq. 1.6}$$

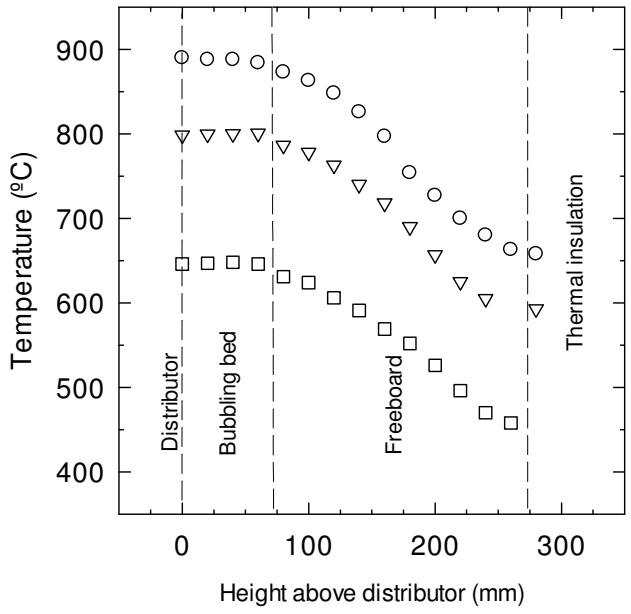

Figure 1.21 - Axial temperature profiles along the fluidized bed reactor. Examples with N_2 fluidizing gas (bubbling regime) and bed temperatures of 650, 800 and 900ºC.

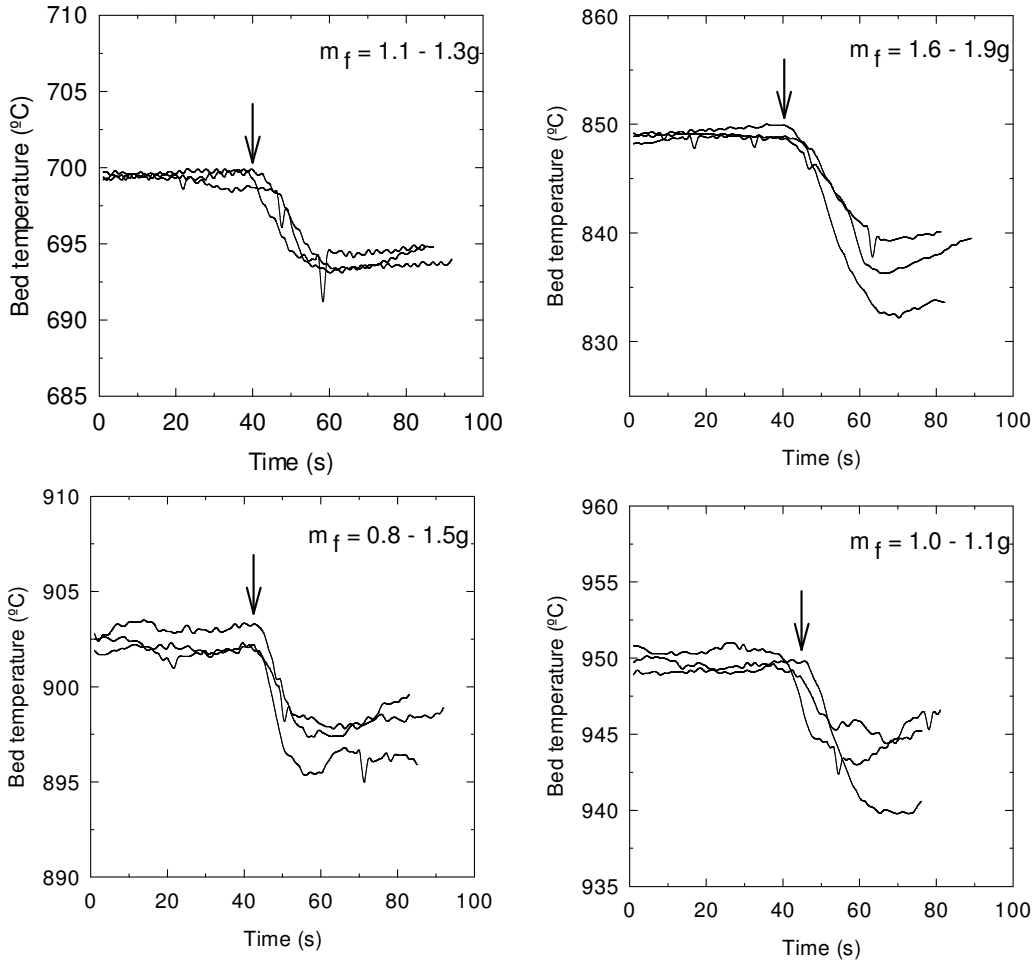

Figure 1.22 – Time-dependent bed temperature (T1) during pyrolysis of typical dry fuel batches (noted m_f). Examples with forest residues pellets at 700, 850, 900 and 950ºC bed temperatures. Arrows indicate the moment of fuel feeding (3 tests *per* temperature level).

1.5.4.2 *Sampling line for the pyrolytic volatiles*

This sampling line is used in Paper V to determine the composition and yields of the volatile species leaving the fluidized bed reactor during pyrolysis of a dry fuel batch. An outline of this line is shown in Figure 1.23, that include a heated particle filter, a condenser, two backup filters, a gas mass-flow meter, various solenoid valves and a gas expansion bag. As stated above, this line connects to the reactor via the side sampling port located on top of the freeboard. Initially, this connection was based on screw fittings but, latter, a flange connection was used instead of the screw fittings. Between the sampling port and the condenser (≈500mm SS tubing), the line is thermally insulated with ceramic wool and heated to around 380ºC by trace heating (0.5kW$_e$). This enabled to remove the particles (e.g. soot) by in-line filter without simultaneous vapor condensation (e.g. tar); the heated particle filter

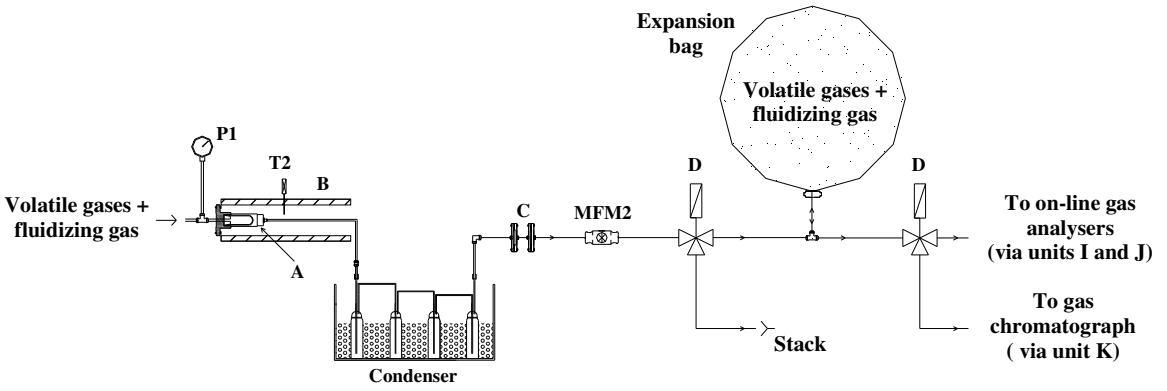

Figure 1.23 – Schematic layout of the sampling line for the pyrolytic volatiles evolved from a fuel batch. A - heated quartz thimble filter, B – 0.5kW$_e$ oven, C – backup quartz filters, D – solenoid valves; P1, T2, MFM2 and units I to K according to Figure 1.18.

was developed during this work and basically consists of a thimble quartz filter (Whatman 603G, 82x22mm) mounted on suitable SS holder. A small thermocouple (K-type) is placed outside the filter holder to monitor the temperature. The volatiles and fluidizing gas leaving this filter goes through the condenser where the liquid species (i.e., pyrolytic water and organics) are collected by condensation in a set of 25mL impinger glass bottles sitting on iced-water. Though, due aerosol forming upon cooling the tars within the bottles, two in-series quartz filters (Schleicher & Schuell, No.8) are placed downstream the condenser; the first filter acts as particle collector while the second one enabled to ascertain the collection efficiency. In general, a negligible mass of aerosols is retained in the second backup filter. Figure 1.24 shows photographs of the impinger bottles and backup filters after passage of the volatiles released from about 5g of fuel. The dry and clean permanent gas (i.e., volatile species + N_2 fluidizing gas) leaving the condenser and backup filters pass through a gas mass-flow meter (MFM2) and are collected in a 10L bag (SKC, H_2 proof). The advantage with this flow meter was that it enabled to monitor the release of the volatiles gases over time after feeding of a fuel batch. As examples, Figure 1.25 shows the time-dependent response of MFM2 as well as those of the sensors measuring the flow rate of N_2 fluidizing gas (MFM1 in Figure 1.18) and pressure in the freeboard (P1) during pyrolysis of typical fuel batches. It can be seen that the response of both MFM2 and P1 initially increase due to the rapid release of the volatiles and then decrease as the fuel particles become exhausted of volatile matter. Once the pyrolysis is complete, the response of MFM2 returns to a value close to that of MFM1 (i.e. only N_2 fluidizing gas is passing) while P1 stabilizes at 200-250mm H_2O due to trapping of aerosols in the thimble filter and backup filters. The pyrolysis time varies somewhat among the experiments but the major differences were found between different particle sizes (here, 8mm *vs.* 6mm OD). Even though this method offers good conditions for evaluating the kinetics of biomass pyrolysis, this issue is beyond the scope of the present work. Here the aim

of this method was only to determine when to stop the collection of the gas into the bag so that dilution of the contents of the bag is minimized. In practice this was done by operating the solenoid valves short after the pyrolysis is complete to discard the remainder gas into the stack (see Figure 1.23).

An automatic gas control and measurement unit was developed to operate the heated sampling line (see section 1.5.4.4). The analysis of the collected pyrolytic volatiles is based on gravimetry for the condensable species and soot, and gas chromatography (sometimes also online gas analyzers) for the permanent gas species (see section 1.5.4.5).

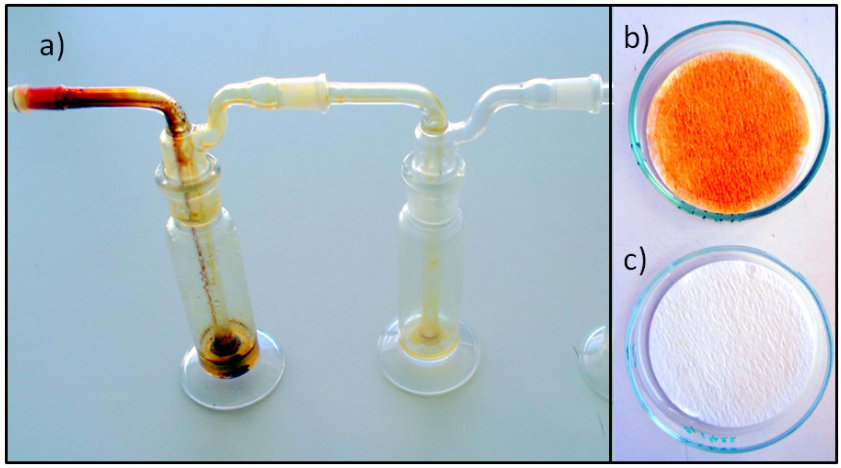

Figure 1.24 – Photographs of the first two impinger bottles (a) and the first (b) and second (c) backup quartz filters after passage of a quantity of pyrolytic volatiles.

1.5.4.3 *Sampling line for the combustion flue gases*

To determine the amount of carbon remaining in-bed after the pyrolytic stage, the fluidizing gas is switched to dry reconstituted air (21%v O_2 in N_2) to burn the char; the carbon is evaluated from the amount of CO_2 leaving the fluidized bed reactor with the flue gases. For that purpose a suitable gas sampling line was developed (Figure 1.26) which basically comprises an on-off valve, a condenser, a particle filter, a volume meter, a pump and a regulating valve, to be able to send a slipstream of the dry and clean flue gases to the online gas analyzers (see section 1.5.4.5). This sampling line is used in experiments described in Papers IV and V.

The combustion flue gases leaving the reactor through the upper port on top of the freeboard are lead by 6mm OD PTFE tube (≈500mm length) to a glass bottle immersed in ice-bath. Trapping of water, if any, is due to condensation in the bottom part of the bottle and adsorption in a fixed-bed of silica gel positioned in the upper part of the bottle. The dry flue

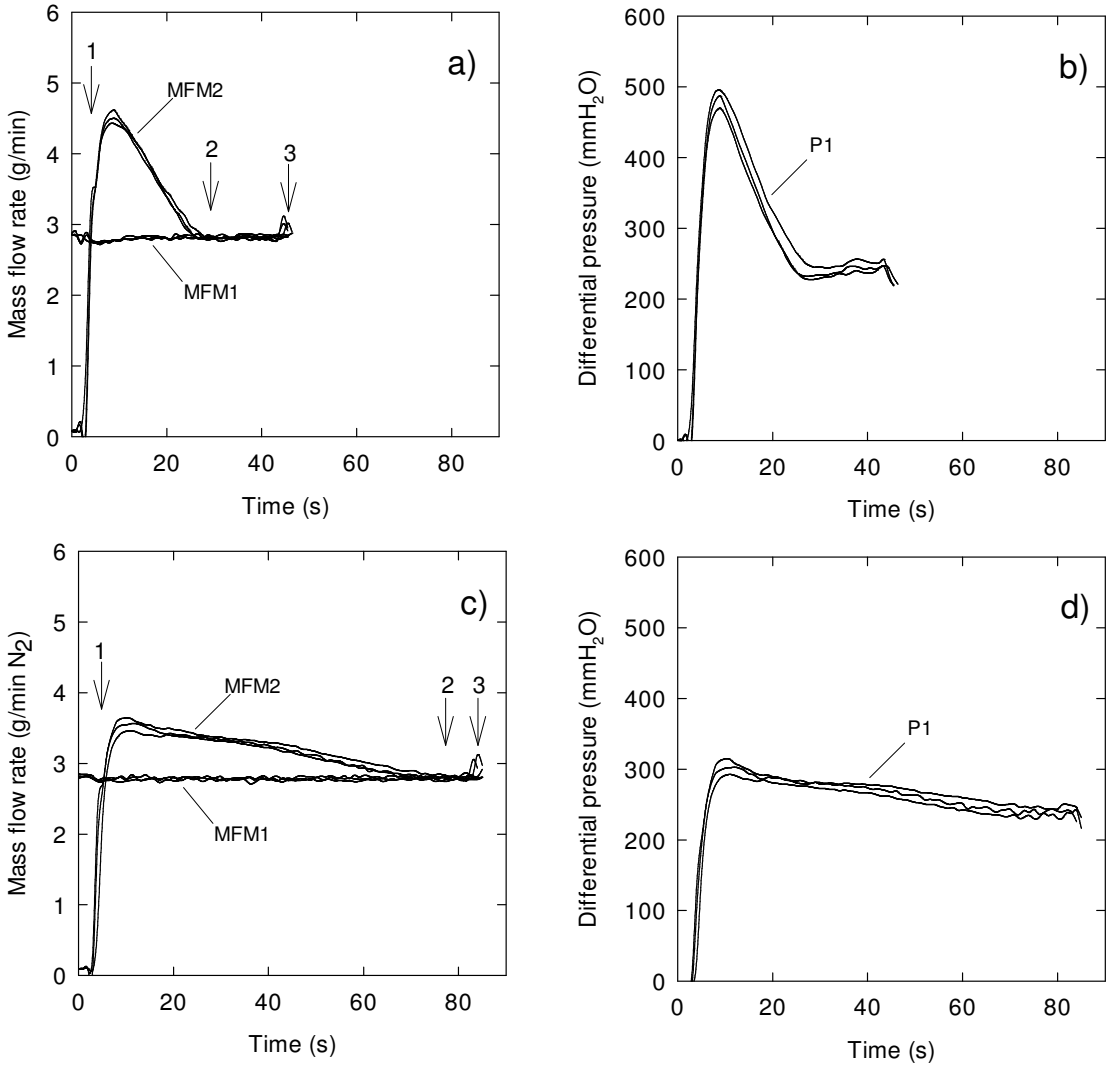

Figure 1.25 – Mass flow rates of the gas streams entering (N_2, MFM1) and leaving (N_2 + volatile gases, MFM2) the fluidized bed reactor and differential pressure in the freeboard relative to the atmosphere (P1) during pyrolysis of typical fuel batches at 700-750ºC bed temperature. Pyrolysis of 6mm OD eucalyptus wood particles (a, b) and 8mm OD wood pellets particles (c, d). Arrows indicate: 1 – fuel feeding, 2 – end of pyrolytic decomposition, 3 – end of gas sampling into the bag.

gases are then passed through an in-line quartz filter (Schleicher & Schuell, No.8) and bellows-type volume meter. This volume meter was used in combination with a timer, manometer and thermocouple to determine the total amount of dry flue gases produced during the burnout of the char. Thereafter, a slipstream of the flue gases is sampled by diaphragm pump and regulating valve while the remainder gas is discarded. In practice, sampling of the dry gas was done by means of gas sampling and distribution units (noted I and J in Figure 1.18) which enabled to put the gas analyzers into service in an automatic manner; a description of these automatic units is provided in the following section.

The concentration of CO_2 in the dry flue gases peaks at about 3-5min after switching the fluidizing gas to dry air, with maximum values of 3-11%v depending on the mass of char under combustion; the process is essentially complete after, say, 15min. Even during combustion experiments with rather high loads of char the concentration of CO in the dry flue gases is typically below 0.15%v. This is because sampling of the flue gases is done on top of the freeboard which permits relatively long gas residence times in the freeboard of the fluidized bed reactor (typically, 3-5s).

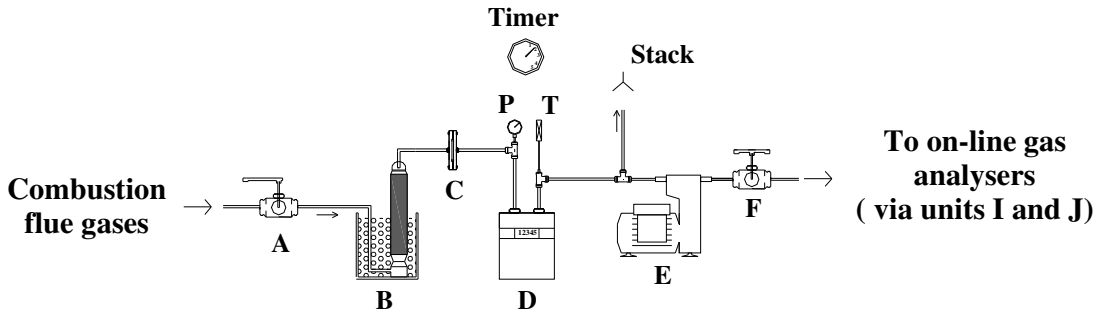

Figure 1.26 - Schematic layout of the sampling line for the combustion flue gas evolved during the burnout of the char. A – on-off valve, B – ice bath with packed bed of silica gel , C – backup quartz filter, D – bellows-type volume meter, E – diaphragm pump, F – regulating valve; P – pressure measurement; T – temperature measurement.

1.5.4.4 *Automatic gas control and measurement units*

For reasons of convenience and mainly due to limited human resources available to conduct the experiments (often one person), the fluidized bed facility should be operated with a high degree of automation. This was made possible by a number of automatic units integrating suitable pneumatics and instrumentation, as shown in Figure 1.18 and 1.27: fluidizing gas control and measurement unit (H), gas sampling and conditioning unit (I), gas distribution unit (J) and volatile gas control and measurement unit (K). Units H to J are part of an existing experimental infrastructure at UA, and were found suitable to be used also in this work; a detailed description of these units can be found in [68] and only a basic outline is provided here. Nevertheless, to implement the method for collecting the volatile gases into the bag, a new unit turned necessary (unit K). The automatic operation of these units is possible by built-in electronics and a computer-based data-acquisition and control system (section 1.5.4.6).

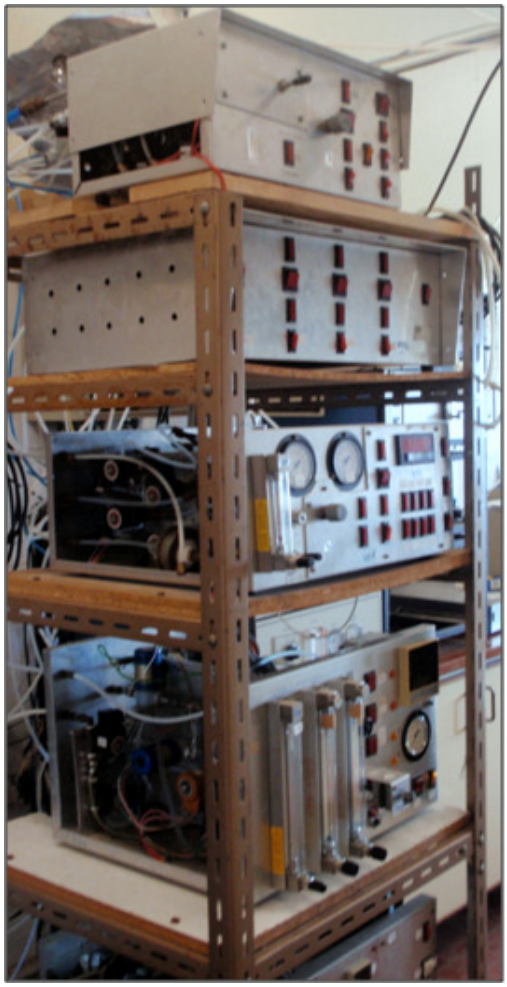

Figure 1.27 – Gas control and measurement units used in the laboratory fluidized bed facility. From top to bottom: volatile gas control and measurement unit (noted K in Figure 1.18), gas distribution unit (J), gas sampling and conditioning unit (I), fluidizing gas control and measurement unit (H).

Fluidizing gas control and measurement unit (H)

The main purpose of using this unit was to select, control and measure the fluidizing gas during the pyrolysis (pure nitrogen) and combustion (reconstituted air) experiments carried out in the small fluidized bed reactor. Also the flow rate of purge gas entering the bottom part of the reactor tube is adjusted through this unit. Selection of the fluidizing gas is accomplished by a multiplexing pneumatic circuit which basically includes on-off solenoid valves, regulating valves, manometers and one mass-flow meter (MFM1 in Figure 1.18). The fluidizing gases are supplied to this unit via gas cylinders. Also integrated in this unit is the power control system for the 2.5kW$_e$ reactor oven (see [68] for a detailed description of this oven), including suitable temperature controller (Shimaden, SR25) and transistor electric power regulator (Shimaden, PAC15P). The temperature controller is connected to thermocouple T0 (K-type, 3mm OD) shown in Figure 1.18 and is also operated via the aforementioned automatic control system.

Gas sampling and conditioning unit (I)

Unit I enables to suck a slipstream of a dry gas (say, 1-3LPM) from several locations around the facility through a multiplexing pneumatic circuit. The gas sample coming from a given location is further conditioned and sent to the online gas analyzers via automatic unit J to which this unit is connected (see Figure 1.18). Both the flue gases leaving the fluidized bed reactor during the burnout of the char and the volatile gases collected in the expansion bag were sampled through this unit. Apart from various flow control devices, the pneumatic circuit includes filters to remove particles and traces of water and a diaphragm pump; an additional 3-way solenoid valve was installed during this work to be able to sample the contents of the bag. Built-in instrumentation includes an absolute pressure sensor for measuring the pressure at the gas sampling point (Keller, PA33).

Gas distribution unit (J)

The dry and clean sample gas coming from unit I can be distributed to up to four online gas analyzers through this unit, which consists of a de-multiplexing pneumatic circuit operated by on-off solenoid valves. This pneumatic circuit is also used to supply zero/reference gas (99.999%v N_2) to the online gas analyzers.

Volatile gas control and measurement unit (K)

Figure 1.28 shows the pneumatic circuit of the volatile gas control and measurement unit developed during this work. This unit enabled to: (1) clean and empty the expansion bag before each pyrolysis test, (2) collect the permanent gas leaving the fluidized bed reactor during pyrolysis of one fuel batch, and (3) operate a dedicated GC system.

The cleaning procedure of the bag consists of various consecutive filling/empting cycles of the bag with pure helium (99.999%v). During the filling step, helium is supplied from a gas cylinder by opening the solenoid valves V1 and V8; the emptying step is accomplished by sucking the gas with small venturi operated with air and opening valve V5 instead. After a series of filling/empting cycles, the bag is emptied under vacuum and sealed by closing the solenoid valves. The sample gas leaving the heated sampling line enters the automatic unit through valve V7 after passing through the mass-flow meter (MFM2 in Figure 1.18). Thereafter, proper operation of valves V1 and V3 enables one to collect the gas into the expansion bag or discard it into the stack. In combination with the time-dependent response of the gas mass-flow meter, which permits to monitor the course of pyrolysis (recall Figure 1.25), this layout makes it easy to collect the gas only during the passage of the pyrolytic volatiles. The total gas collected into the bag is a mixture of volatile gases released from a fuel batch, N_2 fluidizing gas and minor amount of He supplied while cleaning the bag. To analyze the contents of the bag, valve V2 is operated together with the venturi so that a slipstream of

the gas passes through the GC loop. The line connecting the automatic unit to the GC consists of a 1/8''OD SS tube and includes a regulation valve (V10) and flow indicator (rotameter) placed downstream the loop. Calibration of the GC against standard gases is also possible by opening valves V9 and V4 while adjusting the gas flow rate by regulating valve (V11); zero gas (i.e. He) can be provided to the GC loop as well by using valve V8 instead of V9.

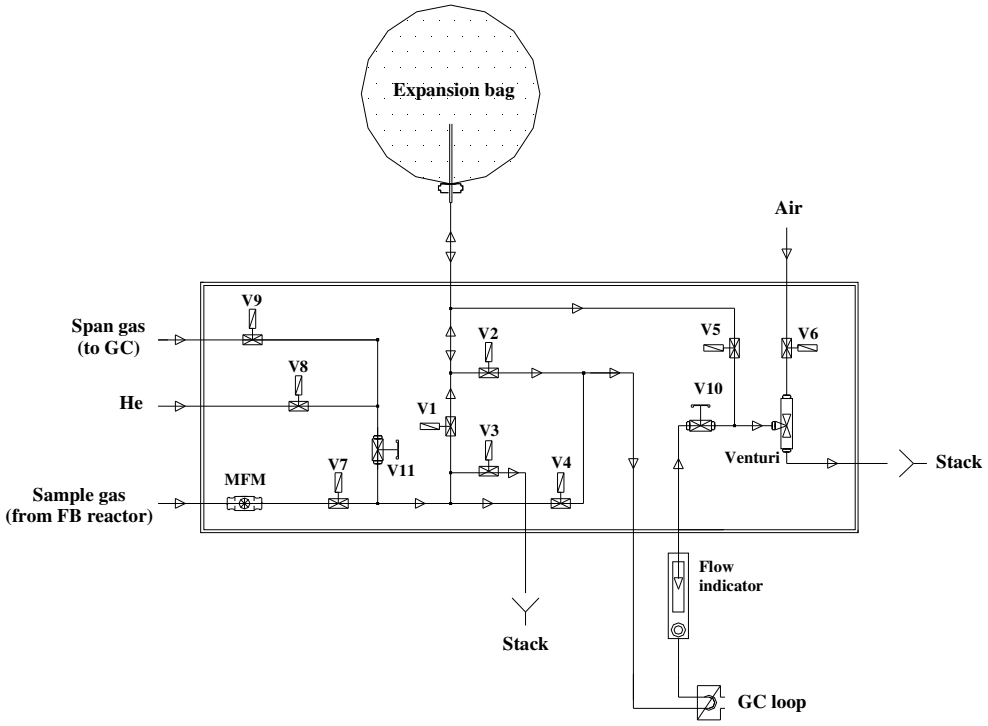

Figure 1.28 – Pneumatics of the automatic volatile gas control a measurement unit. V1 to V9 – solenoid valves, V10 and V11 – regulating valves, MFM – mass flow meter (MFM2 in Figure 1.18).

To control the electric circuit powering the solenoid valves (V1 to V9, 220VAC) within the automatic unit, electromechanical relays (RS1 to RS7, 220VAC) as well as manual switches (S0 to S5) are used, according to the layout shown in Figure 1.29. Note that one of the relays operating the valves V1 and V5 includes a time delay function to be able to realize the consecutive filling/empting cycles of the bag. The electromechanical relays are in turn operated by solid-state relays (SSR1 to SSR7) which are part of the automatic control system.

1.5.4.5 *Measurement systems*

The set measurement systems used in the laboratory fluidized bed facility are described below which includes systems for measuring the gas composition, pressures, temperatures, and gas flow rate and volume. Most of these systems feature electronic transducers to be able to read and save the respective analog output signals via the computer-base data-acquisition system.

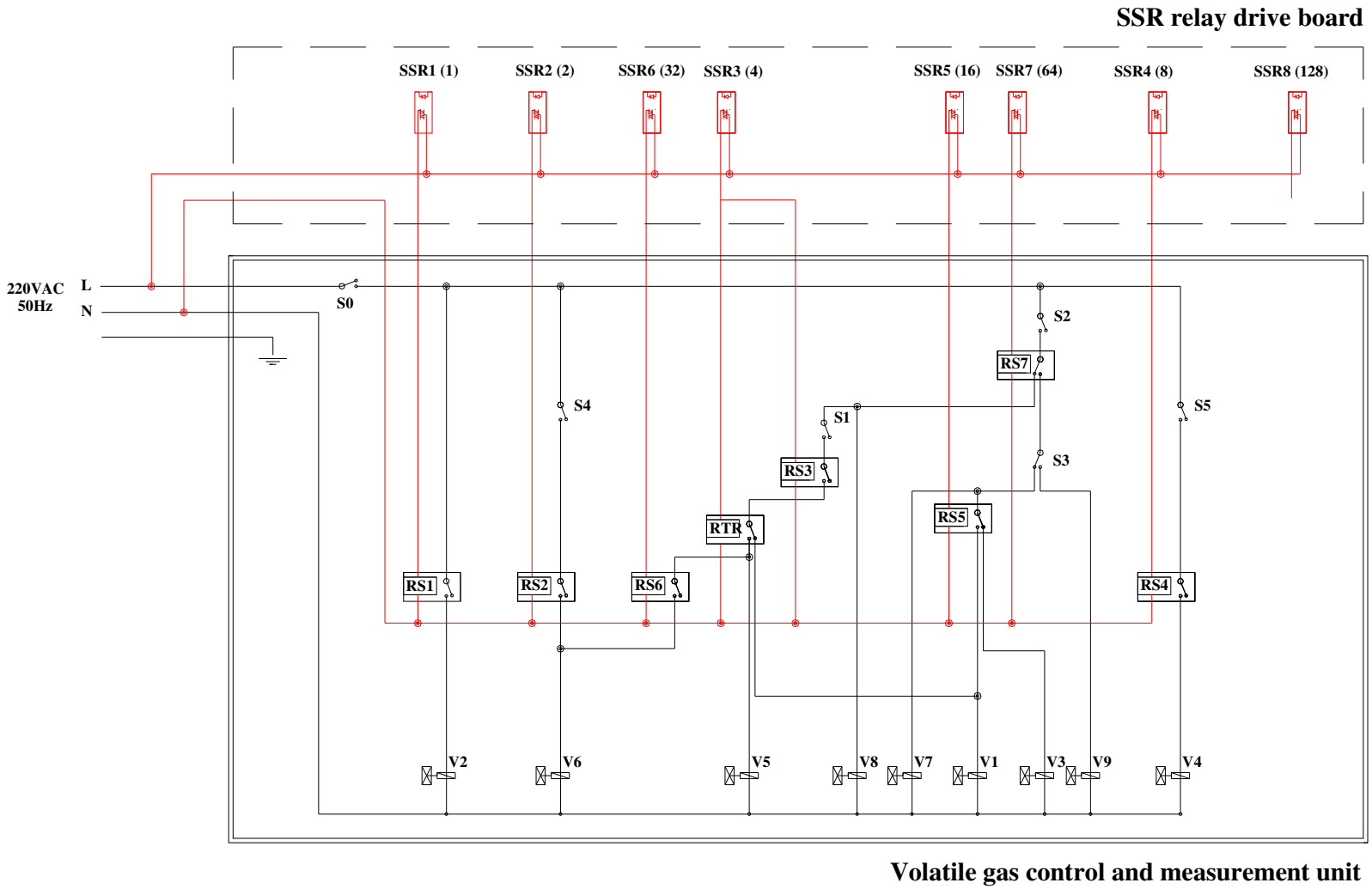

Figure 1.29 – Electric circuit of the automatic volatile gas control a measurement unit. V1 to V9 – 220 VAC solenoid valves; S0 to S5 – manual switches; RS1 to RS7 – electromechanical relays; SSR1 to SSR8 – solid state relays; RTR – solid state relay with timer.

Online gas analyzers

The online gas analyzers were used for measuring the time-dependent composition of the dry and clean flue gases leaving the fluidized bed reactor during the burnout of the char and, sometimes, to ascertain the composition of the gas collected in the expansion bag during the pyrolysis experiments. CO and CO_2 gas analyzers were used in this work, being operated by the automatic gas distribution unit J.

The CO gas analyzer (ADC, 5000) is based on the principle of NDIR (non-dispersive infrared) with a measuring cell for concentrations in the range of 0-30%v; the analogue output is 1-5VDC. This analyzer was mainly used to corroborate the concentration of CO within the expansion bag. Unfortunately, an unstable response was sometimes observed for the CO analyzer which made it unsuitable to be used during some experiments.

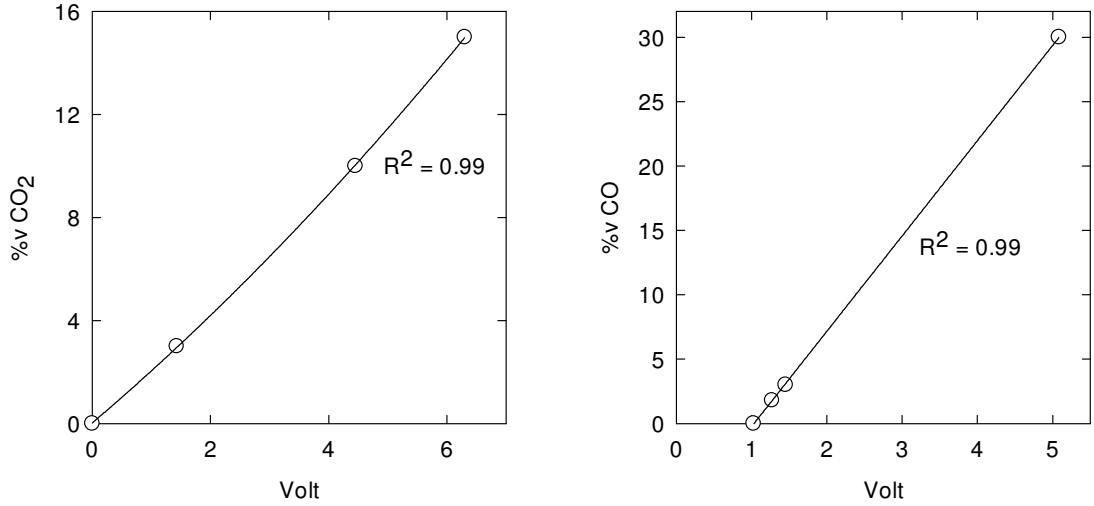

Figure 1.30 - Examples of calibration curves for the CO_2 and CO gas analyzers.

The CO_2 gas analyzer (ADC, 1450 Luft) is also based on NDIR technology; despite of various measuring cells integrated within this analyzer, only the 0-25%v cell was used in this work. A reference cell is continuously purged with pure nitrogen (99.999%v). The analogue output is 0-10VDC. This analyzer was especially suitable to be used during the combustion experiments of the char due to its short response time (t_{90}<5s). Yet, it was sometimes used for measuring the concentration of CO_2 within the expansion bag as well.

Calibration of the gas analyzers was done against standard gases covering the range of concentration of CO and CO_2 in the gas mixtures to be analyzed; the need for adjusting the calibrations was regularly verified. Interferences from other gas species were tested especially in the case of the CO_2 gas analyzer. Figure 1.30 shows typical multipoint calibration curves for the CO and CO_2 analyzers, where the best fits were based on first order and second-order polynomials, respectively.

Shimadzu gas chromatograph

The Shimadzu GC system is fully integrated onto the fluidized bed facility and was applied for measuring the composition of the dry and clean gas collected in the expansion bag. Figure 1.31 shows a photograph of this GC system, which includes the GC itself (GC 15A) and ancillaries for data processing (Chromatopac C-R3A) and an automatic operation of the GC sampling valve (PRG 102A interface).

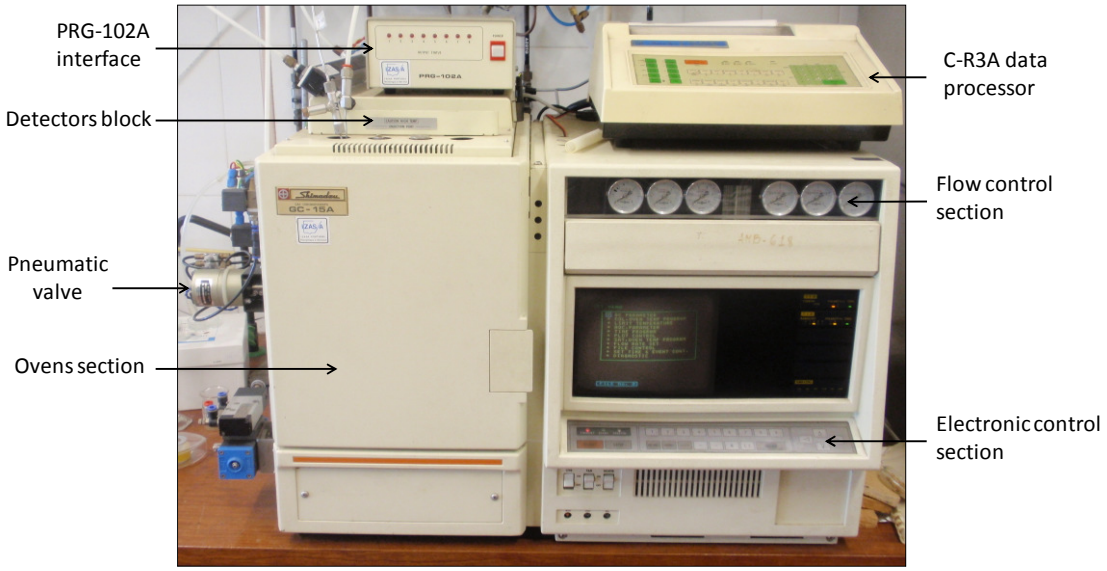

Figure 1.31 – Shimadzu GC-15A system. Gas chromatograph and ancillary equipment for processing chromatograms, computer interface and automated operation.

The GC comprises three main sections: oven section, flow control section and electronic control section. The oven section includes the column oven and detectors block. The column oven accommodates the chromatographic columns plumbed on a 10-port gas sampling valve, and the injection ports for the detectors; a pneumatic valve placed outside the oven drives the 10-port valve in between the "INJECT" and "LOAD" positions. The column oven is capable of furnishing a uniform temperature up to 399ºC following heating ramps up to 40ºC/min. Although two detectors are mounted in the GC, one thermal conductivity detector (TCD) and one flame ionization detector (FID), only the TCD was used in this work. The TCD is contained in its own oven (up to 399ºC) and is of a dual cell type. Two filaments (i.e. resistances) are use in each cell, where one cell serves as reference and the other one as sample. Carrier gas (helium, 99.999%v) flows through the reference cell while carrier gas with eluants flows through the sample cell. A constant current (0-200mA, selectable) is supplied to the filaments in each cell which means that the passage of the eluants can be detected as a variation in the resistances (i.e. voltage) across the filaments. The setting of the carrier gas flow rate across

the TCD cells is done by separated flow regulators and the reading is done by rotameters (0-0.1L/min). The electronic control section includes the switches for powering the ovens, fan and detectors, and built-in keyboard and CRT display for monitoring the operation of the GC system and setting of the analysis parameters (e.g. column oven temperature program).

The TCD analog signal is conditioned and recorded by the C-R3A data processor with a built-in printer for plotting the chromatograms and gas analysis report. The methods for processing the chromatographic peaks and calculating the respective amount of eluants can be adjusted; here the peak areas are measured and are related to the amount of the gas species in the GC loop. The C-R3A apparatus also enables a BASIC program to be executed. Programs for an automated operation of the GC (e.g. for starting the GC analysis via control system) and for communication with computers via RS-232 serial port (e.g. for transmitting the analysis report or starting the GC analysis via control system) were used in this work. One of these programs enabled a time-dependent operation of the pneumatic valve driving the 10-port GC valve for e.g. injecting the contents of the GC loop into the chromatographic columns for separation. This was done via the ancillary PRG 102A interface integrating relays and to which the C-R3A data processor is connected.

A chromatographic method for separating a set of relevant species collected in the expansion bag (N_2, H_2, CO, CO_2, CH_4, C_2H_4, C_2H_6 and C_3H_8) was developed in this work. Figure 1.32 shows the 10-port valve plumbing configuration, including the connections for the GC loop (1mL), chromatographic columns and TCD. The setup enables two columns to be plumbed in-series which offers good flexibility for separating the species of interest by single channel analysis. Methods based on molecular sieves, porous polymers and carbon sieves were investigated in this work. One method was investigated in which one column was packed with 5Å molecular sieve (SS, 1.7m×5mm OD) and the other one with Hayesep Q porous polymer (SS, 1.5m×5mm OD). Combination between these columns enabled an analysis time of ≈10min while reducing the need for column regeneration due to trapping of CO_2 and long hydrocarbons onto the molecular sieve column. Bypassing the molecular sieve column was possible by proper tuning of the 10-port valve which allowed CO_2 and the hydrocarbons to pass directly from the Hayesep Q column to the TCD. However, the method leaded to detection difficulties due to small peaks (e.g. C_2H_4) being processed on the tail of the major N_2 peak. To address this problem, the 5Å molecular sieve column was replaced by a Carbosieve SII column (SS, 2m×1/8'' OD) which is suitable for separating CO_2 and hydrocarbons. Figure 1.33 shows a chromatogram for a standard gas mixture following the modified method, including the retention times for the species. An analysis time below 15min was possible by using temperature program for the column oven and helium flow rate of 25mLPM. In order to fill the GC loop with fresh sample gas, the 10-port valve remains in "LOAD" position until the analysis is started. After stabilization of the contents of the loop to

the atmospheric pressure, the valve is rotated to "INJECT" position at time zero and the sample gas flushed into the Hayesep Q column, which is upstream the Carbosieve SII column; the species H_2, N_2, CO, CH_4 and CO_2 leave the Hayesep Q column unresolved and enter the Carbosieve SII column for separation before being detected. After passage of CO through the TCD cell, the 10-port valve is rotated back to "LOAD" position (see pressure disturbance in the chromatogram) to bypass the Carbonsieve SII column. This allowed the hydrocarbon species eluting from the Hayesep Q column to pass directly to the TCD; in turns, the CH_4 and CO_2 eluting from the Carbosieve SII column pass a second time through the Hayesep Q column before reaching the detector.

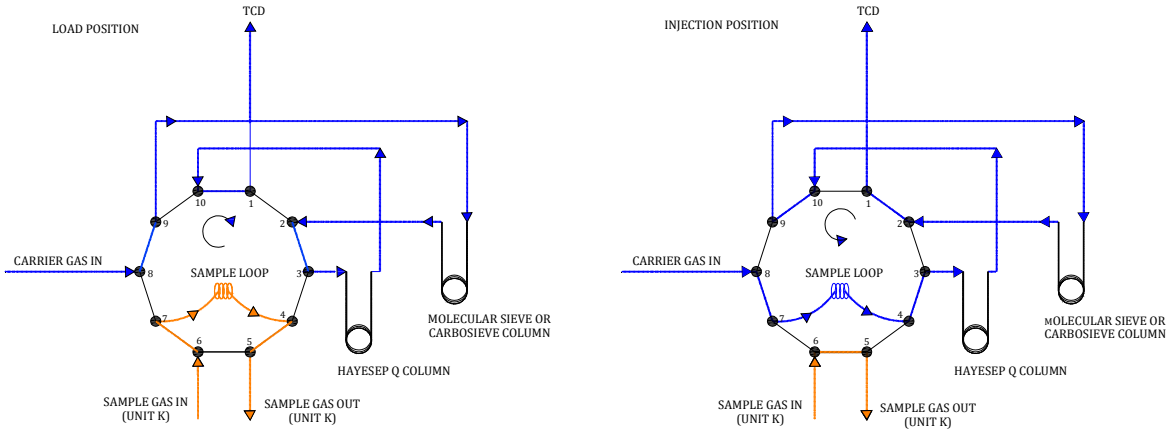

Figure 1.32 – 10-port GC sampling valve with connections to the GC sampling loop, carrier gas intake, volatile gas control and measurement unit (K), chromatographic columns and TCD.

The modified method improved the separation for the aforesaid species even though the analysis time is longer when compared to the case using the 5Å molecular sieve column. Anyway, the operation of the 10-port valve in between the "LOAD" and "INJECT" positions enabled a significant reduction of the analysis time due to bypassing of the Carbosieve SII column for the hydrocarbon species. Further reduction of the analysis time was achieved by heating the columns to 150ºC after elution of CO.

Calibration of the method was done against a set of standard gases supplied from gas cylinders. Figure 1.34 shows multipoint curves in which the volume fraction of the species in the GC loop is plotted against the measured peak areas. The TCD showed a linear response for most species with only H_2 leading to a slight non-linear response. The best-fitting parameters for each species were input to the C-R3A data processor for an automatic calculation of the composition of the sample gas. The calibration of the TCD was checked on a daily basis during the course of the experimental season; the species concentration were corrected for daily variations of the atmospheric pressure according to the ideal gas law (barometric pressure available at e.g. UA Department of Physics, www.ua.pt/fis).

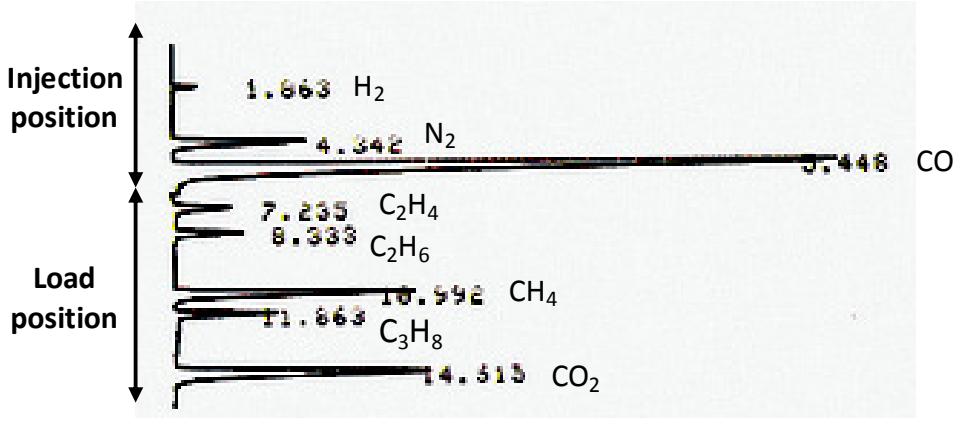

Figure 1.33 – Scan of a typical chromatogram for a standard gas mixture. Columns: Carbosieve SII and Hayesep Q. Carrier gas: He, 25mL/min. Detector: TCD, 100ºC, 100mA. Temperature program: 40ºC for 6min, 20ºC/min to 150ºC and 150ºC till end of analysis.

Figure 1.35 shows an example of a chromatogram and respective analysis report for the gas collected in the bag after pyrolysis of a biomass fuel batch in the fluidized bed reactor. The peaks corresponding to the species used in the calibration of the GC could always be detected, with only the C_3H_8 peaks being dubious due to small adjacent peaks being also detected; to cope with this problem, the C_3H_8 was analyzed by another GC system (see below). Even the H_2, which has a similar thermal conductivity to that of He carrier gas, produced peaks that were easily discerned by the C-R3A data processor. Yet, higher sensitivity for H_2 could be achieved by adjusting the size of the GC loop and/or the operation of the TCD (e.g. current across the filaments). The major chromatographic peak corresponds to N_2, which was used as fluidizing gas during the pyrolysis experiments; N_2 represented typically 60-90%v of the total gas collected in the bag. The respective abundances for the pyrolytic species were typically in range of 1-8%v H_2, 4-18%v CO, 1-6%v CH_4, 1-5%v CO_2, 0.5-2%v C_2H_4 and <0.3%v C_2H_6.

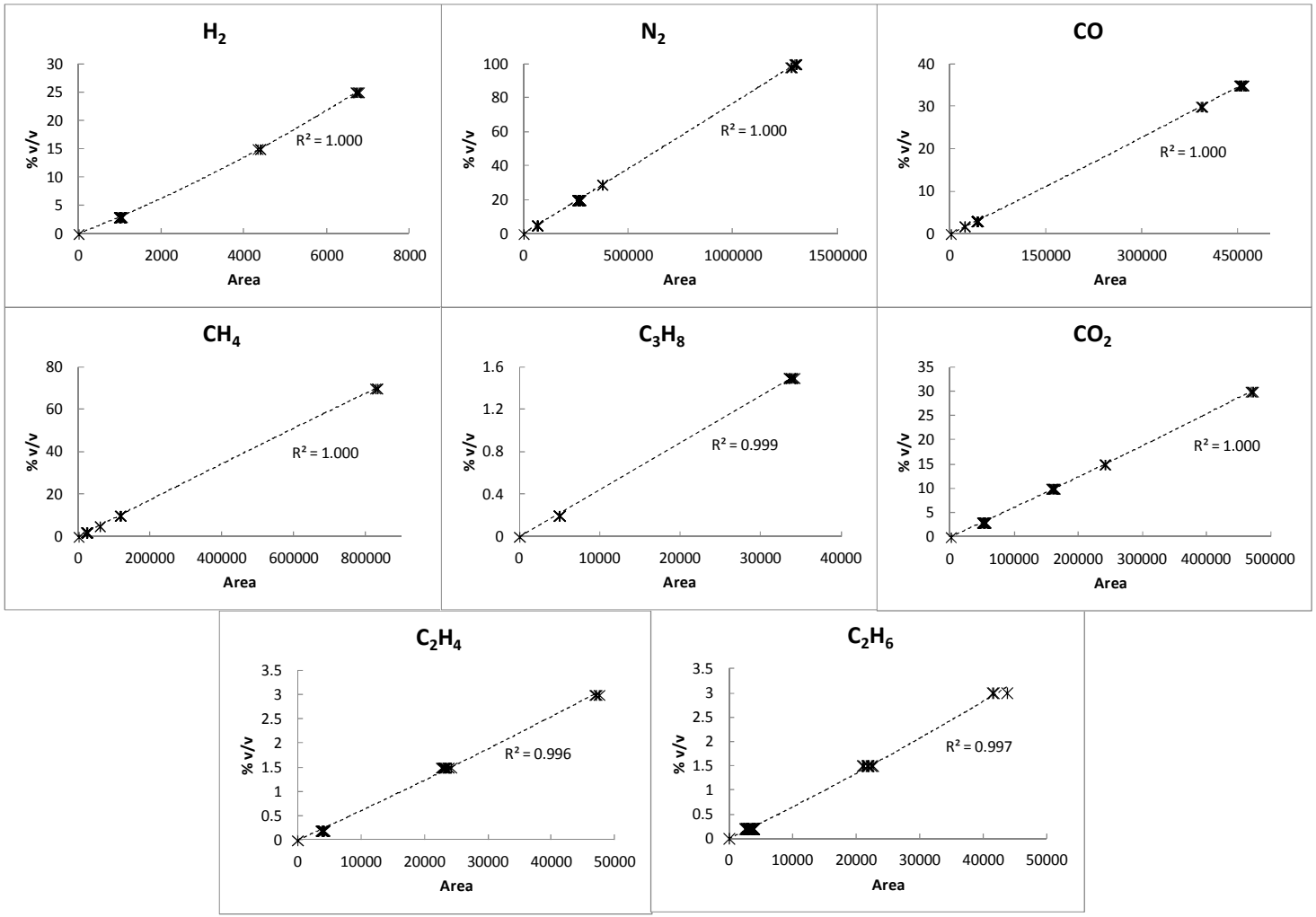

Figure 1.34 – Response of the TCD against the most relevant gas species collected into the expansion bag as obtained by proposed GC method. Summary of the calibration results over the course of the experimental season.

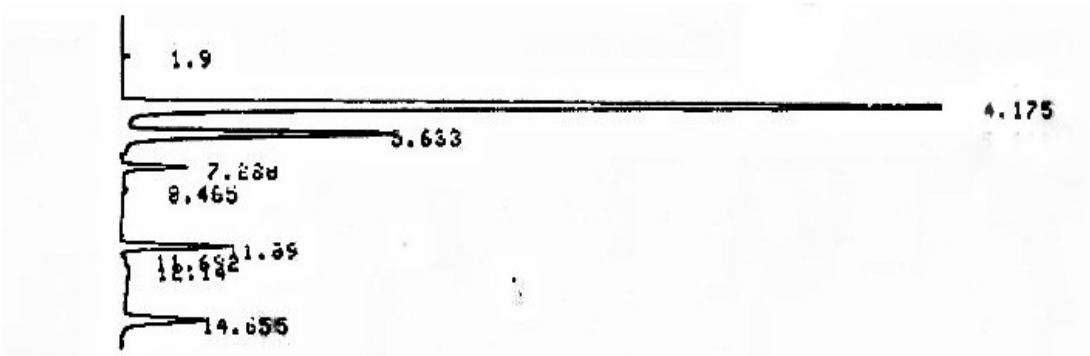

C-ROMATOPAC C-R3A FILE 1
SAMPLE NO 0 METHOD 44
REPORT NO 485 SAMPLE WT 188

PKNO	TIME	AREA	MK	IDNO	CONC	NAME
1	1.9	2693		1	6.9463	H2
2	4.175	829625		2	63.7772	N2
3	5.633	216684	V	3	16.7221	CO
4	7.286	30887		4	2.1662	C2H4
5	8.485	1054		5	0.0576	C2H6
6	11.09	62415		6	5.408	CH4
7	11.692	1383		7	0.0348	C3H8
8	12.14	1521	V	7	0.0627	C3H8
9	14.655	65797		8	3.9186	CO2
	TOTAL	12.5577			99.0854	

Figure 1.35 – Scan of a typical chromatogram and analysis report for the gas collected in the expansion bag during a pyrolysis test. Columns: Carbosieve SII and Hayesep Q. Carrier gas: He, 25mL/min. Detector: TCD, 100ºC, 100mA. Temperature program: 40ºC for 6min, 20ºC/min to 150ºC and 150ºC till end of analysis.

Varian gas chromatograph

A Varian micro-GC (GC 4900) was used in some pyrolysis experiments for analyzing a set of gas species that were difficult to analyze through the Shimadzu GC system. This compact GC system offers the complete analysis solution with built-in autosampler and two GC channels for a separated analysis of the lightest species (He, H_2, O_2, N_2, CO, CH_4) and other species (CO_2, C_2H_4, C_2H_6, C_3H_8); the channels are setup in parallel and include its own injection systems, chromatographic columns and TCDs, and are pre-configured according to an analysis method optimized by the manufacturer. Argon is used as carrier gas in the first channel with the lightest species being separated in a 5Å molecular sieve column (SS, 10m×1/8'' OD); in turns, the second channel uses Helium as carrier gas and a Porapak Q column (SS, 10m×1/8'' OD). Note that the lightest species leave the Porapak Q column unresolved which is the reason to split the gas into a parallel 5Å molecular sieve column. Adsorption of e.g. CO_2 into the molecular sieve column has a limited impact on peak

resolution and many analyses can be done before regeneration is required. Due to the autosampler, the automatic volatile gas control and measurement unit was no longer used for sucking the contents of the sampling bag into the GC loop. The parallel setup of the columns greatly improves the analysis time to about 3min without the need for temperature programming (isothermal analysis).

The micro-GC is connected directly to a laptop computer with suitable software for chromatogram processing and quantitative calculation as well as for instrument control and monitoring. A specific routine for calibration of the GC enables to derive the best-fit parameters for the species to be analyzed; a daily calibration against standard gases was done during the course of the experiments.

Gas flow meters and volume meters

Two gas mass-flow meters (Honeywell, AMW5101, 0-5NLPM) were used for monitoring the flow rate of the gas streams entering and leaving the fluidized bed reactor during pyrolysis of one fuel batch. The entering gas is N_2 fluidizing gas and is measured by the flow meter installed within the automatic unit H (MFM1 in Figure 1.18); the escaping gas is a mixture of N_2 fluidizing gas and pyrolytic gases and is measured by the flow meter within the unit K (MFM2). This type of flow meters is based on micro-bridge silicon technology in which the response of the sensor element depends on both the flow rate and the thermo-physical properties of the gas passing through it.

Calibration of the mass flow meters was done with the help of a drum-type volume meter (Ritter, TG05) according to the procedure described in [78]; both flow meters were calibrated with pure N_2 (99.999%v) at room conditions, as shown in Figure 1.36. The output signal is 1-5VDC and is linearly correlated with the mass gas flow rate.

Whether the passage of the pyrolytic gases increases or decreases the response of MFM2 relative to that against N_2 is difficult to predict based on the existing experimental information. An investigation by [78] showed relatively large differences on the response of this type of flow meters among a limited set of species (CO_2, N_2, O_2, Ar). Since the time-dependent composition of the gas mixture leaving the fluidized bed reactor is unknown, the time-dependent gas flow rate computed from the analog output of MFM2 shall be taken as an approximated value.

Also used in this work was a bellows-type volume meter (Schlumberger, Gallus) to quantify the total amount of the combustion flue gases leaving the fluidized bed reactor during the burnout of the char. This volume meter was calibrated against the reference drum-type meter (Ritter, TG05) with the results showing small differences between the outcomes of both meters (typically within ±3%)

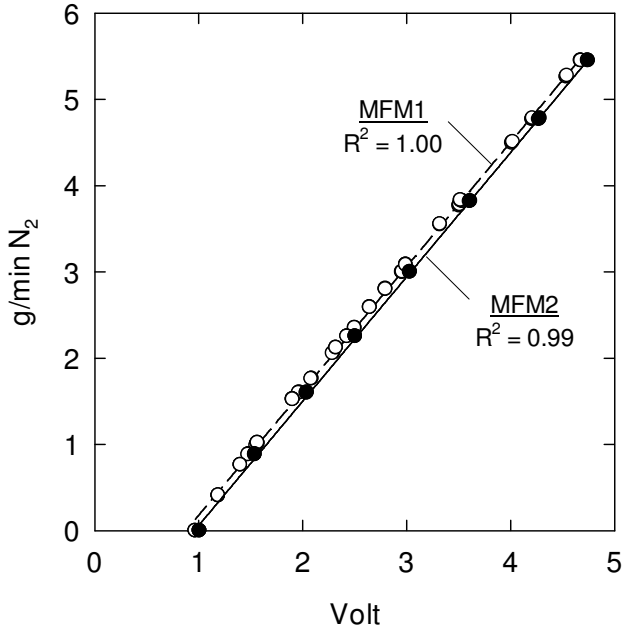

Figure 1.36 – Summary of calibration data for the mass flow meters used for measuring the gas streams entering (MFM1) and leaving (MFM2) the fluidized bed reactor.

Pressure and temperature measurement

A differential piezoelectric pressure sensor (Motorola MPX5010DP, 0-100mmH_2O) was used to monitor the pressure in the freeboard of the fluidized bed reactor during pyrolysis of one fuel batch (see P1 in Figure 1.18). For this purpose, one of the taps of the sensor is connected to exhaust port of the reactor, which is closed during the release of the volatiles whereas the other tap is opened to the atmosphere. This sensor was calibrated with a regular water column gauge (results not shown). The analog output is 0-5VDC and is also linearly correlated to the pressure difference between the two taps of the sensor.

Temperatures were sensed by general purpose K-type thermocouples (NiCr/NiAl) of 1.5 and 3 mm OD and various lengths. The temperature is computed from the output voltage generated by the metal junction according to polynomials, and after cold junction compensation (see [68] for details on the temperature measurement).

1.5.4.6 *Data-acquisition and control system*

An outline of the computer-based system used for data-acquisition and control of the fluidized bed facility is provided in Figure 1.37. A detailed description of this system is out of the scope of this work as it can be found in [68]. Apart from the automatic gas control and measurement units (section 1.5.4.4), the ancillaries of the Shimadzu GC (section 1.5.4.6) and the instrumentation (e.g. thermocouples, mass flow meters), the system includes two electronic command units (noted B and C in Figure 1.37), a multifunction DAQ board (Advantech Mod818H) and a desktop computer running on MS-DOS operating system.

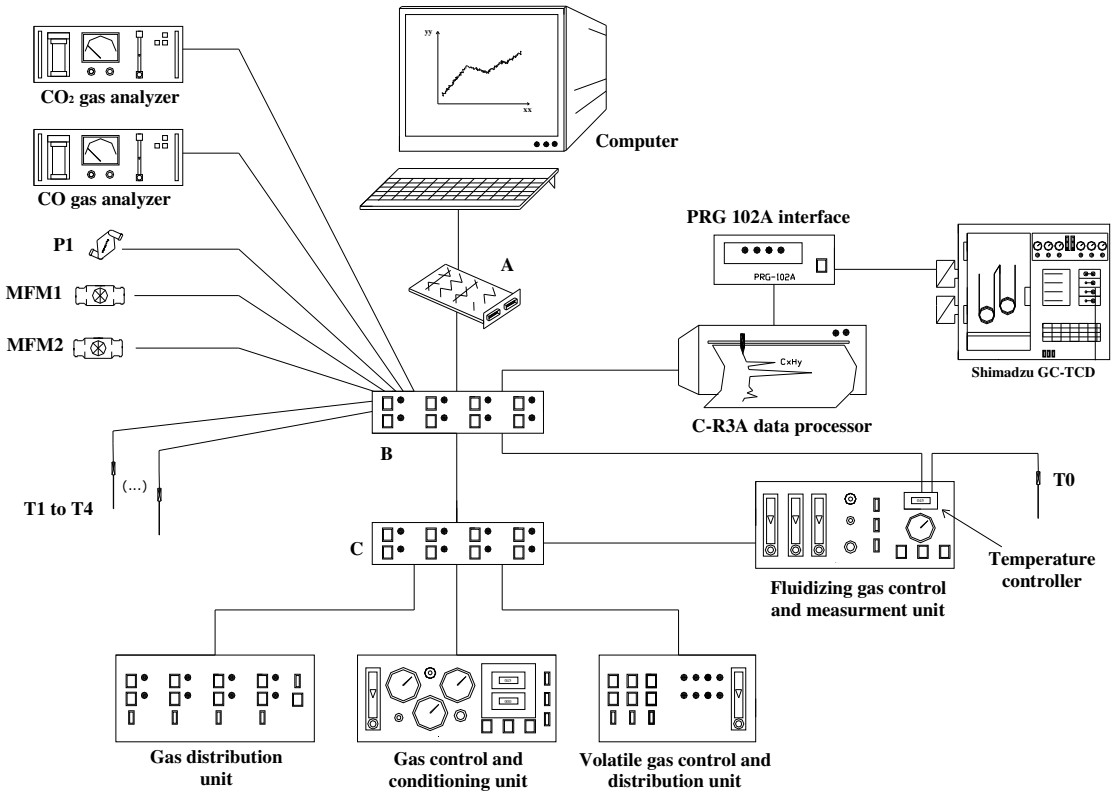

Figure 1.37 – Computer based data acquisition and control system. A - multifunction data acquisition and control board; B and C – electronic command units; P1, MFM1, MFM2, T0 to T4 according to Figure 1.18.

The 12-bit DAQ board includes 8 differential analog input channels (ADC) with gain settings and 16 digital I/O channels (DIO), among other features (e.g. analog output, DAC). The first 2 analog input channels are used for reading the output signals from the pressure sensor and thermocouples; the other six channels are multiplexed in 12 analog input channels to support the reading of the online gas analyzers and mass-flow meters. The digital I/O channels enable to operate printed circuit boards built-in onto the two electronic command units shown in Figure 1.37, which provide interface between the DAQ board and the instrumentation and flow-control devices itself. The electronic unit B comprises the physical connections to the online gas analyzers (plugs), pressure sensor and mass flow-meters as well as up to 16 K-type thermocouples. An analog channel multiplexing and multiple gain amplifier board mounted within this unit enables to connect one out of the 16 thermocouples to the first analog input channel. Unit B also comprises a set of boards which are used to (1) select the set value of the temperature controller for the reactor oven and operate the C-R3A data processor (for e.g. starting the time-dependent GC analysis via computer), and (2) operate SSR driver boards mounted within the second electronic command unit (unit C) to be able to drive AC loads (220VAC) in the automatic gas control and

measurement units. For instance, Figure 1.29 shows the SSR driver board operating the electric circuit of the volatile gas control and measurement unit. In the same vein, another two SSR driver boards enabled to operate the other three automatic gas control and measurement units used in this work.

Microsoft QuickBASIC language was used for programming the DAQ board and for application development. A set of programs developed by Matos [68], including routines provided by the manufacturer of the board, were used here: ARLCAL.BAS and the series INICIO.BAS, SELECT.BAS, CONTRA.BAS and AMOSTR.BAS. Some of these programs were further developed during this work to suit the needs of the experimental procedure. The ARLCAL.BAS program permits to carry out any individual data-acquisition and control tasks among the fluidized bed facility, e.g., measurement of gas-flow-rates, temperatures and pressures, setting of temperatures for the reactor oven, sample and analyze the composition of gases through the online gas analyzers, operate the expansion bag and the Shimadzu GC system, calibrate sensors. The upgrades to this program include routines to operate the volatile gas control and measurement unit and the GC system. A limitation of the ARLCAL.BAS program is that human interface with the computer is always required which made it unsuitable to be used during the pyrolysis experiments. To overcome this, the program series comprising INICIO.BAS, SELECT.BAS, CONTRA.BAS and AMOSTR.BAS programs was used after proper adjustment of the codes. INICIO.BAS enables to list information about the specific experiment to be conducted (e.g. date, file names, fuel, mass of fuel batch, bed temperature), after which the SELECT.BAS program is called for setting the temperature controller for the reactor oven and start heating the fluidized bed reactor. The system proceeds then into CONTRA.BAS which aims at monitoring and controlling the experimental rig during the heating stage of the fluidized bed; during this time, a slipstream of nitrogen is supplied to the reactor via the distributor and the purging line, while leaving through the exhaust port (see Figure 1.19). Modifications to this program include routines to prepare the analysis system during the start-up procedure of the reactor, including the following operations: (1) clean the expansion bag with helium, (2) seal de expansion bag under vacuum, and (3) clean the sampling lines to the GC loop, online gas analyzers and expansion bag. When a steady operation of the reactor is achieved (bed temperature within ±3ºC of set-value) the purging gas is shut-off, the bed is fluidized in bubbling regime and the pneumatics of the volatile gas control and measurement unit are operated so that the incoming sample gas is discarded (valves V3 and V7 opened). With the experimental rig ready, the AMOSTR.BAS program is called for an automatic control of the rig during the pyrolysis experiment. A beep is used to tell the operator to feed in the dry fuel batch; after 2 seconds a second beep indicates that the volatile gas control and measurement unit has been tuned for collecting the incoming gas into the bag (valves V1 and V7 opened, Figure 1.28). Practice was

needed to fit the program design with the operator's performance. Temperatures and gas flow rates (e.g. MFM1 and MFM2) are displayed in the computer to be able to discard the sample gas once the pyrolysis process is finished. A last routine makes it possible to suck the contents of the bag into the GC loop or the online gas analyzers for analysis; in practice, mainly the GC was used due to the small volume of gas collected in the bag (typically 2.5-4.5L) which made it difficult to also purge the sampling line and measuring cells of the online gas analyzers in some experiments.

1.5.5 *Laboratorial quartz-tube pyrolysis facility*

The quartz tube (fixed bed) facility permits to determine the yield of char during fast pyrolysis of biomass at high temperatures (600-1000ºC) in a convenient way. Like the small fluidized bed pyrolysis reactor, fuel particle sizes of practical interest can be used in this facility. An illustration of the fixed-bed pyrolysis apparatus and ancillaries for carrier gas supply and temperature control is provided in Figure 1.38. The core of this facility is the horizontal quartz tube furnace (20mm ID, 300mm length) heated by a 0.5kW_e coil wound uniformly around the tube. The power input to the coil (220VAC) is adjusted by suitable solid state contactor and temperature controller (Shimaden, SR21). The temperature of the furnace is sensed by K-type thermocouple (T0, 1.5mm OD) positioned in the middle of the quartz tube. The furnace is insulated with a cerablanket and the outer shell is made of aluminum. Another quartz tube (10mmID, 350mm length) can be inserted along the tube furnace to be able to suddenly introduce a fuel batch (1-2 fuel particles) in the middle of the furnace. Both ends of the inner tube are insulated with cerablanket plugs followed by SS wires, to hold the fuel particles at a given position within the tube (see photograph in Figure 1.38). Pure N_2 is continuously supplied to the inner tube (≈0.5NLPM) so that the fuel converts under an inert atmosphere. The flow rate of N_2 is regulated via the same automatic unit used in the fluidized bed pyrolysis facility (unit H in Figure 1.18). The temperature of the incoming N_2 stream is measured close to the converting fuel batch by another K-type thermocouple (T1, 1.5mm OD) and is recorded by a data logger (TESTO 176-T4). It takes less than 1min for the gas surrounding the fuel to achieve 90% of the furnace temperature which ensures heating rates of the fuel particles in order to those attained in the small fluidized bed reactor. This follows from e.g. the comparable pyrolysis times that were found in both facilities; a qualitative evaluation of the course of pyrolysis of one fuel batch can be done by observing the white mists escaping the inner tube towards the stack. After 5-10min at peak temperature, the inner tube is moved back to outside the tube furnace so that the char particles cool to room temperature under inert gas and are recovered for gravimetric

analysis. Further details on the measurement procedures for the fixed-bed pyrolysis facility are given in Paper IV.

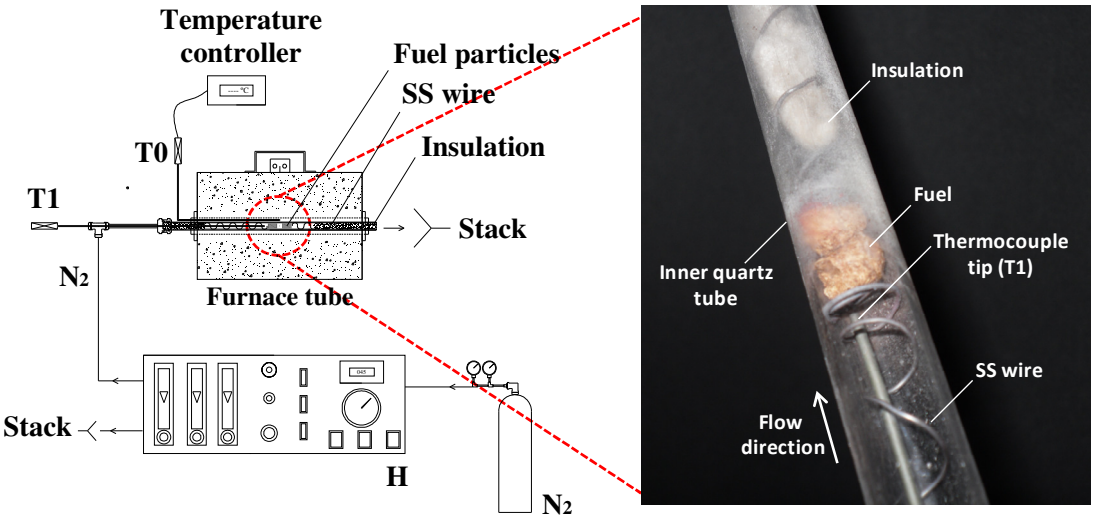

Figure 1.38 – Outline of the laboratorial quartz tube pyrolysis apparatus and ancillaries (left) and photograph of the inner quartz tube with a fuel batch in place (right). Unit H according to Figure 1.18.

1.5.6 *Thermogravimetric analyzer*

To verify the influence of slow heating of biomass on the production of pyrolytic char, a thermogravimetric analyzer (LECO, TGA701) was used; details on this analyzer can be found in website of the manufacturer (www.leco.com). Here, fuel batches of 1-2g were pyrolysed under nitrogen at 5 or 50ºC/min to distinguish from the heating rates attained in the laboratorial fluidized bed and quartz-tube reactors (say, 10^{3}ºC/min). Each experiment starts with a drying stage at 130ºC followed by the heating ramp to a peak temperature of 915ºC. After approximately 7min at 915ºC, the oven is cooled to room temperature always under a sweep of nitrogen. Paper IV provides the experimental procedures and the results from the pyrolysis experiments in the thermogravimetric analyzer.

1.6 *Solid fuels: preparation and analysis*

To cover the range of compositions of most biomass fuels, eleven fuel types were used in the combustion and pyrolysis experiments conducted at UA: pine wood, pine bark, eucalyptus wood, eucalyptus bark, beech wood, gorse wood, oak wood, forest biomass residues pellets (hereinafter referred to as forest pellets), wood pellets, as well as cellulose and one type of lignin. All these fuels were tested in the laboratory fluidized bed and quartz tube pyrolysis

reactors, even though only the forest pellets were used in the pilot scale fluidized bed combustor. The pine, eucalyptus, beech, gorse, oak and forest pellets varieties came from relatively old logs/barks or were supplied from commercial companies in the region of Aveiro (cases of beech and forest pellets); in the case of the woody varieties, the samples were taken from the outer shell of the logs. The wood pellets, cellulose and lignin were taken from Chalmers; the wood pellets correspond to the fuel used as reference in the Chalmers $2MW_{th}$ gasifier.

During the fast pyrolysis experiments the focus was on thermal conditions typical of fluidized bed combustors and gasifiers, which means that the heating of the fuel particles is largely controlled by the intraparticle heat transfer. As a result, particle sizes in range of the industrial practice shall be preferably used, i.e. mm- to cm-sized, which leads intraparticle temperature gradients under the conditions used in this work (see e.g. [79]). Because feeding of fuel particles larger than ≈8mm in diameter to the small fluidized bed reactor was problematic, it was decided to use particles of 6×6mm (diameter × length) which correspond to the size of the forest pellets particles also used in the pilot scale combustor. Therefore, cylindrical particles of ≈6×6mm in size were prepared from the raw materials used at UA by different methods; the exception was the wood pellets which had dimensions of ≈8×8mm (cylindrical).

For the woody materials and the pine bark, the raw materials were first cut into long pieces of ≈100mm^2 cross sectional area. These pieces were then machined in a lathe into 6mm OD rods which were subsequently cut into cylindrical particles of 6mm in length. Figure 1.39-a shows a photograph of the lathe with a piece of wood in place; thousands of cylindrical particles were prepared during the course of this work through this method. For the fragile pine bark a bench grinder was sometimes needed to be able to obtain the cylindrical shape. The eucalyptus bark and cellulose were first ground in a hammer mill (Cullati, MFC) to <2mm in size and then gently compressed into 6×6mm pellets; a special accessory was developed to produce these pellets (Figure 1.39-b). The lignin was supplied as cm-sized, clay-like particles and attempts to prepare pellets from the lignin proved unsuccessful. Therefore, a sharp knife was used to cut cylinder-like particles from the raw lignin particles. Figure 1.40 shows examples of the so obtained cylindrical particles for some of the fuels used in the fast pyrolysis experiments at UA.

An additional five fuels (straw pellets, bark pellets, sawdust, peat, wood chips), as well as the wood pellets tested at UA, were used in the experiments conducted at Chalmers. All these fuels were pyrolysed in the thermobalance; with the exception of the pelletized fuels (≈8×8mm), grinding was of the raw materials was necessary to fit the size of the crucibles used in the thermobalance. Note that this procedure shall have a limited effect on the course of pyrolysis as the heating of the fuels particles in the thermobalance depends mainly of the

extraparticle heat transfer. The wood pellets also correspond to the fuel used during the gasification experiments in the Chalmers 2MW_{th} gasifier.

All the fuels were characterized with respect to ultimate compositions and ash contents (data given in the upcoming chapters). The ultimate analysis was carried out by external laboratories in Portugal (SIIAF-University of Lisbon, DEQ-University of Coimbra) and Sweden, and the ash content was determined in our laboratories at UA and Chalmers following CEN/TS 14775 standard.

(a) (b)

Figure 1.39 – Ancillary equipment for preparation of the 6mmOD fuel particles. Production of 6mm OD wood rods in the lathe (a) and production of 6mm eucalyptus bark particles in a small pelletizer.

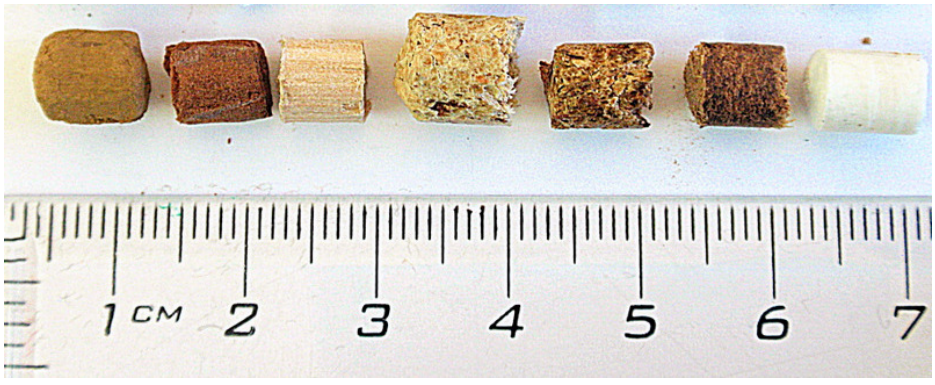

Figure 1.40 – Photograph of typical fuel particles used in the fluidized bed or quartz-tube facilities. From left to right: lignin; pine bark; eucalyptus wood; wood pellets; forest pellets; eucalyptus bark; and cellulose.

1.7 *Outline of this thesis work*

Chapters 2 to 6 of this thesis correspond to the Papers I to V, respectively, and stands by itself. Figure 1.41 shows how these papers have been organized to cope with the objectives of this work, thus providing the framework for the rest of this thesis. The facilities used in the experiments are also described in each chapter, according to Table 1.1 above.

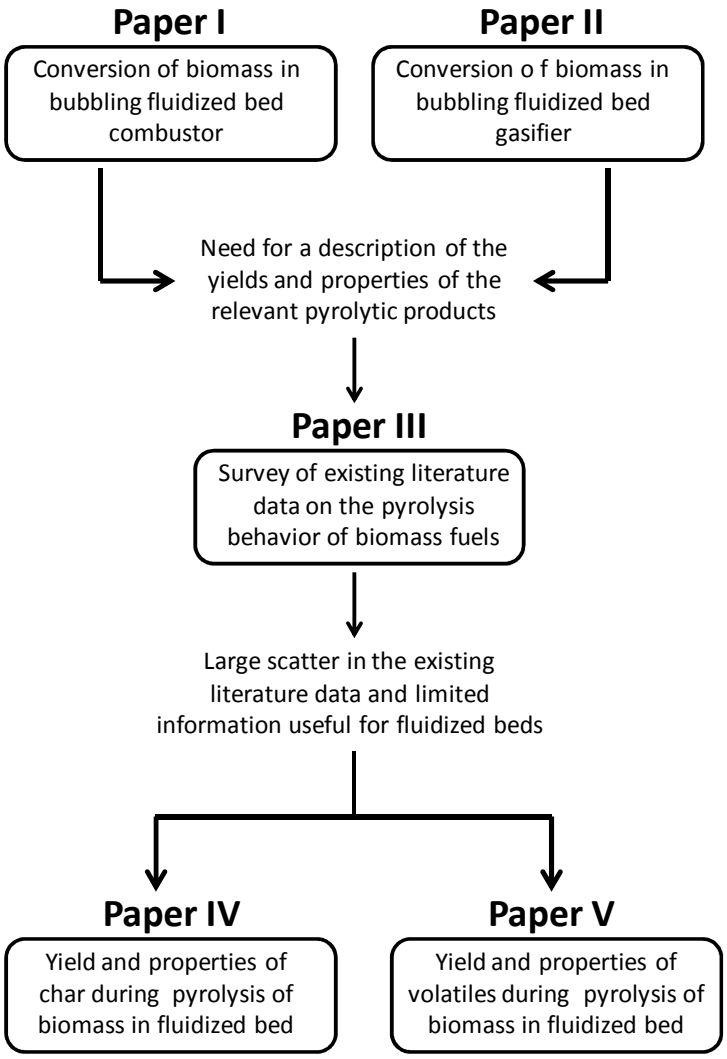

Figure 1.41 - Outline of this thesis work. Papers I to V corresponds to chapters 2 to 6 of this thesis.

Chapter 2 and 3 are based on experimental campaigns carried out in the pilot-scale bubbling fluidized bed combustor and the $2MW_{th}$ dual fluidized bed gasifier, respectively; chapter 3 makes also use of the online gas combustion facility for monitoring the CHON composition of the raw gas leaving the gasifier. The need for a good description of the pyrolytic degradation of biomass to evaluate the operation of combustors and gasifiers is

pointed out in both Chapters 2 and 3 which have motivated one to survey the existing literature data in the field. This is what is done in Chapter 4 where a large set of literature data on the properties of the major pyrolytic products and the stoichiometry of the overall pyrolysis reaction is structured and analyzed. It can be seen that the scatter in the data is large and information specialized for fluidized beds, namely gasifiers, is limited. To cope with these limitations of the literature data, experimental campaigns were done in the laboratorial fluidized bed and quartz tube pyrolysis facilities to elucidate how the composition of fuel and operating conditions influences the pyrolysis process, as shown in Chapters 5 and 6. Chapter 5 describes the dependence of char yield on the composition of parent fuel while Chapter 6 deals with the composition of the evolved pyrolytic volatiles. These experiments were designed to provide data specialized for fluidized beds as well as to verify the trends derived in Chapter 4. In particular, the data obtained on the pyrolysis behavior of the wood pellets have a good deal of usefulness for the evaluation of the conversion process in Chalmers $2MW_{th}$ gasifier.

Chapter 7 provides the conclusions of the present work as and suggestions for future work.

For convenience reasons, the conference papers published on the scope of this thesis work are also provided as appendixes. Papers VI and VII complement the analysis of the Chalmers dual fluidized bed gasification process. Papers VIII and IX complement the analysis of literature data shown in Chapter 4.

1.7.1 *Summary of chapters 2 to 6*

Chapter 2

Chapter 2 is the only one concerned with biomass combustion in fluidized bed. By using the pilot-scale fluidized bed combustor, two major topics are covered within this chapter: (1) evaluation of the progress of biomass conversion along the reactor; and (2) evaluation of the influence of the operating conditions on the exit flue gas emissions. The 6mm OD forest pellets were used as fuel and the combustion conditions were varied considerably (bed temperature of 750 and 800ºC, excess air level within 10-100%). The measurements include values of pressure, temperature and dry gas composition (O_2, CO_2, CO, NO, N_2O, total hydrocarbons) at several locations along the reactor tube as well as at the gas outlet port. This has enabled to investigate the elemental mass balance of the combustion reaction from inside the bed up to the top of the freeboard; the conversion of fuel carbon into CO and CO_2, and fuel nitrogen to NO is provided. The effect of the high volatile matter content of biomass on the operation of the combustor is highlighted in an attempt to convey an important distinction – the difference between using biomass or a fuel like e.g. coal during bubbling

fluidized bed combustion and its implications for reactor control and pollutant mitigation. The operating conditions minimizing the flue gas emissions are analyzed in relation to the Portuguese legal requirements.

Chapter 3

Chapter 3 deals with biomass steam gasification in the Chalmers (2+12)MW_{th} dual fluidized bed installation. An initial issue treated in this chapter is on the measurement of the CHON mass fractions of the raw gas leaving the gasifier as it provides several ways for the operational monitoring of the process. Nevertheless, the composition of the raw gas is rather complex, including variable amounts of permanent gases (e.g. H_2, CH_4), steam and condensable organics (say, tars), and minor amount of soot. Methods currently used for analyzing the CHON composition of the raw gas are surveyed in this chapter. To overcome some major limitations of the available methods, an alternative method is proposed in this chapter which simplifies the analysis and provides results with comparably high temporal resolution. In the proposed method a slipstream of the raw gas is continuously burned into H_2O, CO_2 and N_2, and the CHON contents of the raw gas are retrieved by solving backward the mass balance across the combustor. The online gas combustion facility was used to demonstrate this new method and results showing the accuracy and reliability of the measurements are provided. The second part of Chapter 3 describes the application of the online gas combustion facility in obtaining critical operational parameters of the 2MW_{th} fluidized bed gasifier. A zero-dimensional model of the gasifier is presented which, in combination with the so obtained CHON composition of the produced raw gas, provides simple ways for estimating (1) the degree of biomass and char conversion in the gasifier, (2) the composition of any unconverted char escaping the gasifier towards the boiler, (3) the amount of oxygen transported into the gasifier by a catalyst blended in circulating bed material and (4) the amount of condensables (steam+organics) in the raw gas. Some of these parameters can now be obtained in real-time which represent essential progress towards unattended gasifiers. Moreover, the elemental mass balance across the Chalmers 2MW_{th} gasifier could be closed by the proposed method.

Chapter 4

Chapter 4 lays out the state of knowledge on the experimental investigation and the behavior of biomass conversion upon pyrolysis. For that purpose, several investigations dealing with biomass pyrolysis under inert atmosphere were analyzed and the respective data screened and structured in this chapter. The collected data are concerned with the yields and properties (CHON composition, heating value) of the major product fractions (char, tar, water, permanent gases) together with information about the parent fuels (e.g. CHON

composition), pyrolysis conditions (e.g. peak temperature) and experimental rigs. A range of pyrolysis conditions of practical interest for torrefaction, pyrolysis, gasification or combustion applications is covered by this survey. Apart from a discussion of the major parameters governing the thermal degradation of a fuel particle, correlations were developed among yields of gases, properties of the char, tar and total permanent gas, and temperature, in an attempt of providing mathematical tools useful for engineers. Also developed in this chapter is an empirical model for estimating the stoichiometry of the overall pyrolysis reaction. The outcome of this chapter is a guide on the pyrolysis characteristics of biomass, setting the typical ranges for the yields and properties of the major pyrolytic products and providing insight to the overall mechanism describing the thermal degradation of a biomass fuel particle. While surveys dealing with the pyrolysis kinetics, pyrolysis mechanisms, transport phenomena and reactor modeling were already published [28,29,34,36], a survey structuring the kind of data provided in Chapter 3 was missing. Moreover, Chapter 3 also constitutes a good research starting point as the limitations of the literature data could be addressed thus pointing to where the experimental resources shall be directed.

Chapter 5

Chapter 5 focus on a specific issue which has emerged during the analysis of literature data in Chapter 4: for temperatures typical of fluidized bed combustors and gasifiers (say, >700ºC), the yield of char exhibits a minor temperature dependency but can vary within ≈5-40% among different fuels (mass % of daf fuel). What does govern the production of char under these high temperatures? In an attempt to solve this issue, Chapter 5 follows with a theoretical and experimental investigation on the production of char under operating conditions useful for fluidized beds. The theoretical investigation is based on thermodynamic equilibrium modeling of the distribution of pyrolytic products, in which carbon graphite is used as model compound for the pyrolytic char. To provide an overview of the theoretical yield of carbon graphite for the whole series of charring fuels, literature data on the elemental composition (CHONS) of lignins, biomasses and pyrolytic chars was surveyed. Concerning the experimental investigation, cellulose, lignin and fourteen types of biomass were fast pyrolysed in the laboratorial fluidized bed and quartz tube facilities under nitrogen to peak temperatures within 600-950ºC. Moreover, to verify the influence on char yield of lowering the heating rate of the fuel, additional experiments were carried out in the thermogravimetric analyzer at 5 and 50ºC/min. The results show how the composition of parent fuel, heating rate and temperature influences the yield of char, with a simple model being proposed to estimate the yield of char in fluidized bed combustors and gasifiers.

Chapter 6

To verify the trends on yields and properties of the pyrolytic volatiles derived from literature data in Chapter 3, dedicated experiments were done in Chapter 6 using the laboratorial fluidized bed pyrolysis facility; the information provided in this chapter can also be seen as a complement to Chapter 5, on the production of pyrolytic char, as similar operating conditions were used (i.e. bed temperatures of 600-975ºC, gas residence time <5s, inert atmosphere). However, in Chapter 6 the measurements were restricted to four fuel types, representing woody varieties of interest to large scale applications in Portugal (pine and eucalyptus), the forest pellets tested in the pilot scale fluidized bed combustor (Chapter 2) and the wood pellets used as fuel in the Chalmers $2MW_{th}$ gasifier (Chapter 3). All major product fractions (i.e. char, liquids, permanent gas and soot) were collected to verify the overall mass balance of pyrolysis and the composition of the permanent gas was further resolved into a number of species: H_2, CO_2, CO, C_3H_8, C_2H_6, C_2H_4 and CH_4. Apart from an analysis on how the composition of the pyrolytic volatiles evolve as a function of temperature and composition of the parent fuel, a set of empirical parameters with yields and properties of the permanent gas species are proposed in an attempt to provide data useful for modelers.

Nomenclature

ΔP_b	Pressure drop across the bed, Pa
ΔP_d	Pressure drop across the distributor, Pa
H	Bed height of the fluidized bed, m
H_{mf}	Bed height at minimum fluidization, m
ε_{mf}	Bed voidage at minimum fluidization, -
ρ_p	Bed particle density, kg/m3
ρ_g	Fluidizing gas density, kg/m3
g	Acceleration of gravity, m/s2
N_{or}	Number of orifices of distributor plate, -
d_{or}	Diameter of orifices, m
u_{or}	Gas velocity through an orifice, m/s
u	Superficial fluidization velocity, m/s

u_{mf} Minimum fluidization velocity, m/s

u_t Terminal velocity of a single particle, m/s

u_b Bubble rise velocity in the bed, m/s

Φ_p Spericity of a bed particle, -

m_p Mass of bed material, kg

A_r Cross-sectional area of reactor bed, m2

d_p Bed particle diameter, m

$Re_{p,mf}$ Bed particle Reynolds number at minimum fluidization velocity, -

$C_{d,or}$ Orifice discharge coefficient, -

μ Dynamic viscosity of gas, kg/m·s

References

1. Twidell J., Weir AD. Renewable energy resources: Taylor & Francis Group 2006.
2. Boyle G., Everett B., Ramage J. University O. Energy systems and sustainability: Oxford University Press, Incorporated 2003.
3. European, Commission. EU Energy in Figures 2012: Publications Office of the European Union 2012.
4. BP. BP Statistical Review of World Energy June 2012. 2012.
5. DGEG. Balanço Energético 2010, http://www.dgeg.pt/ 2010.
6. DGEG. Balanço Energético 2005, http://www.dgeg.pt/ 2005.
7. DGEG. Renováveis - Estatísticas Rápidas 2013, http://www.dgeg.pt/ 2013.
8. Patrão G. The Portuguese Energy Strategy and the role of Biomass, Workshop BIOGAIR. Aveiro, Portugal 2011.
9. Monteiro C., Tarelho L., Lopes M., Monteiro A., Cascão P., Miranda A.M. Air pollution impacts from logistics related to forest biomass to energy chain. World Bioenergy 2012 Conference & Exhibition on Biomass for Energy. Jönköping, Sweden 2012.
10. AIFF. Relatório de caracterização da fileira florestal 2010. Portugal 2010.
11. Santos P. O mercado da energia verde e as mecanismos de apoio aos projetos de biomass. Associação de Produtores de Energia e Biomassa. Expo Energia 2011.

12. APREN. Roteiro Nacional das Energias Renováveis - Aplicação da Directiva 2009/28/CE. Portugal 2010.
13. Viana H., Cohen W.B., Lopes D., Aranha J. Assessment of forest biomass for use as energy. GIS-based analysis of geographical availability and locations of wood-fired power plants in Portugal. Appl Energ. 2010;87:2551-60.
14. Ferreira S., Moreira N.A., Monteiro E. Bioenergy overview for Portugal. Biomass and bioenergy 2009;33:1567-76.
15. Bioenergy International. The world of pellets (map), www.bioenergyinternational.com. Stockholm, Sweden 2012.
16. Silva J.S., (Ed.). Árvores e florestas de Portugal. Vol. 8. Lisboa, Portugal: Público & Fundação Luso-Americana 2007.
17. Gil L. Cork powder waste: an overview. Biomass and bioenergy 1997;13:59-61.
18. Vassilev S.V., Baxter D., Andersen L.K., Vassileva C.G. An overview of the chemical composition of biomass. Fuel 2010;89:913-33.
19. Neves D., Thunman H., Matos A., Tarelho L., Gomez-Barea A. Characterization and prediction of biomass pyrolysis products. Prog Energ Combust. 2011;37:611-30.
20. Pettersen R.C. The chemical composition of wood. The chemistry of solid wood 1984;575:57-126.
21. Channiwala S., Parikh P. A unified correlation for estimating HHV of solid, liquid and gaseous fuels. Fuel 2002;81:1051-63.
22. Friedl A., Padouvas E., Rotter H., Varmuza K. Prediction of heating values of biomass fuel from elemental composition. Analytica Chimica Acta 2005;544:191-8.
23. Nunn T.R., Howard J.B., Longwell J.P., Peters W.A. Product Compositions and Kinetics in the Rapid Pyrolysis of Milled Wood Lignin. Ind Eng Chem Proc Dd. 1985;24:844-52.
24. Raveendran K., Ganesh A. Heating value of biomass and biomass pyrolysis products. Fuel 1996;75:1715-20.
25. Savolainen V., Berggren H. Wood fuels basic information pack: BENET 2000.
26. McKendry P. Energy production from biomass (part 2): conversion technologies. Bioresource Technol. 2002;83:47-54.
27. Faaij A.P.C. Bio-energy in Europe: changing technology choices. Energy Policy 2006;34:322-42.
28. Di Blasi C. Modeling chemical and physical processes of wood and biomass pyrolysis. Prog Energ Combust. 2008;34:47-90.

29. Di Blasi C. Combustion and gasification rates of lignocellulosic chars. Prog Energ Combust. 2009;35:121-40.
30. Tang M., Bacon R. Carbonization of cellulose fibers—I. Low temperature pyrolysis. Carbon 1964;2:211-20.
31. Piskorz J., Radlein D., Scott DS. On the mechanism of the rapid pyrolysis of cellulose. J Anal Appl Pyrol. 1986;9:121-37.
32. Brunner P.H., Roberts P.V. The significance of heating rate on char yield and char properties in the pyrolysis of cellulose. Carbon. 1980;18:217-24.
33. Mackay D., Roberts P. The influence of pyrolysis conditions on yield and microporosity of lignocellulosic chars. Carbon. 1982;20:95-104.
34. Di Blasi C. Modeling and simulation of combustion processes of charring and non-charring solid fuels. Prog Energ Combust. 1993;19:71-104.
35. Sreekanth M., Renu Kumar R., Kolar A.K., Leckner B. Estimation of wood char size at the end of devolatilization in a bubbling fluidized bed combustor. Fuel 2008;87:3393-402.
36. Gomez-Barea A., Leckner B. Modeling of biomass gasification in fluidized bed. Prog Energ Combust. 2010;36:444-509.
37. Basu P., Kaushal P. Modeling of pyrolysis and gasification of biomass in fluidized beds: a review. Chemical Product and Process Modeling 2009;4.
38. Carvalho L., Wopienka E., Pointner C., Lundgren J., Verma V.K., Haslinger W., et al. Performance of a pellet boiler fired with agricultural fuels. Appl Energ. 2013;104:286-96.
39. Williams A., Jones J., Ma L., Pourkashanian M. Pollutants from the combustion of solid biomass fuels. Prog Energ Combust. 2012;38:113-37.
40. Yin C., Rosendahl L.A., Kær S.K. Grate-firing of biomass for heat and power production. Prog Energ Combust. 2008;34:725-54.
41. Thunman H., Åmand L-E., Leckner B. A cost effective concept for generation of heat, electricity and transport fuel from biomass in fluidized bed boilers – using existing energy infrastructure. 15th European Biomass Conference & Exhibition. Berlin, Germany 2007.
42. Yang W-C. Handbook of fluidization and fluid-particle systems: CRC Press 2003.
43. Kunii D., Levenspiel O. Fluidization engineering: Butterworth-Heinemann Boston 1991.
44. Werther J., Saenger M., Hartge E.U., Ogada T., Siagi Z. Combustion of agricultural residues. Prog Energ Combust. 2000;26:1-27.
45. Sami M., Annamalai K., Wooldridge M. Co-firing of coal and biomass fuel blends. Prog Energ Combust. 2001;27:171-214.

46. Williams A., Pourkashanian M., Jones J. Combustion of pulverised coal and biomass. Prog Energ Combust. 2001;27:587-610.
47. Hein K., Bemtgen J. EU clean coal technology—co-combustion of coal and biomass. Fuel Process Technol. 1998;54:159-69.
48. Piriou B., Vaitilingom G., Veyssière B., Cuq B., Rouau X. Potential direct use of solid biomass in internal combustion engines. Prog Energ Combust. 2012.
49. El-Rub Z.A., Bramer E.A., Brem G. Experimental comparison of biomass chars with other catalysts for tar reduction. Fuel 2008;87:2243-52.
50. Devi L., Ptasinski K.J., Janssen F.J. A review of the primary measures for tar elimination in biomass gasification processes. Biomass and bioenergy 2003;24:125-40.
51. Abu El-Rub Z., Bramer E., Brem G. Review of catalysts for tar elimination in biomass gasification processes. Ind Eng Chem Res. 2004;43:6911-9.
52. Arias B., Pevida C., Fermoso J., Plaza M., Rubiera F., Pis J. Influence of torrefaction on the grindability and reactivity of woody biomass. Fuel Process Technol. 2008;89:169-75.
53. Antal M.J., Grønli M. The art, science, and technology of charcoal production. Ind Eng Chem Res. 2003;42:1619-40.
54. Gronly M., Antal Jr. M.J., Schenkel Y, Crehay R. The science and technology of charcoal production, In: Fast pyrolysis of biomass: a handbook. CPL Press 2005.
55. Antal M.J., Allen S.G., Dai X., Shimizu B., Tam M.S., Grønli M. Attainment of the theoretical yield of carbon from biomass. Ind Eng Chem Res. 2000;39:4024-31.
56. Wang L., Trninic M., Skreiberg Ø., Gronli M., Considine R., Antal Jr. M.J. Is elevated pressure required to achieve a high fixed-carbon yield of charcoal from biomass? Part 1: Round-robin results for three different corncob materials. Energ Fuel 2011;25:3251-65.
57. Bridgwater A.V., Czernik S., Diebold J. Fast pyrolysis of biomass: a handbook: CPL Press 1999.
58. Bridgwater A.V. Fast Pyrolysis of Biomass 2: A Handbook: CPL Scientific Publishing Services, Limited 2008.
59. Bridgwater A.V. Fast pyrolysis of biomass 3: a handbook: CPL Press 2005.
60. Bridgwater A.V., Peacocke G.V.C. Fast pyrolysis processes for biomass. Renewable and Sustainable Energy Reviews 2000;4:1-73.
61. Bridgwater A.V. An introduction to fast pyrolysis of biomass for fuels and chemicals, In: Fast pyrolysis of biomass: a handbook CPL Press 1999.
62. Knoef H. Handbook Biomass Gasification. Biomass Technology Group. 2005.

63. Henriksen U., Ahrenfeldt J., Jensen T.K., Gøbel B., Bentzen J.D., Hindsgaul C., et al. The design, construction and operation of a 75kW two-stage gasifier. Energy 2006;31:1542-53.
64. Hofbauer H., Rauch R., Löffler G., Kaiser S., Fercher E., Tremmel H. Six years experience with the FICFB-gasification process. 12th European Conference and Technology Exhibition on Biomass for Energy, Industry and Climate Protection. Amsterdam, The Nederlands 2002. p. 982-5.
65. Seemann M.C., Thunman H. The new Chalmers research-gasifier. Proceedings of the International Conference on Polygeneration Strategies. Wien, Austria 2009.
66. Kohl T., Laukkanen T., Järvinen M., Fogelholm C-J. Energetic and environmental performance of three biomass upgrading processes integrated with a CHP plant. Appl Energ. 2013;107:124-34.
67. Levenspiel O. What will come after petroleum? Ind Eng Chem Res. 2005;44:5073-8.
68. Matos M.A.A. Formação e redução de NO_x na combustão de coque em leito fluidizado, PhD Thesis. Aveiro, Portugal: University of Aveiro 1995.
69. Tarelho L.A.C. Controlo de emissões gasosas poluentes resultantes da conbustão de carvão em leito fluidizado, PhD Thesis. Aveiro, Portugal: University of Aveiro 2001.
70. Tarelho L.A.C., Matos M.A.A., Pereira F.J.M.A. Axial and radial CO concentration profiles in an atmospheric bubbling FB combustor. Fuel 2005;84:1128-35.
71. Tarelho L.A.C., Matos M.A.A., Pereira F.J.M.A. Axial concentration profiles and NO flue gas in a pilot-scale bubbling fluidized bed coal combustor. Energ Fuel 2004;18:1615-24.
72. Edvardsson E., Åmand L.E., Thunman H., Leckner B., Johnsson F. Measuring the External Solids Flux in a CFB boiler. Proceedings of the 19th International Conference on Fluidized Bed Combustion. Viena (Austria) 2006.
73. Larsson A., Seeman M., Thunman H. Assessment of mass and energy flows in the Chalmers gasifier. Sweden: Department of Energy and Environment, Chalmers University of Technology 2011.
74. Larsson A., Thunman H., Neves D., Pallarés D., Seemann M. Zero-dimensional modeling of indirect fluidized bed gasification. Proceedings of the XIII Fluidization Conference. Gyeong-ju, Korea 2010.
75. Hermansson S., Lind F., Thunman H. On-line monitoring of fuel moisture-content in biomass-fired furnaces by measuring relative humidity of the flue gases. Chem Eng Res Des. 2011;89:2470-6.
76. Licht W. Air Pollution Control Engineering: Basic Calculations for Particulate Collection: Marcel Dekker Incorporated 1988.

77. Howard J.R. Fluidized Bed Technology: Principles and Applications: Adam Hilger; 1989.
78. Matos M.A.A., Ferreira V. S. Gas mass-flow meters: Principles and applications. Flow Measurement and Instrumentation 2010;21:143-9.
79. Gomez-Barea A., Nilsson S., Vidal Barrero F., Campoy M. Devolatilization of wood and wastes in fluidized bed. Fuel Process Technol. 2010;91:1624-33.

Chapter 2 - Forest biomass waste combustion in a pilot-scale bubbling fluidised bed combustor

Tarelho L.A.C., Neves D.S.F., Matos M.A.A.

University of Aveiro and CESAM

Published in Biomass and Bioenergy. 2011, 35, 4, 1511-23.

Abstract

Combustion experiments of forest biomass waste in a pilot-scale bubbling fluidised bed combustor were performed under the following conditions: i) bed temperature in the range 750-800ºC, ii) excess air in the range 10-100%, and iii) air staging (80% primary air and 20% secondary air). Longitudinal pressure, temperature and gas composition profiles along the reactor were obtained.

The combustion progress along the reactor, here defined as the biomass carbon conversion to CO_2, was calculated based on the measured CO_2 concentration at several locations. It was found that 75-80% of the biomass carbon was converted to CO_2 in the region located below the freeboard first centimetres, that is, the region that includes the bed and the splash zone.

Based on the CO_2 and NO concentrations in the exit flue gas, it was found that the overall biomass carbon conversion to CO_2 was in the range 97.2 to 99.3%, indicating high combustion efficiency, whereas the biomass nitrogen conversion to NO was lower than 8%.

Concerning the Portuguese regulation about gaseous emissions from industrial biomass combustion, namely, the accomplishment of CO, NO and volatile organic compounds (VOC) (expressed as carbon) emission limits, the set of adequate operating conditions includes bed temperatures in the range 750-800ºC, excess air levels in the range 20% to 60%, and air staging with secondary air accounting for 20% of total combustion air.

Keywords

Fluidised bed, Biomass, Combustion, Emission

2.1 *Introduction*

In recent years, pressures on global environment and energy security led to an increasing interest on renewable energy sources, and diversification on world's energy supply. Among these renewable resources, the biomass could exert an important role, since it is considered CO_2 neutral, can be used from a set of multiple biomass resources, and can potentially provide energy for heat, power and transport fuels.

Among others, the technology of Fluidised Bed Combustion (FBC) applied to solid biomass is a proven technology for heat and power production, showing some advantages in operating conditions and fuel flexibility [1-5].

Beyond the main products CO_2 and H_2O, flue gas emissions from biomass combustion include some pollutants, either associated to incomplete combustion (CO, hydrocarbons and carbon particles), or to the operating conditions and fuel properties (NO_x, N_2O, SO_2, HCl, and ash) [2,6-8]. In relation to the nitrogen compounds, whereas the NO_x emission appears to be strongly influenced by the nitrogen content of the biomass fuel [2,3,6], on the other hand the N_2O emission appears to be of minor importance [2,3]. Biomass combustion is an important source of particulate matter (ash and tar), and this is important considering its impact on the performance of the heat recovery equipment, but also on both public health and global climate change. The tar emission includes poliaromatic hydrocarbons (PAH), among them the chlorinated hydrocarbons (PCDD/F), and this is an issue of particular concern during biomass combustion, since these compounds can be subject of bio-accumulation throughout the ecosystems, and are responsible for chronic effects in the public health. Both the characteristics of the biomass fuel feedstock, namely its chlorine content, and the operating conditions determine the formation and emission of these compounds [5,9-13].

An appropriate understanding of the biomass combustion process in fluidised beds is needed to establish proper control of combustion conditions, use of additives, flue gas quenching and flue gas treatment conditions, in order to limit the drawbacks from biomass combustion in fluidised beds, namely the operational problems and environmental impacts.

In what concerns the combustion process, the solid biomass fuels follow generally the same phenomena sequence as any other solid fuel (as for example the coal), when submitted to high temperatures and oxidant atmospheres, that is, drying, devolatilisation, combustion of volatiles and char. There are, however, some significant differences between the solid biomass fuels combustion and that of, for example, coal combustion. Among the factors that contribute for such differences are [3,14]: i) the density of biomass is much lower than that of coal, ii) biomass has in general about 70-80%wt volatile matter content, whereas that of coal is in the range 10-50%wt, iii) the heating value of biomass is significantly lower than that of

coal, iv) the ash content and its composition. An important aspect is that most of the chemical energy contained in solid biomass appears to be converted in thermal energy through volatile matter combustion, rather than from the combustion of the solid fraction (char) remaining after the parent biomass fuel has undergone thermal decomposition on being heated.

As a consequence of such fuel differences, for example, during biomass combustion in Bubbling Fluidised Bed Combustors (BFBC) the highest temperature in the reactor is observed in the freeboard region [2,14-28], irrespective of the biomass feed location (over-bed or under-bed), and not inside the bed as observed in the case of low volatile content coal combustion [29]; higher freeboard temperatures relative to the dense bed have been observed also during co-combustion of biomass with other solid fuels [30-32]. It has been argued that this behaviour is related to the high volatile matter content of biomass fuels, and a consequence of the oxidation of most of the volatile matter in the splash and freeboard regions of a BFBC, even in the case of under-bed feeding, as a result of: i) segregation of fuel particles during devolatilisation at the top of the bed (whatever the feeding option) and ii) very limited in-bed volatile matter combustion [17,22,23,25,33,34]. The segregation of biomass fuel particles at bed surface during devolatilisation has been documented [35,36], and is related with the lift effect that the volatile bubbles can exert on fuel particles. The combustion of some gaseous fuels in the dense bed can be limited due to the quenching effect exerted by bed solid particles on free radicals, as discussed elsewhere [29,33,37-39], and this can also occur during the combustion of volatiles inside the bed.

Nevertheless, energy balances indicate [23] that the major part of the heat released in the splash region is fed back to the bed (the dominant mechanism of heat transfer being solids convection associated with particles ejection/fall-back). Only a small amount of the thermal energy released during biomass volatiles combustion appears to contribute to freeboard over-heating above bed temperature [23].

As a consequence, the specificity of the solid biomass fuel has to be accounted for on the design of technologies dedicated to its energetic conversion. This applies both to the combustion process and respective control variables (as for example the temperature, stoichiometry and gas residence time), and to the measures applied to pollution control (for example, some measures developed for coal combustion could not have the same result in the case of solid biomass fuels combustion). It is recognised that fluidised bed technology is characterised by high rates of heat transfer inside the dense bed, and has proven to be effective in reducing the NO_x concentration in flue gases because of the lower operating temperature and NO_x destruction inside the dense bed (most of it related to heterogeneous and catalytic reactions between the NO and the char). In this context, if most part of the mass of the solid biomass fuel is released as volatiles and would burn in the freeboard region instead of inside the bed, the location of heat transfer devices should be evaluated

accordingly, and the strategies for NO_x abatement should be adapted considering the decrease of importance of the dense bed on the NO_x chemistry.

To evaluate the influence of the solid biomass fuels characteristics on the performance of energy conversion systems, as for example FBC, it is important to understand the fuel combustion behaviour, namely the combustion progress along the reactor. For that purpose it is useful to access and analyse information related with the pressure, temperature and gas composition distribution along the reactor.

The objective of this work is to present and analyse experimental information about values of pressure, temperature and gas composition (concentration of O_2, CO_2, CO, NO and N_2O) at several locations along the reactor during biomass combustion in a pilot-scale BFBC, in order to contribute to a better understanding of the combustion of high volatile fuels (as biomass) in bubbling fluidised bed combustors.

2.2 *Experimental work*

2.2.1 *Fuel characteristics*

The biomass fuel used was prepared from pellets made of forest waste. The biomass pellets were grinded in order to produce biomass particles of smaller size. The biomass particles used in the experiments were in the size range ($1.0x10^{-3}$ m < $d_{p,f}$ < $4.0x10^{-3}$ m). The chemical composition of the solid biomass fuel is presented in Table 2.1.

Table 2.1 - Chemical composition of the solid biomass fuel.

Proximate analysis (%wt, as received)	
Moisture	0.09
Ash	0.02
Volatile Matter	0.70
Fixed C	0.19
Ultimate Analysis (%wt, dry basis)	
Ash	0.025
C	0.498
H	0.067
N	0.030
S	nd
O (by difference)	0.380

nd-Not determined, below detection limit.

2.2.2 *Pilot-scale bubbling fluidised bed combustor*

The biomass combustion experiments were conducted in a pilot-scale Bubbling Fluidised Bed Combustor (BFBC). The reactor is a thermally insulated AISI 310 SS tube with 0.25 m I.D. and 3 m height. The layout of the experimental facility is presented in Figure 2.1. The bed is operated with sieved silica sand ($0.500x10^{-3}$ m < $d_{p,b}$ < $0.710x10^{-3}$ m), with a static height of 0.23 m, of which 0.14 m are located above the fluidising air injectors. The reactor is equipped with a top reactor double screw feeding system for simultaneous and independent solid fuels feeding (two top reactor biomass feeders).

The combustion air was staged, with primary air fed through injectors located in the distributor plate and secondary air above the bed injected at 0.43 m above the distributor plate (that is, 0.20 m above the surface of the static bed). Uncertainties associated with measurements of primary and secondary air flow rates are 3%.

The solid biomass fuel was over-bed fed and was added together with the secondary air through a vertical tube located inside the freeboard (Figure 2.1); thus, the biomass particles are continuously dropped at the bed surface. Uncertainties associated with measurements of fuel feeding rates (screw feeders) are 5%.

Pressure, temperature and combustion flue gas were sampled by means of eight water-cooled probes located at several heights along the reactor, two of which are immersed in the dense bed of particles and the rest located along the freeboard. Each sampling probe is equipped with an external circulating quenching water sleeve, an ice-cooled particle filter, a K-type thermocouple and a cerablanket plug at the tip for particle filtering. A dedicated probe with the tip located inside the reactor at a height of 1.70 m above the distributor plate was used for gas sampling using a 190ºC heated line for total hydrocarbons analysis.

The set of analysers used include: O_2 (paramagnetic, ADC model O_2-700 with a Servomex Module), CO_2 (non-dispersive IR, ADC model 1450 Luft), CO (non-dispersive IR, ADC model RF558), NO (chemiluminescent, ThermoElectron model 10A), N_2O (non-dispersive IR, ADC model RF558), and total hydrocarbons (Dyna-Fid Hydrocarbon Gas Analyser, model SE-310). Uncertainties associated with gas composition measurements in the online analysers for O_2, CO_2, CO, NO and N_2O are 2%.

The operation and monitoring of the reactive system, the gas sampling system and data acquisition (temperature, pressure and gas concentration) system was performed by a computer based control and data acquisition hardware and software system.

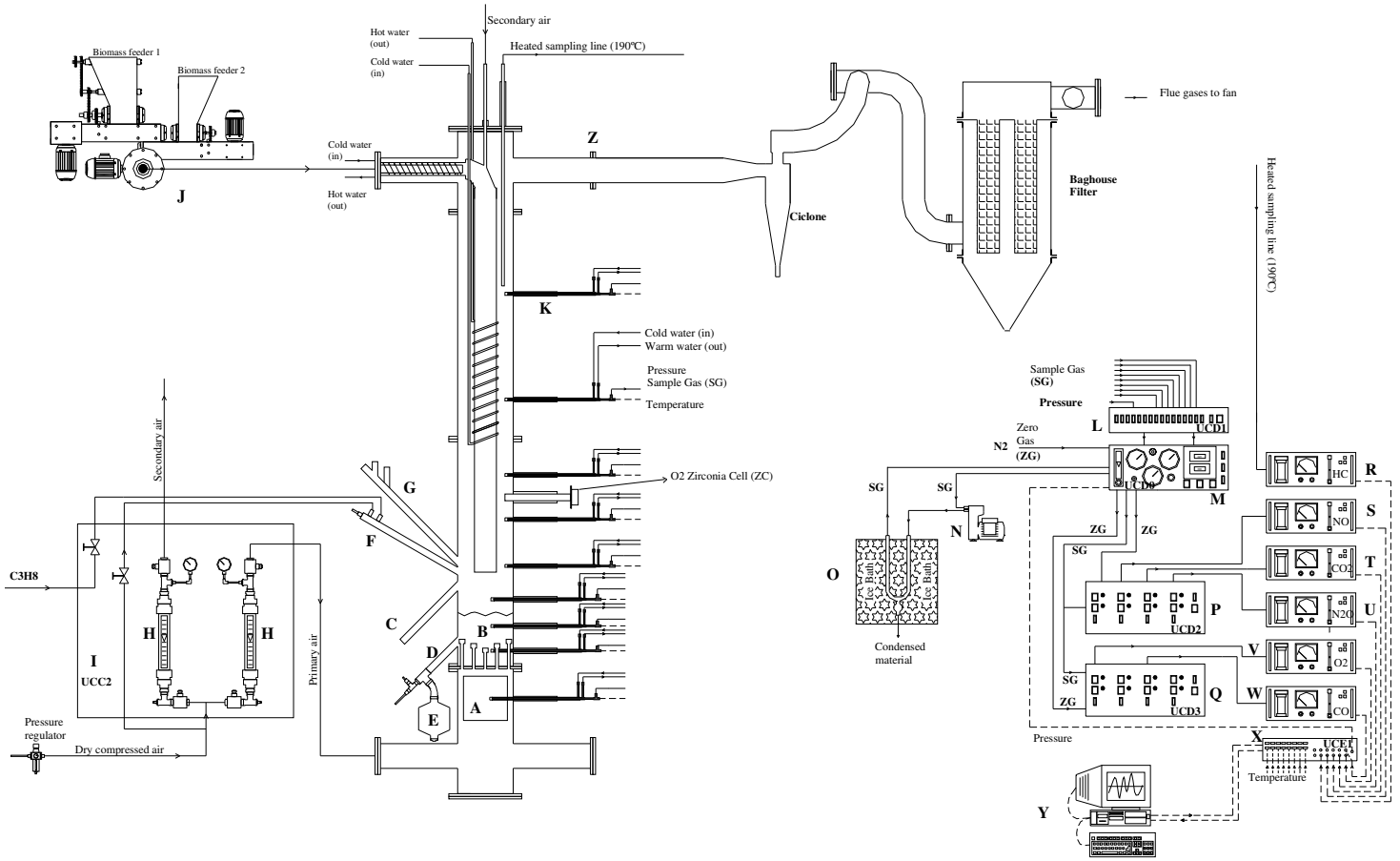

Figure 2.1 - Schematic representation of the pilot-scale installation. Dashed line - Electric circuit, Continuous line - Pneumatic circuit, A - Primary air heating system, B - Sand bed, C - Bed solids level control, D - Bed solids discharge, E - Bed solids discharge silo, F - Propane burner system, G - Port for visualisation of bed surface, H - Air flow meter (primary and secondary air), I - Control and command unit (UCC2), J - Biomass feeder, K – Water-cooled gas sampling probe, L, M, P, Q - Command and gas distribution units (UCD0, UCD1, UCD2, UCD3), N - Gas sampling pump, O - Gas condensation unit for moisture removal, R, S, T, U, V, W - Automatic online gas analysers (HC, NO, CO_2, N_2O, O_2, CO), X - Electronic command unit (UCE1), Y - Computer data acquisition and control system, Z - Exhaust duct to cyclone and bag-house filter.

2.2.3 *Combustion experiments*

The combustion experiments were planned so that the hydrodynamics of the reactor was kept similar during experiments. For that purpose the primary air flow-rate was adjusted in order to keep the fluidising velocity between 2.5 and 3 times the minimum fluidising velocity, that is, between 0.28 and 0.30m·s^{-1} depending on the bed temperature. The secondary air was adjusted in order to represent 20% of total combustion air. On following, the stoichiometry of combustion was established independently by proper adjustment of the solid biomass fuel feed rate. The bed temperature was maintained at the desired level by means of regulating the insertion of a set of eight water-cooled probes located at the bed level. The freeboard temperature was controlled by means of a heat exchanger, operated with liquid water at a constant flow rate of 1L·min^{-1}.

One set of experiments was made in order to evaluate the longitudinal (along the reactor height) concentration profiles of main combustion gases (CO_2, CO, O_2 and NO), with the objective of studying the combustion progress along the BFBC. Another set of experiments were conduced in order to evaluate the influence of excess air in the exit flue gas concentration of CO, NO, N_2O and total hydrocarbons. The set of operating conditions used is presented in Table 2.2.

The monitoring of pressure and temperature, and gas sampling at different heights along the reactor were made with the probes tip at half distance between the reactor wall and the axial line.

All the measurements (pressure, temperature and gas composition) were taken with the reactor operating at pre-set steady state conditions. At specified feeding conditions of air and biomass, the steady state condition was evaluated by monitoring the bed temperature and the exit flue gas composition (in terms of O_2 and CO_2 concentration); the steady state condition was considered as achieved when the bed temperature and the exit flue gas composition were almost constant, and then a complete set of measurements was performed.

Since biomass was continuously added to the bed, it was necessary to control the bed height. Nevertheless, the biomass feed rate was relatively small (30-50g·min^{-1}), and the bed solids level didn't change significantly during an experimental run. However, a procedure of bed renew was implemented in order to prevent the known defluidisation events that occur due to the alkaline content of the ash. For this purpose, periodically openings of the bed discharge port permitted to withdraw a known amount of bed solids, subsequently followed by the feeding of an equivalent amount of fresh sand in order to keep the bed level and the bed particles renovation. Between openings, the bed level did not change more than a few percent of total bed height, and thus the amount of solids extracted was also only a small

fraction of the total bed solids inventory; in this way the steady state was not unduly affected. Besides, the actual measurements of process variables (pressure, temperature and gas composition) were never made during the operations of bed solids withdraw and replenishment.

Table 2.2 - Experimental conditions.

Experiment reference	Bed temperature (ºC)	Total air		First stage stoichiometry[(a)] (-)	Excess air[(b)] (%)
		Primary air (%)	Secondary air (%)		
10-750	750	80	20	0.88	10
15-750	750			0.92	15
20-750	750			0.96	20
35-750	750			1.08	35
40-750	750			1.12	40
50-750	750			1.20	50
55-750	750			1.24	55
40-800	800			1.12	40
60-800	800			1.28	60
100-800	800			1.60	100

[(a)] Primary air flow rate/Stoichiometric air flow rate; [(b)] ((Total air flow rate/Stoichiometric air flow rate)-1)x100.

2.3 *Results and discussion*

The experimental results obtained during biomass combustion in the pilot-scale bubbling fluidised bed combustor include values of pressure, temperature and gas composition along the reactor height.

2.3.1 *Longitudinal pressure and temperature profiles*

Longitudinal pressure and temperature profiles along the reactor height are presented in Figure 2.2.

The pressure has its maximum value at the base of the bed, that is, at the level of the air injectors, then it drops across the fluidised bed and maintains an almost constant value along the freeboard height.

The temperature is at a minimum value in the base of the bed, where there is a fixed bed of sand (below the level of the air injectors), but increases in the fluidised bed region and attains a maximum value near the location of the secondary air and biomass addition point,

decreasing in the space above. A remarkable temperature decrease in the freeboard above 1.00m is due to the existence of a water heat exchanger (where liquid water at a flow rate of 1L·min^{-1} at 102 kPa and 80ºC is removed). Inside the fluidised bed (dense bed) the temperature varies within ±5ºC around the average value presented in Figure 2.2.

Similar longitudinal temperature profiles during biomass combustion in BFBC have been reported in the literature [17,23,25], and the temperature peak observed in the freeboard above the dense bed has been attributed to the characteristic high volatile matter content of biomass fuels and to its release and combustion mostly in the splash region and freeboard instead of inside the dense bed. Besides, the biomass feed point location appears to influence the freeboard temperature, with higher freeboard temperatures during over-bed feeding been reported [23].

Another feature of the longitudinal temperature profiles is that the temperature along the freeboard tends to be lower for the high excess air levels analysed (Figure 2.2). This behaviour can be understood as resulting from lower heat input in the reactor with increasing the excess air level. During the experiments the combustion air flow was maintained constant, and the stoichiometry was modified by changing the biomass feed rate; a higher excess air implies a lower biomass feed rate. Also, with increasing the excess air less unburned species are oxidised along the freeboard, as can be observed in the axial concentration profiles of CO (Figure 2.3), and thus less amount of heat is generated there.

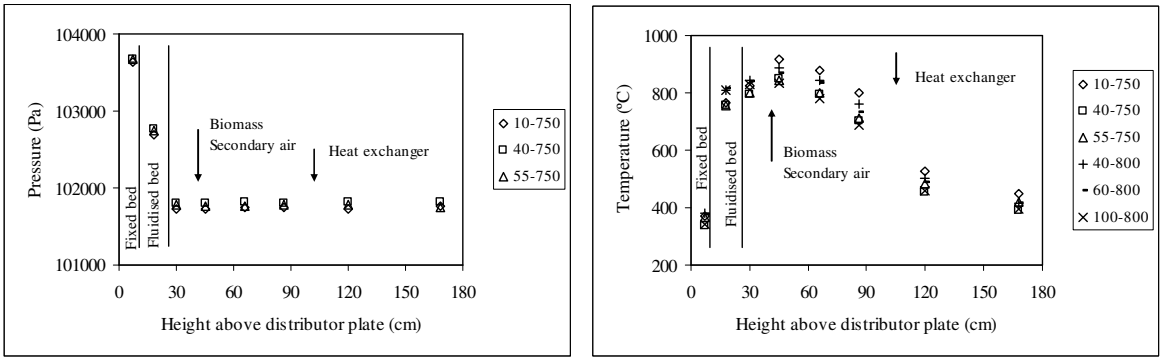

Figure 2.2 - Longitudinal pressure and temperature profiles measured along the pilot-scale BFBC, during biomass combustion. Legend according to experiment reference in Table 2.2.

2.3.2 *Longitudinal gas composition profiles*

Longitudinal concentration profiles of CO_2, O_2, CO and NO during biomass combustion in the bubbling fluidised bed combustor are presented in Figure 2.3.

Inside the bed, it is observed that the concentration of CO_2 in the gas sampled has its minimum value and the concentration of O_2 has its maximum value. The concentration of CO_2

in the gas sampled increases significantly from half bed height (inside the bed) to the bed surface. The O_2 concentration shows a complimentary behaviour of the one observed for CO_2, that is, the O_2 in the gas sampled decreases from half bed height (inside the bed) to the bed surface. Above the splash region and along the freeboard height the CO_2 and O_2 concentrations remain almost unchanged, although some influence of the secondary air injection is observed, more pronounced for the lower excess air presented in Figure 2.3; the CO_2 concentration decreases locally above the secondary air injection, whereas the concentration of O_2 increases. Although there is some degree of reaction, since the concentration of CO decreases upon secondary air injection, the observed influence of secondary air injection should be mostly related with dilution of combustion gases and gas mixing in this region.

As it can be observed in the axial concentration profiles of CO (Figure 2.3), an increase on the excess air results in less unburned species oxidised along the freeboard.

The CO concentration in the gas sampled inside the bed is relatively low, when compared with the values observed during bituminous or anthracite coal combustion in the same BFBC [29]. This could be related with: i) the lower contribution of in-bed biomass combustion when compared with the observed for coal and ii) the catalytic effect of biomass ashes on the CO conversion to CO_2 [40]. It has been argued that, as result of its high content of volatile matter, a significant part of the biomass fuel mass is released to the gas phase and oxidised in the splash region and along the freeboard; thus the contribution of in-bed combustion could represent less conversion of biomass carbon to CO and consequently a relatively low concentration of CO inside the bed. When comparing the longitudinal CO concentration profiles for coal and for biomass combustion under similar experimental conditions in this same BFBC, it can be observed that during coal combustion there is a significant decrease on the CO concentration from within the bed to the splash zone [29], whereas for biomass combustion it is observed an increase of CO concentration from within the bed to the splash region (Figure 2.3). This behaviour during biomass combustion is an indication of the importance of the bed surface (splash zone) for volatiles release and combustion during biomass conversion. In fact, it has been argued that the biomass particles show a tendency to float at bed surface during volatiles evolution [23,36], thus, considering the high volatile matter content of biomass the observed behaviour (Figure 3) is an indication of the importance of volatile matter release and conversion in the splash region and freeboard of a BFBC.

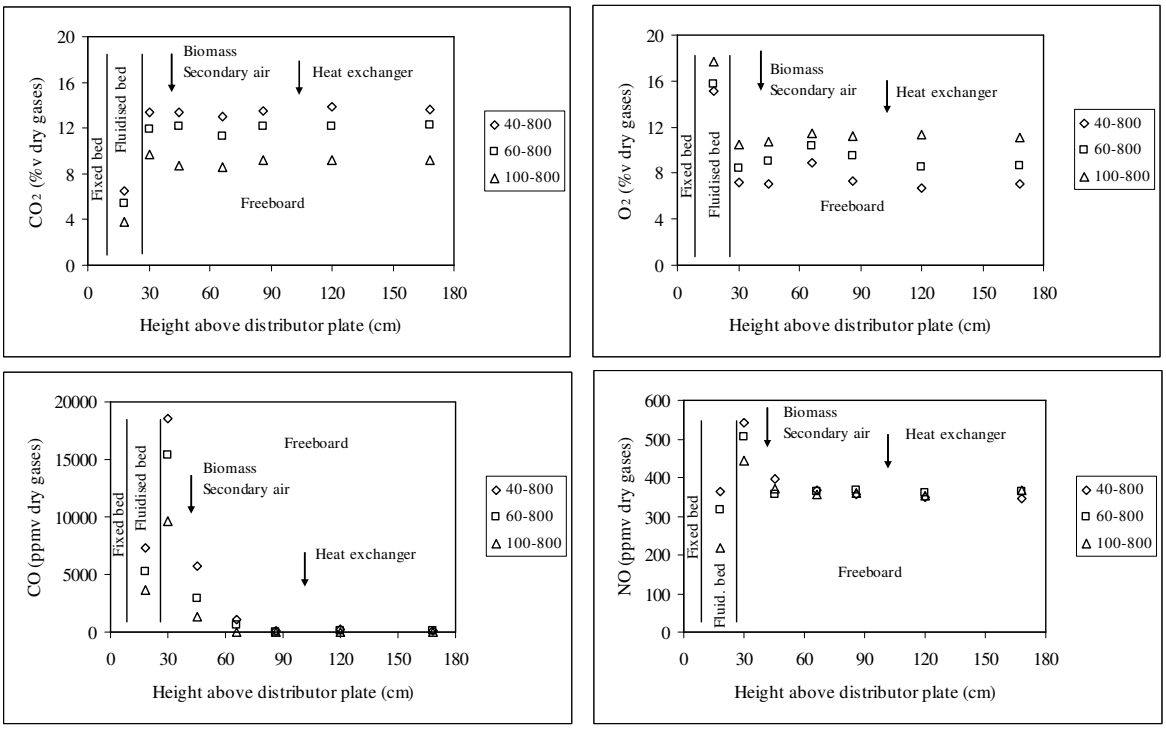

Figure 2.3 - Longitudinal O_2, CO_2, CO and NO concentration profiles in the pilot-scale BFBC, during biomass combustion. Legend according to experiment reference in Table 2.2.

The longitudinal NO concentration profile follows closely the longitudinal CO concentration profile, that is, the NO concentration increases from inside the bed to the splash region, where it attains the highest concentration value, an then decreases in the space above. This NO behaviour during biomass combustion is somewhat distinct from the one observed during coal combustion in the same BFBC [41]; during coal combustion the highest NO concentration observed was within the bed, whereas during biomass combustion the highest NO concentration is observed in the splash region. This behaviour during biomass combustion shows the relevance of the splash region on the NO formation, and can be related to the fact that most of the nitrogen species present in the solid fuel are released with the volatiles (the major part of the solid fuel mass) at bed surface (where the solid fuel is fed) and oxidised in the splash region and freeboard. Further NO destruction in the space above the splash region appears to be of minor importance, since the NO concentration decrease upon injection of the secondary air is mainly related with the dilution effects, as will be analysed latter (see Figure 2.4), rather than a result of NO destruction by reaction.

This observed NO behaviour during biomass combustion can rise questions regarding the recognised relevance of fluidised bed technology on NO-fuel abatement, namely the characteristic heterogeneous environment inside the bed that contributes to NO destruction and thus to low NO emissions [41]. Two reasons can contribute to this: i) since the fixed carbon content of biomass fuels is only a small amount of the solid fuel mass, the char

inventory inside the bed should be reduced when compared to the observed during coal combustion and consequently the relevance of the NO destruction reactions involving the char should be of minor relevance, and ii) if the NO is formed by oxidation of volatiles species above the bed surface, the contribution of the bed for the NO formation and destruction could be of limited importance. Consequently, the measures of NO_x control during biomass combustion in BFBC should be analysed accordingly.

2.3.3 *Fuel conversion along the reactor*

In order to understand the role of the bed and freeboard during the combustion of a biomass fuel in BFBC, it was analysed the biomass carbon conversion to CO_2 and CO based on measured CO_2 and CO concentrations at several heights along the reactor, respectively, as an indicator of the combustion progress along the reactor. The biomass nitrogen conversion to NO was also evaluated, based on measured NO concentration at several heights along the reactor.

The conversion of biomass chemical i^{th} element (C, N) on feeding to the j^{th} gas compound (CO_2, CO or NO) on flue gas was evaluated by using Eq. 2.1 to Eq. 2.4. The j^{th} gas concentration value ($\overline{C}_{j,sample}$) used in conversion calculations at each location z along the reactor height was the value measured experimentally (see Figure 3). Inside the bed, the value of $G_v(z)$ used corresponds to the total volumetric gas flow throughout the bed and was considered equal to the gas flow of primary air measured experimentally, and corresponds to the sum of bubble and emulsion phases volumetric gas flows at level z above the fluidising air injectors, since the temperature and pressure shall be the same. In the freeboard the value of $G_v(z)$ used was the total volumetric gas flow throughout the reactor: i) below the secondary air injection point it was considered that the overall gas flow rate results from the mixture of the bubble and emulsion phases volumetric gas flows emerging from the bed, and ii) above secondary air injection, the overall gas flow rate it was considered the sum of the freeboard gas flow upcoming from the first stage with the gas flow of secondary air injected. The results obtained are presented in Figure 2.4.

A critical issue on this analysis is related to the use of time-mean concentration values measured on mass balance calculations. Whereas the use of time-mean concentration measurements in mass balance in the freeboard appears to be reasonable, inside the bed this procedure could result in a misleading interpretation of experimental data as discussed elsewhere [42, 43].

$$G_{v,j}(z) = \overline{C}_{j,sample}(z) \times G_v(z) \qquad \text{Eq. 2.1}$$

$$G_{m,j}(z) = \frac{G_{v,j}(z) \times P_b(z) \times M_j}{R \times T_b(z)} \quad \text{Eq. 2.2}$$

$$G_{m,i-j}(z) = G_{m,j}(z) \times \frac{M_i}{M_j} \quad \text{Eq. 2.3}$$

$$X_{i-j}(z) = \frac{G_{m,i-j}(z)}{S_{m,i,biomass}} \quad \text{Eq. 2.4}$$

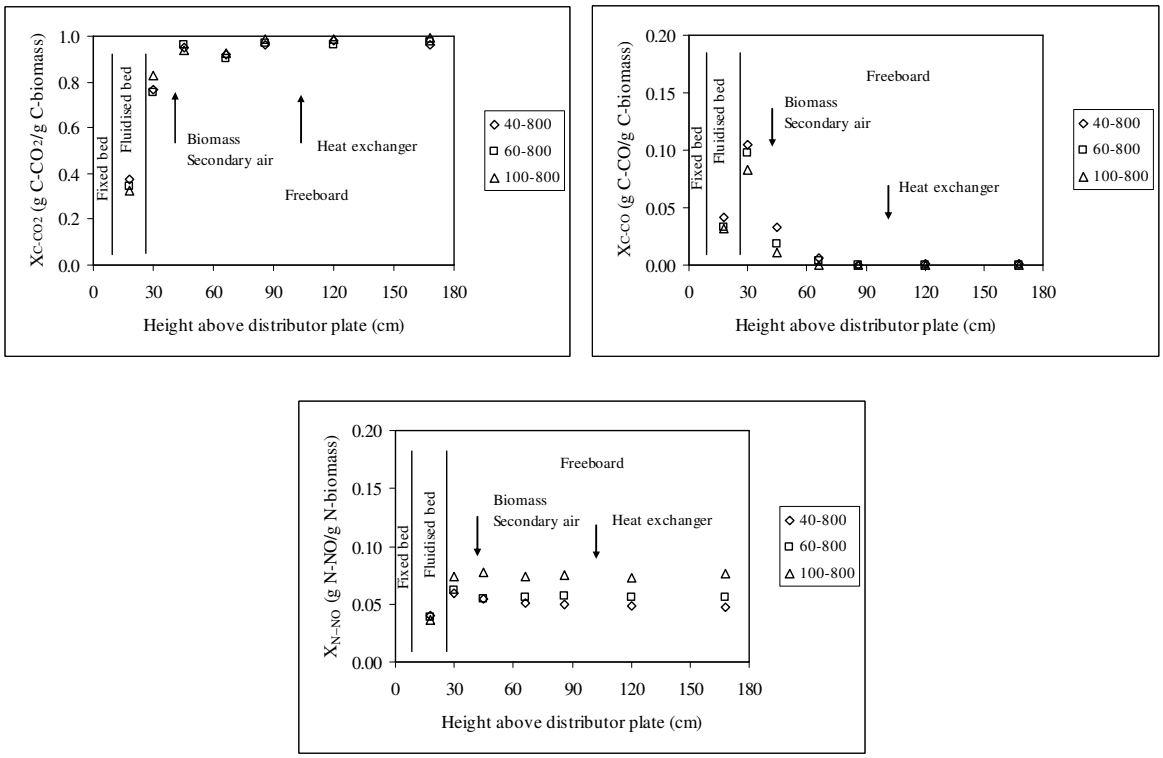

Figure 2.4 - Longitudinal conversion of: biomass carbon to CO_2 (X_{C-CO_2}) and to CO (X_{C-CO}), and biomass nitrogen to NO (X_{N-NO}), in the pilot-scale BFBC. Legend according to experiment reference in Table 2.2.

Assuming the two phase theory of fluidisation [44] for the bubbling bed, the concentration of the jth gas (CO_2, CO, NO) in the gas sampled inside the bed can be regarded as a time-mean concentration of the gas resulting from in-bed constant flow sampling coming from two sources i) the emulsion phase and ii) the bubble phase, as given by Eq. 2.5 [43], where, inside the bed at level z above the fluidising air injectors, $\overline{C}_{j,sample}(z)$ represents the time-mean concentration of the jth gas compound, $C_{j,b}(z)$ and $C_{j,e}(z)$ are the concentrations of the jth gas compound in bubble and emulsion phases, respectively, and $\varepsilon_b(z)$ is the time-mean fraction of bed volume occupied by the bubble phase.

$$\overline{C}_{j,sample}(z) = C_{j,b}(z) \times \varepsilon_b(z) + C_{j,e}(z) \times (1 - \varepsilon_b(z)) \quad \text{Eq. 2.5}$$

On the other hand, in order to evaluate the solid fuel i^{th} chemical element conversion to the gaseous j^{th} chemical compound at each height inside the bed, it must be known the gas flow rate of each phase (emulsion and bubble) and the respective concentration of gaseous j^{th} compound in each gas flow.

In fact, the time-mean concentration $\overline{C}_{j,sample}(z)$ resulting from in-bed constant flow sampling can differ from the time-mean concentration $\overline{C}_{j,flow}(z)$ based on the gas flow through the two phases and calculated by Eq. 2.6 [43], where, inside the bed at level z above the fluidising air injectors, $G_{v,b}(z)$ and $G_{v,e}(z)$ represent the volumetric gas flow associated to the bubble and emulsion phases respectively, and the sum $(G_{v,b}(z)+G_{v,e}(z))$ represents the total volumetric gas flow throughout the bed.

$$\overline{C}_{j,flow}(z)=\frac{C_{j,b}(z)\times G_{v,b}(z)+C_{j,e}(z)\times G_{v,e}(z)}{G_{v,b}(z)+G_{v,e}(z)} \qquad \text{Eq. 2.6}$$

In this context, significant errors can occur when using $\overline{C}_{j,sample}(z)$ in mass balances, because the overall mass flow of the j^{th} gaseous chemical compound inside the bed at level z above the fluidising air injectors can be more, or less, influenced by each of the gas flows (bubble or emulsion) according the respective concentration on each gas phase (bubble or emulsion) [43].

In order to understand the in-bed experimental gas concentration data presented in this work, and the implication of their use in mass balances, a simple numeric model to analyse the bed hydrodynamics was formulated to illustrate the influence of the two distinct flows and concentrations in the two phases (emulsion and bubble) of the bubbling fluidised bed combustor. The objective of the model is not to present the true values of concentration on each phase inside the bed, because this is not possible to observe, but rather to contribute to the understanding of experimental data obtained and to highlight the need of a better knowledge of the bed hydrodynamics of a bubbling fluidised bed in order to interpret experimental data and how can they be used in mass balances.

The model is based on the two phase theory of fluidisation [44] and was developed considering the operating conditions of the actual pilot-scale bubbling fluidised bed combustor. In this simple model it is not considered the existence of the radial concentration gradients inside the bed.

The emulsion phase is considered at the minimum fluidisation velocity, so that the amount of air injected in the bed above the condition of minimum fluidisation flows throughout the bed as bubbles. The voidage fraction in the emulsion phase at the operating conditions (ε_e) remains the same as at the minimum fluidisation condition (ε_{mf}). The equations used in the model for bed hydrodynamics calculations are presented in Table 2.3.

Table 2.3 - Equations used in the hydrodynamic model.

Equation	Reference	Equation
$u_{mf}(z)=\frac{d_{p,b}^2\times(\rho_s-\rho_g(z))\times g\times\varepsilon_{mf}^3(z)\times\varphi_s^2}{150\times\mu_g(z)\times(1-\varepsilon_{mf}(z))}$	[45]	Eq. 2.7
$A_o=\frac{A_t-\frac{N_{nzl}\times\pi\times d_{nzl}^2}{4}}{N_{nzl}}$	[46]	Eq. 2.8
$d_b(z)=\frac{0.54\times(u_0(z)-u_{mf}(z))^{0.4}\times\left(z+4\times\sqrt{A_o}\right)^{0.8}}{g^{0.2}}$	[46]	Eq. 2.9
$u_{bi}(z)=0.711\times\sqrt{g\times d_b(z)}$	[44]	Eq. 2.10
$u_b(z)=u_0(z)-u_{mf}(z)+u_{bi}(z)$	[44]	Eq. 2.11
$\varepsilon_b(z)=\frac{u_0(z)-u_{mf}(z)}{u_b(z)}$	[44,47]	Eq. 2.12

The parameters used and the results from hydrodynamic calculations for the experimental operating conditions used in this work are presented in Table 2.4, at level z=0.09 m above the fluidisation air injectors (location of the in-bed gas sample probe, see Figure 2.1).

To evaluate the influence of bed hydrodynamics and concentration of the jth gaseous chemical compound in each phase (bubble and emulsion) on the calculation of the conversion of the ith chemical element (C, N) in the biomass feed, it will be now defined a ratio ($\phi(z)$) between $C_{j,e}(z)$ and $C_{j,b}(z)$ as given by Eq. 2.13. Based on Eq. 2.5, the time-mean concentration $\overline{C}_{j,sample}(z)$ as a function of both concentration values $C_{j,e}(z)$ and $C_{j,b}(z)$ is then given by Eq. 2.14. Then, using the value of $\overline{C}_{j,sample}(z)$ measured experimentally inside the bed at level z above the fluidising air injectors (see Figure 2.3), the relation between $C_{j,b}(z)$ and $\overline{C}_{j,sample}(z)$ can be estimated based on Eq. 2.15. Using Eq. 2.16 together with Eq. 2.2 to Eq. 2.4, it can be evaluated the influence of the ratio $\phi(z)$ between the concentration of the jth gaseous compound in the emulsion and bubble phases, $C_{j,e}(z)$ and $C_{j,b}(z)$ respectively, on the calculation of the conversion of the ith chemical element (C, N) in the biomass feed on the jth chemical compound (CO_2, CO or NO) present in the combustion flue gas, inside the bed at level z above the fluidising air injectors.

Table 2.4 - Parameters used in the hydrodynamic model and model results, for a bed temperature of 800ºC (1073.15 K), at level z=0.09 m above the fluidising air injectors.

$$z = 0.09\ \text{m}$$

$$T_b(z) = 1073.15\ \text{K}$$

$$\varepsilon_{mf}(z) = 0.400$$

$$\varepsilon_e(z) = \varepsilon_{mf}(z) = 0.400$$

$$\varphi_s = 0.860$$

$$u_{mf}(z) = 0.108\ \text{m/s}$$

$$d_b(z) = 0.048\ \text{m}$$

$$u_{bi}(z) = 0.487\ \text{m/s}$$

$$u_b(z) = 0.642\ \text{m/s}$$

$$\varepsilon_b(z) = 0.241$$

$$C_{j,e}(z) = \phi(z) \times C_{j,b}(z) \qquad \text{Eq. 2.13}$$

$$\overline{C}_{j,sample}(z) = C_{j,b}(z) \times \varepsilon_b(z) + \phi(z) \times C_{j,b}(z) \times (1 - \varepsilon_b(z)) \qquad \text{Eq. 2.14}$$

$$C_{j,b}(z) = \frac{\overline{C}_{j,sample}(z)}{(\varepsilon_b(z) + \phi(z) \times (1 - \varepsilon_b(z)))} \qquad \text{Eq. 2.15}$$

$$G_{v,j}(z) = C_{j,b}(z) \times G_{v,b}(z) + C_{j,e}(z) \times G_{v,e}(z) \qquad \text{Eq. 2.16}$$

The calculated values of biomass carbon conversion to CO_2 inside the bed at level z=0.09 m above the fluidising air injectors applying the above described procedure are presented in Figure 2.5.

For the operating conditions used in the experiments the volumetric gas flow through the bubble phase is 1.4 times the gas flow through the emulsion phase, according to model results. It can be observed (Figure 2.5) that for high gas concentration differences between the bubble and emulsion phases, in particular when the concentration in bubble phase is much higher than that of the emulsion phase (low values of $\phi(z)$), significant differences on calculated values of conversion of biomass carbon to CO_2 and to CO, and also of biomass nitrogen conversion to NO, can be obtained.

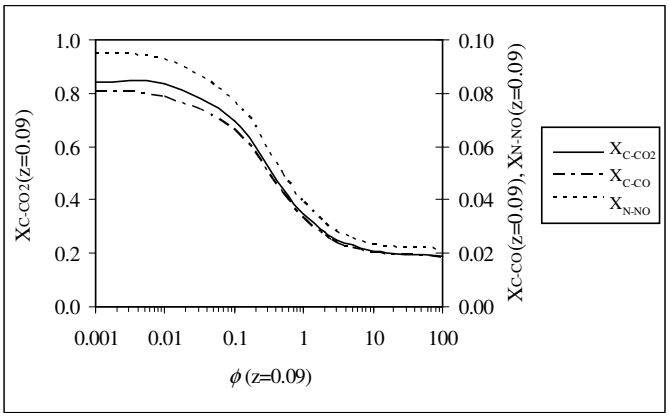

Figure 2.5 - Influence of the ratio ($\phi(z)$) between the concentrations of the j[th] gaseous chemical compound (for CO_2, CO and NO) in the emulsion gas flow and in the bubble gas flow on estimating the conversion of biomass carbon to CO_2 ($X_{C-CO_2}(z)$) and CO ($X_{C-CO}(z)$), and biomass nitrogen to NO ($X_{N-NO}(z)$), at level z=0.09 m above the fluidising air injectors, for the experiment with reference 800-40 (see Table 2.2 and Figure 2.3).

However, the assumption of higher CO_2 concentration in the emulsion phase relative to the bubble phase during solid fuels combustion in bubbling fluidised beds seams to be reasonable [39,48,49]; the same is true for CO and NO [39,48,49]. So, during biomass combustion in BFBC the value of $\phi(z)$ should be higher than unity. For these conditions, according to the simple hydrodynamic model developed the biomass carbon conversion to CO_2 inside the bed at level z=0.09 m above fluidising air injectors should be in the range $0.19 \leq X_{C-CO_2}(z=0.09) \leq 0.35$, for values of $1.0 \leq \phi(z=0.09) < 100.0$ (Figure 2.5). That is, the values of biomass carbon conversion to CO_2 inside the bed ($X_{C-CO_2}(z=0.09)$, Figure 2.4) estimated (Eq. 2.1 to Eq. 2.4) using the time-mean concentration measured experimentally inside the bed (Figure 2.3) and the total volumetric gas flow (emulsion plus bubble phase flows) throughout the bed, such calculation corresponding to $\phi(z=0.09)=1.0$, are slightly overestimated, and should be regarded as an upper limit for that conversion; the true conversion values should be somewhere between 0.20 and 0.30 (Figure 2.5). A similar behaviour is found for the in-bed (at z=0.09 m) biomass carbon conversion to CO and biomass nitrogen conversion to NO (Figure 2.5); it is observed $0.018 \leq X_{C-CO}(z=0.09) \leq 0.033$ for values of $1.0 \leq \phi(z=0.09) < 100.0$, and $0.021 \leq X_{N-NO}(z=0.09) \leq 0.039$ for values of $1.0 \leq \phi(z=0.09) < 100.0$.

The values of biomass carbon conversion to CO_2 and CO inside the bed are lower than the ones observed for bituminous and anthracite coal combustion [39] using the same calculation procedure; also the biomass nitrogen conversion to NO inside the bed is lower than that observed for bituminous and anthracite coal combustion [39].

According to these results it is expected that more than 50% of the biomass carbon is converted to CO_2 in the upper half height of the dense bed and splash region (Figure 2.4); that

is, the dense bed and the splash region are responsible for around 75-80% of the biomass carbon conversion to CO_2. Consequently it can be stated that the dense bed and the splash region still are the main regions responsible for the biomass carbon conversion to CO_2. Between the splash region and a location near the point of addition of secondary air, an additional (around) 15-20% of the biomass carbon is converted in CO_2. This 15-20% of biomass carbon conversion to CO_2 above the splash region should be one of the reasons explaining the temperature peak observed at the location near the secondary air injection point; other reason should be related with heat transfer by radiation from the bed surface and splash region.

It can be observed that the decrease on CO concentration between the bed surface (splash region) and the location near the addition of secondary air (Figure 2.3) results from conversion of CO and not only dilution effect caused by secondary air addition (Figure 2.4). On the other hand, the decrease on the NO concentration between the bed surface (splash region) and the location near the addition of secondary air (Figure 2.3) results mostly from dilution effect of secondary air, since the NO conversion appears to be of minor importance (Figure 2.4).

The biomass carbon conversion to CO_2, calculated based on the CO_2 concentration measured in the combustion flue gases at the top of the freeboard, was in the range 97.2 to 99.3% (Figure 2.4), indicating a high combustion efficiency. The amount of unburned carbon in fly ashes was found to be in the range 3% to 14% (by weight), which accounted for a mass loss of unburned carbon in fly ashes lower than 1% (by weight). The overall biomass carbon conversion calculated based on measured concentrations of CO_2, CO, total hydrocarbons and unburned carbon in fly ash, for the conditions of 40, 60 and 100% excess air was in the range 98.0 to 99.6%, that is, the error on the overall mass balance to the biomass carbon was in the range 0.4 to 2%. This error can result from several uncertainties in measurements related with the reactive system operation and monitoring, as for example biomass feed rates, combustion air flow rates and combustion gas analysis (see section 2.2.2).

The biomass nitrogen conversion to NO, calculated based on the NO concentration measured at the top of the freeboard, is relatively small, always less than 8% for the experimental conditions analysed (Figure 2.4); small biomass nitrogen conversion to NO have been reported by others [17,25,52] during biomass combustion in BFBC.

2.3.4 *CO, total hydrocarbons, NO and N_2O concentration at the exit flue gases*

Besides pollutant emissions, the CO and total hydrocarbons (measured as CH_4) in exit the flue gases also represent a measure of biomass carbon conversion efficiency. It is observed a similar behaviour for these compounds: their concentration decreases with

increasing the oxygen concentration in flue gases (that is, increasing the excess air) (Figure 2.6). It is observed that for O_2 levels above 4%v (dry gases) in the exit flue gases, that is, above 20% excess air, the CO concentration is below the emission value limit from the Portuguese regulation [50]. Low concentrations of CO during biomass combustion in BFBC have been reported by others in result of the high reactivity of biomass char and volatiles [23]. The total hydrocarbons concentration (measured as CH_4) in the exit flue gases is expressed in Figure 2.6 as organic carbon, as a measure of volatile organic compounds (VOC), and under the experimental conditions used it is below the emission value limit from the Portuguese regulation [50,51].

The NO concentration in the exit flue gas increases with increasing the oxygen concentration in flue gases (that is, increasing the excess air) (Figure 2.7). During biomass combustion in BFBC the increase on NO concentration in flue gases with increasing the excess air was also reported by others [15,18,20,23,26,52]. This behaviour can be related with the increase on oxygen availability due to the increase in the excess air and can be attributed to: (i) an increase in the rate of biomass nitrogen oxidation to NO [41], and (ii) a decrease on the concentration of NO reducing compounds as char particles, hydrocarbons and reduced nitrogen compounds [41]. It was considered that at the operating temperature conditions used the thermal-NO formation from nitrogen present in combustion air is of minor importance. The bed temperature (in range 750-800ºC) appears not to influence the NO concentration in the exit flue gases (Figure 2.7).

It is observed that below 8.5%v O_2 (dry gases) in the exit flue gases, that is, below 60% excess air, the NO concentration (expressed as NO_2) is below the emission value limit from the Portuguese regulation [50] (Figure 2.7).

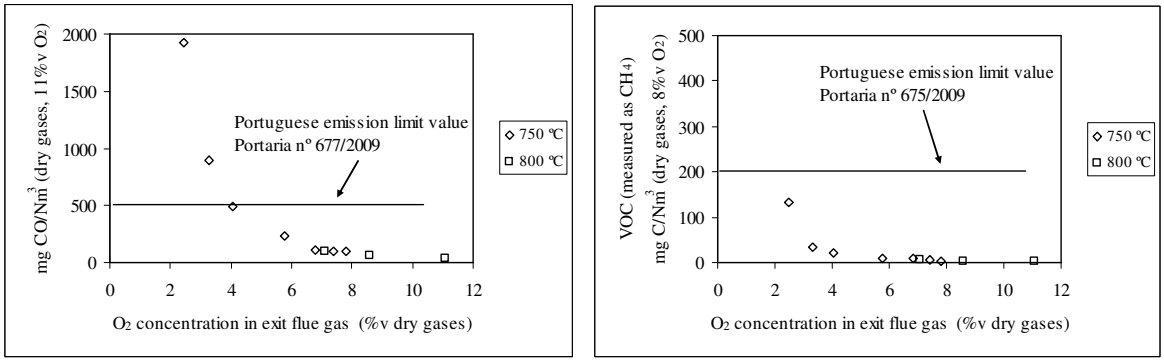

Figure 2.6 - Concentration of CO and total hydrocarbons (measured as CH_4 and expressed as carbon in volatile organic compounds (VOC)) in the pilot-scale BFBC exit flue gases, during biomass combustion. The CO and total hydrocarbons concentrations are corrected to 11%v/v and 8%v/v O_2 (dry gases), respectively.

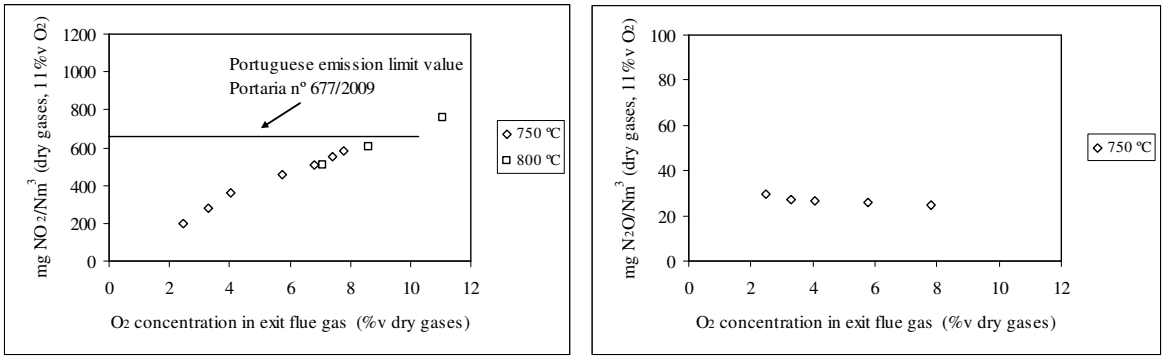

Figure 2.7 - Concentration of NO (expressed as NO_2) and N_2O in the pilot-scale BFBC exit flue gases during biomass combustion. The NO and N_2O concentrations are corrected to 11%v/v O_2 (dry gases).

The NO concentration in the exit flue gases observed during biomass combustion (Figure 2.3 and 2.7) is higher than that observed during coal combustion in the same installation under similar operating conditions [39,41]; this behaviour can be explained as a result of the higher nitrogen content of the biomass fuel when compared with the coal. Nevertheless, it is observed a lower biomass nitrogen conversion to NO (Figure 2.4) when compared with the observed during coal combustion in the same installation under similar operating conditions [39,41]. Lower fuel nitrogen conversion to NO with increasing fuel nitrogen content has also been reported in other studies [52,53]. Several reasons have been proposed to justify the low fuel nitrogen conversion to NO during biomass combustion in BFBC namely: (i) the higher content of volatile matter of biomass [54], (ii) the higher concentration of reduced gaseous nitrogen compounds (as for example the NH_3) that act both as source and sink of NO [5,53], (iii) the higher reactivity of the biomass ashes on destroying the NO [1,5], and (iv) the higher concentration of H and OH radicals in the combustion environment as a result of high O/C and H/C ratios in biomass [5]. It the context of NO destruction during biomass combustion in BFBC the role of biomass char has been suggested of minor importance due to the low inventory of biomass char particles inside the bed [5]. However, it is recognised the high reactivity of biomass chars towards NO destruction [55]. Considering that the most of the NO chemistry occurs in a region of high concentration of bed solids (the bed and the splash region), based on the results presented in this work, the role of the bed solids (ashes and char) should be considered. However, the experimental results presented in this work do not permit to conclude about the relative contribution of each mechanism referred above for the low biomass nitrogen conversion to NO.

The observed N_2O concentration in the exit flue gas is relatively low, as also reported by others during biomass combustion in BFBC [20,26], and appears not to be influenced by the stoichiometry (Figure 2.7). The low N_2O concentration observed during biomass combustion in fluidised beds has been sometimes [2,5] related with the nitrogen functional groups present in biomass fuels, mainly amino groups, and the consequent predominance of NH_3 as

the main nitrogen-containing volatile species. It is recognised [39,48] that NH_3 is mainly oxidised to NO and N_2 instead of N_2O and this has been used [2,5] to explain the low N_2O concentration observed during biomass combustion. However, pyrolysis experiments of different biomass fuels indicate that, beyond NH_3 other gaseous nitrogen compounds such as HCN and HNCO are also present in significant amounts in the volatiles and their relative abundance is dependent on operating conditions, namely the pyrolysis temperature and biomass characteristics [53,56-60]. Alternative reasons, other than the NH_3 as the biomass volatile nitrogen-containing species, should explain the low N_2O concentration observed during biomass combustion in BFBC, considering that: (i) most of the mass of the solid biomass particle is released to the gas phase during pyrolysis, the same happening to the biomass nitrogen, (ii) HCN and HNCO are present in biomass pyrolysis gases in significant amounts, and (iii) HCN and HNCO are recognised important precursors of N_2O throughout the homogeneous path [39,48]. Indeed, some research studies have shown results that can offer additional explanations for the low N_2O concentration, namely: (i) the HCN conversion to NH_3 during biomass pyrolysis [5,59] which can be then oxidised (homogeneously and catalytically) to NO instead of N_2O, (ii) the selectivity of HCN oxidation to NO is strongly enhanced by the presence of biomass ash, while almost no N_2O is formed [40], (iii) the high catalytic activity of biomass ashes on N_2O destruction [40,61], (iv) the presence of higher concentration of H and OH radicals in the combustion environment as a result of high O/C and H/C ratios in the feeding biomass [5], since those radicals are known to be important in N_2O destruction [39,48,53]. Also, the higher concentration of O and OH radicals during biomass combustion due to the high O/C and H/C ratios in biomass, can perhaps influence the called [62] trade-off between NO and N_2O formation from homogeneous HCN oxidation, which in result could be shifted towards the NO formation.

With the results presented in this work it is not possible to conclude about the relative importance of each mechanism responsible for the low N_2O concentration observed during biomass combustion in BFBC. However, considering the results of the present work, that is (i) most (around 75-80%wt) of the biomass fuel is converted in a region containing the dense bed and the splash region (Figure 2.4), and (ii) the NO chemistry occurs mainly within this same region (Figure 2.4), it can be concluded that although most of the biomass solid (and consequently their nitrogen containing species) is rapidly converted in gaseous species (the volatiles) upon devolatilisation as entering the reactor, those gaseous species are subjected to intense contact with the bed solid phase, even in the splash region. Consequently, the bed material (sand particles and biomass ashes) could have an important role on the nitrogen chemistry, namely on the NO and N_2O formation and destruction. That is, among other factors, the catalytic effect of biomass ash may have an important influence on the low N_2O concentration observed during biomass combustion in fluidised bed, since the nitrogen-

containing gaseous species are mostly converted in regions characterised by intense gas-solid contact.

2.4 *Conclusions*

Longitudinal pressure, temperature and gas composition (O_2, CO_2, NO, N_2O and volatile organic compounds) profiles were obtained in a pilot-scale bubbling fluidised bed combustor during biomass combustion.

The biomass carbon conversion to CO_2 along the reactor was calculated based on the measured CO_2 concentration at several locations, and was used as an indicator of the combustion progress along the reactor. It was found that around 75-80% of the biomass carbon was converted to CO_2 in the reactor region located below few centimetres above the bed surface, that is, the region that includes the bed and the splash zone.

Furthermore, based on the CO_2 and NO concentrations in the exit flue gas, it was found that: i) the overall biomass carbon conversion to CO_2 was in the range 97.2 to 99.3%, indicating high combustion efficiency, and ii) the biomass nitrogen conversion to NO is relatively small, always lower than 8% for the experimental conditions analysed.

Concerning the Portuguese regulation about gaseous emissions from industrial biomass combustion, namely, the accomplishment of CO, NO and volatile organic compounds (VOC) (expressed as carbon) emission limits, the set of adequate operating conditions includes bed temperatures in the range 750-800ºC, excess air levels in the range 20% to 60%, and air staging with secondary air accounting for 20% of total combustion air.

Nomenclature

A_o	Superficial area *per* orifice in the distributor plate of fluidising air, $m^2 \cdot orifice^{-1}$
A_t	Cross sectional area of the distributor plate of fluidising air, m^2
$d_b(z)$	Equivalent bubble diameter at level z above the air injectors, m
$d_{p,b}$	Bed particles equivalent diameter, m
$d_{p,f}$	Biomass particles equivalent diameter, m
$C_{j,b}(z)$	Concentration of j^{th} gaseous compound in the bubble phase gas flow inside the bed at level z above the air injectors, at conditions $P_b(z)$ and $T_b(z)$, $m^3_j \cdot m^{-3}_{gas}$
$C_{j,e}(z)$	Concentration of j^{th} gaseous compound in the emulsion phase gas flow inside

	the bed at level z above the air injectors, at conditions $P_b(z)$ and $T_b(z)$, $m^3_j \cdot m^{-3}_{gas}$
$\overline{C}_{j,flow}(z)$	Mean concentration of j^{th} gaseous compound based on gas flow and concentration of emulsion and bubble phases at level z above the air injectors, at conditions $P_b(z)$ and $T_b(z)$, $m^3_j \cdot m^{-3}_{gas}$
$\overline{C}_{j,sample}(z)$	Time-mean concentration of j^{th} gaseous compound in the sample gas at level z above the air injectors, at conditions $P_b(z)$ and $T_b(z)$, $m^3_j \cdot m^{-3}_{gases}$
d_{nzl}	Diameter of orifices of the fluidising air injectors, m
g	Acceleration of gravity, 9.8 $m \cdot s^{-2}$
$G_v(z)$	Total volumetric gas flow rate through the reactor at level z above the air injectors, at conditions $P_b(z)$ and $T_b(z)$, $m^3 \cdot s^{-1}$
$G_{v,b}(z)$	Volumetric gas flow rate in the bubble phase through the bed at level z above the air injectors, at conditions $P_b(z)$ and $T_b(z)$, $m^3 \cdot s^{-1}$
$G_{v,e}(z)$	Volumetric gas flow rate in the emulsion phase through the bed at level z above the air injectors, at conditions $P_b(z)$ and $T_b(z)$, $m^3 \cdot s^{-1}$
$G_{v,j}(z)$	Total volumetric gas flow rate of j^{th} gaseous compound through the reactor at level z above the air injectors, at conditions $P_b(z)$ and $T_b(z)$, $m^3_j \cdot s^{-1}$
$G_{m,i-j}(z)$	Total mass flow rate of i^{th} chemical element present in the j^{th} gaseous compound present in flue gases, through the reactor at level z above the air injectors, $kg_i \cdot s^{-1}$
$G_{m,j}(z)$	Total mass flow rate of j^{th} gaseous compound through the reactor at level z above the air injectors, $kg_j \cdot s^{-1}$
i	i^{th} Chemical element present in biomass: C, N
j	j^{th} Chemical gaseous compound present in combustion flue gases: CO_2, CO, NO
M_i	Molar mass of i^{th} chemical element (C,N), $kg \cdot mol^{-1}$
M_j	Molar mass of j^{th} chemical gaseous compound (CO_2, CO, NO), $kg \cdot mol^{-1}$
N_{nzl}	Number of orifices of the fluidising air injectors in the distributor plate, -
$P_b(z)$	Absolute pressure in the reactor at level z above the air injectors, Pa

R	Constant of ideal gases, 8.314 $J \cdot mol^{-1} \cdot K^{-1}$
$S_{m,i,biomass}$	Mass flow rate of i^{th} chemical element fed with biomass, $kg_{i} \cdot s^{-1}$
$T_b(z)$	Absolute temperature in the reactor at level z above the air injectors, K
$u_b(z)$	Bubble rising velocity at level z above the air injectors, $m \cdot s^{-1}$
$u_{bi}(z)$	Bubble rising velocity for an isolated bubble at level z above the air injectors, $m \cdot s^{-1}$
$u_{mf}(z)$	Minimum fluidization velocity at level z above the air injectors, $m \cdot s^{-1}$
$u_0(z)$	Superficial gas velocity at the operating conditions, at level z above the air injectors, $m \cdot s^{-1}$
$X_{i-j}(z)$	Conversion of i^{th} chemical element present in biomass on the j^{th} chemical gaseous compound present in the combustion gas flow at level z above the air injectors, -
z	Height above fluidising air injectors, m
$\varepsilon_b(z)$	Fraction of bed volume occupied by the bubble phase at the operating conditions, at level z above the air injectors, -
$\varepsilon_e(z)$	Voidage fraction in emulsion phase at the operating conditions, at bed level z above the air injectors, -
$\varepsilon_{mf}(z)$	Voidage fraction in emulsion phase at minimum fluidisation conditions, at level z above the air injectors, -
$\phi(z)$	Ratio between concentration of gaseous compound j in emulsion phase and bubble phase inside the bed, -
φ_s	Sphericity of bed solids, -
π	3.1415, -
$\rho_g(z)$	Volumic mass of fluidising gas at level z above the air injectors, and at conditions $P_b(z)$ and $T_b(z)$, $kg \cdot m^{-3}$
ρ_s	Volumic mass of the bed solid particles, $kg \cdot m^{-3}$
$\mu_g(z)$	Dynamic viscosity of fluidising gas at level z above the air injectors, and at conditions $P_b(z)$ and $T_b(z)$, $kg \cdot m^{-1} \cdot s^{-1}$

Acknowledgements

The authors want to acknowledge the financial support from the project with reference PTDC/AAC-AMB/098112/2008, financed by the Portuguese Foundation for the Science and Technology.

References

1. Werther J., Ogada T. Sewage sludge combustion. Progress in Energy and Combustion Science 1999;25:55.
2. Werther J., Saenger M., Hartge E-U., Ogada T., Siagi Z. Combustion of agricultural residues. Progress in Energy and Combustion Science 2000;26:1.
3. van Loo S., Koppejan J. Handbook of biomass combustion and co-firing. 2nd ed. Earthscan, London, UK 2008.
4. Koornneef J., Junginger M., Faaij A. Development of fluidised bed combustion – An overview of trends, performance and cost. Progress in Energy and Combustion Science 2007;33:19.
5. Khan A.A., de Jong W., Jansens P.J., Spliethoff H. Biomass combustion in fluidized bed boilers: Potential problems and remedies. Fuel Processing Technology 2009;90:21.
6. Winter F., Wartha C., Hofbauer H. NO and N_2O formation during the combustion of wood, straw, malt waste and peat. Bioresource Technology 1999;70:39.
7. Demirbas A. Potential applications of renewable energy sources, biomass combustion problems in boiler power systems and combustion related environmental issues. Progress in Energy and Combustion Science 2005;31:171.
8. Joller M., Brunner T., Obernberger I. Modeling of aerosol formation during biomass combustion for various furnace and boiler types. Fuel Processing Technology 2007;88:1136.
9. Hustad J.E., Skreiberg O., Sonju O.K. Biomass combustion research and utilisation in IEA countries. Biomass and Bioenergy 1995;9:235.
10. Chagger H.K., Kendall A., McDonald A., Pourkashanian M., Williams A. Formation of dioxins and other semi-volatile organic compounds in biomass combustion. Applied Energy 1998;60:101.
11. Lavric E.D., Konnov A.A., Ruyck J. Dioxin levels in wood combustion—a review. Biomass and Bioenergy 2004;26:115.
12. Nussbaumer T. Combustion and co-combustion of biomass: Fundamentals, technologies, and primary measures for emission reduction. Energy and Fuels 2003;17:1510.

13. Cabrita I., Gulyurtlu I., Pinto F., Boavida D., Costa P., Racha L. Formação e destruição das dioxinas em processos de combustão e co-combustão. Revista da Faculdade de Medicina de Lisboa 2003;8:225 (in Portuguese).
14. Demirbas A. Combustion characteristics of different biomass fuels. Progress in Energy and Combustion Science, 2004;30:219.
15. Kaynak B., Topal H., Atimtay A.T. Peach and apricot stone combustion in a bubbling fluidized bed. Fuel Processing Technology 2005;86:1175.
16. Armesto L., Bahillo A., Veijonen K., Cabanillas A., Otero J. Combustion behaviour of rice husk in a bubbling fluidised bed. Biomass and Bioenergy 2002;23:171.
17. Suksankraisorn K., Patumsawad S., Fungtammasan B. Combustion studies of high moisture content waste in a fluidised bed. Waste Management 2003;23:433.
18. Kuprianov V.I., Janvijitsakul K., Permchart W. Co-firing of sugar cane bagasse with rice husk in a conical fluidized-bed combustor. Fuel 2006;85:434.
19. Kouprianov V.I., Permchart W. Emissions from a conical FBC fired with a biomass fuel. Applied Energy 2003;74:383.
20. Permchart W., Kouprianov V.I. Emission performance and combustion efficiency of a conical fluidized-bed combustor firing various biomass fuels. Bioresource Technology 2004;92:83.
21. Kuprianov V.I., Permchart W., Janvijitsakul K. Fluidized bed combustion of pre-dried Thai bagasse. Fuel Processing Technology 2005;86:849.
22. Okasha F. Staged combustion of rice straw in a fluidized bed. Experimental Thermal and Fluid Science 2007;32:52.
23. Miccio F., Scala F., Chirone R. Fluidized bed combustion of a biomass fuel: Comparison between pilot scale experiments and model simulations. Journal of Heat Transfer 2005;127:117.
24. Rao K.V.N.S., Reddy G.V. Effect of distributor design on temperature profiles in fluidized bed during the combustion of rice husk. Combustion Science and Technology 2007;179:1589.
25. Abelha P., Gulyurtlu I., Boavida D., Barros J.S., Cabrita I., Leahy J., Kelleher B., Leahy M. Combustion of poultry litter in a fluidised bed combustor. Fuel 2003;82:687.
26. Chyang C-S., Qian F-P., Lin Y-C., Yang S-H. NO and N_2O emission characteristics from a pilot scale vortexing fluidized bed combustor firing different fuels. Energy and Fuels 2008;22:1004.

27. Sun Z., Jin B., Zhang M., Liu R., Zhang Y. Experimental studies on cotton stalk combustion in a fluidized bed. Energy 2008;33:1224.
28. Ghani W.A.W.A.K., Alias A.B., Savory R.M., Cliffe K.R. Co-combustion of agricultural residues with coal in a fluidised bed combustor. Waste Management 2009;29:767.
29. Tarelho L.A.C., Matos M.A.A., Pereira F.J.M.A. Axial and radial CO concentration profiles in an atmospheric bubbling FB combustor. Fuel 2005;84:1128.
30. Okasha F. Modeling combustion of straw–bitumen pellets in a fluidized bed. Fuel Processing Technology 2007;88:281.
31. Atimtay A.T., Kaynak B. Co-combustion of peach and apricot stone with coal in a bubbling fluidized bed. Fuel Processing Technology 2008;89:183.
32. Gogebakan Z., Gogebakan Y., Selçuk N. Co-firing of olive residue with lignite in bubbling FBC. Combustion Science and Technology 2008;180:854.
33. Scala F. Fluidized bed combustion of high-volatile solid fuels. PhD Thesis. Università degli Studi di Napoli Federico II, Naples, Italy; 1999.
34. Scala F., Salatino P. Modelling fluidized bed combustion of high-volatile solid fuels. Chemical Engineering Science 2002;57:1175.
35. Fiorentino M., Marzocchella A., Salatino P. Segregation of fuel particles and volatile matter during devolatilisation in a fluidised bed reactor – II. Experimental. Chemical Engineering Science 1997;52:1909.
36. Diego L.F., Garcia-Labiano F., Abad A., Gayan P., Adanez J. Coupled drying and devolatilisation of non-spherical wet pine wood particles in fluidised beds. Journal of Analytical and Applied Pyrolysis 2002;65:173.
37. Wu W., Dellenback P.A., Agarwal P.K., Haynes H.W. Combustion of isolated bubbles in an elevated-temperature fluidized bed. Combustion and Flame 2005;140:204.
38. Baron J., Bulewicz E.M., Kandefer S., Pilawska M., Zukowski W., Hayhurst A.N. Combustion of hydrogen in a bubbling fluidized bed. Combustion and Flame 2009:156:975.
39. Tarelho L.A.C. Control of gaseous emissions resulting from coal combustion in fluidized bed. PhD Thesis (in Portuguese). University of Aveiro, Portugal; 2001.
40. Loffler G., Wargadalam V.J., Winter F. Catalytic effect of biomass ash on CO, CH_4 and HCN oxidation under fluidised bed combustor conditions. Fuel 2002;81:711.
41. Tarelho L.A.C., Matos M.A.A., Pereira F.J.M.A. Axial concentration profiles and NO flue gas in a pilot-scale bubbling fluidized bed coal combustor. Energy & Fuels 2004;18:1615.

42. Lyngfelt A., Amand L-E., Leckner B. Progress of combustion in the furnace of a circulating fluidised bed boiler. In: Proceedings of the 26th Symposium (International) on Combustion; 1996. p. 3253-3259.
43. Grace J., Bi H., Zhang Y. Pitfalls in gas sampling from fluidized beds. Chemical Engineering Science 2009;64:2522.
44. Davidson J.F., Harrison D. Fluidized particles. Cambridge University Press, London, UK 1963.
45. Kunni D., Levenspiel O. Fluidization Engineering. 2nd ed. Butterworth-Heinemann Series in Chemical Engineering, Massachusetts Institute of Technology, Stoneham MA, USA 1991.
46. Darton R.C. A bubble growth theory of fluidized bed reactors. Trans. IChemE. 1979;57:134.
47. Xavier A.M., Lewis D.A., Davidson J.F. The expansion of bubbling fluidized beds. Trans. IChemE. 1978;56:274.
48. Jensen A. Nitrogen chemistry in fluidized bed combustion of coal. PhD Thesis. Technical University of Denmark, Denmark 1996.
49. Tarelho L.A.C., Matos M.A.A., Pereira F.J.M.A. Modelling coal combustion in a bubbling fluidised bed, and validation with data obtained in a pilot-scale reactor. In: Proceedings of the 7th European Conference on Industrial Furnaces and Boilers, ISBN 972-99309-1-0; 2006. Paper 69.
50. Portaria n.º 677/2009, de 23 de Junho. Portuguese legislation regarding the emission limits of certain pollutants in flue gases: combustion facilities.
51. Portaria n.º 675/2009, de 23 de Junho. Portuguese legislation regarding the emission limits of certain pollutants in flue gases: emission values of general application.
52. Chyang C-S., Wu K-T., Lin C-S. Emission of nitrogen oxides in a vortexing fluidized bed combustor. Fuel 2007;86:234.
53. Winter F., Wartha C., Hofbauer H. NO and N_2O formation during the combustion of wood, straw, malt waste and peat. Bioresource Technology 1999;70:39.
54. Fryda L., Panopoulos K., Vourliotis P., Pavlidou E., Kakaras E. Experimental investigation of fluidised bed co-combustion of meat and bone meal with coals and olive bagasse. Fuel 2006;85:1685.
55. Garijo E.G, Jensen A.D, Glarborg P. Kinetic study of NO reduction over biomass char under dynamic conditions. Energy and Fuels 2003:17;1429.

56. Leppdahti J., Koljonen T. Nitrogen evolution from coal, peat and wood during gasification: Literature review. Fuel Processing Technology 1995;43:1.

57. Hansson K-M., Samuelsson J., Tullin C., Amand L-E. Formation of HNCO, HCN, and NH_3 from the pyrolysis of bark and nitrogen-containing model compounds. Combustion and Flame 2004;137:265.

58. Jong W., Nola G., Venneker B.C.H., Spliethoff H., Wójtowicz M.A. TG-FTIR pyrolysis of coal and secondary biomass fuels: Determination of pyrolysis kinetic parameters for main species and NO_x precursors. Fuel 2007;86:2367.

59. Becidan M., Skreiberg O., Hustad J.E. NO_x and N_2O precursors (NH_3 and HCN) in pyrolysis of biomass residues. Energy and Fuels 2007;21:1173.

60. Ren Q., Zhao C., Wu X., Liang C., Chen X., Shen J., Tang G., Wang Z. Effect of mineral matter on the formation of NO_x precursors during biomass pyrolysis. Journal of Analytical and Applied Pyrolysis 2009;85:447.

61. Barisic V., Klingstedt F., Kilpinen P., Hupa M. Kinetics of the catalytic decomposition of N_2O over bed materials from industrial circulating fluidized-bed boilers burning biomass fuels and wastes. Energy and Fuels 2005;19:2340.

62. Pels A.J.R., Wójtowicz M.A., Kapteijn F., Moulijn J.A. Trade-off between NO and N_2O in fluidized-bed combustion of coals. Energy and Fuels 1996;9:743.

Chapter 3 -Method for online measurement of the CHON composition of raw gas from biomass gasifier

Daniel Neves[a,b], Henrik Thunman[b], Luís Tarelho[a], Anton Larsson[b], Martin Seemann[b], Arlindo Matos[a]

[a] University of Aveiro and CESAM, [b] Chalmers University of Technology

Published in Applied Energy, 2014, 113, 932-45.

Abstract

For unattended biomass gasification processes, rapid methods for monitoring the elemental composition (CHON) of the raw gas leaving the gasifier are needed. Conventional methods rely on time-consuming and costly laboratory procedures for analysing the condensable part of the raw gas. An alternative method, presented in this work, assesses the CHON composition of raw gas in a "one step" analysis without the need to previously characterise its chemical species composition. Our method is based on the quantitative conversion of a raw gas of complex chemical composition into CO_2, H_2O, and N_2 in a small combustor. The levels of these simple species can be measured with high accuracy and good time resolution, and the CHON composition of the raw gas can be determined from the mass balance across the combustor. To evaluate this method, an online combustion facility was built and used to analyse the raw gas from the Chalmers 2-MW_{th} dual fluidised bed steam gasifier. Test runs of the developed facility demonstrated complete combustion of the raw gas and the measurements were both fast and reliable. The new method used in combination with zero-dimensional reactor modelling provides valuable data for the operational monitoring of gasification processes, such as the degree of fuel conversion, composition of the char exiting the gasifier, oxygen transport by catalytic bed material, and amount of condensables in raw gas.

Keywords

Method, Gas, Tar, Biomass, Gasification, Fluidised bed

3.1 *Introduction*

To accelerate the industrialisation of biomass gasification, various demonstration plants are or have been in operation around the world [1]. Allothermal gasification in a dual fluidised bed (DFB) is one of these processes [2-4] that has enabled essential progress towards the ideal gasification process [5]. The most well-known DFB gasification project is the $8MW_{th}$ CHP plant in Güssing, Austria [4, 6, 7]. In this technology, the bed material is continuously circulated between two interconnected fluidised bed (FB) reactors. Fresh chopped biomass is fed into the first reactor, the steam gasifier, where it is heated and partially converted into gaseous fuel. The remainder of the biomass (i.e., the char) leaves the gasifier in the direction of the second reactor, the air combustor, where it is burned. This enables reheating of the bed material in the combustor, which is subsequently circulated back into the first reactor for endothermic gasification. The gas streams that leave each reactor are streamed off separately which permits to produce a raw gas with low N_2 content (<5%v) and moderate heating value (12-14 MJ/Nm^3) (e.g., [4, 6, 7]). A similar process to the one applied in Güssing was demonstrated at Chalmers University of Technology, Sweden [8, 9], where it was shown how to integrate a bubbling FB steam gasifier onto existing circulating FB boilers; this option minimises investment costs and enables an even more flexible operation of the gasifier [8].

Despite recent progress in gasification technologies, the development of adequate monitoring methods for the composition of the raw gas leaving the gasifier has not kept pace. Indeed, the dry and clean raw gas can be analysed online by, e.g., gas chromatography (GC), although the condensable fraction (i.e., water and organics) is difficult to handle and requires offline procedures (see e.g., [10-14]). As a consequence, it can be problematic, not only in utilizing the raw gas in certain end-user applications [15, 16], e.g., hot gas burners using an open loop control system (see e.g., [17, 18]), but also in understanding the operation of the gasifier itself. The reason for this is that the chemical (i.e., molecular) composition of raw gas is commonly used to calculate the corresponding CHON composition, heating value, and flow rate. In a gasification process, all of this information is needed to establish the mass and energy balances across the gasifier and thereby, the chemical efficiency of the process. Considering that the amount of condensables in the raw gas is significant, a fast measurement of the composition of the raw gas cannot be achieved by currently used methods and valuable information for controlling the operation of the gasifier is lost.

To address this problem, a specialized method for measuring the CHON composition of raw gas is proposed in this work, whereby the analysis is simplified and data with high temporal resolution is obtained. In this method, the entire raw gas is initially converted into

CO_2, H_2O, and N_2 in a small combustion reactor. Thereafter, these simple species are analysed online and, based on the derived composition, the CHON mass fractions of the raw gas are calculated. We tested the application of this method to the raw gas from the Chalmers 2-MW_{th} DFB steam gasifier (hereinafter referred to as the 'Chalmers gasifier') and it is shown how operational data about the process (e.g., the degree of biomass conversion, oxygen transport by catalytic material, amount of condensables in the raw gas) can be obtained from these measurements.

3.2 *Measuring the CHON composition of raw gas*

The ash-free raw gas that exits a biomass gasifier is composed of species that vary considerably with regards to physical properties and chemical functionalities. To simplify the treatment, some of these species are combined into lumps (Figure 3.1). The permanent gas includes inorganic species (e.g., H_2) and hydrocarbons (C_1-C_5 species), the latter being noted as C_xH_y. The condensables include organic species and water. The chemical makeup of the condensable organics formed inside the gasifier is complex [19-22], which has led to inconsistent terminology in the literature (see e.g., [16]); in the present work, the combined organics are assumed to constitute a single 'tar' loop. Soot is particulate carbon that is formed inside the gasifier through reactions between the pyrolytic volatiles. Although the raw gas contains hundreds of chemical species, only carbon, hydrogen, oxygen and nitrogen (CHON) are relevant to consideration of the elemental composition.

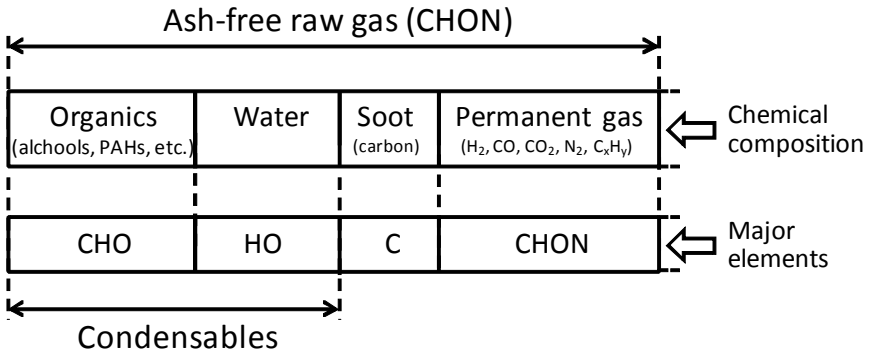

Figure 3.1 - Chemical and elemental compositions of the raw gas from a biomass gasifier.

3.2.1 *Conventional measurement methods*

The CHON composition of raw gas is usually determined from a slipstream according to Eq. (3.1), where $Y_{k,G}$ is the mass fraction of k^{th} species in the raw gas (subscript G) and $Y_{j,k}$ is the mass fraction of j^{th} element in k^{th} species. The problem with this calculation is that the values of $Y_{k,G}$ and $Y_{j,k}$ have to be known for a large number of species present in the raw gas.

$$Y_{j,G} = \sum_{k} Y_{k,G} \cdot Y_{j,k} \qquad j = C,\ H,\ O,\ N \qquad k = CO_2,\ CO, H_2,\ C_xH_y,\ N_2,\ H_2O,\ tar,\ soot \qquad \text{Eq. 3.1}$$

Soot is commonly collected at the beginning of the sampling train using a high-temperature filter (e.g., at 350ºC [10]), thereby avoiding simultaneous vapour condensation. After removal of the soot, the usual procedure for analysing the raw gas is based on the use of cold traps that further separate the condensables from the permanent gas. To obtain a sufficient amount of tar, the sampling period can be several hours [10, 11, 13]. Moreover, the operating conditions in the cold trap (e.g., the solvent used to absorb the tar) vary across the investigations (see e.g. [16]), influencing the nature of the collected liquid. The use of backup filters is also advisable to quantify the aerosols that are formed upon cooling of the tar [10, 13]. For the analysis of the collected liquid, in general, extensive laboratory procedures are used. A widely used method to determine the water content is Karl-Fisher titration [14]. In turns, according to a guideline [10], the gravimetric-tar content is obtained by evaporating the water, solvent and light tar species under specific conditions followed by weighing the heavy residue. Another possibility is to analyse the bulk liquid by GC using a flame ionisation detector (FID) [10]; the so-called GC-tar content is obtained by summing the elution peaks over several tens of minutes. Since, in this method, the heavy tars are retained in the GC column [10], a more satisfactory result is obtained by combining the GC and gravimetric methods [23]. For the analysis of the permanent gas that exits the cold trap various methods are available, while the amount of gas collected can be assessed e.g. using a bellows-type meter; a commonly used method of gas analysis is GC coupled with thermal conductivity detector (TCD). Appropriate selection of GC columns enables quantification of CO_2, CO, H_2, N_2 and light hydrocarbons (C_1-C_3) within a couple of minutes, although the quantification of longer hydrocarbons (up to C_5) takes more time, say, 10–30 minutes [24].

The growing interest in biomass gasification has led to efforts to develop more suitable methods for sampling and analysing the tar. In the SPA method, the raw gas is passed through a solid adsorbent to trap the tar [12, 25]. The solid phase is held in a syringe, which is used to withdraw a small volume of raw gas (100 mL) from the high-temperature line (>300ºC) during about 1 min per sample. The syringe tube is then extracted with solvents to recover the tar, and the bulk liquid solution is analysed by the aforementioned GC-FID technique to quantify the light tars (typically, species up to coronene [25]). Others have modified this procedure by using a thermal desorption technique to recover the tar from the solid phase [26]. A recent review of online tar measurement methods [27] reveals that the most used ones are based on FID [28], photo-ionisation [29], mass spectrometry [30], and laser spectroscopy [31]. For example, the IVD-tar analyser [28] uses a FID to analyse the raw gas and the respective dry raw gas. The organic carbon separated by cold trapping is then

determined by difference and the result is expressed, e.g., as CH_4. Given the various tar measurement methods, it would not be amiss to assume that they produce different results. A comparison of four on-line and off-line methods revealed differences of up to 50% in the tar content of a raw gas [28].

An additional problem associated with determining the CHON composition of a raw gas is that the nature of the lumped tar is largely unknown (i.e., $Y_{j,tar}$ in Eq. 3.1). Literature data [32] suggests that the CHON composition of tar is close to that of the parent fuel (i.e., it is highly oxygenated), although the data show considerable scatter. The most satisfactory way to approximate the CHON composition of lumped tar is by standard method or alternatively, by measuring a large number of tar species using GC analysis. Online tar measurement methods provide little help in this regard, since the nature of the lumped tar is not resolved.

In summary, conventional methods to evaluate the CHON composition of raw gas using Eq. (3.1) are impractical, costly, do not provide rapid feedback, and can easily generate inaccurate results.

3.2.2 *A new measurement method*

In combustion calculations, the aim is often to determine the oxygen requirements and the composition of flue gases formed during complete conversion of a given fuel. It is equally possible to determine the CHON composition of the fuel being burned from the flow rates and chemical compositions of both the oxidiser and combustion flue gases, which is the rationale behind the measurement method proposed in the present work.

3.2.2.1 *Measurement principle*

The combustible elements of raw gas, carbon and hydrogen, are assumed to react with oxygen to yield CO_2 and H_2O, while the nitrogen appears as N_2. In this work the oxidiser is dry atmospheric air and, hence, the combustion reaction of raw gas can be represented by:

$$\nu_{G,A}\,(\text{raw gas}) + \text{air} \longrightarrow \nu_{CO2,A}\,CO_2 + \nu_{N2,A}\,N_2 + \nu_{H2O,A}\,H_2O + \nu_{O2,A}\,O_2\ (+\ \nu_{Ar,A}\,Ar) \qquad \text{Eq. 3.2}$$

where $\nu_{G,A}$ and $\nu_{k,A}$ ($k = CO_2, N_2, H_2O, O_2$) are the stoichiometric coefficients. The stoichiometry is written on a dry air basis (subscript A), since the respective flow rate ($\dot{n}_A$) can be measured accurately. The problem is to determine the amounts of CO_2, N_2, H_2O, and O_2 produced per unit mass of dry air feed ($\nu_{k,A}$, kg k/kg A). These are related to the chemical composition ($y_{k,E}$, mole fraction) and molar flow rate ($\dot{n}_E$) of the combustion flue gases according to Eq. (3.3), in which $\dot{n}_E$ can be derived from the nitrogen balance across the combustor (e.g., Eq. 3.4 [33]). The inclusion of the N/H mass ratio of the raw gas in Eq. (3.4) is

needed to be able to account for the nitrogen entering the combustor with the raw gas. When the raw gas is nitrogen-free or contains a negligible amount of nitrogen, Eq. (3.4) simplifies to $\dot{n}_E = y_{N2,A} \cdot \dot{n}_A / y_{N2,E}$; otherwise, the N/H ratio has to be known to resolve the generalised form. A simple way to measure the N/H ratio of the raw gas being burned is given later on in this paper (Section 3.4.1).

$$\nu_{k,A} = y_{k,E} \cdot \frac{\dot{n}_E}{\dot{n}_A} \cdot \frac{M_k}{M_A} \qquad k = CO_2, N_2, O_2, H_2O \qquad \text{Eq. 3.3}$$

$$\dot{n}_E = \frac{y_{N2,A}}{y_{N2,E} - (Y_{N,G} / Y_{H,G}) \cdot y_{H2O,E} \cdot (2M_H / M_{N2})} \cdot \dot{n}_A \qquad \text{Eq. 3.4}$$

Now the steady-state elemental mass balances to the combustion process can be solved according to Eqs. (3.5) to (3.8), where the left sides represent the mass of the j[th] element supplied with the raw gas per unit mass of dry air; the ratio of raw gas to dry air ($\nu_{G,A}$ in Eq. 3.2) is then the summation value for CHON, i.e. $\nu_{G,A} = \sum_j (Y_{j,G} \cdot \nu_{G,A})$.This makes it possible to compute the CHON mass fractions of the raw gas being burned ($Y_{j,G}$) using Eq. (3.9). It shall be stressed that, when a measurement of the H/C ratio of raw gas is enough, it can be approximated directly from the concentrations of H_2O and CO_2 in the combustion flue gases without the need to solve Eqs. (3.3) to (3.9).

$$Y_{C,G} \cdot \nu_{G,A} = \nu_{CO2,A} \cdot \frac{M_C}{M_{CO2}} - y_{CO2,A} \cdot \frac{M_{CO2}}{M_A} \qquad \text{Eq. 3.5}$$

$$Y_{H,G} \cdot \nu_{G,A} = \nu_{H2O,A} \cdot \frac{M_{H2}}{M_{H2O}} \qquad \text{Eq. 3.6}$$

$$Y_{O,G} \cdot \nu_{G,A} = \nu_{O2,A} + \nu_{CO2,A} \cdot \frac{M_{O2}}{M_{CO2}} + \nu_{H2O,A} \cdot \frac{M_{O2}}{M_{H2O}} - y_{O2,A} \cdot \frac{M_{O2}}{M_A} \qquad \text{Eq. 3.7}$$

$$Y_{N,G} \cdot \nu_{G,A} = \nu_{N2,A} - y_{N2,A} \cdot \frac{M_{N2}}{M_A} \qquad \text{Eq. 3.8}$$

$$Y_{j,G} = \frac{Y_{j,G} \cdot \nu_{G,A}}{\sum_j (Y_{j,G} \cdot \nu_{G,A})} \qquad j = C, H, O, N \qquad \text{Eq. 3.9}$$

3.3 *Zero-dimensional model of dual fb gasifier*

To show how the CHON composition of the raw gas can be used for monitoring the operation of a DFB gasifier, a zero-dimensional reactor model is presented below. For the sake of clarity, the streams across the gasifier are illustrated in Figure 3.2. Note that the total

entering char comprises both unburnt char from the boiler (subscript ch1) and pyrolytic char (subscript ch) formed inside the gasifier during pyrolysis of fresh biomass. Therefore, the unconverted char leaving the gasifier together with the circulating bed material (subscript ch2) is also a mixture of unburnt char and pyrolytic char. The purge gas (subscript P) refers to some unknown quantity of gas leakage as, for example, flue gases from the boiler or ambient air. Me_xO_y and Me_xO_{y-1} represent different oxidation states of a suitable in-bed catalyst, which can lead to selective oxygen transport from the boiler (oxidation zone) to the gasifier (reduction zone).

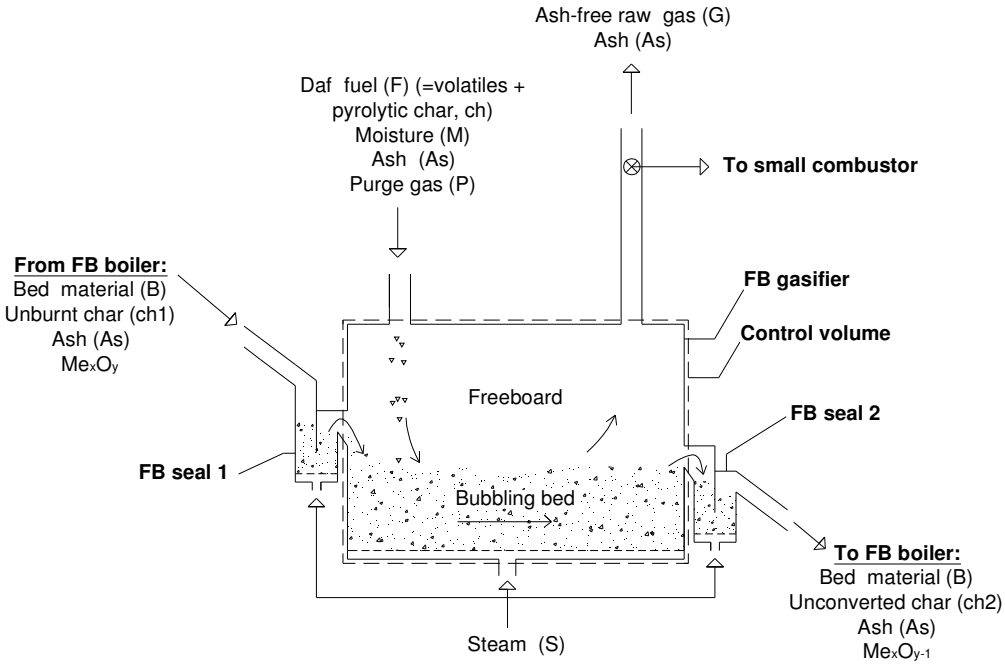

Figure 3.2 - Illustration of the main streams across a bubbling DFB biomass gasifier. Abbreviations used are those listed in the nomenclature.

3.3.1 *Degrees of fuel and char conversion*

In the simplified model presented here, the same degree of gasification (χ) is assumed for the two types of char, as shown in Eq. (3.10). The simplest way to evaluate χ is to monitor the H/C mass ratio of the raw gas ($Y_{H,G}/Y_{C,G}$). Indeed, the gas-phase reactions that occur in the gasifier do not alter the CHON contents of the raw gas, and the respective H/C ratio depends only on the streams entering the reactor and the amount of char converted, as in Eq. (3.11), where $Y_{i,F}$ is the mass ratio of the i^{th} stream to the daf fuel feed (subscript F) and $Y_{j,i}$ is the mass fraction of the j^{th} element in the i^{th} stream.

$Y_{ch,F}$ is essentially independent of the steam-fuel ratio ($Y_{M,F}+Y_{S,F}$) and can be estimated by separate pyrolysis experiments conducted at a temperature close to that used in the gasifier.

In turns, the inflows of unburnt char ($Y_{ch1,F}$) and purge gas ($Y_{P,F}$) are difficult to measure but, they are generally minor streams that can either be neglected or combined with the major streams to simplify the treatment (see [33]). In the first limiting case, in which only devolatilisation occurs, the H/C ratio is determined by setting χ=0 in Eq. (3.11); in the other limiting case, the fuel is completely gasified and χ=1. In practice, the degree of char conversion in the gasifier is obtained by searching the value of χ that fits the measured H/C ratio of the raw gas. Note that χ can also be obtained from the O/C ratio of the raw gas if the gasifier is operated without in-bed metal oxide.

$$\chi = \frac{Y_{ch,F} - \left(Y_{ch2,F} - Y_{ch1,F}\right)}{Y_{ch,F} + Y_{ch1,F}} \qquad \text{Eq. 3.10}$$

$$\frac{Y_{H,G}}{Y_{C,G}} = \frac{Y_{H,F} + \left(Y_{M,F} + Y_{S,F}\right) \cdot Y_{H,H2O} + Y_{ch,F} \cdot Y_{H,ch} \cdot \left(\chi - 1\right) + Y_{ch1,F} \cdot Y_{H,ch1} \cdot \chi}{Y_{C,F} + Y_{P,F} \cdot Y_{C,P} + Y_{ch,F} \cdot Y_{C,ch} \cdot \left(\chi - 1\right) + Y_{ch1,F} \cdot Y_{C,ch1} \cdot \chi} \qquad \text{Eq. 3.11}$$

When a measurement of the flow rate of the raw gas ($Y_{G,F}$) is available, an alternative method to determine the amount of char that is converted is through the CHON balances across the gasifier, as shown for carbon, hydrogen, oxygen, and nitrogen in Eq. (3.12), where $Y_{i,F}$ is a positive or negative value depending on whether the i^{th} stream is entering or leaving the gasifier (see Figure 3.2). The difference between the amounts of char moving out and into the gasifier is obtained by summing the left side of Eq. (3.12) for CHON (Eq. 3.13), and the obtained difference $Y_{ch2,F}$ - $Y_{ch1,F}$ is related to χ by Eq. (3.10) (see also Table 1).

$$Y_{ch2,F} \cdot Y_{j,ch2} - Y_{ch1,F} \cdot Y_{j,ch1} = Y_{j,F} + \sum_i Y_{i,F} \cdot Y_{j,i} \qquad j=C,H,O,N \qquad i=P,G,M,S \qquad \text{Eq. 3.12}$$

$$Y_{ch2,F} - Y_{ch1,F} = \sum_j \left(Y_{ch2,F} \cdot Y_{j,ch2} - Y_{ch1,F} \cdot Y_{j,ch1}\right) \qquad j = C, H, O, N \qquad \text{Eq. 3.13}$$

Table 3.1 - Fuel conversion in the DFB gasifier as a function of the operational parameter $Y_{ch2,F}$-$Y_{ch1,F}$.

Condition	Char conversion, χ
$Y_{ch2,F} - Y_{ch1,F} = Y_{ch,F}$	χ=0
$-Y_{ch1,F} < Y_{ch2,F} - Y_{ch1,F} < Y_{ch,F}$	0<χ<1
$Y_{ch2,F} - Y_{ch1,F} = -Y_{ch1,F}$	χ=1
$Y_{ch2,F} - Y_{ch1,F} > Y_{ch,F}$	Fuel is partially devolatilized

3.3.2 *Composition of the char leaving the gasifier*

The elemental composition of the escaping char (ch2) can be estimated from the CHON balances across the gasifier. Here, it is given by the balances for carbon and oxygen, although depending on the accuracy of the measurements, the analysis can be extended to hydrogen and nitrogen. Starting from Eqs. (3.12) and (3.13), it can be shown that the carbon and oxygen contents of ch2 are within the ranges given by Eqs. (3.14) and (3.15), respectively, so that the condition $Y_{ch1,F} \geq 0$ is fulfilled. The maximum value for carbon content and the minimum value for oxygen content of the escaping char are established by those of the unburnt char coming from the boiler. This is expected, since the reactor temperature has a positive effect on the carbon content of chars [32]. As a practical matter, the carbon and oxygen contents of the escaping char can be approximated from the equalities in Eqs. (3.14) and (3.15), as minor differences are obtained in the composition of chars formed at high temperature (say, >750ºC) [32] and the contribution of the unburnt char to the total escaping char is small as compared to that of the pyrolytic char.

$$\frac{Y_{ch2,F} \cdot Y_{C,ch2} - Y_{ch1,F} \cdot Y_{C,ch1}}{Y_{ch2,F} - Y_{ch1,F}} \leq Y_{C,ch2} < Y_{C,ch1} \qquad \text{Eq. 3.14}$$

$$Y_{O,ch1} < Y_{O,ch2} \leq \frac{Y_{ch2,F} \cdot Y_{O,ch2} - Y_{ch1,F} \cdot Y_{O,ch1}}{Y_{ch2,F} - Y_{ch1,F}} \qquad \text{Eq. 3.15}$$

3.3.3 *Oxygen transport by catalytic material*

The amount of oxygen transported by the catalytic material to the gasifier ($Y_{O^*,F}$) can be investigated from the O/C mass ratio of the raw gas (Eq. 3.16) once the degree of char conversion (χ) has been measured. A simple way to obtain χ is to also measure the H/C mass ratio of the raw gas, as shown in Eq. (3.11). However, during the reduction of the metal oxide in the gasifier, elemental carbon can form over the surface of the catalyst which lead to higher H/C (and O/C) ratio for the raw gas due to recirculation of carbon to the boiler via the catalytic bed. Previous investigations have shown that carbon deposition is highly dependent upon the nature of the catalyst [34-36] and can be avoided by using an iron-based catalyst. Therefore, for those cases in which the catalyst does not form carbon, Eq. (3.11) can be used in combination with Eq. (3.16) to estimate the oxygen transport in a DFB system. Similar to the O/C ratio of the raw gas, the oxygen balance across the gasifier (Eq. 3.12) also provides a measurement of the incoming oxygen if a comparison is made between gasification experiments with and without the catalytic bed material.

$$\frac{Y_{O,G}}{Y_{C,G}}=\frac{Y_{O,F}+\left(Y_{M,F}+Y_{S,F}\right)\cdot Y_{O,H2O}+Y_{P,F}\cdot Y_{O,P}+Y_{ch,F}\cdot Y_{O,ch}\cdot\left(\chi\text{-}1\right)+Y_{ch1,F}\cdot Y_{O,ch1}\cdot\chi+Y_{O^*,F}}{Y_{C,F}+Y_{P,F}\cdot Y_{C,P}+Y_{ch,F}\cdot Y_{C,ch}\cdot\left(\chi\text{-}1\right)+Y_{ch1,F}\cdot Y_{C,ch1}\cdot\chi} \qquad \text{Eq. 3.16}$$

3.3.4 *Flow rate and amount of condensables in raw gas*

To get a measurement of the mass flow rate of raw gas leaving the gasifier, a known flow rate of an inert gas, e.g., helium, is mixed with the gasification agent, to allow correlating the measured CHON mass fractions of raw gas with the unit mass of helium fed to the gasifier. In a similar manner, a rapid measurement of the amount of condensables (tar + water) leaving the gasifier can be obtained if a second slipstream of the raw gas is dried and cleaned and subsequently burned in a second combustion reactor. Then, the CHON contents of the dry and clean raw gas can also be related to the unit mass of helium fed to the gasifier, so that the amount of condensables in the raw gas can be estimated by difference. For instance, the carbon and hydrogen removed by cold trapping can be rapidly evaluated by relating the amounts of CO_2 and H_2O in the flue gases from each combustor to the unit mass of helium.

3.4 *Experimental*

The experimental setup, including an online combustion facility and ancillary systems, used to demonstrate the measurement method for the CHON composition of raw gas is described in this section. The Chalmers DFB gasifier is also briefly addressed because it was used to test the method with a real raw gas.

3.4.1 *Online monitoring combustion facility and ancillaries*

The combustion facility developed in this work is outlined in Figure 3.3; its overall dimensions are 2.0×0.9×0.6 m. The main purpose of the reactor is to assure complete combustion of the raw gas. It consists of a 253 MA stainless steel (SS) tube with an outer diameter (OD) of 33.4 mm and length of 770 mm, and it is operated at atmospheric pressure and temperatures within 800–950ºC. For that purpose, the reactor is positioned within a 2.8-kW_e oven and the temperature is monitored by thermocouples (K-type, 1.5-mm OD) placed in the middle (T1, Figure 3.3) and bottom exit (T2) of the reactor. The top and bottom joints of the reactor are flange-type and extend ≈50 mm out of each side of the oven. No combustion catalyst is used.

The temperature of the raw gas is kept at 360–390ºC along the pathway between the sampling port (at ≈700–800ºC and ≈ -1kPa relative to the atmospheric pressure) and the combustion chamber, thus limiting the chemical reactions among the raw gas components and avoiding tar condensation [10]. The larger particles are initially separated in a ceramic

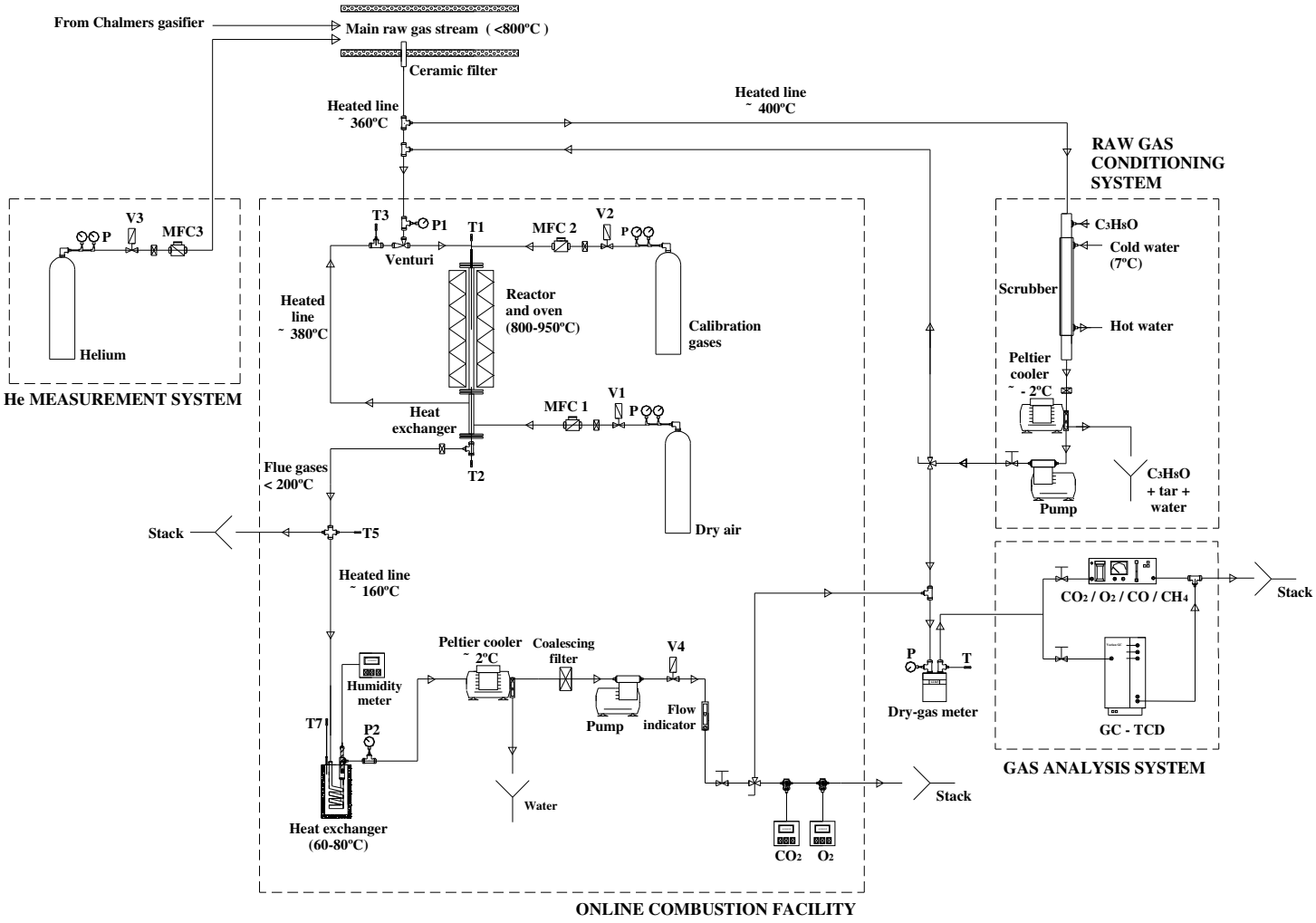

Figure 3.3 - Process schematic of the online monitoring combustion facility and ancillary equipment. T, temperature measurement; P, pressure measurement; MFC, mass-flow controller; V, solenoid valves.

filter attached to the sampling port. A flexible heating hose (0.28 kW/m, 360ºC, SS 8-mm OD inner tube) is then used to lead a slipstream of the raw gas to the vacuum side of a 316L SS all-welded venturi. To suck the raw gas into the venturi, a known flow rate of dry air is injected into the respective pressure side. The ratio of vacuum to pressure flow rates is a function of the amount of gas entering the pressure side and, in practice, this enables to control the air-fuel ratio in the small combustor [33]. Moreover, the vacuum generated (P1) is continuously monitored. Heat is furnished to the venturi and the incoming dry air by trace heating (0.25 kW/m), with the temperature (≈380ºC) monitored by a thermocouple (K-type, 1.5-mm OD) placed at 10 mm from the pressure side of the venturi (T3). The raw gas/air mixture moves then into the side port of a gas burner attached to the reactor top flange and finally, it goes down into the combustion chamber; a perforated nozzle is attached to the burner tip to help in spreading the flame. The flange and the burner are well-insulated and heated to approximately 390ºC using the heating tape already used to heat the venturi.

The flue gases that leave the combustion chamber pass through the inner tube (33.4 mm OD, 350 mm length) of a counter-flow heat exchanger, while dry combustion air flows up through the outer tube (48.3 mm OD). The heat exchanger is attached to the reactor bottom flange and is used to: (i) rapidly cool the combustion flue gases to < 200ºC; and (ii) preheat the dry air moving into the venturi. Thereafter, a slipstream of flue gases is sampled (2-4 NLpm) and the remaining gas is discarded. The temperature of the flue gases is measured by a thermocouple (K-type, 1.5-mm OD) inserted into the exhaust pipe (T5). Another flexible heating hose (0.14 kW/m, PTFE 6-mm OD inner tube) is used to lead the slipstream of flue gases at about 160ºC to an online moisture measurement system [37]. In this system, the gases are further cooled in a submerged tube heat exchanger (oil bath) before entering a measurement cell, which includes in situ humidity (capacitive thin-film polymer) and temperature (PT100) sensors and a side connection to an absolute pressure transducer (P2). In practice, the temperature of the oil bath is adjusted to 60–80ºC (T7) so that the relative humidity of the flue gases rises to within 40–80%. The flue gases are then transported by insulated PTFE tube to a Peltier cooler (≈2ºC) where the condensable species (mainly water) are trapped. Trace vapours and aerosols are further removed in a coalescing filter. The dry and clean combustion flue gases are finally displaced by a diaphragm pump into the gas analysis system.

Apart from the thermocouples, the instrumentation used in the combustion facility comprise: i) two absolute pressure transducers (P1 and P2, WIKA S10, 0–1.6 bar); ii) two mass-flow controllers (MFC1 and MFC2, Bronkhorst EL-FLOW, 0-29 NLpm and 0-5 NLpm, respectively); iii) a moisture measurement system (Vaisala HMT338, 0–100% RH); iv) an O_2 gas sensor (electrochemical cell, Figaro KE-25, 0–100%v); and v) a CO_2 gas sensor (silicon-

based NDIR, Vaisala GMT220, 0–10%v). A real-time control and data acquisition system (NI CompactRIO) is used to operate the pneumatics and read the sensor signals.

One of the mass-flow controllers is used to measure the flow rate of dry combustion air (MFC1, 0-29 NLpm), ensuring an uncertainty bellow 1% of reading. The humidity cell was factory calibrated up to 94% RH and the results show a typical uncertainty of 1% of reading. In a set of combustion experiments, the response of the humidity cell was compared to the mass of condensate trapped in the cooler, as provided in Figure 3.4. Note that the comparison shall be qualitative due to errors affecting the gravimetric method, such as condensate build-up in the cooler and the trapping of unburnt species during transient operation of the combustor. Nevertheless, a good agreement between the online method and the gravimetric method is seen. The O_2 and CO_2 gas sensors enabled to control the excess air in the combustion chamber within a few seconds; the O_2 cell is particularly suitable for this purpose due to its short response time (t_{90} <15s). However, for the evaluation of the measurement method proposed in this work, the dry and clean flue gas is directed by SS tube to an ancillary gas analysis system (Section 3.4.1.1).

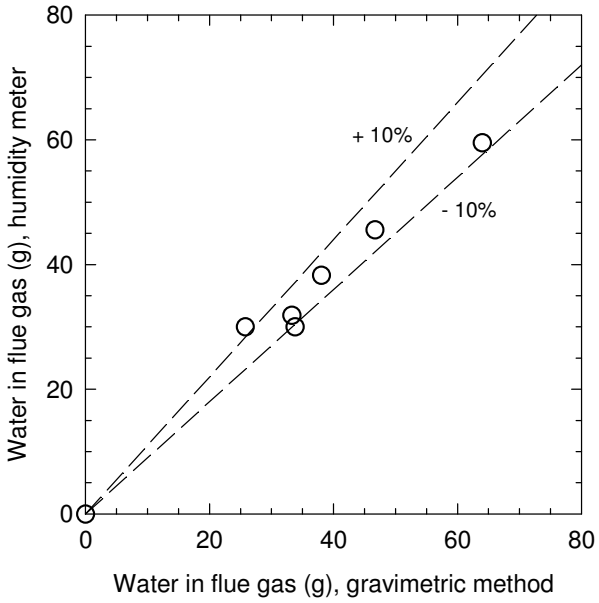

Figure 3.4 - Comparison of the online humidity meter and gravimetric methods. The amounts of water exiting the small combustor in experiments with or without raw gas are shown.

3.4.1.1 *Ancillary systems*

The ancillary systems used in this work include: (i) a helium measurement system; (ii) a raw gas conditioning system; and (iii) a dry gas analysis system.

The helium measurement enables to use a tracer gas across the Chalmers gasifier. In the present work, helium is supplied from a series of gas cylinders and mixed with the fluidising

steam of the gasifier at a known flow rate by a mass-flow controller (MFC3, Bronkhorst, 0–100 NLpm).

The raw gas conditioning system enables to dry and clean of a slipstream of the raw gas. It consists of a separate heating hose (0.28 kW/m, SS inner tube) attached to the ceramic filter that leads the raw gas at ≈400ºC to a scrubber operated with isopropanol at ≈7ºC; here, the main part of the tar is absorbed and the steam is condensed. The gas that leaves this scrubber is further cooled to -2ºC in a Peltier cooler and filtered.

The gas analysis system is used to measure the composition of either the dry raw gas leaving the gasifier or the dry flue gases leaving the small combustor. This system comprises a multi-component gas analyser (Rosemount MLT, 0–100%v CO_2, 0–25%v O_2, 0–1%v CO, and 0–10%v CH_4) and a µGC (Varian GC4900). The µGC measures the concentrations of N_2 and He every 3 minutes, where the species are separated in a 5Å molecular sieve column (1/8'' OD, 10-m length, argon carrier gas) and quantified by TCD.

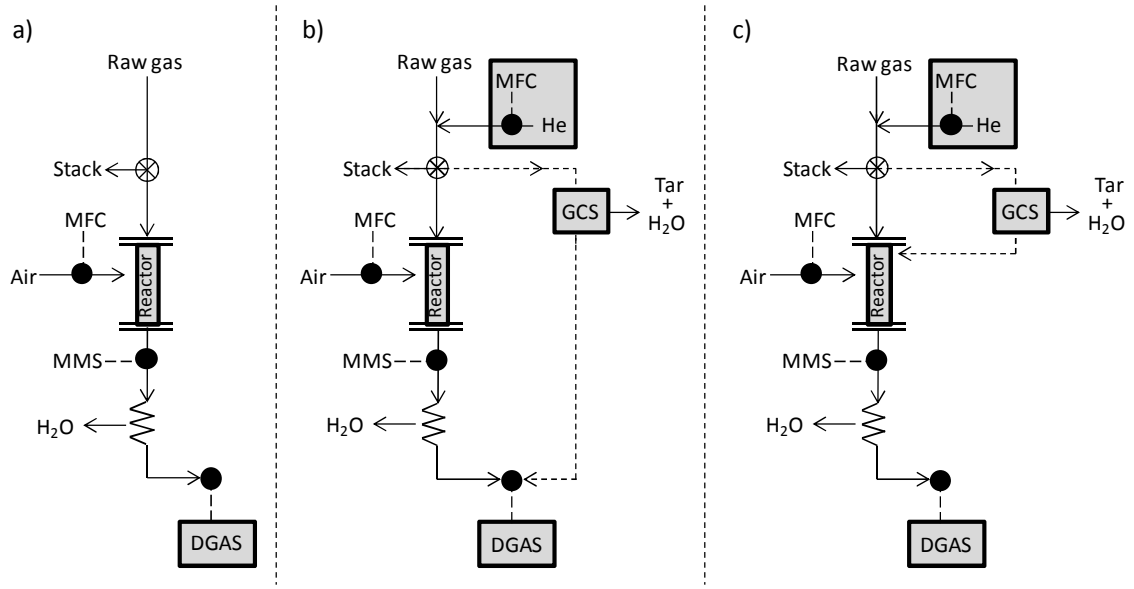

Figure 3.5 - Investigated measurement setups for: (a) the H/C ratio of raw gas; (b) the CHON composition and flow rate of raw gas; and (c) the amount of condensables in raw gas. MFC, mass-flow controller; MMS, moisture measurement system; GCS, raw gas conditioning system; DGAS, dry gas analysis system.

The ways these systems were combined with the online combustion facility is depicted in Figure 3.5. Real-time monitoring of the H/C ratio of the raw gas is carried out using the basic setup shown in Figure 3.5-a, whereby this ratio is approximated from the amounts of H_2O and CO_2 in the combustion flue gases. To derive the CHON contents and flow rate of the raw gas the setup shown in Figure 3.5-b is used; in this case, between 25 and 100 NLpm of helium are mixed with the fluidising steam of the gasifier. The raw gas sample is then divided

into two streams: one stream is lead into the small combustor and the other stream is lead into the raw gas conditioning system. The H/He ratio of the incoming raw gas sample is determined from the amounts of H_2O and He in the combustion flue gases while the respective N/He ratio is approximated from the amounts of N_2 and He in the dry and clean raw gas. This enables to compute the N/H mass ratio of the raw gas and solve the elemental balances across the combustor (see Section 3.2.2). In the setup shown in Figure 3.5-c the raw gas and the respective dry gas are burned in consecutive steps to be able to compute the amount of condensables in the raw gas by difference (see Section 3.3.4).

3.4.2 *The Chalmers gasifier*

A description of the Chalmers DFB process is available elsewhere [8, 9, 38] and only a basic outline is provided here. Fresh biomass is fed at a constant flow rate (±1% of the average value) by a screw feeder and rotary valves over the surface of the bubbling bed operating at preset temperature. Given that the gasifier operates at a slight under-pressure (≈-1 kPa relative to the atmospheric pressure), a small amount of purge gas (dry flue gases from the boiler) is used in the fuel feeding system to minimise ambient air leakage. The flow rate of the fluidising steam is measured by venturi meter and adjusted according to the preset steam-fuel ratio. The bed material is silica sand with an average particle diameter of 270μm. The circulation rate of the bed material and the respective flow direction is secured by FB seals operated with steam; previous measurements based on distinct methods yielded circulation rates between 14000 and 25000 kg bed/h [38-40], depending on the operating conditions. The bed temperature is monitored by PT100 probes.

3.4.2.1 *Fuel*

Wood pellets of 8mm diameter and 10mm length were used in the gasifier. The elemental composition, ash content, and moisture content of the pellets were measured by standard methods (typical values in Table 3.2). The amount of char formed during the thermal decomposition of the pellets was determined in pyrolysis experiments carried out under a sweep of nitrogen and temperature in range of the gasifier. Pyrolysis under fast heating rates (10^2–10^3ºC/min) was achieved in a laboratory-scale bubbling FB and quartz-tube reactors. In both cases, a known mass of dry pellets was instantaneously fed into the preheated reactor (600–950ºC) and the char particles were recovered for analysis. To test whether the heating rate affects the yield of char, experiments were performed in a thermobalance (LECO, TGA 701) at 50ºC/min up to 915ºC. A sample of the char formed in the laboratory-scale FB reactor was sent for ultimate analysis (see Table 3.2).

Table 3.2 - Proximate and ultimate analyses of wood pellets and respective pyrolytic char formed under fast heating.

Wood pellets[a]	Mass %, as received basis[d]
Ash	0.5 ± 0.0
Carbon	46.4 ± 0.3
Hydrogen	5.6 ± 0.1
Nitrogen	0.1 ± 0.0
Oxygen[c]	39.6 ± 0.3
Moisture	7.8 ± 0.7
Pyrolytic char, 835ºC[a,b]	**Mass %, daf basis[d]**
Carbon	93.1 ± 0.6
Hydrogen	1.2 ± 0.1
Nitrogen	0.4 ± 0.1
Oxygen[c]	5.3 ± 0.6

[a] Sulphur content was not determined or was <100 ppm;[b] Char produced in the laboratory-scale bibbling FB reactor ;[c] Difference method; [d] Average value ± one standard deviation (for the wood pellets, the variation is related to a set of analysis carried out during the course of the gasification experiments).

3.4.3 *Overview of the experiments*

The initial experiments were aimed at evaluating the operation of the combustion facility and validating the measurement method for the CHON composition of the raw gas (Section 3.5.2). This was done by burning standard gases, as well as the raw gas leaving the Chalmers gasifier under a given operating condition.

Then, experiments to show the application of the method for evaluating the operation of DFB gasifiers were done (Section 3.5.3). For this purpose, a slipstream of raw gas from the Chalmers gasifier was burned in the small combustor while varying the gasification condition (runs #1 to #6 in Table 3.3). The degrees of fuel and char gasification and the composition of the escaping char were evaluated during runs #1 to #4, whereby runs #1 to #3 tested the effect of varying the steam-fuel ratio (0.7–1.05 kg/kg) and run #4 tested the effect of varying the bed temperature (830ºC *vs.* 775ºC). Selective oxygen transport from the boiler to the gasifier was evaluated during runs #5 and #6, in which a known amount of ilmenite (Ti-Fe oxide) was mixed with the bed material. The amount of condensables in the raw gas was evaluated during run #6.

Due to measurement problems during run #1, the H/He ratio of the raw gas could not be determined according to Section 3.4.1.1. The alternative was to compute the hydrogen outflow through a simplification of the hydrogen balance across the gasifier, as shown in Eq. (3.17). Figure 3.6 plots the results obtained using Eq. (3.17) against those obtained using the

helium method, where it covers the gasification conditions in runs #2 to #6. The simplified hydrogen balance provides results that are in close agreement with those from the helium method and, thus, it provides a good alternative to approximate the N/H ratio of the raw gas.

Table 3.3 - Summary of the operational conditions used for the Chalmers gasifier.

Run No.	Bed temperature[a]	Fuel feeding rate (arb[b])	Fuel moisture content (arb)	Steam feeding rate[c]	Steam-fuel ratio[d]	Bed material
	ºC	kg/h	Mass %	kg H_2O/h	kg H_2O/kg F	Mass %
#1	835	389-396	7.61	295	0.89-0.91	100% sand
#2	835	398	7.61	350	1.04	100% sand
#3	830	405-412	6.83	240	0.70-0.71	100% sand
#4	775	397-409	6.83	240	0.70-0.72	100% sand
#5	830	377-398	8.51	350	1.06-1.11	≈ 98% sand, 2% ilmenite
#6	830	394-400	8.51	240	0.75-0.76	≈ 88% sand, 12% ilmenite

[a] Average value close to the bed material and fuel inlet; [b] The term "arb" refers to the "as received basis"; [c] Includes steam supplied through the distributor and FB seals 1 and 2 (excluding fuel moisture); [d] Includes steam and fuel moisture, $Y_{S,F}+Y_{M,F}$.

$$Y_{G,F} \cdot Y_{H,G} \approx Y_{H,F} + \left(Y_{M,F} + Y_{S,F} \right) \cdot Y_{H,H2O} \qquad \text{Eq. 3.17}$$

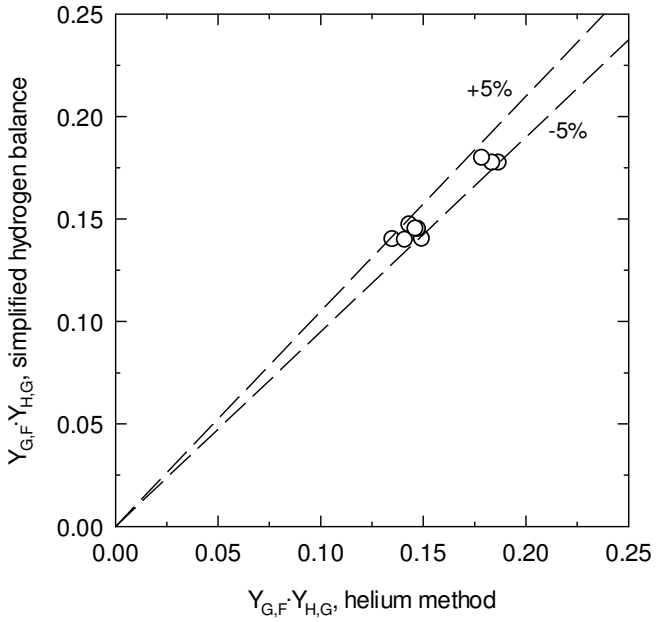

Figure 3.6 - Comparison of the simplified hydrogen balance across the gasifier (Eq. 3.17) and the measurements obtained from the combustion experiments with raw gas (see section 3.4.3).

3.5 *Results and discussion*

3.5.1 *Sensitivity analysis*

A sensitivity analysis to the general setup in Figure 3.5-b is carried out, whereby the influence of the measurement uncertainties on the solution of Eq. (3.9) is shown. This is illustrated by considering a typical composition of raw gas from a DFB gasifier (e.g., 20% C, 10% H, 65% O and 5% N, mass %) and assuming a value for the flow rate of helium mixed with the fluidizing steam. The theoretical composition of the flue gases leaving the small combustor is calculated from Eq. (3.2) considering that the raw gas burns under 100% excess air, and is taken as Case A in the analysis. Then, it is investigated how the predicted CHON contents of the raw gas vary when the measurement parameters are varied in 2% of Case A (Figure 3.7). Cases B to F test the influence of an uncertainty in the composition of the combustion flue gases, respectively for the concentrations of H_2O, CO_2, O_2, N_2 and He. Cases G and H test the influence of an uncertainty in the concentrations of He and N_2 in the dry raw gas leaving the ancillary gas conditioning system, respectively. The outcome is that the new method provides stable solution for the CHON contents of raw gas, being always predicted within ±3% of Case A. For engineering applications, only the concentrations of H_2O, CO_2 and O_2 need to be measured in the flue gases as the concentration of N_2 can be approximated by difference.

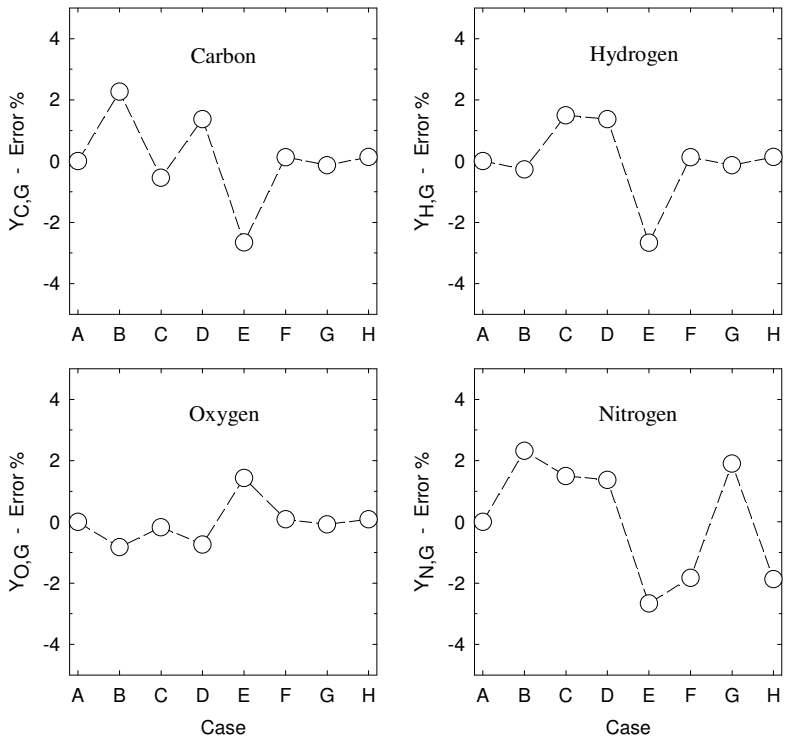

Figure 3.7 - Sensitivity analysis for the determination of CHON composition of raw gas following the setup in Figure 3.5-b.

3.5.2 *Accuracy and precision*

Table 4 shows the accuracy of the proposed method for samples of known composition. The initial testing was done with a non-combustible gas, CO_2, which was sucked into the venturi while varying the flow rate of dry air entering the pressure side. The gas stream leaving the small combustor was analysed and the elemental composition of CO_2 was recalculated from the measurements. This initial test showed that the mass fractions of carbon and oxygen could be predicted within a ±5% error, even though this error decreased to below ±1% when using high CO_2/air ratios. The tendency to over-predict the oxygen content was compatible with a ±3% error in the measured concentrations of CO_2 and O_2. Following this, the system was tested with a dry combustible gas of 43.3 %C, 5.4 %H, and 51.3 %O (mass %), that was burned under ≈50% excess air. In this case, the flue gases were analysed for CO_2, O_2, H_2O, CO and CH_4, while the N_2 was determined by difference. CO and CH_4 were found at ppm levels, indicating efficient combustion. Despite the approximation used, the CHO composition was predicted within a ±4% error and the result could be further improved by decreasing the excess air level [33]. These experimental results are clearly in line with the sensitivity analysis shown in Figure 3.7.

Table 3.4 - Results obtained using the proposed method for samples of known composition.

	Measured composition of flue gases (%v, wet basis)				CHO composition – Error %		
Sample	O_2	N_2	CO_2	H_2O	C	H	O
100% CO_2	20.1	73.7	5.3	0.0	-4.8	0.0	+1.8
100% CO_2	19.3	70.6	9.7	0.0	-2.4	0.0	+0.9
100% CO_2	19.1	70.0	10.5	0.0	-2.2	0.0	+0.8
100% CO_2	18.6	66.5	14.8	0.0	-3.4	0.0	+1.3
100% CO_2	16.5	60.3	22.1	0.0	-0.9	0.0	+0.4
100% CO_2	16.3	59.6	22.9	0.0	-1.0	0.0	+0.4
100% CO_2	16.0	58.5	24.5	0.0	-0.8	0.0	+0.3
100% CO_2	14.9	53.5	30.6	0.0	-1.2	0.0	+0.5
Combustible gas[b]	5.6	70.2[a]	13.8	10.4	+2.8	+4.1	-2.8

[a] Calculated by difference method; [b] 43.3 %C, 5.4 %H, and 51.3% O (mass %).

During the testing of the method with raw gas from the Chalmers gasifier, the operating conditions in the small combustor were widely varied without compromising the combustion efficiency. The variations included temperature within the range of 800–950ºC, flow rate of dry air within the range of 6–12 NLpm (excess air as low as 10%) and gas residence time below 0.5 s. As an example, Figure 3.8 shows a dynamic combustion experiment in which the gasifier was run under stable operation and the small combustor was operated under varying

stoichiometric conditions (time periods I to VI). Sampling of the flue gases started at minute 2, leading to a step-like increase of T5, which is the temperature at the entrance of the 160ºC heating hose. One minute later, the 360ºC line for the raw gas was intermittently connected to the venturi, which explains the peak-like behaviours of T1, P1, and $y_{H2O,E}$. This line was permanently connected to the venturi in period II, leading to prone ignition (see e.g., T1) and stable combustion. In periods II to VI, the amount of dry air entering the venturi was varied from 7 to 10 NLpm, resulting in an inverse variation of the vacuum P1. As a result, the excess air in the chamber varies inversely with the flow rate of dry air, as indicated by T1 and $y_{H2O,E}$. The two-step increase of T1 in period III was due to a slight change in the thermocouple position. In general, a more stable combustion was achieved by increasing the vacuum in the venturi.

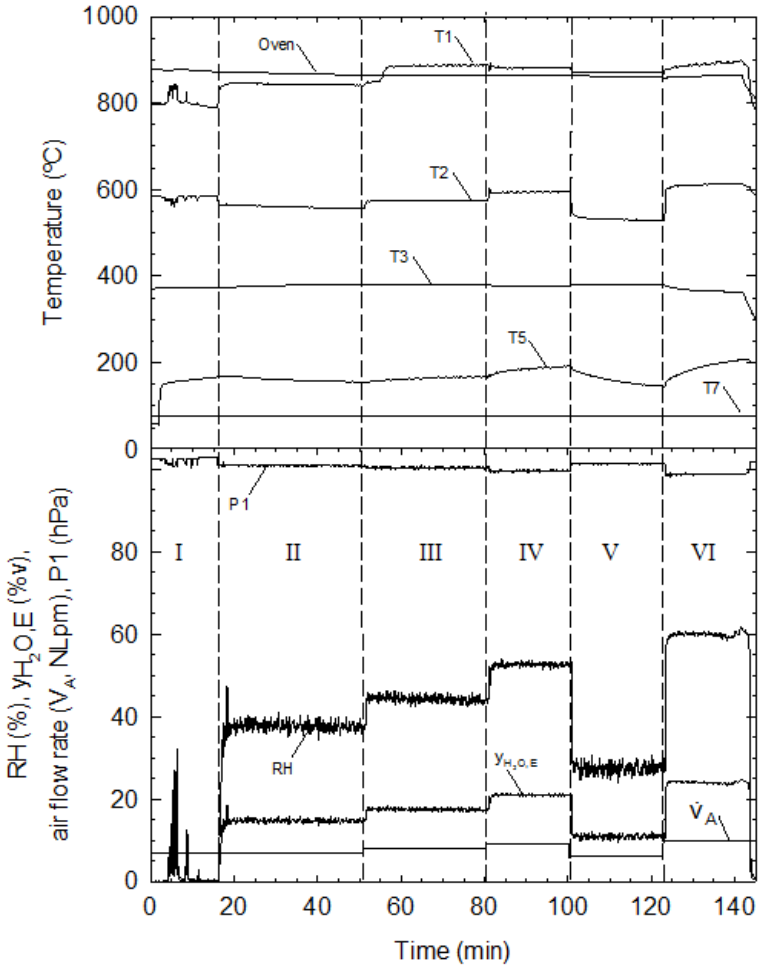

Figure 3.8 - Operational conditions in the online combustion facility during experiments with raw gas from the Chalmers gasifier (run #1). The average compositions of the flue gases are shown in Table 3.5. The temperature and pressure taps are according to Figure 3.3.

The average compositions of the flue gases in periods II to VI are given in Table 3.5. Once again, CO and CH_4 were found at ppm levels, verifying efficient combustion. Although the

level of excess air varied widely in periods II to VI, the measured H/C ratio of the raw gas was stable (≈0.45 kg/kg), which shows that the method is reliable. By the end of period VI, the heating elements (e.g., oven) were turned off and the line for the raw gas was disconnected from the venturi. Ambient air was then sucked into the combustor, resulting in a step-like decrease in the response of the humidity cell.

Table 3.5 - Average composition of the combustion flue gases in the experiment shown in Figure 3.8.

Variable / Period	II	III	IV	V	VI
$\dot{V}_A$ (NLpm)	7.0	8.0	9.0	6.0	10.0
$y_{O2,E}$ (%v, wet gas)[a,c]	11.1	9.5	7.7	13.0	5.9
$y_{CO2,E}$ (%v, wet gas) [a,c]	5.4	6.4	7.8	4.2	8.9
$y_{H2O,E}$ (%v, wet gas)[b,c]	14.8	17.5	20.9	10.9	24.0
$Y_{H,G}$ / $Y_{C,G}$ (kg H/kg C)[d]	0.46	0.45	0.45	0.44	0.45

[a] Measured by the multi-component gas analyser; [b] Measured by the moisture measurement system; [c] Balance to 100%v is N_2 and He as given by GC-TCD analysis; [d] Approximated from the H/C mass ratio of the flue gases.

3.5.3 *Application in monitoring of Chalmers DFB gasifier*

To evaluate the operation of the Chalmers gasifier one turns to the zero-dimensional model described in Section 3.3. Apart from the CHON contents of the pellets and pyrolytic char (Table 3.2), the inflows of pyrolytic char ($Y_{ch,F}$), unburnt char ($Y_{ch1,F}$), and purge gas ($Y_{P,F}$) are inputs to this model and are evaluated below.

Figure 3.9 shows the yield of pyrolytic char arising from the wood pellets as a function of peak temperature and heating rate of fuel. The data relative to fast heating show that the yield of char is roughly constant under temperatures typical of DFB gasification and, in comparison to the results obtained with the thermobalance, it is seen that a one-fold variation in the heating rate of fuel has also a small effect. Thus, given the narrow range of gasification conditions tested in the present work (Table 3.3), the amount of pyrolytic char formed inside the Chalmers gasifier is estimated within 16–18% of the daf fuel feed.

The unburnt char emerging from the boiler was estimated in previous work in the Chalmers gasifier where a crude estimate based on the operation of the gasifier without fuel feeding is that $Y_{ch1,F} \approx 0.15$ [39]; though a more recent analysis of the incoming bed material indicates that this value is one-fold lower.

The flow rate of purge gas used in the fuel feeding system of the gasifier can be evaluated based on the quantity of nitrogen leaving with the raw gas. The latter was found to be stable during runs #1 to #6 with values in range of 0.033–0.041 kg N/kg F (see Section 3.4.1.1 for method). Since the chars represent minor contributions to the total quantity of nitrogen

across the DFB gasifier, the respective nitrogen balance (Eq. 3.12) can be simplified into Eq. (3.18). The nitrogen content of the purge gas ($Y_{N,P}$) was about 0.73 kgN/kgP and thus, $Y_{P,F}$ was estimated as being 0.045–0.056 kg P/kg F throughout the gasification experiments.

$$Y_{P,F} \cdot Y_{N,P} \approx Y_{G,F} \cdot Y_{N,G} - Y_{N,F} \qquad \text{Eq. 3.18}$$

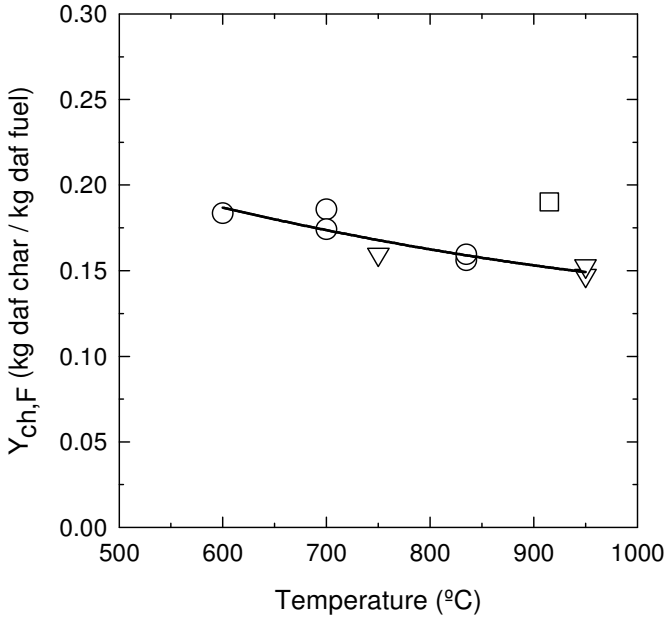

Figure 3.9 - Yield of pyrolytic char ($Y_{ch,F}$) for the wood pellets as a function of reactor peak temperature in experiments carried out under an inert atmosphere. Symbols used: ○, fast pyrolysis in the FB reactor; ∇, fast pyrolysis in the quartz-tube reactor; □, slow pyrolysis in the thermobalance (50ºC/min). The solid line represents the trend for the fast pyrolysis conditions.

3.5.3.1 *Degree of fuel conversion (runs #1 to #4)*

The experimental H/C and O/C mass ratios of the raw gas are provided in Figure 3.10, which also shows the theoretical pyrolysis (χ=0) and gasification (χ=1) ratios for the wood pellets; the range shown for the case of pyrolysis is due to the uncertainty in $Y_{ch,F}$, i.e., 16–18% of daf fuel. The value of $Y_{ch1,F}$ is unknown and was not accounted for in the theoretical ratios. However, it must be emphasised that $Y_{ch1,F}$ does not influence the pyrolysis lines, whereas it decreases the slopes of the gasification lines. The experimental data for runs #1 to #3 follow closely the pyrolysis line using $Y_{ch,F}$ = 0.16, which is approximately the yield of char released from the pellets under fast heating. Even if the pyrolytic char is taken as $Y_{ch,F}$ = 0.18 the char conversion in the gasifier would not exceed 10%. Thus, the measured H/C and O/C ratios indicate that the composition of the raw gas is closely given by the CHO contents of the pyrolytic volatiles together with the steam added to the gasifier. Moreover, for a bed

temperature of 830ºC, variation of the steam-fuel ratio between 0.7 and 1.1 kg/kg does not significantly alter this behaviour. A decrease in the gasification temperature in run #4 (775ºC) yielded a raw gas with slightly higher H/C and O/C ratios, indicating that a smaller fraction of the fuel carbon is converted into gaseous fuel. This can be explained by the more favourable charring conditions in run #4, i.e., the lower peak temperature attained by the pellets [32]. To fit the H/C and O/C ratios in run #4, an additional 2–3% char shall be formed at 775ºC relative to 830ºC (runs #1 to #3), which is roughly in line with the measurement uncertainties shown in Figure 3.9.

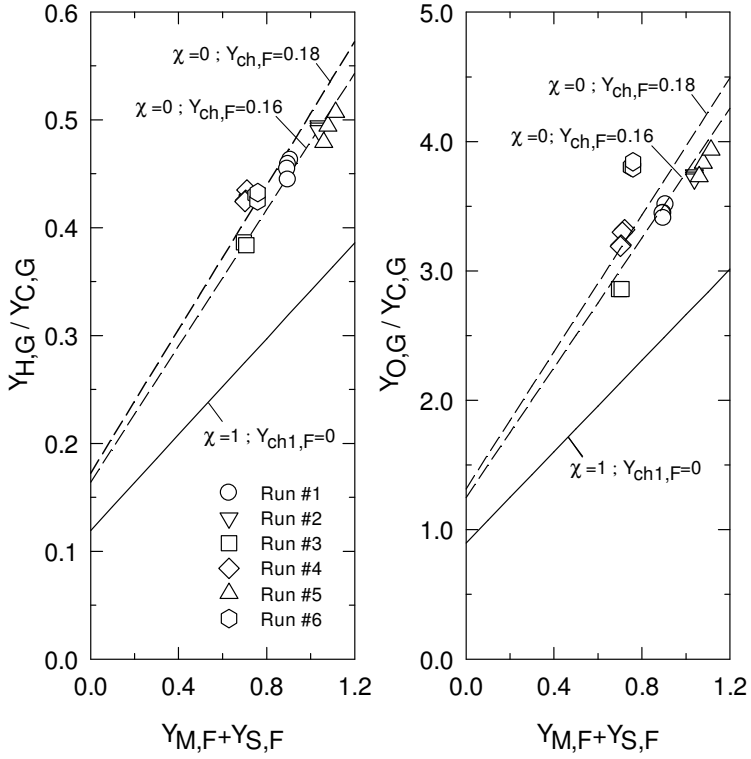

Figure 3.10 - H/C and O/C mass ratios of raw gas from the Chalmers gasifier as a function of the steam-fuel ratio. The lines represent the theoretical pyrolysis (χ=0, dashed) and gasification (χ=1, solid) ratios according to Eq. 3.11 and Eq. 3.16.

The other way to examine the degree of fuel conversion is through the elemental balances across the gasifier (Eq. 3.12). However, since the balances for hydrogen and nitrogen can be simplified into Eqs. (3.17) and (3.18), respectively, the operational parameter $Y_{ch2,F}$ - $Y_{ch1,F}$ defined in Eq. (3.13) is approximated from the carbon and oxygen balances. These are provided in Figure 3.11 as a function of the steam-fuel ratio.It is clear that in runs that use 100% sand the difference between the amounts j^{th} element in ch2 and ch1 is closely given by the amount of j^{th} element being supplied with the pyrolytic char arising from the pellets. For instance, in runs #1 to #3, the carbon leaving with ch2 minus the carbon entering with ch1 is within the range of 0.14–0.16 kgC/kgF, whereas with respect to the oxygen this

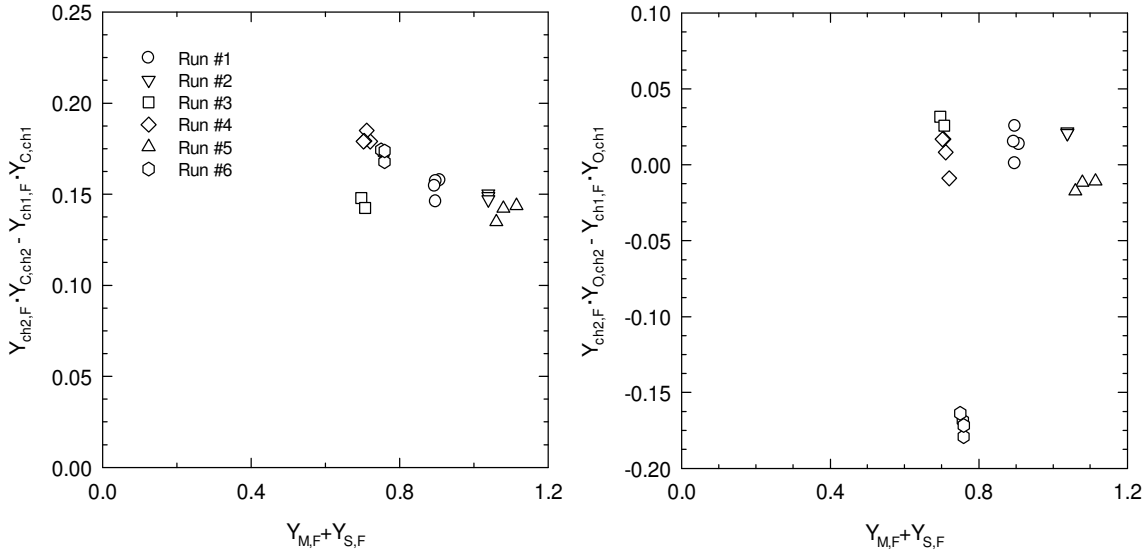

Figure 3.11 - Carbon and oxygen mass balances across the Chalmers gasifier as a function of the steam-fuel ratio. The quantities of carbon or oxygen entering the gasifier with fuel, steam, and purge gas minus the respective quantities leaving with the raw gas are indicated (see Eq. 3.12).

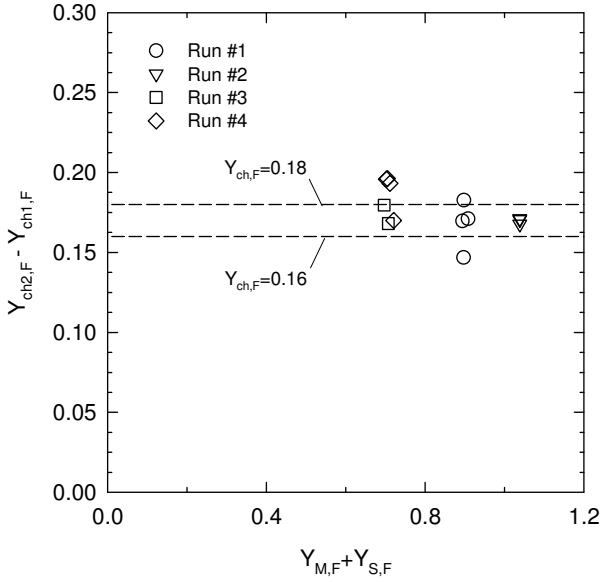

Figure 3.12 - Differences in the quantities of char moving out and into the Chalmers gasifier (see Eq. 3.13) as a function of the steam-fuel ratio. Char entering is unburnt char from the boiler ($Y_{ch1,F}$) and char leaving is unconverted char from the gasifier ($Y_{ch2,F}$). The dashed lines indicate the range for the yield of pyrolytic char supplied by the pellets ($Y_{ch,F}$).

difference is within about 0–0.03 kgO/kg F; the corresponding amounts of carbon and oxygen supplied with the pyrolytic char were estimated as ≈0.15 kgC/kgF and ≈0.01 kgO/kgF, respectively (Figure 3.9 and Table 3.2), which are in the range of the values obtained from the elemental balances across the gasifier. This further confirms that the amount of char escaping the gasifier is approximately given by the amount of unburnt char coming from the boiler

plus the pyrolytic char arising from the pellets, i.e., $Y_{ch2,F}$ - $Y_{ch1,F}$ ≈ $Y_{ch,F}$, as shown in Figure 3.12.

3.5.3.2 *Composition of the escaping char (runs #1 to #4)*

According to Section 3.3.2, the carbon and oxygen contents of the escaping char (ch2) can also be estimated from the material balances across the gasifier (Figs. 3.11 and 3.12). With respect to the gasification experiments conducted at 830ºC (runs #1 to #3), a minimum carbon content for the escaping char of 89±5% and maximum oxygen content of 11±5% (mass% of ch2) were obtained. The respective values at 775ºC (run #4) were 93±2% carbon and 7±2% oxygen, which are within the range of the values at 830ºC. The influence of the steam-fuel ratio was also negligible. It is clear that the balances across the gasifier provide results for the elemental composition of the escaping char that are in good agreement with the values obtained by standard ultimate analysis of the pyrolytic char arising from the wood pellets (Table 3.2).

3.5.3.3 *Effect of blending ilmenite with the bed material (runs #5 and #6)*

The effect of ilmenite addition on the CHON composition of the raw gas is shown in Figure 3.10. For instance, the utilisation of 12% ilmenite in run #6 led to a much higher O/C ratio of raw gas than in experiments that used 100% sand (i.e., runs #1 to #3 at ≈830ºC). However, unlike the O/C ratio, the H/C ratio for ilmenite in the bed was roughly in the range of the values obtained with 100% sand, which clearly indicates selective oxygen transport by ilmenite. The experiments using ilmenite gave negative values for the oxygen balance across the gasifier (Figure 3.11), since the release of oxygen during the reduction stage of the metal oxide is not accounted for in Eq. (3.12). For instance, the average value of the oxygen balance in the case of 12% ilmenite was -0.17 kgO/kgF, and this included both the oxygen supplied with the ilmenite and pyrolytic char. Therefore, this quantity shall be recalculated by comparison with experiments that used 100% sand, where the oxygen balance was ≈0.02 kgO/kgF. The outcome is that the oxygen entering the gasifier with ilmenite in run #6 is about 0.19 kgO*/kgF. During this process, a small quantity of carbon is likely to form over the surface of the reduced ilmenite, as indicated by the slightly higher values for the carbon balance in run #6 relative to runs #1 to #3 (Figure 3.11). Nevertheless, the effect is small, which is in line with dedicated investigations [34-36] of iron-based catalysts. The effect of ilmenite on the composition of the raw gas is also seen in run #5, although it is difficult to quantify due to the low concentration of ilmenite.

The oxygen transported *per* unit mass of fresh ilmenite can be estimated from the circulation rate of the bed material between the interconnected FB reactors, i.e. 14000–

25000 kg bed/h, and the concentration of ilmenite used in the experiments (Table 3.3). Following this, a crude estimate of the mass ratio of ilmenite to daf fuel feed in run #6 was 4.7–8.3 kg/kg F. With a value for the oxygen entering the gasifier of 0.19 kgO^*/kgF, the oxygen transport capacity of fresh ilmenite is estimated as ≈2–4% (mass %), which is in agreement with the results from reduction/oxidation experiments described in the literature [41-43].

3.5.3.4 *Amounts of condensable organics and steam in the raw gas (run #6)*

One combustion experiment was done during run #6, whereby the amounts of carbon and hydrogen leaving the gasifier with the raw gas and the respective dry raw gas were related to the unit mass of helium fed to the gasifier (see setup in Figure 3.5-c). The results from this experiment are provided in Table 3.6.

The initial result was that ≈8% of the total carbon in the raw gas was removed by cold-trapping, which represents less than 2% of the whole raw gas (mass %). According to the terminology used in this work, the whole condensing carbon is ascribed to lumped tar (see Figure 3.1). The tar content of raw gas is higher than that of tar-bound carbon, since lumped tar is highly oxygenated [20, 21]. Literature data reveals that the carbon content of tar is frequently within a range defined by the carbon content of fuel multiplied by a factor of 1.0 to 1.3 [32]. Thus, after the carbon removed by cold trapping has been measured by the method outlined above, the plausible range for the amount of tar leaving the Chalmers gasifier is estimated at between 4 and 6% of the daf fuel feed (mass %), which corresponds to roughly 50–80 g/Nm^3 of dry raw gas. Despite the widely varying tar measurement methods currently in use (see Section 3.2.1), this result is comparable to literature values for FB steam gasifiers, where the crude range is 1–50 g/Nm^3 (often <10g/Nm^3 when using a catalyst) for DFB gasifiers and up to 100 g/Nm^3 for other types of FB gasifiers [2, 16].

Also noteworthy is the massive quantity of hydrogen that is separated upon cooling of the raw gas: ≈75% of the total hydrogen in the raw gas (Table 3.6). The major part of the condensing hydrogen is likely due to steam. This can be evaluated from the yield of tar given above and the typical hydrogen content of pyrolytic tar [32]; it follows that tar-bound hydrogen is likely to be less than 5% of the total mass of condensing hydrogen. Thus, if all the condensing hydrogen is attributed to steam, a crude approximation of the steam that leaves the gasifier in run #6 is about 0.99 kg steam/kg F, which is greater than the amount of steam added to the gasifier via the fluidising agent and fuel moisture (≈0.75 kg/kg, Table 3.3). However, two additional sources of steam must be accounted for in run #6. These include the pyrolytic water formed from the converting pellets (up to 0.2 kg/kg daf fuel [32]) and the water formed from the oxygen added with the ilmenite and purge gas (up to 0.22 kg/kg daf fuel if all the incoming oxygen yield water). These additional sources of steam can easily

offset the steam consumed during the gas-phase reforming of the volatiles (e.g., the water-gas shift reaction), and can play a decisive role in relation to the large amount of steam leaving the gasifier during run #6.

Table 3.6 - Characteristics of the raw gas and respective dry gas from the Chalmers gasifier (run #6).

Parameter	Raw gas	Dry gas	Tar + water
kg H/kg C	0.43	0.12	--
kg C/kg F[a]	0.34	0.31	0.03
kg H/kg F[a]	0.15	0.04	0.11

[a] Mass of element leaving the DFB gasifier with the raw gas or the respective dry gas *per* unit mass of dry ash-free fuel feed (F).

3.6 *Conclusions*

For convenience and for economic reasons, current methods used to determine the CHON composition of raw gas from biomass gasifiers need to be simplified. With this in mind, a method was developed in which the raw gas is converted into CO_2, H_2O, and N_2 in a small combustor before the analysis of the CHON composition is undertaken. Based on our evaluation of the method with standard gases combined with a sensitivity analysis, the error in the CHON mass fraction of raw gas can be reduced to ±3% through appropriate adjustment of the excess air condition. The results of the combustion experiments with raw gas further underline the reliability of the method. A recently developed moisture measurement system [37] coupled with IR gas analysers enables real-time monitoring of the H/C ratio of raw gas, while the respective CHON composition can be resolved by GC analysis with a measurement time of 3 minutes.

In combination with mass balance reactor model, the new method provides simple routes to evaluate the operation of biomass gasifiers. The straightforward way to monitor the degrees of fuel and char gasification is to analyse the H/C ratio of the raw gas. An alternative approach is to establish the elemental balances across the gasifier once the CHON composition and flow rate of the raw gas have been measured. Detection and quantification of oxygen transport by in-bed catalyst is also shown to be feasible, as evidenced by the higher O/C mass ratio of the raw gas and the oxygen balance across the gasifier. An estimate of the amount of condensables leaving the gasifier is possible by analysing both the raw gas and the respective dry gas.

The proposed method can be applied to determine the CHON composition of raw gas from any gasifier. In the present work, it was applied to the Chalmers gasifier and the outcomes of these experiments lead to the following conclusions: (1) the fuel is completely devolatilised in the gasifier but char gasification is limited; (2) char gasification is not

significantly influenced by the steam-fuel ratio, which means that the primary pyrolysis and gas-phase reactions of the volatiles are the main processes occurring in the gasifier; (3) char gasification (including plausible mass transport effects) is rate-determining when compared to fuel devolatilisation and solid mixing in the bed; and (4) blending ilmenite in the circulating bed material provides a large quantity of oxygen into the gasifier without inherent dilution of the raw gas by nitrogen.

Nomenclature

$Y_{i,F}$	Mass of i^{th} stream *per* unit mass of dry ash-free fuel, kg i/kg F
$Y_{j,i}$	Mass fraction of j^{th} chemical element in i^{th} stream, kg j/kg i
$Y_{k,i}$	Mass fraction of k^{th} chemical species in i^{th} stream, kg k/kg i
$Y_{j,k}$	Mass fraction of j^{th} chemical element in k^{th} chemical species, kg j/kg k
$y_{k,i}$	Molar fraction of k^{th} species in i^{th} stream, kmole k/ kmole i
$\nu_{G,A}$	Stoichiometric coefficient in Eq. 3.2, mass of raw gas *per* unit mass of dry air, kg G/kg A
$\nu_{k,A}$	Stoichiometric coefficient in Eq. 3.2, mass of k^{th} species *per* unit mass of dry air, kg k/kg A
χ	Degree of conversion of incoming char, dimensionless
RH	Relative humidity of the wet flue gases leaving the small combustor, %
$\dot{n}_i$	Molar flow rate of i^{th} stream, kmol i/s
M_k	Molar mass of k^{th} chemical species, kg k/kmol k
M_j	Molar mass of j^{th} chemical element, kg j/kmol k
$\dot{v}_i$	Volume flow rate of i^{th} stream, NLpm

Subscripts

i	i^{th} stream (As, B, ch, ch1, ch2, F, G, E, A, P, M, S, O*)
k	k^{th} chemical species (CO_2, CO, H_2, N_2, CH_4, C_xH_y, H_2O, tar, soot, Ar, O_2, He)
j	j^{th} chemical element (C, H, O, N)
As	Ash

B Bed material

ch Pyrolytic char resulting from the pyrolysis of fresh fuel within the gasifier, daf

ch1 Unburnt char transported from the boiler into the gasifier, daf

ch2 Unconverted char leaving the gasifier towards the boiler, daf

F Biomass fed to the gasifier, daf

G Raw gas from the biomass gasifier

E Wet flue gases leaving the small combustor

A Dry atmospheric air

P Purge gas (dry flue gases from FB boiler)

M Fuel moisture

S Fluidising steam (excluding moisture)

O* Oxygen transport by catalytic material to the gasifier

Abbreviations

daf Dry ash-free basis

Db Dry basis

arb As-received basis

Acknowledgements

The financial support provided by the Fundação para a Ciência e a Tecnologia (FCT), Portugal, through PhD grant SFRH/BD/39567/2007 and research project PTDC/AAC-AMB/098112/2008 (Bias-to-soil), and the Swedish Energy Agency, is acknowledged. The operation of the gasifier was performed through the co-operation of Akademiska Hus, Göteborg Energi, Metso Power, and the Swedish National Gasification Centre (SFC).

References

1. Knoef H. Handbook on biomass gasification. Biomass Technology Group (BTG). Enschede, The Netherlands: GasNet; 2005.

2. Corella J, Toledo JM, Molina G. A review on dual fluidized-bed biomass gasifiers. Ind Eng Chem Res. 2007;46:6831-9.
3. Goransson K, Soderlind U, He J, Zhang WN. Review of syngas production via biomass DFBGs. Renew Sust Energ Rev. 2011;15:482-92.
4. Pfeifer C, Koppatz S, Hofbauer H. Steam gasification of various feedstocks at a dual fluidised bed gasifier: Impacts of operation conditions and bed materials Biomass Conversion and Biorefinery 2011;1:39-53.
5. Levenspiel O. What will come after petroleum? Ind Eng Chem Res. 2005;44:5073-8.
6. Hofbauer H, Rauch R, Löffler G, Kaiser S, Fercher E, Tremmel H. Six years experience with the FICFB-gasification process. 12th European Conference and Technology Exhibition on Biomass for Energy, Industry and Climate Protection. Amsterdam, The Nederlands2002. p. 982-5.
7. Hofbauer H, Rauch R. Stoichiometric water consumption of steam gasification by the FICFB-gasification process. In: Bridgwater AVE, Blackwell Science, Ltd., editor. Thermochemical Biomass Conversion, Proceedings of the International Conference, Innsbruck, Austria, 2000. London2001. p. 99-208.
8. Thunman H, Åmand L-E, Leckner B. A cost effective concept for generation of heat, electricity and transport fuel from biomass in fluidized bed boilers – using existing energy infrastructure. 15th European Biomass Conference & Exhibition. Berlin, Germany2007.
9. Seemann MC, Thunman H. The new Chalmers research-gasifier. Proceedings of the International Conference on Polygeneration Strategies. Wien, Austria2009.
10. Good J, Ventress L, Knoef H, Zielke U, Hansen PL, van de Kamp W, et al. Sampling and analysis of tar and particles in biomass producer gases – Technical report. CEN BT/TF 143 "Organic Contaminants ("Tar") in Biomass Producer Gases". 2005.
11. Simell P, Stahlberg P, Kurkela E, Albrecht J, Deutsch S, Sjostrom K. Provisional protocol for the sampling and anlaysis of tar and particulates in the gas from large-scale biomass gasifiers. Version 1998. Biomass Bioenerg. 2000;18:19-38.
12. Brage C, Yu QZ, Chen GX, Sjostrom K. Use of amino phase adsorbent for biomass tar sampling and separation. Fuel. 1997;76:137-42.
13. Hasler P, Nussbaumer T. Sampling and analysis of particles and tars from biomass gasifiers. Biomass Bioenerg. 2000;18:61-6.
14. Oasmaa A, Peacocke C. A guide to physical property characterization of biomass-derived fast pyrolysis liquids. Espoo, Finland: Technical Research Centre of Finland 2001.

15. Devi L, Ptasinski KJ, Janssen FJJG. A review of the primary measures for tar elimination in biomass gasification processes. Biomass Bioenerg. 2003;24:125-40.
16. Milne TA, Evans RJ, Abatzoglou N. Biomass gasifier "tars": their nature, formation and conversion. Colorado, U.S.: National Renewable Energy Laboratory; 1998.
17. Lewis J, Marsh R, Sevcenco Y, Morris S, Griffiths A, Bowen P. The effect of variable fuel composition on a swirl-stabilised producer gas combustor. Energy Conversion and Management. 2012;64:52-61.
18. Al-attab KA, Zainal ZA. Design and performance of a pressurized cyclone combustor (PCC) for high and low heating value gas combustion. Applied Energy. 2011;88:1084-95.
19. Branca C, Blasi CD, Elefante R. Devolatilization and Heterogeneous Combustion of Wood Fast Pyrolysis Oils. Ind Eng Chem Res. 2005;44:799-810.
20. Elliott DC. Relation of Reaction-Time and Temperature to Chemical-Composition of Pyrolysis Oils. Acs Sym Ser. 1988;376:55-65.
21. Evans RJ, Milne TA. Molecular Characterization of the Pyrolysis of Biomass .1. Fundamentals. Energ Fuel. 1987;1:123-37.
22. Font Palma C. Modelling of tar formation and evolution for biomass gasification: A review. Applied Energy. 2013;111:129-41.
23. Coda B, Zielke U, Suomalainen M, Knoef HAM, al. e. Tar measurement standard: a joint effort for the standardization of a method for measurement of tars and particulates in biomass producer gas. Proceedings of the 2nd World Biomass Conference. Italy2004.
24. Eugene F. Barry PD, Robert L. Grob PD. Columns for Gas Chromatography: Performance and Selection: John Wiley & Sons; 2007.
25. Brage C, Yu QZ, Chen GX, Sjostrom K. Tar evolution profiles obtained from gasification of biomass and coal. Biomass Bioenerg. 2000;18:87-91.
26. Dufour A, Girods P, Ravel S, Bernard C, Lédé J, Rogaume Y, et al. A new analytical method to quantify tar at very low concentration ranges (0.01 to 100 mg/Nm3). 17th European Biomass Conference & Exhibition. Hamburg, Germany2009.
27. Meng XM, Mitsakis P, Mayerhofer M, de Jong W, Gaderer M, Verkooijen AHM, et al. Tar formation in a steam-O2 blown CFB gasifier and a steam blown PBFB gasifier (BabyHPR): Comparison between different on-line measurement techniques and the off-line SPA sampling and analysis method. Fuel Process Technol. 2012;100:16-29.
28. Moersch O, Spliethoff H, Hein KRG. Tar quantification with a new online analyzing method. Biomass Bioenerg. 2000;18:79-86.

29. Knoef HAM, van de Beld L, Ahmadi M, Sjöstrom K, Brage C, Liliedahl T. Development of an online tar measuring method for quantitative analysis of biomass producer gas. Proceedings of the 17th European Biomass Conference & Exhibition. Hamburg, Germany2009. p. 884-8.
30. Carpenter DL, Deutch SP, French RJ. Quantitative Measurement of Biomass Gasifier Tars Using a Molecular-Beam Mass Spectrometer: Comparison with Traditional Impinger Sampling. Energ Fuel. 2007;21:3036-43.
31. Karellas S, Karl J. Analysis of the product gas from biomass gasification by means of laser spectroscopy. Optics and Lasers in Engineering. 2007;45:935-46.
32. Neves D, Thunman H, Matos A, Tarelho L, Gomez-Barea A. Characterization and prediction of biomass pyrolysis products. Prog Energ Combust. 2011;37:611-30.
33. Neves D, Thunman H, Tarelho L, Larsson A, Seemann M, Matos A. On-line measurement of raw gas elemental composition in fluidized bed biomass steam gasification. World Bioenergy 2012 Conference & Exhibition on Biomass for Energy. Jönköping, Sweden2012.
34. Cho P, Mattisson T, Lyngfelt A. Carbon formation on nickel and iron oxide-containing oxygen carriers for chemical-looping combustion. Ind Eng Chem Res. 2005;44:668-76.
35. Mendiara T, Johansen JM, Utrilla R, Geraldo P, Jensen AD, Glarborg P. Evaluation of different oxygen carriers for biomass tar reforming (I): Carbon deposition in experiments with toluene. Fuel. 2011;90:1049-60.
36. Mendiara T, Johansen JM, Utrilla R, Jensen AD, Glarborg P. Evaluation of different oxygen carriers for biomass tar reforming (II): Carbon deposition in experiments with methane and other gases. Fuel. 2011;90:1370-82.
37. Hermansson S, Lind F, Thunman H. On-line monitoring of fuel moisture-content in biomass-fired furnaces by measuring relative humidity of the flue gases. Chem Eng Res Des. 2011;89:2470-6.
38. Larsson A, Seeman M, Thunman H. Assessment of mass and energy flows in the Chalmers gasifier. Sweden: Department of Energy and Environment, Chalmers University of Technology; 2011.
39. Larsson A, Thunman H, Neves D, Pallarés D, Seemann M. Zero-dimensional modeling of indirect fluidized bed gasification. Proceedings of the XIII Fluidization Conference. Gyeong-ju, Korea2010.
40. Edvardsson E, Åmand LE, Thunman H, Leckner B, Johnsson F. Measuring the External Solids Flux in a CFB boiler. Proceedings of the 19th International Conference on Fluidized Bed Combustion. Viena (Austria)2006.

41. Leion H, Lyngfelt A, Johansson M, Jerndal E, Mattisson T. The use of ilmenite as an oxygen carrier in chemical-looping combustion. Chem Eng Res Des. 2008;86:1017-26.
42. Cuadrat A, Abad A, Garcia-Labiano F, Gayan P, de Diego LF, Adanez J. Ilmenite as oxygen carrier in a Chemical Looping Combustion system with coal. Enrgy Proced. 2011;4:362-9.
43. Bidwe AR, Mayer F, Hawthorne C, Charitos A, Schuster A, Scheffknecht G. Use of ilmenite as an oxygen carrier in Chemical Looping Combustion-Batch and continuous dual fluidized bed investigation. Enrgy Proced. 2011;4:433-40.

Chapter 4 - Characterization and prediction of biomass pyrolysis products

Daniel Neves[a,b], Henrik Thunman[b], Arlindo Matos[a], Luís Tarelho[a], Alberto Gómez-Barea[c]
[a]University of Aveiro and CESAM, [b]Chalmers University of Technology, [c]University of Seville
Published in Progress in Energy and Combustion Science, 2011, 37, 611-20.

Abstract

In this study some literature data on the pyrolysis characteristics of biomass under inert atmosphere were structured and analyzed, constituting a guide to the conversion behavior of a fuel particle within the temperature range of 200-1000ºC. Data is presented for both pyrolytic product distribution (yields of char, total liquids, water, total gas and individual gas species) and properties (elemental composition and heating value) showing clear dependencies on peak temperature. Empirical relationships are derived from the collected data, over a wide range of pyrolysis conditions and considering a variety of fuels, including relations between the yields of gas-phase volatiles and thermochemical properties of char, tar and gas. An empirical model for the stoichiometry of biomass pyrolysis is presented, where empirical parameters are introduced to close the conservation equations describing the process. The composition of pyrolytic volatiles is described by means of a relevant number of species: H_2O, tar, CO_2, CO, H_2, CH_4 and other light hydrocarbons. The model is here primarily used as a tool in the analysis of the general trends of biomass pyrolysis, enabling also to verify the consistency of the collected data. Comparison of model results with the literature data shows that the information on product properties is well correlated with the one on product distribution. The prediction capability of the model is briefly addressed, with the results showing that the yields of volatiles released from a specific biomass are predicted with a reasonable accuracy. Particle models of the type presented in this study can be useful as a submodel in comprehensive reactor models simulating pyrolysis, gasification or combustion processes.

Keyword

Biomass, Volatiles, Char, Pyrolysis, Gasification, Combustion, Model, Review

4.1 *Introduction*

Biomass is a solid fuel which, in relation to coal, has high moisture and volatile content. Therefore, when the parent solid is heated, most of its mass is released as a result of drying and pyrolysis, making the description of both processes of paramount importance during the thermochemical conversion of biomass fuels. The description of the pyrolysis process is particularly challenging because it evolves a great deal of physical and chemical transformations and produces a large number of product species. As a result, existing models aiming to predict the rates or yields of the released pyrolytic volatiles are still supported by empirical data (e.g. [1]).

The yield and composition of volatiles leaving the fuel particle surface can be considered independent of the composition of the surroundings, provided that there is enough high outflow of volatiles to prevent the surrounding gas to be transported to the fuel particle. These volatiles can be characterized through dedicated experiments, where a specific biomass fuel is pyrolysed under inert atmosphere. Because there isn't further interaction of volatiles with steam, air, etc., this experimental information can be scaled-up to different situations, including pyrolysis, gasification and combustion applications. Consequently, structuring the existing literature data on biomass pyrolysis is useful to empirically describe the quantities of pyrolytic products released from specific fuels under various operating conditions.

Much work has been published on biomass pyrolysis, regarding models, mechanisms, kinetics and product distribution. Different rigs have been used and the operating conditions, fuel type, methodologies and measurements have varied widely among investigations. There is much reported data on the yields of main products (char, total liquids and total gas) and also of individual species. Product property data, such as proximate and elemental compositions and heating value, are also found in the literature. Some information on product yields and properties, resulting from pyrolysis experiments under inert atmosphere, has been structured [2]; the analysis of this data shows that, despite of the variety of biomasses, reactors, experimental conditions and methodologies, there are general trends for both product distribution and properties as a function of temperature. This general conversion behavior makes sense considering that the elemental composition of biomass fuels fits within a relatively narrow range (perhaps,40-60% carbon, 30-50%oxygen and 5-8%hydrogen, mass % of dry ash-free fuel). However, the chemical elements are bound in the fuel in the form of various chemical structures (for instance, cellulose, lignin and hemicellulose) that are present in variable quantities in different fuels [4]. Since each of these chemical structures has its own

pyrolysis behavior, the composition of volatiles for a particular fuel is a combination of the volatiles resulting from the conversion of the individual chemical structures [3,4].

The results of Neves et al. [2] suggest that empirical relationships can be developed to approximate the pyrolysis behavior of most biomasses. Moreover, the literature data structured by the authors is related to a wide range of operating conditions, being therefore useful to various thermochemical applications. Therefore, models aiming at predicting product yields over a wide range of operating conditions can be developed if, in addition to energy and elemental balances to the pyrolysis process, experimentally-based closure relationships are derived from the database. The model of Thunman et al. [5] is an example of this type of particle model, where the overall energy and elemental mass balances were used with two additional empirical relationships, forming a system of six equations to predict the yields of six volatile species. By doing so, the conversion of the fuel particle is treated as a black-box since the complex processes occurring while it undergoes pyrolysis are not considered. Only the final stoichiometry of the pyrolysis process is predicted, being the empirical parameters used in the model to solve the composition of volatiles in a relevant number of species. However, the parameters used in [5] were derived from a particular set of experimental data and have a restricted range of validity. These simplified particle models are useful because it can be readily used in a comprehensive reactor model [6], although one would desire to be supported by more general empirical relationships.

The aim of this study is to provide a guide on the pyrolysis characteristics of biomass, covering conditions typically found in pyrolysis (400-700ºC), gasification (700-900ºC) and combustion (800-950ºC), which can be useful for engineering applications. To achieve it, a great deal of pyrolysis data were screened and structured. The collected data are concerned with the overall stoichiometry of the pyrolysis process (i.e. the mass balance), including the accumulated (or final) yields and also relevant thermochemical properties of pyrolytic products; the detailed mechanisms and the kinetics of biomass pyrolysis are beyond the scope of this study. Empirical relationships are derived from the collected data over the temperature range of 200-1000ºC. An empirical model is developed to describe the general trends of product distribution as a function of temperature, which is made of elemental balances, energy balance and empirical relationships. This empirical model is a way of compiling the collected experimental data in a structured tool that can be effectively used to analyze the biomass pyrolysis process. The composition of volatiles is represented by seven species (five permanent gases, tar and pyrolytic water). Comparison between model results and experimental measurements was done to show its predictive capability for specific biomass fuels.

4.2 *Biomass pyrolysis measurements*

In this section a brief analysis of the thermal conversion of solid biomass is presented, including the primary degradation of a fuel particle and the secondary reactions of volatiles, as extensive surveys of the involved physical and chemical processes, mechanisms, kinetics and models are already available [6-13]. Despite of this, the proposed analysis is here useful for a better understanding of the pyrolysis behavior of biomass feedstocks, as discussed later in this study based on the collected literature data. The experimental analysis of biomass pyrolysis is here emphasized, including a discussion of the influence of the operating conditions on the observed yields of pyrolytic products (section 4.2.2) and a overview of experimental methods commonly used in biomass pyrolysis measurements (section 4.2.3).

4.2.1 *Thermal degradation of solid biomass*

Biomass pyrolysis is induced by the heat transported from the surrounding gas to the fuel particle, causing it to thermal decompose into a huge number of products. Figure 4.1 illustrates the processes occurring after introducing a wet solid fuel particle in a hot environment. During transient heating of the particle, temperature increases locally, leading first to the evaporation of moisture (drying stage) and then to the progressive release of pyrolytic volatiles (primary pyrolysis stage). The primary volatiles (denoted by "1" in Figure 4.1) are produced from the thermal scission of chemical bonds in the individual constituents of biomass, which are cellulose, hemicellulose, lignin and extractives, and comprise permanent gas species (e.g. CO_2, CO, CH_4) and condensable species at ambient conditions (several organic compounds and water). Although each of the biomass constituents decompose at faster rates in different temperature ranges, the overall primary pyrolysis stage is complete at relatively low temperatures (say, <500ºC), yielding a carbon-rich non-volatile solid that is called char or charcoal (denoted by "1" in Figure 4.1). The produced char also contain a significant part of the mineral matter originally present in the parent fuel. Nevertheless, if the fuel is converted at higher temperatures some of the primary volatiles released inside the particle can further participate in a variety of secondary reactions to form product "2" (see Figure 4.1). Serial and parallel reactions can take place, occurring either heterogeneously or homogeneously, as for example cracking, reforming, dehydration, condensation, polymerization, oxidation and gasification reactions [4,11]. The distinction between intraparticle/primary pyrolysis and extraparticle/secondary pyrolysis is not perfect as the secondary reactions of volatiles can occur both in the pores of the particles and/or in the bulk gas. Thus, the primary and secondary reactions can occur simultaneously in different parts of a fuel particle. The char resulting from the primary pyrolysis stage can also be active

during the secondary reactions, namely by catalyzing the conversion of organic vapors into light gases (cracking reactions) and secondary char (polymerization reactions). In addition, the char can itself be converted into gas species by gasification reactions with H_2O and CO_2 (just to mention the main reactants during pyrolysis experiments). However, the rates of char gasification with H_2O and CO_2 are orders of magnitude lower than those of primary pyrolysis so the conversion of char formed is limited during the release of volatiles within the particle. In comparison, the secondary conversion of the primary volatiles is a rapid process and, depending on the operational conditions of a given experiment, it can exert modest to major influence on the final composition and yields of the volatiles (see section 4.2.2). Primary fragmentation and shrinkage of the fuel particles can also occur in parallel with the described physicalchemical processes (Figure 4.1).

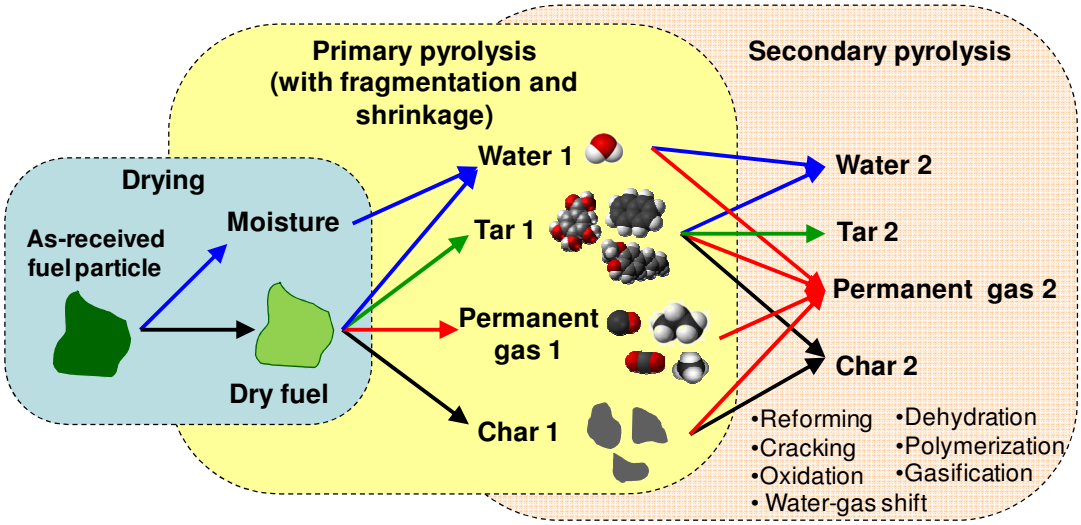

Figure 4.1 - Thermal degradation of a solid biomass particle under inert atmosphere: drying, primary pyrolysis and secondary pyrolysis. The arrows indicate the main routes for the formation of products.

The composition of pyrolytic volatiles, including the combined effect of both primary pyrolysis and secondary conversion, is here outlined by means of the following most relevant components: H_2O, CO_2, CO, H_2, CH_4, other light (non-condensable) hydrocarbons (C_xH_y) and condensable (liquids at ambient conditions) organic compounds. Condensable organics are a complex mixture containing several chemicals with a wide range of molecular weights and boiling points. For the sake of simplicity, in this study the condensable organics are conveniently lumped into a group and referred to as “tar”.

4.2.2 *Main factors governing biomass pyrolysis*

4.2.2.1 *Particle size*

Particle size has a major influence on the heating rate of solid fuel, making it an important parameter controlling the rates of drying and primary pyrolysis and to what extent these processes overlap during fuel decomposition. Because of negligible extraparticle and intraparticle heat transfer resistance, for fine particles there is a uniform heating rate, enabling the drying and primary pyrolysis to occur more or less uniformly throughout the particle, rapidly and in sequence. This enables the moisture and the primary volatiles to leave the particle with minor interaction between each other and with a hot char layer, thus limiting the extent of the secondary reactions inside the particle. However, as particle size increases the overall rate of drying and primary pyrolysis decreases. Due to non-uniform heating, both processes can happen simultaneously in different parts of the particle. Drying and primary pyrolysis fronts move in sequence, progressively from the particle outer surface (at higher temperature) towards its centre (at lower temperature). Consequently, as fuel decomposition progresses, different zones can appear within a larger fuel particle: an outer zone completely exhausted of moisture and volatiles (char layer), an intermediate zone where dry fuel reacts to yield primary volatiles, and an inner zone consisting of more or less virgin fuel and where drying occurs. Intraparticle secondary reactions involving moisture and newly formed volatiles are expected to become more significant as particle size increases. On the one hand, the species generated in the drying and primary pyrolysis fronts has to pass through an external hot char layer to leave the particle; on the other hand, the transport time of these species through the porous char structure is increased in a larger particle. This enhances the possibility of both homogeneous and heterogeneous reactions to occur inside the particle. Moreover, since the thickness of the char layer increases with time, the heterogeneous reactions of volatiles with the char surfaces might become more effective as fuel conversion proceeds in a large particle.

In fact, lower yields of liquids were measured when pyrolysing larger fuel particles [14,15], as a result of the particle size effect on the secondary reactions of volatiles. For example, Nik-Azar et al. [15] found that an increase of particle size from 53-63 mm to 270-500 mm leads to a decrease of the maximum tar yield from 53% to 38% (mass % of parent fuel). In fluidized bed experiments at 500ºC [16], the effect of particle size on the secondary conversion of tars was also suspected during pyrolysis of fine fuel particles (3-12 mm). Because below around 500ºC there is minor possibility of homogeneous tar cracking, the increased tar conversion as particle size increased can be partially attributed to the catalytic cracking in the char layer. This is supported by dedicated experiments on the cracking of

biomass derived tars [17] showing that even below 500ºC a fraction of tars is highly susceptible to char-induced cracking while being highly resistant to gas-phase cracking. Indeed, a compilation of literature data at around 500ºC [18] showed that the yield of pyrolytic water increases significantly with fuel particle size increase, being this behavior also attributed to the increased conversion of newly formed tars (i.e. dehydration) during its passage through the hot char layer formed around the larger particles, which acts as a catalyst. However, in other experiments at 400-600ºC [17,21], changes in the yield of water due to tar cracking over char surfaces were found to be of little significance.

Char-induced conversion of tars was found to produce coke (i.e. secondary char) in addition to light gases [17]. Thus, during tar release inside a larger particle, the coking can also lead to higher yields of (secondary) char. This could have occurred during fluidized bed pyrolysis of wood at 850ºC [5], where an increase of particle size from around 6 to 20 mm resulted in higher yields of char by about 6% (mass % of parent fuel).

However, product distribution was also found dependent on the heating rate of solid fuel, which, in turns, is inversely proportional to particle size. In general, fast heating rates lead to higher yields of liquids and lower yields of char [19]. For example, the increase of heating rate from 1 to 1000K/s was observed to result in higher yields of tar by about 10% (mass % of fuel) [20]. Experiments performed in a fluidized bed at 500ºC [21] confirmed the decrease in the yield of liquids when fuel particle size was increased from 0.3 to 1.5 mm. Though, this behavior was attributed to the change in heating rate between different particle sizes instead of the increased secondary conversion of volatiles (i.e. tars) as it flows through the pore structure of the larger particles. Accordingly, it was proposed that the higher heating rates favor bond-scission reactions to form tar fragments while the lower heating rates favor the recombination of tar fragments on the biomass matrix (charring reactions) [21].

High internal pressure caused by a rapid release of volatiles at the pore structure can break the initial fuel particles into fragments (see Figure 4.1). For a given severity of the thermal treatment (imposed external temperature and heat flux), the primary fragmentation is more significant for larger particles [22]. Thus, if breakage of particles into smaller fragments is significant before the end of primary pyrolysis, particle size can lead to an opposite influence on the secondary conversion of volatiles to what was discussed above. This is because formation of small fragments and surface fissures in the initial stage of pyrolysis enables the volatiles released within the particle to escape immediately, without further intraparticle secondary reactions.

4.2.2.2 *Temperature, gas dilution and residence time*

When performing pyrolysis experiments, inert carrier gas is provided to the reaction vessel. With flowing carrier gas the volatiles leaving the surface of fuel are rapidly swept from

the high temperature region. Carrier gas also causes an extensive dilution of volatiles which reduces the rate of homogeneous reactions (reforming, water-gas shift, etc.). Reduced residence time at the higher temperatures and reduced concentration of volatiles can limit the conversion of permanent gases and water vapor but, presumably, it has little effect on the gas-phase cracking of the primary tars. Experiments on the gas-phase cracking of highly diluted tars, in the temperature range of 500-800ºC and residence time of 0.9-2.2s, showed tar conversions from5% up to 88% (relative mass % of tar) [23]. Tars released from a fixed bed of wood at 500ºC were also found prone to gas-phase conversion if further heated up to above 650ºC, even at residence time below 0.2s (highest tar conversion of 88% at 990ºC) [24]. Gilbert et al. [25] have also found that the gas-phase cracking of tars exhibits a strong dependence of temperature, in the range of 500-800ºC. In turns, high yields of liquids were obtained at 400-450ºC even if the gas residence time was as high as 10s [26]. This leads to the conclusion of that primary tars are not easily cracked in the gas-phase at temperatures below around 500ºC but an increasing fraction of tar is readily converted at higher temperatures even if highly diluted and the residence time is very low. According to Antal et al. [9] this gas-phase conversion of the primary tar can be described as two parallel reactions to form light gases and refractory tar, which is harder to crack than the primary tar. Indeed, attempts were made to describe the sequential transformation of the primary tars in the gas-phase as a function of temperature [27], where it proceeds through a stage of light hydrocarbons and oxygenates to the ultimate formation of small quantities of polynuclear aromatics. In addition, the secondary tar-cracking process can lead to the formation of soot (secondary char), through a gas-phase nucleation mechanism that is also favored at high temperatures [24,27].

4.2.2.3 *Amount of fuel*

The mass of fuel used in pyrolysis experiments can influence the extent of secondary reactions outside the particles as it influences the amount of char in the reactor. Tars are known to break down when contacting with hot surfaces of char [17,25]. Therefore, increasing the char hold-up in fluidized beds or the bed depth in fixed beds can be effective in reducing the amount of tar in volatiles. It was reported [17] that a fraction up to 35% of tars released from wood pyrolysis is highly susceptible to catalytic cracking when passed through a bed of char, even at low temperatures (400-600ºC) and residence time of 2.5 ms. In fact, the heterogeneous conversion of tars was shown to increase with initial bed height during fixed bed pyrolysis of biomass at 500ºC [17]. Fixed beds of small particles can have a similar effect on the conversion of tars since the available char surface area *per* unit volume of bed increases. However, different conclusions were drawn during fluidized bed pyrolysis of wood

at 500ºC [21], where the increase of the amount of char in the bed was not found to increase the conversion of tar within the reactor.

4.2.2.4 *Summary*

During biomass pyrolysis experiments the secondary reactions of newly formed volatiles can be affected in many different ways. This might influence the measurements since product yields are, to a given extent, dependent on the specific experimental conditions (particle size, initial amount of fuel, residence time, etc.) even if the fuel, external heating rate and peak temperature are the same. Among the primary volatiles, tars are particularly vulnerable to further conversion into light gases [17,23-25], secondary char (coke and soot) [17,24], water [16,18,21,24] and refractory tar [9] (see Figure 4.1). Since tars are one of the major products of primary pyrolysis, its secondary conversion can influence significantly the final composition of volatiles. Experimental work clearly shows that secondary reactions of tars are enhanced with the increase of temperature [17,23-25,28] and the char availability for catalytic cracking [17,25]. In a number of references [14-16,21,29] the yield of liquids was also observed to decrease by using larger particle sizes. Nevertheless, the influence of particle size on product distribution is still poorly understood. From a review of 21 investigations on this issue, the influence particle size was reported in fifteen studies [5,14-16,21,29-38] while in the remaining six studies [39-44] no influence was found. Further work is also necessary to ascertain how particle size influences the yield of pyrolytic water. Changes on product yields due to particle size can be related to the homogeneous and heterogeneous reactions of newly formed tars as it escapes from the particle; nevertheless, it was also suggested that the heating rates experienced by different particle sizes can be a major factor in determining the yield of liquids, where fast heating rates (i.e. fine particles) favor bound scission (formation of tar) over recombination (formation of char) reactions [21]. Both gas-phase and catalytic cracking of tars is effective even for residence time below 0.2s [17,24]. Since the gas residence time in pyrolysis experiments is most often above this threshold, it is reasonable to conclude that the secondary reactions of primary tars are much significant in investigations performed at high temperature (say, >500ºC).

4.2.3 *Practices of biomass pyrolysis*

A simplified concept of an experimental setup for biomass pyrolysis is outlined in Figure 4.2. In the literature the experiments are most often carried out batchwise (e.g. [5,16,30,39,40]) although there are also rigs designed for continuous operation (e.g. [18,29,34,46,47]). In both cases, generally, a known amount of as received or dry fuel is fed to the reaction vessel under a continuous sweep of inert carrier gas (usually N_2 or He). Here the

fuel particles are dried and pyrolysed under specific conditions (heating rate, temperature, bed depth, etc.) to yield a given amount of char and volatiles. The flowing carrier gas provides an inert atmosphere for fuel decomposition and rapidly transports moisture and pyrolytic volatiles away from the hot region towards the hot particle separator and subsequent gas cooling and cleaning system. Nevertheless, in experiments conducted above approximately 500ºC, it is difficult to avoid the secondary reactions of volatiles before quenching.

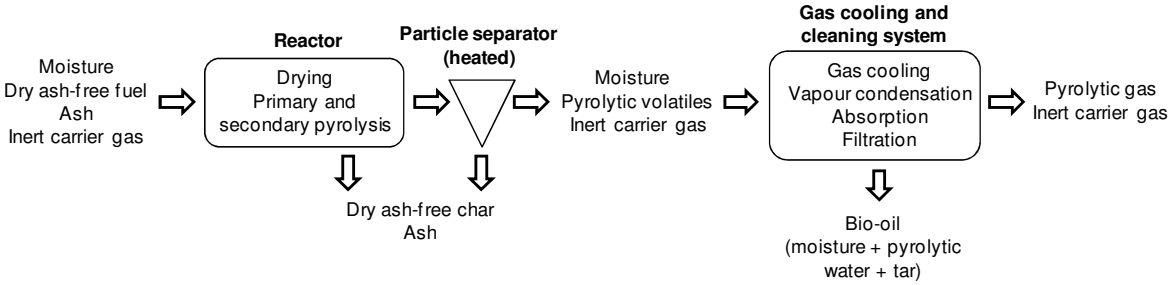

Figure 4.2 - Principles of biomass pyrolysis experiments (simplified scheme).

The char is usually referred as the mass of solid remaining after the pyrolysis is complete at a given peak temperature, including both that remaining in-vessel and that captured in the particle separator (Figure 4.2), i.e. cyclone or filter. To avoid significant tar condensation over the captured char particles, the particle separator must be heated above 350ºC [54]. The yield of char is frequently assessed through gravimetric methods (e.g. [35,36,48]). In few investigations, the yield of char is determined by a mass balance to ash (e.g. [49]) assuming that all ash in feed fuel remains in char. Another method to determine the yield of char is to measure the carbon release during a subsequent burnout of the char (e.g. [5]), providing that the carbon content in char is known or simply considering that char is merely comprised of carbon and ash.

There is some confusion in the literature about the meaning of "bio-oil", for which it is possible to find different synonyms (tars, pyrolytic liquids, bio-crude, etc.). The most used definition is that bio-oil refers to the whole liquid fraction, that is organic compounds + pyrolytic water + moisture (e.g. [4,45]). Thus, according to Figure 4.3, the yield of bio-oil in dry ash-free (daf) fuel basis ($Y_{bio\text{-}oil,F}$) is given by $Y_{tar,F} + Y_{H2O,F} + Y_{M,F}$. The sampling and analytical methods used for bio-oil, tars and water deserve yet great deal of research and, together with a consensus about the definitions, some ambiguities in the comparison of liquid yields could be avoided. For instance, according to some studies [50,51], the observed yields of liquids depends on the measurement methods used. In order to reduce the inaccuracies that the measurement of liquids always comport, some guidelines for their sampling and analysis were proposed [52-54]. The measurement method for the yield of bio-oil can make use of condensers and filters (Figure 4.2) and further gravimetric analysis (e.g. [16,46,55]). The tars retained in the condensers and filters can be recovered by washing with solvent (e.g.

acetone [46]), separated through evaporation techniques and quantified by gravimetric analysis. Gas-chromatography coupled with appropriate detectors (usually MS or FID) can be used to quantify specific tar species. The configuration of the sampling train, the nature of solvent and the temperature at which the condensers are operated vary widely among investigations [50] and this definitively affects the nature of bio-oil and the observed yields. Alternative methods for tar sampling and analysis were developed [51,56,57].

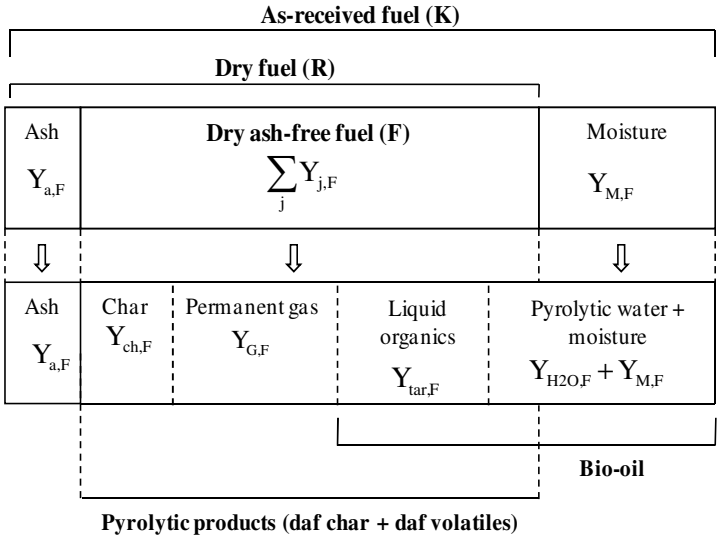

Figure 4.3 - Overall mass balance to the biomass pyrolysis process. The quantities presented in each box are mass ratios (Y) referred to the dry ash-free part of fuel (subscript "F"), kg/kg daf fuel. The length of each box is only illustrative.

There are two sources of water during the thermal decomposition of a wet biomass (Figure 4.1 and 4.3): (i) free water evaporated during drying (subscript "M") and (ii) chemically bound water released during pyrolysis of the dry ash-free fuel (subscript "H_2O"). If as-received biomass is used in pyrolysis experiments, the quantity of moisture driven-off from the fuel (typically 5-20%, dry basis, db) can be similar to the yield of pyrolytic water (typically 12% of dry fuel [45]), making it very important to analyze carefully whether moisture in the parent fuel is or not quoted as pyrolytic product. During pyrolysis experiments water can be subject of both heterogeneous and homogeneous conversion. On the one hand, measurements were published suggesting that water is not easily converted heterogeneously [17]. In these experiments, highly diluted volatiles leaving a fixed bed of wood (heated up to 450ºC) were further passed through a bed of char, the temperature of which was adjusted up to 600ºC. Comparison of runs with/without the bed of char showed that the yield of water did not change by more than 1-2% in relation to the parent fuel (mass %) [17]. On the other hand, the homogeneous conversion of water was investigated during the thermal treatment of a reconstituted pyrolysis gas within 1000-1400ºC and gas residence time of 2s [13], where little conversion of water was observed. These findings [13,17]

suggests that the conversion of water outside the fuel particle might be of little significance during pyrolysis experiments. Furthermore, most investigations use fine particles (mm-sized or even μm-sized) so the intraparticle reactions of water are also limited. Therefore, it is reasonable to consider that water is not appreciably converted during pyrolysis experiments, thus, providing a way to distinguish fuel moisture from pyrolytic water. Accordingly, to calculate the yield of pyrolytic water according to Figure 4.3 ($Y_{H2O;F}$) one need to subtract the moisture content of fuel from the water present in the bio-oil:

$$Y_{H20,F} = Y_{M,bio-oil} \cdot Y_{bio-oil,F} - Y_{M,F} \qquad \text{Eq. 4.1}$$

where $Y_{M,bio\text{-}oil}$ is the moisture content of bio-oil, $Y_{bio\text{-}oil,F}$ is the yield of bio-oil in daf fuel basis and $Y_{M,F}$ is the moisture content of fuel in daf fuel basis. The moisture content of bio-oil can be determined through titration techniques [52].

Pyrolytic gas and carrier gas are obtained once the bio-oil is removed in the condensers (Figure 4.2). Measurement of total gas volume leaving the system can be made by using expansion bags (e.g. [58]) or continuously through diverse methods (for instance, orifice plates [18] and dry gas meters [46]). In combination with a mass balance to the inert carrier gas, this allows to calculate the yields of pyrolytic gas species (e.g. [58]). Sometimes a specific gas tracer is mixed with carrier gas to facilitate the quantification of pyrolytic gas through gas chromatography (e.g. [17]). The composition of pyrolytic gas can be evaluated online through gas analyzers (single gas analyzers, FID analyzers, FTIR analyzers). Gas chromatography (generally using TCD and/or FID detectors) is also widely used in combination with different offline methods. In some investigations (e.g. [41,59]) only two of the main products (char, bio-oil or total gas) are measured while the third one is obtained by difference when closing the overall mass balance to the pyrolysis process.

Biomass pyrolysis experiments are designed for: (i) controlled heating of the reaction environment to a given peak temperature, where the fuel is previously introduced at ambient conditions and heated up according to the surrounding conditions (typically conducted in thermogravimetric systems and fixed beds), or (ii) isothermal reaction environment, where the fuel is suddenly introduced to achieve faster heating rates (such as in fluidized beds and drop-tube reactors). In any case, the actual heating rate experienced by the fuel particles is dependent on the specific heat transport conditions, both in the gas film-layer and inside the particles, and can only be estimated by modeling. Nevertheless, experiments with packed beds of cm-sized particles may be representative of “slow” heating rates (e.g. [37]) whereas fluidized bed experiments with mm-sized particles can be considered to occur at “fast” heating rates (e.g [16].). In fact, the boundary between “slow” and “fast” is somewhat arbitrary. It is accepted that experiments conducted below 10^1-10^2ºC/s belongs to “slow”

[12,60,61] whereas heating rates above 10^{2}-10^{3}ºC/s belongs to "fast" [61], often referred to as "flash" pyrolysis. Note that in this study "slow" and "fast/flash" heating rate do not refer to the technical processes employed to maximize the char yield and liquid and/or gas yields, respectively.

4.3 *Structured collection of literature data*

Data from a set of investigations [5,16,28,30,31,34-41,43-49, 55,59,61-105], including more than 60 different biomass samples (see Table 4.1), particles having a variety of shapes and sizes (between roughly 10^{-1} and 10^{2} mm) and reactor peak temperature within 200-1000ºC were analyzed. These data were structured in a worksheet, consisting of a unique multi-field table where filters can be applied to sort data according to specific criteria. The following information was recorded from each investigation analyzed: (i) reactor type (e.g. fluidized bed), (ii) reactor scale (industrial, pilot or laboratory), (iii) type of biomass (e.g. pine), (iv) nature of the fuel using wood as reference (wood *vs.* nonwood), (v) specific value of the heating rate (e.g. 500ºC/min), (vi) classification of heating rate according to "slow" *vs.* "fast", (vii) fuel properties (moisture content, ash content, elemental composition, particle size and heating value), (viii) the dependence of product yields and respective properties on reactor peak temperature and (ix) a variety of observations (residence time, catalyst, etc.). Structuring this information was challenging because the way it is reported in the literature is very heterogeneous and often ambiguous; in addition, most of the collected data is presented in the form of graphics in the original references, which makes difficult to read accurately the values in some investigations. The collected information on product distribution refers to the quantities of products formed after the pyrolysis process is complete at a given peak temperature. In many investigations analyzed it is indicated whether the experiments performed are representative of "slow" or "fast" pyrolysis conditions, even if the specific heating rate is unknown, so the respective data were structured accordingly in this study. This is for example the case of experiments carried out in fluidized beds which were classified according to "fast" pyrolysis conditions. On the contrary, in experiments where a fuel sample is heated at a controlled rate from ambient conditions to a given peak temperature, the distinction between "slow" and "fast" pyrolysis was based on a arbitrary threshold for the heating rate. For instance, the heating rate used in these experiments varies considerably among investigations, being frequently in the range of 10^{-1} to 10^{2}ºC/s. In this study, the classification of this kind of experiments according to "slow" or "fast" pyrolysis was based on the threshold of 10^{1}ºC/s.

Table 4.1 - Proximate and ultimate analysis (mass % of dry fuel) and higher heating value (HHV, MJ/kg dry fuel) of a set of biomass samples used in this study.

Fuel	C	H	O	N	S	Ash	Moisture	HHV	Reference
Birch wood	49.05	6.28	44.17	0.16		0.30		18.40	[5]
Spruce wood	50.00	6.27	43.33	0.10		0.40		18.80	[5]
Pine wood	49.90[a]	5.95[a]	44.05[a]	0.10[a]			7.50		[16]
Beech wood	48.42[a]	6.01[a]	45.42[a]	0.15[a]			7.30		[16]
Bamboo wood	48.62[a]	5.90[a]	45.15[a]	0.33[a]			5.80		[16]
Rice husks	48.36	5.13	32.79	0.72	0.31	12.50	6.80	16.79	[30]
Rape seed	58.51	8.57	23.46	3.67		5.78	5.15	26.70[b]	[31]
Birch wood	48.45	5.58	45.46	0.20		0.30	5.26	17.02	[34]
Walnut Shell	50.58	6.41	41.21	0.39		1.40	8.11	19.20[b]	[35]
Safflower seed	59.05	8.87	26.72	3.03		2.33	6.04	23.86[b]	[36]
Sesame stalk	48.62	5.65	37.89	0.57		7.26	9.53	19.10[b]	[39]
Olive bagasse	50.88	7.15	35.63	1.62		4.72	7.30	20.00[b]	[41]
Soybean cake	52.46	6.17	26.51	8.72		6.15	9.15	23.23[b]	[43]
Cardoon	42.78	4.40	43.69	0.64	0.09	8.40		18.20	[44]
Hybrid poplar wood	49.40	6.00	43.10	0.23	0.05	1.20	5.00	19.74	[46]
Switchgrass	46.90	5.80	42.00	0.58	0.11	4.60	5.00	19.53	[46]
Corn stover	46.00	5.90	41.40	0.88	0.12	5.00	5.40	18.62	[46]
Mixed wood	47.58	5.87	42.10	0.20	0.03	2.10	7.76		[47]
Sweet gum wood	49.50[a]	6.10[a]	44.60[a]						[48]
Apricot pulp	48.98	5.43	38.31	2.38		4.70	10.30	18.40	[55]
Peach pulp	44.51	6.73	45.38	0.88		2.40	9.30	15.40	[55]
Coir pith	44.03	4.70	43.44	0.70		7.10		18.07	[59]
Corn cob	47.60	5.01	44.60	0.00		2.80		15.65	[59]
Groundnut shell	48.27	5.70	39.40	0.80		5.90		18.65	[59]
Rice husks	38.89	5.10	32.00	0.60		23.50		15.29	[59]
Rice straw	36.89	5.00	37.89	0.40		19.80		16.78	[59]
Subabul wood	48.20	5.90	45.19	0.00		0.90		19.78	[59]
Wood	45.68	6.30	47.42	0.30		0.30		18.99	[62]
Coconut shell	47.97	5.88	45.57	0.30		0.50		19.45	[62]
Straw	42.69	6.04	47.11	0.46		3.70		17.53	[62]
Pine wood	45.92	5.27	48.24	0.22		0.35	7.99	18.98[b]	[63]
Almond shell	47.63	5.71	44.48			2.18			[64]
Hazelnut shell	49.94	5.65	42.81	0.27		1.33			[64]
Beech wood	47.91	5.90	44.71			1.46			[64]
Beech sawdust	48.60[a]								[65]
Fir wood	46.40	5.90	47.17	0.09	0.00	0.45	8.00		[67]
Wheat straw	43.60	6.20	44.32	0.30	0.08	5.50	7.00		[67]
Olive husks	50.90	6.30	38.60	1.37	0.03	2.80	8.50		[67]

Grape residues	47.90	6.20	38.60	2.11	0.09	5.10	9.00		[67]
Rice husks	40.30	5.70	38.37	0.30	0.03	15.30	7.00		[67]
Beech wood	46.00	6.46	46.94	0.07	0.03	0.50	5-6		[68]
Quebracho blanco wood	57.47	6.27	34.96	0.90		0.40			[69]
Timber wood	47.72	5.54	44.85	0.89		1.00			[69]
Hazelnut shell	50.08	5.13	41.99	1.38		1.42	9.53	18.50[b]	[70]
Mixed wood	45.16	5.63	45.85			1.62	8.11		[72]
Forestry residue	51.40	6.00	40.00	0.50		2.10	8.81	20.80	[75]
Pine sawdust	50.30	6.00	43.50	0.10		0.20	3.41	20.60	[75]
Poplar-aspen wood	49.41	6.09	43.53	0.56		0.39	5.19		[76]
Poplar-aspen bark	48.77	6.12	40.26	0.51		4.38	8.17		[76]
Maple wood	48.21	6.06	44.64	0.50		0.59	5.63		[76]
Wheat straw	48.50	5.13	41.30	0.50		4.60	6.95		[76]
Corn stover	50.10	5.01	33.00	0.93		11.00	9.89		[76]
Bagasse	44.58	5.00	46.31	0.00	0.19	3.92	5.82		[76]
Oak sawdust	47.00	5.60	41.80			5.60			[79]
Pine wood	47.79	5.85	45.31	0.10	0.10	0.86	7.53		[80]
Tobacco stalk	48.95	5.75	39.59	2.05		2.50			[85]
Yellow pine wood	51.79	6.18	41.04	0.40		0.40			[85]
Cottonseed cake	49.29	5.59	38.67	1.23		5.22	6.50	18.00[b]	[86]
Cotton straw and stalk	46.42	4.95	42.45	1.13		5.05	7.96	15.98[b]	[87]
Spurge	43.52	5.45	43.33	1.69		6.00	8.81	15.88[b]	[90]
Hazelnut shell	50.94	4.97	42.90	0.50		0.70	7.53	15.49[b]	[92]
Safflower seed	48.02	6.69	39.38	2.91		3.00	6.38	24.80	[93]
Paper waste	40.78	5.73	51.28	0.00		1.18	12.60		[94]
Hazelnut shell	50.34	5.84	42.33	0.40		1.10		19.90	[95]
Peanut Shell	46.59	6.00	43.65	2.06		1.70		18.60	[95]
Pistachio shell	49.26	6.07	41.66	1.57		1.45	7.98		[96]
Tobacco residues	45.40	5.45	35.25	1.80		12.10	8.39	19.19[b]	[98]
Beech wood	49.47	5.57	44.39	0.16	0.02	0.47	7.80	19.30	[101]
Pine sawdust	44.70	6.55	48.38	0.05	0.10	0.22	16.28		[102]
Sunflower shell	47.4	5.80	41.40	1.40	0.05	4.00		18.00	[105]
Minimum	36.89	4.40	23.46	0.00	0.00	0.20	3.41	15.29	
Average	47.87	5.86	41.39	0.93	0.08	3.88	7.61	18.96	
Maximum	59.05	8.87	51.28	8.72	0.31	23.50	16.28	26.70	

[a] Dry ash-free basis; [b] Assumed higher heating value in a dry basis.

In the following (section 4.3.1) some considerations about the overall mass balance to the biomass pyrolysis process are presented, which will be useful in understanding how the literature data were implemented in the worksheet (section 4.3.2).

4.3.1 *Overall mass balance to the pyrolysis process*

The organic part of biomass consists mainly of carbon, oxygen and hydrogen, while the nitrogen, sulfur and chlorine contents are much lower. The other parts of biomass are moisture and a minor quantity of ash. The thermal decomposition of the as-received fuel (subscript "K", Figure 4.3), including both drying and pyrolysis steps, is represented by Eq. 4.2, which also takes the secondary reactions of primary volatiles into account. According to the discussion above, the moisture (subscript "M") present in the as-received fuel is considered conservative and it is distinguished from pyrolytic water in volatiles (subscript "H_2O", see Eq. 4.1). The daf part of fuel (subscript "F") decomposes into pyrolytic volatiles (subscript "V" and yield $Y_{V,F}$) and daf char (subscript "ch" and yield $Y_{ch,F}$) (see Figure 4.3). The yield of volatiles is divided in two parts, one belonging to liquids at ambient conditions (tars and H_2O) and other to permanent gases (C_xH_y, CH_4, CO, CO_2, and H_2), as given by Eq. 4.3 and Eq. 4.4. Since ash is not accounted for in $Y_{ch,F}$ (kg daf char/kg daf fuel), the ash content of fuel appears in both sides of Eq. 4.2 and is denoted by $Y_{a,F}$ (kg ash/kg daf fuel).

$$\left(\sum_j Y_{j,F} + Y_{a,F}\right) \cdot \frac{1}{1 - Y_{M,K}} = Y_{ch,F} + Y_{V,F} + Y_{M,F} + Y_{a,F} \qquad \text{Eq. 4.2}$$

$$Y_{V,F} = Y_{tar,F} + Y_{H2O,F} + Y_{G,F} \qquad \text{Eq. 4.3}$$

$$Y_{G,F} = Y_{CxHy,F} + Y_{CH4,F} + Y_{CO,F} + Y_{CO2,F} + Y_{H2,F} \qquad \text{Eq. 4.4}$$

4.3.2 *Data implementation*

4.3.2.1 *Char*

In the literature the yield of char is usually reported as the mass of solid residue remaining after pyrolysis is complete and expressed on a dry fuel mass basis. As a result, it accounts for both organic material (mainly carbon) and ash. One of the ways the yield of char was recorded in the database is kg of solid residue *per* kg of dry fuel ($Y_{S,R}$). However, since the ash content of solid residue is sometimes reported, the yield of char can also be recorded according to Eq. 4.2 and Figure 4.3, which relates the daf part of char to the daf part of fuel ($Y_{ch,F}$, kg daf char/kg daf fuel), as follows

$$Y_{ch,F} = Y_{S,R} \cdot \left(\frac{1 - Y_{a,S}}{1 - Y_{a,R}}\right) \qquad \text{Eq. 4.5}$$

where $Y_{S,R}$ is the yield of solid residue in a dry fuel basis, $Y_{a,S}$ is the ash content of solid residue and $Y_{a,R}$ is the ash content of fuel in a dry basis. Nevertheless, as the ash content of solid residue is not always reported, to ensure consistency it was here assumed that all ash in parent fuel remains in the solid residue, so the yield of ash free char can be calculated according to

$$Y_{ch,F} = \frac{Y_{S,R} - Y_{a,R}}{1 - Y_{a,R}} \qquad \text{Eq. 4.6}$$

Figure 4.4 shows a compilation of some literature data concerning the mass ratio of ash content in solid residue to the ash content in parent fuel ($Y_{a,S}/Y_{a,R}$) [37,40,44,48, 55,62,64,67,69,70,74,84,95,105], where it is observed an increase of $Y_{a,S}/Y_{a,R}$ with temperature increase. Furthermore, the inverse of the data presented in Figure 4.4 is actually the yield of solid residue, since $Y_{a,S}/Y_{a,R}=1/Y_{S,R}$. Thus, from this data, it can be concluded that the yield of solid residue decreases from roughly 40-80% at 400ºC to a value below 40% above 800ºC (mass % of fuel) which is in agreement with diverse measurements on the yield of solid residue and suggests that most of ash in parent fuel effectively remains in the solid residue.

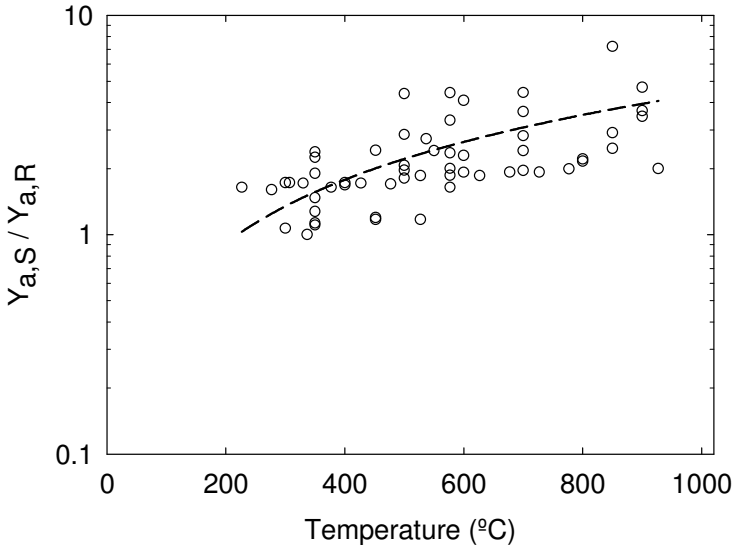

Figure 4.4 - Ratio of ash content in char ($Y_{a,S}$, dry basis) to the ash content in parent fuel ($Y_{a,R}$, dry basis) as a function of pyrolysis peak temperature. Dashed line is a trendline. Data-points from [37,40,44,48,55,62,64,67,69,70,74,84,95,105].

The elemental composition of char was recorded on a daf char basis and often just for carbon, hydrogen and oxygen. There are situations where the basis used to report this data is not explicitly given in the original reference. Nonetheless, it can be often assessed from the

mass balance of the char (for example, on a dry char basis, the sum of daf char and ash is equal to unity). Concerning the heating value of char, the higher heating value (HHV) is frequently reported, expressed on a dry char basis. In few investigations there is no reference to the basis used to express the heating value of char, so it was assumed to be on a dry basis. Ambiguous terms like "calorific value" can be found in the literature and, here, it was also assumed to be HHV. Actually, the most usual information saved in the worksheet is HHV on a dry char basis [2].

4.3.2.2 *Liquids*

The yields of liquids were recorded in a daf fuel basis and structured according to Figure 4.3: (i) total liquids (bio-oil, $Y_{tar;F} + Y_{H2O;F} + Y_{M;F}$), (ii) total pyrolytic liquids ($Y_{bio\text{-}oil,F} - Y_{M,F}$), (iii) organic liquids (tar, $Y_{tar,F}$) and (iv) pyrolytic water ($Y_{H2O;F}$). There is not a uniform method of expressing these yields in the literature. The main difficulty in structuring these data was to understand whether the moisture in fuel was or not quoted as pyrolytic product. Sometimes $Y_{M,F}$ is even missed so the reported data on the yields of liquids could not be managed to fit to all the fields of the worksheet (for example, in these situations, the yield of total pyrolytic liquids could not be estimated); in such situations, data were saved as reported (for example, the yield of bio-oil). The elemental composition of tar (mostly C, H and O) was recorded on a daf tar basis. In few cases this information was derived from the elemental composition of bio-oil, by using Eq. 4.7-Eq. 4.9, as long as the moisture content of bio-oil ($Y_{M,bio\text{-}oil}$) was reported.

$$Y_{C,tar} = Y_{C,bio-oil} \cdot \frac{1}{1 - Y_{M,bio-oil}} \quad \text{Eq. 4.7}$$

$$Y_{O,tar} = \left(Y_{O,bio-oil} - \frac{16}{18} \cdot Y_{M,bio-oil}\right) \cdot \frac{1}{1 - Y_{M,bio-oil}} \quad \text{Eq. 4.8}$$

$$Y_{H,tar} = \left(Y_{H,bio-oil} - \frac{2}{18} \cdot Y_{M,bio-oil}\right) \cdot \frac{1}{1 - Y_{M,bio-oil}} \quad \text{Eq. 4.9}$$

In the literature, there is data for both HHV and LHV of tar and bio-oil. To derive the heating value of tar (organic part of bio-oil) from the one of bio-oil, information on the moisture content of bio-oil is also required. In addition, the hydrogen content of the organic fraction is needed to changeover between HHV and LHV. As a result, the developed worksheet contains data for both the HHV and LHV of tar [2].

4.3.2.3 *Gas*

Information relative to the production of total permanent gas is often reported as yields (see Figure 4.3, $Y_{G,F}$) or, in a few investigations, as Nm^3 gas/kg fuel. The data expressed as yields allows studying the stoichiometry of biomass pyrolysis (Eq. 4.2) whereas it cannot be evaluated from Nm^3 gas/kg fuel if the gas composition is unknown. As long as possible, data was recorded as $Y_{G,F}$ (kg total gas/kg daf fuel) but, when it is not the case, then data was also recorded as reported. The composition of pyrolysis gas is usually reported using: (i) yields of the individual gas species (kg species/kg fuel) or (ii) volume or mass fractions of the individual gas species in the total gas (kmol species/kmol total gas or kg species/kg total gas). Again, the second method is not so useful since the yields of the individual gases cannot be evaluated if the yield of total gas is missed. For example, to convert from mass fraction of i^{th} gas in total gas ($Y_{i,G}$) into yield of i^{th} gas in a daf fuel basis ($Y_{i,F}$) one need to perform

$$Y_{i,F} = Y_{i,G} \cdot Y_{G,F} \qquad \text{Eq. 4.10}$$

As far as possible, the literature information about the composition of total gas was recorded by means of yields on a daf fuel basis ($Y_{i,F}$). In addition, when literature data could not be evaluated to fit this representation then it was also recorded as reported. The recorded information concerned the following gases: CO, CO_2, H_2, CH_4 and other light hydrocarbons (non condensable, here lumped into a single group, referred as C_xH_y). The most frequently reported light hydrocarbons (apart from CH_4) are C_2 species and sometimes C_3 species. Thus, the recorded data on the yield of C_xH_y can be viewed as a rough approximation for the yield of the smaller hydrocarbons (mainly C_2 species) but it might underestimate the yield of the whole non-condensable light hydrocarbons. The heating value of total permanent gas is seldom reported so, here, the chemical composition of gas was used to approximate its LHV.

4.4 *An empirical model for the composition of volatiles*

In the following an empirical pyrolysis model to predict the yields of main volatile species arising from the thermal conversion of a biomass particle is presented. In the adopted modeling approach, the fuel particle is treated as a black box as the physical-chemical processes occurring within it are not considered in the model. Instead, elemental mass balances are established to the overall pyrolysis process which, in combination with experimentally-based closing parameters (see section 4.4.1), enables to establish a system of equations to predict the accumulated yields of a relevant number of volatiles (see section

4.4.2). The pyrolysis model is here looked as a mode of compiling the collected experimental data in a tool that can be effectively used to investigate the general pyrolysis behavior of biomass feedstocks (see analysis in section 4.5).

4.4.1 *Empirical data for modeling*

The empirical relationships used in the pyrolysis model were derived from the collected literature data. It can be used to relate the yields of various gas-phase volatiles and to approximate relevant thermochemical properties of char, tar and total permanent gas. The selection of the regression mathematical models used to fit the literature data was based on a trial-and-error strategy. First, to decide among the most suitable types of regression models, the shape of the relationship between the dependent and independent variables was considered. Thereafter, the regression model giving higher prediction performance, here measured by the squared correlation coefficient (R^2), was adopted.

4.4.1.1 *Relations between the yields of gas-phase volatiles*

The ratio between gaseous products arising from pyrolysis of a given quantity of biomass were investigated [3,9,67,76,77,107]. Selected ratios were correlated over a range of temperature, showing a similar behavior for different biomasses. In addition, yields of various gases were correlated against the yield of a specific gas [76,107]; particle size, heating rate and reactor type were found to be of limited influence on these empirical relationships [107] although it seems slightly dependent on the biomass being pyrolysed [76]. Yields of CO, CO_2, CH_4 and other light hydrocarbons have received particular interest.

The mass ratio of H_2 to CO ($Y_{H2,F}/Y_{CO,F}$) is plotted against temperature in Figure 4.5, which is a compilation of some literature data [16,34,44,47,62,67,72,76], using various fuels, reactors and operating conditions (heating rate, particle size, etc.). It is worth to point out that Figure 4.5 includes the activity of both the primary release of volatiles and secondary reactions. An increase of the $Y_{H2,F}/Y_{CO,F}$ ratio was observed, from below 0.002 kg H_2/kg CO to almost 0.06 kg H_2/kg CO when the temperature increases from 350 to 1000ºC. A plateau seems to be attained as temperatures increases above 800ºC. This ratio was selected as an empirical closing parameter because its trend on temperature dependence can be outlined from both the experience and theory. On the one hand, experiments at low temperature have shown very low H_2 formation below 500ºC (e.g. [67,76]) while CO is noticeably formed, resulting in a decrease of $Y_{H2,F}/Y_{CO,F}$ when temperature decreases. On the other hand, chemical equilibrium modeling shows that both H_2 and CO are thermodynamically stable at high temperature [111]; hence, as temperature increases, the hydrogen in the parent fuel is mostly converted into H_2 while almost all the oxygen and a significant fraction of the carbon

react to form CO; the remaining quantity of carbon in the fuel react to form char with a carbon content close to 100% (mass % of daf char). Accordingly, at high temperatures and chemical equilibrium conditions, the distribution of pyrolytic products can be approximated as follows: $Y_{H2;F} \approx Y_{H;F}$; $Y_{CO,F} \approx Y_{O,F} \times 28/16$ and, in case of biomasses with negligible nitrogen content, $Y_{ch,F} \approx 1 - Y_{H,F} - Y_{O,F} \times 28/16$. Indeed, if one for example take a biomass with 50% carbon, 44% oxygen and 6% hydrogen (mass %, daf basis), the ratio $Y_{H2,F}/Y_{CO,F}$ would approach 0.078 kg H_2/kg CO as temperature increases, which is in accordance with the trend shown in Figure 4.5. From the present compilation of data (Figure 4.5), the following temperature-dependent ratio is proposed

$$\frac{Y_{H2,F}}{Y_{CO,F}} = 3 \cdot 10^{-4} + \frac{0.043}{1 + (T/632)^{-7.23}} \qquad R^2 = 0.73 \qquad \text{Eq. 4.11}$$

where T (ºC) is the pyrolysis peak (i.e. reactor) temperature, within 350-1000ºC.

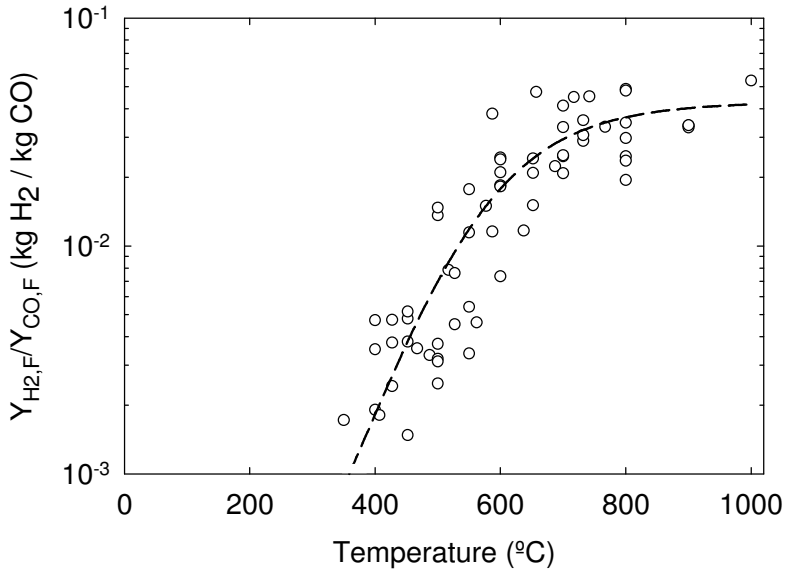

Figure 4.5 - Mass ratio of the yield of hydrogen ($Y_{H2,F}$) to the yield of carbon monoxide ($Y_{CO,F}$) as a function of pyrolysis peak temperature. Dashed line is given by Eq. 4.11. Data-points from [16,34,44,47,62,67,72,76].

Previous studies [3,76,77,107] have investigated the relation between the yields of CH_4 and CO, developing approximate relationships between them. In this respect, Figure 4.6 presents the recorded data on $Y_{CH4,F}$ as a function of $Y_{CO,F}$, taken from [16,34,44, 46,47,62,66,67,72,76,77]; literature relations of $Y_{CH4,F}$ *vs.* $Y_{CO,F}$ [76] are also presented in the figure. It is observed that experimental data for biomass pyrolysis fits between the relations for lignin and cellulose pyrolysis. This indicates that the chemical composition of fuel (for instance, the proportions of cellulose and lignin) influences the pyrolytic product

distribution; moreover, in general, the collected data seems closer to the pyrolytic behavior of cellulose. Qualitatively, the data shows that the yields of CH_4 and CO have similar behavior over a wide range of temperature. The observed trend in the data is here fitted by Eq. 4.12, which can be used for CO yields up to 0.55 kg CO/kg daf fuel; Eq. 4.12 show a lower slope than other relationships developed in the literature for specific fuels [76] being likely a result of the variety of biomasses accounted for in Figure 4.6.

$$Y_{CH4,F} = -2.18 \cdot 10^{-4} + 0.146 \cdot Y_{CO,F} \qquad R^2 = 0.88 \qquad \text{Eq. 4.12}$$

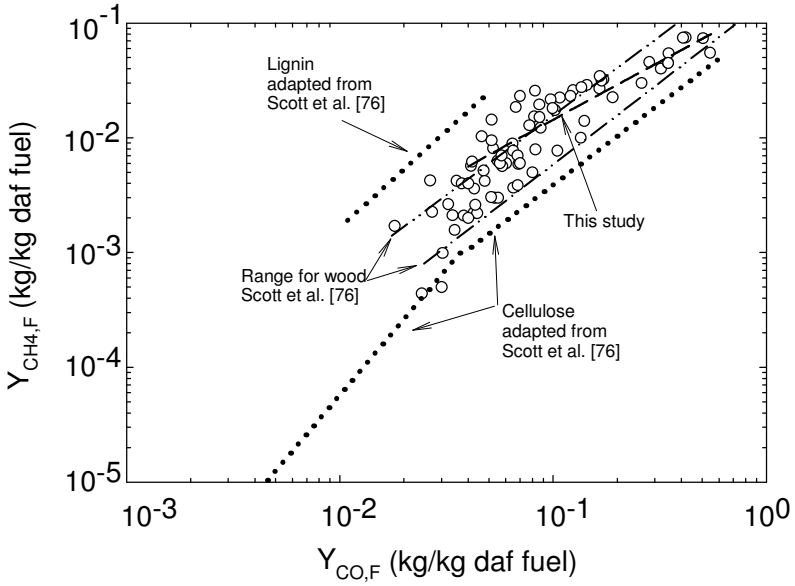

Figure 4.6 - Yield of methane ($Y_{CH4,F}$) as a function of the respective yield of carbon monoxide ($Y_{CO,F}$). The dashed line relative to this study is given by Eq. 4.12. Data-points from [16,34,44,46,47,62,66,67,72,76,77].

4.4.1.2 *Product properties*

Figure 4.7 provides a compilation of some literature data [16,34,40,44,46,62,66, 67,72,76,80] on the lower heating value of total pyrolytic (permanent) gas (LHV_G) as a function of reactor temperature (ºC). The LHV_G increases almost linearly from 2-5 MJ/kg to 15-18 MJ/kg with the temperature increase from 300 to 900ºC. At low temperature, the heating value of pyrolysis gas compares with that of a blast furnace gas, while it approaches that of a carbureted water gas above 800ºC [110]. The trend of LHV_G above 900ºC can be investigated through chemical equilibrium modeling since at those thermal conditions (say 1200ºC), and given enough residence time for the volatiles, the composition of the pyrolysis gas becomes closer to the equilibrium composition, where H_2 and CO are by far the most important gases [111]. Accordingly, following the discussion at section 4.4.1.1, if one take

again for example a biomass with 50% carbon, 44% oxygen and 6% hydrogen (mass % of daf fuel), then the equilibrium gas composition at very high temperature is around $Y_{H2,F}$ = 6% and $Y_{CO,F}$ = 77% (mass % of daf fuel), which gives a LHV_G close to 18 MJ/kg. If this procedure is repeated for different fuel compositions, covering a range of CHO contents typical of biomass fuels, the figure is that the LHV_G at equilibrium conditions is in the range of 16-21 MJ/kg. This brief analysis clearly shows that the LHV_G will tend to a plateau as temperature increases above 900ºC. Within the temperature range of 300-900ºC, the collected data on the lower heating value of total pyrolysis gas can be fitted by Eq. 4.13.

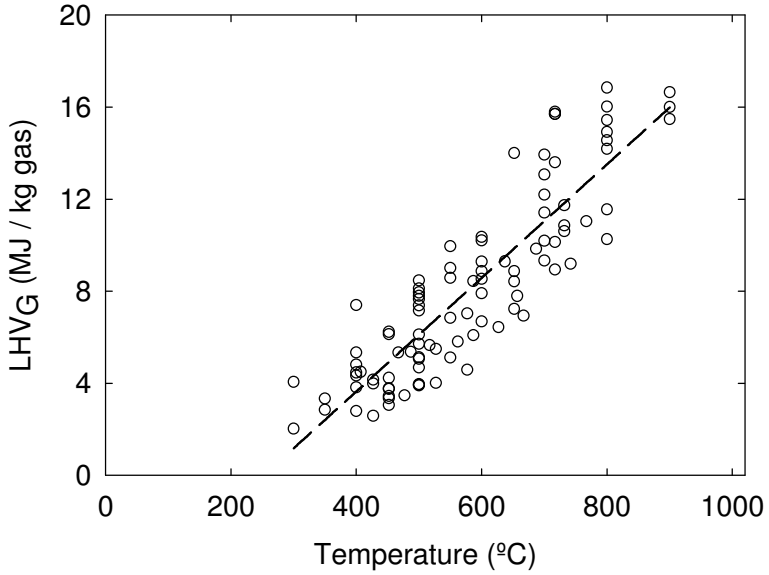

Figure 4.7 - Lower heating value of pyrolysis gas (LHV_G) as a function of peak temperature. Dashed line is given by Eq. 4.13. Data-points from [16,34,40,44,46,62,66,67,72,76,80].

$$LHV_G = -6.23 + 2.47 \cdot 10^{-2} \cdot T \qquad R^2 = 0.78 \qquad \text{Eq. 4.13}$$

The data on the elemental composition of char (C, H and O) is presented in Figure 4.8, taken from [16,31,35-38,40,41,48,62,64,65,67,69,70,72,79,84,87,95,98,101,104,105]. The elemental composition of char varies roughly from the one of parent fuel to the one of graphite (i.e. 100% carbon), being highly dependent on the pyrolysis conditions. From the present set of literature data, the carbon content of char increases rapidly with temperature increase, being typically in the range of 85-95% (mass %, daf char basis) above 800ºC. The enrichment in carbon is accompanied by a loss of oxygen and hydrogen, the value of which decreases to 5-15% and <2%, respectively. Moreover, changes in CHO composition of chars occurs largely below around 600ºC corresponding to the temperature window where the fuel undergoes primary pyrolysis. A slight tendency for non-woody fuels to generate chars with

higher carbon content is observed, which can be partially related to the high carbon contents that are, in general, present in these fuels. A temperature-dependent CHO composition of chars ($Y_{j,ch}$, j = C, H, O) is here given by Eq. 4.14-Eq. 4.16, in the temperature range of 250-1000ºC.

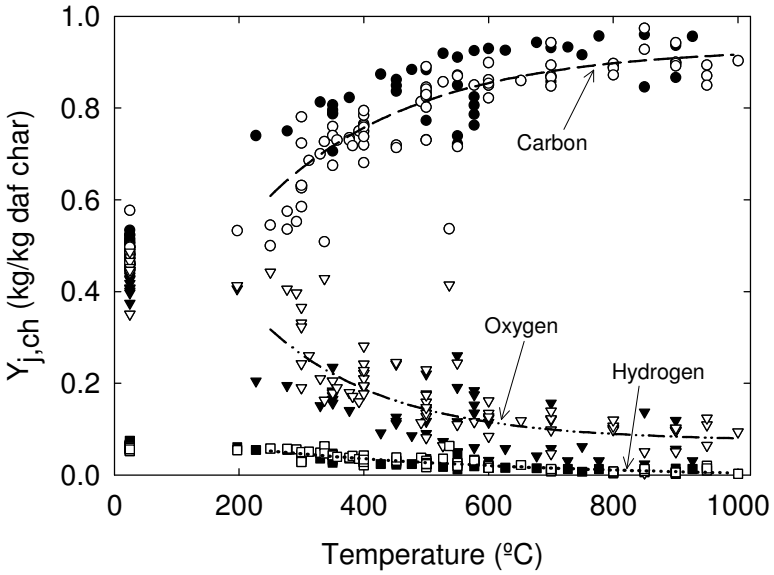

Figure 4.8 - Elemental composition of dry ash-free chars ($Y_{j,ch,}$ j=C,H,O) as a function of pyrolysis peak temperature. Data-points at 25ºC refer to the elemental composition of parent fuels ($Y_{j,F}$, j=C,H,O). Dashed lines are given by Eq. 4.14 - Eq. 4.16; solid symbols – non-wood; open symbols – wood. Data-points from [16,31,35-38,40,41,48,62,64,65,67,69,70,72,79,84,87,95,98,101,104, 105].

$$Y_{C,ch} = 0.93 - 0.92 \cdot \exp(-0.42 \cdot 10^{-2} \cdot T) \qquad R^2 = 0.65 \qquad \text{Eq. 4.14}$$

$$Y_{O,ch} = 0.07 + 0.85 \cdot \exp(-0.48 \cdot 10^{-2} \cdot T) \qquad R^2 = 0.56 \qquad \text{Eq. 4.15}$$

$$Y_{H,ch} = -0.41 \cdot 10^{-2} + 0.10 \cdot \exp(-0.24 \cdot 10^{-2} \cdot T) \qquad R^2 = 0.75 \qquad \text{Eq. 4.16}$$

The data on the elemental composition of tar was collected from [16,31,35,36,38,39,41, 43,46,48,55,62,72-76,78-80,82,86,87,92,94,96,98,99,101,104]. In this study, the C, H and O contents of tar were normalized to the respective contents of parent fuels (i.e. $Y_{j,tar}/Y_{j,F}$, j = C, H, O), being represented as a function of reactor peak temperature (ºC) in Figure 4.9. The tar composition is here expressed on a water-free basis (i.e. just considering the organic part of bio-oil, see Eq. 4.7-Eq. 4.9). Data are more abundant below 600ºC since investigations usually are focused on the characterization of liquid products at operating conditions that maximize the yield of bio-oil. Although there is considerable scatter in the collected data, the CHO composition of lumped tar seems relatively close to that of parent fuel, being highly

oxygenated. This indicates that biomass undergoes low temperature decomposition (i.e. primary pyrolysis) into smaller tar molecules without significant change of the original chemical structure. Nevertheless, the oxygen content of tar seems to decrease slightly with increasing temperature, whereas the carbon and hydrogen contents increase slightly. Therefore, during secondary pyrolysis, lumped tar become enriched in less oxygenated and likely more stable species. This can be also interpreted as a transformation towards more aromatic tars [106]. In the range of 250-1000ºC, temperature-dependent elemental mass ratios ($Y_{j,tar}/Y_{j,F}$) are here given by Eq. 4.17-Eq. 4.19. Contrasting with the behavior of char (Figure 4.8), there is a weak relationship between the elemental composition of tar and pyrolysis temperature. This further suggests averaging all the data provided in Figure 4.9, yielding the following empirical mass ratios: $Y_{C,tar}/Y_{C,F}$ = 1.14, $Y_{O,tar}/Y_{O,F}$ = 0.80 and $Y_{H,tar}/Y_{H,F}$ = 1.13.

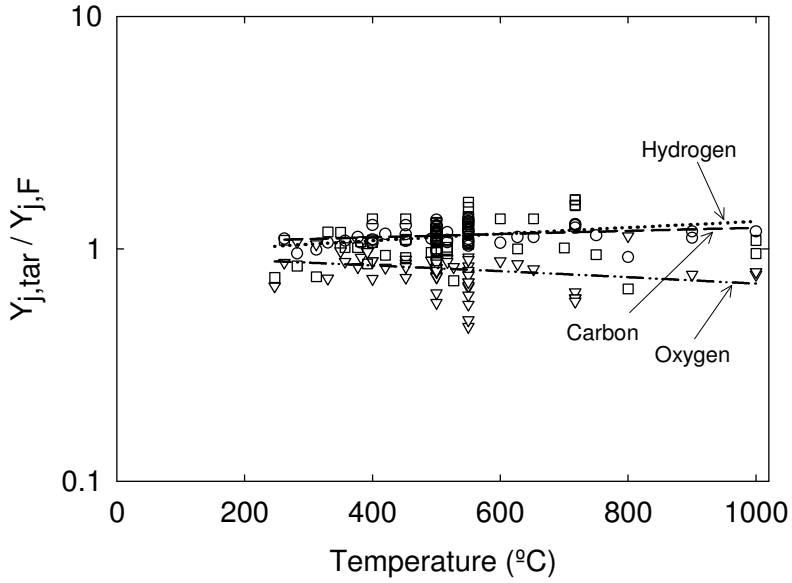

Figure 4.9 - Mass ratios of carbon, oxygen and hydrogen content in tar ($Y_{j,tar}$, j=C,H,O) to the respective content in parent fuels ($Y_{j,F}$, j=C,H,O), as a function of pyrolysis peak temperature. Dashed lines are given by Eq. 4.17 to Eq. 4.19. Data-points from [16,31,35,36,38,39,41,43,46,48,55, 62,72-76,78-80,82,86,87,92,94,96,98,99,101,104].

$$\frac{Y_{C,tar}}{Y_{C,F}} = 1.05 + 1.9 \cdot 10^{-4} \cdot T \qquad R^2 = 0.07 \qquad \text{Eq. 4.17}$$

$$\frac{Y_{O,tar}}{Y_{O,F}} = 0.92 - 2.2 \cdot 10^{-4} \cdot T \qquad R^2 = 0.07 \qquad \text{Eq. 4.18}$$

$$\frac{Y_{H,tar}}{Y_{H,F}} = 0.93 + 3.8 \cdot 10^{-4} \cdot T \qquad R^2 = 0.06 \qquad \text{Eq. 4.19}$$

4.4.2 *Empirical model*

The aim is to predict the (accumulated) yields of the main volatile species resulting from the thermal conversion of the dry ash-free (daf) part of biomass relative to carbon, hydrogen and oxygen. The mass balances of nitrogen, sulfur and chlorine are not considered in the model. Both volatiles and char are dry ash-free. The composition of volatiles is here defined by the following species: tar, C_xH_y, CH_4, CO, CO_2, H_2O and H_2. Tar is assumed to be composed only of carbon, oxygen and hydrogen. Evaporative moisture released from the as-received fuel is not included as a volatile species (see section 4.3.1).

The overall elemental mass balances to the pyrolysis process are expressed by Eq. 4.20-Eq. 4.22, respectively for carbon, oxygen and hydrogen. These balances establish that the total quantities of elements appearing in the volatiles can be calculated as a difference between the respective quantities originally present in fuel and those remaining in char after pyrolysis. Therefore, to solve the balances, it is necessary to know the yield of daf char ($Y_{ch,F}$) and the CHO composition of both parent fuel (given by a standard elemental analysis) and daf char (here approximated by Eq. 4.14-Eq. 4.16). In addition, to establishing the distribution of the elements among the considered volatiles (5 permanent gases, tar and H_2O), the CHO composition of each of the volatiles is also needed in Eq. 4.20-Eq. 4.22. With this concern, the carbon and oxygen contents of tar are here roughly approximated by Eq. 4.17 and Eq. 4.18 and the respective hydrogen content is calculated by difference. The elemental composition of lumped non-methane light hydrocarbons (C_xH_y) is here estimated from its chemical composition. Light hydrocarbons are relatively minor pyrolytic products and literature data on the yields of individual species or groups of species is limited [16,34,46-48,62, 67,72,76,77].Here it was found reasonable to approximate the elemental composition of lumped C_xH_y by that of ethylene ($Y_{C,CxHy}$ = 24/28; $Y_{H,CxHy}$ = 4/28), since its yield was found relatively higher than other C_2 or C_3 hydrocarbons [18,48,76]. It is worth to point out that, by doing so, the equivalent molecule of light hydrocarbons (i.e., x and y in C_xH_y molecule) is not defined in the model. This also applies to tars, for which Eq. 4.17-Eq. 4.19 define its CHO composition but not the respective equivalent "tar molecule".

$$\begin{aligned} Y_{C,V} \cdot Y_{V,F} &= Y_{C,F} - Y_{C,ch} \cdot Y_{ch,F} \\ &= Y_{C,tar} \cdot Y_{tar,F} + Y_{C,CxHy} \cdot Y_{CxHy,F} + Y_{C,CH4} \cdot Y_{CH4,F} + Y_{C,CO} \cdot Y_{CO,F} \\ &\quad + Y_{C,CO2} \cdot Y_{CO2,F} \end{aligned} \qquad \text{Eq. 4.20}$$

$$\begin{aligned} Y_{O,V} \cdot Y_{V,F} &= Y_{O,F} - Y_{O,ch} \cdot Y_{ch,F} \\ &= Y_{O,tar} \cdot Y_{tar,F} + Y_{O,CO} \cdot Y_{CO,F} + Y_{O,CO2} \cdot Y_{CO2,F} + Y_{O,H2O} \cdot Y_{H2O,F} \end{aligned} \qquad \text{Eq. 4.21}$$

$$Y_{H,V} \cdot Y_{V,F} = Y_{H,F} - Y_{H,ch} \cdot Y_{ch,F} = Y_{H,tar} \cdot Y_{tar,F} + Y_{H,CxHy} \cdot Y_{CxHy,F} + Y_{H,CH4} \cdot Y_{CH4,F} + Y_{H,H2O} \cdot Y_{H20,F} + Y_{H,H2} \cdot Y_{H2,F} \quad \text{Eq. 4.22}$$

Since the heating value of total gas can be approximated by Eq. 4.13, it is possible to include the energy balance of total gas (Eq. 4.23) in the pyrolysis model. However, Eq. 4.23 cannot be used directly because the yield of total gas ($Y_{G,F}$) is an unknown to be solved. Therefore, from the overall mass balance to the pyrolysis process (Eq. 4.2), an alternative form for the energy balance of total gas is here used (Eq. 4.24), where the yield of daf char ($Y_{ch,F}$) is used instead of the yield of total gas. Apart from the heating value of CH_4, CO and H_2, the heating value of C_xHy is also needed, being here roughly approximated by that of ethylene. Advantageously, the heating value of tar and the heat of pyrolysis reaction are not used in the empirical model.

$$Y_{G,F} \cdot LHV_G = Y_{CxHy,F} \cdot LHV_{CxHy} + Y_{CH4,F} \cdot LHV_{CH4} + Y_{CO,F} \cdot LHV_{CO} + Y_{H2,F} \cdot LHV_{H2} \quad \text{Eq. 4.23}$$

$$\left(\sum_j Y_{j,F} - Y_{ch,F} \cdot \sum_j Y_{j,ch}\right) \cdot LHV_G = \left(Y_{tar,F} + Y_{H2O,F}\right) \cdot LHV_G + Y_{CxHy,F} \cdot LHV_{CxHy} + Y_{CH4,F} \cdot LHV_{CH4} + Y_{CO,F} \cdot LHV_{CO} + Y_{H2,F} \cdot LHV_{H2} \quad \text{j=C, H, O} \quad \text{Eq. 4.24}$$

Since there is one more unknown than there are equations in the system formed by Eq. 4.11, Eq. 4.12, Eq. 4.20-Eq. 4.22 and Eq. 4.24, a seventh equation is needed in the model to solve for the yields of the 7 volatile species. Here, the final equation is an empirical correlation to approximate the yield of hydrogen ($Y_{H2,F}$) as a function of peak temperature (ºC). This correlation is based on some experimental data obtained in various investigations [16,34,44,47,62,67,72,76], being expressed by Eq. 4.25 and represented in Figure 4.10. It is valid in the temperature range of 350-1000ºC. Eq. 4.25 was selected because it provides a good description of the collected data, which shows a clear relationship between the yield of hydrogen and peak temperature.

$$Y_{H2,F} = 1.145 \cdot \left(1 - exp(-0.11 \cdot 10^{-2} \cdot T)\right)^{9.384} \qquad R^2 = 0.94 \quad \text{Eq. 4.25}$$

A model consisting of a system of linear equations is finally obtained to approximate the yields of pyrolytic volatiles (Eq. 4.26), where $\Omega_1 = Y_{H2,F}/Y_{CO,F}$ is given by Eq. 4.11 and $\Omega_2 = Y_{H2,F}$ is given by Eq. 4.25, with T the pyrolysis peak (i.e. reactor) temperature in ºC. The model

requires few input data: (i) the CHO composition of parent fuel ($Y_{j,F}$, j = C,H,O), (ii) the yield of daf char ($Y_{ch,F}$) and (iii) the temperature of pyrolysis (T, ºC). The remaining information needed solve Eq. 4.26 is provided along section 4.4. The yields of H_2, CO and CH_4 are obtained once the temperature is specified, as given by Eq. 4.11, Eq. 4.12 and Eq. 4.25. In turns, the yields of tar, C_xH_y, CO_2 and H_2O are calculated by solving the system of linear equations (Eq. 4.26). The correlations for the CHO composition of char (Eq. 4.14-Eq. 4.16) and tar (Eq. 4.17-Eq. 4.19) were developed from experimental data within 250-1000ºC. The correlation for the yield of hydrogen (Eq. 4.25) and the mass ratio of H_2 to CO (Eq. 4.11) can be used within 350-1000ºC. Eq. 4.11 and Eq. 4.25 give a yield of CO of almost 0.6 kg CO/kg daf fuel at 1000ºC. As a result, the correlation for the yield of CH_4 as a function of CO (Eq. 4.12) can be also used up to around 1000ºC. However, the information on the lower heating value of total gas (Eq. 4.13) limits the application of the empirical model up to a temperature of 900ºC.

$$\begin{bmatrix} Y_{C,tar} & Y_{C,CxHy} & Y_{C,CH4} & Y_{C,CO} & Y_{C,CO2} & 0 & 0 \\ Y_{O,tar} & 0 & 0 & Y_{O,CO} & Y_{O,CO2} & Y_{O,H2O} & 0 \\ Y_{H,tar} & Y_{H,CxHy} & Y_{H,CH4} & 0 & 0 & Y_{H,H2O} & Y_{H,H2} \\ 0 & 0 & 0 & -\Omega_1 & 0 & 0 & 1 \\ 0 & 0 & -1 & 0.146 & 0 & 0 & 0 \\ LHV_G & LHV_{CxHy} & LHV_{CH4} & LHV_{CO} & 0 & LHV_G & LHV_{H2} \\ 0 & 0 & 0 & 0 & 0 & 0 & 1 \end{bmatrix} \cdot \begin{bmatrix} Y_{tar,F} \\ Y_{CxHy,F} \\ Y_{CH4,F} \\ Y_{CO,F} \\ Y_{CO2,F} \\ Y_{H2O,F} \\ Y_{H2,F} \end{bmatrix} = \begin{bmatrix} Y_{C,F} - Y_{C,ch} \cdot Y_{ch,F} \\ Y_{O,F} - Y_{O,ch} \cdot Y_{ch,F} \\ Y_{H,F} - Y_{H,ch} \cdot Y_{ch,F} \\ 0 \\ 2.18 \cdot 10^{-4} \\ \left(\sum_j Y_{j,F} - Y_{ch,F} \cdot \sum_j Y_{j,ch} \right) \cdot LHV_G \\ \Omega_2 \end{bmatrix} \quad j = C, H, O \qquad \text{Eq. 4.26}$$

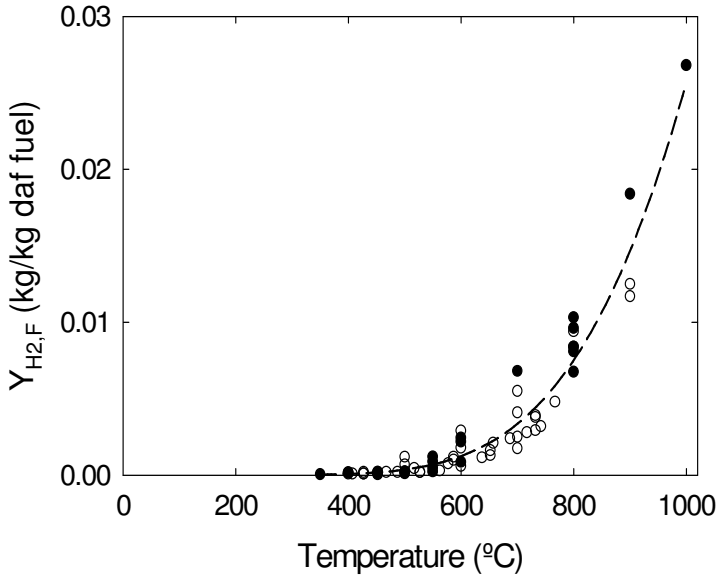

Figure 4.10 - Yield of hydrogen ($Y_{H2,F}$) as a function of pyrolysis peak temperature. ● -"fast heating rate"; ○ -"slow heating rate"; dashed line is given by Eq. 4.25. Data-points from [16,34,44,47,62,67,72,76].

4.5 *General trends of pyrolytic product distribution*

Here the influence of the thermal conditions on the yields of pyrolytic products is summarized and discussed, focusing on the effect of temperature and heating rate. Initially, the analysis of product distribution is based on the collected literature data, where the data for char, total liquids, total gas and water is provided in subsection 4.5.1 and the data for individual gas species in section 4.5.2. A brief analysis on the quality of data is also presented in beginning of section 4.5.1. Thereafter, in section 4.5.3, a second approach is used to investigate the mass balance of biomass pyrolysis which completes the analysis done in sections 4.5.1 and 4.5.2. It consists in using the empirical model developed in section 4.4 to predict the general trends of product distribution as a function of temperature. Finally, in section 4.5.3.1, the predictive capability of the model with a specific biomass is briefly analyzed, although it plays a secondary role in this study.

4.5.1 *Yields of main products*

The recorded data on product distribution as a function of reactor peak temperature, including data for dry ash-free char, total pyrolytic (permanent) gas, total pyrolytic liquids and pyrolytic water are presented in Figure 4.11. The data were collected from [5,16,30,31,34-41,43-47,55,59,61-63,65-68,70-73, 75-77, 79-81, 85-87, 89, 90,92-94, 96-102, 105] regardless of biomass type, reactor and experimental conditions. In the figure, product

yields are expressed in a dry ash-free fuel basis (kg product/kg daf fuel). Each subplot of Figure 4.11 is made of two data-series, one belonging to "slow heating rates" and another to "fast heating rates" (see section 4.3). It is worth to point out that not all experiments are represented in all subplots of Figure 4.11 due to lack of data in some of the investigations analyzed.

For a given product and temperature, the variability in data in Figure 4.11 is high, with differences between the lowest and largest yield as high as 60% of parent fuel (mass %). The variability is high even if the data for "slow" and "fast" heating rates are analyzed separately. The variability in data doesn't seem to depend on the observable (char, total liquids, total gas) although it is higher when product yields are also high. The variability in data can be explained by differences in feedstock, reactor, pyrolysis conditions (particle size, bed depth, residence time, heating rate, etc., see section 4.2.2) and experimental procedures (temperature of cold traps, etc., see section 4.2.3). An example on how differences in fuel can influence product distribution is [108], where high-temperature (750-900ºC) fast-pyrolysis of five distinct biomasses was found to result in differences of char yield up to 10% and differences of total liquids and total gas up to 20% (mass % of parent fuel). These differences obtained from pyrolysis of only five biomasses [108] are comparable to the variability in data found in Figure 4.11 for a huge number of biomasses. On the other hand, the influence of pyrolysis conditions can be found, for example, in [5], where for a given fuel feed and temperature, changes of char yield due to particle size were found as high as 6% (mass % of parent fuel).

Further, each data-point in Figure 4.11 is itself an average value taken from the results of a limited number of replicated experiments. Pyrolysis tests are time consuming and, generally, each experiment is perhaps repeated only two or three times (e.g. [16,90,96]). The quality of data for a given experiment depends on the apparatus and the experimental procedures. The need to consider precision arises because pyrolysis experiments on identical materials and, presumably, identical conditions do not, in general, yield identical results. Random errors are inherent to any experiment and always introduce some variability in data. The reproducibility of the experimental methods is seldom discussed in the literature and the precision of the measurements is not always reported. In a number of references [16,18,25,47,90,92,99] precision has been provided by means of the standard deviation of experimental results or error bars. If the results of a particular experiment are normally distributed then about 99.7% of the observations lie within ±3 standard deviations from the average value. Wang et al. [16] reports an indicative standard deviation of 0.4-1.4% for measurements of liquid yields with an average of 61-65%; thus, if one accounts for ±3 standard deviations from the average, the uncertainty of their measurements is up to ±7% (i.e., ±1.4% × 3/61%). Further analysis of the literature [18,25,47,99] suggests that data on

the yields of main products (char, total liquids, total gas) are often uncertain in roughly ±5-20% of the reported values. However, there are situations where the uncertainty of data is higher as error bars as high as around ±40% of average value can be found [18]. Moreover, a review of some literature [16,18,25,46,48,109] shows a mass balance closure of pyrolysis experiments within 86-108% of parent fuel feed (mass %). The mass closure is the sum of product recoveries expressed as a *per* cent value of parent fuel feed. This constitutes an overall checking to the accuracy of the measurements as the true value is known (i.e. 100%). A mass balance closure within 86-108% gives the impression that random variation is comparable to the inaccuracy of measurements.

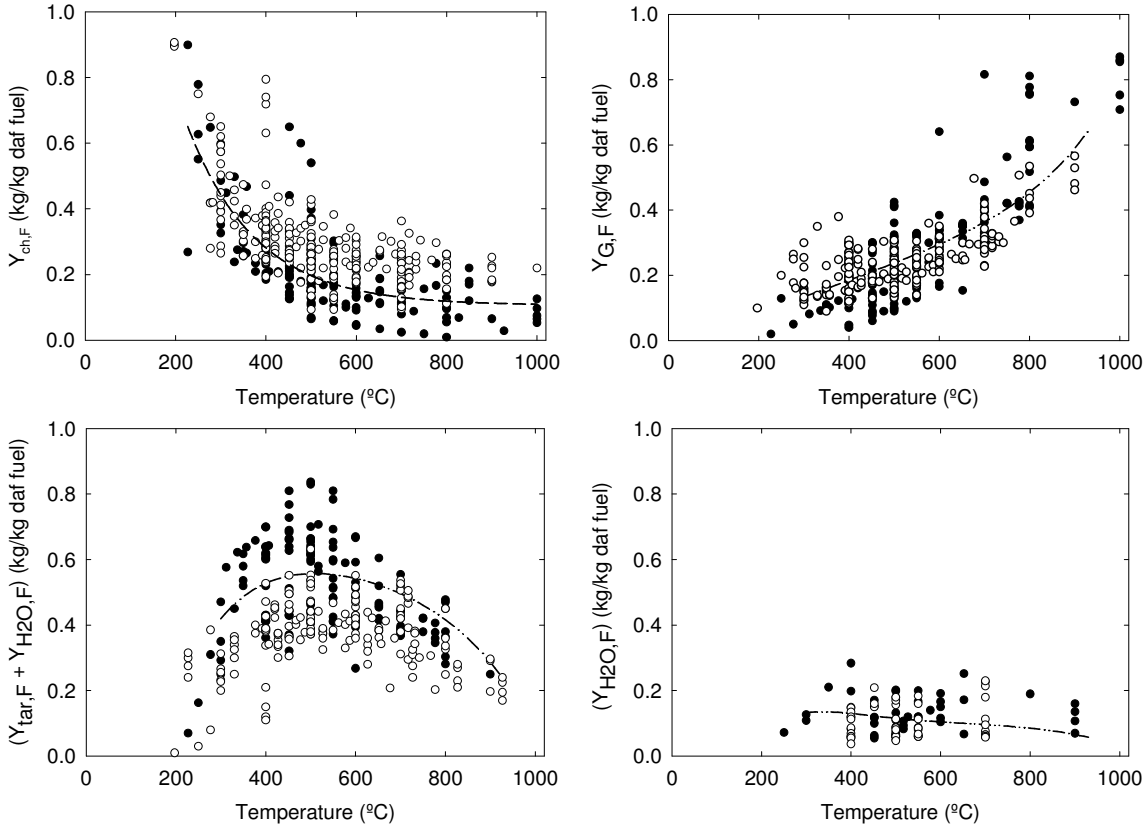

Figure 4.11 - Yields of daf char ($Y_{ch,F}$), total pyrolytic gas ($Y_{G,F}$), total pyrolytic liquids ($Y_{tar,F}$+$Y_{H2O,F}$) and pyrolytic water ($Y_{H2O,F}$) as a function of pyrolysis peak temperature. ● - "fast heating rate"; ○ - "slow heating rate"; ··–·· empirical model (Eq. 4.26) based on a biomass with 49% carbon, 44% oxygen and 5.90% hydrogen (mass % of daf fuel) and a yield of daf char given by Eq. 4.27; – – yield of daf char for "fast heating rate" conditions given by Eq. 4.27. Data-points from [5,16,30,31,34-41,43-47,55,59,61-63,65-68,70-73,75-77,79-81,85-87,89,90,92-94,96-102,105].

A global analysis of Figure 4.11 shows that temperature and heating rate are important process parameters on determining the yields of char, total gas and total liquids. At the lowest temperatures (<300ºC) char is the main product; at middle range temperatures (450-550ºC) a maximum of total liquids is observed; in turn, at the highest temperatures (>800ºC)

the production of light gases is favored. Qualitatively, these general trends in product yields as a function of temperature are the same for both slow and fast heating rates (Figure 4.11). The influence of the heating rate in the yields of main products seems dependent on the temperature of pyrolysis. On heating up to around 450-550ºC (i.e. before secondary reactions of volatiles become active), slow heating rates gives more char and fewer liquids than fast heating rates. Apparently, at these low temperatures, the heating rate of solid fuel exerts little influence on the yield of total gas. As temperature increases above 450-550ºC variations in the yield of char are small, with slow heating rates also associated with higher yields of char, despite of the considerable variability in data. However, a positive relationship seems to appear between the yield of gas and the heating rate. The influence of the heating rate on the yield of total liquids becomes of less importance for the highest temperatures analyzed (>800ºC).

The observed decrease in the yield of char as temperature increases (Figure 4.11) indicates that the major part of fuel mass loss occurs in the range of 200-600ºC. This low temperature stage of biomass thermal decomposition can be referred as the primary pyrolysis stage. This behavior is also observed in Figure 4.12, providing a compilation of some literature data on the quantities of carbon, oxygen and hydrogen remaining in char *per* unit mass of parent fuel [16,37,40,62,63,65,67,72,79,101,104]. Above 600ºC, a rough estimate is that only 10-20% of carbon, 1-5% of oxygen and less than 0.5% of hydrogen (both in mass % of parent fuel) are in char while the remaining quantities of elements were released from solid fuel as primary volatiles (Figure 4.12). These primary volatiles consist mainly of liquids, that is, tars and pyrolytic water. This is explained by observing that the yield of total gas does not change significantly below 600ºC (typically below 40% of daf fuel) while the yield of total liquids increases rapidly (Figure 4.11). For fast heating rates the maximum of liquid yield is roughly in the range of 45-75% whereas for slow heating rates it is roughly in the range of 35-55%. Furthermore, under fast heating rates, the collected data suggests that the primary pyrolysis of wood gives rise to higher yields of total liquids than non-woody biomasses. The yield of pyrolytic water is roughly within 5-20% over the whole temperature range. There appear that almost all pyrolytic water is formed in the beginning of pyrolysis (e.g. dehydration of the chemical structures of fuel), even below 300ºC. An almost constant yield of pyrolytic water as a function of temperature indicates that the increase of total liquids up to 450-550ºC is due to the release of primary tars from solid fuel.

Above 450-550ºC, the yield of pyrolytic liquids starts to decrease (Figure 4.11), caused by the secondary conversion of the primary volatiles. At 900ºC the yield of liquids is typically below 30% which is similar to the yield of pyrolytic water. Because the secondary formation/destruction of pyrolytic water cannot be distinguished from the collected data, the decrease in the yield of liquids above 450-550ºC is attributed to the secondary pyrolysis of

tars. The reduction in liquid products is compensated by the production of light gases; the yield of char is approximately constant above 600ºC (roughly within 5-20% for fast-pyrolysis and 10-30% for slow-pyrolysis) (Figure 4.11). This also explains that, at high temperatures, fast heating rates tends to yield more gas than slow heating rates; indeed, below 450-550ºC, fast-pyrolysis gives rise to a larger quantity of primary tars which, in turns, originate a larger quantity of light gas due to thermal cracking at the higher temperatures.

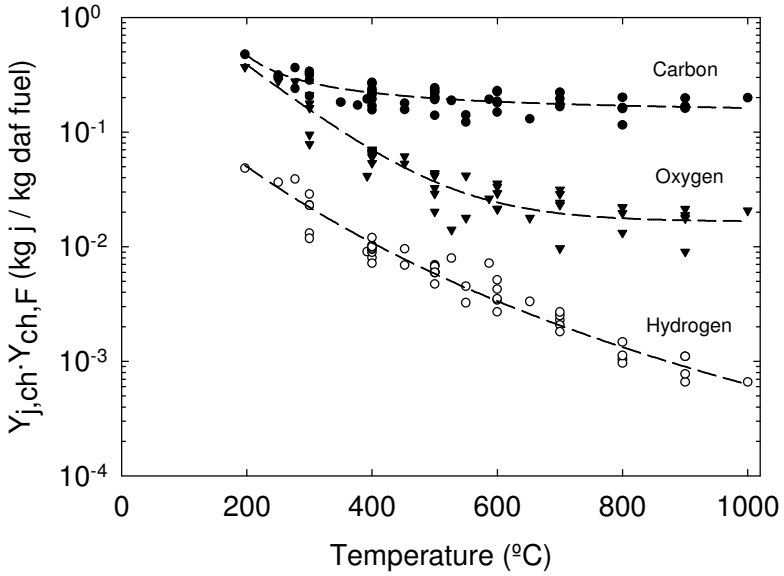

Figure 4.12 - Quantities of carbon, oxygen and hydrogen remaining in dry ash-free char *per* unit mass of dry ash-free fuel ($Y_{j,ch} \cdot Y_{ch,F,}$ j=C,H,O) as a function of pyrolysis peak temperature. Dashed lines are trendlines. Data-points from [16,37,40,62,63,65,67,72,79,101,104].

4.5.2 *Yields of gas-phase products*

The yields of specific (permanent) gases as a function of peak temperature are provided in Figure 4.10 and 4.13, concerning H_2, CO_2, CO, CH_4 and other light hydrocarbons (C_xH_y), based on some data collected from [16,34,44,46,47,62,66,67,72,76,77], involving also various biomasses, reactors and experimental conditions. On a mass basis, the pyrolysis gas consists mainly of CO_2 and CO, with lower amounts of C_xH_y, CH_4 and H_2. Based on the collected data, the heating rate seems of little effect on determining the composition of the pyrolysis gas. The yields of CO, CH_4 and H_2 show a similar pattern of change as a function of temperature but the observed trend of CO_2 is different. The yield of CH_4 + C_xH_y (where, C_xH_y accounts mainly for C_2 hydrocarbons) appears linearly dependent on the yield of CH_4. This relationship suggests that similar formation pathways exist for both CH_4 and C_xH_y hydrocarbons.

Below around 450-550ºC, that is, when the activity of secondary reactions of volatiles is negligible, most of permanent gases might result directly from degradation of the chemical

structures of solid biomass. Within this low temperature range, the collected literature data show a weak relationship between temperature and the production of light gases (Figure 4.13). CO_2 and CO are the main gas species arising from the primary decomposition, although CH_4 seems also to be produced in small quantities. This is in agreement with dedicated experiments [107] showing that during the initial stages of primary pyrolysis the production of CO_2, CO and CH_4 is well correlated with the fuel mass loss. The observed trend on the yield of H_2 as a function of temperature (Figure 4.10) indicates that its production during primary pyrolysis is very small. As a rough indication, below around 450ºC, CO_2 accounts for two thirds of total gas and the remaining gas consists mainly of CO (mass fractions of total permanent gas).

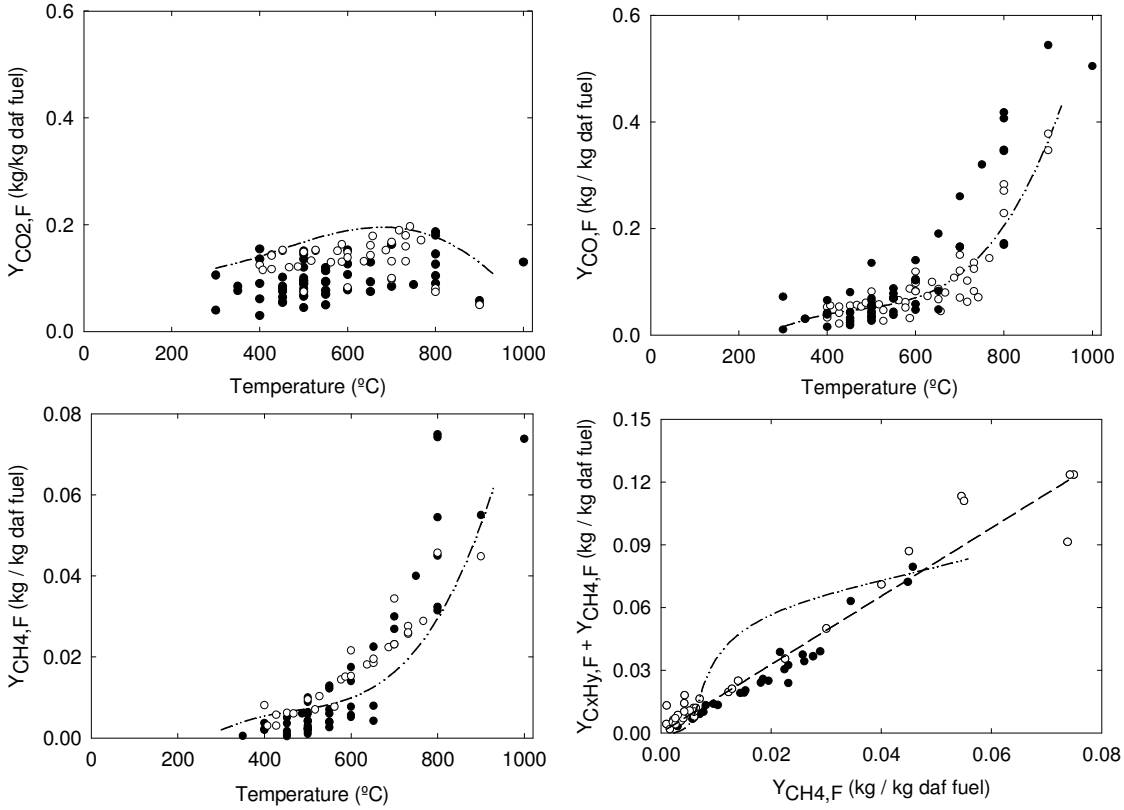

Figure 4.13 - Yields of CO_2, CO and CH_4 as a function of pyrolysis peak temperature and yield of (C_xH_y + CH_4) as a function of the yield of CH_4. ● -"fast heating rate"; ○ -"slow heating rate"; – – trendline;···–··· empirical model (Eq. 4.26) based on a biomass with 49% carbon, 44% oxygen and 5.90% hydrogen (mass % of daf fuel) and a yield of daf char given by Eq. 4.27. Data-points from [16,34,44,46,47,62,66,67,72,76,77].

However, as temperature increases above 450-550ºC, the yields of combustible gases (CO, CH_4, C_xH_y and H_2) become a strong function of temperature. The yield of CO can be

roughly estimated to increase from 2-15% (mass % of daf fuel), at 450-550ºC, to 30-55% at temperatures higher than 850ºC. The increase of CO is roughly compensated by the decrease in pyrolytic liquids(Figure 4.11 and 4.13), which is an indication of that CO is a major gas species resulting from the secondary reactions of tars. Most of the remaining tars convert into CH_4 and C_xH_y and, together, this yield increases from roughly 1% at 450-550ºC to above 10% at temperatures higher than 850ºC (Figure 4.13). This behavior is in accordance with dedicated experiments [17], where the gas-phase cracking of wood pyrolysis tars showed that CO accounts for almost 65% of the tar lost and CH_4 + C_2H_2 for an additional 20% (mass % of tar). The yield of H_2 increases from <0.2% at 450-550ºC to >1% above around 850ºC (Figure 4.10) and this behavior is also linked with the secondary conversion of tars. Due to the rapid increase of CO and H_2 when the activity of secondary reactions is higher (say, above 500ºC), both gases have been suggested as indicators for tar conversion [24]. Between 450-550ºC to around 800ºC, temperature as a limited influence on the yield of CO_2 suggesting that it is produced in small quantities from the secondary reactions of volatiles.

4.5.3 *Fitting the trends of product yields with the empirical model*

In this study the empirical model Eq. 4.26 is used to predict the general trends of product distribution as a function of temperature, as showed in Figure 4.11 and 4.13, under "fast heating rate" conditions. It is worth it because it enables (i) to verify the consistency between the empirical data used for modeling (e.g. the properties of char, tar and gas) and the data on product distribution and (ii) to predict the trends of product yields that are not clear from the collected experimental data (e.g. the trend of CO_2 and H_2O). The yields of volatile species are predicted from the set of equations used in the model, establishing (i) the overall elemental mass balance to the pyrolysis process and (ii) the trends of selected empirical data as a function of temperature. Because the yield of char is an input in the empirical model, the observed trend in Figure 4.11, for "fast heating rates", is fitted by Eq. 4.27. The output of Eq. 4.27 (i.e. the yield of daf char) is then used as input in Eq. 4.26, thus, providing a guideline to the corresponding yields of volatiles as a function of temperature. The CHO composition of biomass is also an input in Eq. 4.26 being here used the following: 49% carbon, 44% oxygen and 5.90% hydrogen (mass % of daf fuel) which is close to the average composition of all biomasses used in the scope of Figure 4.11 and 4.13, under fast-pyrolysis conditions.

$$Y_{ch,F} = 0.106 + 2.43 \cdot exp(-0.66 \cdot 10^{-2} \cdot T) \qquad R^2 = 0.56 \qquad \text{Eq. 4.27}$$

A sensitiveness analysis of model results in relation to the yield of char and the CHO composition of biomass (i.e. the inputs used to fit the trends in Figure 4.11 and 4.13) is

preformed according to Table 4.2, with the predicted yields of volatiles at 500ºC and 850ºC presented in Figure 4.14. Firstly, the yield of char is varied in ±0.05 kg/kg daf fuel in relation to the yield given by Eq. 4.27 (case A, B and C); then, the composition of biomass is varied instead (case A, D, E and F). According to model Eq. 4.26, the yields of tar and total gas vary inversely with the yield of char but the yield of pyrolytic water varies proportionally. Changes in the yield of total gas are due to changes in the yields of CO_2 and C_xH_y since in the empirical model the yields of H_2, CO and CH_4 are fixed at a given temperature. While the yield of tar is more sensitive to the yield of char at low temperature (i.e. 500ºC in Figure 4.14), the yield of gas becomes increasingly sensitive to it as temperature increases (i.e. 850ºC in Figure 4.14). Changes in the CHO composition of fuel can also lead to rapid variation in the predicted yields and unrealistic values can be obtained; in particular, the yield of C_xH_y can easily take unrealistic values when a solution is searched close to the lowest temperatures analyzed in this study (say, <400ºC). In Figure 4.14 it is shown that a variation of the carbon to oxygen mass ratio in fuel (from 1.02 to 1.21 kgC/kgO, Case A, D and E) lead to significant variations in the yields of tar and gas but negligible variation in the yield of water. The increase of the carbon to oxygen ratio raises the yield of tar and lowers the yields of CO_2 and C_xH_y. If instead the mass fraction of hydrogen in fuel is varied from 5.90% to 6.30% (Case A and F), the predict yield of water increases; an increase of the hydrogen content in fuel also raises the yield of tar and lowers the yields of CO_2 and C_xH_y.

Table 4.2 - Data used in the sensitivity analysis of empirical model predictions (Eq. 4.27). Influence of the yield of char and the elemental composition of biomass.

Variable / Case	A	B	C	D	E	F
$Y_{ch,F}$ (kg/kg daf fuel)[a]	Eq. 4.27	Eq. 4.27 + 0.05	Eq. 4.27 - 0.05	Eq. 4.27	Eq. 4.27	Eq. 4.27
$Y_{C,F}$ (kg C/kg daf fuel)	0.49	0.49	0.49	0.47	0.51	0.49
$Y_{O,F}$ (kg O/kg daf fuel)	0.44	0.44	0.44	0.46	0.42	0.44
$Y_{H,F}$ (kg H/kg daf fuel)	0.059	0.059	0.059	0.059	0.059	0.063
$Y_{C,F}/Y_{O,F}$ (kg C/kg O)	1.11	1.11	1.11	1.02	1.21	1.11

[a] In case A, D, E and F the yield of char is given by Eq.27. In case B and C it is added or subtracted 0.05kg char/kg daf fuel in relation to the yield given by Eq. 4.27, respectively.

In the following, Eq. 4.26 is used to predict the composition of volatiles resulting from fast-pyrolysis of an hypothetical biomass (49% carbon, 44% oxygen and 5.90% hydrogen, mass % of daf fuel) with a temperature-dependent yield of char given by Eq. 4.27. The results of the empirical model applied to the cited case are also presented in Figure 4.11 and 4.13, being discussed hereafter. Comparison of model results with the collected literature data show that the empirical relationships developed for modeling (Eq. 4.11-Eq. 4.19 and Eq. 4.25) are in good agreement with the observed trends of product yields as a function of temperature; in particular, this agreement corroborates the trends shown in section 4.4.1.2 for the properties of char, tar and gas.

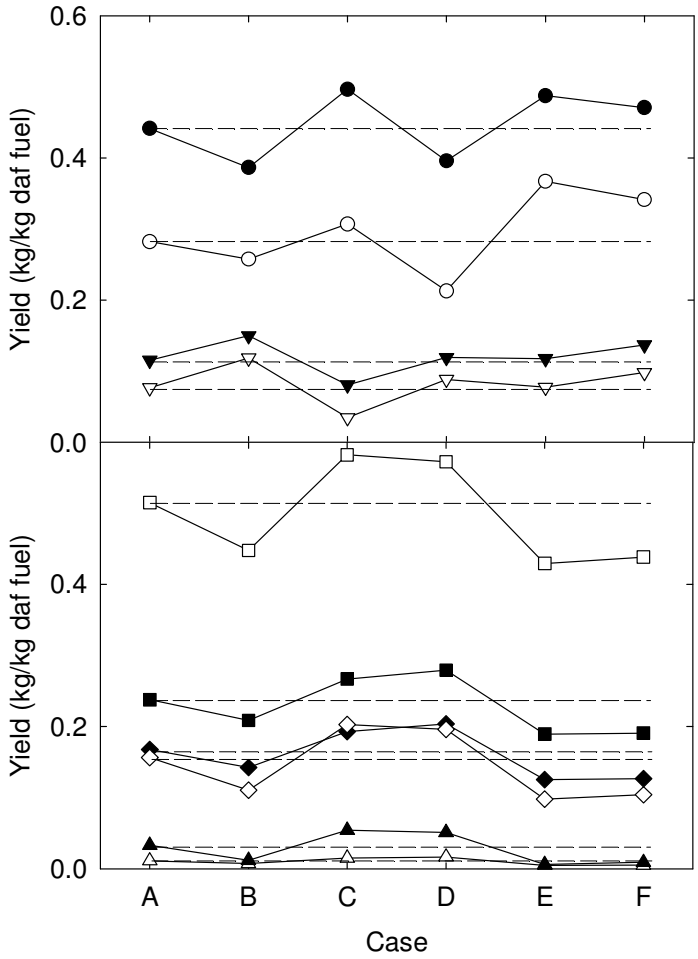

Figure 4.14 - Predicted yields of volatiles according to Eq. 4.26 and the data for sensitivity analysis presented in Table 4.2. Solid symbols – results at 500ºC; open symbols – results at 850ºC; ○ - tar; ▽ - H_2O; □ - total pyrolytic gas; ◇ - CO_2; △ - C_xH_y. Dashed lines are the reference case.

According to Eq. 4.26 and considering the cited case, the yield of CO_2 decreases above around 700ºC, although the present set of literature data does not permits to ascertain this behavior (Figure 4.13). A decreasing yield of CO_2 at high temperature was found in [62], starting to decrease even below 700ºC. The collected data on the CO/CO_2 mass ratio and the respective trend predicted by the model are presented in Figure 4.15. Below 600-700ºC, both literature data and model results show a ratio below 2 kg CO/kg CO_2 but for higher temperature the ratio increases rapidly. A CO/CO_2 mass ratio with a vertical asymptote at high temperature corroborates the decrease of CO_2 shown in Figure 4.13. The predicted trend of CO_2 suggests that a destruction pathway of CO_2 is enhanced at high temperature, which can be linked to the secondary reactions of tars and/or light hydrocarbons. Indeed, the thermal treatment of a reconstituted pyrolysis gas in the temperature range of 1000-1400ºC showed that CO_2 is very active in the oxidation of light hydrocarbons into CO [13]. A similar

mechanism can be responsible for the conversion of CO_2 in a real pyrolysis gas where the concentration of light hydrocarbons is higher than in the cited experiments [13]. The predicted temperature dependence for the yield of total liquids is parabolic-like and peaks at around 500ºC (Figure 4.11); a similar behavior is predicted for the yield of tars (not shown). The predicted yield of pyrolytic water is in the range of 6-13% (mass % of daf fuel), although it decreases slightly with temperature increase (Figure 4.11). Accordingly, the model results suggest that pyrolytic water is not noticeably formed or destroyed during the secondary reactions of volatiles. In the cited case, the model predicts a peak of light hydrocarbons (C_xH_y) when the yield of CH_4 is roughly 2% of parent fuel (mass %, daf basis), which is achieved at around 700-750ºC (Figure 4.13). This trend is not recognizable from the collected literature data, where only the smaller hydrocarbons are accounted for (mainly C_2 species). Thus, the predicted peak of C_xH_y can be related to $>C_3$ light hydrocarbons; nevertheless, the model results tend to the experimental data at the higher temperatures (roughly, >850ºC) which can be viewed as the conversion of $>C_3$ species into smaller hydrocarbon species. It is worth to point out that, according to the model and the cited case, the peaks of tar, C_xH_y and CH_4 occur in sequence: first the peak of tar at ≈500ºC; secondly the peak of light hydrocarbons at ≈700-750ºC and finally the peak of methane above 900ºC. These findings suggest a multistep conversion of tars into light gases as a function of temperature. Apart from the conversion towards CO, as temperature increase above 450-500ºC, tars are subject of bound cleavage into progressively smaller hydrocarbons (first to C_xH_y and then to CH_4). Also CH_4 will further convert to H_2 and CO at higher temperatures (say, > 1000ºC) [13], to match a condition where the composition of volatiles is close to that predicted by chemical equilibrium modeling. Indeed, CO and H_2 are known as high temperature recipients of carbon, oxygen and hydrogen originally present in parent fuel.

Before secondary reactions become active (say at around 500ºC), the empirical model predicts that, in the cited case, the elements released from the parent fuel are mainly converted into liquids, CO_2 and CO: around 75% of the released mass of carbon converts into tar, 15% into CO_2 and less than 10% into CO (mass %); concerning oxygen, almost 65% of the released mass appears as pyrolytic liquids (tars þ pyrolytic water), 30% as CO_2 and the remaining as CO. At such low temperatures, the predicted composition of pyrolysis gas is roughly 70% CO_2, 20% CO and minor quantity of CH_4 (mass % of total gas) (Figure 4.16), which gives a lower heating value of around 5 MJ/kg gas (see Figure 4.7). CO_2 is the main gas species below around 750ºC but its mass fraction in pyrolysis gas decreases with temperature increase (Figure 4.16). Conversely, the mass fraction of CO increases with temperature. CO is predicted as the main gas-phase product under conditions typical of gasification or combustion applications, followed by CO_2 and CH_4 (Figure 4.16).

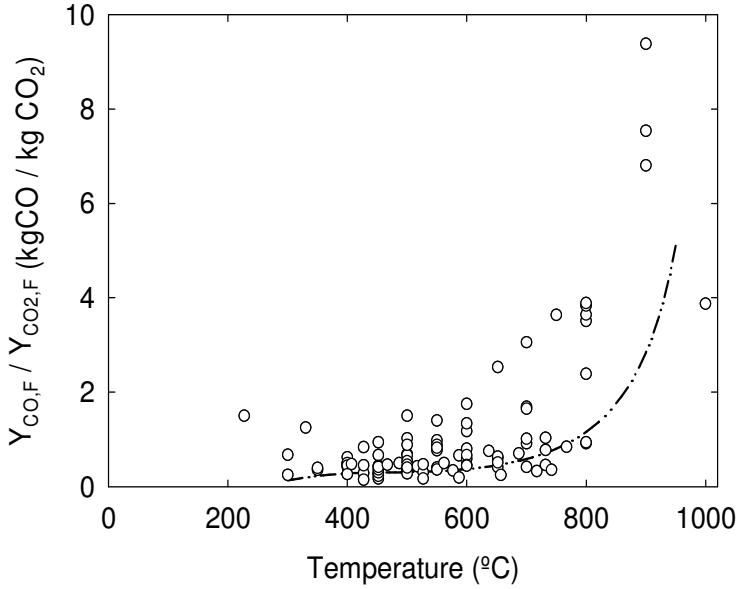

Figure 4.15 - Mass ratio of the yield of CO ($Y_{CO,F}$) to the yield of CO_2 ($Y_{CO2,F}$) as a function of pyrolysis peak temperature. ···-···empirical model (Eq. 4.26) based on a biomass with 49% carbon, 44% oxygen and 5.90% hydrogen (mass % of daf fuel) and a yield of daf char given by Eq. 4.27. Data-points from [16,34,44,46,47,62,66,67,72,76,77].

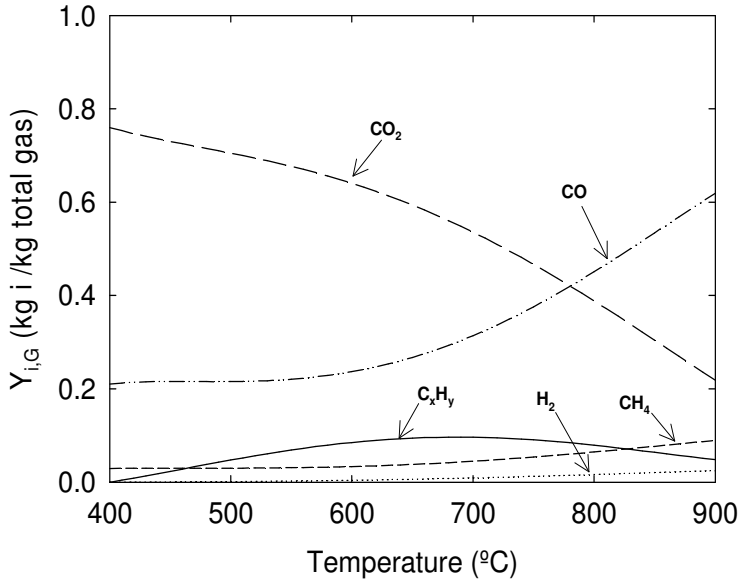

Figure 4.16 - Composition of pyrolysis gas (mass fractions) as a function of peak temperature as given by empirical model (Eq. 4.26) and based on a biomass with 49% carbon, 44% oxygen and 5.90% hydrogen (mass % of daf fuel) and a yield of daf char given by Eq. 4.27.

4.5.3.1 *Comparison of model results and measurement data: a case study*

Although the model presented in Eq. 4.26 use empirical relationships derived from data on the pyrolysis characteristics of a variety of biomasses, including experiments in various reactors and under various operating conditions, in the following it is used to predict the yields of volatiles arising from pyrolysis of a specific fuel (melee eucalypt wood) in a fluidized bed reactor at temperatures between 350 and 580ºC [18]; the measurement data reported in this investigation were not used to derive the empirical relationships used in Eq. 4.26. To apply the model, the following input data were taken from [18]: (i) the elemental composition of biomass (48.4% carbon, 45.2% oxygen, 6.3% hydrogen, mass % of daf fuel), (ii) the yield of char and (iii) reactor temperature. A comparison of predicted and measured yields of pyrolytic product is provided in Figure 4.17, where it was focused the yields of total liquids, total gas, tar, water, and CO_2. As already observed, these yields are predicted by solving Eq. 4.26, i.e. it is not given by the empirical relationships.

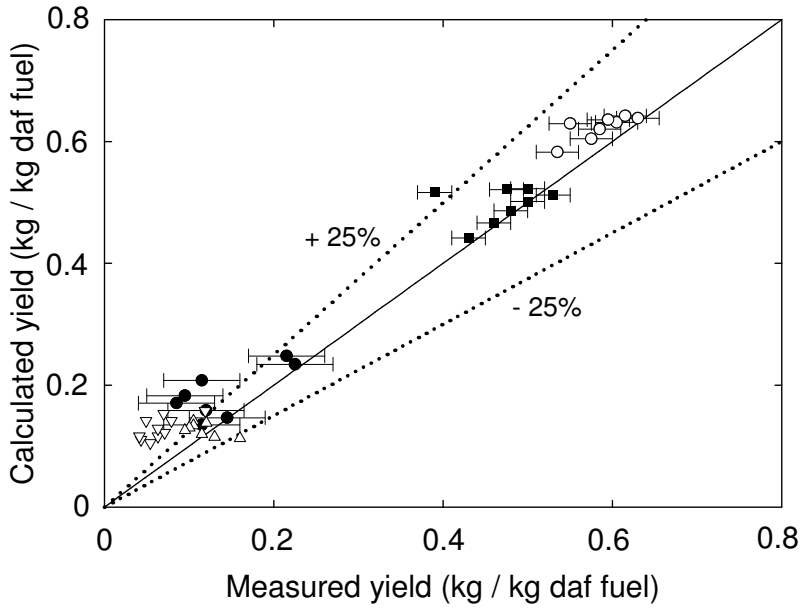

Figure 4.17 - Comparison between the results of empirical model (Eq. 4.26) and measurement data on the pyrolysis of woody biomass in the temperature range of 350-575ºC [18]. ○ - total pyrolytic liquids; ■ - tar; ● - total pyrolytic gas; ▽ - CO_2; △ - H_2O.

The model predicts most of measured yields within ±25% accuracy and the predictions are often within the uncertainty of the measurements. In general, the model overestimates the measurement data with the predicted yields of CO_2 significantly higher than the observed ones. The agreement is very reasonable for the yields of tar, water and total liquids. The difference between the predicted and modeled yields is less than 10% for both total liquids and total gas (both in mass % of daf fuel). The overall overestimation of the measured yields

is in the range of 3-12% of parent fuel which is in close agreement with the mass balanced closure reported in the cited experiments (86-96 mass % of parent fuel) [18]. Nevertheless, it is worth to point out that deviation on the modeled composition of volatiles can be obtained if the parameters of Eq. 4.26 are varied. A parameter that has great effect on the solution, even if it is varied marginally, is the CHO composition of tar that is here roughly approximated by empirical relationships (see section 4.4.1.2). By varying slightly the composition of tar, the figure is that a better prediction of gas is coupled with a worst prediction of liquids and vice-versa, since the overall overestimation of the measurements is maintained.

4.6 *Summary and conclusions*

In this study, investigations on biomass pyrolysis under inert atmosphere, including experiments with more than 60 different biomasses (woody and non-woody) in a variety of reactors and over a wide range of temperatures (200-1000ºC) were analyzed, and the respective data were screened and structured. The experimental data on pyrolytic product distribution and properties were collected together with information concerning the experimental rigs, operating conditions and fuel properties. The pyrolytic products were characterized by means of seven volatile species (tar, H_2, H_2O, CO, CO_2, CH_4 and other light hydrocarbons) and dry ash-free char.

Two regions of temperature corresponding to distinct stages of biomass thermal conversion were identified from the collected literature data. In the low temperature region (typically below 500ºC) the parent solid fuel decomposes into primary volatiles. The rapid decrease of the yield of char with temperature increase is compensated by the production of liquid products (i.e. tars and pyrolytic water). The yield of tar can increase to a value above 50% (mass % of daf fuel) at 450-550ºC but the yield of pyrolytic water is roughly constant. Variations in the yield of total permanent gas due to temperature increase are also small. The production of tars (depolymerization reactions) and pyrolytic water (dehydration reactions) seems complete within this low temperature region. The CHO contents of tar are largely dependent on the composition of parent biomass while those of char are very sensitive to the temperature of pyrolysis. The permanent gas is mainly composed CO_2 and CO. In the high temperature region (typically above 500ºC) the primary volatiles are further subject of secondary pyrolysis which has a great impact on the final composition of volatiles. Here the yield of pyrolytic liquids decreases rapidly with temperature increase, which is compensated by an increase in the yield of total permanent gas. Variations in the yield of char and pyrolytic water are comparatively small. It seems that the carbon and hydrogen contents of tar increases slightly while the oxygen content decreases. The elemental composition of char tends to a plateau and is much enriched in carbon. Tars are converted into a variety of

gaseous species, specially CO and light hydrocarbons. A multistep conversion of tars into smaller hydrocarbons was identified as a function of temperature. The yields of CO, H_2 and CH_4 show a similar pattern of change with temperature and are characterized by an exponential-like increase up to around 1000ºC. The yield of CO_2 increases slowly with temperature up to around 700-800ºC. The yield of the smaller light hydrocarbons (mainly C_2 species) seems to be linearly correlated with the yield of CH_4.

These general trends of pyrolytic product distribution as a function of temperature were fitted with an empirical model, consisting of system of equations where elemental and energy balances to the pyrolysis process are combined with empirical parameters. The model predicts the composition of pyrolytic volatiles by means of seven species (tar, H_2, H_2O, CO, CO_2, CH_4 and C_xH_y). The empirical relationships used in the model were derived from the collected literature data, including relations between the yields of gas-phase volatiles (H_2, CO and CH_4), product properties (elemental composition of char and tar and heating value of total gas) and the yield of hydrogen. These empirical data are well correlated with the collected data on product distribution, since the model predicts the correct trends of product yields as a function of temperature. This also shows that the kind of empirical relationships used in the model (i.e. the structure of the model) is adequate for biomass pyrolysis predictions. The model was here used as a complementary tool to further analyzing and checking the consistency of the collected data, while its prediction capability for specific fuels play a secondary role. However, comparison between model results and measurement data on the conversion of a woody biomass showed also a good agreement. The uncertainty on the elemental composition of lumped tar is still a major limitation in predicting the stoichiometry of the pyrolysis process for specific fuels. The model requires few input data, which is easily obtained: (i) the elemental composition of biomass, (ii) the yield of dry ash-free char and (iii) reactor temperature. In turns, it predicts the yields of volatile products that are difficult to measure (e.g. the yield of tar). The effect of operating parameters other than temperature (e.g. heating rate) are indirectly accounted for in the model as it influences the yield of char. It is concluded that empirical models of the type presented in this study, if conveniently modified by specific measurements with the fuel to be analyzed, can be useful as a submodel in comprehensive reactor models simulating pyrolysis, gasification or combustion processes.

Nomenclature

$Y_{i,F}$, $Y_{i,R}$, $Y_{i,K}$	yield of i^{th} product, dry ash-free fuel basis (kg i/kg dry ash-free fuel F), dry fuel basis (kg i/kg dry fuel R) or as-received fuel basis (kg i/kg as-received fuel K)
$Y_{j,F}$, $Y_{j,R}$, $Y_{j,K}$	mass fraction of j^{th} element in fuel, dry ash-free fuel basis (kg j/kg dry ash-

	free fuel F), dry fuel basis (kg j/kg dry fuel R) or as-received fuel basis (kg i/kg as-received fuel K)
$Y_{j,i}$	mass fraction of j^{th} element in i^{th} product, kg j/kg i
$Y_{a,F}$, $Y_{a,R}$, $Y_{a,K}$	ash content in fuel, dry ash-free fuel basis (kg ash/kg dry ash-free fuel F), dry fuel basis (kg ash/kg dry fuel R) or as-received fuel basis (kg ash/kg as-received fuel K)
$Y_{a,i}$	ash content in i^{th} product, kg ash/kg i
$Y_{M,F}$, $Y_{M,R}$, $Y_{M,K}$	moisture content in fuel, dry ash-free fuel basis (kg moisture/kg dry ash-free fuel F), dry fuel basis (kg moisture/kg dry fuel R) or as-received fuel basis (kg moisture/kg as-received fuel K)
$Y_{M,i}$	moisture content in i^{th} product, kg moisture/kg i
LHV_i	lower heating value of i^{th} product, MJ/kg i
T	pyrolysis (reactor) peak temperature, ºC
R^2	square of the correlation coefficient

Subscripts

i	i^{th} pyrolysis product (V, G, ch, S, tar, H_2O, bio-oil, C_xH_y, H_2, CO, CO_2, CH_4)
V	pyrolytic volatiles (tar + pyrolytic water + total permanent gas)
G	total pyrolytic (permanent) gas
ch	dry ash-free char
S	solid residue (dry ash-free char + ash)
Tar	lumped condensable organic compounds (liquids at ambient conditions)
H_2O	pyrolytic water
bio-oil	tar + pyrolytic water + moisture
C_xH_y	lumped non-methane light hydrocarbons (noncondensable at ambient conditions)
H_2	molecular hydrogen

CO	carbon monoxide
CO_2	carbon dioxide
CH_4	Methane
j	chemical elements
C	Carbon
H	Hydrogen
O	Oxygen
F	dry ash free fuel
R	dry fuel basis
K	as received fuel basis
M	Moisture
a	Ash

Abbreviations

arb	as-received basis
db	dry basis
daf	dry ash-free
LHV	lower heating value
HHV	higher heating value

Acknowledgement

It is gratefully acknowledged the financial support through a grant to Daniel Neves (ref. SFRH/BD/39567/2007) from the Fundação para a Ciência e a Tecnologia (FCT), Portugal.

References

1. Niksa S. Predicting the rapid devolatilization of diverse forms of biomass with bio-flashchain. Proc Combust Inst 2000;28:2727-33.

2. Neves D., Thunman H., Seeman M., Ideias P., Matos A., Tarelho L. et al. A database on biomass pyrolysis for gasification applications. In: Proceedings of the 17th European Biomass Conference & Exhibition: 1018-28. Hamburg, Germany 2009.
3. Di Blasi C., Branca C., Santoro A., Hernandez E.A. Pyrolytic behavior and products of some wood varieties. Combust Flame 2001;124:165-77.
4. Mohan D., Pittman C.U., Steele P.H. Pyrolysis of wood/biomass for bio-oil: a critical review. Energy & Fuels 2006;20:848-89.
5. Thunman H., Niklasson F., Johnsson F., Leckner B. Composition of volatile gases and thermochemical properties of wood for modeling of fixed or fluidized beds. Energy & Fuels 2001;15:1488-97.
6. Gómez-Barea A., Leckner B. Modeling of biomass gasification in fluidized bed. Prog Energy Combust Sci 2010;36:444-509.
7. Kersten S.R.A., Wang X., Prins W., van Swaaij W.P.M. Biomass pyrolysis in a fluidized bed reactor. Part 1: literature review and model simulations. Ind Eng Chem Res 2005;44:8773-85.
8. Roberts A.F. A review of kinetics data for the pyrolysis of wood and related substances. Combust Flame 1970;14:261-72.
9. Antal Jr. MJ. Effects of reactor severity on the gas-phase pyrolysis of cellulose and Kraft lignin-derived volatile matter. Ind Eng Chem Prod Res Dev 1983;22:366-75.
10. Ranzi E., Cuoci A., Faravelli T., Frassoldati A., Migliavacca G., Pierucci S., et al. Chemical kinetics of biomass pyrolysis. Energy & Fuels 2008;22:4292-300.
11. Di Blasi C. Modeling chemical and physical processes of wood and biomass pyrolysis. Prog Energy Combust Sci 2008;34:47-90.
12. Di Blasi C. Modeling and simulation of combustion processes of charring and non-charring solid fuels. Prog Energy Combust Sci 1993;19:71-104.
13. Dufuor A., Valin S., Castelli P., Thiery S., Boissonnet G., Zoulalian A., et al.Mechanisms and kinetics of methane thermal conversion in a syngas. Ind Eng Chem Res 2009;48:6564-72.
14. Scott D.S., Piskorz J. The continuous flash pyrolysis of biomass. Can J Chem Eng 1984;62:404-12.
15. Nik-Azar M., Hajaligol M.R., Sohrabi M., Dabir B. Effects of heating rate and particle size on the products yields from rapid pyrolysis of beech-wood. Fuel Sci Technol Int 1996;14:479-502.

16. Wang X., Kersten S.R.A., Prins W., van Swaaij W.P.M. Biomass pyrolysis in fluidized bed reactor. Part 2: experimental validation of model results. Ind Eng Chem Res 2005;44:8786-95.
17. Boroson M.L., Howard J.B., Longwell J.P., Peters W.A. Heterogeneous cracking of wood pyrolysis tars over fresh char surfaces. Energy & Fuels 1989;3:735-40.
18. Garcia-Perez M., Wang X-S., Shen J., Rhodes M.J., Tian F.J., Lee W.J., et al. Fast pyrolysis of oil mallee woody biomass: effect of temperature on the yield and quality of pyrolysis products. Ind Eng Chem Res 2008;47:1846-54.
19. Di Blasi C. Combustion and gasification rates of lignocellulosic chars. Prog Energy Combust Sci 2008;35:121-40.
20. Fraga A.R., Gaines A.F., Kandiyoti R. Characterization of biomass pyrolysis tars produced in the relative absence of extraparticle secondary reactions. Fuel 1991;70:803-9.
21. Shen J., Wang X-S., Garcia-Perez M., Mourant D., Rhodes M.J., Li C-Z. Effects of particle size on the fast pyrolysis of oil mallee woody biomass. Fuel 2009;88:1810-7.
22. Sreekanth M., Kumar R.R., Kolar A.K., Leckner B. Estimation of wood char size at the end of devolatilization in a bubbling fluidized bed combustor. Fuel 2008;87:3393-402.
23. Boroson M.K., Howard J.B., Longwell J.P., Peters A.W. Product yields and kinetics from the vapor phase cracking of wood pyrolysis tars. AIChE J 1989;35:120-8.
24. Morf P., Hasler P., Nussbaumer T. Mechanisms and kinetics of homogeneous secondary reactions of tar from continuous pyrolysis of wood chips. Fuel 2002;81:843-53.
25. Gilbert P., Ryu C., Sharifi V., Swithenbank J. Tar reduction in pyrolysis vapours from biomass over a hot char bed. Bioresour Technol 2009;100:6045-51.
26. Scott D.S., Majerski P., Piskorz J., Radlein D. A second look at fast pyrolysis of biomass - the RTI process. J Anal Appl Pyrolysis 1999;51:23-37.
27. Evans R.J., Milne T.A. Molecular characterization of the pyrolysis of biomass. 1. Fundamentals Energy Fuels 1987;1:123-37.
28. Yu Q., Brage C.,Chen G., Sjöström K. Temperature impact on the formation of tar from biomass pyrolysis in a free-fall reactor. J Anal Appl Pyrolysis 1997;40-41:481-9.
29. Kang B-S., Lee K.H., Park H.J., Park Y-K., Kim J-S. Fast pyrolysis of radiate pine in a bench scale plant with a fluidized bed: influence of a char separation system and reaction conditions on the production of bio-oil. J Anal Appl Pyrolysis 2006;76:32-7.
30. Tsai W.T., Lee M.K., Chang Y.M. Fast pyrolysis of rice husks: product yields and compositions. Bioresour Technol 2007;98:22-8.

31. Onay O., Beis S.H., Kockar O.M. Fast pyrolysis of rape seed in a well-swept fixed bed reactor. J Anal Appl Pyrolysis 2001;58-59:995-1007.
32. Shinogi Y., Kanri Y. Pyrolysis of plant, animal and human waste: physical and chemical characterization of the pyrolytic products. Bioresour Technol 2003;90:241-7.
33. Acikgoz C., Onay O., Kockar O.M. Fast pyrolysis of linseed: product yields and compositions. J Anal Appl Pyrolysis 2004;71:417-29.
34. Zanzi R., Sjöström K., Björnbom E. Rapid pyrolysis of agricultural residues at high temperature. Biomass & Bioenergy 2002;23:357-66.
35. Onay O., Beis S.H., Koçkar O.M. Pyrolysis of walnut shell in a well-swept fixed bed reactor. Energy Sources 2004;26:771-82.
36. Beis S.H., Onay O., Koçkar O.M. Fixed-bed pyrolysis of safflower seed: influence of pyrolysis parameters on product yields and compositions. Renewable Energy 2002;26:21-32.
37. Valenzuela C., Bernalte A., Gómez V., Bernate M. Influence of particle size and pyrolysis conditions on yield, density and some textural parameters of chars prepared from holm-oak wood. J Anal Appl Pyrolysis 1987;12:61-70.
38. Onay Ö., Koçkar Ö. Production of bio-oil from biomass: slow pyrolysis of rapeseed (Brassica napus L.) in a fixed-bed reactor. Energy Sources 2003;25:879-92.
39. Ates F., Putun E., Putun A.E. Fast pyrolysis of sesame stalk: yields and structural analysis of bio-oil. J Anal Appl Pyrolysis 2004;71:779-90.
40. Figueiredo J.L., Valenzuela C., Bernalte A., Encinar J.M. Pyrolysis of holm-oak wood: influence of temperature and particle size. Fuel 1989;68:1012-6.
41. Sensöz S., Demiral I., Gerçel H.F. Olive bagasse (Olea europea L.) pyrolysis. Bioresour Technol 2006;97:429-36.
42. Encinar J.M., Beltran F.J., Bernalte A., Ramiro A., Gonzalez J.F. Pyrolysis of two agricultural residues: olive and grape bagasse: influence of particle size and temperature. Biomass Bioenergy 1996;11:397-409.
43. Uzun B.B., Pütün A.E., Pütün E. Fast pyrolysis of soybean cake: product yields and compositions. Bioresour Technol 2006;97:569-76.
44. Encinar J.M., González J.F., González J. Fixed-bed pyrolysis of *Cynara cardunculus* L. Product yields and compositions. Fuel Process Technol 2000;68:209-22.
45. Bridgwater A.V., Meier D., Radlein D. An overview of fast pyrolysis of biomass. Org Geochem 1999;30:1479-93.

46. Agblevor F.A., Besler S., Wiselogel A.E. Fast pyrolysis of stored biomass feedstocks. Energy & Fuels 1995;9:635-40.
47. Dupont C., Commandré J.M., Gauthier P., Boissonnet G., Salvador S., Schweich D. Biomass pyrolysis experiments in an analytical entrained flow reactor between 1073K and 1273K. Fuel 2008;87:1155-64.
48. Nunn T., Howard J.B., Longwell J.P., Peters W.A. Product compositions and kinetics in the rapid pyrolysis of sweet gum hardwood. Ind Eng Chem Process Des Dev 1985;24:836-44.
49. Zanzi R., Sjöström K., Björnbom E. Rapid high-temperature pyrolysis of biomass in a free-fall reactor. Fuel 1996;75:545-50.
50. Milne T.A., Evans R.J., Abatzoglou N. Biomass gasifier "tars": their nature, formation and conversion. Colorado, U.S: National Renewable Energy Laboratory 1998. NREL/TP-570-25357.
51. Moersch O., Spliethoff H., Hein K.R.G. Tar quantification with a new online analyzing method. Biomass & Bioenergy 2000;18:79-86.
52. Oasmaa A., Peacocke C. A guide to physical property characterization of biomass-derived fast pyrolysis liquids, vol. 450. Espoo, Finland: VTT Publications 2001. Technical Research Centre of Finland.
53. Hasler P, Salzmann R, Kaufmann HP, Nussbaumer T. Method for the sampling and analysis of particles and tars from biomass gasifiers. In: Biomass for Energy and Industry. Proceedings of the 10th European Conference and Technology Exhibition, Würzburg, Germany 1998.
54. Good J., Ventress L., Knoef H., Zielke U., Hansen P.L., van de Kamp W., et al. Sampling and analysis of tar and particles in biomass producer gases. Technical report. CEN BT/TF 143. In: Organic Contaminants ("Tar") in Biomass Producer Gases 2005.
55. Özbay N., Apaydin-Varol E., Uzun B.B., Pütün A.E. Characterization of bio-oil obtained from fruit pulp pyrolysis. Energy 2008;33:1233-40.
56. Brage C., Yu Q., Chen G., Sjöström K. Use of amino phase adsorbent for biomass tar sampling and separation. Fuel 1997;76:29-37.
57. Knoef H.A.M., van de Beld L., Ahmadi M., Sjöstrom K., Brage C., Liliedahl T. Development of an online tar measuring method for quantitative analysis of biomass producer gas. In: Proceedings of the 17th European Biomass Conference & Exhibition; 884-88. Hamburg, Germany 2009.
58. Dufour A., Girods P., Masson E., Rogaume Y., Zoulalian A. Synthesis gas production by biomass pyrolysis: effect of reactor temperature on product distribution. Int J Hydrogen Energy 2009;34:1726-34.

59. Raveendran K., Ganesh A., Khilar K.C. Pyrolysis characteristics of biomass and biomass components. Fuel 1996;75:987-98.
60. Maschio G., Lucchesi A., Stoppato G. Production of syngas from biomass. Bioresour Technol 1994;48:119-26.
61. Demirbas A., Arin G. An overview of biomass pyrolysis. Energy Sources 2002;24:471-82.
62. Fagbemi L., Khezami L., Capart R. Pyrolysis products from different biomasses: application to the thermal cracking of tar. Appl Energy 2001;69:293-306.
63. Sensöz S., Can M. Pyrolysis of pine (Pinus Brutia Ten.) Chips: 1. Effect of pyrolysis temperature and heating rate on the product yields. Energy Sources 2002;24:347-55.
64. Balci S., Dogu T., Yücel H. Pyrolysis kinetics of lignocellulosic materials. Ind Chem Res 1993;32:2573-9.
65. Barooah J.N., Long V.D. Rates of thermal decomposition of some carbonaceous materials in a fluidized bed. Fuel 1976;55:116-20.
66. Beaumont O., Schwob Y. Influence of physical and chemical parameters on wood pyrolysis. Ind Eng Chem Process Des Dev 1984;23:637-41.
67. Di Blasi C., Signorelli G., Di Russo C., Rea G. Product distribution from pyrolysis of wood and agricultural residues. Ind Eng Chem Res 1999;38:2216-24.
68. Di Blasi C., Branca C. Kinetics of primary product formation from wood pyrolysis. Ind Eng Chem Res 2001;40:5547-56.
69. Della Roca P.A., Cerrella E.G., Bonelli P.R., Cukierman A.L. Pyrolysis of hardwoods residues: on kinetics and chars characterization. Biomass and Bioenergy 1999;16:79-88.
70. Demirbas A. Properties of charcoal derived from hazelnut shell and the production of briquettes using pyrolytic oil. Energy 1999;24:141-50.
71. Gray M.R., Corcoran W.H., Gavalas G.R. Pyrolysis of a wood-derived material. Effects of moisture and ash content. Ind Eng Chem Process Des Dev 1985;24:646-51.
72. Horne P.A., Williams T. Influence of temperature on the products from the flash pyrolysis of biomass. Fuel 1996;75:1051-9.
73. Islam M.N., Zailani R., Ani F.N. Pyrolytic oil from fluidized bed pyrolysis of oil palm shell and its characterization. Renewable Energy 1999;17:73-84.
74. Nunn T., Howard J.B., Longwell J.P., Peters W.A. Product compositions and kinetics in the rapid pyrolysis of milled wood lignin. Ind Eng Chem Process Des Dev 1985;24:844-52.
75. Oasmaa A., Kuoppala E. Fast pyrolysis of forestry residue. 3. Storage stability of liquid fuel. Energy & Fuels 2003;17:1075-84.

76. Scott D.S., Piskorz J., Radlein D. Liquid products from the continuous flash pyrolysis of biomass. Ind Eng Chem Process Des Dev 1985;24:581-8.
77. Scott D.S., Piskorz J., Bergougnou M.A., Graham R., Overend R.P. The role of temperature in the fast pyrolysis of cellulose and wood. Ind Chem Res 1988;27:8-15.
78. Sipilä K., Kuoppala E., Fagernäs L., Oasmaa A. Characterization of biomass based flash pyrolysis oils. Biomass and Bioenergy 1998;14:103-13.
79. Thurner F., Mann U. Kinetic investigation of wood pyrolysis. Ind Eng Chem Process Des Dev 1981;20:482-8.
80. Williams P.T., Besler S. The influence of temperature and heating rate on the slow pyrolysis of biomass. Renewable Energy 1996;7:233-50.
81. Xianwen D., Chuangzhi W., Haibin L., Yong C. The fast pyrolysis of biomass in CFB reactor. Energy & Fuels 2000;14:552-7.
82. Shihadeh A., Hochgreb S. Diesel engine combustion of biomass pyrolysis oils. Energy & Fuels 2000;14:260-74.
83. Shuanging X., Zhihe L., Boaming L., Weiming Y., Xueyuan B. Devolatilization characteristics of biomass at flash heating rate. Fuel 2006;85:664-70.
84. Channiwala S.A., Parikh P.P. A unified correlation for estimating HHV of solid, liquid and gaseous fuels. Fuel 2002;81:1051-63.
85. Demirbas A. Analysis of liquid products from biomass via flash pyrolysis. Energy Sources 2002;24:337-45.
86. Özbay N., Pütün A.E., Uzun B.B., Pütün E. Biocrude from biomass: pyrolysis of cottonseed cake. Renewable Energy 2001;24:615-25.
87. Pütün A.E. Biomass to bio-oil via fast pyrolysis of cotton straw and stalk. Energy Sources 2002;24:275-85.
88. Çaglar A., Dermibas A. Conversion of cotton cocoon shell to hydrogen rich gaseous products by pyrolysis. Energy Conversion Manage 2002;43: 489-97.
89. Güllü D. Effect of catalyst on yield of liquid products from biomass via pyrolysis. Energy Sources 2003;25:753-65.
90. Tuncel F., Gerçel H.F. Production and characterization of pyrolysis oils from Euphorbia Macroclada. Energy Sources 2004;26:761-70.
91. Demirbas A. Pyrolysis and steam gasification processes of black liquor. Energy Conversion Manage 2002;43:877-84.
92. Pütün A.E., Özcan A., Pütün E. Pyrolysis of hazelnut shells in a fixed-bed tubular reactor: yields and structural analysis of bio-oil. J Anal Appl Pyrolysis 1999;52:33-49.

93. Sensöz S., Angin D. Pyrolysis of safflower (*Chartamus tinctorius* L.) seed press cake: Part 1. The effects of pyrolysis parameters on the product yields. Biosource Technol 2008;99:5492-7.
94. Li L., Zhang H., Zhuang X. Pyrolysis of waste paper: characterization and composition of pyrolysis oil. Energy Sources 2005;27:867-73.
95. Bonelli P.R., Cerrella E.G., Cukierman A.L. Slow pyrolysis of nutshells: characterization of derived chars and of process kinetics. Energy Sources 2003;25:767-78.
96. Apaydin-Varol E., Pütün E., Pütün A.E. Slow pyrolysis of pistachio shell. Fuel 2007;86:1892-9.
97. Zandersons J., Gravitis J., Kokorevics A., Zhurinsh A., Bikovens O., Tardenaka A., et al. Studies of the Brazilian sugarcane bagasse carbonization process and products properties. Biomass and Bioenergy 1999;17:209-19.
98. Pütün A.E., Önay E., Uzun B.B., Özbay N. Comparison between the 'slow' and 'fast' pyrolysis of tobacco residue. Ind Crops Prod 2007;26:307-14.
99. Miao X., Wu Q. High yield bio-oil production from fast pyrolysis by metabolic controlling of Chorella protothecoides. J Biotechnol 2004;110:85-93.
100. Tsai W.T., Lee M.K., Chang Y.M. Fast pyrolysis of rice straw, sugarcane bagasse and coconut shell in an induction-heating reactor. J Anal Appl Pyrolysis 2006;76:230-7.
101. Schröder E. Experiments on the pyrolysis of large beechwood particles in fixed beds. J Anal Appl Pyrolysis 2004;71:669-94.
102. Aguado R., Olazar M., José M.J.S., Aguirre G., Bilbao J. Pyrolysis of sawdust in a conical spouted bed reactor. Yields and product composition. Ind Eng Chem Res 2000;39:1925-33.
103. Raveendran K., Ganesh A. Heating value of biomass and biomass pyrolysis products. Fuel 1996;75:1715-20.
104. Sensöz S., Can M. Pyrolysis of pine (*Pinus Brutia* Ten.) Chips: 2. Structural analysis of bio-oil. Energy Sources 2002;24:357-64.
105. Demirbas A. Effect of temperature on pyrolysis products from four nut shells. J Anal Appl Pyrolysis 2006;76:285-9.
106. Elliot D.C. Relation of reaction time and temperature to chemical composition of pyrolysis oils. In: Soltes ED, Milne TA, editors. Pyrolysis oils from biomass: Producing, analyzing and Upgrading (ACS Symposium series 376). Washington D.C: ACS 1998.
107. Funazukuri T., Hudgins R.R., Silveston P.L. Correlation of volatile products from fast cellulose pyrolysis. Ind Eng Chem Process Des Dev 1986;25:172-81.

108. Gómez-Barea A., Nilsson S., Barrero F.V., Campoy M. Devolatilization of biomass and waste in fluidized bed. Fuel Process Technol 2010;91:1624-33.

109. Piskorz J., Majerski P., Radlein D., Scott D.S., Bridgwater A.V. Fast pyrolysis of sweet sorghum and sweet sorghum bagasse. J Appl Anal Pyrolysis 1998; 46:15-29.

110. Culp A.W. Principles of Energy Conversion. 2nd ed. McGraw-Hill 1991.

111. Pereira M.R.C. Projecto de um gasificador de biomassa. MSc thesis 2009. University of Aveiro, Aveiro, Portugal.

Chapter 5 - Dependence of char yield on the elemental composition of biomass

Daniel Neves[a,b], Arlindo Matos[a], Luís Tarelho[a], Henrik Thunman[b], Anton Larsson[b], Martin Seemann[b]

[a] University of Aveiro and CESAM, [b] Chalmers University of Technology

Submitted for publication in Biomass & Bioenergy.

Abstract

The yields and properties of the primary products of pyrolysis are critical parameters for evaluating thermochemical conversion of biomass. How these parameters are influenced by fuel and operating conditions is currently poorly understood. In the present work, we investigated how one of the products, the char, is affected by the composition of fuel under operating conditions typical of fluidised bed combustors and gasifiers. For this purpose, the carbonisation of 14 biomasses, cellulose, and lignin (6×6 mm cylindrical particles) was investigated under nitrogen and with peak temperatures within 600–950ºC. Fast heating was achieved in a small fluidised bed and quartz tube reactors, while the effect of less severe heating (5 or 50ºC/min) was tested in a thermobalance. The char from the rapidly carbonised fuels exhibited minor mass loss at temperatures >600ºC and this process yielded high carbon content chars at the higher temperatures. As the properties of char tend to those of graphite as the temperature increases, also the respective yields tended to asymptotes that approached the theoretical equilibrium values predicted for graphite. In practice, the production of char in fluidised beds is largely governed by the composition of the fuel and in the manner described by a model proposed in this work.

Keywords

Biomass, Char, Pyrolysis, Gasification, Combustion, Fluidised bed

5.1 *Introduction*

Thermal degradation of solid biomass can be viewed as a two-stage process [1-3]. During primary pyrolysis numerous volatile products are released from the parent fuel, to yield a carbon-rich char. Some of these volatiles are thermally unstable and undergo secondary pyrolysis into light gases, refractory tars and eventually, soot (i.e. carbon) [4-8]. At a given temperature, the overall pyrolysis reaction ultimately drives the distribution of products towards the equilibrium composition. However, the process is often kinetically controlled, and with short residence time can be plotted as a function of temperature (Figure 5.1). Only at the highest temperatures (e.g., >1300ºC) is the fuel likely to be converted to equilibrium in a short time, yielding a rather simple composition of the volatiles (mainly H_2 and CO). This process is typified by the case [9] in which a surrogate pyrolysis gas is seen to approach the equilibrium composition through thermal treatment at 1370ºC and a 2s residence time; similar conditions have been applied in a pilot process to convert the raw gas from a fluidised bed steam gasifier mainly into H_2 and CO [10]. However, as the temperature decreases, more time is needed to attain the equilibrium, with the consequence that the composition of the volatiles becomes more complex. At 500-600ºC, the secondary reactions are sufficiently slow [1] so that the process is governed by primary degradation. Several studies have shown that primary pyrolysis produces between 60 and 95% volatiles as the biomass heats up to 600ºC (Figure 5.2-a). However, further heating leads to a relatively small additional loss of mass (see also e.g., [11-13]). The apparent asymptotic yield of char at temperatures >600ºC suggests that the secondary reactions are a minor source/sink of char, although these reactions are effective in pushing the composition of the primary volatiles towards equilibrium. It is noteworthy that the carbon content and heating value of char also exhibit an asymptotic behaviour as a function of temperature (Figure 5.2-b, -c), approaching the values for carbon graphite (100%C, 32.8MJ/kg), at temperatures above 600ºC. The accompanying structural transformations of the char were investigated (e.g. [14]) using infrared (IR) and X-ray analyses which revealed increasing carbon aromatisation towards the stable graphite structure as the temperature increased above 400ºC.

As the properties of char tend to those of graphite as the temperature increases, it is hypothesised that the asymptotic yield of char also approaches the equilibrium value for graphite under certain conditions. In the present work, we tested this hypothesis in relation to the fast carbonisation of fuel at high temperature, based on literature data and experiments with a set of biomasses, cellulose, and lignin. Carbonisation of fuel particles of a practical size was performed in a small fluidised bed and fixed bed quartz-tube reactors operated at atmospheric pressure and temperatures in the range of 600-950ºC. To test the

effect of slow heating (<50ºC/min) on the charring process, some experiments were performed in a thermobalance. The results demonstrate how the composition of biomass affects the yield of char under conditions typically used for fluidised bed combustors and gasifiers.

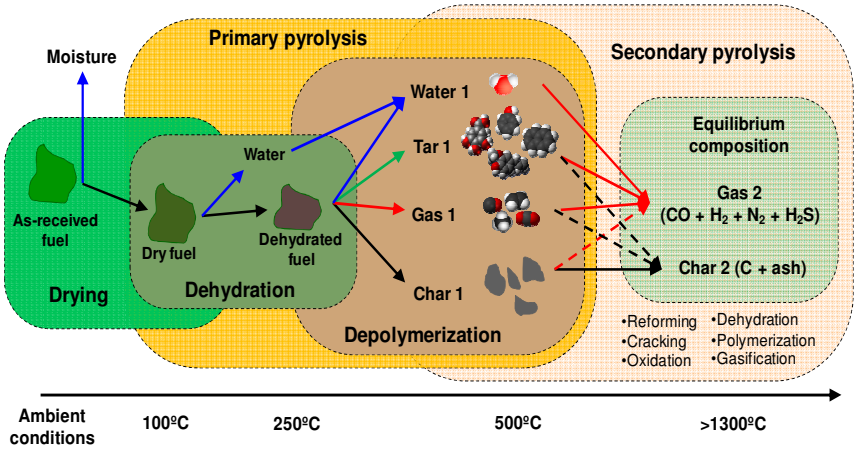

Figure 5.1 - Pyrolysis pathways for a fresh biomass particle towards the equilibrium composition. Staged conversion is shown as a function of temperature and with a short residence time (say, <5s). Lumped tar refers to all organic compounds that condense under ambient conditions.

5.2 *Parameters that influence the asymptotic yield of char*

The scatter in the yields of char obtained at temperatures >600ºC (Figure 5.2-a) can be partially due to variations in the composition of the biomass. It is emphasised that this scatter (from 5 to 40% of daf fuel) is within the range obtained for the pyrolysis of cellulose and lignin under various conditions; ultimate yields of char of 3-28% have been reported for cellulose [4,15-25], while yields for lignins are in the range of 15-46% [4,15,16,22,26-31]. The positive effect of lignin on the formation of char has been shown [32-34], and has led to models in which the yield of char from a given fuel is predicted based on the respective contents of lignin, hemicellulose, cellulose, and eventually extractives (e.g., [22,33,35]). For the pyrolysis of 20 biomasses at 500ºC, a positive effect of the carbon content of the fuel on the yield of char has been also shown [33]. More recently, Antal et al. [34] noted that for some fuels the yield of char could be approximated from the ultimate analysis (i.e., equilibrium values) if the pyrolysis was carried out at 450ºC and 1 MPa and if the char obtained in this way was further heated to 950ºC under atmospheric pressure. Therefore, the range of char yields shown in Figure 5.2-a for temperatures >600ºC is in some way related to variations in the structural and elemental compositions of the biomass. Not unexpectedly, the structural and elemental compositions are also correlated given the high carbon content of lignins (59-67% of daf fuel [4,15,16,22,26-31]) compared with cellulose (44.4%).

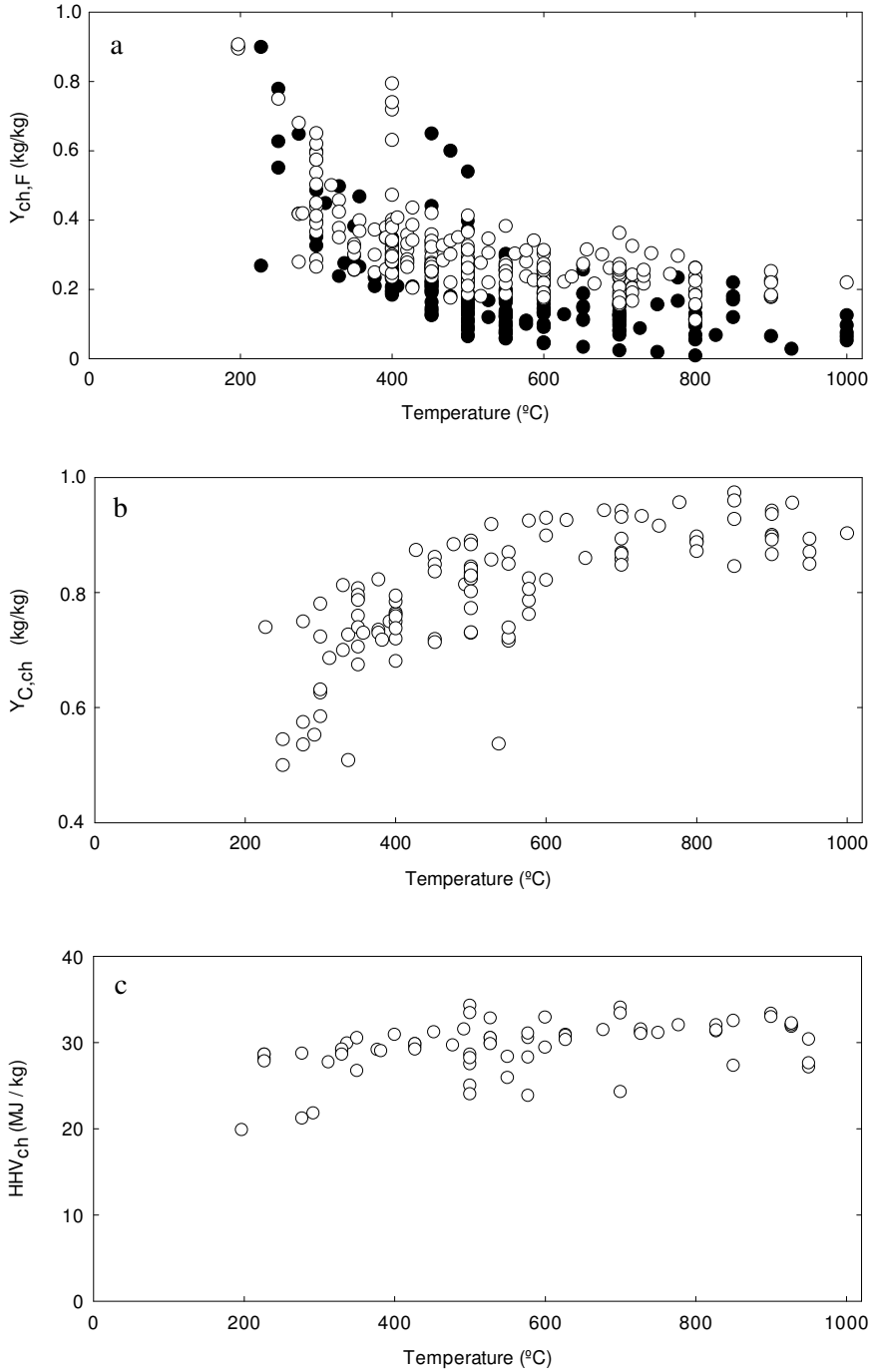

Figure 5.2 - Overview of literature data regarding the yields (a, $Y_{ch,F}$), carbon contents (b, $Y_{C,ch}$), and heating vales (c, HHV_{ch}) of biomass chars as a function of pyrolysis peak temperature [3,67]. The data for the yields are structured according to slow (open symbols) and fast heating (filled symbols).

In addition, the influence of the operating conditions must be recognized [36], e.g., the higher yields of char generated by slow heating (Figure 5.2-a). This outcome may be due to re-polymerisation of the newly formed volatiles (e.g., tar) within or between the charring particles, which means that conditions such as slow heating, large fuel particle size, and high

external pressure, may favour the production of secondary char from the volatiles [13,36,37]. There are notable examples of how the yield of char varies depending on the manipulation of the volatiles [34,37,38]. Moreover, studies of the pyrolysis mechanism of cellulose (see reviews [1,7,39]) show that the operating conditions can also influence the primary production of char. The current consensus is that cellulose degradation involves an early stage of dehydration, which is followed by depolymerisation. Dehydration is the rate-limiting step at temperatures <250ºC, and the outcome is a more stable dehydrated structure than the parent cellulose. Accordingly, when dehydration is almost complete before the onset of depolymerisation, the net volatilisation is reduced, which may explain the more favourable charring conditions observed for slow heating [13,24,25]. For instance, the above mechanism has been invoked to explain the increase in char yield from 11 to 28% (mass % of fuel) when the heating rate of cellulose is decreased from 70 to 0.03ºC/min [25]. This may also explain the positive effect of ash on the char yield [13,25], as some minerals that occur naturally in biomass can catalyse dehydration. We note that owing to the segregation of the dehydration reaction during slow heating, the residue that is undergoing depolymerisation no longer has the same properties as the parent fuel. For example, the rapid cleavage of cellulose starts at 240ºC and the IR spectrum at 280ºC is no longer that of the carbohydrate [14]. Thus, under slow pyrolysis, the production of primary char becomes a function of the heating history [24], and the composition of the fuel plays a secondary role.

In summary, the yield of char obtained at high temperature (i.e., >600ºC) is influenced by both the composition of the fuel and the operating conditions. Unless the formation of secondary char from the gas-phase reactions of volatiles is promoted (by e.g. increasing the residence time or pressure), the competing dehydration and depolymerisation reactions determine the quantity of char arising from a given fuel (see Figure 5.1). We further hypothesise that depolymerisation at an early stage of pyrolysis attributes no “memory” to the conversion history. Therefore, the composition of the fuel is likely to be the main parameter that determines the asymptotic yield of char under fast heating.

5.2.1 *Yield of char under the equilibrium condition*

Thermodynamics allows the analysis of the influence of fuel composition on the yield of char. In the present work, this is investigated with the Gaseq equilibrium software [40] and using carbon graphite (noted C_g) as a model compound for the char. Figure 5.3 shows the temperature-dependent equilibrium composition of the pyrolytic products for one type of biomass that contains significant amounts of CHONS. Similar trends are obtained for any biomass, cellulose or lignin. Note that only a few species are relevant for the mass balance, i.e., CO_2, CO, H_2O, H_2, N_2, H_2S, CH_4, and C_g, even though other volatile species were considered

in the analysis. Large amounts of CO_2, H_2O, CH_4, and Cg are predicted at temperatures below ≈500ºC, while at higher temperatures (say, >1000ºC), CO, H_2 and Cg are the preferred products. The yields of N_2 and H_2S are rather stable over the entire temperature range analysed. Carbon graphite undergoes major changes in the temperature range of 500-900ºC and, outside this range, the yield is also stable; the plateau being attained at temperatures >1000ºC (≈15.6% in Figure 5.3; hereinafter denoted as $Y^*_{Cg,F}$) is emphasized since we hypothesizes that the asymptotic yield of char shown in Figure 5.2-a approaches this value when the fuel is converted with fast heating. Therefore, an approximated model that computes $Y^*_{Cg,F}$ is proposed in the following.

Figure 5.3 shows that at high temperature and under an excess of carbon and hydrogen, the fuel is converted according to a simple scheme (e.g., the reaction at 1200ºC): (i) the oxygen is mainly incorporated into CO; (ii) most of the hydrogen is converted into H_2, with the remainder forming H_2S; and (iii) the nitrogen becomes N_2. Since other volatile species can be neglected at this high temperature, the plateau values for the yields of CO, H_2, H_2S, and N_2 under the equilibrium condition ($Y^*_{i,F}$) can be approximated by Eq. 5.1 to Eq. 5.4, respectively, and the corresponding yield of carbon graphite can be obtained by the difference method, as expressed in Eq. 5.5 and Eq. 5.6 for a daf fuel basis and fuel carbon basis, respectively.

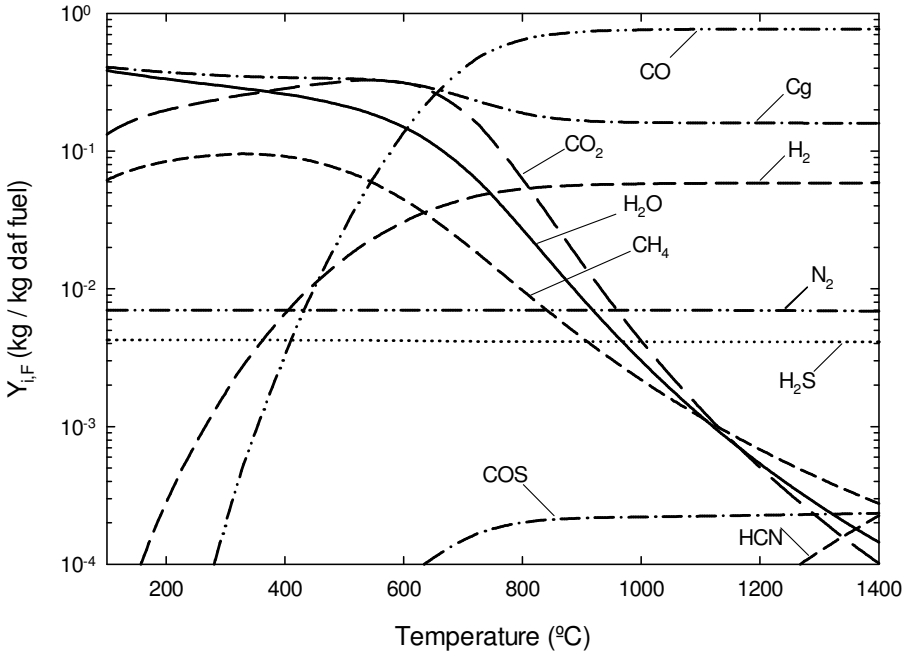

Figure 5.3 - Equilibrium composition of pyrolytic products as a function of temperature and atmospheric pressure. Example for one lignocellulosic biomass with significant amounts of CHONS (48.7%C, 6.2%H, 44.0%O, 0.7%N, 0.4%S). Species below <0.01% of the daf fuel are not shown.

$$Y^{*}_{CO,F} \approx Y_{O,F} \cdot \frac{M_{CO}}{M_{O}} \quad \text{Eq. 5.1}$$

$$Y^{*}_{H_2,F} \approx Y_{H,F} - Y_{S,F} \cdot \frac{M_{H_2S}}{M_{S}} \quad \text{Eq. 5.2}$$

$$Y^{*}_{H_2S,F} \approx Y_{S,F} \cdot \frac{M_{H_2S}}{M_{S}} \quad \text{Eq. 5.3}$$

$$Y^{*}_{N_2,F} \approx Y_{N,F} \quad \text{Eq. 5.4}$$

$$Y^{*}_{Cg,F} \approx Y_{C,F} + \left(1 - \frac{M_{CO}}{M_{O}}\right) \cdot Y_{O,F} \quad \text{Eq. 5.5}$$

$$\frac{Y^{*}_{Cg,F}}{Y_{C,F}} \approx 1 + \left(1 - \frac{M_{CO}}{M_{O}}\right) \cdot \frac{Y_{O,F}}{Y_{C,F}} \quad \text{Eq. 5.6}$$

To provide an overview of $Y^{*}_{Cg,F}$ and $Y^{*}_{Cg,F}/Y_{C,F}$ among charring fuels, literature data on the CHONS composition of biomasses, lignins, and chars were surveyed; existing datasets were used for biomasses [3,41], while the data for lignins [4,15,16,22,26-31] and chars (Table 5.1) [12,42-62] were structured in the present work. The values predicted by Eq. 5.5 and Eq. 5.6 are shown in Figure 5.4 as function of the O/C mass ratio of fuel, providing the series of fuels structured according to its ability to form carbon graphite. The maximum and minimum values of $Y^{*}_{Cg,F}$ (and $Y^{*}_{Cg,F}/Y_{C,F}$) correspond to pure carbon (O/C=0, $Y^{*}_{Cg,F}$=1) and glucose (O/C=1.33, $Y^{*}_{Cg,F}$=0), respectively. Pyrolysis of glucose does not produce carbon under equilibrium because it has the same O/C ratio as carbon monoxide. However, the elimination of one molecule of water from glucose yields cellulose with an O/C ratio of 1.11 kg/kg, which enables the process to proceed under an excess of carbon. Thus, cellulose yields 0.074 kg/kg of carbon graphite under the equilibrium condition (fuel-basis). Likewise, for hemicellulose (in the present instance, xylan) one predicts $Y^{*}_{Cg,F}$=0.09, while for lignins, the compositions of which vary across biomasses, the corresponding values range from 0.33 to 0.48 kg/kg. As expected, the theoretical values for biomass lie approximately between those for the major structural components, i.e., cellulose and lignin, whereas biomass chars give values that range from those of lignins (case for low-temperature chars) to almost unity (case for high-temperature chars).

Table 5.1 - Survey of some literature data regarding the compositions of chars formed from the pyrolysis of biomass.[a]

Parent fuel	T_{peak} (ºC)	Mass fraction, mass% of daf-fuel					Ash (db)	Ref.
		Carbon	Hydrogen	Oxygen	Nitrogen	Sulphur		
Wood	500	89.0	2.8	8.2	--	--	0.6	[42]
	700	94.2	1.1	4.7	--	--	1.1	
	900	94.2	0.6	5.1			1.1	
Coconut shell	500	88.4	2.6	9.0	--	--	1.4	[42]
	700	93.1	1.1	5.8	--	--	1.4	
	900	93.6	0.7	5.6	--	--	1.7	
Straw	500	82.8	2.7	11.7	--	--	16.3	[42]
	700	85.8	1.3	15.7	--	--	16.4	
	900	86.7	1.4	11.9	--	--	17.4	
Fir wood	577	85.0	3.2	11.6	0.2	0.0	2.0	[43]
Wheat straw	577	78.6	2.9	17.5	0.6	0.4	18.3	[43]
Olive husks	577	82.5	3.0	13.5	1.0	0.0	4.6	[43]
Grape residues	577	76.3	2.9	18.4	2.3	0.1	10.2	[43]
Rice husks	577	80.6	3.3	15.3	0.7	0.0	36.1	[43]
Mixed waste wood	400	68.1	3.2	28.1	--	--	--	[44]
	450	71.9	3.2	24.2	--	--	--	
	500	73.0	3.2	22.9	--	--	--	
	550	71.6	2.7	24.4	--	--	--	
Hazelnut shell	197	53.3	6.1	40.6	--	--	--	[45]
	277	75.0	5.5	19.5	--	--	2.3	
	377	82.3	3.6	14.1	--	--	2.3	
	477	88.4	2.4	8.6	--	--	2.4	
	577	92.5	1.9	6.0	--	--	2.7	
	677	94.3	1.5	4.2	--	--	2.7	
	777	95.7	1.3	3.1	--	--	2.8	
Hardwood	350	76.0	4.4	17.9	1.7	--	0.9	[46]
	850	97.4	0.9	0.5	1.2	--	4.3	
Hardwood	350	74.0	4.3	20.5	1.2	--	1.9	[46]
	850	92.8	1.3	5.1	0.8	--	7.2	
Almond shell	350	78.9	2.7	18.4	0.0	--	2.4	[47]
	452	86.2	2.3	11.3	0.3	--	2.4	
Hazelnut shell	350	80.7	3.4	15.7	0.2	--	1.5	[47]
	452	84.9	2.9	11.7	0.5	--	1.6	
Beech shell	350	79.6	3.1	17.3	0.0	--	1.7	[47]

	452	83.7	2.6	12.6	0.6	--	1.7	
Oak sawdust	330	70.0	4.9	21.0	--	--	--	[48]
	357	73.0	4.0	19.0	--	--	--	
	377	73.5	3.8	18.0	--	--	--	
	392	75.0	3.5	16.0	--	--	--	
Sweet gum wood	337	50.9	6.3	42.8	--	--	1.5	[49]
	537	53.7	6.4	41.4	--	--	4.1	
Pine wood	250	50.0	5.8	44.2	--	--	--	[12]
	400	72.0	3.8	24.2	--	--	--	
	550	87.0	2.0	11.0	--	--	--	
	652	86.0	2.2	11.8	--	--	--	
	800	89.0	0.8	10.2	--	--	--	
Subabul wood	950	87.0	2.0	10.9	0.0	--	4.0	[50]
Casuria wood	950	89.4	1.1	6.5	3.1	--	13.2	[50]
Eucalyptus wood	950	85.0	1.5	12.4	1.1	--	10.5	[50]
Coconut shell	750	91.6	0.8	6.2	1.4	--	2.9	[50]
Cotton straw/stalk	550	72.2	1.2	26.0	--	--	--	[51]
Safflower seed	500	77.4	2.2	16.2	4.2	--	--	[52]
Olive bagasse	500	73.1	2.3	22.0	2.6	--	--	[53]
Rape seed	550	87.2	2.4	5.0	5.4	--	--	[54]
Pine wood	500	84.5	2.7	12.8	0.0	--	--	[55]
Walnut shell	500	77.3	3.5	17.7	1.5	--	--	[56]
Peanut shell	350	78.7	4.5	16.5	0.5	--	1.4	[57]
	600	93.0	2.2	3.2	0.7	--	4.5	
	850	96.0	0.6	2.4	0.6	--	3.2	
Hazelnut shell	350	70.6	4.7	23.5	1.2	--	2.5	[57]
	600	85.0	2.2	11.5	1.2	--	3.9	
	850	84.6	0.8	13.7	0.9	--	4.2	
Tobacco residue	550	73.9	4.7	19.1	2.3	--	--	[58]
Rape seed	550	91.10	2.70	5.10	1.10	--	--	[62]
Beech wood	277	53.6	5.7	40.5	0.2	--	--	[59]
	292	55.3	5.6	39.7	0.2	--	--	
	312	68.6	5.1	26.1	0.3	--	--	
	337	72.7	4.8	16.3	0.2	--	--	
	382	71.8	4.2	17.1	0.3	--	--	
	400	76.2	4.3	19.2	0.3	--	--	
	452	71.4	3.8	24.5	0.3	--	--	
	492	81.4	3.8	11.5	0.2	--	--	

	527	85.7	3.6	6.4	0.3	--	--	
	197	53.3	5.4	41.3	--	--	2.2	
	300	62.6	4.3	33.1	--	--	5.4	
	400	75.0	2.8	22.2	--	--	5.9	
	500	83.4	2.3	14.3	--	--	6.7	
Holm oak	600	89.9	1.7	8.4	--	--	5.5	[60]
	700	89.4	0.8	9.8	--	--	4.7	
	800	89.7	0.4	9.9	--	--	5.2	
	900	90.0	0.3	9.7	--	--	5.7	
	1000	90.3	0.3	9.4	--	--	5.0	
	300	58.5	5.0	36.5	--	--	3.6	
	400	73.8	3.4	22.0	--	--	7.3	
	500	80.2	2.4	17.4	--	--	8.7	
Holm oak	600	82.2	1.6	16.2	--	--	10.2	[61]
	700	84.8	1.3	13.9	--	--	10.6	
	800	87.2	0.8	12.0	--	--	12.0	
	900	89.2	0.6	10.2	--	--	11.5	

[a] Within a given reference, only one temperature series is shown for each fuel.

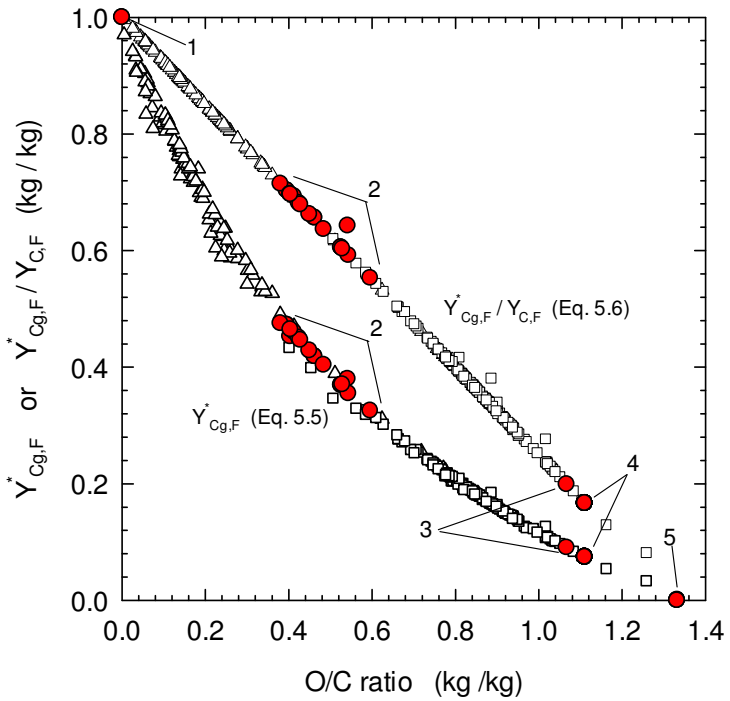

Figure 5.4 - Yield of carbon graphite under the equilibrium condition as a function of the O/C mass ratio of the parent fuel (see Eq. 5.5 and Eq. 5.6). Data points: 1, pure carbon; 2, lignins (data from [4,15,16,22,26-31]); 3, hemicellulose (xylan); 4, cellulose; 5, glucose; Δ, pyrolytic chars from lignocellulosic biomasses (data from [12,42-62]); □, lignocellulosic biomasses (data from [3,41]).

5.2.1.1 *Comparisons with literature data*

An initial insight into the relationship between the asymptotic yield of char and the elemental composition of fuel is provided in Figure 5.5, which is based on published data and also includes the theoretical values for $Y^{*}_{Cg,F}$ (see Eq. 5.5). The data on biomasses were taken from a survey conducted by Vassilev et. al. [41] and are related to the fixed carbon content of fuel (daf basis), as obtained by standard proximate analysis; the widely used procedures described in ASTM E872 and CEN/TS 15148 consist of heating the fuel sample in tapped crucibles to 900–950ºC and holding at this temperature for 6–7 minutes. Both methods assure fast heating and a reducing atmosphere, which means that the analysis provides a good estimate of the asymptotic yield of char under fast heating. In turns, the data for lignins and cellulose were derived from investigations in which pyrolysis was carried out under an inert gas and the heating rates ranged from 5ºC/min to fast [4,15-31].

Despite the large variations in pyrolysis conditions and measurement methods, the collected data render a function of the O/C ratio of the fuel and are typically within ±25% of the equilibrium values predicted for carbon graphite. Only a few investigations have reported data well beyond this range (Figure 5.5). The scatter in the data is also attributed to two major concerns regarding the measurements: 1) the uncertainty associated with standard ultimate analysis of fuel; and 2) the uncertainty associated with the measured yields of char (or fixed carbon content). Ultimate analyses of replicate fuel samples commonly yield errors of, say, ±3% for the carbon and oxygen contents (e.g., [24,37]), which means that the uncertainty with regard to the O/C mass ratio of the fuel is typically ±5%. As a result, the uncertainty for the theoretical value of $Y^{*}_{Cg,F}$ calculated from the elemental composition of fuel (see Eq. 5.5) is ±5–20%, depending on the fuel under investigation. Moreover, exposure of the fuel samples to moist ambient air before they are fed into the elemental analyser cannot be ruled out, and this may also lead to inaccurate results [24]. Secondly, the measurement methods for the yield of char may also lack precision. Indeed, a round-robin study among eight laboratories that measured mass-loss curves of cellulose using thermogravimetry [18] showed widely scattered results; under moderate heating (40ºC/min), the asymptotic yield of char reported for different fractions of the same sample of cellulose varied from 2.9 to 10.5% (mass % of fuel). When the yield of char is approximated from the standard proximate analysis of the fuel, the results are uncertain in typically ±5–10% of the mean value. In light of this, it can be stated that the differences between the measured yields of char and the theoretical yields of carbon graphite in Figure 5.5 are frequently within the measurement uncertainties. However, given the inherent features in the collected literature data (e.g., different heating rates of fuel), the scatter remains large and the relationship needs to be further verified. This was the motivation for

the experiments carried out in this work, which were conducted with a broad range of fuels and under conditions that enhance the effect of fuel composition in the charring process.

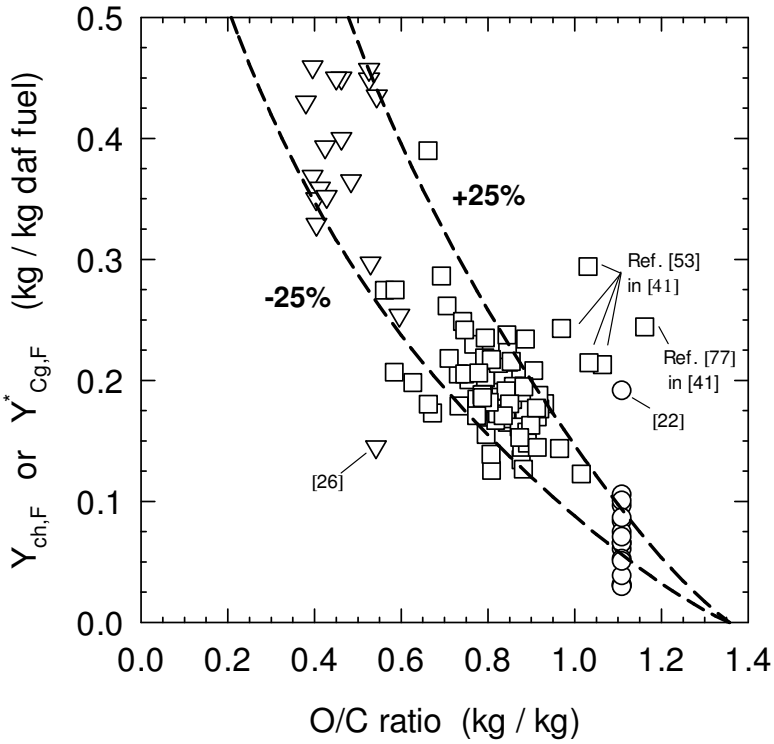

Figure 5.5 - Asymptotic yield of char as a function of the O/C mass ratio of the parent fuel. Comparison of literature data [4,15-31,41] and the equilibrium values for carbon graphite; the ±25% range is relative to the result given by Eq. 5.5. □, Lignocellulosic biomass; ▽, lignin; ○, cellulose (assumed as $C_6H_5O_{10}$).

5.3 *Experimental*

The materials and experimental equipment used in this work are described below. The equipment includes facilities that are designed to achieve fast heating (atmospheric bubbling fluidised bed and quartz-tube reactors) or slow heating (thermobalance) of the fuel to high temperatures (600–950ºC).

5.3.1 *Fuels*

Fourteen biomasses, lignin and cellulose were used in this work. At the University of Aveiro, a 11 materials, pine wood, pine bark, eucalyptus wood, eucalyptus bark, beech wood, gorse wood, oak wood, forest biomass residues pellets (hereinafter referred to as forest pellets), wood pellets, cellulose, and lignin, were pyrolysed with fast heating. To minimise the influence of the variability of particle size among the fuels, cylindrical particles of about 6×6

mm were prepared from the raw materials (with the exception of the wood pellets, which had dimensions of 8×8 mm). The woody materials and the pine bark were cut into ≈100 mm^2 parallelepipeds before the cylindrical shape was formed using a lathe or bench grinder. The eucalyptus bark and cellulose were ground in a hammer mill to <2 mm and gently compressed into 6×6mm pellets. The lignin was supplied as cm-sized, clay-like particles. As attempts to prepare pellets from the lignin proved unsuccessful, a sharp knife was used to cut cylinder-like particles from the raw particles. The forest pellets (≈6×6 mm) and wood pellets (≈8×8 mm) were supplied by a company. An additional five fuels (straw pellets, bark pellets, sawdust, peat, and wood chips) and the wood pellets were tested at Chalmers University of Technology at slow heating rates using a thermobalance. For this purpose, the pelletised fuels were not ground, as grinding was found to have no effect on the results; the other fuels were ground to fit the size of the crucibles used in the thermobalance.

The ultimate compositions and ash contents of the fuels are summarised in Table 5.2; the ultimate analysis was carried out by external laboratories, while the ash content was determined in our laboratories following a standard method (CEN/TS 14775).

Table 5.2 - Ash contents and ultimate compositions of the fuels used in this work. The results shown are the mean values for replicate samples (± one standard deviation for some fuels).

	Mass fraction, mass % of dry fuel					
Fuel	Carbon	Hydrogen	Oxygen[a]	Nitrogen	Sulphur	Ash
Pine wood	48.0±1.2	6.3±0.1	45.1±1.2	0.1±0.0	nd	0.5±0.0
Pine bark	54.0±0.6	5.8±0.1	38.7±1.2	0.1±0.1	nd	0.8±0.1
Eucalyptus wood	46.3±0.5	6.4±0.1	46.8±0.6	0.1±0.0	nd	0.4±0.0
Eucalyptus bark	47.9	6.6	40.2	0.5	nd	4.7±0.9
Beech wood	47.6±1.4	6.2±0.1	45.7±1.4	0.1±0.1	nd	0.4±0.0
Gorse wood	47.9±0.3	6.3±0.2	44.9±0.4	0.2±0.1	nd	0.5±0.0
Oak wood	48.4±0.9	6.0±0.2	45.2±1.0	0.2±0.0	nd	0.2±0.0
Forest pellets	49.8±0.8	6.3±0.1	42.7±0.8	0.3±0.0	nd	1.0±0.0
Wood pellets	49.1±1.0	6.6±0.1	43.5±1.1	0.1±0.0	0.0	0.7±0.0
Straw pellets	46.7	5.8	42.0	0.4	0.1	5.0
Bark pellets	51.9	5.4	37.8	0.5	nd	4.4
Sawdust	49.9	6.0	43.8	nd	nd	0.3
Peat	54.6	5.8	32.4	2.6	0.3	4.3
Wood chips	49.6	6.3	43.4	nd	nd	0.7
Cellulose	43.0±0.2	6.4±0.1	49.9±0.9	0.0±0.1	nd	0.1±0.0
Lignin	64.2±0.6	5.9±0.0	29.5±0.6	0.1±0.0	nd	0.4±0.0

[a] Determined by difference method; nd Not determined or <100 ppm.

5.3.2 *Facilities and methods*

5.3.2.1 *Bubbling fluidised bed*

A schematic of the fluidised bed facility is shown in Figure 5.6-a. The main body of the reactor consists of a AISI 310 SS tube (920 mm in length and 70 mm ID) heated by a 3kW$_e$ oven. The oven furnishes heat to the central part of the tube (≈200 mm in length), which comprises the preheating zone for the fluidising gas, the distributor, dense bed, and splash region. Heat losses in the lower and upper parts of the reactor are minimised by using thermal insulation both inside and outside the tube. Under regular operation, a thermocouple (T1, K-type, 3mm OD) is inserted through the reactor top flange, to measure the temperature in the middle of the bed. The bed is held at a point half the height of the reactor by means of a concentric SS tube (62mm ID), which includes a distributor plate of 29 0.6mm holes. The bed operates with 250 g of round silica sand that was sieved to particles sizes in the range of 180–250 μm (Sauter diameter of 205 μm), yielding a static bed height of 55 mm. The minimum fluidisation velocity of these particles is about 0.04 m/s under room conditions. The fluidising gas is selected in an automatic unit (H) that incorporates a mass flow meter (Honeywell, 0-5NLpm) and a regulating valve; the typical uncertainty for this flow meter is ±2.5% of the reading [63]. During the experiments, the bed was operated at 3- to 4-times the minimum fluidising velocity, thereby ensuring a well-developed bubbling bed with nearly isothermal conditions. The bed and freeboard extend ≈270 mm to the insulating material placed in the upper part of the reactor tube.

The fuel was oven-dried at 105ºC to a constant weight and stored in desiccators until the experiments. Gravimetric analysis of the dry fuel samples was performed in a controlled-humidity room using a precision balance (Mettler Toledo, readability of 0.1 mg). The fuel feeding system (A) basically consists of a ball valve (placed outside the reactor) attached to a 12mm OD SS tube, which is inserted down through the reactor top flange to the top of the freeboard. With this system, up to five fuel particles (<2 g) can be fed simultaneously over the hot bed (N_2 carrier gas, 99.999%v) in less than 1s. Only the fragile lignin particles were problematic to feed with this system, and therefore they were not tested in this facility. Pyrolysis proceeds at atmospheric pressure while the bed temperature decreases at less than 2% of the set value. The release of volatiles ceases in 30–90 s, depending on the fuel and bed temperature; this process can be evaluated by observing the white mists escaping the reactor towards the stack. Since the fuel heats up to the temperature of the bed during this period of time, the average heating rate of the fuel is above 10^{2}ºC/min, or even 10^{3}ºC/min. After 5–10 min at the peak temperature, the reactor oven is turned off and the bed is allowed to cool overnight under a flow of nitrogen. The char particles are recovered by sieving the bed

material (250μm mesh), cleaned of silica adhered to the external surfaces of the particles, and dried at 105ºC prior to gravimetric analysis. To compute the yield of daf char ($Y_{ch,F}$, kg daf char/kg daf fuel) it is assumed that the whole ash content of the dry fuel ($Y_{a,R}$) is retained in the char, Eq. 5.7, whereby $Y_{S,R}$ is the mass of dry char (subscript S) recovered from the bed *per* unit mass of dry fuel feed (subscript R). The measurements were sometimes repeated, albeit not more than twice for a given fuel and operating condition.

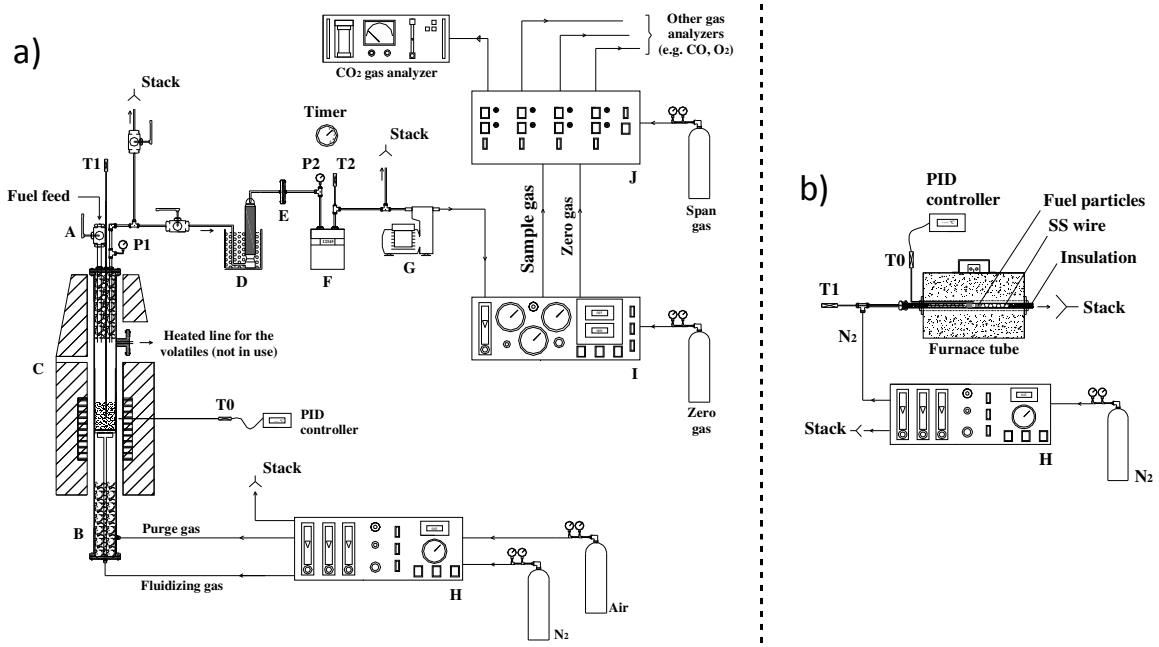

Figure 5.6 - Fast pyrolysis facilities developed at the University of Aveiro. a) Bubbling fluidised bed; and b) horizontal quartz tube (fixed bed). A, Fuel feeding system; B, bubbling fluidised bed reactor; C, furnace and thermal insulation; D, cold trap; E, quartz filter; F, bellows-type volume meter; G, diaphragm pump; H, automatic gas control and measurement unit; I, automatic gas sampling and conditioning unit; J, automatic gas distribution unit; T0 to T2, temperature measurement points; P1 and P2, pressure measurement points.

$$Y_{ch,F} = \frac{Y_{S,R} - Y_{a,R}}{1 - Y_{a,R}} \qquad \text{Eq. 5.7}$$

A second type of experiment was carried out in the fluidised bed facility with the aim of assessing the pyrolytic carbon remaining in-bed using a combustion method. For this purpose, after the volatiles have been released, the fluidising gas is switched from nitrogen to reconstituted air (see unit H in Figure 5.6-a). The combustion flue gases that exit the top of the freeboard are led to a cold trap (D), which consists of a glass bottle sitting in an ice bath at 0ºC, for condensing out the water; it is followed of a packed bed of desiccant and backup quartz filter (E) to remove aerosols and traces of water. The total flow rate of the dry and

clean flue gases leaving the reactor is determined using a bellows-type volume meter (F) and timer. A slipstream of this gas (≈1NLpm) is sampled using a diaphragm pump (G) and gas conditioning unit (I) and sent to the online gas analysers (selection by automatic de-multiplexing unit, J). In the present work, a CO_2 gas analyser (ADC, NDIR 0-25%v) was used owing to the negligible amounts of unburnt gas species in the flue gases; this analyser was calibrated against standard gases and showed a typical uncertainty of ±3% of the reading.

A typical combustion experiment of the char is shown in Figure 5.7, in which the initial pyrolysis step was conducted at 850ºC. The combustion flue gases enter the sampling train at the beginning of the experiment, causing a slight overpressure of ≈95 mmH_2O in the freeboard (see P1). The major part of the char burns in the 10-min period, as indicated by the concentration of CO_2, and the experiment ends after 20 min. Thereafter, the reactor is opened to the atmosphere, resulting in a steep decrease in the response of the pressure transducer. The amount of carbon that leaves the reactor during the experiment is given by the outflow of CO_2, which make it possible to determine the yield of carbon (kgC/kgF) from Eq. 5.8, in which $\dot{n}_{Ed}$ is the molar flow rate of dry flue gases, $y_{CO2,Ed}$ is the molar fraction of CO_2 in the dry flue gases, t_b is the burnout time, and m_F is the mass of daf fuel that is subjected to pyrolysis. In the present work, $\dot{n}_{Ed}$ has a constant value due to the constant flow rate of combustion air and the near-quantitative conversion of O_2 into CO_2.

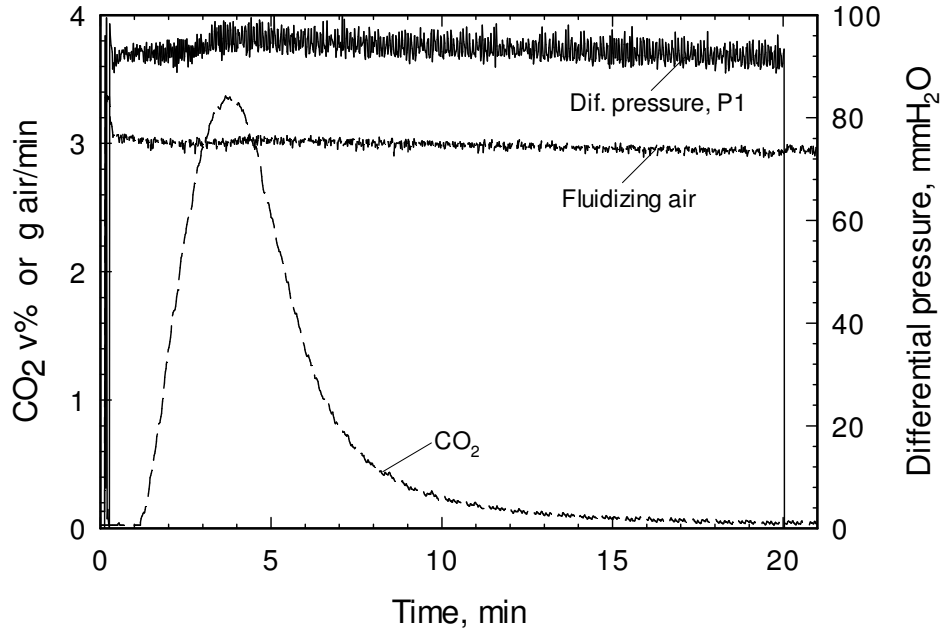

Figure 5.7 - Online monitoring of char combustion in the bubbling fluidised bed, through measurements of the flow rate of dry combustion air, differential pressure in the freeboard relative to the atmosphere, and the volume-fraction of CO_2 in the dry flue gases. The experiment was conducted with char particles produced from ≈1.7g of dry eucalyptus wood at 850ºC.

$$Y_{ch,F} \cdot Y_{C,ch} = \frac{M_C}{m_F} \cdot \int_0^{t_b} \dot{n}_{Ed} \cdot y_{CO_2,Ed} \cdot dt \qquad \text{Eq. 5.8}$$

5.3.2.2 *Horizontal quartz tube*

The amount of char formed with fast heating is readily determined with an apparatus such as that depicted in Figure 5.6-b, and it takes less than 1 hour to perform one experiment. In this case, the furnace consists of a 20mm ID quartz-glass tube heated by a 0.5kW heating coil. Although the coil is wound uniformly around the tube, it does not furnish a uniform temperature along its entire length. Thus, the power input to the coil is adjusted so that the temperature at the centre of the tube is maintained at a preset value, as monitored using a K-type thermocouple (T0, 1.5mm ID) that is placed inside the tube. The heating tube is well-insulated with a cerablanket and the outer shell of the furnace is made of a suitable metal. The fuel sample is placed within the inner reaction tube, which is also made of quartz glass with 10mm ID and 350mm length. Both ends of the reaction tube are insulated with a 50mm cerablanket plug followed by ≈110mm SS wire, which is used to hold the sample in the centre of the tube. A tee assembly attached to the inlet of the reaction tube enables insertion another thermocouple (T1, K-type, 1.5mm ID) at a distance of approximately 3mm from the sample while the tube is flushed with nitrogen (≈0.5NLpm, measurement through unit H).

With the reaction tube placed outside the furnace, 2 or 3 fuel particles (<1.5 g) are put in place. These particles have been previously oven-dried at 105ºC to a constant weight and subjected to gravimetric analysis in the aforementioned precision balance (±0.1mg). The tube is then inserted into the furnace at the preset temperature, so that the sample is batch-pyrolysed in the middle of the furnace. The volatiles and carrier gas rapidly exit the reaction tube and are discarded. After 5–10 min at the peak temperature, the reaction tube is moved back outside the furnace and the char particles are cooled under nitrogen. These particles are carefully recovered from the reaction tube into small glass boxes and immediately subjected to gravimetric analysis; this procedure avoids exposure to moist ambient air, which makes it straightforward to determine the yield of daf char using Eq. 5.7. The heating rate of the fuel particles is in the order of that obtained in the fluidised bed (>10^{2}ºC/min). Replicates of the experiments were performed for each fuel under some operating condition.

5.3.2.3 *Thermobalance*

The char yield during pyrolysis at a slow heating rate was determined using a thermogravimetric analyser (LECO, TGA 701). This system allows for multiple fuel samples, a controlled atmosphere, and heating rates in the range of 5–50ºC/min. Before the

experiments, the fuel samples were oven-dried for 24 hours at 105ºC. Each experiment was initiated with a 2-hour step at 130ºC under inert atmosphere (N_2, 7 Lpm). Then, the samples were heated in closed crucibles at a constant heating rate to a peak temperature of 915ºC also under N_2 gas; after 7 minutes at 915ºC, the oven was cooled to the room temperature. For each fuel type, between four and six samples of 1-2g each were analysed.

5.4 *Results and discussion*

In total, 72 experiments were performed in the fluidised bed facility described in the present work. Of these, 31 experiments were aimed at determining the yield of char by gravimetric analysis, while the remaining 41 experiments were to determine the yield of pyrolytic carbon by burning the char. To complement and verify the results obtained with the fluidised bed, an additional 39 experiments were carried out in the quartz-tube facility, in which the yield of char is also obtained by gravimetric analysis. Moreover, a few experiments were performed in the thermobalance, aimed at determining the sensitivity of the charring process to significantly lower heating rates of fuel.

5.4.1 *Evaluation of the measurements in the fast pyrolysis facilities*

Recovery of the char particles from the fast pyrolysis facilities was, in general, easily accomplished. Fragmentation was mainly dependent upon the nature of the parent fuel and, to a lesser extent, upon the type of reactor. Among the biomasses and cellulose samples tested, only pine bark underwent significant fragmentation to coarse char particles, which were easily recovered. The woody materials showed negligible fragmentation, while the pelletised materials produced a low number of mm-sized fragments in the case of the fluidised bed. In a few experiments, the char fines remaining in-bed after pyrolysis of pelletised materials was determined by burning the sieved bed in a muffle, which revealed that the fines were a minor quantity (<0.5% of daf fuel, mass%). With respect to the lignin, it produced chars that were problematic to recover from the quartz-tube reactor. Indeed, lignin was observed to melt at relatively low temperatures and fuse into rather fragile char particles, which expanded considerably relative to the parent particles and became attached to the internal walls of the quartz tube. Fragmentation was also observed during the heating of lignin, and some char fines could not be recovered. Figure 5.8 shows a photograph of typical char particles arising from selected fuels. With the exceptions of lignin and pine bark, the char particles maintained the cylindrical shape but shrank in volume by ≈50% compared with the parent fuel particles.

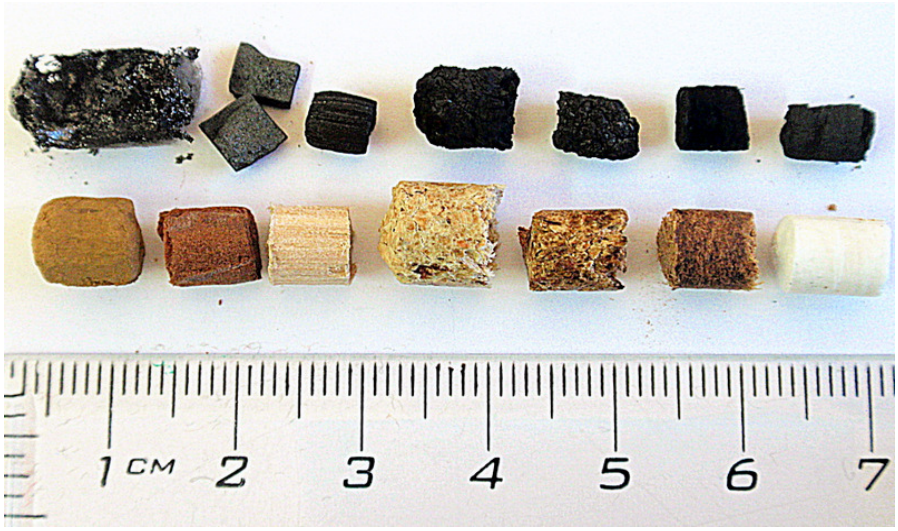

Figure 5.8 - Photograph of typical fuel particles and the respective char particles recovered from the fluidised bed or quartz-tube facilities. From left to right: lignin; pine bark; eucalyptus wood; wood pellets; forest pellets; eucalyptus bark; and cellulose. For the pine bark, two char fragments are shown, while for the other fuels the fragments, if any, are not shown.

The adequacy of the sieving procedure to recover the char particles from the fluidised bed is depicted in Figure 5.9, which provides a comparison of the yields of char (Eq. 5.7) and the respective yields of pyrolytic carbon (Eq. 5.8) for some fuels. The results show that the yields of pyrolytic carbon increase towards those of the char as the temperature increases, and that approximated values are obtained at 950ºC ($Y_{ch,F} \cdot Y_{C,ch} \approx 0.95 \cdot Y_{ch,F}$). Since the chars formed at high temperature are composed predominantly of carbon (see also Figure 5.2-b), it can be concluded that the results obtained using the combustion method corroborate those obtained from the gravimetric analysis of the char particles.

Table 5.3 shows the yields of char obtained for various fractions of the same fuel sample (wood pellets or forest pellets) in experiments that were carried out on different dates, so as to verify the repeatability of the results obtained with the fast pyrolysis facilities. There was good agreement between the results obtained for the replicate fuel samples, with values typically within ±5% of the mean values. In addition, for the conditions used in the experiments, the differences in the results from these facilities were often within the measurement uncertainties (Figure 5.10), which confirms the reliability of the measurements. The similarity of the results obtained in the fluidised bed and quartz-tube facilities can be understood from the thermal Biot number of the fuel particles. For a 6mm sized fuel particle that is suddenly fed into the preheated reactors (600–950ºC), one estimate is that the effective heat transfer coefficient between the hot surroundings and the particle can easily exceed 10^2 W/m^2/K; as an example, experiments carried out by others [12] under conditions relevant to the present work showed that the heat transfer coefficient for a 10mm

fuel particle converting in the splash region or the dense phase of a fluidised bed is within the range of 400–475 W/m²/K. Thus, given the relatively low thermal conductivity of solid biomass (0.1–0.25 W/m/K), the Biot number is estimated as being >1 (albeit not a high value), which means that the external rate of heat transfer tends to be higher than the internal rate of heat transfer. Therefore, the choice of reactor to be used in the fast pyrolysis experiments is of limited importance.

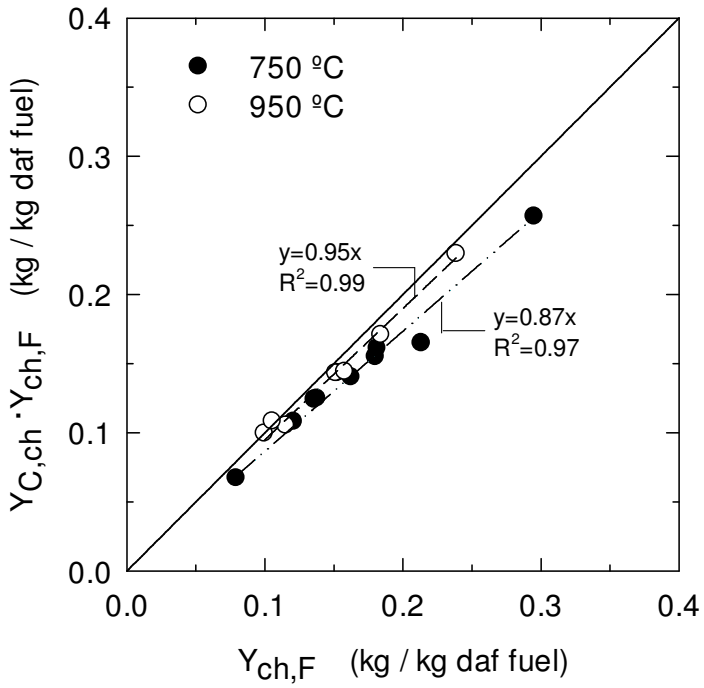

Figure 5.9 - Yield of pyrolytic carbon ($Y_{C,ch}$·$Y_{ch,F}$) as a function of the respective yield of char ($Y_{ch,F}$) for a set of fuels. The experiments were conducted in the fluidised bed at peak temperatures of 750 and 950ºC.

Table 5.3 - Yields of char as determined by gravimetric analysis of the char particles recovered from the fast pyrolysis facilities. Results for replicate samples of forest pellets (6×6mm cylinders) or wood pellets (8×8mm cylinders).

Fuel	Facility	T_{peak} (ºC)	Sample No.	$Y_{ch,F}$ (kg/kg)
Forest pellets	Quartz tube	950	#1	0.163
			#2	0.159
			#3	0.165
			#4	0.170
			#5	0.169
Wood pellets	Fluidised bed	700	#6	0.186
			#7	0.174
		835	#8	0.156
			#9	0.160

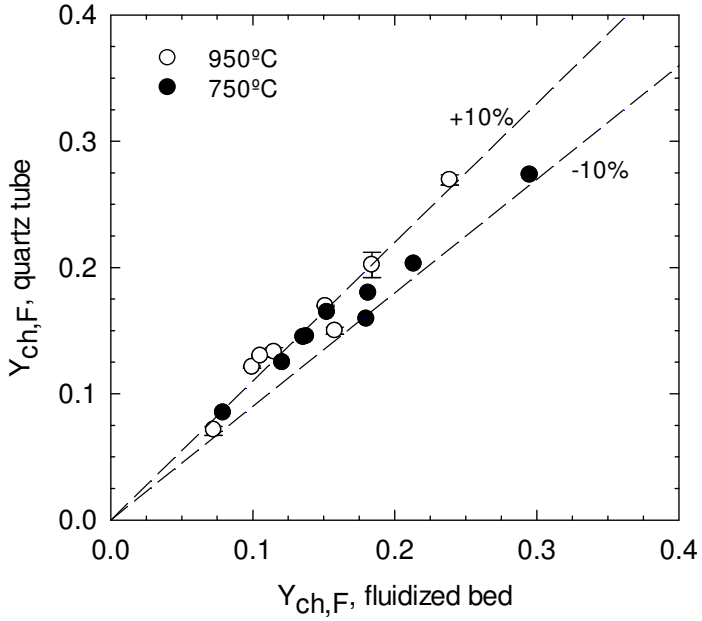

Figure 5.10 - Comparison between the yields of char obtained in the fluidised bed and quartz-tube facilities for a set of fuels. The experiments were conducted at peak temperatures of 750 and 950ºC.

5.4.2 *Effect of peak temperature with fast heating rate*

The fast-pyrolysis experiments carried out in the range of 600–950ºC revealed that for all the fuels used in this work there was a small effect of peak temperature on the yield of char. For instance, this was investigated in detail for a set of fuels for which the yield of char was measured in small temperature steps (Figure 5.11-a); note that in this figure the peak temperature refers to T1 in Figure 5.6-a and -b. Although variations in temperature intervals of <100ºC were difficult to measure using the proposed methods, the trends indicate that the chars generated at high heating rates experienced an average mass loss of only ≈1%/100ºC (mass% of daf fuel) up to the highest temperature analysed. The yield *vs.* temperature dependencies are roughly independent of the fuel, which suggests that the variation in the yield of char among fuels, e.g., 8 to 19% at 750ºC, are mainly due to reactions that occur below 600ºC (for corroborative findings see e.g. [13]). Of course, in the present work, the composition of fuel should be the major parameter governing the formation of char at temperatures <600ºC, since the experiments were performed with fuel particles of near-identical size. Moreover, the results indicate that the re-deposition of carbon due to secondary reactions among the volatiles, as for example tar cracking in the interior of the charring particles, is of minor importance. Indeed, a varied body of evidence indicate that native tars are prone to conversion as the temperature increases above 500ºC [3], especially in the presence of hot char surfaces, whereas the yields of char obtained in this work showed

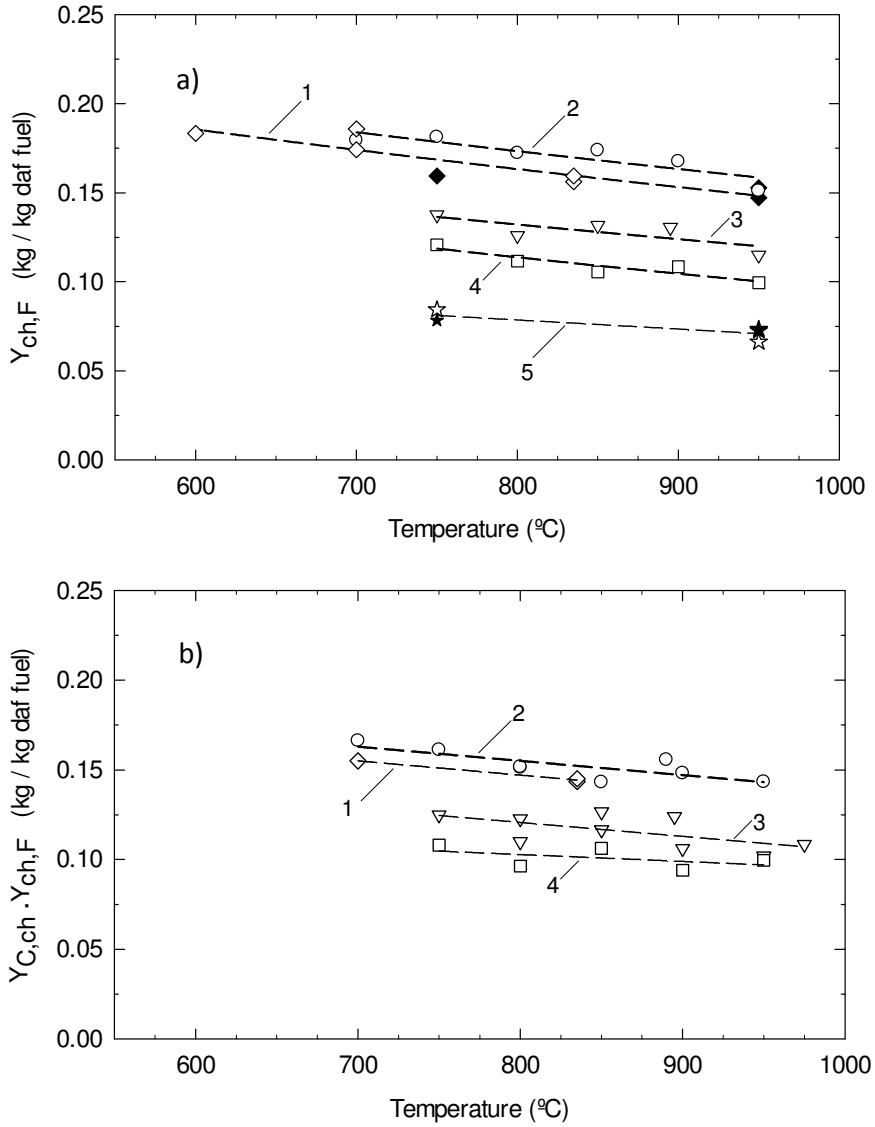

Figure 5.11 - Yield of char (a, $Y_{ch,F}$) and yield of pyrolytic carbon (b, $Y_{C,ch}$·$Y_{ch,F}$) from a set of fuels used in the present work, as a function of reactor peak temperature. 1, Wood pellets; 2, forest pellets; 3, pine wood; 4, eucalyptus wood; 5, cellulose. Results are from the fluidised bed (open symbols) and quartz-tube (filled symbols) facilities.

a slightly negative temperature dependence. At first glance, the decreasing yields of char can result from a combination of other effects: 1) the utilisation of preheated reactors, which causes the heating rate of the fuel feed to increase with increases in reactor temperature; and 2) the release of residual volatiles as the temperature increases above 600ºC. To distinguish between these possibilities, one refers to experiments in which cellulose was pyrolysed at a constant heating rate (70ºC/min) to temperatures that ranged from 700 to 900ºC [25]; these experiments showed rates of mass loss (≈1.5%/100ºC) similar to those found in the present study. Therefore, the slightly decreasing yields of char shown in Figure 5.11-a should be attributed mainly to ongoing volatilisation. Whether this is caused by the release of carbon

can be examined from the burnout experiments conducted in the fluidised bed (Figure 5.11-b). It turns out that the amount of pyrolytic carbon remaining in-bed also decreases with increases in temperature, although the slopes are less pronounced (typically <1%/100ºC, mass % of daf-duel) than those for the char (Figure 5.11-a). To compensate for the slightly faster decrease in char yield, as compared with the pyrolytic carbon yield, the release of carbon at high temperatures should be accompanied by the release of minor amounts of oxygen and/or hydrogen in a manner that causes the carbon content of chars to increase as the temperature increases (see Figure 5.10); carbon contents of >90% (mass % of daf-char) can be obtained at high temperatures, i.e., >800ºC.

While the results obtained with fast heating and at atmospheric pressure show that, for engineering purposes, the pyrolytic mass loss of the chars is negligible above, say, 800ºC, an analysis of how the mass that remains at these high temperatures is affected by the heating rate of fuel is presented in the following section.

5.4.3 *Effect of heating rate*

The effect of heating rate was analysed based on the results with cellulose, which is frequently taken as a model compound for lignocellulosic biomasses and has a well-known elemental composition (O/C ratio of 1.11 kg/kg). Figure 5.12 summarises the yields of char obtained from cellulose under a wide range of conditions, combining literature data relative to slow to moderate heating [25] and the results obtained in the present work with fast heating. It is clear that the yield of char tends to asymptotes as the temperature increases and that it varies considerably depending on the heating rate; with extremely slow heating (0.03ºC/min in the figure), the ultimate yield of char from cellulose is 28% [25], and the yield decreases to ≈7% when the heating rate exceeds a certain threshold (see the results from this work). It is noteworthy that under fast heating conditions the sensitivity of the yield of char with respect to the heating rate of the fuel is relatively low. For instance, an increase in the heating rate of cellulose from 11 to 70ºC/min results in a 10% decrease in the asymptotic yield of char (from 20% to 10% of the daf-fuel in Figure 5.12), whereas under the more severe conditions typical of fluidised beds (say, 10^3ºC/min), an additional decrease of <5% of the fuel is obtained. To examine this behaviour with respect to a lignocellulosic biomass, experiments were conducted in the thermobalance with the wood pellets (Table 5.4). Fast heating of the pellets to high temperature realised char yields of 16%, and these rose to only 19% when the heating rate decreased to 50ºC/min. This result is consistent with those obtained for cellulose, and further indicates that the fast pyrolysis process realises stable values for the asymptotic yield of char even if the fuel is subjected to relatively large variations in heating rate. This is also in agreement with the near-constant yields of char

shown in Figure 5.11, given that the heating rate of the fuel feed depends upon the temperature of the preheated reactors. For essentially the same reasons, the effect of particle size on the yield of char should be also small, at least up to certain particle sizes (see e.g., [12]), even though this behaviour is difficult to evaluate from the data available in the literature [3].

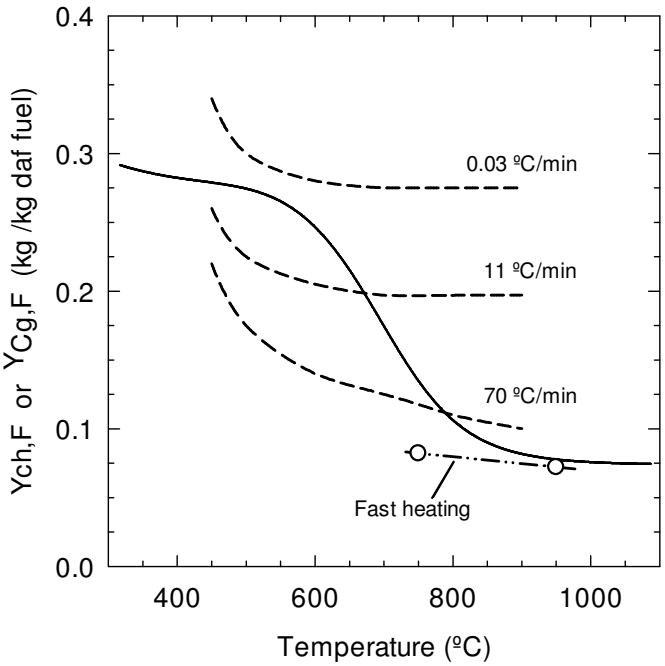

Figure 5.12 - Yield of char from cellulose as a function of peak temperature and atmospheric pressure. The dashed lines represent data from the literature for various heating rates [25]. The data-points and trend-line for fast heating are from experiments conducted in the fluidised bed and quartz-tube facilities; solid line, yield of carbon graphite from cellulose under the equilibrium condition.

Also worthy of note is the theoretical yield of carbon graphite predicted for cellulose as a function of temperature (Figure 5.12). The low-temperature plateau given by theory (≈28%) agrees rather well with the detailed reaction mechanism postulated in [14], which describes the degradation of two cellulose units into a stable graphite array at extremely slow heating rates; in turn, the high-temperature plateau (7.4%, noted for $Y^{*}_{Cg,F}$) can be approximated using Eq. 5.5. These results reveal that the optimal conditions for the yield of char to approach the theoretical values for carbon graphite are dependent upon the temperature. In a low-temperature process (e.g., 500ºC), the high yields predicted by theory are difficult to achieve in practice. This may require very slow heating of the fuel so that the dehydration and depolymerisation reactions partially decouple, therefore limiting the release of volatile fragments at temperature above, say, 250ºC. Moreover, with slow heating rates, the escaping volatiles re-polymerise more effectively within the pores of the charring particles, so as to form additional (secondary) char. If the processing time is short, pressurised reactors are

needed for the low-temperature process [34,36,37]. Indeed, pyrolysis of four wood varieties at 450ºC and 0.1 MPa realised yields of char in the range of 28.9–33.0%, with yields increasing to 34.6–37.5% when the volatiles remained captive at 1 MPa [34]. This indicates that the conversion of the native volatiles into secondary char is needed to approach the high yields predicted for carbon graphite at low temperature. Conversely, in a high-temperature process (e.g., >800ºC) the fuel must be converted instantaneously and the formation of secondary char from the volatiles does not appear to be necessary to approach the theoretical yields; in practice, this can be achieved in a preheated reactor operating at atmospheric pressure with fuel particle sizes of practical relevance, as evident from the results obtained in this work. Though, further work is needed to verify the range of particle sizes for which the theoretical yield of carbon graphite is meaningful in a high-temperature process.

Table 5.4 - Yields of char during pyrolysis of wood pellets at various heating rates.

Heating rate	Rapid heating[a]	50ºC/min[b]	5ºC/min[b]
$Y_{ch,F}$ (kg/kg F)	0.16	0.19	0.23

[a] Average value for the fluidised bed and quartz-tube facilities for peak temperatures of 750 to 950ºC; [b] Thermobalance at peak temperature of 915ºC.

5.4.4 *Effect of fuel composition*

Following the analysis conducted for cellulose, it was of interest to investigate how the asymptotic yield of char depends on the composition of lignocellulosic biomasses. The results of this work are summarised in Figure 5.13 which provide the yield of char as a function of the O/C ratio of the parent fuel. For the fast pyrolysis facilities, the data obtained at 750ºC and 950ºC are presented, as it was difficult to distinguish the yields of char for smaller temperature intervals (see Table 5.3 and Figure 5.11). Unlike cellulose, the elemental composition of biomass varies considerably (see e.g., Figure 5.4) and has to be determined for each fuel by standard ultimate analysis; as noted before, measurements of replicate samples may differ considerably, as indicated by the error bars in Figure 5.13. As in Figure 5.5, the theoretical values for carbon graphite, $Y^{*}_{Cg,F}$ in Eq. 5.5, are provided as a ±15% range.

At 750ºC, the average yields of char (kg daf char *per* kg daf fuel, %) obtained with the fast pyrolysis facilities ranged from 8.2% for cellulose to 43.3% for lignin, whereas at 950ºC the yields ranged from 7.1% for cellulose to 39.0% for lignin. For the biomasses, the yields of char showed a much narrower range, from roughly 12% for eucalyptus wood to 20% for eucalyptus bark (average values at 750ºC and 950ºC); only the pine bark gave yields outside this range (average of about 27%). This can make it difficult to evaluate how the yield of char varies among fuels with similar compositions (e.g., woody varieties), as the uncertainty

associated with the O/C ratio of the fuel may overlap the narrow range for the corresponding yields of char. However, by considering the extreme values for lignin and cellulose, it is clear that the production of char is highly dependent upon the elemental composition of the fuel.

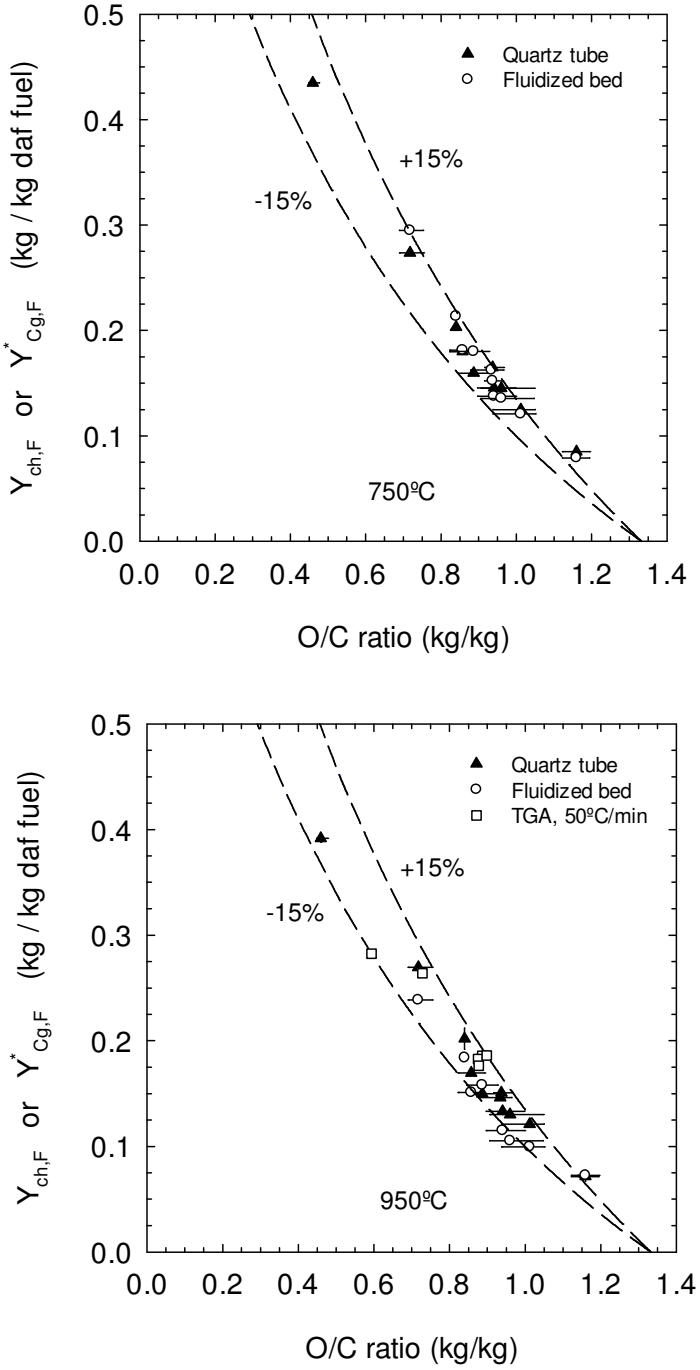

Figure 5.13 – Yields of char ($Y_{ch,F}$) measured for the fuels used in the present work at 950ºC (the data from TGA are for yields at 915ºC) and 750ºC as a function of the respective O/C mass ratios. The ±15% range is relative to the equilibrium values predicted for carbon graphite at high temperatures ($Y^*_{Cg,F}$, Eq. 5.5). The error bars for the O/C ratios give the maximum and minimum values from the ultimate analysis.

Moreover, the experimental char yield *vs.* O/C ratio relationship follows approximately the theoretical line predicted for the yield of carbon graphite. The experimental yield of char for cellulose at 950ºC agrees reasonably well with the yield of carbon graphite derived based on the theoretical O/C ratio of cellulose (1.11 kg/kg), although it slightly overestimates the yield based on the experimental O/C ratio (1.16 kg/kg; Table 5.2). It is worth noting the remark made by [24] that the theoretical O/C ratio of cellulose may only be approximated by correcting the result from the ultimate analysis (1.18 kg/kg in [24]) for the amount of water adsorbed onto the sample before analysis; a similar deviation for the O/C ratio of cellulose was obtained in the present work. Whether this effect contributes to the deviations between the measured and theoretical yields could not be resolved and cannot currently be ruled out. For the remaining fuels, the deviations seen at 950ºC were almost always within the experimental errors; the small deviation for lignin, 39.2% at 950ºC *vs.* 42.2% under equilibrium is possibly related to the poor recovery of the char particles from the quartz tube reactor. In addition, the thermobalance experiments (50ºC/min to 915ºC) showed good agreement with values of char yield that are generally above the theoretical ones; the exception is the result for peat (≈28%), which is ≈15% less than the equilibrium value. The widely varying ash contents of the fuels used in the present work (up to ≈5% of the dry fuel) has no measurable effect on the yield *vs.* O/C ratio relationship, once the results are corrected to a dry ash-free fuel basis according to Eq. 5.7. This further reinforces the notion that the CHONS composition of the parent fuel is the major parameter governing the formation of char under fast heating conditions, thus corroborating and improving the results derived from the literature (Figure 5.5).

5.5 *Remarks on application for modelling*

To describe the conversion of biomass in combustors and gasifiers, several models that predict the kinetics and stoichiometry of the pyrolysis step have been proposed, and these often involve parameters adjusted by experiments. One parameter that is often needed to characterise the distribution of the primary pyrolytic products is the yield of char. For instance, the empirical models derived previously [3,64] predict the accumulated yields of the most relevant volatile species from the elemental composition of the fuel and the yield of char. Simplified models of this type are useful when the devolatilisation of the fuel particle can be assumed to be instantaneous, which is often the case when evaluating fluidised bed processes [65,66]. To reduce the need for measurements, simple predictive tools for the yield of char are needed. One approach is to calculate the yield of char as a summation of the contributions from the major structural components of biomass, lignin, cellulose,

hemicelluloses, and extractives, where the yield of char from each component is given as an input (e.g., [22,33,35]). Although this approach gives satisfactory results it has certain limitations, such as the need for a detailed structural analysis of the biomass, which is not common practice. Nevertheless, the results presented in Figure 5.13 offer strong support on that the yield of char can alternatively be approximated from the equilibrium values for carbon graphite, which means that only a standard ultimate analysis of the fuel is needed, in accordance with the approximated model proposed in the present work (see Eq. 5.5). To be consistent with this, a further simplification is to assume that the dry char is composed simply of carbon and ash. The alternative is to estimate the yield of char through dedicated experiments or standard proximate analysis, even though the accuracy is not greatly improved relative to the result obtained from Eq. 5.5. When the results from both the ultimate and proximate analyses of the fuel are available, we believe that the CHONS contents will be in agreement with the respective fixed carbon content, thus providing an overall check of the measurements that are preformed.

5.6 *Conclusions*

An investigation of the carbonisation characteristics of biomasses, cellulose and lignin is presented here, with the focus on operating conditions typical for fluidised bed combustors and gasifiers. Pyrolysis experiments were conducted in atmospheric laboratory scale facilities (fluidised bed and quartz-tube), enabling temperatures in the range of 600–950ºC and high heating rates typical of fluidised beds. Moreover, to elucidate the influence on char yield of lowering the heating rate of the fuel, separate experiments were conducted in a thermobalance. In addition to the experimental analysis, the present work is supported by a large body of literature data.

Pyrolytic volatilisation of solid biomass is mostly complete at temperatures of around 600ºC. Higher temperatures lead to marginal mass loss at about 1% of daf-fuel *per* 100ºC, the value of which is roughly independent of the composition of the parent fuel. These results provide strong support for the idea that the charring process is mainly due to reactions that occur below 600ºC under the conditions of the experiments, and that the formation of secondary carbon inside the fuel particles by reactions among the volatiles is of minor importance. The slightly decreasing yield of char as the temperature increases is mainly due to carbon loss at a rate that leads to about 95%C chars at the higher temperatures analysed.

For engineering purposes, the yield of char attains asymptotic values above, say, 800ºC, since further increases in temperature lead to variations that are within the measurement uncertainties. At sufficiently high heating rates, e.g., when the fuel is fed into isothermal reactors, the asymptotic yields are strongly correlated with the O/C mass ratio of fuel, which

was achieved in the present work with thermally-tick fuel particles of 6–8 mm in diameter. Given the broad range of fuels used in this work, which included varieties with O/C ratios ranging from 0.46 to 1.16 kg/kg and ash contents up to 5% (dry-fuel basis), it is likely that this char yield *vs.* O/C ratio relationship applies to the majority of biomasses, although further work is needed to resolve this issue.

The asymptotic yields of char were typically within ±15% of the theoretical minimum predicted for carbon graphite under thermodynamic equilibrium, thus providing a simple way to relate the yield of char to the composition of biomass when conversion takes place under conditions typical for fluidised beds. A simple model is proposed in the present work to compute the theoretical yield of carbon graphite from the O/C mass ratio of fuel, which can be useful in combination with suitable particle models that simulate the pyrolysis of biomass in gasification and combustion processes carried out in fluidised beds.

Nomenclature

$Y_{i,F}$	yield of i^{th} product on a dry ash-free fuel basis, kg i/kg F
$Y^{*}_{i,F}$	high temperature plateau value for the yield of i^{th} product on a dry ash-free fuel basis, kg i/kg F
$Y_{i,R}$	yield of i^{th} product on a dry fuel basis, kg i/kg R
$Y_{a,R}$	mass fraction of ash in dry fuel, kg a/kg R
$Y_{j,F}$	mass fraction of j^{th} element in dry ash-free fuel, kg j/kg F
$Y_{j,i}$	mass fraction of j^{th} element in i^{th} product, kg j/kg i
M_i	molar mass of i^{th} product, kg i/kmol i
M_j	molar mass of j^{th} chemical element, kg j/kmol j
m_F	mass of dry ash-free fuel feed, kg F
$y_{CO2,Ed}$	molar fraction of CO_2 in the dry flue gases from the burnout of the char, kmol CO_2/kmol Ed
$\dot{n}_{Ed}$	molar flow rate of dry flue gases from the burnout of the char, kmol Ed/s
HHV	higher heating value, MJ/kg

Subscripts

R dry fuel

F dry and ash-free fuel

a Ash

ch dry and ash-free char

S dry char (dry ash-free char plus ash)

Ed dry flue gases from the burnout of the char

Cg carbon graphite

C Carbon

H Hydrogen

O Oxygen

N Nitrogen

S Sulphur

Acknowledgements

We acknowledge the financial support provided by the Fundação para a Ciência e a Tecnologia (FCT), Portugal, through PhD grant SFRH/BD/39567/2007 and research project PTDC/AAC-AMB/098112/2008 (Bias-to-soil - Biomass ash: Characteristics in relation to its origin, treatment and application to soil), and by the Swedish Gasification Centre (SFC).

References

1. Di Blasi C. Modeling chemical and physical processes of wood and biomass pyrolysis. Prog Energ Combust. 2008;34:47-90.
2. Di Blasi C. Combustion and gasification rates of lignocellulosic chars. Prog Energ Combust. 2009;35:121-40.
3. Neves D., Thunman H., Matos A., Tarelho L., Gómez-Barea A. Characterization and prediction of biomass pyrolysis products. Progress in Energy and Combustion Science. 2011;37:611-30.
4. Antal M.J. Effects of reactor severity on the gas-phase pyrolysis of cellulose- and kraft lignin-derived volatile matter. Industrial & Engineering Chemistry Product Research and Development. 1983;22:366-75.

5. Elliott Douglas C. Relation of Reaction Time and Temperature to Chemical Composition of Pyrolysis Oils. Pyrolysis Oils from Biomass: American Chemical Society; 1988. p. 55-65.
6. Evans R.J., Milne T.A. Molecular Characterization of the Pyrolysis of Biomass .1. Fundamentals. Energ Fuel. 1987;1:123-37.
7. Diblasi C. Modeling and Simulation of Combustion Processes of Charring and Non-Charring Solid Fuels. Progress in Energy and Combustion Science. 1993;19:71-104.
8. Morf P., Hasler P., Nussbaumer T. Mechanisms and kinetics of homogeneous secondary reactions of tar from continuous pyrolysis of wood chips. Fuel 2002;81:843-53.
9. Dufour A., Valin S., Castelli P., Thiery S., Boissonnet G., Zoulalian A., et al. Mechanisms and Kinetics of Methane Thermal Conversion in a Syngas. Ind Eng Chem Res. 2009;48:6564-72.
10. Valin S., Ravel S., Castelli P., Masson E., Dufour A., Defoort F. Connecting a steam fluidized bed to a high temperature gas reactor to reduce the methane and tar content of biomass syngas. 17th European Biomass Conference & Exhibition. Hamburg, Germany 2009. p. 936-9.
11. Dufour A., Girods P., Masson E., Rogaume Y., Zoulalian A. Synthesis gas production by biomass pyrolysis: Effect of reactor temperature on product distribution. Int J Hydrogen Energ. 2009;34:1726-34.
12. Wang X.Q., Kersten S.R.A., Prins W., van Swaaij W.P.M. Biomass pyrolysis in a fluidized bed reactor. Part 2: Experimental validation of model results. Ind Eng Chem Res. 2005;44:8786-95.
13. Mackay D.M., Roberts P.V. The Influence of Pyrolysis Conditions on Yield and Microporosity of Lignocellulosic Chars. Carbon. 1982;20:95-104.
14. Tang M.M., Bacon R. Carbonization of Cellulose Fibers .1. Low Temperature Pyrolysis. Carbon. 1964;2:211-&.
15. Yang H.P., Yan R., Chen H.P., Lee D.H., Zheng C.G. Characteristics of hemicellulose, cellulose and lignin pyrolysis. Fuel 2007;86:1781-8.
16. Cordero T., Rodriguez-Maroto J.M., Rodriguez-Mirasol J., Rodriguez J.J. On the Kinetics of Thermal-Decomposition of Wood and Wood Components. Thermochim Acta. 1990;164:135-44.
17. Varhegyi G., Antal M.J., Jakab E., Szabo P. Kinetic modeling of biomass pyrolysis. J Anal Appl Pyrol. 1997;42:73-87.
18. Gronli M., Antal M.J., Varhegyi G. A round-robin study of cellulose pyrolysis kinetics by thermogravimetry. Ind Eng Chem Res. 1999;38:2238-44.

19. Banyasz J.L., Li S., Lyons-Hart J.L., Shafer K.H. Cellulose pyrolysis: the kinetics of hydroxyacetaldehyde evolution. J Anal Appl Pyrol. 2001;57:223-48.
20. Jakab E., Meszaros E., Borsa J. Effect of slight chemical modification on the pyrolysis behavior of cellulose fibers. J Anal Appl Pyrol. 2010;87:117-23.
21. McGrath T.E., Chan W.G., Hajaligol M.R. Low temperature mechanism for the formation of polycyclic aromatic hydrocarbons from the pyrolysis of cellulose. J Anal Appl Pyrol. 2003;66:51-70.
22. Cagnon B., Py X., Guillot A., Stoeckli F., Chambat G. Contributions of hemicellulose, cellulose and lignin to the mass and the porous properties of chars and steam activated carbons from various lignocellulosic precursors. Bioresource Technol. 2009;100:292-8.
23. Dobele G., Rossinskaja G., Telysheva G., Meier D., Faix O. Cellulose dehydration and depolymerization reactions during pyrolysis in the presence of phosphoric acid. J Anal Appl Pyrol. 1999;49:307-17.
24. Broido A., Nelson M.A. Char Yield on Pyrolysis of Cellulose. Combust Flame. 1975;24:263-8.
25. Brunner P.H., Roberts P.V. The Significance of Heating Rate on Char Yield and Char Properties in the Pyrolysis of Cellulose. Carbon. 1980;18:217-24.
26. Nunn T.R., Howard J.B., Longwell J.P., Peters W.A. Product Compositions and Kinetics in the Rapid Pyrolysis of Milled Wood Lignin. Ind Eng Chem Proc Dd. 1985;24:844-52.
27. Sharma R.K., Wooten J.B., Baliga V.L., Lin X.H., Chan W.G., Hajaligol M.R. Characterization of chars from pyrolysis of lignin. Fuel 2004;83:1469-82.
28. Caballero J.A., Font R., Marcilla A. Study of the primary pyrolysis of Kraft lignin at high heating rates: Yields and kinetics. J Anal Appl Pyrol. 1996;36:159-78.
29. Liu Q., Wang S.R., Zheng Y., Luo Z.Y., Cen K.F. Mechanism study of wood lignin pyrolysis by using TG-FTIR analysis. J Anal Appl Pyrol. 2008;82:170-7.
30. Ferdous D., Dalai A.K., Bej S.K., Thring R.W. Pyrolysis of lignins: Experimental and kinetics studies. Energ Fuel. 2002;16:1405-12.
31. Jakab E., Faix O., Till F., Szekely T. Thermogravimetry Mass-Spectrometry Study of 6 Lignins within the Scope of an International Round-Robin Test. J Anal Appl Pyrol. 1995;35:167-79.
32. Demirbas A. Effects of temperature and particle size on bio-char yield from pyrolysis of agricultural residues. J Anal Appl Pyrol. 2004;72:243-8.
33. Mackay D.M., Roberts P.V. The Dependence of Char and Carbon Yield on Lignocellulosic Precursor Composition. Carbon. 1982;20:87-94.

34. Antal M.J., Allen S.G., Dai X.F., Shimizu B., Tam M.S., Gronli M. Attainment of the theoretical yield of carbon from biomass. Ind Eng Chem Res. 2000;39:4024-31.
35. Ouensanga A., Largitte L., Arsene M.A. The dependence of char yield on the amounts of components in precursors for pyrolysed tropical fruit stones and seeds. Micropor Mesopor Mat. 2003;59:85-91.
36. Antal M.J., Gronli M. The art, science, and technology of charcoal production. Ind Eng Chem Res. 2003;42:1619-40.
37. Wang L., Trninic M., Skreiberg O., Gronli M., Considine R., Antal M.J. Is Elevated Pressure Required To Achieve a High Fixed-Carbon Yield of Charcoal from Biomass? Part 1: Round-Robin Results for Three Different Corncob Materials. Energ Fuel 2011;25:3251-65.
38. Mok W.S.L., Antal M.J. Effects of Pressure on Biomass Pyrolysis .I. Cellulose Pyrolysis Products. Thermochim Acta. 1983;68:155-64.
39. Antal M.J., Varhegyi G. Cellulose Pyrolysis Kinetics - the Current State Knowledge. Ind Eng Chem Res. 1995;34:703-17.
40. Morley C. Gaseq version 0.79. Available from: http://www.c.morley.dsl.pipex.com/.
41. Vassilev S.V., Baxter D., Andersen L.K., Vassileva C.G. An overview of the chemical composition of biomass. Fuel 2010;89:913-33.
42. Fagbemi L., Khezami L., Capart R. Pyrolysis products from different biomasses: application to the thermal cracking of tar. Appl Energ. 2001;69:293-306.
43. Di Blasi C., Signorelli G., Di Russo C., Rea G. Product distribution from pyrolysis of wood and agricultural residues. Ind Eng Chem Res. 1999;38:2216-24.
44. Horne P.A., Williams P.T. Influence of temperature on the products from the flash pyrolysis of biomass. Fuel 1996;75:1051-9.
45. Demirbas A. Properties of charcoal derived from hazelnut shell and the production of briquettes using pyrolytic oil. Energy 1999;24:141-50.
46. Della Rocca P.A., Cerrella E.G., Bonelli P.R., Cukierman A.L. Pyrolysis of hardwoods residues: on kinetics and chars characterization. Biomass Bioenerg. 1999;16:79-88.
47. Balci S., Dogu T., Yucel H. Pyrolysis Kinetics of Lignocellulosic Materials. Ind Eng Chem Res. 1993;32:2573-9.
48. Thurner F., Mann U. Kinetic Investigation of Wood Pyrolysis. Ind Eng Chem Proc Dd. 1981;20:482-8.
49. Nunn T.R., Howard J.B., Longwell J.P., Peters W.A. Product Compositions and Kinetics in the Rapid Pyrolysis of Sweet Gum Hardwood. Ind Eng Chem Proc Dd. 1985;24:836-44.

50. Channiwala S.A., Parikh P.P. A unified correlation for estimating HHV of solid, liquid and gaseous fuels. Fuel 2002;81:1051-63.
51. Putun A.E. Biomass to bio-oil via fast pyrolysis of cotton straw and stalk. Energ Source. 2002;24:275-85.
52. Beis S.H., Onay O., Kockar O.M. Fixed-bed pyrolysis of safflower seed: influence of pyrolysis parameters on product yields and compositions. Renew Energ. 2002;26:21-32.
53. Sensoz S., Demiral I., Gercel H.F. Olive bagasse (*Olea europea* L.) pyrolysis. Bioresource Technol. 2006;97:429-36.
54. Onay O., Kockar O.M. Production of bio-oil from biomass: Slow pyrolysis of rapeseed (*Brassica napus* L.) in a fixed-bed reactor. Energ Source 2003;25:879-92.
55. Sensoz S., Can M. Pyrolysis of pine (*Pinus brutia* Ten.) chips: 2. Structural analysis of bio-oil. Energ Source 2002;24:357-64.
56. Onay Z., Beis S.H., Kockar O.M. Pyrolysis of walnut shell in a well-swept fixed-bed reactor. Energ Source 2004;26:771-82.
57. Bonelli P.R., Cerrella E.G., Cukierman A.L. Slow pyrolysis of nutshells: Characterization of derived chars and of process kinetics. Energ Source 2003;25:767-78.
58. Putun A.E., Onal E., Uzuna B.B., Ozbayc N. Comparison between the "slow" and "fast" pyrolysis of tobacco residue. Ind Crop Prod. 2007;26:307-14.
59. Schroder E. Experiments on the pyrolysis of large beechwood particles in fixed beds. J Anal Appl Pyrol. 2004;71:669-94.
60. Valenzuela C., Bernalte A., Gomez V., Bernalte J. Influence of Particle-Size and Pyrolysis Conditions on Yield, Density and Some Textural Parameters of Chars Prepared from Holm-Oak Wood. J Anal Appl Pyrol. 1987;12:61-70.
61. Figueiredo J.L., Valenzuela C., Bernalte A., Encinar J.M. Pyrolysis of Holm-Oak Wood - Influence of Temperature and Particle-Size. Fuel 1989;68:1012-6.
62. Onay O., Beis S.H., Kockar O.M. Fast pyrolysis of rape seed in a well-swept fixed-bed reactor. J Anal Appl Pyrol. 2001;58:995-1007.
63. Rodrigues N. Metrologia aplicada ao desenvolvimento de sistemas de medição. MSc thesis. Universidade de Aveiro 2009.
64. Thunman H., Niklasson F., Johnsson F., Leckner B. Composition of volatile gases and thermochemical properties of wood for modeling of fixed or fluidized beds. Energ Fuel 2001;15:1488-97.
65. Gomez-Barea A., Leckner B. Modeling of biomass gasification in fluidized bed. Prog Energ Combust. 2010;36:444-509.

66. Gómez-Barea A., Leckner B. Estimation of gas composition and char conversion in a fluidized bed biomass gasifier. Fuel 2013;107:419-31.

67. Neves D., Thunman H., Seeman M., Ideias P., Matos A., Tarelho L. et al. A database on biomass pyrolysis for gasification applications. 17th European Biomass Conference & Exhibition. Hamburg, Germany 2009. p. 1018-28

.

Chapter 6 - Volatile gases from biomass pyrolysis under conditions relevant for fluidized bed gasifiers and combustors

Daniel Neves[a,b], Arlindo Matos[a], Luís Tarelho[a], Henrik Thunman[b], Anton Larsson[b], Martin Seeman[b]

[a] University of Aveiro and CESAM, [b] Chalmers University of Technology

Submitted for publication in Fuel.

ABSTRACT

The evaluation of fluidized bed gasifiers and combustors benefits of knowledge on the composition of the volatile products released from a converting biomass particle. These volatile products can be investigated through detailed biomass pyrolysis experiments. In this work a laboratorial fluidized bed reactor operated with inert gas was used to simulate the pyrolysis of biomass under conditions relevant for fluidized bed gasifiers and combustors. Two types of wood (eucalyptus and pine) and two types of pellets (forest residues and wood) with thermally thick particles of 6 to 8mm in diameter were fed over the hot bubbling bed at temperatures within 600-975ºC. The resultant major pyrolytic products (char, soot, liquids and permanent gas) were collected to verify the overall mass balance, and the composition of the permanent gas was resolved in a number of species (CO_2, CO, C_3H_8, C_2H_6, C_2H_4, CH_4, H_2). Primary pyrolysis of biomass is essentially complete at 600ºC and further increase of the temperature mainly leads to a progressive conversion of the volatiles towards the more stable species. Our results show that the yields of carbon dioxide and light hydrocarbons go through maxima at distinct temperatures to give rise to CO and H_2 at the higher temperatures. Although the gas release does not attain thermodynamic equilibrium under fluidized bed conditions, the yields of various gas species were found well correlated to each other, which make extrapolation of data among operating conditions feasible; moreover a relation between the yields of H_2 and CO was found also dependent on the composition of the parent fuel.

Kewords

Biomass, Volatiles, Gas, Pyrolysis, Gasification, Combustion, Fluidized bed

6.1 *Introduction*

As a consequence of the will to reduce the emissions of carbon dioxide to the atmosphere, the interest on biomass gasification and combustion is increasing. Combustion of biomass is to be considered a commercial process, whereas gasification to produce synthetic biofuels in large scale still is waiting for its commercial breakthrough. Although various gasification technologies for biofuel production are available [1-6], there are two major tracks; the first is the high temperature gasification (typically, >1300ºC) in entrained-flow gasifiers and the second is the low temperature gasification (typically, 700-925ºC) in fluidized bed gasifiers.

In an entrained-flow gasifier the extensive need of fuel pretreatment, together with the high temperatures and the use of pure oxygen, lead to an efficiency penalty for the process. Also, if the aim is to produce a substitute for natural gas (SNG), the high temperatures mean that methane, which is the wanted product and is formed in large amounts during the pyrolytic degradation of biomass, is broken into hydrogen and carbon monoxide. In this regard, fluidized bed gasifiers offer the advantages of lower operating temperatures and the possibility of using untreated chopped biomass. Moreover, an indirect (or allothermal) gasification process can be done by using two interconnected fluidized bed reactors [4, 7-9], whereby a high quality product gas is obtained without the need for pure oxygen. In this case, one reactor is operated with steam and the endothermal pyrolysis and gasification reactions of biomass take place. In the other reactor operated with air, some of the fuel is burned to provide the heat needed for the gasifier via the circulating bed material.

Considering the operating condition in the different gasifiers, the need for information on the pyrolytic products released from biomass varies. For the entrained-flow gasifiers the information given by standard proximate and ultimate analysis of fuel is enough as the process is under thermodynamic control (e.g. [6, 10]). For the fluidized bed gasifiers the operating temperature is below 925ºC, which mean that the reaction rates are slower and the chemical equilibrium is not reached. As a result, the information from standard analysis of fuel has to be complemented by the composition of the pyrolytic volatiles to be able to evaluate the operation of fluidized bed gasifiers. This also applies to fluidized bed combustors, which typically also are operated below 925ºC.

In a fluidized bed reactor the rapid release of the volatiles from the converting fuel particles prevents the bulk gas to diffuse to the fuel surface [11, 12]. This means that the complementary information can be obtained by pyrolysis experiments conducted under inert gas and using operating conditions (e.g. temperature, fuel particle size, residence time) similar to those in the gasifier or combustor [5]. This kind of information was reviewed in

[13], showing that, even if there are clear trends on how the volatiles evolve as a function of the operating conditions, the scatter in the data is large and data useful for fluidized bed reactors is scarce. Since extrapolation of data among fuels and operating conditions is difficult, specialized experiments are often needed. However, pyrolysis experiments usually suffer of inaccurate mass balance, which leads to uncertainties regarding the yields of the volatiles released within the gasifier or combustor. To overcome these limitations, an alternative proposed in [14] resorts to simplified pyrolysis models in which the yields of the volatiles are estimated by mass and energy balances in combination with empirical parameters that are easier to measure. These include property data of the major pyrolytic products and ratios between yields of volatile gases. Indeed, findings by [15-19] showed approximated relations among the yields of carbon monoxide and various light hydrocarbons that seem weakly dependent on the operating conditions (e.g. temperature, heating rate, particle size, [15]) and, hence, can be useful to close the conservation equations describing the pyrolysis process.

In this work, a method to investigate the pyrolysis of biomass under operating conditions interesting for fluidized bed gasifiers and combustors is presented. Even though yields of char, soot and volatiles (liquids and permanent gases) were obtained, our focus is on the composition and properties of the permanent gas. This investigation also verifies and expands the dataset and the empirical parameters derived in previous work [13].

6.2 *Experimental*

Pyrolysis of four biomass fuels under fast heating rates and peak temperatures within 600-975ºC was achieved in a small bubbling fluidized bed reactor. The characteristics of the fuels and a description of the experimental rig, procedures and measurements are given in this section.

6.2.1 *Fuels*

The fuels used in this work are forest biomass residues pellets (hereinafter referred to as forest pellets), wood pellets, eucalyptus wood and pine wood. The forest pellets are a heterogeneous material containing wood and also dark-brown grains of, possibly, barks; the particles are cylindrical with around 6×6mm in size. The wood pellets consist mainly of spruce with cylindrical particles of around 8×8mm in size. The eucalyptus wood came from an old log of ≈80mm in diameter that was debarked and cut into cylindrical particles of 6×6mm in size with the help of a lathe. The pine wood was supplied as pieces of ≈400mm^2

cross section that were also cut into cylindrical particles of 6×6mm in size. A photograph with examples of the fuel particles used in this work is shown in Figure 6.1.

Air-dried fuel samples were ground in a hammer mill to < 250μm in size and sent for standard ultimate analyses in an external laboratory, while the ash content was determined in house following CEN/TS 14775 standard. The properties of the dry fuels used in this work are summarized in Table 6.1.

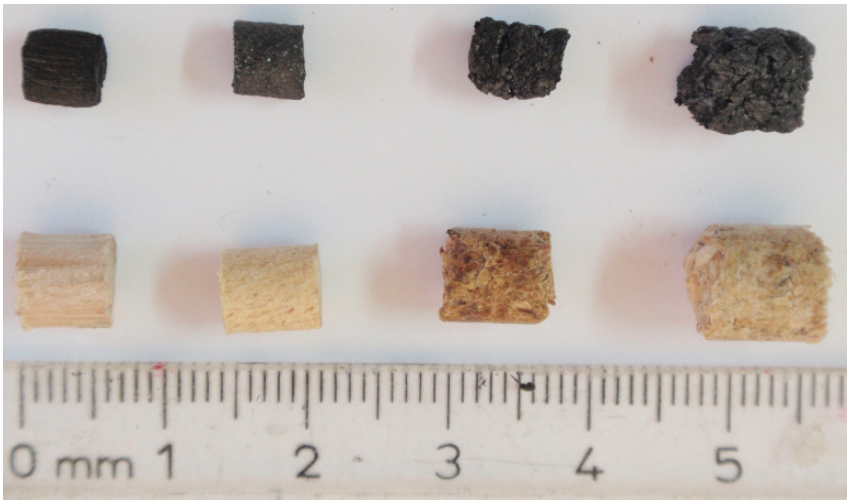

Figure 6.1 - Photograph with examples of the fuel particles used in this work and respective char particles formed at 850ºC. From left to right: eucalyptus wood, pine wood, forest pellets and wood pellets.

Table 6.1 - Ultimate composition and ash content of the fuels used in this work.

	Mass fraction, mass % of dry fuel					
Fuel	Carbon[a]	Hydrogen[a]	Oxygen[a,b]	Nitrogen[a]	Sulfur[a]	Ash[a]
Eucalyptus wood	46.3±0.5	6.4±0.1	46.8±0.6	0.1±0.0	Nd	0.4±0.0
Pine wood	48.0±1.2	6.3±0.1	45.1±1.2	0.1±0.0	Nd	0.5±0.0
Wood pellets	49.1±1.0	6.6±0.1	43.5±1.1	0.1±0.0	0.0	0.7±0.0
Forest pellets	49.8±0.8	6.3±0.1	42.7±0.8	0.3±0.0	nd	1.0±0.0

[a] Mean value ± one standard deviation of replicate samples; [b] Determined by difference method; nd below detection limit (<100ppm).

6.2.2 *Fluidized bed facility*

Figure 6.2 outlines the experimental facility used in this work. It comprises a stationary fluidized bed reactor and ancillary systems for fuel feeding, fluidizing gas measurement and control and flue gas conditioning and analysis. Two types of experiments were conducted in this facility: (1) fast-pyrolysis of batches of solid biomass under inert atmosphere and (2) combustion of the char formed during the previous pyrolysis stage.

The reactor main body consists of an AISI 310 refractory steel tube (700mm ID, 920mm length) sealed by flanges. It is placed within a $3kW_e$ oven that furnishes heat over ≈200mm height at the central part of the tube. The bed is held at middle height of the reactor by a concentric tube (62mm ID) welded onto a distributor plate with 29 holes of 0.6mm in diameter. The bed and freeboard extends over ≈270mm up to the insulating material (Cerablanket wool) placed in the upper part of the reactor tube. On top of the freeboard the escaping gases can divert into two alternative sampling lines (Figure 6.2): (1) the pyrolytic volatiles go through the side port into the high temperature line, and (2) the flue gases formed during the burnout of the char enter the upper port and are cooled in the other line. This upper port is also used as (1) pressure tap during the pyrolysis experiments (P1 in Figure 6.2) or (2) gas exhaust port. Also on top of the freeboard is the fuel discharge tube, which is attached to a ball valve placed outside the reactor; up to 5 fuel particles can be fed at once over the bed through this system. A third hole on the reactor top flange accommodates a K-type thermocouple to ascertain the temperature inside the bed (T1). The side port in the bottom of the reactor tube is used to purge the whole reactor vessel with inert gas.

Round silica sand with particle sizes in the range of 180-250μm (mean Sauter diameter of 205μm) is used as bed material. 250g of bed material are fed into the inner reactor tube leading to a static bed height of ≈55mm. The theoretical minimum fluidization velocity (u_{mf}) for this bed is ≈0.04m/s at room conditions. However, during the experiments the fluidizing velocity is adjusted to bubbling regime. The flow rate of fluidizing gas is measured by mass-flow meter (MFM1, Honeywell, 0-5NLpm) with typical uncertainty of 2.5% of the reading [20]. During pyrolysis the bed is operated with nitrogen (99.999%v) while dry reconstituted air is used during the subsequent burnout of the char; switching from N_2 to reconstituted air is done by automatic gas control unit H incorporating solenoid valves (Figure 6.2). The fluidizing gas pass through a preheating zone at the bottom part of the reator tube before reaching the distributor plate. De-fluidization of the bed due to e.g. accumulation of ash from consecutive char combustion experiments, can be checked out visually through the fuel discharge tube.

The heated sampling line for the volatiles firstly comprises an in-line quartz thimble filter (C, Whatman 603G) to remove carbon soot without vapor condensation (e.g. tars); the filter is heated to 380ºC by trace heating (0.25 kW/m) and the temperature is monitored by a thermocouple (T2). The pyrolysis liquids (i.e., condensable volatile species comprising organics and water) are collected downstream the heated filter by passing the filtered volatiles through a series of impinger bottles (4×25mL) sitting on iced water (F); these bottles are equipped with glass joints and do not use solvent. It follows two quartz filters in-series (G, Schleicher & Schuell No.8) to collect any escaping aerosols that might be formed inside the impinger train. The dry and filtered permanent gas (i.e. volatile gases released

from a fuel batch and N_2 fluidizing gas) is then lead by a Teflon (PTFE) tube to another mass-flow meter (MFM2, Honeywell, 0-5NLpm) and is collected in a 10L sampling bag (SKC FlexFoil, H_2 proof) for later analysis by gas chromatography (GC) (see Section 6.2.3). The operation of this bag is done by an automatic gas control unit I featuring suitable pneumatics and solenoid valves (Figure 6.2).

During the burnout of the char the combustion flue gases enter the second sampling line comprising an ice bath trap with silica gel (D, Figure 6.2), backup quartz filter and bellows-type volumeter (E). A slipstream of the dry and clean flue gas is extracted by a diaphragm pump (J) and sent to a CO_2 gas analyzer (ADC NDIR, model LUFT, 0-25%v) by suitable gas conditioning and distribution units (L and M).

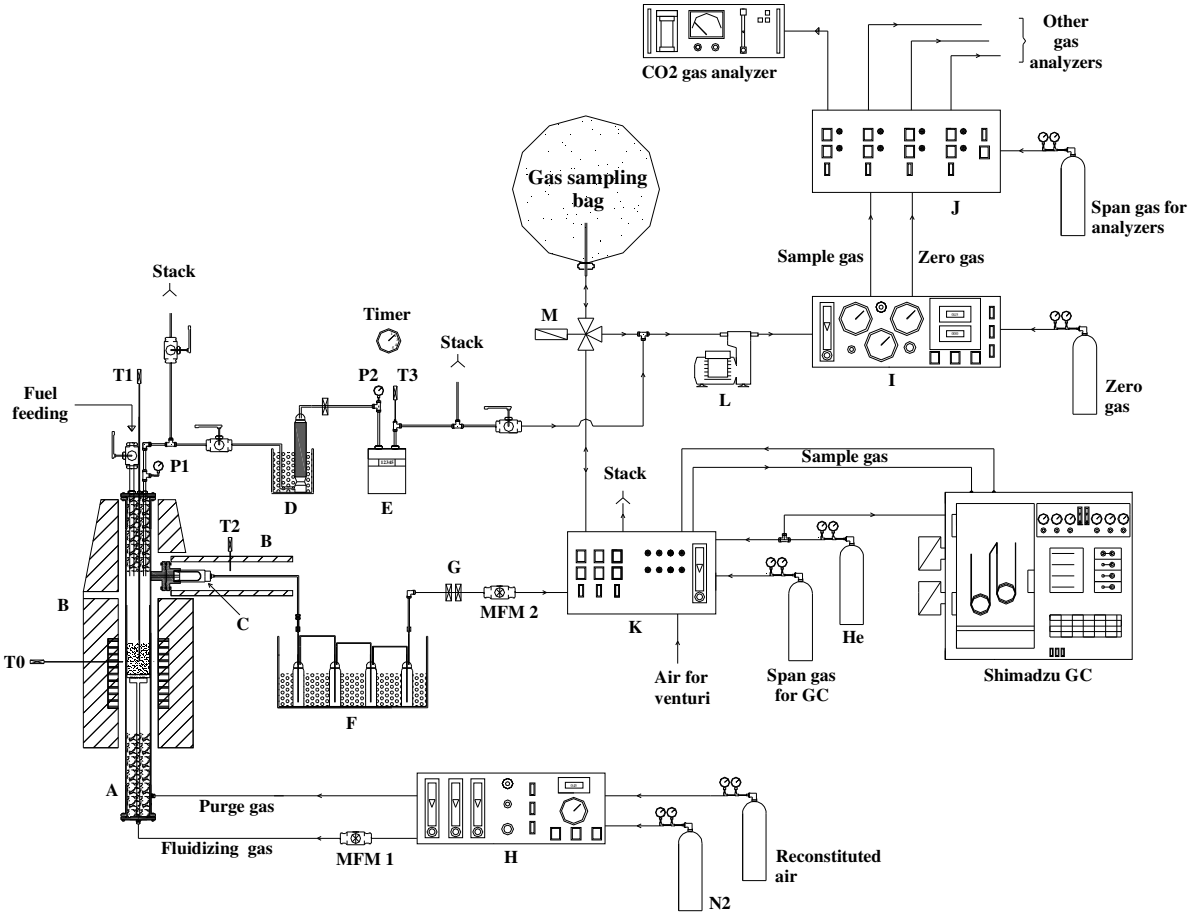

Figure 6.2 - Schematic layout of the laboratorial-scale fluidized bed facility at the University of Aveiro. A – bubbling fluidized bed reactor, B – electrically heated ovens, C – heated quartz thimble filter, D – ice bath with silica gel tower, E – bellows-type volume meter, F – ice bath with impinger bottles, G – quartz backup filters, H - automatic gas control and measurement unit, I – automatic unit to operate the gas sampling bag and GC-TCD system, J – diaphragm pump, K – 3-way solenoid valve, L – automatic gas sampling and conditioning unit, M – automatic gas distribution unit, P1 and P2 – pressure measurement points, T0 to T3 – thermocouples.

6.2.3 *Chromatographic procedures*

The gas collected in the sampling bag was analyzed by a dedicated Shimadzu 15A GC system or a μGC (Varian GC4900). In the Shimadzu GC system the gas sample is loaded into the GC loop by ⅛ in. SS tube with the help of a small venturi placed downstream of the loop; the sample is left to equilibrate to the atmospheric pressure before injection into the chromatographic columns. Separation is done in a Carbosieve SII (2m, ⅛ in.) and Hayesep Q (1.5m, packed) columns plumbed in-series on a 10 port GC sampling valve. Proper tuning of this valve enables H_2, N_2, CO and CH_4 to elute from the Carbosieve SII column while CO_2 and other hydrocarbons (in this GC system, C_2H_4 and C_2H_6) elute from the Hayesep Q column. The analysis time is 15min using temperature programming, helium carrier gas and thermal conductivity detection (TCD). During the wood pellets experiments the μGC was available that in addition to the species that could be measured by the Shimadzu GC system also can analyze C_3H_8 and He. The μGC is equipped with a molecular sieve 5Å (10m, ⅛ in.) and Porapak Q (10m, ⅛ in.) columns using argon and helium as carrier gas, respectively. Due to a parallel setup of the columns the analysis time is ≈3min under isothermal condition (TCD detection). Both GC systems are calibrated against standard gases covering the range of concentration of the species collected in the sampling bag.

6.2.4 *Test procedure*

For each bed temperature and fuel type, the experiment is done according to the following procedure:

1. The impinger bottles and backup filters are weighted in a precision balance (Mettler Toledo) with a readability of 0.01mg for the filters and 0.1mg for the bottles. The gas sampling bag is purged with helium during 20-30min and its cleanness is verified by GC analysis; the sampling bag is then emptied under vacuum and sealed.

2. The reactor and thimble filter are heated up and the bed fluidized with a known flow rate of N_2 (see MFM1 in Figure 6.2). Nearly the same flow rate of N_2 is used in the experiments, which means that the fluidizing velocity depends somewhat on the reactor temperature (usually, between 3 and 4 times the values of u_{mf}).

3. A batch of fresh biomass (<2g) is oven dried at 105ºC to constant weight, cooled to room temperature in a desiccator with silica gel and weighted (readability of 0.1mg).

4. The dry fuel batch is fed over the hot bubbling bed and the ball valve (see Figure 6.2) is immediately closed. The volatiles and inert fluidizing gas pass through the heated thimble, impinger train, backup filters and are collected into the sampling bag. When the response of the MFM2 returns to a value corresponding to the flow rate of the fluidizing gas (typically 30-90s after fuel feeding) the bag is sealed and the remainder inert gas is discarded.

5. The first backup quartz filter is recovered into a Petri box and re-weighted immediately. The composition of the gas collected in the sampling bag is analyzed at least three times using GC-TCD.

6. A new backup filter is weighted and put in place and the gas sampling bag is cleaned with helium and sealed again. The procedure given in points 3 to 5 is repeated for another two batches of the same fuel sample.

7. The thimble filter is recovered in a crucible and burned in a muffle to determine the amount of organics being trapped. The external walls of the impinger bottles are dried and the bottles are re-weighted. The second backup filter is re-weighted to verify the collection efficiency of the aerosols escaping the impinger train.

8. After the three pyrolysis experiments, the fluidizing gas is switched to reconstituted air to burn the char remaining in-bed. In separate experiments the bed material is left to cool overnight under nitrogen; the char particles are carefully recovered by sieving the bed and then oven dried at 105ºC and weighted (± 0.1mg).

6.2.5 *Treatment of data*

The distribution of pyrolytic products is reported as yields, $Y_{i,F}$, having units of kg i/kg daf fuel feed. The yield of daf char ($Y_{ch,F}$) is determined from the mass of dry char particles recovered from the bed ($Y_{S,R}$) and assuming that all the ash in the parent fuel ($Y_{a,R}$) remains in the char, as shown in Eq. (6.1). In turns, the amount of carbon in the char ($Y_{ch,F}$·$Y_{C,ch}$, kg C/kg daf fuel) is determined during the combustion experiments according to Eq. (6.2), where m_F is the mass of daf fuel feed, $\dot{n}_{Ed}$ the molar flow rate of dry flue gases leaving the reactor, $y_{CO2,Ed}$ the molar fraction of CO_2 in the dry flue gases and t_b the char burnout time. Further details on the measurement procedure for $Y_{ch,F}$·$Y_{C,ch}$ are given in [21]. The material trapped in the heated thimble filter is ascribed to soot, $Y_{soot,F}$. The material trapped in the impinger train and the two backup filters is defined as pyrolytic liquids, $Y_{L,F}$, and includes organic compounds and water. The sampling bag contains the integrated amounts of permanent volatile gases released from a fuel batch, N_2 fluidizing gas and minor amount of helium used in the cleaning procedure of the bag. The yields of the gas species are determined from a known amount of inert gas injected into the bag and the results of the GC analysis. The inert gas is the N_2 fluidizing gas entering the sampling bag together with the volatile gases as quantified by mass flow-meter (MFM1); following this route, the yield of i^{th} gas species is computed by Eq. (6.3), where $y_{i,bag}$ and $y_{N2,bag}$ are the molar fractions of i^{th} species and N_2 in the bag, respectively, $\dot{m}_{N2}$ the mass flow rate of fluidizing gas and t_s the sampling time. However, in the experiments using the μGC (pyrolysis of wood pellets) helium was used as inert gas instead of N_2. Following this route, after the volatiles and N_2 fluidizing gas were

collected, an additional 0.5-1L of helium was injected into the sampling bag in order to relate the amount of each gas species in the bag to the unit mass of helium. The amount of dry helium injected into the bag is given by drum-type volumeter (±0.2% accuracy) and is corrected for the residual amount of helium added during the cleaning procedure of the bag.

$$Y_{ch,F} = \frac{Y_{S,R} - Y_{a,R}}{1 - Y_{a,R}} \quad \text{Eq. 6.1}$$

$$Y_{ch,F} \cdot Y_{C,ch} = \frac{M_C}{m_F} \cdot \int_0^{t_b} \dot{n}_{Ed} \cdot y_{CO2,Ed} \cdot dt \quad \text{Eq. 6.2}$$

$$Y_{i,F} = \frac{y_{i,bag}}{y_{N2,bag}} \cdot \frac{M_i}{M_{N2}} \cdot \frac{1}{m_F} \cdot \int_0^{t_s} \dot{m}_{N2} \cdot dt \quad \text{Eq. 6.3}$$

6.3 *Results and discussion*

6.3.1 *Temperatures, gas residence time and kinetics*

Apart from the flow rate of the N_2 fluidizing gas, the residence time of the escaping volatiles in the reactor is dependent on the temperature profile along the reactor (see Figure 6.3), the mass of the fuel batch and the pyrolysis kinetics. Based on the typical flow rate of N_2, the gas residence time in the freeboard is estimated to be within 4-5s for bed temperatures in the range of 650-900ºC, but it decreases once the volatiles start to evolve from the fuel particles. The release rate of the volatile gases is exemplified in Figure 6.4, where the time-dependent bed temperature (T1), differential pressure in the freeboard (P1) and flow rates of the gas streams entering (N_2, MFM1) and leaving (N_2 + volatile gases, MFM2) the reactor during pyrolysis of batches of eucalyptus wood are shown. During the first ≈3-4s of the experiments the fluidizing gas is discarded into the stack (see e.g. P1). The dry fuel batch is then dropped into the reactor and the volatiles plus the fluidizing gas lead through the heated line towards the sampling bag. The rapid release of the volatiles causes the responses of P1 and MFM2 to peak seconds later and decrease slowly thereafter; in the experiments shown in Figure 6.4, both sensors indicate that the bulk of pyrolysis of the 6mm OD wood particles occurs within 30s. For the 8mm OD wood pellets this period of time increases to about 80s. During the release of the volatiles the bed temperature does not decreases below ≈1-2% of the set value, but the gas residence time in the freeboard can easily fall to below 3s. Once the pyrolysis is complete the response of MFM2 returns to a value close to that of MFM1 and the overpressure in the freeboard stabilizes at ≈200-250 mmH_2O, due to the aerosols trapped in the thimble filter and backup filters. To ensure that all volatile gases are collected, the reactor and heated line are purged for 10-15s before the sampling bag is sealed.

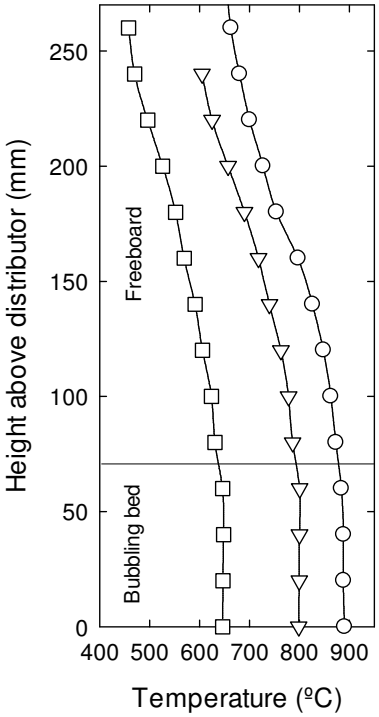

Figure 6.3 - Axial temperature profiles along the bubbling bed and freeboard. Measurements carried out during experiments with inert fluidizing gas at 650, 800 and 900ºC bed temperatures.

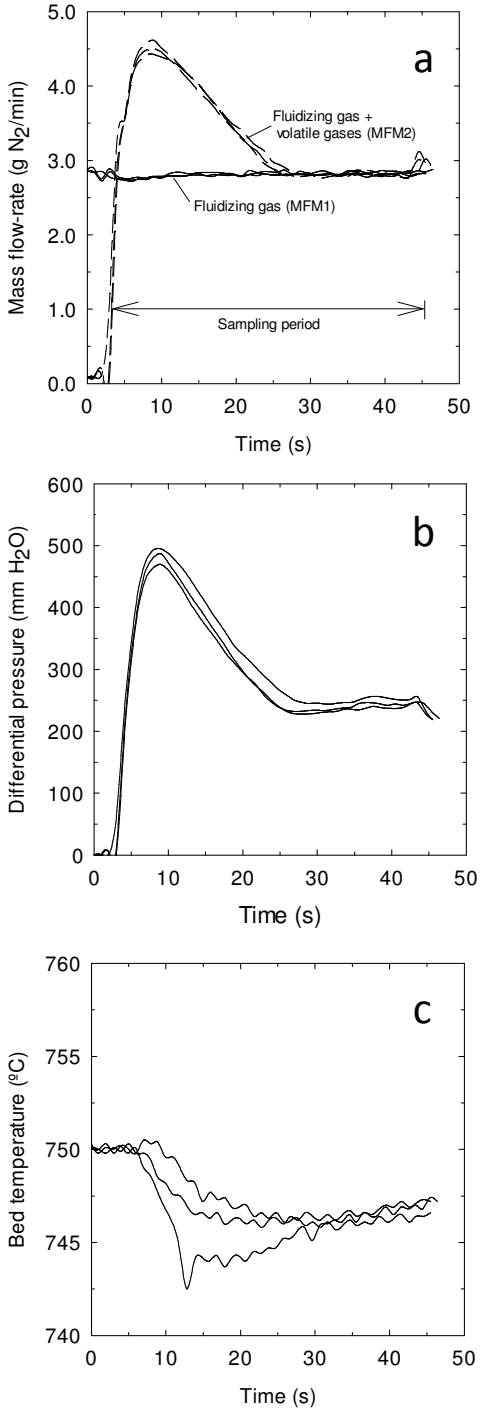

Figure 6.4 - Pyrolysis of three batches of ≈0.63g of eucalyptus wood (6×6mm cylindrical particles, dry) at 750ºC bed temperature. Mass flow-rates of gas streams entering (N_2, MFM 1) and leaving (N_2+volatiles, MFM2) the reactor (a), differential pressures in the freeboard relative to atmosphere (b) and temperatures at middle height of the bubbling fluidized bed (c) as a function of time.

6.3.2 *Overall mass balance*

As an example of the overall mass balance, Table 6.2 provides the measurements relative to the experiments shown in Figure 6.4. In general, fragmentation was negligible in the case of woody materials but it leads to a number of mm-sized char particles in the case of pellets. Anyhow, the char particles were easily recovered from the bed and the amount of char fines remaining in-bed after the sieving procedure is <0.5% of daf fuel feed (mass %). Figure 6.1 also shows typical char particles recovered from the bed which are relatively smaller than those of parent fuel (roughly 20% smaller in both the diameter and length). The major part of the pyrolytic liquids released from a fuel batch is collected in the first impinger bottle, representing typically 80-90% (84% in Table 6.2) of the total mass of liquids collected in the impinger train; nevertheless, the contribution of the first bottle decreased with pyrolysis temperature increase. The aerosols formed upon cooling the volatiles could be seen on top of the bottles escaping towards the two backup filters. The mass of aerosols trapped in the first backup filter is higher than the mass of liquids collected in the last three impinger bottles, and is proportional to the total amount of liquids collected; it varied from as much as 12% of daf fuel at 600ºC to ≈3% at the higher temperatures tested (4.1% in Table 6.2). The first backup filter turned orange after the passage of the volatiles, but the second filter keeps the original white color due to negligible amount of aerosols collected. The orange color of the deposits in the first backup filter is similar to that of the tars trapped in the impinger bottles; however, the first filter turns brown within a couple of days which, together with a slight mass loss at room conditions, indicate that low vapor pressure species are collected. In turn, the weight increase of the 380ºC thimble filter is due to non-volatile black deposits. Figure 5-a shows a scanning electron micrograph (SEM) of the thimble deposit. Clusters of nm-sized spheres can be seen, which seem combined into large synthetic aggregates; no filamentous carbon, char fines or bed solids were found in the thimbles. Energy dispersive spectrometer (EDS) analysis shows that the deposits are composed mainly of carbon (Figure 5-b). There is a relatively large scatter in the amount of material trapped in the thimble filters, but the trends indicate that it increases with pyrolysis temperature increase, up to ≈2% of daf fuel (0.7% in Table 6.2), and correlates positively with the yield of total permanent gas (see Figure 6.6). This suggests that the collected carbon is a result of gas-phase polymerization reactions among the volatiles [22-26], namely tars. Regarding the permanent gas collected in the sampling bag, in general, between 96 and 99% by volume could be identified by GC-TCD analysis. The measured pyrolytic gases corresponds to typically 10-40%v of the total collected gas and the remainder gas is N_2 fluidizing gas, unmeasured pyrolytic species (e.g. >C_3 light hydrocarbons), and He (<1%v).

Table 6.2 – Mass balance of replicate pyrolysis experiments with eucalyptus wood at 750ºC (see time-dependent release of volatiles in Figure 6.4).

			Impinger bottle (g)[b]				Backup filter (g)[b]		Bag composition (%v)									
Replicate no.	Fuel (g)[a]	Soot (g)[b]	#1	#2	#3	#4	#1	#2	H_2	CO	CO_2	CH_4	C_2H_4	C_2H_6	N_2	m_G (g)[c]	m_{ch}(g)[d]	Sum
#1	0.6372	--	--	--	--	--	0.02729	--	1.53	8.51	1.79	2.05	0.78	0.12	83.20	0.308	--	--
#2	0.6164	--	--	--	--	--	0.02522	--	1.53	8.06	1.88	1.98	0.72	0.12	84.00	0.295	--	--
#3	0.6325	--	--	--	--	--	0.02527	--	1.54	7.62	1.88	1.92	0.69	0.13	81.67	0.302	--	--
Overall (g)[f]	1.8861	0.01395	0.3540	0.0506	0.0122	0.0068	0.07778	0.00001	--	--	--	--	--	--	--	0.905	--	--
Mass %	--	**0.7**	**18.8**	**2.7**	**0.6**	**0.4**	**4.1**	**0.0**	**--**	**--**	**--**	**--**	**--**	**--**	**--**	**48.0**	**12.1**	**87.4**

[a] Mass of the fuel batch fed into the reactor (dry ash-free); [b] Mass of material (liquids or aerosols) accumulated after pyrolysis of each fuel batch or all three fuel batches; [c] Mass of permanent gas based on the species analyzed; [d] Dry ash-free char particles recovered from the bed as determined in a separate pyrolysis experiment.

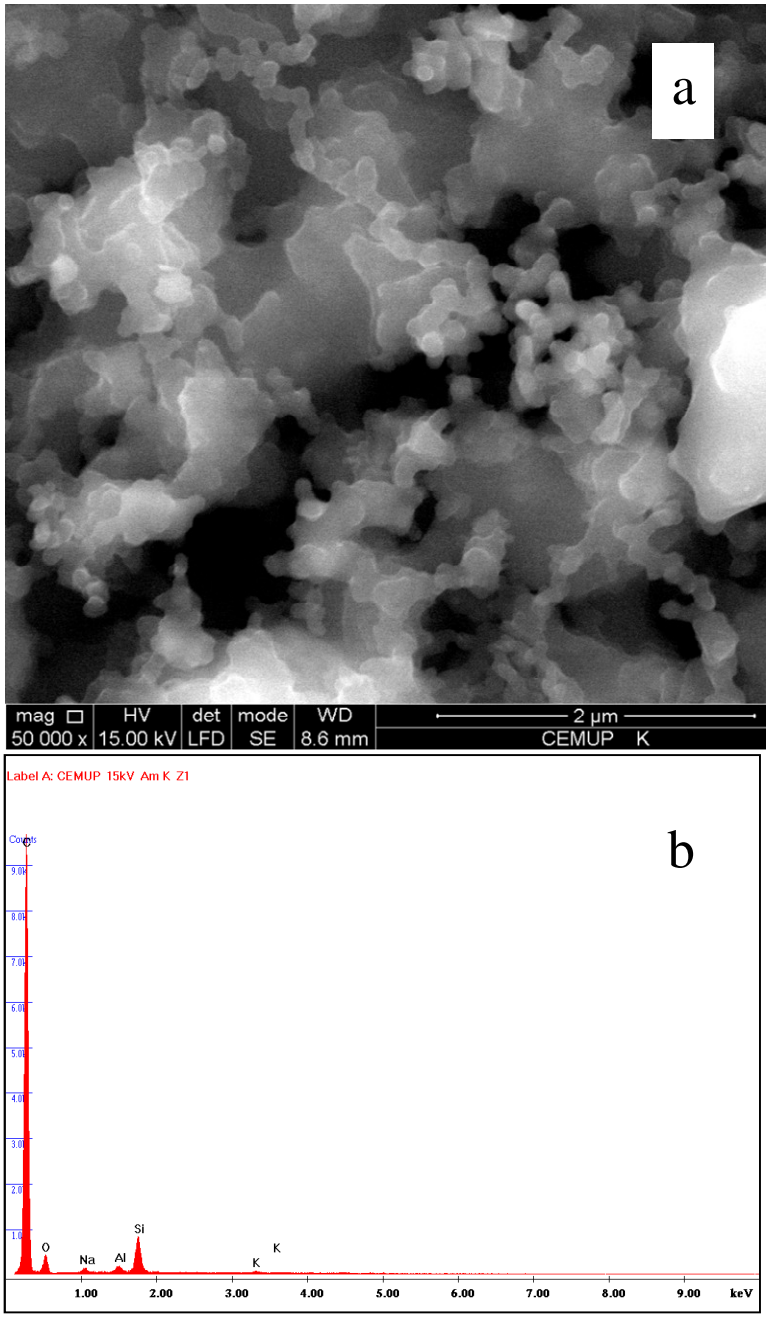

Figure 6.5 - Scanning electron micrograph (SEM, a) and energy dispersive spectrum (EDS, b) of the material collected over the heated quartz thimble filter (≈380ºC) after passage of the pyrolytic volatiles.

Figure 6.7-a provides all mass balance results obtained in this work. Note that, although the mass balance for the wood pellets was checked only at 600 and 700ºC, the composition of the volatile gases was analyzed in a broader temperature range (see Section 6.3.4). The mass balance closure was most often between 85 and 103% of daf fuel with only one value outside this range (i.e. 107% for the pine wood at 975ºC). These results compare well with literature values of 86 to 108% [13], as obtained in various experimental rigs.

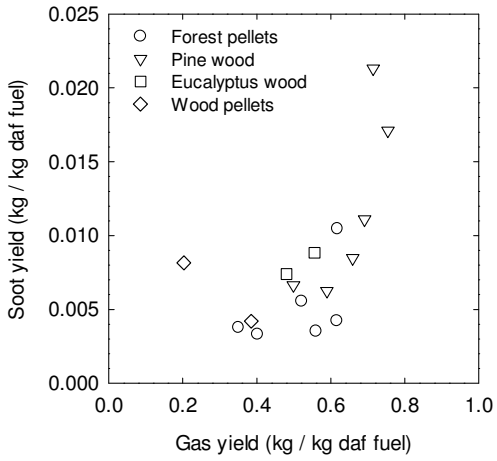

Figure 6.6 - Amount of soot collected in the quartz thimble filters against the respective amount of total permanent gas during pyrolysis experiments with bed temperatures within 600-975ºC.

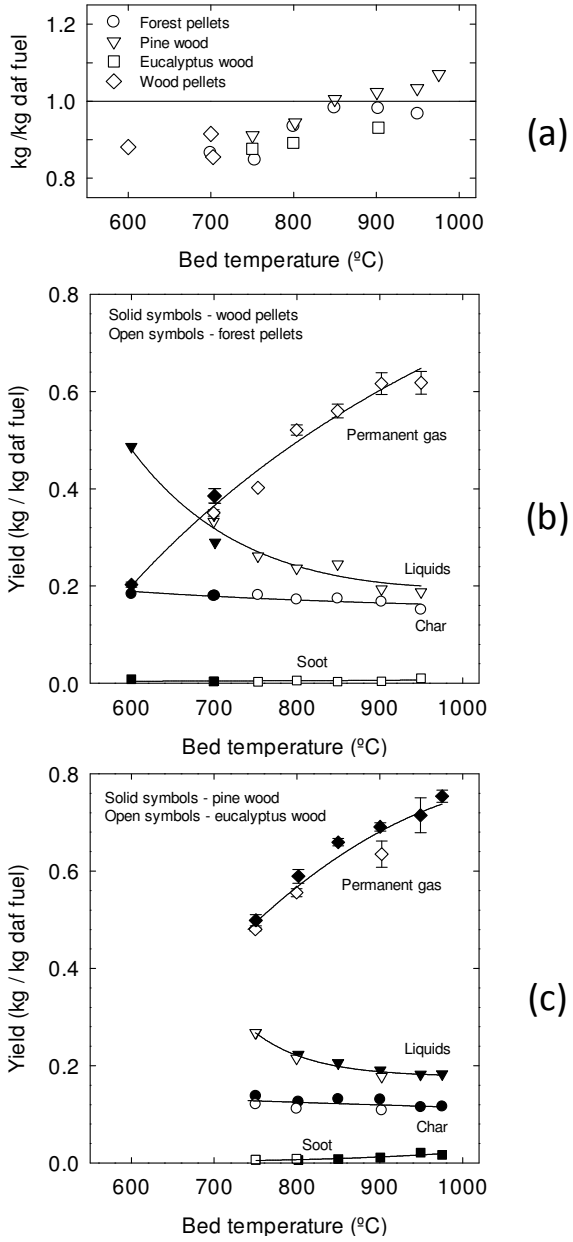

Figure 6.7 - Mass balance closures (a), and yields of major product fractions from the pellets (b) and wood (c) as a function of bed temperature. Mass balance is the sum of the yields of char, soot, liquids (organics + water) and permanent gases (H_2, CO, CO_2, CH_4, C_2H_4 and C_2H_6). Solid lines show the average trends for the pellets and wood.

6.3.2.1 *Evaluation of the measurements*

To understand the values shown in Figure 6.7-a, an evaluation of the uncertainty of the measurements was done. Concerning the yields of permanent volatile gases, a comparison is made between the results of two experiments conducted with the wood pellets at 750ºC in

which the yields were determined using different methods. The first experiment was based on the N_2 method (see Section 6.2.5) with the gas collected in the bag analyzed using the Shimadzu GC; the second experiment was done months later following the He method and using the Varian μGC. The results from these two experiments are presented in Figure 6.8, showing that differences in the yields of gases are typically within ±10%. Moreover, following one of these methods (i.e. under repeatability conditions) the yield of total gas among replicate fuel samples varies less than ±5% of the mean values (see e.g. Table 6.2 following the N_2 method).

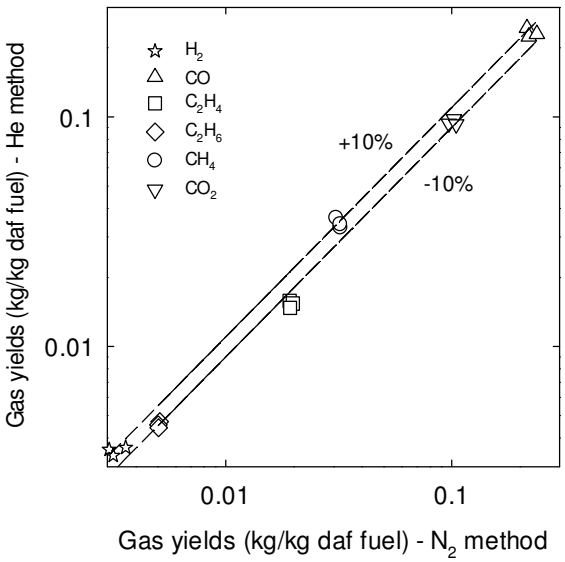

Figure 6.8 - Yields of gas species determined through the He method and using the Varian μGC system against those determined through the N_2 method and using the Shimadzu GC system, during pyrolysis experiments with wood pellets at a bed temperature of 750ºC.

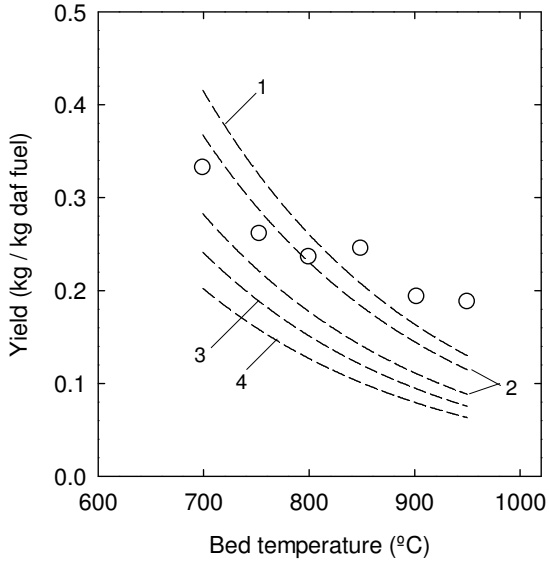

Figure 6.9 - Measured yields of total pyrolytic liquids (circles) and calculated yields of organic liquids (lines) as a function of bed temperature. Carbon content of the organic liquids varied from that of levoglucosan (1), range given by [13] (2), phenol (3) and toluene (4).

In relation to the yields of char, previous investigation showed that repeated experiments in the fluidized bed reactor also lead to variations below ±5% of the mean values [21]. When the yields of char obtained in the fluidized bed were compared to those obtained in a quartz tube reactor offering similar heating rates of fuel, the differences were below ±10% [21]. The aerosols trapped in the first backup filter were measured three times per experimental condition (i.e. temperature and fuel, see e.g. Table 6.2) thus providing an indication of the variability of the measured yields of liquids. It turns out that the aerosols trapped in this filter vary in less than ±10% among replicated fuel samples. Thus, considering the variability in the measured yields of permanent gases, char and liquids, an upper bond for the variability in the mass balance closures is around ±10%. Accordingly, the deviations from

100% obtained in experiments above 800ºC (see Figure 6.7-a) are roughly within the measurement uncertainties. However, at lower temperatures, the mass closures (typically <90%) can hardly be explained by experimental errors and are also likely due to unmeasured product species.

One aspect that can contribute to the temperature dependency of the mass balance closures is the limited set of light hydrocarbons measured in this work. The values in Figure 6.7-a are based on six gas species (H_2, CO, CO_2, CH_4, C_2H_4 and C_2H_6) while there are many light hydrocarbons that were not measured. To investigate the possible role of the unmeasured light hydrocarbons, the μGC was used in some experiments to additionally measure C_3H_8. According to the results, the yields of C_3H_8 peak at temperatures below 800ºC and reach up to 2% of daf fuel. Findings by [27, 28] suggest that the yields of C_3H_6 are in range of those of C_3H_8 during fluidized bed pyrolysis of wood, and a simulation based on an empirical pyrolysis model indicates that the yield of total non-methane light hydrocarbons can easily reach a few percent of daf fuel at temperatures of 700-750ºC [13]. Hence, the lower closures shown in Figure 6.7-a below 800ºC can be partially due to unmeasured light hydrocarbons (i.e. C_3 to C_5) that are unstable at higher temperatures.

In addition, an underestimation of the liquids formed below 800ºC, due to e.g. evaporation of light organics before weighting the impinger train and backup filters and/or deposition of heavy organics in the sampling line cannot be ruled out. To ascertain this possibility, the amount of carbon condensing was calculated as a difference between the carbon in dry fuel and the carbon measured in the gas-phase (i.e., CO, CO_2, CH_4, C_2H_4, C_2H_6), soot and char, the later being determined according to Eq. 6.2. Considering that all condensing carbon is due to organics, this procedure also provides an estimate for the yield of organic liquids as long as their carbon content is known. Previous works [24, 29] have shown the maturation of the organic compounds during biomass pyrolysis, in which mild temperatures of, say, <600ºC, give rise to low-carbon compounds (e.g. levoglucosan 44.4%C) while higher temperatures cause a transition to high-carbon secondary (e.g. phenol 76.6%C) and tertiary (e.g. toluene 91.3%C) compounds. This can be compared to the data summarized in [13, 30] showing also a slight positive temperature dependency of the carbon content of the organic liquids even though the values lie often within 1 to 1.3 times the carbon content of the parent fuel (typically 50-70%C, mass % of lumped organics). These results indicate that the organic liquids formed at low temperatures are highly oxygenated, which more or less corresponds to the temperatures yielding the lower mass balance closures in Figure 6.7-a. Thus, under the aforesaid difference method, Figure 6.9 shows the calculated yields of organic liquids for the case of the forest pellets, in which the carbon content of the organics was varied from that of levoglucosan to that of toluene. The outcome is that the calculated yields of organic liquids at high temperature are about half of the measured yields of total

liquids (i.e. organics + water); however, for the low temperatures conducive to the formation of highly oxygenated organics, the calculated yields approach or exceed those of the total liquids. Considering that an overwhelming part of the total liquids is water (typically 10-20% of daf fuel [13]), the mass balance closures found below 800ºC could easily approach 100% if all missing carbon was attributed to highly oxygenated organics. This further suggests that the temperature-dependent mass balance closures shown in Figure 6.7-a are due to a combination of the effects of the unmeasured light hydrocarbons and organic liquid compounds.

6.3.3 *Yields of the major product fractions*

Figs. 7-b and -c provides the yields of the major product fractions (char, soot, liquids and permanent gas) as a function of bed temperature (T1 in Figure 6.2) with the results from the pellets and woody materials grouped for the sake of clearness. Notice that the data is not normalized and shall be analyzed in combination with the mass balance closures provided in Figure 6.7-a.

A global result from Figs. 6.7-b and -c is that mainly the yields of liquids and permanent gas vary as a function of temperature while the yields of char vary much less. Yields of gas increase with temperature increase and yields of liquids decrease; the variations in the yields of gas and liquids do not perfectly match probably due to unmeasured species at low temperatures as discussed in Section 6.3.2. The results indicate that pyrolysis proceeds mainly in the gas-phase with the less stable liquid species (e.g. tars) being progressively converted into permanent gases and minor amounts of soot. Nevertheless, at temperatures above, say, 800ºC, the yield of liquids decreases more slowly which suggests that a fraction of the liquids is rather difficult to convert under the range of residence times used in this work. For instance, the yields of liquids at ≈800ºC are within 20-25% of daf fuel and do not decrease to below ≈18% for any higher temperatures tested. The liquids surviving at high temperatures shall comprise refractory tars [19] and water. For instance, water was found to be stable even for temperatures within 1000-1300ºC and 2s residence time during the thermal cracking of a surrogate pyrolysis gas [31], which is in agreement with the review by [13] showing that the yield of water is stable at temperatures within 300-900ºC.

Despite the yields of char exhibit a small temperature dependency under the conditions of the present work, they depend somewhat on the fuel being converted. Indeed, the two types of pellets clearly produce more char (≈16-19% of daf fuel) than the two types of wood (≈10-14%). The results from the char burnout experiments further underline this behavior since the total amount of carbon remaining in-bed consistently increased with the carbon content of the fuel (Figure 6.10): eucalyptus wood < pine wood < wood pellets < forest

pellets. Therefore, despite the fact that the yield of char is not notably influenced by the reactor temperature, more favorable charring conditions are obtained for fuels with higher carbon contents. In this work, the variations in the yield of char among fuels are mainly balanced by variations in the respective yields of permanent gases (Figure 6.7-b and -c) as the fuel dependency of the yields of liquids are comparatively low.

Overall, our results regarding the yields of the major product fractions compare well with the results from a review of literature data in [13] and, in particular, with data from other fluidized bed reactors [27, 28, 32, 33].

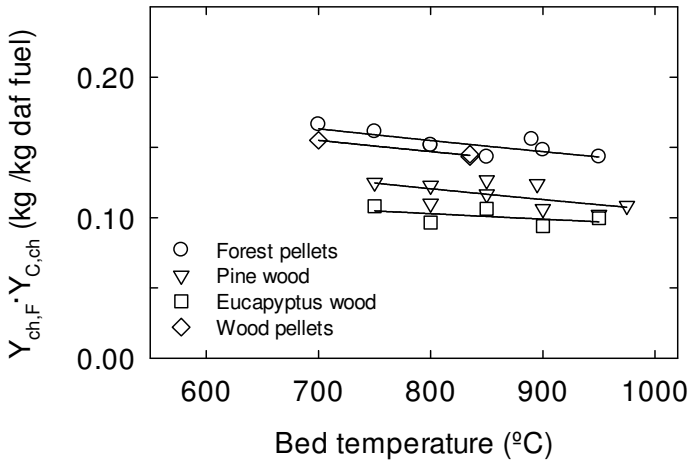

Figure 6.10 - Amount of carbon remaining in bed as char per unit mass of daf fuel (see Eq. 6.2) as a function of bed temperature.

6.3.4 *Yields of permanent volatile gases*

The yields of the bulk of the permanent gases CO_2, CO, CH_4 and H_2 are shown in Figure 6.11 as a function of temperature. It shall be noted that devolatilization is roughly complete at temperatures above 600ºC as indicated by the yields of char in Figure 6.9 and, hence, the temperature dependency of the gas yields in Figure 6.11 is mainly due to gas-phase reactions. Also, note that the residence time of the volatiles decreases considerably as the temperature increases from 600 to 950 ºC, which might also have a bearing on the gas yields.

Carbon monoxide is by far the major gas species and its production is a strong function of temperature; above 900ºC it represents within 35-50% of daf fuel feed, or 30-45% and 45-60% of the total carbon and oxygen in fuel, respectively. Carbon dioxide is the gas species with the second largest yields (7-15% of daf fuel), but in comparison with carbon monoxide exhibits a weak temperature dependency; it is a product of the gas-phase reactions because the yields initially increase with temperature increase above 600ºC, but it becomes unstable at relatively low temperatures. In this work the yields of carbon dioxide apparently go

through maximum values of ≈12-15% of daf fuel at temperatures in the range of 850-950ºC. An investigation by [31] highlights that carbon dioxide is likely to partake in the oxidation of hydrocarbons during the thermal treatment of a surrogate pyrolysis gas, being a major donor of hydroxyl radicals (CO_2+H → CO+OH). It is likely that this mechanism also governs the decreasing yields of carbon dioxide found in this work above ≈850ºC. Methane behaves like carbon monoxide over a wide temperature range with yields increasing from ≈1% at 600ºC to as much as 6-8% at 975ºC (Figure 6.11). During the experiments with the forest pellets the yields of methane were observed to become constant or start to decrease above ≈950ºC; in the case of pine wood, methane seems to increase up to 975ºC but this may be due in part to an overestimation of the overall mass balance as shown in Figure 6.7-a. The decomposition of methane ultimately yields thermodynamically stable species, CO and H_2, through a complex mechanism which also produces other light hydrocarbons [31, 34]. The results provided in Figure 6.11 also clearly indicate that hydrogen is an important product from the gas-phase reactions among the volatiles with yields steadily increasing from <0.5% at 700ºC to ≈1.5% at 975ºC (Figure 11), which represent an overwhelming part of the hydrogen in fuel feed.

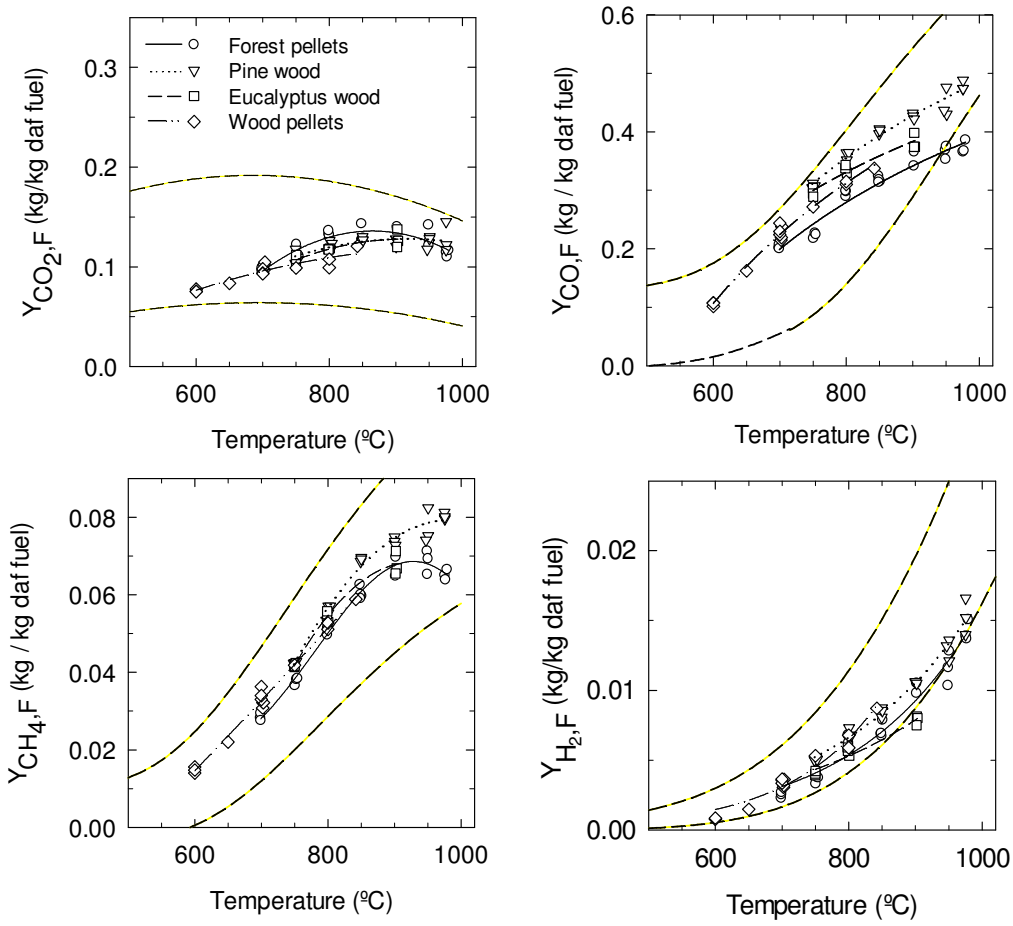

Figure 6.11 - Yields of carbon dioxide, carbon monoxide, methane and hydrogen as a function of bed temperature. Dashed lines give the ranges derived in [13] after a survey of literature data.

The yields of the minor measured componets C_3H_8, C_2H_6 and C_2H_4 are shown in Figure 6.12. Yields of ethylene are relatively high compared to those of the saturated species and show a similar temperature dependency as the yields of methane. It is evident that ethylene starts to convert above around 900ºC. In turns, the yields of propane and ethane peak at lower temperatures (700-750ºC) with maximum values of ≈2% and ≈0.5% of daf fuel, respectively. Noteworthy, some findings show that propane and ethane start to evolve at high rates at ≈500ºC [27, 28] while the results from this work suggest that its conversion is rather high at temperature approaching 1000ºC. The main products from the thermal cracking of propane and ethane are methane, hydrogen and minor amounts of other hydrocarbons (e.g. propylene) [35, 36] together with carbon monoxide if oxygen is present.

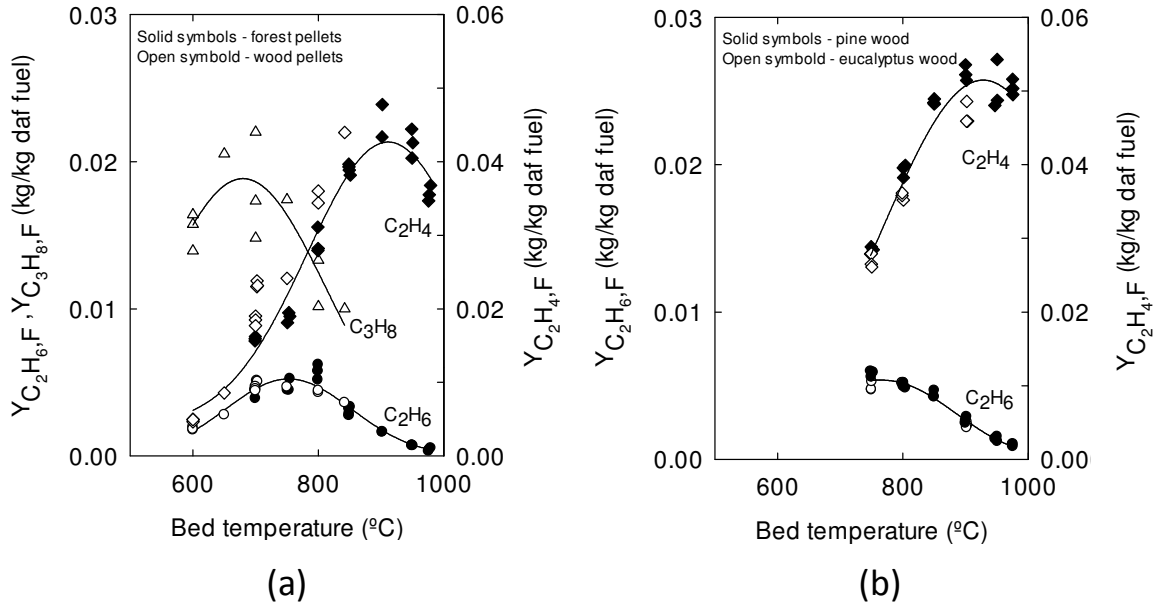

Figure 6.12 - Yields of propane, ethane and ethylene from pellets (a) and wood (b) as a function of bed temperature. Solid lines show the average trends for the pellets and wood.

6.3.4.1 *Comparison with thermodynamic equilibrium*

If the yields of the gas species would be under thermodynamic control, light hydrocarbons would be minor species at temperatures above, say, 900 ºC [21]. Since, this is not the case (see Figures 6.11 and 6.12), the yields are kinetically controlled and it becomes of interest to compare them to the equilibrium values. For a given fuel and pressure, the yields of volatiles under equilibrium condition also depend on the temperature, but the values for the major gases approach asymptotes at relatively low temperatures [21, 37]. Above, say, 1000ºC, stable yields are predicted for carbon monoxide and hydrogen, while the yields of other species (e.g. CO_2, CH_4) are negligible. The asymptotic values predicted for the yields of carbon monoxide and hydrogen can be estimated from the elemental composition of

the fuel (noted $Y^*_{i,F}$ for the ith product), $Y^*_{CO,F} \approx Y_{O,F} \times M_{CO} / M_O$ and $Y^*_{H2,F} \approx Y_{H,F}$ [13, 21], yielding values within 75-82 %CO and 6.3-6.6 %H_2 (mass % of daf fuel) for the fuels listed in Table 6.1. It is seen that, even at the highest temperatures tested, the measured yields of carbon monoxide and hydrogen are much lower than the asymptotic yields predicted under equilibrium condition. Despite of this, the trends shown in Figs. 6.7, 6.11 and 6.12 indicate that the composition of the volatiles evolves towards equilibrium as temperature increases. Yields of carbon monoxide and hydrogen always increase with temperature increase and the yields of liquids and other gases decrease above certain temperatures: (i) yields of total liquids star to decrease at temperatures as low as ≈500ºC [13], (ii) yields of propane and ethane decrease above ≈750ºC, (iii) yields of carbon dioxide decrease above ≈850ºC, and (iv) yields of ethylene and methane decrease above ≈900-950ºC.

6.3.4.2 *Influence of fuel type*

In general, the woody materials produce higher amounts of combustible gases (CO, CH_4, C_2H_6, C_2H_4) than the pellets (Figs. 6.11 and 6.12). This behavior is especially evident from the results for carbon monoxide, showing consistently higher yields as follows: forest pellets < wood pellets < woody materials. The higher yields of carbon monoxide afforded by wood are in agreement with the higher equilibrium values predicted for fuels with higher oxygen content (see Section 6.3.4.1). The inconsistent result is that pine wood gives slightly higher yields of carbon monoxide than the eucalyptus wood, despite the higher oxygen content of the later (Table 6.1); however, the small number of data points together with the lower mass balance closures obtained for the eucalyptus wood does not allow a clear conclusion. The yields of carbon dioxide exhibit a distinct behavior compared to those of carbon monoxide as higher yields were found for the forest pellets which exhibits the lower oxygen content. It is worth to note that a comparison between pyrolysis of woody and non-woody fuels made in [18, 32] also showed that wood leads to higher yields of carbon monoxide but lower yields of carbon dioxide. However, differences in the yields of carbon dioxide among the fuels tested here are small and further work is needed to ascertain this issue. The composition of parent fuel has also a small effect on the yields of hydrogen under the conditions of this work.

6.3.5 *Relations between yields of volatile gases*

The comparisons of yields of pyrolytic products from different fuels and operating conditions must be done with caution since variations in the mass balance closures can lead to misinterpretations. A better approach is to compare relations between yields of products because the effect of experimental errors (e.g. gas leakage) can be minimized in this way. The distribution of products can be retrieved from this kind of relations with the help of the

conservation equations describing the pyrolysis process, as discussed in detail in [13, 14]. Given that similar yields *vs.* temperature curves were found in this work for CO, H_2, CH_4 and C_2H_4 (Figs. 6.11 and 6.12), relations between the yields of these species are discussed below.

6.3.5.1 *Light hydrocarbons versus methane*

Figure 6.13-a plots the yields of selected light hydrocarbons against the respective yields of methane. The yields of C_2H_4+CH_4 are well correlated with those of methane and similar relations are obtained for all fuels tested here. Moreover, when the yields are plotted in this way, there is practically no effect of the operating conditions, such as bed temperature (and residence time). Also shown in the figure is a relation derived from literature data representing various biomasses, reactors and pyrolysis conditions [13], in which C_xH_y refers to a limited number of light hydrocarbons (mainly C_2 species). Despite of this, the relation based on literature data follows closely the results from this work which further confirms its usefulness for predicting results. However, it shall be stressed that, when C_xH_y accounts for C_3–C_5 species the relation with the yields of methane might change since these longer species can exhibit a distinct yield *vs.* temperature behavior (see e.g. Figure 6.12 for yields of C_3H_8). This is especially the case of processes carried out at low temperatures, e.g. <800ºC, which permits high yields of long light hydrocarbons other than methane and C_2H_4. Under these conditions the adequacy of the literature relation showed in Figure 6.13-a for predicting the yields of total light hydrocarbons (C_xH_y+CH_4) must be carefully addressed. This behavior was illustrated in [13], where the yield of total light hydrocarbons is predicted by an empirical pyrolysis model, showing that the yields of C_xH_y+CH_4 approach those of C_2+CH_4 only for the highest yields of methane, i.e. at sufficiently high temperatures.

6.3.5.2 *Methane versus carbon monoxide*

Yields of methane are plotted against those of carbon monoxide in Figure 6.13-b; this particular relation has been analyzed in previous investigations [13, 15, 17] with the results also shown in the figure. Literature data indicates linear dependencies on logarithmic coordinates [15, 17] even though the data obtained here can also be well represented by straight lines on linear coordinates. Data for cellulose and lignin, i.e. the two major structural components of biomass, show that the composition of fuel influences the CH_4 *vs.* CO relations. Pyrolysis of cellulose yields higher amounts of carbon monoxide relative to methane than lignin does. This behavior can be also related to the higher oxygen content of cellulose (49.3%O *vs.* 25-35%O for lignin, mass% [21]) which was found to positively affect the yields of carbon monoxide (see Section 6.3.4.2). On the whole, the data for biomasses scatters within the lines for cellulose and lignin as indicated by a survey of eleven references in [13],

and a relation derived from this literature data also holds well for the fuels used in this work (Figure 6.13-b). The CH_4 *vs.* CO yields were here found little dependent on the composition of fuel and, taking into consideration that the composition of typical biomasses lies within a relatively narrow range (45-55%C, mass% of daf fuel [13, 21]), the relation derived in [13] shall provide good results in most cases. However, one recalls that the yields of methane apparently broaden at temperatures above ≈950ºC under the conditions used in the small fluidized bed (see Figure 6.11) and, hence, a slope change in the CH_4 *vs.* CO relation might become evident for yields of carbon monoxide exceeding those in Figure 6.13-b.

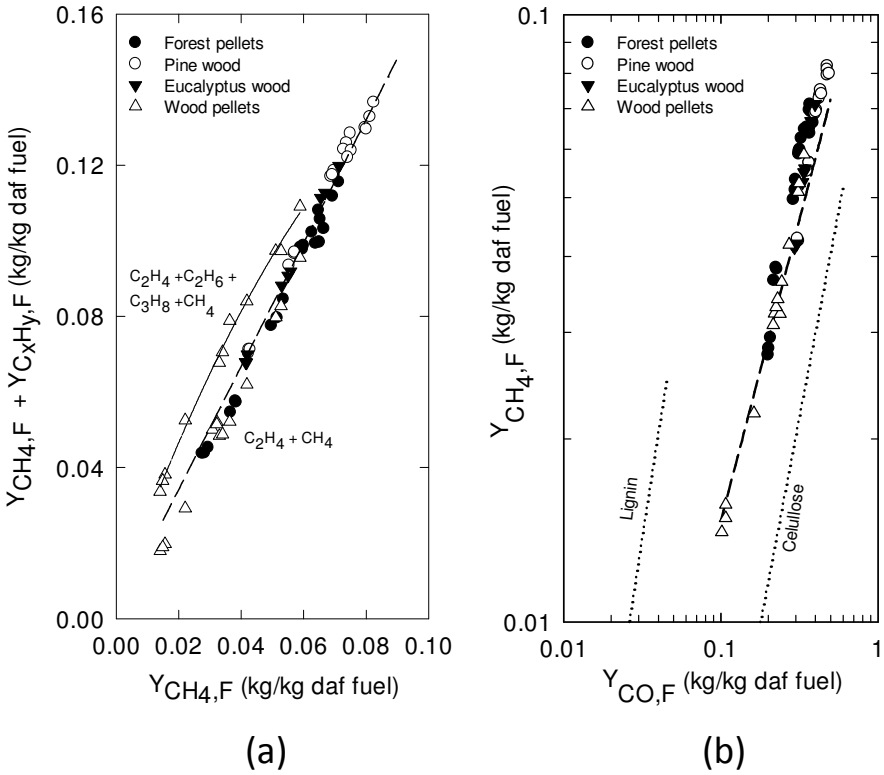

Figure 6.13 - Yields of light hydrocarbons as a function of the respective yields of methane (a) and yields of methane as a function of the respective yields of carbon monoxide (b). The solid line is a trend line for wood pellets, dotted lines are correlations for lignin and cellulose [15, 17] and, dashed lines are correlations based on literature data for various biomasses [13]. C_xH_y is non-CH_4 light hydrocarbons.

6.3.5.3 *Hydrogen versus carbon monoxide*

Relations between yields of hydrogen and carbon monoxide are of utmost importance because these are thermodynamically stable species and major products from the secondary gas-phase reactions. As a result, the H_2 *vs.* CO yields might monotonically tend to the equilibrium values predicted from the composition of parent fuel. To demonstrate this behavior, the measurement data relative to the forest pellets is compared to the respective equilibrium values in Figure 6.14-a, where the calculations were done within the temperature

range of 600 to 1300ºC using the Gaseq equilibrium software [38]. It is seen that the equilibrium H_2 *vs.* CO yields increase to a point which mainly depends on the hydrogen and oxygen contents of the pellets and this point is approximately given by $Y^*_{H2,F}=Y_{H,F}$ and $Y^*_{CO,F}=Y_{O,F}\times M_{CO}/M_O$. As noted before, this follows from the fact that the yields of hydrogen and carbon monoxide under equilibrium become nearly constant above, say, 1000ºC. In general, the measurements show much lower yields of hydrogen relative to carbon monoxide than those predicted by equilibrium, but they also tend to the theoretical $Y^*_{H2,F}$ vs. $Y^*_{CO,F}$ values. Similar trends are obtained for all fuels used here with the data showing non-linear H_2 *vs.* CO relations (Figure 6.14-b). Funazukuri et al. [15] has related the yields of various gases against those of carbon monoxide by relations of the type $Y_{i,F}=A\cdot(Y_{CO,F})^B$ but, unfortunately, the H_2 *vs.* CO yields were not studied by them. Nevertheless, relations of this type also work very satisfactorily for the experimental H_2 *vs.* CO yields shown in Figure 6.14. Least square analysis of the $Y_{H2,F}$ *vs.* $Y_{CO,F}$ values together with the $Y^*_{H2,F}$ vs. $Y^*_{CO,F}$ values results in R^2 above 0.99 for all fuels tested. Note that different relations are obtained for each fuel, in accordance to the respective hydrogen and oxygen contents, but the slopes are similar.

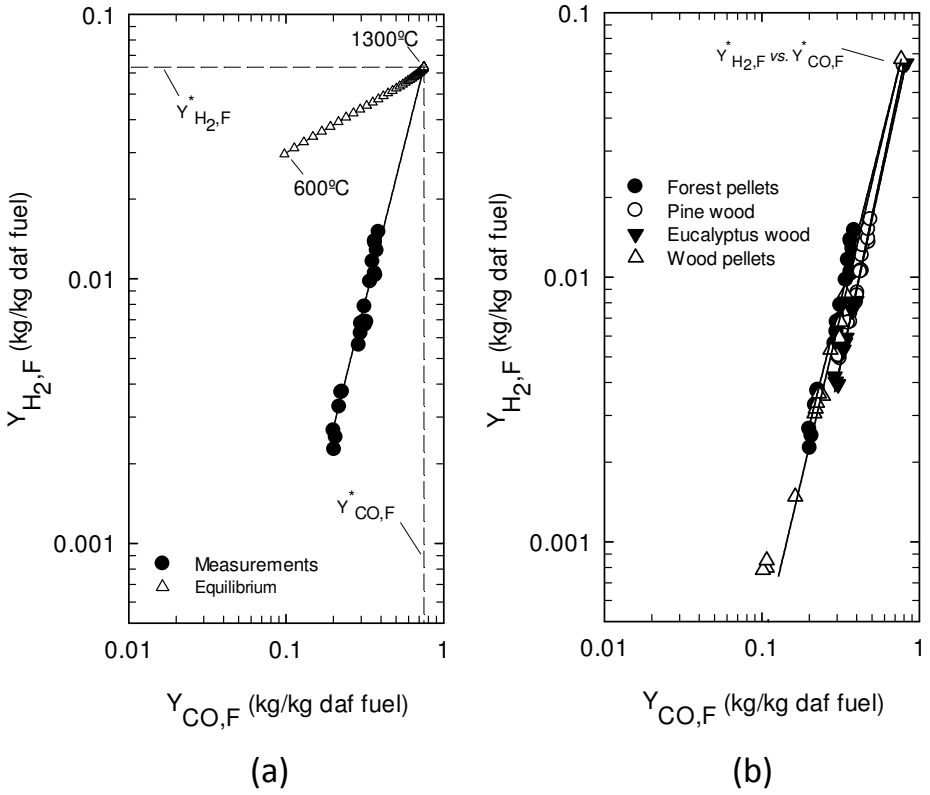

Figure 6.14 - Yields of hydrogen as a function of the respective yields of carbon monoxide. Comparison between thermodynamic equilibrium (calculations within 600-1300ºC at 10ºC/step, 101.3hPa) and measurements during pyrolysis of the forest pellets (a), and a compilation of the measurements for the fuels tested in this work (b). Solid lines are trend lines based on the measurements and the values of $Y^*_{H2,F}$ *vs.* $Y^*_{CO,F}$ under equilibrium condition.

6.3.6 *Properties of total volatile gas*

This section presents the heating value and molar mass of the total permanent gas as calculated from the measured gas yields. The experimental values are further compared to those calculated from the equilibrium gas composition.

6.3.6.1 *Lower heating value*

The lower heating value of total permanent gas (LHV_G) is plotted against the respective yields of carbon monoxide in Figure 6.15-a, which also includes the asymptotic values given by the thermodynamic equilibrium model at sufficiently high temperature (noted LHV_G^* and calculated from the values of $Y_{H2,F}^*$ and $Y_{CO,F}^*$). Similar LHV_G *vs.* temperature relations were found for all fuels tested here, where the LHVG increases from ≈10-12MJ/kg at 600ºC to ≈16-18MJ/kg above 900ºC (see Figures 6.11 and 6.15-a). However, note that the values at lower temperatures can be less accurate due to the plausible role of unmeasured light hydrocarbons (see Section 6.3.2). On the whole, the results obtained in this work are in the range of values obtained during pyrolysis of a variety of woody and non-woody fuels [13]. The permanent gas produced from both types of pellets exhibit slightly higher heating values than that produced from the woody materials. This can be linked to the lower amounts of oxygen relative to hydrogen of the pellets and is in agreement with the theoretical results. The values of LHV_G calculated from the measured yields of gas tends to the respective values of LHV_G^* as the yields of carbon monoxide increase (i.e., when the temperature increases). However, unlike the yields of the permanent gas species, the lower heating value of the total gas measured at ≈900-975ºC is already close to the maximum attainable equilibrium values of 18-19MJ/kg, indicating that a plateau shall be reached above ≈1000ºC under the conditions of this work. Then, despite the processes occurring above ≈1000ºC have a rather large influence on the yield and composition of the total permanent gas, they lead to a small variation in the respective lower heating value.

6.3.6.2 *Molar mass*

Figure 6.15-b shows the dependence of the molar mass of total permanent gas (M_G) to the yields of carbon monoxide. The molar mass exhibited a small temperature dependency with values typically within 20-25g/mol for temperatures ranging from 750 to 975ºC. The dependency of M_G on the composition of fuel is also small and opposite to that observed for the lower heating value; both the measurements and the theory show that the molar mass of the total permanent gas increases with the oxygen content of fuel. The M_G *vs.* CO yields

indicate a decreasing linear relationship which tends to the thermodynamic equilibrium values ($M_G^* \approx 14$g/mol, as calculated from $Y_{i,F}^*$) as the yields of carbon monoxide increase.

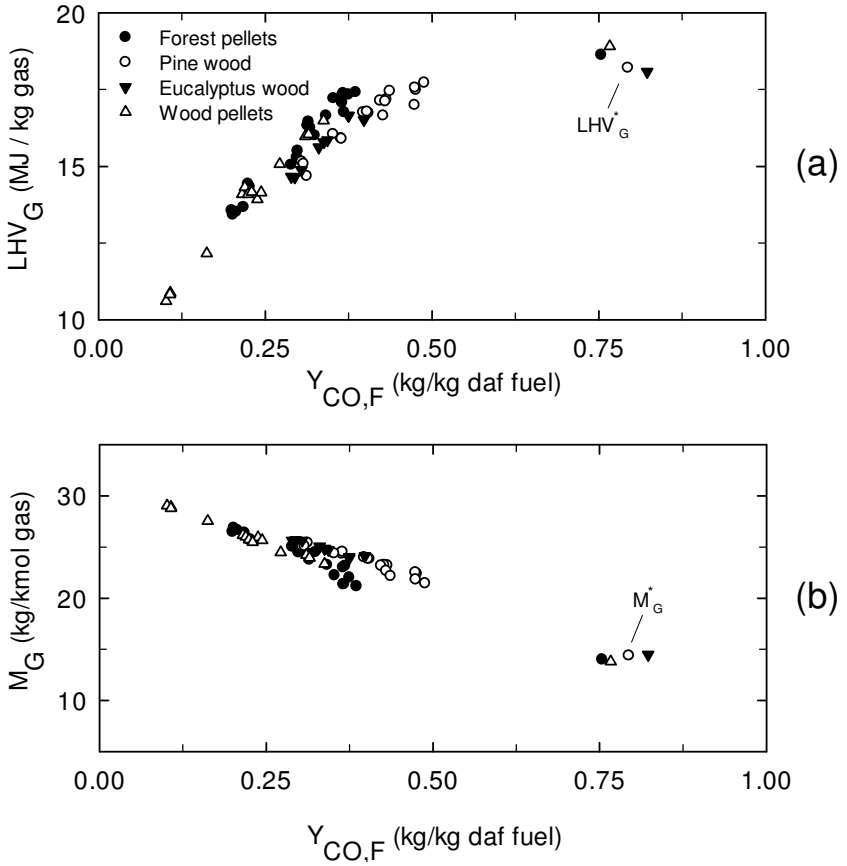

Figure 6.15 - Lower heating value (a) and molar mass (b) of the total permanent gas as a function of the respective yields of carbon monoxide. Values of LHV_G^* and M_G^* are calculated from the asymptotic yields of gas species ($Y_{i,G}^*$) predicted by thermodynamic equilibrium at high temperature (say, >1000ºC).

6.4 *Conclusions*

A laboratorial-scale fluidized bed facility was used to investigate the pyrolysis of biomass under conditions of interest for fluidized bed gasifiers and combustors. The reactor was operated with batches of dry fuel and the resulting pyrolytic products (char, soot, liquids and permanent gas) were collected for analysis. These product fractions were subjected to gravimetric analysis to verify the mass balance of biomass pyrolysis. The composition of the permanent pyrolysis gas was further resolved in a number of species (CO_2, CO, C_3H_8, C_2H_6, C_2H_4, CH_4 and H_2) as a function of temperature (600-975ºC) and fuel type (eucalyptus wood,

pine wood, forest pellets and wood pellets). The results of this work compare well and complement the results from a previous survey of literature data [13].

Under the range of temperatures used in this work (i.e., within 600-975 ºC) the following conclusions are drawn:

- The total amount of volatiles (i.e. permanent gases + liquids) released from biomass is weakly dependent on the temperature, but exhibits a positive dependency on the oxygen content of parent fuel. In turn, the composition of the volatiles changes continuously as temperature increases, in which variations in the yields of liquids (i.e. organics + water) closely match the variations in the yields of permanent gases. A fraction of the liquids (≈18% of daf fuel in this work) was found to be stable even at 975ºC bed temperature.
- The composition of the permanent gas is also a strong function of temperature and is under kinetic control. Yields of carbon monoxide and hydrogen steadily increase with temperature increase, whereas the yields of other gas species (here, CO_2, C_3H_8, C_2H_6, C_2H_4, CH_4) become constant or start to decrease above certain temperatures. Qualitatively, the composition of the permanent gas shows similar temperature dependencies for all fuels tested. Major differences were found for the yields of CO which correlates positively with the oxygen content of fuel.
- Cross plotting of yields of the major gas species has the advantage of reducing the effects of the experimental errors, operating conditions and fuel type. In particular, yields of C_2H_4+CH_4 *vs.* CH_4, CH_4 *vs.* CO and H_2 *vs.* CO are well correlated over a wide temperature range. Approximated relations involving the lower heating value and molar mass of the total permanent gas were also found. The effect of fuel composition on relations involving yields of H_2 and CO as well as the heating value and molar mass of total permanent gas can be accounted for through thermodynamic equilibrium modeling.
- Empirical parameters for describing the pyrolysis of biomass during conversion in fluidized beds can be developed from the results of this work. The need for experiments is also reduced since extrapolation of data among operating conditions is feasible.

Nomenclature

$Y_{i,F}$ Mass of i^{th} product species *per* unit mass of dry ash-free fuel (F), kg i/kg F

$Y^{*}_{i,F}$ high temperature plateau value for the yield of i^{th} product on a dry ash-free fuel basis, kg i/kg F

$Y_{S,R}$ Mass of dry char particles recovered from the bed *per* unit mass of dry fuel fed (R), kgS/kg R

$Y_{a,R}$ Ash content of fuel on a dry basis, kg a/kg R

$Y_{j,i}$ Mass fraction of j^{th} chemical element in i^{th} product species, kg j/kg i

$y_{i,bag}$ Molar fraction of i^{th} species in total gas collected in the bag, kmole i/ kmole gas bag

$y_{N2,bag}$ Molar fraction of N_2 fluidizing gas in total gas collected in the bag, kmole N_2/ kmole gas bag

$Y_{CO2,Ed}$ Molar fraction of CO_2 in the dry combustion flue gases (Ed) leaving the reactor, kmol CO_2/kmol Ed

$\dot{m}_{N2}$ Mass flow-rate of N_2 fluidizing gas, kg N_2/s

$\dot{n}_{Ed}$ Molar flow-rate of dry combustion flue gases leaving the reactor, kmol Ed/s

M_i Molar mass of i^{th} product species, kg i/kmol i

M_{N2} Molar mass of N_2 fluidizing gas, kg N_2/kmol N_2

M_j Molar mass of j^{th} chemical element, kg j/kmol j

m_F Mass of the fuel batch (dry ash-free) fed into the reactor for pyrolysis, kg F

t_b Burnout time of the char remaining in-bed, s

t_s Time of gas sampling into the bag, s

u_{mf} Minimum fluidizing velocity, m/s

Subscripts

i i^{th} product species (ch, H_2, CO, CO_2, C_3H_8, C_2H_6, C_2H_4, CH_4, C_xH_y)

j j^{th} chemical element (C, H, O, N)

C_xH_y Lumped non-methane light hydrocarbon species

ch Dry ash-free char recovered from the bed

S Dry char recovered from the bed

a Ash

N_2 nitrogen fluidizing gas

He Helium inert gas

F Dry ash-free fuel

Ed Dry flue gases leaving the reactor during the burnout of the char

bag permanent gas collected into the bag (volatiles + N_2 fluidizing gas + He inert gas)

Abbreviations

daf Dry ash-free basis

db Dry basis

Acknowledgment

The financial support by Fundação para a Ciência e a Tecnologia (FCT), Portugal, throught a PhD grant SFRH/BD/39567/2007 and research project PTDC/AAC-AMB/116568/2010 (BiomAshTech), and the Swedish Gasification Centre (SFC), is acknowledged.

References

1. Knoef, H., Handbook Biomass Gasification. Biomass Technology Group.2005.
2. Bridgwater, A.V., The Technical and Economic-Feasibility of Biomass Gasification for Power-Generation. Fuel, 1995. 74(5): p. 631-653.
3. Beenackers, A.A.C.M. and A.V. Bridgwater, Gasification and Pyrolysis of Biomass in Europe, in Pyrolysis and Gasification, G.L. Ferrero, Editor 1989.
4. Basu, P., Combustion and gasification in fluidized beds2006, Boca Raton FL: CRC Press.
5. Gomez-Barea, A. and B. Leckner, Modeling of biomass gasification in fluidized bed. Progress in Energy and Combustion Science, 2010. 36(4): p. 444-509.
6. Van der Drift, A., et al., Entrained flow gasification of biomass, in ECN Biomass2004.
7. Corella, J., J.M. Toledo, and G. Molina, A review on dual fluidized-bed biomass gasifiers. Industrial & Engineering Chemistry Research, 2007. 46(21): p. 6831-6839.
8. Goransson, K., et al., Review of syngas production via biomass DFBGs. Renewable & Sustainable Energy Reviews, 2011. 15(1): p. 482-492.
9. Pfeifer, C., S. Koppatz, and H. Hofbauer, Steam gasification of various feedstocks at a dual fluidised bed gasifier: Impacts of operation conditions and bed materials Biomass Conversion and Biorefinery 2011. 1(1): p. 39-53.
10. Couhert, C., S. Salvador, and J. Commandre, Impact of torrefaction on syngas production from wood. Fuel, 2009. 88(11): p. 2286-2290.

11. Di Blasi, C., Modeling and simulation of combustion processes of charring and non-charring solid fuels. Progress in Energy and Combustion Science, 1993. 19(1): p. 71-104.
12. Broido, A. and M.A. Nelson, Char Yield on Pyrolysis of Cellulose. Combustion and Flame, 1975. 24(2): p. 263-268.
13. Neves, D., et al., Characterization and prediction of biomass pyrolysis products. Progress in Energy and Combustion Science, 2011. 37(5): p. 611-630.
14. Thunman, H., et al., Composition of volatile gases and thermochemical properties of wood for modeling of fixed or fluidized beds. Energy & Fuels, 2001. 15(6): p. 1488-1497.
15. Funazukuri, T., R.R. Hudgins, and P.L. Silveston, Correlation of volatile products from fast cellulose pyrolysis. Industrial & Engineering Chemistry Process Design and Development, 1986. 25(1): p. 172-181.
16. Scott, D.S., et al., The role of temperature in the fast pyrolysis of cellulose and wood. Industrial & Engineering Chemistry Research, 1988. 27(1): p. 8-15.
17. Scott, D.S., J. Piskorz, and D. Radlein, Liquid products from the continuous flash pyrolysis of biomass. Industrial & Engineering Chemistry Process Design and Development, 1985. 24(3): p. 581-588.
18. Di Blasi, C., et al., Product distribution from pyrolysis of wood and agricultural residues. Industrial & Engineering Chemistry Research, 1999. 38(6): p. 2216-2224.
19. Antal Jr, M.J., Effects of reactor severity on the gas-phase pyrolysis of cellulose-and kraft lignin-derived volatile matter. Industrial & Engineering Chemistry Product Research and Development, 1983. 22(2): p. 366-375.
20. Rodrigues, N., Metrologia aplicada ao desenvolvimento de sistemas de medição, in DAO2009, Universidade de Aveiro.
21. Neves, D., et al., Dependence of char yield on the elemental composition of biomass. Submitted to Biomass and Bioenergy., 2013.
22. Morf, P., P. Hasler, and T. Nussbaumer, Mechanisms and kinetics of homogeneous secondary reactions of tar from continuous pyrolysis of wood chips. Fuel, 2002. 81(7): p. 843-853.
23. Boroson, M.L., et al., Heterogeneous cracking of wood pyrolysis tars over fresh wood char surfaces. Energy & Fuels, 1989. 3(6): p. 735-740.
24. Evans, R.J. and T.A. Milne, Molecular Characterization of the Pyrolysis of Biomass .1. Fundamentals. Energy & Fuels, 1987. 1(2): p. 123-137.
25. Fitzpatrick, E., et al., Mechanistic aspects of soot formation from the combustion of pine wood. Energy & Fuels, 2008. 22(6): p. 3771-3778.

26. Valin, S., et al., Upgrading biomass pyrolysis gas by conversion of methane at high temperature: Experiments and modelling. Fuel, 2009. 88(5): p. 834-842.
27. Wang, X.Q., et al., Biomass pyrolysis in a fluidized bed reactor. Part 2: Experimental validation of model results. Industrial & Engineering Chemistry Research, 2005. 44(23): p. 8786-8795.
28. Garcia-Perez, M., et al., Fast pyrolysis of oil mallee woody biomass: effect of temperature on the yield and quality of pyrolysis products. Industrial & Engineering Chemistry Research, 2008. 47(6): p. 1846-1854.
29. Elliott Douglas, C., Relation of Reaction Time and Temperature to Chemical Composition of Pyrolysis Oils, in Pyrolysis Oils from Biomass1988, American Chemical Society. p. 55-65.
30. Neves D, T.H., Seeman M, Ideias P, Matos A, Tarelho L et al. A database on biomass pyrolysis for gasification applications. in 17th European Biomass Conference & Exhibition. 2009. Hamburg, Germany.
31. Dufour, A., et al., Mechanisms and Kinetics of Methane Thermal Conversion in a Syngas. Industrial & Engineering Chemistry Research, 2009. 48(14): p. 6564-6572.
32. Gomez-Barea, A., et al., Devolatilization of wood and wastes in fluidized bed. Fuel Processing Technology, 2010. 91(11): p. 1624-1633.
33. Di Blasi, C., Combustion and gasification rates of lignocellulosic chars. Progress in Energy and Combustion Science, 2009. 35(2): p. 121-140.
34. Warnatz, J., U. Maas, and R.W. Dibble, Combustion: physical and chemical fundamentals, modeling and simulation, experiments, pollutant formation2006: Springer.
35. Buekens, A.G. and G.F. Froment, Thermal Cracking of Propane. Kinetics and Product Distributions. Industrial & Engineering Chemistry Process Design and Development, 1968. 7(3): p. 435-447.
36. Froment, G.P., et al., Thermal cracking of ethane and ethane-propane mixtures. Industrial & Engineering Chemistry Process Design and Development, 1976. 15(4): p. 495-504.
37. Pereira, M.R.C., Projecto de um gasificador de biomassa, in DAO2009, University of Aveiro.
38. Morley, C. Gaseq version 0.79. Available from: http://www.c.morley.dsl.pipex.com/

Chapter 7 -Conclusions

The main conclusions from the results obtained in Chapters 2 to 6 are summarized as follows:

Chapter 2

The operation of the pilot-scale fluidized bed combustor at UA with forest pellets feed leads to high values of temperatures and CO and NO concentrations in a narrow region above the surface of the bed. This is the opposite of what has been observed during coal combustion in the same facility in which the temperature and CO and NO concentrations peak within the dense bed. These different modes of solid fuel conversion along the combustor are due to the high volatile matter content of biomass in relation to coal. For biomass the major fraction of the dry fuel feed (≈80% by mass for the pellets) is released as pyrolytic volatiles as the fuel particles experience the high temperatures at the bed surface; the resultant volatiles mix with the bulk air and burn above this level during transport along the freeboard. This conversion behaviour of biomass fuels has some implications concerning both the reactor control and pollutant mitigation. For instance, it can be challenging to keep the freeboard temperature below acceptable values during biomass combustion which is problematic due to e.g. the aggressive nature of the biomass ashes. Also, measures that were proven for pollutant control during coal combustion in fluidized beds, e.g. NO_x abatment by the char within the bed, has to be readdressed for the case of biomass combustion. Indeed, the splash region and the bottom part of the freeboard seems to play the larger part in the formation/destruction of pollutants during biomass combustion.

Chapter 3

A black-box modelling approach was presented to evaluate the operational performance of biomass gasifiers. One of the parameters used in the model is the CHON composition of the raw gas leaving the gasifier. A survey of methods to accomplish the required measurements revealed that the analysis is often controversial and the techniques employed are both time-consuming and costly. The outcome is that the CHON composition of the raw gas cannot be analyzed online by current methods and valuable information for the operational control of the gasifier is lost. To overcome this problem a measurement method based on a small gas combustor was developed; the evaluation of this method during the operation of the $2MW_{th}$

Chalmers gasifier showed that the measurement of the CHON composition of the raw gas can be done in a fast, reliable and unattended way. The analysis time was reduced from several hours (or days) in case of the current methods to a couple of minutes in the case of the new method. In combination with the black-box reactor model, this new method showed that the CHON composition of the raw gas leaving the Chalmers gasifier is closely given by the composition of pyrolytic volatiles together with the steam added to the gasifier. This shows that the relatively rapid solid mixing in the gasifier enables the major part of the char to escape the gasifier unconverted, regardless of the bed temperatures, steam-fuel ratio, and amount of catalyst blended in the bed material. This also opens new possibilities to optimize the integrated combustion/gasification process as the char escaping the gasifier is used as fuel in the boiler, and this can be monitored with high temporal resolution by proposed method.

Chapter 4

The way the literature data on biomass pyrolysis are reported is very heterogeneous and needs to be structured to highlight its most important features and compare the data among different works. This task was accomplished in this work and made it possible to obtain the general trends on both product yields and properties as a function of temperature, heating rate and fuel type. Though, the scatter in the data is still large and the data is more abundant at low temperatures since works mainly focus on conditions useful for pyrolysis processes.

The analysis of the collected data showed two main temperature ranges corresponding to distinct stages of biomass pyrolysis. Below about 500ºC the parent fuel undergoes primary decomposition into volatiles and char. The rapid fuel mass loss is mainly compensated by the release of organic liquids, whereas the production of water and permanent gas species is comparatively small. The CHO composition of the organic liquids always resembles the one of the parent fuel (i.e. highly oxygenated lump) but, in comparison, the CHO composition of the char is a strong function of the temperature. Above 500ºC the organic liquids start to convert into permanent gases (mainly CO, H_2 and CH_4) while the yield of char and water seems little dependent of the temperature. Also the CHO composition of the char flats out, being much enriched in carbon. This suggests that, at these high temperatures, the secondary reactions among the volatiles are a minor source/sink of char and water. There are very approximated relationships among the yields of the major volatile gases, namely CH_4, H_2 and CO, which seems little sependent of the operating conditions. Proper combination of these empirical relationships with the conservation equations describing the pyrolysis permits to estimate the yields of the relevant volatile species (H_2O, tar, CO, CO_2, H_2, CH_4, other light hydrocarbons) as a function of temperature, yield of char and the CHON composition of parent biomass. Despite models of this type are useful to estimate the volatile species released from biomass

in a thermochemical reactor, in this chapter it enabled to elucidate the yields of species that are difficult to measure (e.g. tars, H_2O) and also show that the collected literature data on product yields and properties are consistent.

Chapter 5

Experiments conducted in the fast pyrolysis rigs with 6-8mm OD fuel particles confirm that heating of biomass to above 600ºC leads to a marginal mass loss of roughly 1%/100ºC; this rate of mass loss appears little dependent of the composition of the parent fuel but the asymptotic char yields vary widely among different fuel types. The results show that under fluidized bed conditions the O/C ratio of fuel is a major parameter governing the formation of char, with experimental values ranging from about 7% for cellulose (O/C=1.11kg/kg), 10-30% for biomass (say, 0.6<O/C<1.1/kg), and up to 45% for lignins (O/C<0.6kg/kg). This relation seems not influenced by the ash content of fuel nor by relatively large variation of the heating rate of fuel. It is worth noting that, under the aforesaid conditions, the experimental char yield *vs.* O/C ratio is typically within ±15% of the theoretical yield of carbon graphite predicted under termodinamic equilibrium, as long as a sufficiently high temperatures (say, >1000ºC) are used for modeling. As a practical matter, the experimental results obtained in this chapter offer strong support on that the production of char in fluidized bed combustors and gasifiers is intimately related to the CHON composition of fuel feed. Note that knowledge of the yield of char provides as well information about the total amount of volatiles released from the fuel particles.

Chapter 6

Pyrolysis experiments conducted in the laboratory fluidized bed with both woody and pelletized materials showed that, despite the secondary pyrolysis reactions proceeding above 600ºC are a minor source /sink of char, they lead to progressive conversion of the primary volatiles evolved from solid fuel into more stable species: (1) the yields of pyrolytic liquids start decreasing at ≈500ºC, (2) the yields of C_3H_8 and C_2H_6 decrease above ≈750ºC, (3) the yields of CO_2 decrease above ≈850ºC, (4) the yields of C_2H_4 and CH_4 decrease above ≈900-950ºC, while (5) the yields of H_2 and CO always increase with temperature increase. At 950-975ºC the yields of H_2 and CO attained values of ≈1.0-1.7% and ≈35-50% of daf fuel (mass%), respectively, depending on the fuel under concern. Though, a fraction of the liquids is very difficult to convert even at tempearures of 950ºC and a couple of seconds residence time. Although the yields of certain gases increase and those of other gases decrease as a function of temperature, the lower heating value of the total permanent gas steadly increases from ≈10-12MJ/kg at 600ºC to close to 18MJ/kg at 975ºC. It is worth nothing that further increase of the temperature has a small effect on the heating value of the gas, despite its effect on the

respective composition of the gas is large. Like it was observed for the yields of char, the CHON composition of fuel also influences the yields of gas species, especially the yields of CO that were found positively correlated with the oxygen content of fuel. Yields of CH_4, C_2H_4, H_2 and CO are well correlated and little dependent on the operating conditions. Although the composition of the pyrolysis gas cannot be determined from the CHON composition of fuel by thermodynamic equilibrium modelling, a way for accounting for CHON composition of fuel in the H_2 *vs.* CO relationships is proposed. This type of relationships are useful as it makes the extrapolation of data from one operating condition to another one feasible.

Future work

The results form this thesis work can be combined in different ways to achieve a better description of the pyrolytic degradation of biomass in fluidized be combustors ans gasifiers. Nevertheless, the experimental facilities and models developed during this work can be used and/or further developed in the future to investigate a number of issues that has emerged. A selection of proposals for future work is:

Issues based on the online gas combustion facility:

- Develop a compact combustion unit that can serve as an online "CHON analyzer" as well and "heating value analyzer" suitable to monitor the raw gas from all kinds of gasifiers;
- Evaluation of the degree of biomass conversion, steam consumption or production, and amount of tars across the Chalmers $2MW_{th}$ gasifier, including measurements with the online combustion facility both inside the bed and along the freeboard.

Issues based on the laboratory fluidized bed pyrolysis facility:

- Further investigation of the mass balance of biomass pyrolysis by improving the current experimental setup. An improvement that was accomplished but need to be tested is the flanged connection to the heated sampling line for the volatiles;
- The sampling and analysis methods used for the yields and composition of the pyrolitc liquids deserve yet great deal of research; one idea around the evaluation of the CHON composition of the tar lump is to pyrolyze tar samples and investigate the amount of char that is formed.
- Get a good description of the stoichiometry of cellulose pyrolys; the results from this work suggest that a number of features related to the pyrolysis of biomass fuels can be obtained by using the pyrolysis behaviour of cellulose as reference.
- Evaluation of the kinetics and amount of volatile gases released from biomass based on the response of gas mass flow meters.
- Evaluation of the effect of particle size on yields and properties of pyrolytic products;

- Analyze the huge amount of char samples that were collected during the course of this work.

Issues based on the collected literature data and the proposed empirical pyrolysis model:

- Integrate the models accounting for the CHON composition of fuel in the yield of char and properties of the volatile gas (e.g. H_2 *vs.* CO yields) on the empirical pyrolysis model;
- Investigate the heat of pyrolysis as a function of temperature, yield of char and fuel type, togheter with a sensitivity analysis.

Appendix I – Zero-dimensional modeling of indirect fluidized bed gasification

XIII Fluidization Conference – Gyeong-Ju, Korea, 2010

ZERO-DIMENSIONAL MODELING OF INDIRECT FLUIDIZED BED GASIFICATION

XIII FLUIDIZATION CONFERENCE – GYEONG-JU, KOREA, 2010

Anton Larsson[a], David Pallarés[a], Daniel Neves[a,b], Martin Seemann[a], H. Thunman[a]

[a] Chalmers University of Technology, Department of Energy and Environment, SE-412 96 Goteborg, Sweden.

[b] University of Aveiro, Department of Environment and Planning, Campus Universitário de Santiago, 3810-193 Aveiro, Portugal.

ABSTRACT

Zero-dimensional models has been developed to investigate mass balance and fuel (biomass) conversion in Chalmers 2-4 MWfuel indirect fluidized bed gasifier. Results from this work indicate that more than 95%mass of the tars is converted in the gasifier and that the water gas shift reaction is far from equilibrium.

INTRODUCTION

Gasification is used to convert solid fuel, such as biomass, into a combustible product gas. The main components of the product gas are H_2O, H_2, CO, CO_2, CH_4 and N_2. This can be used in downstream processes for the production of, for example, various biofuels. The type of gasification concept investigated in the present work is the indirect fluidized bed gasification technique, where the gasification reactor is heated indirectly, see Fig.1a. At Chalmers a 2-4MW indirect bubbling fluidized bed (BFB) gasifier has been installed in connection to the 12 MW Chalmers circulating fluidized bed (CFB) boiler (1), see Fig.1b. The CFB boiler provides hot bed material to the gasifier through a particle distributor and a particle seal. Another particle seal is located after the gasifier, before the bed material reenters the boiler. The bed material flow through particle seals (fluidized with steam), while mixing of gas between the two reactors are prevented.

The present work is focused on the use of zero-dimensional modeling to investigate the performance of this type of gasifiers. Here, Chalmers gasifier is compared with the 8 MW gasifier in Güssing (2) and the 100 kW research gasifier at Vienna University of Technology (3). A major difference between Chalmers gasifier and the other two, is that the Chalmers gasifier is a retrofit on an existing boiler. The boiler can still be operated as a standalone boiler for heat production only or, with the gasifier in operation, for combined heat and gas production. The combustion

part of the system is in this configuration much larger than is needed for the production of the heat for the gasification process, which leads to a more stable operation.

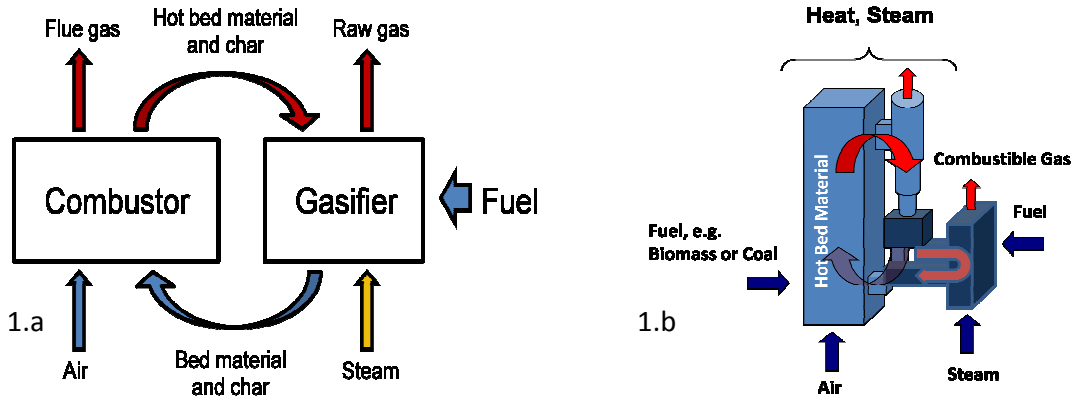

Figure 1.a(Left): Principle of indirect gasification. 1.b(Right): Scheme of the Chalmers gasifier and its integration with the previously existing CFB boiler.

CHAR CONVERSION

To determine the char conversion, measurements of the gas composition at the surface of the bed were carried out. No fuel (other than char entering from the boiler) was fed to the gasifier; hence the measured gas composition is a result of char gasification. This gives the ratio of char conversion *per* mass unit of steam. Thus, knowing the mass flow of steam, an average ratio of char conversion in the gasifier can be estimated. From measurements performed in this work the ratio of char conversion were estimated to 0.05 kgchar/kgsteam.

The external solid flux is estimated to 3 kg/m^{2}s (corresponding to 25,000 kg/h) based on a correlation (4) where the solid flux is related to primary air flow in Chalmers CFB. The char content in the circulated flow is estimated to 0.25% mass percentage. This is based on measurements from the cyclone leg in experiments using similar fuel and operating conditions as the one used here (5). With this, the char flow entering the gasifier corresponds to 60 kg/h, the steam flow was 270 kg/h, which lead to a char conversion of around 20%.

MASS BALANCE OVER THE GASIFIER

A mass balance of the gasifier has, here, been established. This mass balance is calculated through a system of equations based on measured and calculated compositions of in and out going flows, as illustrated in Fig.2. The char composition is taken from Thunman et al. (6). Furthermore, the

composition and mass flow of the dry raw gas and the steam content are measured. Also, leakage into the gasifier is indicated by the presence of nitrogen in the raw gas. These leakages, which can consist of air and/or flue gas, are estimated from the mass balance.

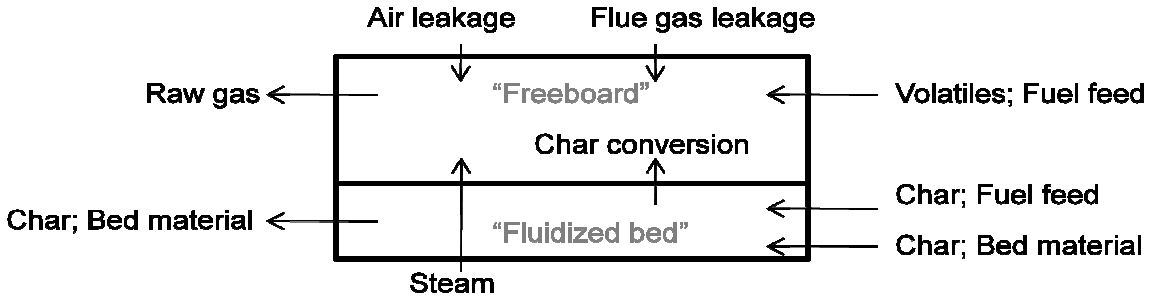

Figure 2. Mass input/output scheme for the Chalmers gasifier. The fuel feeding is illustrated as two streams; one for volatiles and one for char.

GASIFICATION MODEL

A gasification model has been developed to be used to investigate the performance of the Chalmers gasifier. The model is built on three submodels covering respectively: the conversion of a biomass particle, the composition of the volatiles originated from the fuel particles and the homogenous reactions.

Particle model

The particle model is based on the conversion of a moist (> 10%) thermally large particle. The rate of the release of volatiles and moisture are given from known input parameters. For further details see (7).

Volatile Composition

The submodel for the volatile composition is based on the elemental species C,H,O balances together with the energy balance. The product distribution is outlined by means of dry ash free (daf) char and daf volatiles. The volatiles are characterized by CO_2, CO, H_2O, H_2,CH_4, C_xH_y (other light hydrocarbons than CH_4) and $C_nH_mO_k$ (tars). Input data to this submodel are the C,H,O daf contents and the heating value of fuel and pyrolytic products. The lower heating value (LHV) of tar is calculated from the C,H,O composition (8). The elemental composition of C_xH_y is set to concur with the measured raw gas composition from the Chalmers gasifier.

To close the system of equations the four balance equations are complemented with three empirical correlations.

$$Y_{H2} = 1{,}145 \cdot \left(1 - \exp\left(-\,0{,}0011 \cdot T\right)\right)^{9{,}384} \quad \text{(i)}$$

$$Y_{CO} = Y_{H2} \Big/ \left(0.0003 + 0.0429/\left(1 + \left(T/632\right)\right)^{-\,7.228}\right) \quad \text{(ii)}$$

$$Y_{CH4} = -0.0895 + 0.1445 \cdot Y_{CO} \quad \text{(ii)}$$

These correlations are derived from data presented by Neves et al (9). The first two correlations are based on the mass ratios H_2 to CO and CH_4 to CO. These two ratios has been found to only depend on the temperature in the range of 700-900ºC, hence, independent of particle size, heating rate and reactor type (10). The correlation of the mass ratio of CH_4 to CO is in accordance with data presented in (11). The third closure equation is given by an empirical correlation for the yield of H_2 as a function of temperature (9).

Homogenous Reactions

The global homogenous reaction of the gasification process is, here, described by:

R.1) Tars + H_2+ CO_2+ H_2O + CO + CzH_w -> H2O + H_2 + CO + CO_2 + C_zH_w

The above global reaction is here broken down into three parallel reactions:

R.2) Tars + H_2 -> C_zH_w + H_2O

R.3) C_zH_w + H_2O -> CO + H_2

R.4) CO + H_2O <-> CO_2 + H_2

The reactions are controlled by the degree of conversion denoted ηtar, ηC_zH_w and ηWGSR for R.2, R.3 and R.4 respectively. R.2 describes the conversion of tars and R.3 describes the conversion of C_zH_w. Reaction R.4 describes the water gas shift reaction (WGSR). It also balances the products of R.2 and R.3. The degree factors of conversion (ηtar and ηC_zH_w) are defined as the ratio of the mass yields of tar and C_zH_w in the gas to those predicted in the devolatilization submodel denoted $Y_{tar,}0$ and $Y_{CzHw,0}$ i.e.:

$$\eta_{tar} = 1 - \frac{Y_{tar}}{Y_{tar,0}} \quad \text{(iv)}$$

$$\eta_{CzHw} = 1 - \frac{Y_{CzHw}}{Y_{CzHw,0}} \quad \text{(v)}$$

Table 1. Input data gasification model.

Input data	Used value
Process parameters	
Fuel feed	340 kg/h
Steam feed	270 kg/h
Mean bed temperature	791ºC
Mean freeboard temperature	766ºC
Fuel properties	
Proximate analysis	
Moisture	8.0%mass (wet fuel)
Char	18.0%mass (dry fuel)
Volatiles	81.7%mass (dry fuel)
Ash	0.3%mass (dry fuel)
Ultimate analysis	
C	49.9%mass (daf)
H	6.1%mass (daf)
O	43.9%mass (daf)
Mean particle size:	8.2 mm
Initial temperature	25ºC
Density, wet	1125 kg/m^3
Thermal conductivity	0,12 W/m K
Specific heat capacity, dry	1000 J/kg K
Emissivity	0,9
Bed material	
Mean particle size	0.27 mm
Density	2650 kg/m^3
Other	
Fluidization velocity	0.5 m/s
Char conversion	20 %
Leakage	-
C_zH_w	$C_{1,6}H_{4,6}$
Gasifier geometry(W/D/H)	1800/800/1809 mm
Leakage	
Mass flow flue gas	24 kg/h
Mass flow air	19 kg/h

Table 2. Assumptions for gasification model.

Assumption
• the temperature of the bed is uniformed.
• the temperature of the freeboard is homogenous.
• the process operates at steady state.
• the particle size can be represented by an equivalent diameter of a spherical particle.
• fuel nitrogen, sulfur and other minor components are neglected.
• perfect mixture of the gases leaving the gasifier.
• fuel particles undergoing drying and devolatilization float on the bed surface.
• heat transfer reduction due to gases leaving through a particle are neglected
• the composition of volatiles are constant with time.
• longer hydrocarbons C_4-C_8 around 10g/Nm^3 dry raw gas.

The degree of conversion of the WGSR is defined as the degree of equilibrium:

$$\eta_{\mathrm{WGSR}} = \frac{C_{CO2,eq} - X}{C_{CO2,eq}} \qquad \text{(vi)}$$

where X represents the mol fraction to be shifted to reach equilibrium and CCO_2,eq is the mol fraction of CO_2 at equilibrium. The mole fraction X is calculated from the equilibrium constant, Kp, of the WGSR reaction as follows:

$$Kp = \frac{(C_{CO} - X)\cdot(C_{H2O} - X)}{(C_{CO2} + X)\cdot(C_{H2} + X)} = 33.7 \cdot e^{\left(\frac{-4094}{T}\right)} \qquad \text{(vii)}$$

where the empirical correlation for Kp is based on data from (12).

Input Data and Assumptions for the Gasification Model

Input data for the gasification model are listed in Table 1. The determination of the conversion of char is described above. The composition of C_zH_w is estimated from measured amount of C_1 to C_3 hydrocarbons in the raw gas, complemented with an approximated amount of longer hydrocarbons (C_4-C_8). Assumptions made in the model are listed in Table 2.

RESULTS AND MODEL PREDICTION

The mass balance over the gasifier was closed according to the above-described procedure. The output of the closure was that the leakage mass flows of flue gas and air were 24 kg/h and 19 kg/h respectively. With the input data from Table 1 the composition of the devolatilization products was predicted. The resulting mass fractions in percentage of the volatiles released from the fuel particles are as following; H_2O 19.5, CO 25.0, H_2 0.9, CO_2 10.2, C_xH_y 3.7, CH_4 3.7, and "tars" 37.0. The measured composition of the raw gas in mole and mass fraction, with operating conditions according to Table 1, is given in Table 3. The thermo-gravimetric tar analysis gave a tar content of around 10 g/Nm^3.

Table 3. Measured gas composition of the raw gas in percent of volume and percent of mass

Species	H_2O	CO	H_2	CO_2	C_zH_w	N_2
Vol %	58.9	12.7	10.0	6.4	6.4	4.2
Mass %	53.8	18.0	1.0	14.3	7.7	5.1

The conversion factors were calculated for the measured raw gas composition in regard to the predicted composition of the devolatilization products, yielding:

η_{tar} = 97 %
η_{CzHw} = -200 %
η_{WGSR} = 42 %

This means that more or less all of the tar compounds leaving the virgin fuel particle were converted to lighter hydrocarbons, H_2, CO, CO_2 or H_2O. The conversion of the light hydrocarbons is negative, which is due to a larger production of light hydrocarbons from the conversion of tars, here, described by reaction R.2. This production is much larger than the consumption described by reaction R.3. The conversion factor of the WSGR is a measure of temperature, mixture in the freeboard and residence time of the gases.
The value indicates that the gas is rather far from equilibrium, which means that the gas is rich of CO and H_2O.

SENSITIVITY ANALYSIS

The closure of the mass balance was found to be very sensitive for variations of the hydrogen content of the fuel and the hydrogen content of the light hydrocarbons (value of w in C_zH_w). In Fig.3 it can be seen how the estimated leakage flows of air and flue gases are influenced by a change of ±1% of these two input data. The sensitivity of the degree of conversion factors, η_{tar}, η_{CzHw}, η_{WGSR} was in comparison to these very low, a 10 % change resulted in less than a 10 % response.

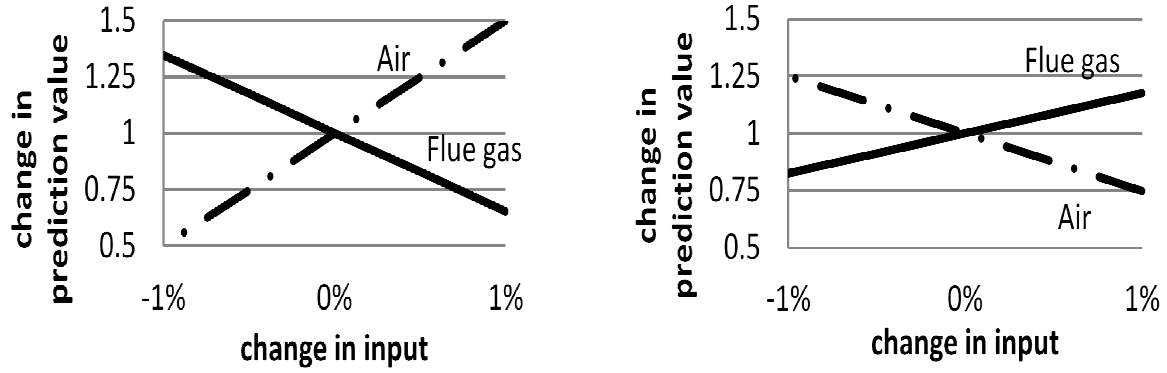

Figure 3. Sensitivity of the mass flows of the leakage of air and flue gas for changes in the H contents of the fuel (left) and the value of w for C_zH_w (right).

DISCUSSION

The system of equations describing the closure of the mass balance is solvable only within very limited value ranges for some parameters. The most critical parameters indentified were the H contents of the fuel, the H contents, denoted as w, in C_zH_w. The composition of the lumped light hydrocarbons is approximated from measurements of CH_4 and C_2-C_3 hydrocarbons. However, longer hydrocarbons (C_4-C_8) are not detected in these measurements, due to the present measurement setup. Therefore, subindices in C_zH_w should have slightly higher values than those given by the measurement of C_1 to C_3 as species such as benzene and other hydrocarbons, not defined as tars, should be included. The strict range of values of the hydrogen contents of the fuel and the light hydrocarbons point out the need for special attention to these parameters. For example, a 0.1% deviation in the content of hydrogen in the fuel will have a significant influence on the mass balance. Also the hydrocarbons should be carefully measured.

From the calculated conversion factors of tars and light hydrocarbons it could be noticed that there are a high conversion of the tars, above 95%. The increase of light hydrocarbons by 200% shows that the major part comes from conversion from tars. It also indicates a slower conversion of the light hydrocarbons than the tars.

Table 4. Comparison of the degree of conversion of the WGSR and values used for calculation.

Species	Chalmers (% mol wet)	100 kW (% mol wet)	Güssing (% mol wet)	Chalmers (% mol dry)	100 kW (% mol dry)	Güssing (% mol dry)
H_2	10.0	21.6[3]	24[3]	24.5	36[1]	35-45
CO_2	6.4	11.4[3]	15[3]	15.8	19[1]	20-30
CO	12.7	16.8[3]	12[3]	31.2	28[1]	15-25
CH_4	4.7	6[3]	6[3]	11.6	10[1]	8-12
N_2	4.2	<3[2]	2,4[3]	10.3	<5[1]	3-5
H_2O	58.9	40[1]	40[2]	-	-	-
Temperature, (C)	791	800-850[1]	>800	791	800-850[1]	>800[2]
η_{WGSR} (%)	43	65	76	-	-	-

[1] *From the work of H.Hofbauer and R.Rauch (3) with a steam-fuel ratio of 0,63 and recalculated to include the water content.*

[2] *Based on the assumption that the Güssing plant reaches the same water contents as the 100kW research facility using the same steam-fuel ratio 0.6(2), (3).*

[3] *Recalculated from the mean values for the composition of the dry gas*

Finally, the performance of the Chalmers gasifier was compared with the 100 kW research gasifier at Vienna University of Technology (3) and the gasifier in Güssing (2), see Table 4. To do the comparison the water content in raw gas from the gasifier in Güssing was assumed to be the same as the one in 100 kW unit. The η_{WGSR} values are calculated at 800 ºC and the results show that the WGSR has gone at least 20 %-units further towards equilibrium in the 100 kW and the gasifier in Güssing than in the Chalmers gasifier, see Table 4. This lower degree of equilibrium is a consequence of differences in parameters such as reactor temperature, gas residence time at high temperature, gas-solid contact, bed material and fuel. The gas residence time depends on the geometry and fluid dynamics of the gasifier and further work is needed to describe this in detail. However, a significant role is thought to be played by the lower contact between pyrolysis products and bed material (since in-bed feeding is not used at Chalmers) and the choice of an inert bed material.

CONCLUSIONS

The conclusions drawn from this work are

- The presented zero-dimensional models are power full tools to evaluation the indirect gasification process
- The conversion of char entering the gasifier with bed material from the boiler is approximately 20%mass
- The leakage of air or flue gas can be estimate by the established mass balance
- The closure of the mass balance is most sensitive to the composition of lumped hydrocarbons and the hydrogen content in the fuel
- The degree of conversion from the predicted volatiles is above 95%mass for tars.
- The degree of conversion predicted for the light hydrocarbons is -200%mass. The negative value implies an increase of the amount of light hydrocarbons resulting from the conversion of the tars.
- The degree of equilibrium for the WGSR was 42%.
- The WGSR at the Chalmers gasifier is shown to be significant further from equilibrium than has been calculated for comparable gasifiers in literature.
- To properly investigate the resulting degree of conversion and evaluate the chemical mechanism used in this work, a more detailed model, including geometrical and fluid dynamical aspects, should be implemented.

ACKNOWLEDGEMENT

This work has been support by Akademiska Hus, Göteborg Energi, METSO, the Swedish Energy Agency and Fundação para a Ciência e a Tecnologia (SFRH/BD/39567/2007), Portugal.

REFERENCES

1. Thunman H, Seemann M, C. First Experience with the new Chalmers gasifier. Proceedings of the 20th International Conference on Fluidized Bed Combustion: 659-663. Xi'an, China, 2009.
2. Hofbauer H, Rauch R, Bauch R. Biomass CHP plant Guessing–a success story. Pyrolysis and Gasification of Biomass and Waste, 2003: p. 371-383.
3. Hofbauer H, Rauch R. Stoichiometric water consumption of steam gasification by the FICFB-gasification process. Progress in thermochemical biomass conversion, 2001: p. 199.
4. Edvardsson E, Åmand L-E, Thunman H, Leckner B, Johnsson F. External Solids Flux Measurements in a CFB boiler. Proceedings of the 19th International Conference on Fluidized Bed Combustion. Vienna, Austria, 2006.
5. Åmand L-E, Lyngfelt A, Karlsson M, Leckner B. Fuel Loading of a Fluidized Bed Combustor Burning Bituminous Coal, Peat or Wood Chips. Report A97-221, Departrment of Energy Conversion, Chalmers University of Technology, Goeteborg, Sweden, 1999.
6. Thunman H, Niklasson F, Johnsson F, Leckner B. Composition of volatile gases and thermochemical properties of wood for modeling of fixed or fluidized beds. Energy & Fuels 2001;15:1488-1497.
7. Palchonok G, Dikalenko V.I, Kovensky V.I, Leckner B. Mechanisms of Drying and Pyrolysis in Combustion of Wood Cylinder. Proceedings of Nordic Seminar of Thermochemical Conversion of Solid Fuels, Gothenburg, Sweden, 1997.
8. Channiwala SA, Parikh PP. A unified correlation for estimating HHV of solid, liquid and gaseous fuels. Fuel 2002; 81:1051-1063.
9. Neves D, Thunman H, Seeman M, Ideias P, Matos A, Tarelho L, Gómez-Barea A. A database on biomass pyrolysis for gasification applications. Proceedings of the 17th European Biomass Conference & Exhibition: 1018-1028. Hamburg, Germany, 2009.
10. Funazukuri T, Hudgins RR, Silveston PL. Correlation of volatile products from fast cellulose pyrolysis. Ind. Eng. Chem. Process. Des. Dev. 1986;25:172-181.
11. Scott DS, Piskorz J, Radlein D. Liquid products from the continuous flash pyrolysis of biomass. Ind. Eng. Chem. Process Des. Dev. 1985;24:581-588.
12. Kanury A.M. Introduction to Combustion Phenomena, Gordon and Breach Science Publishers, New York, 1977.

Appendix II – Online measurement of raw gas elemental composition in fluidized bed biomass steam gasification

World Bioenergy, Conference & Exhibition on Biomass for Energy– Jönköping, Sweden, 2012

WORLD BIOENERGY 2012
Conference & Exhibition on Biomass for Energy
29 - 31 MAY 2012, JÖNKÖPING - SWEDEN

ONLINE MEASUREMENT OF RAW GAS ELEMENTAL COMPOSITION IN FLUIDIZED BED BIOMASS STEAM GASIFICATION

D. Neves[a,b], H.Thunman[b], L. Tarelho[a], A. Larsson[b], M. Seemann[b], A. Matos[a]
[a] Department of Environment and Planning, Centre of Environmental and Marine Studies, University of Aveiro, Campus Universitário de Santiago, PT 3810-193 Aveiro, Portugal; [b] Department of Energy and Environment, Chalmers University of Technology, SE-412 96 Goteborg, Sweden

ABSTRACT: At the present stage of technology development pursuing to achieve unattended gasification processes, the available methods to determine the CHON composition of raw gas involve a great deal of laboratory tasks, making it unpractical, time-consuming and costly. For instance, there are available analyzers to measure the chemical composition of dry raw gas but offline methods are used to determine the liquids (organic compounds + water). An alternative that is investigated in this work is to convert the raw gas first into simple product species that are easily analyzed. The straighforward way to achieve this is to burn the gas with proper amount of oxygen to assure quantitative conversion into CO_2, H_2O and N_2. This method is demonstrated here by monitoring the CHON composition of raw gas with high temporal resolution from Chalmers 2MW_{th} FB gasifier.

Keywords: gasification, gas, tar, biomass conversion, fluidized bed

1 INTRODUCTION

Environmental and social concerns, energy security and fossil fuel prices are driving increased R&D and technological interest on renewable bioenergy. In particular, biomass gasification technologies have been actively discussed over the past decades as a route for producing a raw gas that can be used directly or as a starting feedstock for a whole set of synthetic fuels. Concepts were investigated to achieve a cost-effective and flexible gasification process and improved raw gas quality [1-4]. For example, a dual-FB steam gasification process was demonstrated in Chalmers (Sweden) where an existing 12 MW_{th} FB boiler was retrofitted with a 2 MW_{th} FB gasifier producing a raw gas with heating value up to 15 MJ/kg (dry basis) [5, 6].

With increasing utilization of biomass gasification, fast and reliable monitoring methods are needed to optimize the process. With this in mind, knowledge about the elemental composition of raw gas is crucial for estimating the degree of fuel conversion in the gasifier. Due to the short residence time (<5s) and excess of steam in allothermal gasification, the raw gas is a complex mixture containing permanent gases, tars and water. Thus, a number of problems in assessing its elemental composition can be foreseen. Today this is achieved by extensive sampling and analysis procedures (e.g. [7-10]).

In this work an alternative measurement method for the CHON composition of raw gas is proposed that simplifies the analysis and give data with comparably high time resolution. The principle of the method is based on the continuous high-temperature sampling of the gas and controlled conversion into CO_2, H_2O and N_2 by oxygen or air in a small combustor. These gas species can, thereafter, be measured with high accuracy and high time resolution and the CHON composition of the raw gas calculated by mass balance across the combustor.

The feasibility of the method is shown by a set of combustion experiments with the raw gas produced from Chalmers 2MW_{th} gasifier. The initial result from these experiments shows that the method is fast and reliable. The evaluation of the results also show how operational data such as degree of fuel conversion, oxygen transport by catalytic material and the quantity of tar in raw gas can be obtained by the method.

2 MEASUREMENT METHOD

2.1 Mass balance

For biomass fuels with only trace levels of sulfur and chlorine the combustion of ash-free raw gas with dry atmospheric air is given by

$$\nu_{G,A}\ (\text{raw gas}) + \text{air} \rightarrow \nu_{CO2,A}\ CO_2 + \nu_{N2,A}\ N_2 + \nu_{H2O,A}\ H_2O + \nu_{O2,A}\ O_2 + \nu_{Ar,A}\ Ar \qquad \text{Eq. (1)}$$

where $\nu_{G,A}$ and $\nu_{k,A}$ (k= CO_2, N_2, H_2O, O_2, Ar) are the stoichiometric coefficients. Notice that the raw gas contains an unknown number of compounds. To avoid condensation of heavy organics between the gasifier and the small combustor the temperature of the sampling line is kept above 350 ^{0}C [8]. This makes it difficult to make direct measurement of the flow-rate of raw gas and hence the mass balance across the combustor has to be solved backward. The stoichiometry of Eq. (1) is then written per unit mass of dry air (subscript A) given that it can be measured accurately. The coefficients for the product species are given by Eq. (2), where nE is the flow-rate of wet flue gases (subscript E) and $y_{k,E}$ the mole fraction of k^{th} product species in flue gases.

$$\nu_{k,A} = y_{k,E}\frac{n_E}{n_A}\frac{M_k}{M_A} \quad k = CO_2, N_2, O_2, H_2O \qquad \text{Eq. (2)}$$

In this work the moisture content of flue gases ($y_{H2O,E}$) is measured online with capacitive thin-film humidity sensor [11]; after that, the water is removed in a cold-trap and the dry gas analyzed by traditional methods (IR gas analyzers, GC). The flow-rate of flue gases is calculated from a known quantity of inert gas injected at a given position in the system according to layouts given in Fig. 1.

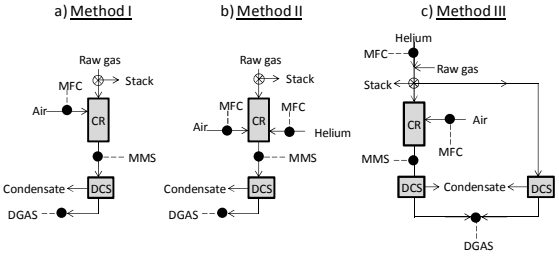

Figure 1: Methods to quantify the flue gases during the combustion of raw gas with dry air. MFC – mass-flow controller; CR – combustion reactor; MMS – moisture measurement system; DCS – gas drying and cleaning system; DGAS – dry gas analysis system.

The intuitive inert gas is, of course, nitrogen which anyway is supplied to the combustor with dry air, method I. This provides the simplest way to calculate n_E as given by the mass balance to the inert gas in Eq. 3, where n_{IG} is the flow-rate of inert gas and $y_{IG,Ed}$ the respective mole fraction in dry flue gases. The drawback of method I is that the measurement becomes restricted to the CHO composition of raw gas. However, most gasifiers have some unknown amount of nitrogen in the raw gas, which mainly comes from the fuel feeding system. This makes it necessary to use another inert gas than nitrogen that can be measured in a simple way. One alternative inert gas considered in this work is helium. In method II a small amount of helium is supplied to the combustor and the flow-rate of flue gases also given by Eq. (3).

$$n_E = \frac{n_{IG}}{y_{IG,Ed}}\left(1 + \frac{y_{H2O,E}}{1 - y_{H2O,E}}\right) \qquad \text{Eq. (3)}$$

To also get a measurement of the quantity of raw gas leaving the gasifier, the inert gas, preferably helium, is mixed with the gasification agent (steam), method III. By doing so, the amount of CHON in raw gas can be related to the unit mass of inert gas. To solve the mass balance to the combustor in Method III one needs again to quantify the flue gases (see Eq. 2). Now, some sort of information about the quantity of nitrogen in the raw gas is necessary. One possibility is to measure the N/H mass ratio of raw gas according to setup given in Fig. 1-c. In this setup the sample is divided into two flows. The first flow is lead to the combustor and the H/He mass ratio of raw gas determined from the amounts of H_2O and He in the produced flue gases (Eq. 4). The second flow is dried in a separate line in order to determine the N/He mass ratio. It is sound to approximate the total nitrogen content of raw gas from the amount of N_2 in the dry gas owing to the low nitrogen content of the fuel used here (section 5) and also that a significant part of fuel nitrogen is likely to convert to N_2 [12-14]. Moreover, previous investigation in the Chalmers $2MW_{th}$ gasifier [15, 16] showed that fuel nitrogen is around 1-2% (mass %) of the total nitrogen leaving the gasifier as N_2. To calculate the N/He ratio from the composition of dry gas (subscript Gd) one can use Eq. (5). The N/H ratio of raw gas is then calculated from the result of Eq. (4) and (5) which makes it possible to determine the quantity of flue gases according to Eq. (6). Note that Eq. (6) is the general form of Eq. (3) in case where the inert gas is supplied with both dry air and raw gas. The drawback in method III is the quantity of helium needed.

$$\frac{Y_{H,G}}{Y_{He,G}} = \frac{Y_{H,E}}{Y_{He,E}} = \frac{y_{H2O,E}M_{H2}}{(1 - y_{H2O,E})y_{He,Ed}M_{He}} \qquad \text{Eq. (4)}$$

$$\frac{Y_{N,G}}{Y_{He,G}} \approx \frac{Y_{N,Gd}}{Y_{He,Gd}} = \frac{y_{N2,Gd}M_{N2}}{y_{He,Gd}M_{He}} \qquad \text{Eq. (5)}$$

$$n_E = \left(\frac{y_{N2,A}M_{N2}}{y_{N2,E}M_{N2} - (Y_{N,G}/Y_{H,G})y_{H2O,E}M_{H2}}\right)n_A \qquad \text{Eq. (6)}$$

Once the composition and flow-rate of flue gases in methods I to III have been determined, the quantities of CHON supplied with raw gas to the small combustor can be obtained from the respective elemental mass balances, Eq. (7) to (10), where $\nu_{k,A}$ (k=CO_2, H_2O, O_2, N_2) are the stoichiometric coefficients given by Eq. (2). The ratio of raw gas to dry air ($\nu_{G,A}$) is calculated by summing up the left sides of the equations and the CHON mass fractions of the raw gas given by Eq. (11).

$$Y_{C,G}\nu_{G,A} = \nu_{CO2,A}\frac{M_C}{M_{CO2}} - y_{CO2,A}\frac{M_{CO2}}{M_A} \qquad \text{Eq. (7)}$$

$$Y_{H,G}\nu_{G,A} = \nu_{H2O,A}\frac{M_{H2}}{M_{H2O}} \qquad \text{Eq. (8)}$$

$$Y_{O,G}\nu_{G,A} = \nu_{O2A} + \nu_{CO2A}\frac{M_{O2}}{M_{CO2}} + \nu_{H2OA}\frac{M_{O2}}{M_{H2O}} - y_{O2A}\frac{M_{O2}}{M_A} \qquad \text{Eq. (9)}$$

$$Y_{N,G}\nu_{G,A} = \nu_{N2,A} - y_{N2,A}\frac{M_{N2}}{M_A} \qquad \text{Eq. (10)}$$

$$Y_{j,G} = \frac{Y_{j,G}\nu_{G,A}}{\sum_j (Y_{j,G}\nu_{G,A})} \quad j = C, H, O, N \qquad \text{Eq. (11)}$$

2.2 Sensitivity analysis

To analyze the uncertainty of the measurement ($Y_{j,G}$) a sensitivity analysis with respect to the three suggested setups is carried out.

The combustion of a nitrogen-free raw gas with dry air is first analyzed and hence method I can be used. The CHO composition of raw gas is taken as 25.0% C, 10.0% H and 65.0% O (mass %). The theoretical composition of flue gases is calculated for two percentages of excess-air (10 and 100%) and is taken as the base cases (A) in the analysis. The sensitivity of $Y_{j,G}$ is investigated by varying the measurement parameters in -2% of case A; cases B to E for variations in $y_{H2O,E}$, $y_{CO2,Ed}$, $y_{O2,Ed}$ and $y_{N2,Ed}$, respectively. Case F tests the situation where the mole fraction of N_2 is given by difference method ($y_{N2,Ed}$=1-$y_{CO2,Ed}$-$y_{O2,Ed}$). The results are shown in Fig. 2-a in terms of the H/C and O/C mass ratios of raw gas. These ratios are always predicted within ±5% of base case regardless

the measurement parameter that is varied. The variations in the CHO mass fractions are also small, being predicted within ±3% of case A (not shown). One remarks that the H/C ratio of raw gas is closely given by the amounts of H_2O and CO_2 in the flue gases (cases B and C).

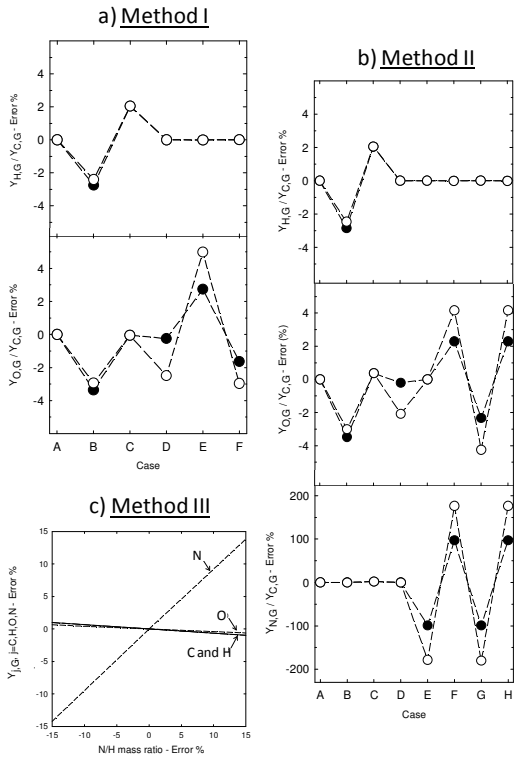

Figure 2: Sensitivity analysis for the CHON composition of raw gas according to proposed method (see also Fig. 1). ● - 10% excess-air; ○ - 100% excess-air.

To illustrate method II the typical gas composition is considered: 20.0% C, 10.0% H, 65.0% O and 5.0% N (mass %). The flow-rate of helium (inert gas) supplied to the small combustor is taken as 0.05 mol He/mol air. The theoretical composition of flue gases under 10% and 100% excess-air is again the base cases. In cases B to H the measurement parameters are varied in -2% of case A, respectively for $y_{H2O,E}$, $y_{CO2,Ed}$, $y_{O2,Ed}$, $y_{N2,Ed}$, $y_{IG,Ed}$, n_{IG} and n_A. The resulting variations in the predicted H/C, O/C and N/C mass ratios of raw gas are shown in Fig. 2-b. It can be seen a low sensitivity with respect to $y_{H2O,E}$, $y_{CO2,E}$ and $y_{O2,E}$ (case B to D). However, similar variations in $y_{N2,Ed}$, $y_{IG,Ed}$, n_{IG} and n_A (cases E to H) leads to excessive variation in the N/C ratio, with values up to ±180% of case A. For the CHON mass fractions the same qualitative behavior is observed. Hence, there are major concerns in the utilization of method II to predict the composition of raw gas since very accurate measurements are needed. For instance, to approximate the nitrogen content of raw gas within ±5% error one needs to reduce the error in cases E to H to below ±0.05%. The high sensitivity of $Y_{N,G}/Y_{C,G}$ (and $Y_{N,G}$) is because the nitrogen leaving the combustor is closely the nitrogen supplied with dry air, $v_{N2,A} \approx Y_{N2,A}$. This also explains the lower sensitivity of the N/C ratio in case of 10% excess-air. Lower excess-air means a higher ratio of raw gas to dry air ($v_{G,A}$) so it contains a larger fraction of the total incoming nitrogen. Thus, the excess-air in the combustor shall be minimized so that the measurement uncertainty (Eq. 12) is also minimized.

This further suggests that a lower sensitivity can be attempted in method II by burning the raw gas with pure oxygen. Therefore, the sensitivity analysis shown in Fig. 2-b was recalculated, now using pure oxygen instead of dry air. The results show a low sensitivity of the H/C, O/C and N/C ratios in relation to any of the measurement parameters. The CHON mass fractions of raw gas do not vary in more than ±6% of the theoretical values when the measurement parameters are varied in -2% of base case (results not shown). Considering that all the hydrogen, nitrogen and carbon entering the combustor come from the raw gas, the respective H/C and N/C ratios becomes only dependent on the composition of flue gases.

Now the case is treated where the N/H mass ratio of raw gas is used to quantify the flue gases (method III, Eq. 6). As noted before, method III is the general form of method I and hence the sensitiveness of both methods with respect to uncertainties in the composition of flue gases is similar (see Fig. 2-a for method I). Therefore, the interest is to investigate the influence of an error in the N/H ratio on the predicted CHON composition of raw gas. This evaluation is done in Fig. 2-c, where the N/H ratio is varied in ±15% of base case while using the theoretical values for the composition of flue gases. It can be seen that the error in the predicted CHON mass fractions is smaller than the error in the N/H ratio. Moreover, the sensitiveness of carbon, hydrogen and oxygen is much lower than that of nitrogen. For instance, in the present example a ±15% error in the N/H ratio results in ±14% error in the nitrogen content of raw gas (variation between 0.043 and 0.057 kg N/kg G) while the error in the respective CHO contents is below ±1%. As described above, the N/H mass ratio is determined from Eq. (4) and (5) and, for example, a ±2% variation in the respective input data leads to a ±5% variation in the N/H ratio. Thus, in practice the uncertainty in the N/H ratio is likely below the ±15% variation shown in Fig. 2-c.

2.2.1 Summary

In case of nitrogen-free raw gas, method I offers the best alternative to measure its CHO composition and one does not need highly accurate measurements to attain a reasonably accuracy (say, ±5% error). For engineering purposes, it is sufficient to characterize the flue gases in terms of H_2O, CO_2 and O_2 and take the concentration of N_2 by difference method; further improvement can be obtained by using reconstituted air instead of atmospheric air. If the mass fraction of nitrogen in the raw gas is to be determined, method II can be used if the combustion is carried out with pure oxygen. If dry air is to be used instead of pure oxygen, then method III provides the alternative to approximate the CHON composition of raw gas within a reasonable accuracy (say, ±5% error).

3 MONITORING COMBUSTION FACILITY

The measurement setup used in the present work can be seen in Fig. 3. The overall size of the facility is around 2.0×0.9×0.6 m. Monitoring, data-acquisition and control systems have been thought for standalone operation. Nevertheless, it can easily be connected to the monitoring

systems of the gasifier. Through the developed facility any of the measurement layouts shown in Fig. 1 can be tested.

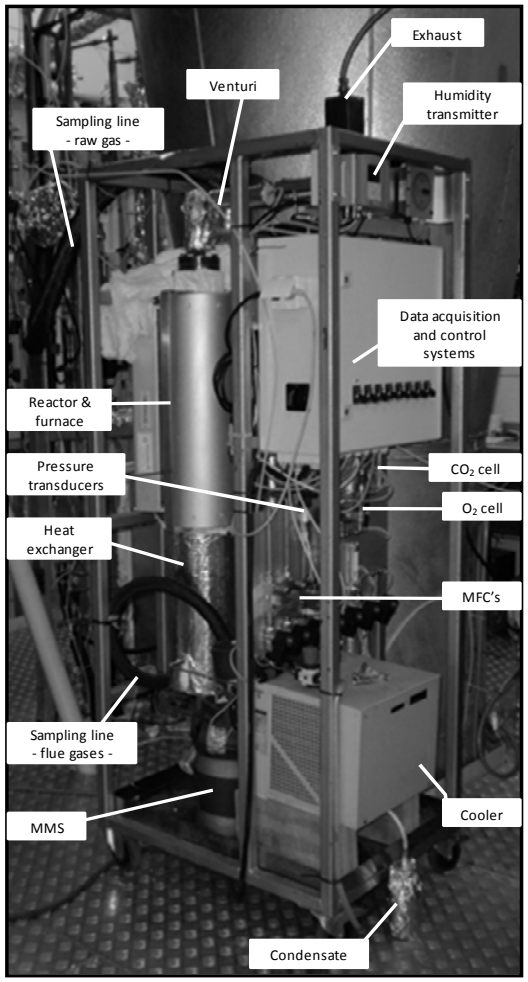

Figure 3: Online monitoring combustion facility. See Fig. 1 for abbreviations.

The combustion reactor is a stainless steel (SS) tube with 33.4 mm OD and 770 mm lenght. It is operated at atmospheric pressure and in the temperature range of 800 to 950ºC. The tube is placed in an electrically heated oven (2.8 kW) and the temperature is monitored by two thermocouples (K-type, 1.5 mm OD) placed in the middle (T1) and close to the bottom exit (T2) of the tube. The top and bottom joints are of a flange type extending 50 mm out of each side of the oven and are thermally insulated. The purpose of the reactor is to assure complete combustion of raw gas; no catalyst was used.

To avoid vapor condensation (e.g. tar), the raw gas is lead by heated line (360-380ºC) to the combustion chamber. A ceramic filter is attached to the sampling port to separate the larger particles from the raw gas and is completely covered with thermal insulation. A flexible heating hose (0.28 kW/m, SS 8 mm OD inner tube) is then used to secure that the temperature of raw gas is above 360ºC all the way into the combustion facility. The hose is connected to the vacuum side of a 316L SS all welded venturi. Dry combustion air is injected into the pressure side of the venturi forcing the raw gas to move into the vacuum port and mix with the dry air. A tee-assembly makes it possible to monitor the vacuum generated (P1). Heat is furnished to the venturi and the dry air stream by winding a heating tape around (0.25 kW/m) and using thermal insulation. A thermocouple (K-type, 1.5 mm OD) is placed at closely 10 mm from the pressure side (T3) to ascertain the temperature of incoming dry air (≈ 380ºC). The raw gas/air mixture moves then into a side port of a gas burner and finally down into the combustion chamber. To accommodate the burner in a vertical position, a suitable hole was bored through the top flange of the reactor and a joint was welded. A nozzle is connected to the bottom end of the burner and drilled with twenty 2.5 mm-holes in order to spread the flame. In the upper part of the burner a second port enables different operation opportunities. One operating condition is when the inert gas (e.g. helium) is supplied through this port and mixed with the raw gas/air mixture. In another operating condition a combustible gas is mixed with dry air before it undergoes combustion. The reactor top flange and the gas burner are also heated to roughly 390ºC by means of the same heating tape used to heat the venturi and are well insulated.

The produced flue gases pass through the inner tube (33.4 mm OD, 350 mm height) of a counter-flow heat exchanger while dry combustion air flows up through the outer tube (48.3 mm OD, 290 mm length). The heat exchanger is used to (i) cool down rapidly the flue gases to bellow 200ºC and (ii) pre-heat the dry air moving into the venturi. Downstream of the heat exchanger a small stream of flue gases is continuously sampled (2-4 NLpm) and the remaining gas is discarded off. A thermocouple (K-type, 1.5 mm OD) is inserted into the exhaust pipe to ascertain the temperature of flue gases (T4). A flexible heating hose (0.14kW/m, PTFE 6 mm OD inner tube) heats the inner tube to ≈160ºC and leads the flue gases to the online moisture measurement system [11]. In this system, the gas is further cooled down by means of an oil bath. A measurement probe with humidity (capacitive thin-film polymer) and temperature (PT 100) sensors is used to monitor the relative humidity of flue gases. In order to determine the partial pressure of water, the absolute pressure of flue gases is also measured. In practice, the temperature of the oil bath (T5) is adjusted to roughly 60-80ºC so that the relative humidity increases to within 55-75%. The flue gas is then lead by insulated PTFE tube to the Peltier cooler (≈2ºC) where the liquids (mainly water) are trapped and collected. Trace vapors and aerosols are further removed in a coalescing filter. The dry and clean flue gas is finally pumped through a flow indicator and sent to the gas analysis system.

The monitoring systems used in the facility are summarized as follows: i) two absolute pressure transducers (WIKA S10, 0-1.6 bar); ii) two mass-flow controllers (Bronkhorst EL-FLOW, 0-29 NLpm and 0-5 NLpm); iii) relative humidity and temperature measurement system (Vaisala HMT338, 0-100% RH, <180ºC); iv) O_2 gas sensor (electrochemical cell, Figaro KE-25, 0-100% O_2); and v) CO_2 gas sensor (silicon-based NDIR, Vaisala GMT220, 0-10% CO_2). A real-time control and data acquisition system (NI CompactRIO) is connected to a host computer to read the sensor signals, operate the pneumatics and save the data.

At present, the O_2 and CO_2 sensors are used to monitor the operating condition in the combustor. In this work mainly the O_2 cell was used due to its short response time (t_{90}<15s). Some response fluctuations were observed for this sensor possibly due to daily fluctuation in ambient temperature. The CO_2 sensor shows a larger response time (t_{90}>30s) and due to its narrow measurement range (0-10% CO_2) was little used in this work. For the evaluation of the setup the dry and clean flue gas was lead by SS 6 mm OD tube to online gas analyzer (Rosemount NGA 2000, 0-100% CO_2, 0-25% O_2, 0-1% CO, 0-10% CH_4) and micro-GC (Varian GC4900). This gas analysis system is far from the monitoring facility and thus the measurement signal is delayed a few minutes. The GC is used to measure the concentration of N_2 and He. These gases are separated in a molecular sieve 5Å column using argon as carrier gas and quantified with TCD. The micro-GC was calibrated by multi-point fit covering the typical range of concentration of N_2 (60-80 %, v/v) and He (<8.0 %, v/v) in dry flue gases.

To control the excess-air in the combustion reactor, advantage is taken from the operating characteristics of the venturi (Fig. 4). The ratio between the vacuum and pressure flow-rates is a strong function of the amount of gas entering the pressure side. In practice, that means the air-fuel ratio can be varied by varying the flow-rate of dry combustion air. For instance, a richer fuel mixture can be prepared by increasing the flow-rate of dry air and vice-versa.

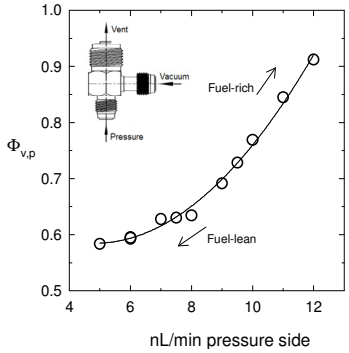

Figure 4: Operating characteristics of the venturi at ≈360ºC. Φv,p is the volume ratio of vacuum to pressure flow-rates.

4 EVALUATION OF THE METHOD

Dry atmospheric air (78.08% N_2, 20.95% O_2, 0.93% Ar and 0.04% CO_2, v%) was used as oxidizer. Following the sensitivity analysis (section 2), method I or III was tested. Table I shows the CHO mass fractions obtained for samples of know composition and indicates the accuracy of the proposed method. The initial test of the system was done with CO_2, which was supplied to the vacuum side of the venturi while varying the amount of air. The gas leaving the small combustor was measured and the elemental composition of CO_2 was recalculated from the measurement. The tests showed that the amount of carbon and oxygen could be predicted within ±5% of the theoretical values although the error decreases to below ±1% in case of high CO_2/air ratios. There was a trend to overpredict the oxygen content in the tests using CO_2. Following this initial tests a combustible gas having 43.3 %C, 5.4 %H and 51.3% O (mass %) was burned under ≈50% excess-air. Here, the flue gases are analyzed for CO_2, O_2, H_2O, CO and CH_4 while N_2 was taken by difference. CO and CH_4 were only found at ppm levels in flue gases which provide proof of complete combustion. Despite the approximation used, the CHO composition of the gas being burned is predicted within ±4% error and the result can be further improved by decreasing the excess-air and/or using reconstituted air instead of dry atmospheric air.

Table I: Results obtained by proposed measurement method on samples of known composition.

	Measured composition of flue gases (%v, wet basis)				CHO composition Error %		
Spl[a]	O_2	N_2	CO_2	H_2O	C	H	O
#1	20.14	73.71	5.32	0.00	-4.8	0.0	+1.8
#1	20.09	73.54	5.53	0.00	-4.5	0.0	+1.7
#1	19.26	70.56	9.66	0.00	-2.4	0.0	+0.9
#1	19.12	70.04	10.54	0.00	-2.2	0.0	+0.8
#1	18.55	66.48	14.77	0.00	-3.4	0.0	+1.3
#1	16.47	60.32	22.05	0.00	-0.9	0.0	+0.4
#1	16.29	59.55	22.90	0.00	-1.0	0.0	+0.4
#1	15.97	58.46	24.48	0.00	-0.8	0.0	+0.3
#1	15.92	58.26	24.69	0.00	-0.8	0.0	+0.3
#1	14.87	53.49	30.57	0.00	-1.2	0.0	+0.5
#2[c]	5.60	70.20[b]	13.80	10.40	+2.8	+4.1	-2.8

[a] Samples: #1 – 100% CO2; #2 – combustible gas.
[b] Calculated by difference method.
[c] 43.3 %C, 5.4 %H and 51.3% O (mass %).

A dynamic combustion experiment using the raw gas produced in the Chalmers gasifier is presented in Fig. 5. Notice that the FB gasifier was under stable operation during the whole experiment. Time periods A to D shows different operating conditions in the combustion reactor. The heated line for the raw gas (≈ 360ºC) is connected to the venturi in the beginning of period A (see resulting vacuum P1). Prone ignition of the raw gas/air mixture is indicated e.g. by temperature increase in the combustion chamber (T1). It was tried to simultaneously sample the raw gas to various measurement systems during period A, but it causes excessive pressure drop in the ceramic filter and leads to unstable operation in the small combustor. Thus, only the combustor was operated afterward. In periods B and C the facility was running according to the sketch shown in Fig. 1-c. Note that the flow-rate of dry air entering the venturi is varied from 10 to 9 Nlpm in periods B to C, respectively, causing the vacuum (P1) to vary inversely. The combustion proceeds then under a higher percentage of excess-air in period C (see also Fig. 4). The effect of the variation of the excess-air can be seen in Table II. As noted before, the H/C ratio of raw gas is closely given by the H_2O and CO_2 contents of flue gases, which results in similar values of H/C in periods B and C. To further test the reliability of the measurements, the side port of the burner was used to supply a sweep of He to the combustor in period D. The dilution caused by He is immediately seen from the concentration of H_2O, CO_2 and O_2 (Fig. 5), although exactly the same H/C ratio is obtained. Thus, the method reliably indicates the steady-state operation of the FB gasifier. By the end of period D the heating elements (e.g. oven) are turned off and the sampling line for the

raw gas is disconnected from the venturi. Ambient air is then sucked into combustor causing P1 to approach atmospheric pressure. One remarks the step-like decrease in the response of the humidity cell to mention that the results given by online moisture measurement system [11] are in close agreement with traditional gravimetric method.

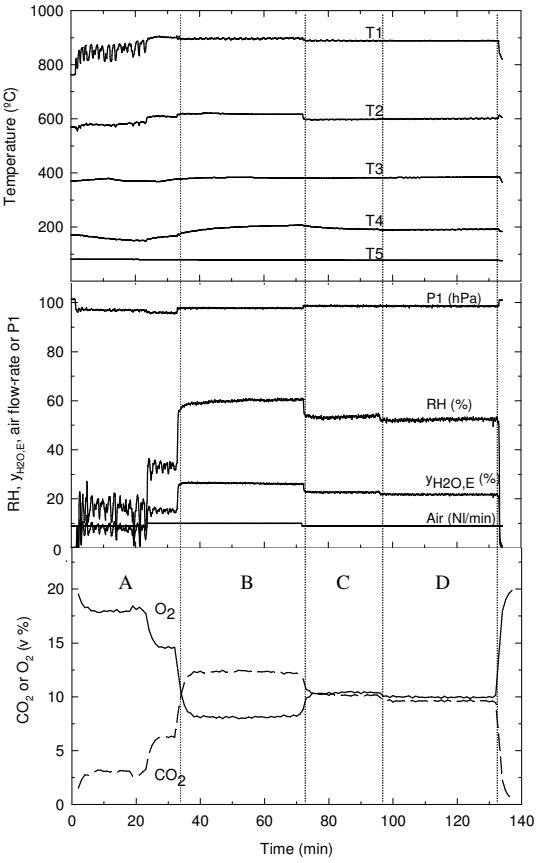

Figure 5: Operating condition in the combustion facility during experiment with raw gas from Chalmers FB gasifier. Average composition of flue gases in Table II.

Table II: Average composition of flue gases in experiment shown in Fig. 5.

Variable / Period	B	C	D
Air flow-rate (Nl/min)	10.0	9.0	9.0
$y_{O2,Ed}$ (v%, dry basis)	8.11	10.38	9.95
$y_{CO2,Ed}$ (v%, dry basis)	12.22	10.09	9.49
$y_{N2,Ed}$ (v%, dry basis)	79.26	79.07	75.11
$y_{He,Ed}$ (v%, dry basis)	0.28	0.24	5.25
$y_{H2O,E}$ (v%,wet basis)	26.33	22.68	21.79
$Y_{H,G}$ / $Y_{C,G}$[a]	0.49	0.49	0.49

[a] Approximated by the H/C mass ratio of flue gases.

5 MONITORING OF DUAL-FB GASIFIER

During the testing of the method with raw gas the operating condition of the Chalmers gasifier was varied. During each condition 2 to 5 combustion experiments were performed resulting in a total of 17 experiments. The conditions in the small combustor were varied widely without compromising the complete combustion, including variation of temperature within 800-950ºC, flow-rate of dry air within 6-12 NLpm (excess-air as low as 10%) and residence time below 0.5s. The CHON composition of raw gas was for these tests determined according to method III (see section 2).

5.1 OPERATING CONDITIONS AND FUEL

An overview of the Chalmers gasification process is found elsewhere [5, 6, 15] while the operating conditions used in this study are summarized in Table III. The circulating bed material between interconnected reactors is silica sand with a average diameter of around 270 µm. In two of the experiments ilmenite is added to the bed. The dense bed was operated at around 830ºC while variyng the steam-fuel ratio between 0.7 and 1.1 kg/kg. The fuel used in the gasifier was wood pellets. Ultimate analysis of fuel yields the following composition ($Y_{j,F}$): 50.6 %C, 6.1 %H, 0.1 %N (mass %, dry ash-free). Periodic measurements are carried out to ascertain the moisture content of pellets, with typical values of 6.8 to 8.5% (mass %, as received). The ash-free char formed after the thermal decomposition of fuel at ≈830ºC was measured under inert atmosphere with values in range of 16-18% (mass % of dry ash-free fuel). Char samples were also sent for ultimate analysis in external laboratory ($Y_{j,ch}$): 93.1 %C, 1.2 %H, 0.4 %N (mass %, dry ash-free).

Table III: Operating conditions in Chalmers 2MW_{th} FB gasifier. Bed temperature ≈830ºC; pressure ≈-1 kPa.

Run No.	Fuel feeding[a]	Steam-fuel ratio[b]	Bed material
	kg/h	kg/kg	Mass %
#1	389-396	0.89-0.91	100% sand
#2	398	1.04	100% sand
#3	405-412	0.70-0.71	100% sand
#4	377-398	1.06-1.11	≈ 98% sand + 2% ilmenite
#5	394-400	0.75-0.76	≈ 88% sand + 12% ilmenite

[a] As received basis.
[b] Includes fluidizing steam and fuel moisture ($Y_{st,F}$).

5.2FUEL CONVERSION AND OXYGEN FLYWHEEL

The wood pellets entering the FB gasifier are rapidly heated to 830ºC causing it to thermal decompose into volatiles and char. Fuel devolatilization is a rapid process (typically <1.5min for cm-sized particles [17]) but the gasification of char is slow. Thus, unconverted char is likely to escape with the circulating bed material towards the FB boiler. Furthermore, selective oxygen transport from the boiler to the gasifier can be attempted by adding suitable catalyst to bed material. A low cost natural ore (ilmenite) proven suitable in chemical looping technologies [18] was here used for evaluating this behaviour. In the following we propose simple method to monitor the functioning of FB gasifier based on the results from the combustion experiments with raw gas.

The gas-phase reactions occurring in the gasifier (e.g. water-gas shift) do not alter the elemental composition of

raw gas and the respective H/C and O/C mass ratios are determined by the quantities of steam and pellets entering the reactor and the fraction of fuel that is converted. The leakage (dry flue gases) and unburnt char recirculated to the gasifier are minor streams and have little influence on these ratios. Accordingly, the theoretical H/C and O/C mass ratios of raw gas can be approximated by simplified zero-dimentional modeling, as given in Eq. (12) and (13),

$$\frac{Y_{H,G}}{Y_{C,G}} = \frac{Y_{H,F} + Y_{ch,F}Y_{H,ch}(\chi - 1) + Y_{st,F}Y_{H,H2O}}{Y_{C,F} + Y_{ch,F}Y_{C,ch}(\chi - 1)} \quad \text{Eq. (12)}$$

$$\frac{Y_{O,G}}{Y_{C,G}} = \frac{Y_{O,F} + Y_{ch,F}Y_{O,ch}(\chi - 1) + Y_{st,F}Y_{O,H2O}}{Y_{C,F} + Y_{ch,F}Y_{C,ch}(\chi - 1)} \quad \text{Eq. (13)}$$

where $Y_{ch,F}$ is the yield of pyrolytic char (see section 5.1) and χ the degree of char conversion in the gasifier. In the limiting case where only devolatilization occurs, the H/C and O/C ratios are determined by setting χ=0 in Eq. (12) and (13), respectively; in other limiting case, the fuel is completely gasified and then one sets χ=1. Note that $Y_{ch,F}$ is considered independent of steam/fuel ratio ($Y_{st,F}$) since the bed is always operated at 830ºC (Table III). The degree of char conversion can be estimated by using the proper values for the parameters in Eq. (12)-(13) and the H/C and O/C ratios given by proposed method. This is illustrated in Fig. 6, where the experimental results are compared to theoretical ratios describing the pyrolysis and gasification of wood pellets; the range shown in case of pyrolysis is due to the uncertainity in $Y_{ch,F}$. The data for runs #1 to #3 clearly shows that the H/C and O/C ratios of raw gas are closely given by the elemental composition of pyrolytic volatiles and taking into account the dilution caused by steam. The wood pellets are then completely devolatilized at 830ºC but the gasification of char is limited. Moreover, variation of the steam-fuel ratio from 0.7 to 1.1 kg/kg does not notably alter the carbon conversion. Notice that the H/C ratio of the flue gases leaving the combustor provide reliable results for the H/C ratio of the raw gas being burned making it possible to monitor the fuel conversion in the gasifier without the need to solve the balance to the combustion process. The utilization of 12% ilmenite in run #5 is seen to increase the O/C ratio due to selective oxygen transport to the gasifier. Notice the consistent values in run #4 comparatively to runs #1 to #3, in light of a minor quantity of ilmenite being used in the former. To further illustrate the effect of ilmenite, the quantity of raw gas produced in run #5 is compared to that produced in case of 100% sand (run #3) in Fig. 7. The higher production of raw gas in run #5 is shown to result from an additional oxygen inflow of ≈0.19 kgO/kgF, after the difference given in Fig. 7 is corrected for the slightly different steam-fuel ratios (Table III). To convert this value into a per unit mass of ilmenite one needs the circulation rate of bed material. This was done in previous investigation [15], showing that a circulation rate of ≈14000 kg/h is needed in order to keep the gasification temperature at ≈830ºC. Thus, a crude estimate for the mass ratio of ilmenite to daf fuel feed in run #5 is 4.7 kg/kg; the oxygen transport capacity of ilmenite is then estimated to be roughly 4% (mass %) which is in agreement to values found by experiments in laboratorial rigs [18].

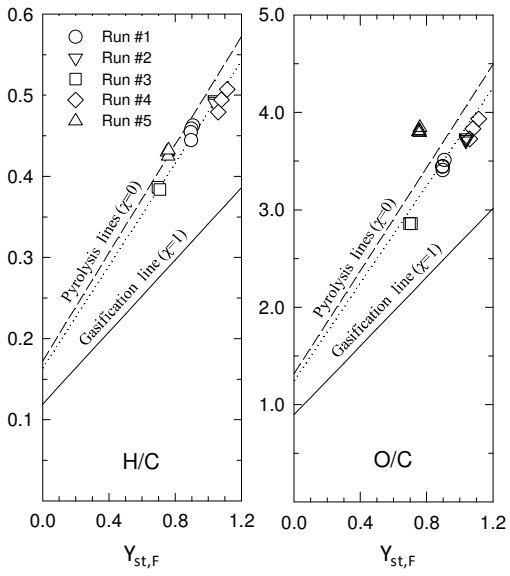

Figure 6: H/C and O/C mass ratios of raw gas leaving the Chalmers FB gasifier as a function of steam-fuel ratio ($Y_{st,F}$). Lines give the theoretical ratios according to Eq. (12) and (13); – – $Y_{ch,F}$ = 0.18; ··· $Y_{ch,F}$ = 0.16.

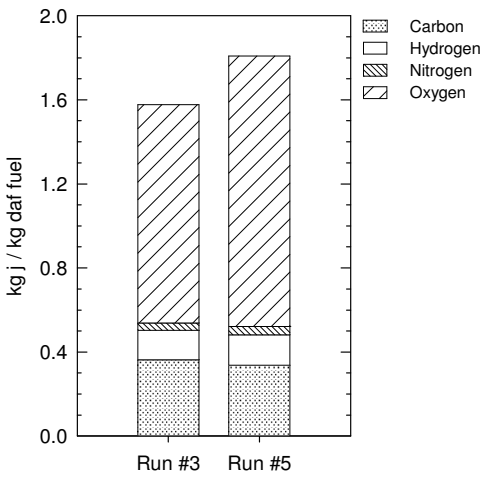

Figure 7: Quantity and CHON composition of raw gas produced in Chalmers FB gasifier.

5.3 AMOUNT OF TAR IN RAW GAS

In operational monitoring of gasifiers, the lumped organic compounds condensing at ambient conditions are commonly refered to as tar. The physical properties and chemical functionalities of tar species varies widely [19, 20] and hence it shows a wide range of stability as a function of reactor severity. Tar cracking is effective above 500ºC [21, 22] but it forms refractory species that are hard to convert in a short residence time [23]. The tar formed in the gasifier is problematic in process equipment and end-use application [24] thus demanding fast measurement methods. Relevant developments in the field include both offline (gravimetry or GC method [8], SPA method [7]) and online (e.g. IVD-analyzer [25], photo-ionization detector [26]) methods. A widely used procedure is based on cold traps andparticle filters to firstly separate water and tar from dry raw gas; the

amount of tar condensing is afterward determined by GC analysis or gravimetry [8]. Though, the most satisfactory estimate of tar is obtained by combining the gravimetric and GC results [27], due to tar species being lost in both methods (e.g. retention of heavy-tars in the GC column).

An option to rapidly estimate the tar condensed can be affordded by using the monitoring combustion facility (Fig. 3 and 8). Helium is once more injected at a know flow-rate into the gasifier. The raw gas/helium mixture is burned at first following the base setup given in Fig. 8-a. Then one splits to dry gas/helium mixture after the water and tar has been removed in the cold trap (Fig. 8-b). By using helium as a tracer gas in the combustion process, the quantities of elements removed in the cold trap can be determined by difference method. The carbon difference is of utmost importance as the total condensing carbon is ascribed to tar. One can rapidly approximate the carbon difference since the C/He mass ratios of raw gas/helium mixture and respective dry gas/helium mixture are closely given by the concentrations of CO_2 and He in flue gases. In the same vein, the hydrogen difference between raw gas and dry raw gas can be approximated from the H_2O and He concentrations.

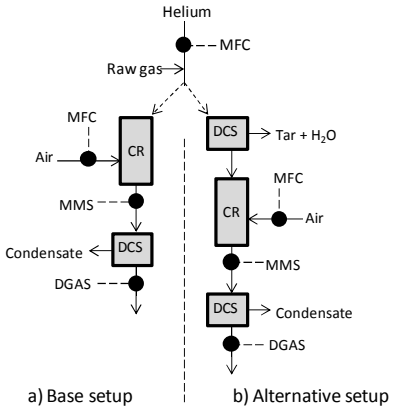

Figure 8: Measurement setups to estimate the amount of elements removed from raw gas by cold trapping. See Fig. 1 for abbreviations.

The measurement procedure was tested during the gasification experiment described in run #5 (Table III) and the results are provided in Table IV. Tar-bound carbon is estimated as 8.2% of total carbon in raw gas or around 1.5% of whole raw gas (mass %). The tar content of raw gas shall be noticeably higher since lumped tar is rich in oxygenated species [19, 20]. A survey of literature data suggests that the elemental composition of pyrolytic tar is highly dependent on that of parent fuel [21]; in particular, the carbon content is frequently within a range defined by the carbon content of fuel times 1 to 1.3 [21]. Therefore, after the carbon difference is measured by procedure given in Fig. 8, the plausible range for the amount of tar moving out the gasifier can be obtained. According to data in Table IV the tar formed in Chalmers gasifier is then estimated within 4.2 and 5.6 % of daf fuel (mass %) which is in range of literature values abtained upon FB biomass gasification (see e.g. survey in [24]).

It is worth to note the massive quantity of hydrogen separated upon cooling-down the raw gas (≈75% of total hydrogen, Table IV). Apart from a small contribution of tar-bound hydrogen, the major part of hydrogen is due to steam condensation. In fact, tar-bound hydrogen is likely below 5% (mass %) of the total mass condensing, owing to the yield of tar given above and the typical hydrogen content of pyrolytic tar [21]. Thus, the proposed method can also help in estimating the steam content of raw gas. A crude approximation of the steam leaving the gasifier in run #5 is then 0.97 kg/kg daf fuel (=0.108×18/2) corresponding to ≈0.54 kg steam/kg raw gas.

Table IV: Characteristics of raw gas and respective dry gas produced in Chalmers FB gasifier (run #5, Table III).

Parameter	Raw gas[b]	Dry gas[c]	Tar + water
kg H/kg C	0.426	0.119	--
kg C/kg F[a]	0.340	0.312	0.028
kg H/kg F[a]	0.145	0.037	0.108

[a] Mass of element leaving the FB gasifier *per unit* mass of dry ash-free fuel feed (F).
[b] Measurement according to base setup, Fig. 8-a.
[c] Measurement according to alternative setup, Fig. 8-b.

6 FUTURE DEVELOPMENTS

Future work shall provide an alternative to evaluate the N/H ratio of raw gas avoiding the need of using huge amount of helium in the gasifier in method III. One option is to build a second chamber to burn the raw gas with pure oxygen. By doing so all the carbon, hydrogen and nitogen leaving this chamber is due to raw gas. To further simplify the method, the N/C ratio of raw gas can be used in a similar maner to the N/H ratio (Eq. 6) so that one needs only the amounts of CO_2 and N_2 in flue gases.

7 SUMMARY AND CONCLUSIONS

- Online monitoring of the elemental composition of raw gas can be done by quantitative conversion of the gas into simple product species (CO_2, H_2O and N_2) that are easy to analyze. The CHON mass fractions of the gas being burned are then determined by solving backward the balances to the combustion reaction.
- The method is demonstrated in this work by using new combustion reactor and ancilary's. High temperature sampling (>350ºC) prevents tar and steam condensation and is feasible by using heated lines for the raw gas and oxidizer and heated venturi as a pump. For engineering purposes, complete combustion of raw gas with dry air was achieved in a wide range of conditions, including temperature of 800-950ºC, excess-air as low as 10% and residence time below 0.5s.
- The accuracy of proposed method was tested against samples of known composition. By proper adjustment of excess-air and oxidizer, the error in the CHO mass fractions can easely reduce to below ±3%. Also, in case of using air as oxidizer, sensitivity analysis show that the error for nitrogen is given by the accuracy of the method used to determine the N/H ratio of raw gas.
- A moisture measurement system coupled with IR gas analyzers enables real-time monitoring of the H/C ratio of raw gas by proposed method. To resolve the CHON composition it takes 3 min by instrumentation used in this study (i.e. micro-GC) which is sufficient to monitor

the time-averaged functioning of gasifiers. The time-resolution can, however, be improved.

- The degree of fuel conversion in dual-FB gasifier can be evaluated by zero-dimensional modelling and using the H/C ratio of raw gas as given by proposed method. In the same vein, selective oxygen transport by catalitic material from boiler to gasifier can be evalued from the O/C ratio of raw gas as shown in this study.
- The measurement method developed here can be used to evaluate the amount of tar and steam in raw gas if one manage to analyze the CHON composition of both raw gas and respective dry gas.

8 NOMENCLATURE

$\nu_{G,A}$ Stoichiometric coefficient in Eq. (1), mass of raw gas per unit mass of dry air, kg G/kg A
$\nu_{k,A}$ Stoichiometric coefficient in Eq. (1), mass of k^{th} species per unit mass of dry air, kg k/kg A
$y_{k,i}$ Molar fraction of k^{th} species in i^{th} stream, kmole k/ kmole i
$Y_{j,I}$ Mass fraction of j^{th} element in i^{th} stream, kg j/kg i
$Y_{i,F}$ Mass of i^{th} stream per unit mass of dry ash-free biomass fuel, kg i/kg F
$Y_{k,i}$ Mass fraction of k^{th} species in i^{th} stream, kg k/kg i
n_i Molar flow-rate of i^{th} stream, mol i/s
M_k Molar mass of k^{th} species, kg k/kmol k
χ degree of conversion of pyrolytic char, dimensionless

Subscripts

i i^{th} stream (F, ch, G, Gd, st, A, E, Ed, IG)
j j^{th} chemical elements (CHON)
k k^{th} chemical species (CO_2, N_2, H_2O, O_2, Ar, CO, H_2, CH_4, C_xH_y, tar, He, IG)
F Dry ash-free biomass fuel
ch Char resulting from pyrolysis of biomass
G Ash-free raw gas (tar+water+permanent gases)
Gd Dry ash-free raw gas (without tar and water)
st Total steam entering the FB gasifier (includes fuel moisture)
A Dry atmospheric air
E Wet flue gases leaving the small combustor
Ed Dry flue gases leaving the small combustor
IG Inert gas (nitrogen, helium)

9 ACKNOWLEDGMENT

It is acknowledged the financial support by Fundação para a Ciência e a Tecnologia (FCT), Portugal, throught PhD grant SFRH/BD/39567/2007 and research project PTDC/AAC-AMB/098112/2008 (Bias-to-soil - Biomass ash: Characteristics in relation to its origin, treatment and application to soil), and Swedish Energy Agency. The operation of the gasifier was done within the co-operation between Akademiska Hus, Göteborg Energi, Metso Power and SFC, Swedish national gasification center.

10 REFERENCES

1. Knoef, H., Handbook on biomass gasification. Biomass Technology Group (BTG)2005, Enschede, The Netherlands: GasNet.
2. Corella, J., J.M. Toledo, and G. Molina, A review on dual fluidized-bed biomass gasifiers. Industrial & Engineering Chemistry Research, 2007. 46(21): p. 6831-6839.
3. Goransson, K., et al., Review of syngas production via biomass DFBGs. Renewable & Sustainable Energy Reviews, 2011. 15(1): p. 482-492.
4. Pfeifer, C., S. Koppatz, and H. Hofbauer, Steam gasification of various feedstocks at a dual fluidised bed gasifier: Impacts of operation conditions and bed materials. Biomass Conversion and Biorefinery, 2011. 1(1): p. 39-53.
5. Thunman H, Å.L.-E., Leckner B, A cost effective concept for generation of heat, electricity and transport fuel from biomass in fluidized bed boilers – using existing energy infrastructure, in 15th European Biomass Conference & Exhibition2007: Berlin, Germany.
6. Seemann MC, T.H., The new Chalmers research-gasifier, in Proceedings of the International Conference on Polygeneration Strategies2009: Wien, Austria.
7. Brage, C., et al., Use of amino phase adsorbent for biomass tar sampling and separation. Fuel, 1997. 76(2): p. 137-142.
8. Good J, V.L., Knoef H, Zielke U, Hansen PL, van de Kamp W et al. , Sampling and analysis of tar and particles in biomass producer gases – Technical report. CEN BT/TF 143 "Organic Contaminants ("Tar") in Biomass Producer Gases", 2005.
9. Oasmaa A, P.C., A guide to physical property characterization of biomass-derived fast pyrolysis liquids, 2001, Technical Research Centre of Finland Espoo, Finland.
10. Hasler, P. and T. Nussbaumer, Sampling and analysis of particles and tars from biomass gasifiers. Biomass & Bioenergy, 2000. 18(1): p. 61-66.
11. Hermansson, S., F. Lind, and H. Thunman, On-line monitoring of fuel moisture-content in biomass-fired furnaces by measuring relative humidity of the flue gases. Chemical Engineering Research & Design, 2011. 89(11A): p. 2470-2476.
12. Leppalahti, J., Formation and Behavior of Nitrogen-Compounds in an Igcc Process. Bioresource Technology, 1993. 46(1-2): p. 65-70.
13. Zhou, J.C., et al., Release of fuel-bound nitrogen during biomass gasification. Industrial & Engineering Chemistry Research, 2000. 39(3): p. 626-634.
14. Pereira, M., Projecto de um gasificador de biomassa, 2009, University of Aveiro: Aveiro, Portugal.
15. Larsson A, S.M., Thunman H, Assessment of mass and energy flows in the Chalmers gasifier, 2011, Department of Energy and Environment, Chalmers University of Technology: Sweden.
16. Larsson A, T.H., Neves D, Pallarés D, Seemann M., Zero-dimensional modeling of indirect fluidized bed gasification, in Proceedings of the XIII Fluidization Conference2010: Gyeong-ju, Korea.
17. Sreekanth, M., et al., Modelling and experimental investigation of devolatilizing wood in a fluidized bed combustor. Fuel, 2008. 87(12): p. 2698-2712.

18. Leion, H., et al., The use of ilmenite as an oxygen carrier in chemical-looping combustion. Chemical Engineering Research & Design, 2008. 86(9A): p. 1017-1026.
19. Evans, R.J. and T.A. Milne, Molecular Characterization of the Pyrolysis of Biomass .1. Fundamentals. Energy & Fuels, 1987. 1(2): p. 123-137.
20. Elliott, D.C., Relation of Reaction-Time and Temperature to Chemical-Composition of Pyrolysis Oils. Acs Symposium Series, 1988. 376: p. 55-65.
21. Neves, D., et al., Characterization and prediction of biomass pyrolysis products. Progress in Energy and Combustion Science, 2011. 37(5): p. 611-630.
22. Di Blasi, C., Modeling chemical and physical processes of wood and biomass pyrolysis. Progress in Energy and Combustion Science, 2008. 34(1): p. 47-90.
23. Antal, M.J., Effects of Reactor Severity on the Gas-Phase Pyrolysis of Celulose-Derived and Kraft Lignin-Derived Volatile Matter. Industrial & Engineering Chemistry Product Research and Development, 1983. 22(2): p. 366-375.
24. Milne TA, E.R., Abatzoglou N, Biomass gasifier "tars": their nature, formation and conversion, 1998, National Renewable Energy Laboratory: Colorado, U.S.
25. Moersch, O., H. Spliethoff, and K.R.G. Hein, Tar quantification with a new online analyzing method. Biomass & Bioenergy, 2000. 18(1): p. 79-86.
26. Knoef HAM, v.d.B.L., Ahmadi M, Sjöstrom K, Brage C, Liliedahl T, Development of an online tar measuring method for quantitative analysis of biomass producer gas, in Proceedings of the 17th European Biomass Conference & Exhibition2009: Hamburg, Germany. p. 884-888.
27. Coda B, Z.U., Suomalainen M, Knoef HAM, et al, Tar measurement standard: a joint effort for the standardization of a method for measurement of tars and particulates in biomass producer gas, in Proceedings of the 2nd World Biomass Conference2004: Italy.

Appendix III - A database on biomass pyrolysis for gasification applications

17th European Biomass Conference & Exihibition – Hamburg, Germany, 2009

A DATABASE ON BIOMASS PYROLYSIS FOR GASIFICATION APPLICATIONS

17th BIOMASS CONFERENCE – HAMBURG, GERMANY, 2009

D. Neves[a,b], H. Thunman[b], M. Seemann[b], P. Ideias[a], A. Matos[a], L. Tarelho[a], A. Gómez-Barea[c]

[a] Department of Environment and Planning, University of Aveiro, Campus Universitário de Santiago, 3810-193 Aveiro, Portugal. Tel.: +351234370349, Fax: +351234370309.

[b] Department of Energy and Environment, Chalmers University of Technology, SE-412 96 Goteborg, Sweden. Tel.: +46317721000, Fax: +46317723592.

[c] Bioenergy Group, Chemical and Environmental Engineering Department, Escuela Superior de Ingenieros (University of Seville), Camino de los Descubrimientos s/n, 41092-Seville, Spain. Tel.: +34954487223, Fax: +34954461775.

ABSTRACT: This work presents a first analysis of data on biomass pyrolysis collected in a database. Data from literature have been screened and structured, containing information about the parent fuel, experimental rig, operating conditions as well as product distribution and properties. From this data the behaviour of biomass pyrolysis within the temperature range 200-1000ºC is characterized. Data on product distribution is recorded through yields (kg product/kg fuel) and includes: char, total liquids (or pyrolytic liquids + water in feed), pyrolytic liquids (or organic liquids + pyrolytic water), organic liquids, pyrolytic water and total permanent (light) gas. The composition of pyrolysis gas includes data of: CO, CO_2, H_2, CH_4 and the remaining light hydrocarbons. Property data included are ash content, elemental composition (by means of CHO) and heating value of char and organic liquids.

Keywords: database, pyrolysis, gasification, yield, tar.

1 INTRODUCTION

Biomass is a solid fuel, which in relation to coal has high moisture and volatile content. Thus, when the parent solid is heated, most of the mass is released as a result of drying and pyrolysis (or devolatilisation, if it occur in an oxidizing environment). This process will evolve in someway regardless of surrounding composition, as long as heat is transport to the fuel particles. Hence, the process is important to describe and understand in the scope of thermo-chemical applications. For example, prediction of the composition of volatiles for different biomasses is a critical issue in gasification systems, demanding proper description of the pyrolysis stage at high temperature.

The composition of volatiles may be reasonably assessed through pyrolysis experiments under inert atmosphere (i.e. without interaction with steam, air, etc.). Consequently, a database structuring the existing experimental data would be a useful tool to empirically predict the distribution of pyrolytic products for specific fuels and for various operating conditions. This information can be integrated into more advanced reactor models for biomass gasification.

Much work has been published on biomass pyrolysis, regarding models, kinetics and product distribution. Several fuels and different parameters have been tested, typically heating rate and temperature. The reported data is usually related to the yields of the main products (char, liquids and gas), although sometimes there is also information about the release of specific species. Property data related to fuel and products, such as proximate and elemental compositions and heating value, may be also found. In the investigations, different types of reaction vessels has been used, the pyrolysis conditions, the fuel type and the measurements has varied, resulting in an large quantity of information.

To screen and structure the literature-derived data on product yields and composition is an investigation rout with great potential. Accordingly, this work aims at presenting a database on biomass pyrolysis, where the available data is being continuously added-on. The collected data already enables to establish general trends of biomass conversion during pyrolysis. Trends of the product yields to the heating rate, temperature and type of fuel are presented, as well as some product property data. This provides information needed for design, modelling and scale-up of gasification systems. Only a few limited efforts have previously been made to summarize the existing experimental data e.g. [1,2].

2 THEORETICAL CONSIDERATIONS

Pyrolysis is the thermal decomposition of the fuel into a huge number of products. As heat is transferred to the fuel particle its temperature increases leading to the release of moisture (drying) and pyrolytic volatiles. The remaining carbonaceous solid is called char. The fuel particle itself may experience severe structural changes. Moreover, at high enough temperatures some of those volatiles (namely the heavier hydrocarbons) may decompose in the reaction environment into low-molecular weight gases. Indeed, secondary reactions [3], including cracking, reforming and polymerization, as the possibility to further convert the primary products to a significant extent. Secondary reactions may occur both heterogeneously, as the volatiles flow out of the fuel particle (although transport of volatiles from the main stream to react at particle surfaces is also possible) and homogeneously, as long as the volatiles are exposed to high temperatures.

Although dependent on diverse factors, the rates of drying and devolatilisation can be approximated by empirical correlations, for instance in the form of a power function of particle size [4,5]. Moreover, to what extent drying and pyrolysis overlap during fuel decomposition depends also on particle size. For small particles these processes are expected to occur very quickly and in sequence. This enables the volatiles to leave the fuel particle with minor interaction between them and with the hot char surface. In contrast, drying and pyrolysis become slower and occur simultaneously for large particles. A hot char layer is formed at outer particle

surface, through which all the volatiles needs to goes through. Thus, intraparticle secondary reactions are expected to become more significant as particle size increases. The effect of the secondary reactions on the composition of the volatiles as function of particle size has been shown by Scott and Piskorz [6], finding a lower yield of liquids (i.e. water and heavy hydrocarbons that condense at ambient temperature) as particle size increases. Also Wang et al. [7] confirmed this tendency through experiments in a fluidized bed reactor at 500ºC, where secondary cracking of organic liquids has been observed even for mm-sized particles. Since, char gasification rate with steam is considerably slower [1] than cracking rate of heavy hydrocarbons [8], the decrease of liquids with particle size should be related to the conversion of the organic fraction. However, for cm-sized particles, breakage of initial particles into smaller fragments, during the pyrolysis stage, may have the opposite effect. For instance, this enables the volatiles released at the pore structure to leave the particle through the cracks, without contact with the hot char.

During pyrolysis experiments, inert carrier gas is provided to the system, transporting the volatiles away form the fuel particle as they volatilises. The rate of carrier gas affects the residence time of volatiles through the vessel and, therefore, the extent of secondary reactions. Carrier gas also dilutes the primary volatiles, reducing the rate of homogeneous reactions (reforming, water-gas shift, etc.). This affects the reactions involving permanent species, but presumably has small effect on the conversion of the heavier hydrocarbons. Boroson et al [9] conducted experiments on gas-phase cracking of highly diluted organic liquids from wood pyrolysis in the temperature range of 500-800ºC and residence time of 0,9-2,2s, reporting conversions from 5% to 88%, whilst the coke formation was negligible. In a subsequent study [10], it was confirmed that organic liquids are extremely labile at temperatures higher than 600ºC. The effect of carrier gas is expected to be more significant during batch-wise experiments, which is the usual procedure for pyrolysis tests.

The initial mass of fuel used in pyrolysis tests may also have a role in secondary reactions. On the one hand, the cracking of hydrocarbons is enhanced by contact with hot char; On the other hand, increasing the mass of fuel may increase the resulting gas velocity and thus, it may decrease the homogeneous reactions of volatiles due to the decrease of gas residence time. It has been reported [10] that a fraction up to 35% of the organic liquids released from wood pyrolysis is highly susceptible to catalytic cracking when passed though a char bed, even at low temperatures (400-600ºC), whereas the homogeneous cracking is not significant bellow 600ºC. It is also important to consider the reactor specific gas-solid contact, for instance, the bed depth in packed beds, the state of fluidization in FB, etc.

In summary, the homogeneous and heterogeneous (during both intraparticle and interparticle transport) cracking of the organic liquids clearly have an important role on the distribution and composition of pyrolytic products. It seems that conversion of primary volatiles is enhanced with increasing particle size (say, >1mm) [6,7], temperature (say, >500ºC) [9,10] and the amount of char in the reactor. It is also important to consider the residence time of the gas. Secondary reactions seem to proceed fast enough to attain significant conversion for residence time bellow 1s. Since the gas residence time in pyrolysis experiments is most often above 1s, it is reasonable to conclude that the extent of secondary reactions must be significant in most investigations.

A special issue is related to the yield of water. Reported data usually shows 5-20% moisture in fuel (dry basis, db) before testing, which compares to the rule of thumb of 12% (db) of pyrolytic water [11]. It is believed that moisture in the parent fuel is not significantly converted during thermal decomposition and, hence, it should be distinguished from direct pyrolytic products [11]. Pyrolysis experiments are usually made using small particles (mm-sized or even µm-sized) so the drying does not overlap with the release of volatiles. As a result, intraparticle reactions involving the moisture released during drying are expected to be limited.

3 METHODOLOGY

3.1 Definitions

The overall pyrolysis process of the as-received fuel is represented by the following reaction:

$$\left(1+\frac{Y_a}{1-Y_a}\right)\cdot\frac{1}{1-Y_m} = Y_C + Y_L + Y_W + Y_G + \frac{Y_a}{1-Y_a}$$

where it consider both the release of primary volatiles and secondary reactions. Y_a is the ash content of fuel in db, Y_m is the moisture content of fuel in as-received basis and on the left side, the successive terms refers to yields in daf fuel basis (kg/kg daf fuel): Y_C for char, Y_L for organic liquids, Y_W for water, Y_G for total permanent gas and $Y_a/(1-Y_a)$ for ash. It is worth to point out that: (i) both moisture water and pyrolytic water are quoted as Y_W; (ii) Y_C does not include ash, which has been intentionally included in both sides of the reaction; and (iii) permanent gas includes the different individual species (CO, CO_2, H_2 and light hydrocarbons).

There is no consensus in the literature about the meaning of "bio-oil", for which it is possible to find diverse synonyms (tars, pyrolytic liquids, bio-crude, etc.) [12]. The most used definition is that "bio-oil" refers to the whole liquid fraction (organic liquid + pyrolytic water + moisture water in feed) (e.g. [11,12]). Thus, according to Fig.1, the yield of "bio-oil" would correspond to (Y_L + Y_W) while for the yield of "tar" is Y_L. Hence, hereafter in this work no distinction is made between "tars", "organic liquids" and "heavy hydrocarbons". On the other hand, the yield of pyrolytic water on daf fuel basis (Y_{WV}) can be calculated from following equation:

$$\underbrace{Y_{WV}}_{\text{pyrolytic water}} = \underbrace{Y_W}_{\text{total water}} - \underbrace{\frac{Y_m}{1-Y_m}\cdot\left(1+\frac{Y_a}{1-Y_a}\right)}_{\text{water from fuel mosisture}}$$

The sampling and analytical methods used for "bio-oil", "tars" and water deserve yet great deal of research and, together with a consensus about the definitions, most of the ambiguities in the analysis and comparison of product yields would be avoided. For instance, according to some studies [13,16], the experimental results depends

on the measurement methods used. As a result, in an effort to reduce the inaccuracies that its measurements always comport, guidelines have been proposed for sampling and analysis of liquids [17,18].

The measurement method for the yield of "bio-oil" may evolve cold traps filled with solvent, and subsequent gravimetric analysis (e.g. [26]). Both the nature of solvent and the temperature at which the traps are maintained vary among investigations [13]. This definitively affects the nature and the observed yield of liquids. The "tar" content in "bio-oil" may be assessed using extraction techniques and further gravimetric analysis or gas-chromatography coupled with appropriate detectors (mass spectrometer, etc.); alternative methods for tar sampling and analysis were developed by Moersch et al. [16] and Brague et al. [28]. The yield of water is usually assessed through the analysis of water content in "bio-oil" (e.g. [22]), for which titration techniques may be used [17].

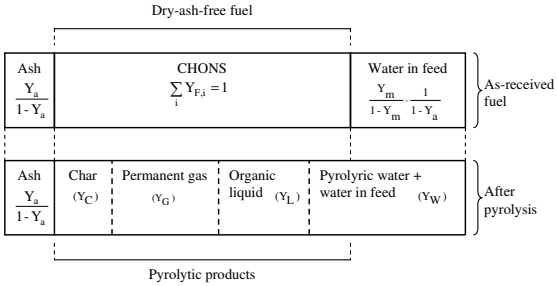

Figure 1: Global mass balance to the pyrolysis process. The quantities provided in each box are in daf fuel basis.

Pyrolytic gas (including the carrier gas) is obtained once the "bio-oil" has been removed in the cold traps. Collection of this gas can be made by using expansion bags or continuously by using diverse methods. Mass balances are thereafter used to calculate the pyrolytic gas yield (e.g. [22]). Dry gas meters may be also used to integrate the total volume of gas, instead of expansion bags (e.g. [14,23]).

The char yield, usually referred as the mass of solid remaining after pyrolysis (including the inventory of in-vessel and that captured in separators, such as cyclones or filters) is usually assessed through gravimetric methods (e.g. [20,21,27]). In few investigations it is determined by a mass balance to the ash (e.g. [19]), assuming that all ash in feed remains in char. Another method to determine the char yield is to measure the carbon release during a subsequent burnout of the char (e.g. [15]), providing that the carbon content in char is known or simply assuming that char is merely comprised of carbon and ash.

In some works (e.g. [24-26]) only two of the main products (char, permanent gas and "bio-oil") are quantified, and the third is given by difference.

Biomass pyrolysis experiments may be designed for: (i) controlled heating of the reaction environment to a given peak temperature, where the fuel is previously introduced and heated according to the surroundings (typically conducted in thermogravimetic systems and packed beds), or (ii) isothermal reaction environment, where the fuel is suddenly introduced to achieve faster heating rates such as in fluidized beds and free-fall reactors. In any case, the actual heating rate experienced by the fuel particles is dependent on the specific heat-transport conditions, both in the film-layer and inside the fuel particles. As a result, tests with packed beds of cm-sized particles may be representative of "slow heating rates" (e.g. [29]) whereas fluidized bed experiments at 700-950ºC with mm-sized particles can be considered to occur at "fast heating rates" (e.g. [7]). In fact, the threshold for "slow heating rate" *versus* "fast heating rate" is somewhat arbitrary. It is accepted that tests conducted between 10^1 and 10^2ºC/s belong to "slow heating rate" [8,30,31], whereas heating rates above 10^3ºC/s belongs to "flash pyrolysis conditions" [31]. It must be pointed out that, here, "slow heating rate" and "fast heating rate" do not refers to processes, pursuing to maximize the char yield and liquid and/or gas yields, respectively. Moreover, these processes are generally conducted bellow 700ºC while for gasification and combustion, the interest is to describe the thermal decomposition of the fuel in the range of 800-950ºC.

3.2 Structured collection of literature-derived data

This first version of the database is being developed in a single MSExcell® worksheet, consisting of a unique multi-field table where different screening rules have been applied to sort data according to specific criteria. For each investigation it has been recorded (i) reactor type (e.g. fluidized bed), (ii) reactor scale (industrial, pilot or laboratory), (iii) type of fuel (e.g. spruce, pine, ...), (iv) nature of the fuel taken wood as reference (wood vs. non-wood), (v) value of the heating rate (e.g. 500ºC/min), (vi) classification of heating rate according to "slow heating rate" *vs.* "fast heating rate", (vii) fuel properties (moisture content, ash content, elemental composition, particle size and heating value), (viii) the dependence of product yields and properties on temperature and (ix) a variety of observations like: residence time, use of catalyst, etc. Currently, the data base includes data from 71 studies [7,11,14,15,20,21,23-27,29,31-89], including around 70 different biomasses (woody and non-woody) and fuel particles having a variety of shapes and sizes (between 0,05 to 100mm), and vessel temperature in the range of 200-1000ºC.

Most of these works states whether the performed tests are representative of "slow heating rate" or "fast heating rate", even if the specific heating rate is unknown. However, when it is not the case, here the distinction was based on the threshold of 1000ºC/min. Nevertheless, the database allows selecting specific thresholds for the heating rate, since this parameter is saved as long as it is reported and filters may be applied to the worksheet. Both "fast" and "flash" heating rates are here considered as "fast heating rates".

3.2.1 Char

As discussed, the char yield is usually reported as the mass of solid remaining after the thermal decomposition of fuel and expressed on a dry feed basis. As a result, it contains organic material (mainly carbon) and ash. One of the ways the char yield has been recorded in the database is kg of solid residue *per* kg of dry fuel. However, since the ash content of char is sometimes reported, the char yield may be also expressed as in Fig.1, which relates the daf part of char to the daf part of parent fuel. So, the char yield has also been recorded as

kg of daf char *per* kg of daf fuel. To secure consistency, when the ash content of char is not reported, it was assumed that the initial ash content of the biomass remains in the char. In the results presented in the following, the char yield always refers to Y_C (thus, without ash, see Fig.1).

The elemental composition of char is recorded on daf basis and often just for carbon, hydrogen and oxygen. There are situations where the basis used to report this data is not explicitly given but it can be often assessed from the mass balance. For example, on a dry char basis, the sum of daf char and ash is equal to unity.

Concerning heating value of char, the most usual reported figure is the higher heating value (HHV), often expressed in db. In few investigations there is no reference to the basis used to express the heating value, so it was assumed to be in dry basis. Ambiguous terms like "calorific value" may be found and, here, it is assumed to be HHV. Actually, the information saved in the database is almost HHV in db. To change between HHV and LHV is straightforward by using the elemental composition of char.

3.2.2 Liquid

The yields are recorded in a daf feed basis and structured according to Fig.1: (i) total liquids (or "bio-oil", Y_L+Y_W), (ii) total pyrolytic liquids (Y_L+Y_{WV}), (iii) organic liquids (or "tar", Y_L) and (iv) pyrolytic water (Y_{WV}). The records are dependent on the reported data in each investigation. To collect these data from literature has been challenge, because there is not a uniform method of expressing these yields. The main difficulty has been to know whether the moisture in feed fuel (Y_m) is included in the pyrolytic products. Sometimes Y_m is even missed so data for all the fields of the database cannot be established. In these situations, the yield of total pyrolytic liquids cannot be estimated because it is not possible to subtracted the moisture water from total liquids; then, data is saved as reported (for example, as total liquids in dry fuel basis).

The elemental composition of "tars" (mostly CHO) is recorded on daf basis. In few cases this information is derived from the elemental composition of "bio-oil" as long as its water content is reported.

In the literature, there is data for HHV and LHV for the organic liquids and "bio-oil". To derive the heating value of organic liquid from that of "bio-oil", information on the water content is required. Yet, the elemental composition of organic liquids is needed to changeover between HHV and LHV. As a result, there is recorded data for HHV as well as for LHV in the database.

3.2.3. Permanent gas

In the literature the yield of total gas is given as in Fig.1 (Y_G) or, in few investigations, expressed as Nm^3/kg fuel feed. The first method is more useful when studying the mechanism of pyrolysis and cannot be evaluated from Nm^3/kg if the gas composition is not reported. In such situations, data is saved in the database as reported. The composition of pyrolysis gas is usually presented by means of: (i) yields for the specific gas species (kg species/kg fuel feed) or (ii) volume or mass fractions of each species in the total gas (kmol species/kmol total gas or kg species/kg total gas). The last method is not so useful because if Y_G is missed then the yields of the specific gases cannot be evaluated. As far as possible, the available information about total gas and respective components has been evaluated and saved by means of yields on a daf fuel feed basis. In addition, when literature data cannot be evaluated to fit this representation it is saved as reported.

The specific gases, considered in this work, are CO, CO_2, H_2, CH_4 and other light hydrocarbons (non condensable). Here, light hydrocarbons different from CH_4 were lumped into a single group, referred as C_xH_y. The most frequently reported light hydrocarbons (excluding CH_4) are C_2 and, sometimes, C_3. Thus, the recorded data on C_xH_y yield can be viewed as a good estimate for the yield of C_2 and, to some extent, for the yield of C_2+C_3 hydrocarbons.

The heating value of permanent gas is not commonly reported so, here, the composition of gas is used to calculate the LHV.

4 RESULTS

4.1 Yields of main products

In what follows, product yields are always expressed as kg product/kg daf fuel (in %). Fig.2 presents the yields of char, total permanent gas, total pyrolytic liquids and pyrolytic water, as a function of vessel peak temperature. It includes data from 57 studies [7,11,14,15,20,21,23-27,29,31,33 - 36,38 - 44,46,47,49,50,52,56,60 - 73,75,77 - 85,87 - 89], regardless of biomass type, reactor type and experimental conditions. Each subplot contains two data-series, one belonging to "slow heating rates" and other to "fast heating rates". It is worth to point out that, in Fig.2, the points in a given subplot sometimes have not corresponding points in the other subplots. This is because the reported data on product distribution is sometimes incomplete (for example, some investigations reports just the char yield).

Comparing the subplots of Fig.2, a consistent behaviour in what concerns the global mass balance is observed. The char yield decreases with temperature, being the dominant product at the lowest temperature. Conversely, the total gas yield increases with temperature, becoming the main product at the highest temperatures. The yield of total liquids shows a maximum at intermediate temperature (450-550ºC).

The major part of devolatilisation occurs in the temperature range of 200-600ºC. Within this range, the char yield decreases exponentially, reaching a minimum typically bellow 30% (Fig.2). At higher temperature region (> 600ºC) the char yield remains roughly constant.

The volatiles consist mainly of liquids (organic liquid + pyrolytic water) explained by observing that the yield of total gas does not evolve significantly bellow 550-600ºC. Indeed, the yield of pyrolytic liquids increases quickly from 200ºC to peak at 450-550ºC (Fig.2): (i) for "slow heating rates" it increases to around 35-45% (middle of range) which compares to the decrease of char yield from approximately 70-80% at 200-250ºC to around 20-30% at 450-550ºC; (ii) for "fast heating rates" the increase of pyrolytic liquids is to almost 55-65% (middle of range) which roughly corresponds to the decrease of char yield from around 70-80% to 15-25%.

Moreover, Fig.2 shows that the yield of pyrolytic water is in the range of 5-20% and clearly fits bellow the data points in the subplot for total liquids. Because, the yield of pyrolytic water seems to be roughly constant (average of 12%), the increase of total liquids in the temperature range of 200ºC to 450-550ºC should be related to the release of organic liquids.

At temperatures above 450-550ºC the yield of total pyrolytic liquids decreases consistently (Fig. 2), from around 35-45% or 55-65%, respectively for "slow heating rates" and "fast heating rates", to a minimum of around 20% at 900ºC, which fits approximately to the yield of pyrolytic water. Since peak temperature has minor effect on the yield of pyrolytic water, this suggests that the decrease of total pyrolytic liquids between 450-550ºC and 900ºC is related to the conversion of "tars".

As already referred, the char yield seems almost constant above 550-600ºC, which means that "tars" are mainly converted into low-molecular weight gases as temperature increases above this temperature. This is suggested by comparing the subplots of total pyrolytic liquids and that of total gas in Fig.2. This behaviour agrees with past observations on the variation of "tar" yield at high temperature [9, 10].

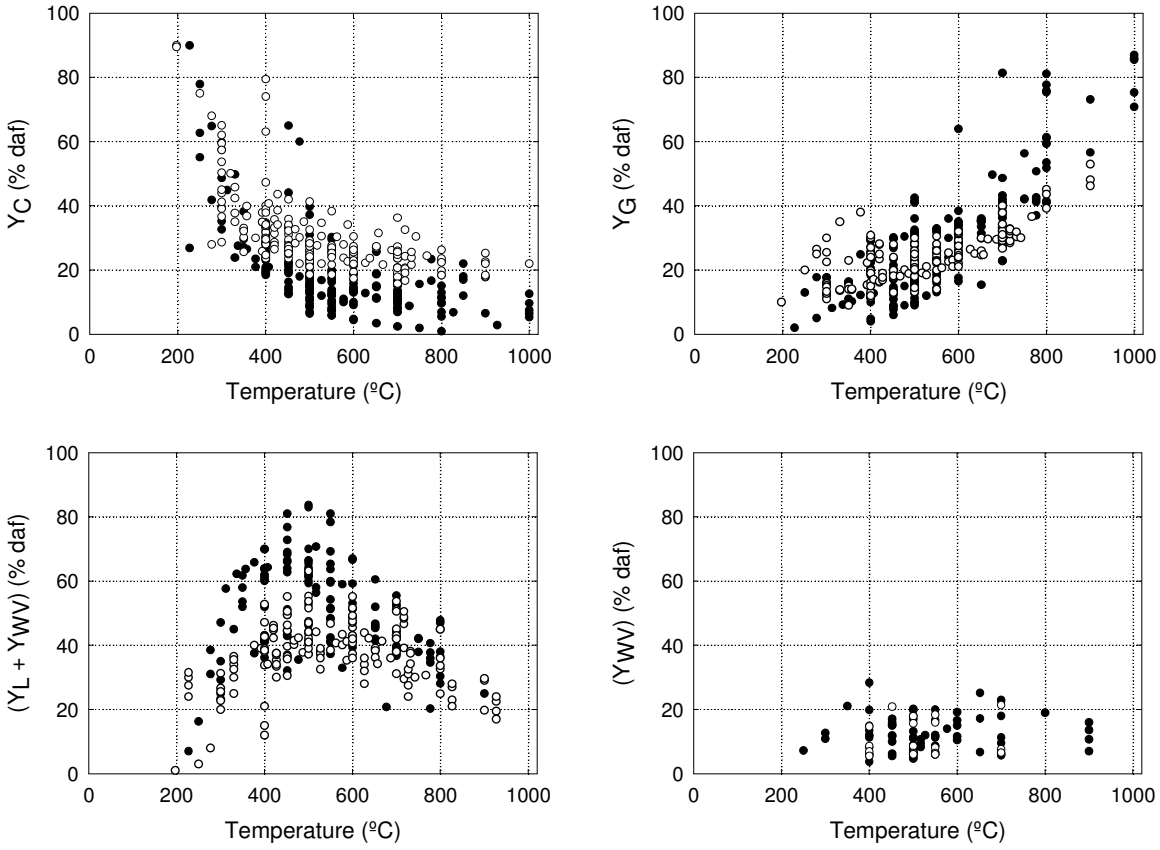

Figure 2: Yields of daf char (Y_C), total gas (Y_G), total pyrolytic liquids (Y_L+Y_{WV}) and pyrolytic water (Y_{WV}) for almost 40 biomasses (both woody and non-woody). [● -"fast heating rate"; ○ -"slow heating rate"].

The data of total pyrolytic liquids for "fast heating rates" in Fig.2 is also provided in Fig.3, distinguishing between woody and non-woody materials. The two data-series are quite different showing that pyrolysis of woody materials gives rise to larger yields of liquids. Between 400 and 600ºC the difference in average values may be as high as 20% (Fig.3). Higher yields of liquids for woody biomasses must be balanced with lower yields of char or gas. This is in agreement with the lower yield of liquids found during pyrolysis of non-woody biomasses when compared to woody biomasses [35,46,73], which has been attributed to higher lignin and/or ash contents of non woody biomasses.

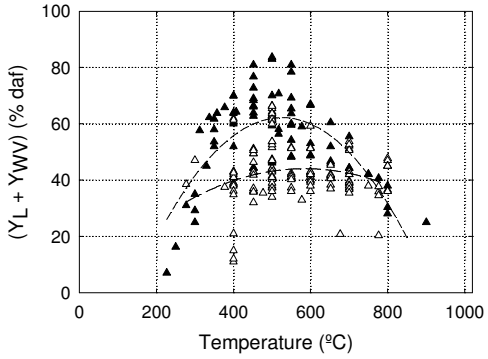

Figure 3: Yield total pyrolytic liquids for "fast heating rate" conditions. [▲ - "woody biomasses"; Δ - "non-woody biomasses"].

4.2 Yields of gas species

The yields of specific gas species are provided in Fig.4 (kg species/kg daf fuel), including CO_2, CO, H_2 and total light hydrocarbons (CH_4+C_xH_y). To draw the figure, data from 11 studies have been accounted for [14,21,23,34,35, 39,41,43,46,47,69], involving pyrolysis of around 15 different materials in different reactors, under specific experimental conditions. Data was found more abundant below 800ºC.

On a mass basis, the pyrolysis gas consists mainly of CO_2, CO, CH_4 and other light hydrocarbons, with lower amounts of H_2. Yields of CO, CH_4+C_xH_y and H_2 show an exponential increase in the temperature range of 350-1000ºC. The behaviour of CO_2 is different, showing a slow increase with temperature until 800ºC; thereafter there is a lack of data and no general behaviour can be postulated. However, there is some evidence that the yield of CO2 decreases with temperature, starting even bellow 800ºC [14].

The heating rate seems to affect the composition of the pyrolysis gas. The available data suggests that "slow heating rates" generally gives rise to large yields of CO_2 (Fig.4). It seems to exist an inverse trend for CO, H_2 and CH_4+C_xH_y, with lower yields for "slow heating rates" (Fig.4), but this are not so evident.

As anticipated, above 550-600ºC permanent gases seems to result mainly from the conversion of "tars" and, accordingly to Fig.4, CO seems to be the major product from "tar" conversion. In fact, between 550-600ºC to around 900ºC, the yield of CO evolves from 5-15% to 40-50%, which compares with the decrease of the pyrolytic liquids (see Fig.2). Most of the remaining "tars" is expected to be converted to CH_4+C_xH_y, which yield increases from 2% to around 12% (Fig.4). This is supported by experiments in [9], where vapour phase cracking of wood pyrolysis "tars" showed that CO accounts for almost 65% of the "tar" lost and CH_4+C_2H_2 for additional 20%. The knowledge of "tar" conversion and the products generated during fuel decomposition at high temperatures is crucial for the analysis and modelling gasification systems.

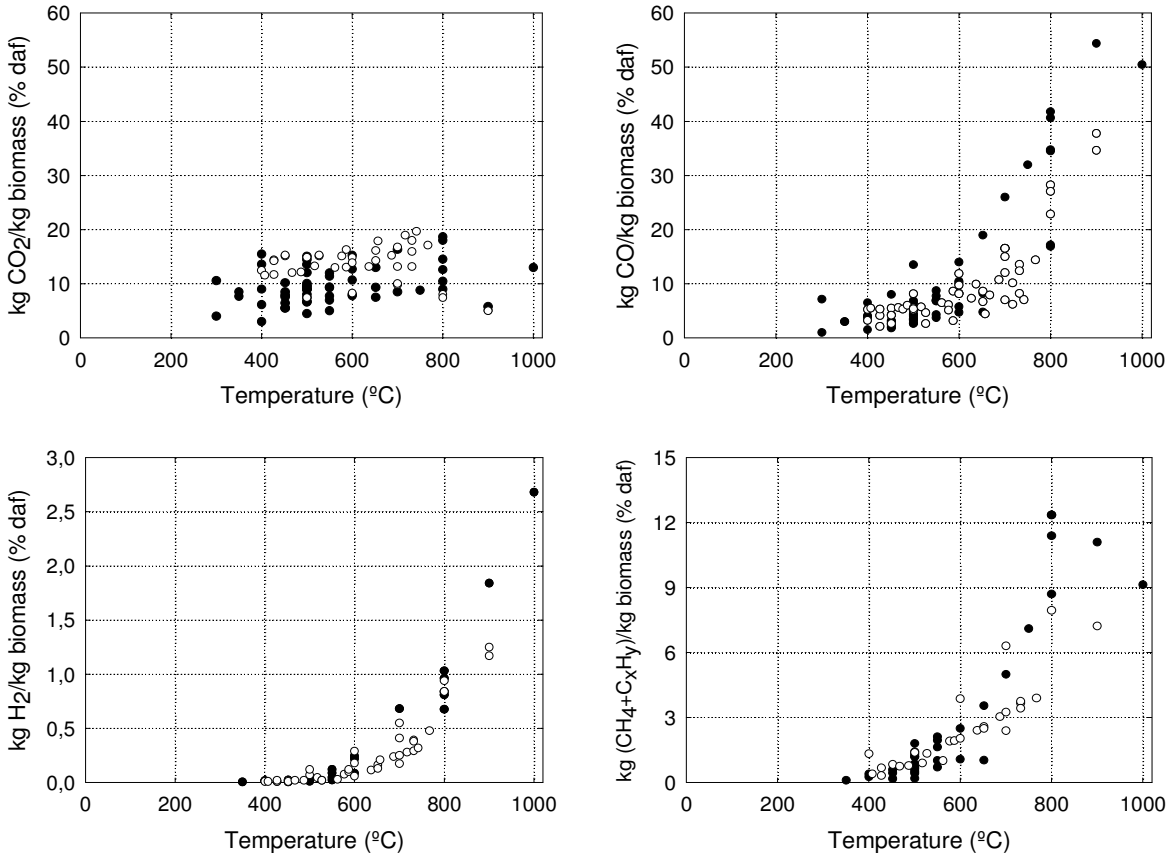

Figure 4: Yields of CO_2, CO, H_2 and total hydrocarbons (CH_4+C_xH_y) for almost 15 biomasses (both woody and non-woody) [● -"fast heating rate"; ○ -"slow heating rate"].

Moreover, below the maximum of pyrolytic liquid yield (around 450-550ºC) most of permanent gases seem to result directly from the devolatilisation of the parent fuel. Below 450-550ºC the yield of total gas is typically bellow 30% (Fig.2) and CO_2 and CO are the most abundant gases (Fig.4). As a rough indication within this temperature region, CO_2 may account for two-thirds of total gas and the remaining shall consist almost of CO (both in mass fraction basis in total gas).

4.3 Product properties

Besides pyrolytic product distribution, it is useful for modelling to collect data of product properties, including: the elemental composition of char and organic liquids

and their heating values and specific heats. Additional information like surface area, effective diffusivity, etc. may be necessary for particle models, but these are beyond the scope of the present work (see [1,15,92] for additional information).

4.3.1 Elemental composition

Fig.5 presents the recorded data on the CHO composition of chars and organic liquids as a function of temperature. It includes data from 25 investigations [7,14,20,21,24,27,29,32,33,35,37,38,41,43,46,49,58,62, 65,66,68,74,79,87,89], where around 30 different biomasses have been pyrolysed in different reactors and operating conditions. In the figure, a distinction was made between woody and non-woody biomasses.

The type of fuel does not seem to affect significantly the CHO composition of char, although it was observed that non-woody biomasses tend to generate char with slightly higher carbon and lower oxygen content. This may be related to the ash content and/or the relative amount of cellulose, lignin and hemicellulose in this type of fuels. Anyway, with rising final pyrolysis temperature the carbon content of char increases towards a plateau between 85-95%. This increase in carbon is coupled with an effective loss of oxygen and hydrogen, which stabilizes at 5-15% and < 2%, respectively (Fig.5-a,b). Furthermore, the main change in CHO composition of char occurs between 200ºC and 600ºC, which is the temperature window where the fuel particle losses most of its mass (Fig.2).

The available information on the database concerning the CHO composition of organic liquids is more abundant for temperatures bellow 600ºC. This is because investigations generally focus on the chemical analysis of "bio-oil" at temperatures where the maximum yield of "bio-oil" is obtained.

The composition of organic liquid (thus excluding water) is dependent on the parent fuel. At Fig.5-c, data-points in the range of 500-550ºC, showing carbon content well above 60% and oxygen content well bellow 30%, are related to non-woody biomasses, including seeds, shells, husks, olive bagasse, etc. However, for woody biomasses then most of such dispersion disappears (Fig.5-d).

The data analysed suggest that chemical composition of organic liquids does not vary significantly with temperature (Fig.5-c,d). It is observed, nevertheless, a slight tendency to larger carbon and hydrogen contents and smaller oxygen content as temperature increases (Fig.5-d). Therefore, "tars" are becoming enriched in less oxygenated and likely more stable species. This can be interpreted as a transformation towards highly aromatic structure of tars as a function of temperature [93].

If data provided at Fig.2 and Fig.5 is used to asses the amounts of carbon, oxygen and hydrogen that remains in the char per kilogram of parent fuel, then, the results for temperatures above 600ºC would tend to 10% carbon, 1% oxygen and 0,1% hydrogen. This amount of elements lost from the solid until around 600ºC is mainly transferred to pyrolytic liquids but, also, to permanent gases (mainly CO_2 and CO). In fact, as a rough estimate, 75-80% of carbon released during devolatilisation appears in "tars" and the remaining is transferred to gases; for oxygen, almost 60-65% appears in total liquids ("tars" + pyrolytic water) whereas 35-40% in gases.

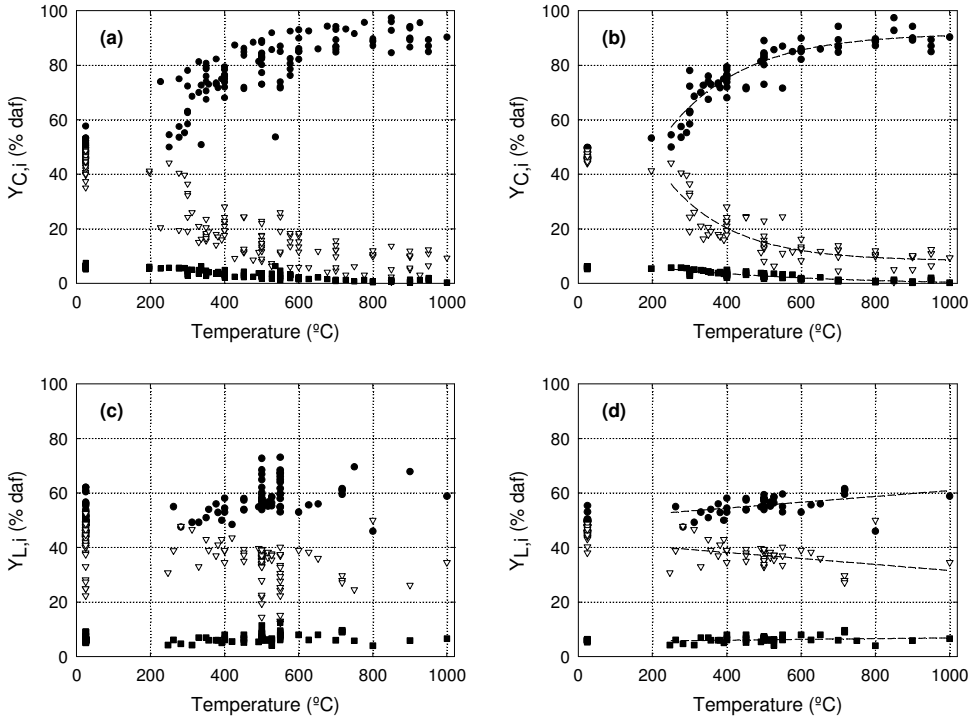

Figure 5: Mass fractions of elements i=C,H,O in chars ($Y_{C,i}$) and organic liquids ($Y_{L,i}$) on a daf basis. Subplots (a) and (c) contain all the recorded data and subplots (b) and (d) contain the recorded data for woody biomasses. Data at 25ºC refers to the parent fuels. [● - "carbon", □ - "oxygen", ■ - "hydrogen"].

4.3.2 Heating value

The recorded data is provided in Fig.6 as follows: (i) data for char come from 13 studies [14,20,27,35,38, 41,58,66,74,78,80,81,87] with around 20 biomasses, (ii) data for organic liquids come from 21 studies [14,20,23, 26,27,41,42,44,48,53,61,62,66,68,70,78,79,82,83,90,91] with around 25 biomasses, and (iii) data for total gas is a compilation of 11 studies [7,14,23,34,35,39, 41,46,50,73, 89] using 18 biomasses.

Above 600ºC the HHV of char most probably fills in the range of 30-35 MJ/kg (Fig.6), which compares with the heating value of some solid fossil fuels. It also fits with the heating value of graphite (33MJ/kg), suggesting that char consists more or less just carbon. A plateau is observed above 600ºC, showing the same trend as char yield (Fig.2) and char CHO composition (Fig.5) (thus, change occurs mainly bellow 600ºC).

With rising temperature from 300ºC to 900ºC the heating value of total permanent gas increases almost linearly, from 2-5MJ/kg to 15-18MJ/kg (Fig.6). At low temperature, the heating value compares with blast furnace gas, while above 800ºC, the heating value is similar to the carburetted water gas [94].

Concerning organic liquids, there is a correspondence between data showing very high carbon content at Fig.5-c and data showing heating values well above 27-28MJ/kg at Fig.6. This information is most often related to specific non-woody biomasses (shells, seeds, etc.). Based on the recorded data, the heating value of organic liquids of woody biomasses is in the range 18-28MJ/kg. This compares with those of alcohol fuels (e.g. ethanol) but is much lower than those of liquid fossil fuels. Since, for woody biomasses, the temperature effect on the CHO composition of organic liquids was found of little importance (Fig.5), it is expected that its heating value remains roughly in the range of 18-28MJ/kg for temperatures typical of gasification systems.

5 CONCLUSIONS

A database on biomass pyrolysis has been presented, where data from 71 investigations and including almost 70 different biomasses, has been structured. In addition to the distribution of the main products (char, total liquids and total gas), data has been collected for pyrolytic water, "tars" and the most relevant light gases: CO_2, CO, H_2, CH_4 and other light hydrocarbons (C_xH_y). The composition and heating value of chars and "tars" has also been summarized.

The essential motivation behind the present database is to achieve a good description of the global mechanism of biomass pyrolysis. Moreover, the collected data will support the development of empiric models to predict the composition of the volatiles. These models are applicable in a number of different situations, since data has been collected from pyrolysis tests under inert atmosphere. Models can be established as function of the fuel composition, heating rate conditions and temperature.

From the present database, data can be especially selected to suit to combustion and gasification conditions. Specific empiric models can be designed from the collected data to describe the volatiles leaving the fuel particles at these conditions. This information is especially useful for comprehensive reactor models.

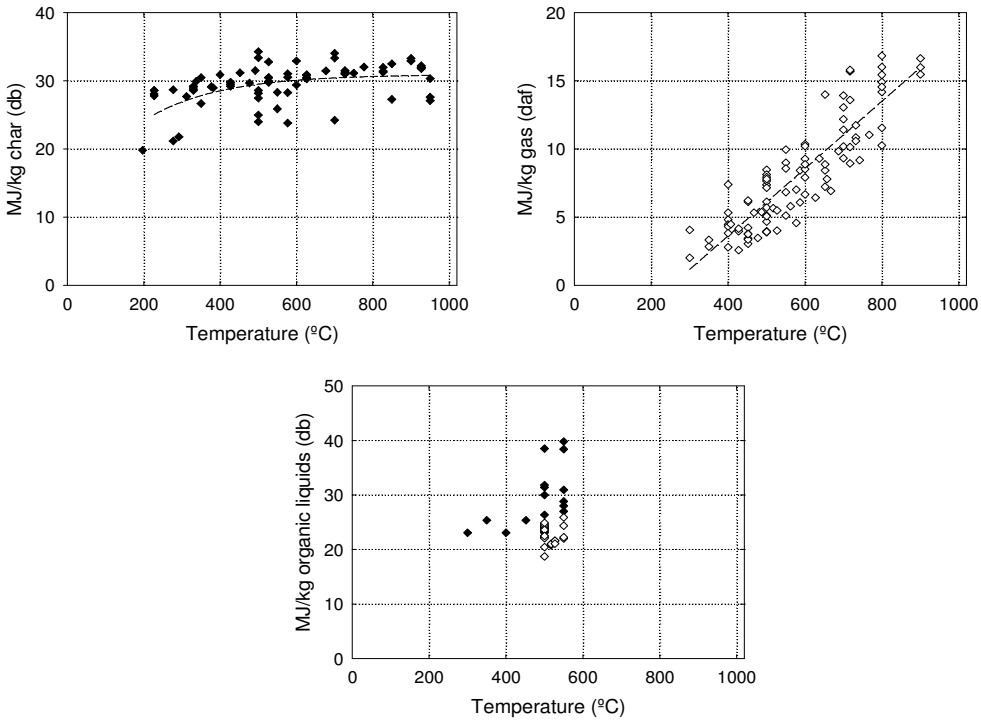

Figure 6: Heating values for char, total permanent gas and organic liquids. [• - "HHV"; ◊ -"LHV"].

For gasification applications, above 800ºC, most of the volatile gases are derived from the conversion of "tars", which seem to be produced at lower temperatures (say <500ºC) directly from fuel decomposition. In fact, the char yield and composition does not evolve appreciably above 600ºC, while the gas yield and composition was found to change rapidly. The "tar" yield is very sensitive to peak temperature but, conversely, it is always highly oxygenated and its composition resembles the one of the parent fuel. In contrast to the other main products, the yield of pyrolytic water seems to remain at around 5-20% within the range of 300-900ºC.

Despite of the variety of fuels, reactors, experimental conditions and testing methodologies, the analysed set of literature-derived data shows that, in general terms, there are tendencies for the most important pyrolysis variables as a function of temperature. For a given temperature, the fuel type and heating rate seem to be the main reason for the dispersion found in data. The effect of other process variables, for example, the amount of sample, particle size, gas residence time, etc., shall be of less importance. The terminology used for liquids ("bio-oil", "tar", water) is not well defined in literature and, coupled with the lack of uniformity of the sampling methods, this introduces some more scattering in the data. In addition, there is yet the uncertainty associated to the measurements.

6 NOMENCLATURE

Y_a - ash content of parent fuel in dry basis, kg/kg dry fuel
Y_m - moisture content of parent fuel in as-received basis, kg/kg as-received fuel
Y_C - yield of dry ash-free char based on dry ash-free fuel, kg/kg daf fuel
Y_L - yield of dry ash-free organic liquids based on dry ash-free fuel, kg/kg daf fuel
Y_W - yield of total dry ash-free water based on dry ash-free fuel, kg/kg daf fuel
Y_G - yield of total dry ash-free pyrolytic gas based on dry ash-free fuel, kg/kg daf fuel
Y_{WV} - yield of dry ash-free pyrolytic water based on dry ash-free fuel, kg/kg daf fuel
$Y_{F,i}$ - mass fraction of element i=CHONS in dry ash-free fuel, kg/kg daf fuel
$Y_{C,i}$ - mass fraction of element i=CHONS in dry ash-free char, kg/kg daf char
$Y_{L,i}$ - mass fraction of element i=CHONS in dry ash-free organic liquids, kg/kg daf char

7 REFERENCES

[1] Di Blasi C. (2008). Combustion and gasification of lignocellulosic chars. Prog. Energy Combust. Sci., 35, 121-140.

[2] Richard N., Thunman H. (2002). General equations for biomass properties. Department of Energy and Environment, Chalmers University of Technology, Sweden.

[3] Di Blasi C. (2008). Modelling chemical and physical processes of wood biomass pyrolysis. Prog. Energy Combust. Sci., 34, 47-90.

[4] Scott S.A., Davidson J.F., Dennis J.S., Hayhurst A.N. (2007). The devolatilisation of particles of a complex fuel (dried sewage sludge) in a fluidised bed. Chem. Eng. Sci., 62, 584-598.

[5] de Diego L.F., García-Labiano F., Abad A., Gayán P., Adánez J. (2003). Effect of moisture content in devolatilisation times of pine wood perticles in a fluidized bed. Energy & Fuels, 17, 285-290.

[6] Scott D.S., Piskorz J. (1984). The continuous flash pyrolysis of biomass. Can. J. Chem. Eng., 62 (3), 404-412.

[7] Wang X., Kersten S.R.A., Prins W., van Swaaij W.P.M. (2005). Biomass pyrolysis in a fluidized bed reactor. Part 2: Experimental validation of model results. Ind. Eng. Chem. Res., 44, 8786-8795.

[8] Di Blasi C. (1993). Modelling and simulation of combustion processes of charring and non-charring solid fuels. Prog. Energy Combust. Sci., 19, 71-104.

[9] Boroson M.L., Howard J.B., Longwell J.P., Peters W.A. (1988). Product yields and kinetics from the vapour phase cracking of wood pyrolysis tars. AIChE J., 35, 120-128.

[10] Boroson M.L., Howard J.B., Longwell J.P., Peters W.A. (1989). Heterogeneous cracking of wood pyrolysis tars over fresh wood char surfaces. Energy & Fuels, 3, 735-740.

[11] Bridgwater A.V., Meier D., Radlein D. (1999). An overview of fast pyrolysis of biomass. Organic Geochemistry, 30, 1479-1493.

[12] Mohan D., Pittman C.U., Steele P.H. (2006). Pyrolysis of wood/biomass for bio-oil: a critical review. Energy & Fuels, 20, 848-889.

[13] Milne T.A., Evans R.J., Abatzoglou N. (1998). Biomass gasifier "tars": their nature, formation and conversion. National Renewable Energy Laboratory, NREL/TP-570-25357, Colorado, U.S.

[14] Fagbemi L., Khezami L., Capart R. (2001). Pyrolysis products from different biomasses: application to the thermal cracking of tar. Applied Energy, 69, 293-306.

[15] Thunman H., Niklasson F., Johnsson F., Leckner B. (2001). Composition of volatile gases and thermochemical properties of wood for modelling of fixed or fluidized beds. Energy & Fuels, 15, 1488-1497.

[16] Moersch O., Spliethoff H., Hein K. R. G. (2000). Tar quantification with a new online analysing method. Biomass & Bioenergy, 18, 79-86.

[17] Oasmaa A., Peacocke C. (2001). A guide to physical property characterisation of biomass-derived fast pyrolysis liquids. Technical Research Centre of Finland, VTT Publications 450, Espoo, Finland.

[18] Hasler Ph., Salzmann R., Kaufmann H.P., Nussbaumer Th. (1998). Method for the sampling and analysis of particles and tars from biomass gasifiers. In: Biomass for Energy and Industry. 10th European Conference and Technology Exhibition, Würzburg, Germany, June 8-11, 1998.

[19] Zanzi R., Sjöström K., Björnbom E. (1996). Rapid high-temperature pyrolysis of biomass in a free-fall reacto. Fuel, 75, 545-550.

[20] Onay Ö., Beis S.H., Koçkar Ö. M. (2004). Pyrolysis of walnut shell in a well-swept fixed-bed reactor. Energy sources, 26, 772-778.

[21] Nunn T., Howard J.B., Longwell J.P., Peters W.A. (1985). Product compositions and kinetics in the

rapid pyrolysis of sweet gum hardwood. Ind. Eng. Chem. Process Des. Dev., 24, 837-841.
[22] Dufour A., Girods P., Masson E., Rogaume Y., Zoulalian A. (2009). Synthesis gas production by biomass pyrolysis: Effect of reactor temperature on product distribution. International Journal of Hydrogen Energy, 34 (4), 1726-1734.
[23] Agblevor F. A., Besler S., Wiselogel A.E. (1995). Fast pyrolysis of stored biomass feedstocks. Energy & Fuels, 9, 3, 637-639.
[24] Sensoz S., Can M. (2002). Pyrolysis of pine (Pinus Brutia Ten.) Chips: 1. Effect of pyrolysis temperature and heating rate on the product yields. Energy Sources, 24, 347-355.
[25] Raveendran K., Ganesh A., Khilar K.C. (1996). Pyrolysis characteristics of biomass and biomass components. Fuel, 75, 8, 988-990.
[26] Özbay N., Apaydin-Varol E., Uzun B.B., Pütün A. E. (2008). Characterization of bio-oil obtained from fruit pulp pyrolysis. Energy, 33, 1234-1236.
[27] Beis S.H., Onay Ö., Koçkar Ö.M. (2002). Fixed-bed pyrolysis of safflower seed: influence of pyrolysis parameters on product yields and compositions. Renewable Energy, 26, 23-29.
[28] Brage C., Yu Q., Chen G., Sjöström K. (1997). Use of amino phase adsorbent for biomass tar sampling and separation. Fuel, 76 (1), 29-37.
[29] Valenzuela C.C., Bernalte G.A., Gómez S.V., Bernalte G.M.J. (1987). Influence of particle size and pyrolysis conditions on yield, density and some textural parameters of chars prepared from holm-oak wood. J. Anal. Appl. Pyrolysis, 12, 61-70.
[30] Maschio, G., Lucchesi, A., Stoppato, G. (1994). Production of syngas from biomass. Bioresource Technology, 48, 119–126.
[31] Demirbas A., Arın G. (2002). An overview of biomass pyrolysis. Energy Sources, 24, 471–482.
[32] Balci S., Dogu T., Yücel H. (1993). Pyrolysis kinetics of lignocellulosic materials. Ind. Chem. Res., 32 (11), 2574-2575.
[33] Barooah J.N., Long V.D. (1976). Rates of thermal decomposition of some carbonaceous materials in a fluidized bed. Fuel, 55, 116-118.
[34] Beaumont O., Schwob Y. (1984). Influence of physical and chemical parameters on wood pyrolysis. Ind. Eng. Chem. Process Des. Dev., 23, 638-640.
[35] Di Blasi C., Signorelli G., Di Russo C., Rea G. (1999). Product distribution from pyrolysis of wood and agricultural residues. Ind. Eng. Chem. Res., 38, 2216-2224.
[36] Di Blasi C., Branca C. (2001). Kinetics of primary product formation from wood pyrolysis. Ind. Eng. Chem. Res., 40, 5550-5554.
[37] Della Roca P.A., Cerrella E.G., Bonelli P.R., Cukierman A.L. (1999). Pyrolysis of hardwoods residues: on kinetics and chars characterization. Biomass and Bioenergy, 16, 80-82.
[38] Demirbas A. (1999). Properties of charcoal derived from hazelnut shell and the production of briquettes using pyrolytic oil. Energy, 24, (2), 142-149.
[39] Encinar J.M., González J.F., González J. (2000). Fixed-bed pyrolysis of Cynara cardunculus L. Product yields and compositions. Fuel Processing Technology, 68, 211- 216.
[40] Gray M.R., Corcoran W.H., Gavalas, G.R. (1985). Pyrolysis of a wood-derived material. Effects of moisture and ash content. Ind. Eng. Chem. Process Des. Dev., 24, 647-650.
[41] Horne P.A., Williams T. (1996). Influence of temperature on the products from the flash pyrolysis of biomass. Fuel, 75 (9), 1052-1054.
[42] Islam M.N., Zailani R., Ani F.N. (1999). Pyrolytic oil from fluidized bed pyrolysis of oil palm shell and its characterization. Renewable Energy, 17, 74-83.
[43] Nunn T., Howard J.B., Longwell J.P., Peters W.A. (1985). Product compositions and kinetics in the rapid pyrolysis of milled wood lignin. Ind. Eng. Chem. Process Des. Dev., 24, 845-850.
[44] Oasmaa A., Kuoppala E. (2003). Fast pyrolysis of forestry residue. 3. Storage stability of liquid fuel. Energy & Fuel, 17, 1076-1079.
[45] Reina J., Velo, E., Puigjaner, L. (1998). Kinetic study of the pyrolysis of waste wood. Ind. Chem. Res., 37, 4291-4291.
[46] Scott D.S., Plskorz J., Radiein D. (1985). Liquid products from the continuous flash pyrolysis of biomass. Ind. Eng. Chem. Process Des. Dev., 24, 581-586.
[47] Scott D.S., Piskorz J., Bergougnou M.A., Graham R., Overend R.P. (1988). The role of temperature in the fast pyrolysis of cellulose and wood. Ind. Chem. Res., 27, 9-14.
[48] Sipilä K., Kuoppala E., Fagernäs L., Oasmaa A. (1998). Characterization of biomass-based flash pyrolysis oils. Biomass and Bioenergy, 14 (2), 106-111.
[49] Thurner F., Mann U. (1981). Kinetic investigation of wood pyrolysis. Ind. Eng. Chem. Process Des. Dev., 20, 482-487.
[50] Williams P.T., Besler S. (1996). The influence of temperature and heating rate on the slow pyrolysis of biomass. Renewable Energy, 7 (3), 234-239.
[51] Chen Y., Charpenay S., Jensen A., Wójtowicz M.A. (1998). Modeling of biomass pyrolysis kinetics. Twenty-Seventh Symposium (International) on Combustion. The combustion Institute, 1328-1331.
[52] Xianwen D., Cguangzhi W., Haibin L., Yong C. (2000). The fast pyrolysis of biomass in CFB reactor. Energy & Fuels, 14, 552-554.
[53] Shihadeh A., Hochgreb S. (2000). Diesel engine combustion of biomass pyrolysis oils. Energy & Fuels, 14, 260-261.
[54] Jenkins B.M., Baxter L.L., Miles Jr, T.R. (1998). Combustion properties of biomass. Fuel processing Technology, 54, 22-27.
[55] Winter F., Prah M.E., Hofbauer H. (1997). Temperatures in a fuel particle burning in a fluidized bed: the effect of drying, devolatilization and char combustion. Combustion and Flame, 108, 303-305.
[56] Dupond C., Commandré J., Gauthier P., Boissonnet G., Salvador S., Schweich D. (2008). Biomass pyrolysis in a analytical entrained flow reactor between 1073K and 1273K. Fuel, 87, 1156-1159.
[57] Shuanging X., Zhihe L., Boaming L., Weiming Y., Xueyuan B. (2006). Devolatilization characteristics of biomass at flash heating rate. Fuel, 85, 665-668.

[58] Channiwala S.A., Parikh P.P. (2002). A unified correlation for estimating HHV of solid, liquid and gaseous fluels. Fuel, 81, 1055-1056.
[59] Parikh J., Channiwala S.A., Ghosal G.K. (2005). A correlation for calculating HHV from proximate analysis of solid fuels. Fuel, 84, 489-491.
[60] Demirbas A. (2002). Analysis of liquid products from biomass via flash pyrolysis. Energy sources, 24, 339-341.
[61] Özbay N., Pütün A.E., Uzun B.B., Pütün E. (2001). Biocrude from biomass: pyrolysis of cottonseed. Renewable Energy, 24, 617-622.
[62] Pütün A.E. (2002). Biomass to bio-oil via fast pyrolysis of cotton straw and stalk. Energy Sources, 24, 276-281.
[63] Çaglar A., Dermibas A. (2002). Conversion of cotton cocoon shell to hydrogen rich gaseous products by pyrolysis. Energy Conversion Management, 43, 491-492.
[64] Güllü D. (2003). Effect of catalyst on yield of liquid products from biomass via pyrolysis. Energy Sources, 25, 755-757.
[65] Uzun B.B., Pütün A.E., Pütün E. (2006). Fast pyrolysis of soybean cake: product yields and compositions. Biosource Technology, 97, 570-573.
[66] Sensöz S., Demiral I., Gerçel F. (2006). Olive bagasse (Olea europea L.) pyrolysis. Biosource Technology, 97, 430-432.
[67] Tuncel F., Gerçel H.F. (2004). Production and characterization of pyrolysis oils from Euphorbia Macroclada. Energy Sources, 26, 762-767.
[68] Onay Ö., Koçkar Ö.M. (2003). Production of bio-oil from biomass: slow pyrolysis of rapeseed (Brassica napus L.) in a fixed-bed reactor. Energy Sources, 25, 880-886.
[69] Dermibas A. (2002). Pyrolysis and steam gasification processes of black liquor. Energy Conversion Management, 43, 879-882.
[70] Pütün A.E., Özcan A., Pütün E. (1999). Pyrolysis of hazelnut shells in a fixed-bed tubular reactor: yields and structural analysis of bio-oil. J. Anal. Appl. Pyrolysis, 52, 35-39.
[71] Sensöz S., Angin D. (2008). Pyrolysis of safflower (Chartamus tinctorius L.) seed press cake: part 1. The effects of pyrolysis parameters on the products yields. Biosource Technology, 99, 5493-5496.
[72] Li L., Zhang H., Zhuang X. (2005). Pyrolysis of waste paper: characterization and composition of pyrolysis oil. Energy Sources, 27, 869-870.
[73] Zanzi R., Sjöström K., Björnbom E. (2002). Rapid pyrolysis of agricultural residues at high temperature. Biomass and Bioenergy, 23, 358-362.
[74] Bonelli P.R., Cerrella E.G., Cukierman A.L. (2003). Slow pyrolysis of nutshells: characterization of derived chars and of process kinetics. Energy Sources, 25, 770-772.
[75] Apaydin-Varol E., Pütün E., Pütün A.E. (2007). Slow pyrolysis of pistachio shell. Fuel, 86, 1895-1896.
[76] Zandersons J., Gravitis J., Kokorevics A., Zhurinsh A., Bikovens O., Tardenaka A., Spince B. (1999). Studies of the Brazilian sugarcane bagasse carbonization process and products properties. Biomass and Bioenergy, 17, 210-217.
[77] Niksa S. (2000). Predicting the rapid devolatilization of diverse forms of biomass with bio-flashchain. Proc. Comb. Inst., 28, 2729-2732.
[78] Pütün A.E., Önay E., Uzun B.B., Özbay N. (2007). Comparison between the 'slow' and 'fast' pyrolysis of tobacco residue. Industrial Crops and Products, 26, 308-312.
[79] Onay Ö, Beis S.H., Koçkar Ö.M. (2001). Fast pyrolysis of rape seed in a well-swept fixed-bed reactor. J. Anal. Appl. Pyrolysis, 58, 996-1002.
[80] Tsai W.T., Lee M.K., Chang Y.M. (2007). Fast pyrolysis of rice husk: product yields and compositions. Biosource Technology, 98, 22-28.
[81] Tsai W.T., Lee M.K., Chang Y.M. (2006). Fast pyrolysis of rice straw, sugarcane bagasse and coconut shell in an induction-heating reactor. J. Anal. Appl. Pyrolysis, 76, 231-234.
[82] Ates F., Pütün E., Pütün A.E. (2004). Fast pyrolysis of sesame stalk: yields and structural analysis of bio-oil. Anal. Appl. Pyrolysis, 71, 779-790.
[83] Miao X., Wu Q. (2004). High yield bio-oil production from fast pyrolysis by metabolic controlling of Chorella protothecoides. Journal of Biotechnology, 110, 87-90.
[84] Jong W., Pirone A., Wójtowicz M.A. (2008). Pyrolysis of miscanthus gianteus and wood pellets: TG-FTIR analysis and reaction and reaction kinetics. Fuel, 82, 1140-1143.
[85] Tsai W.T., Lee M.K., Chang Y.M. (2006). Fast pyrolysis of rice straw, sugarcane bagasse and coconut shell in an induction-heating reactor. J. Anal. Appl. Pyrolysis, 76, 230-237.
[86] Yu Q., Brage C., Chen G., Sjöström K. (1997). Temperature impact on the formation of tar from biomass pyrolysis in a free-fall reactor. J. Anal. Appl. Pyrolysis, 40-41, 481-489.
[87] Schröder E. (2004). Experiments on the pyrolysis of large beechwood particles in fixed beds. J. Anal. Appl. Pyrolysis, 71, 669-694.
[88] Aguado R., Olazar M., José M.J.S., Aguirre G., Bilbao J. (2000). Pyrolysis of Sawdust in a Conical Spouted Bed Reactor. Yields and Product Composition. Ind. Eng. Chem. Res., 39, 1925-1933.
[89] Figueiredo J.L., Valenzuela C., Bernalte A., Encinar J.M. (1989). Pyrolysis of holm-oak wood: influence of temperature and particle size. Fuel, 68, 1012-1016.
[90] Raveendran K., Ganesh A. (1996). Heating value of biomass and biomass pyrolysis products. Fuel, 75 (15), 1715-1720.
[91] Sensoz S., Can M. (2002). Pyrolysis of pine (Pinus Brutia Ten.) Chips: 2. Structural Analysis of Bio-oil. Energy Sources, 24, 357-364.
[92] Thunman H., Leckner B. (2002). Thermal conductivity of wood – models for different stages of combustion. Biomass & Bioenergy, 23, 47-54.
[93] Elliot D.C. (1988). Relation of Reaction Time and Temperature to Chemical Composition of Pyrolysis Oils. In Pyrolysis Oils from Biomass: Producing, Analysing and Upgrading (ACS Symposium Series 376); Soltes E.D., Milne T.A. Ed., ACS, Washington D.C., 1998.
[94] Culp A. W. (1991) Principles of Energy Conversion, 2nd Edition, McGraw-Hill.

8 ACKNOWLEDGEMENTS

This work has been financially supported by a grant from the Fundação para a Ciência e a Tecnologia (FCT), Portugal (SFRH/BD/39567/2007).

Appendix IV - Empirical correlations for biomass pyrolysis predictions

18th European Biomass Conference & Exhibition – Lyon, France, 2010

EMPIRICAL CORRELATIONS FOR BIOMASS PYROLYSIS PREDICTIONS

18th BIOMASS CONFERENCE – LYON, FRANCE, 2010

D. Neves[a,b], H. Thunmanb, A. Matos[a], L. Tarelho[a], A. Gómez-Barea[c]

[a] Department of Environment and Planning and Centre of Environmental and Marine Studies, University of Aveiro, Campus Universitário de Santiago, 3810-193 Aveiro, Portugal. Tel.: +351234370349, Fax: +351234370309; [b] Department of Energy and Environment, Chalmers University of Technology, SE-412 96 Goteborg, Sweden. Tel.: +46317721000, Fax: +46317723592; [c] Bioenergy Group, Chemical and Environmental Engineering Department, Escuela Superior de Ingenieros (University of Seville), Camino de los Descubrimientos s/n, 41092-Seville, Spain. Tel.: +34954487223, Fax: +34954461775.

ABSTRACT: This work provides literature data on the characteristics of biomass pyrolysis. It is analyzed the behavior of product yields and properties on pyrolysis peak temperature dependence (within 200-1000ºC). Empirical relationships are derived from the collected data, which can be used to approximate the elemental composition and heating value of chars, tars and total permanent gas as well as yields of carbon monoxide, hydrogen and light hydrocarbons. Some of these relationships seem valid for almost any biomass and are roughly independent of the pyrolysis conditions. Since pyrolysis is a common stage on the thermo-chemical conversion of solid biomass, the information provided here can be applied in the scope of pyrolysis, gasification and combustion applications.

Keywords: volatiles, char, tar, pyrolysis, gasification, combustion.

1 INTRODUCTION

Thermo-chemical conversion of solid carbonaceous fuels evolves a set of sequential stages that includes drying, pyrolysis (or devolatilization) and gasification or combustion. Drying and pyrolysis are driven by heat transport (i.e. temperature) to the fuel particles causing it to thermal decompose into moisture, pyrolytic volatiles and char. Due to high volatile matter content, pyrolysis is a key stage on the conversion of solid biomass leading to a significant mass loss of the parent fuel particles. The release of volatiles from the solid fuel can be seen as the primary pyrolysis step, to distinguish from the secondary conversion of the primary products. While primary pyrolysis is complete bellow around 500-600ºC, the secondary reactions are only active at higher temperature. Under inert atmosphere (i.e. only by temperature effect), secondary reactions include mainly thermal cracking of selected volatiles but, under O_2, H_2O or CO_2 enriched atmospheres, there is further reforming, combustion and gasification reactions of volatiles and/or char. Knowledge on the quantities and composition of pyrolytic products (i.e., those resulting from the thermal decomposition of parent fuel and including the effect of secondary reactions) is needed for a better understanding of solid biomass thermo-chemical conversion, especially during pyrolysis and gasification applications.

A huge amount of literature data has been produced on the behavior of biomass upon pyrolysis, regarding kinetics, product yields and product properties. The experimental rigs, operating conditions, biomass type, methodologies and measurements have varied widely among investigations. A common feature is that biomass is thermally converted under a sweep of inert carrier gas and the volatiles are rapidly cooled down. Therefore, the resulting experimental data has good deal of usefulness in different situations since the pyrolytic products were not further reacted with O_2, H_2O, CO_2, etc. to a significant extent. Some literature data on the pyrolysis of a variety of solid biomasses has been structured in a database in a previous work [1]. The analysis of the collected data has shown that: (i) general trends exist for product yields and properties as a function of reactor peak temperature, (ii) for a given peak temperature, the heating rate and fuel type (wood *vs.* non-wood) explains most of variability in data, and (iii) simplified particle models, based on mass and energy balances and empirical relationships, can be developed to predict the yields of volatiles released from specific biomass under various pyrolysis conditions.

In this work it is presented some literature data on the composition of char, tar and permanent pyrolysis gas. Empirical relationships are derived from the collected data. The information provided has practical use in engineering applications where first estimates of pyrolytic product yields and properties are necessary.

2 METHODS

The database developed consists of a MSExcell® worksheet, where it is structured data collected from 66 investigations [2-67], including a huge number of solid biomasses (woody and non-woody) having particles of a variety of shapes and sizes (between 0.05 to 100mm), and reactor peak temperature within 200-1000ºC. For each investigation, the recorded information includes: (i) reactor type (e.g. fixed bed), (ii) reactor scale (industrial, pilot or laboratory), (iii) type of biomass (e.g. spruce, pine), (iv) nature of the biomass, taken wood as reference (wood *vs.* non-wood), (v) value of the heating rate (e.g. 500ºC/min), (vi) classification of heating rate according to "slow" *vs.* "fast", (vii) fuel properties (ash content, moisture content, elemental composition, particle size and heating value), (viii) the dependence of product yields and properties on peak temperature and (ix) a variety of observations like residence time, catalyst, etc. A description on how the literature data has been implemented in the referred database can be found elsewhere [1]. A simplified description of pyrolytic volatiles has been accomplished by lumping a huge number of individual species into few groups: H_2O, CO_2, CO, H_2, CH_4, non-methane light (non-condensable) hydrocarbons (C_xH_y) and condensable (liquids at ambient conditions) organic compounds (here simply referred as "tars"). Mass product yields have been expressed on a

dry ash-free (daf) fuel basis. The distinction between "slow heating rates" and "fast heating rates" is here based on the threshold of 1000ºC/min. The selection of regression models was done by a trial-and-error strategy, where the observed trends were taken in account. Models with higher squared correlation coefficient (R^2) were selected.

3 RESULTS

3.1 Product property

3.1.1 Elemental composition

The normalized C, H and O composition of parent biomasses and respective chars and tars produced under diverse pyrolysis conditions is presented in Fig. 1. The data has been collected from various investigations [2,4, 6-8,11-13,15,16,18,20,21,24-28,30-32,34,37,39,40,43,44, 47,49,51,52,54,55,58,59,61,63,65,67], regardless of fuel, reactors and pyrolysis conditions. While the composition of parent fuels ranges within roughly 45-65% carbon, 5-10% hydrogen and 25-50% oxygen, the one of tars is within 45-75% carbon, 5-15% hydrogen and 10-50% oxygen, and the one of chars within 50-99% carbon, 0.3-8% hydrogen and 0.5-45% oxygen (mass %, daf basis). The CHO composition of tars is relatively close to the one of parent fuels. However, ultimate analysis of chars varies widely: roughly from the composition of biomass to the one of graphite (i.e. 100% carbon). On a first glance, there appears that the composition of tars is mainly dependent on the composition of parent biomass while the composition of chars is more sensitive to the pyrolysis conditions. In Fig.2 the mass ratios of carbon content of tars and chars to the respective carbon content of parent fuels are plotted against peak temperature. Although there is some scatter in the collected data, it can be observed that at progressively higher temperatures the produced chars are more enriched in carbon than tars. Above 800ºC the carbon content of char roughly doubles the one of parent fuel while the collected data for tars is always within 0.92-1.35 kgC/kgC (average of 1.14) A common aspect among chars and tars is that the carbon mass ratios tend to the unity as temperature decreases. Temperature (ºC) dependent carbon ratios are expressed here arbitrarily by Eq. 1 and 2, respectively for char and tar.

$$Y_{C,ch} \Big/ Y_{C,F} = 2.051 - 1.594 \cdot \exp(-0.26 \cdot 10^{-2} \cdot T)$$

n=85 R^2=0.58 Eq.1

$$Y_{C,tar} \Big/ Y_{C,F} = 1.047 + 1.9 \cdot 10^{-4} \cdot T$$

n=67 R^2=0.07 Eq.2

General relationships for the O/C and H/C mass ratios of chars and tars as a function of respective carbon contents are presented in Fig.3. For carbon contents bellow 60%, the H/C and O/C ratios of tars are similar to those of chars. The increase of carbon content of chars with increasing peak temperature (Fig.2) is coupled with a massive loss of hydrogen and oxygen; however, the sharp increase of carbon content of tars is couple with a decrease of oxygen and increase of hydrogen. Anyway, lumped tars are highly oxygenated. Fig.1 to 3 suggests that the primary tars released from solid fuel are progressively converted into more aromatic structures as temperature increases. This can be seen as a conversion towards more thermally stable tars [68]: examples of low temperature tars (<650ºC) are guaicols and phenols while at high temperature (>900ºC) it can appear some poli-aromatic hydrocarbons. Better fitting of O/C and H/C mass ratios vs. carbon content of char or tar were achieved by relationships with the form of Eq.3, with coefficients, range of validity and R^2 given in Table I.

$$\frac{Y_{j,i}}{Y_{C,i}} = k1 + \frac{k2 \cdot Y_{C,i}}{k3 + Y_{C,i}} \qquad j=H,O \quad i=tar,char \quad \text{Eq. 3}$$

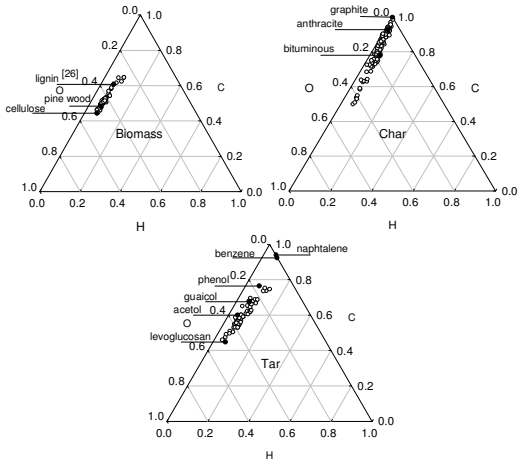

Figure 1: Normalized C,H and O composition of parent biomasses, chars and tars (mass fractions).

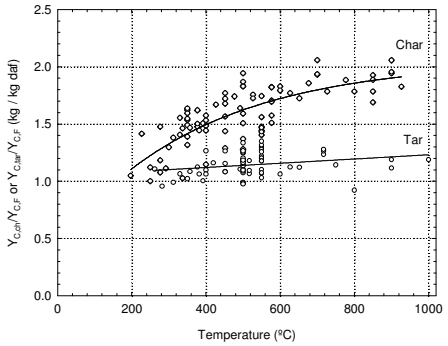

Figure 2: Mass ratios of carbon content in char ($Y_{C,ch}$) and tar ($Y_{C,tar}$) to the respective carbon content in parent fuels ($Y_{C,F}$), as a function of pyrolysis peak temperature. Solid lines are given by Eq.1 and 2.

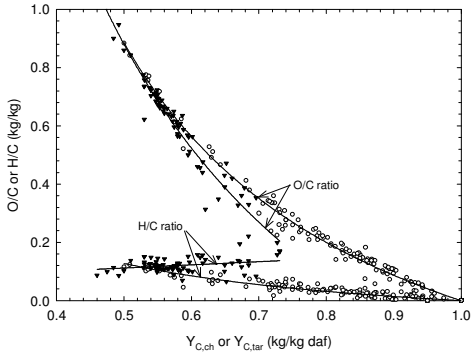

Figure 3: O/C and H/C mass ratios of chars and tars as a function of carbon content of char ($Y_{C,ch}$) or tar ($Y_{C,tar}$), respectively [○ –char, ▼ – tar]. Solid lines are given by Eq.3 with coefficients according to Table I.

Table I: Coefficients of the non-linear fits to plots of O/C or H/C mass ratios of chars and tars vs. respective carbon contents. [k1, k2 and k3 according to Eq.3. R^2 is the square of correlation coefficient for the result of curve fitting to n data-points].

i	Ratio (kg j/kg C)	k1	k2	k3	$Y_{C,i}$ (kg C/kg i)	n	R^2
Char	$Y_{O,ch}/Y_{C,ch}$	-6.135	5.446	$-1.121\cdot10^{-1}$	0.5 to 0.99	116	0.99
	$Y_{H,ch}/Y_{C,ch}$	-274.822	274.694	$-4.646\cdot10^{-4}$	0.5 to 0.99	120	0.90
Tar	$Y_{O,tar}/Y_{C,tar}$	-895.258	894.0	$-1.192\cdot10^{-3}$	0.5 to 0.73	74	0.94
	$Y_{H,tar}/Y_{C,tar}$	$5.718\cdot10^{-2}$	$2.152\cdot10^{4}$	$1.971\cdot10^{5}$	0.5 to 0.73	74	0.10

3.1.2 Heating value

The collected data on the heating value of chars, tars and total permanent pyrolysis gas [2,4,6,8,11,12,17,18, 21,22,24,25,28,30,32,34,37,39,40,44,47,50,51,54-59,61, 63-65,67] are provided in Fig. 4 to 6, again related to diverse biomasses, reactors and operating conditions. Data for chars and total gas are available over a wide temperature range but data for tars are concentrated within 450-550ºC. This is because investigations focus on the characterization of tars at temperatures that yields more bio-oil. The scatter in the collected data is high, namely concerning the data for tars which shows variations up to 20MJ/kg (Fig.5).

Dashed lines in Fig. 4 and 5 are given by an empirical correlation [37] to predict the HHV of fuels from the respective elemental composition. This correlation has been used here with the aim of drawing the trends of the HHV of chars and tars based on data presented in Fig. 2, for which two biomasses with carbon content (denoted $Y_{C,F}$) of 0.47 kgC/kgF and 0.52 kgC/kgF (daf mass basis) were considered as example. Therefore, Eq. 1 to 3 were used to predict the CHO composition of respective chars and tars as function of peak temperature. Since the nitrogen and sulphur contents are inputs in the quoted correlation for HHV [37], here the nitrogen content was calculated by difference based on the dry ash-free parts of chars and tars and the sulphur content was neglected. The results are in good agreement with the collected data for chars (Fig. 4). It also indicates that the HHV of tars increase with increasing peak temperature (Fig.5), although the collect data do not permit to ascertain this behavior on temperature dependence.

The heating value of chars compares with those of solid fossil fuels, namely above around 600ºC where it is most probably within 30-35 MJ/kg (Fig 4). The drawn dashed lines tend to the HHV of graphite (≈33 MJ/kg) as temperatures increases. Concerning tars, data showing heating values above 35MJ/kg refers to pyrolysis of high carbon seeds (>60% carbon, mass % daf basis) [12,55,67] (Fig.5). Conversely, the collected data for wood derived tars is within 18-28 MJ/kg. Therefore, the heating value of tars compares with those of alcohol fuels but, typically, it is lower than those of liquid fossil fuels.

The lower heating value (LHV) of total permanent gas increases with rising pyrolysis peak temperature (Fig. 6). Bellow 400ºC it is typically within 2-5 MJ/kg, which compares with a blast furnace gas, but above 800ºC it increases to roughly 12-18 MJ/kg. Therefore, at the highest temperatures, the heating value of a pyrolysis gas can approach the one of a carbureted water-gas but it is always much lower than those of gaseous fossil fuels. Moreover, it appears that woody biomasses generate a pyrolysis gas with higher heating value than non-woody biomasses (Fig.6). A temperature-dependent LHV of pyrolysis gas (LHV_G) is here arbitrarily given by Eq. 4.

$$LHV_G = -6.23 + 0.0247 \cdot T \qquad n=98 \qquad R^2=0.78 \quad \text{Eq.4}$$

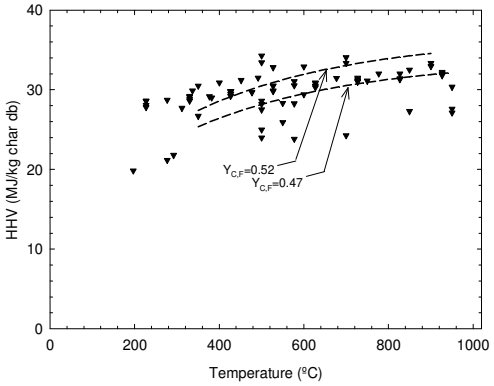

Figure 4: Heating value of chars (dry basis) as a function of pyrolysis peak temperature. Dashed lines are given by an empirical correlation [37], based on the Eq. 1 and 3 for the CHO composition of char.

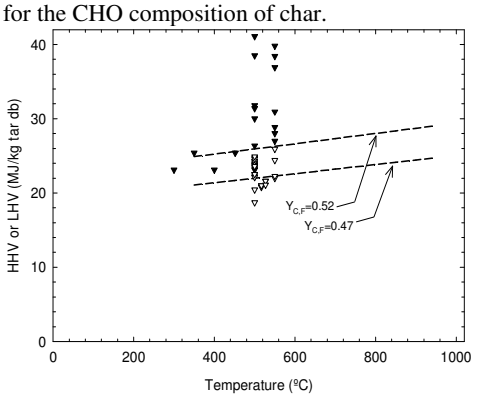

Figure 5: Heating value of tars (dry basis) as a function of pyrolysis peak temperature. Dashed lines are given by an empirical correlation [37], based on the Eq. 2 and 3 for the CHO composition of tar. [▼ - HHV; □ - LHV].

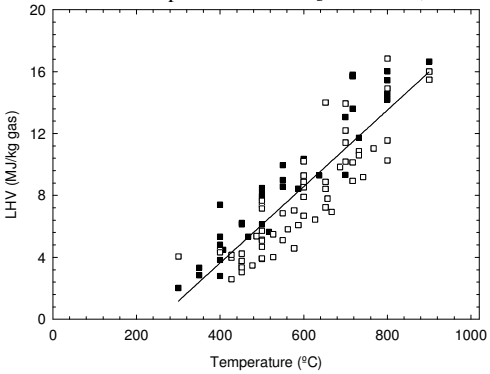

Figure 6: Heating value of total permanent gas as a function of pyrolysis peak temperature. Solid line is given by Eq. 4. [■ - wood; □ - non-wood].

3.2 Yield of main combustible gases

The collected data on the yields of CO, H_2, CH_4 and C_xH_y [4,7,8,17,18,22,24,26,28,29,46] are plotted in Fig. 7 and 9. As before, these data are relative to various biomass fuels, reactors and operating conditions. Apart from CH_4, typically the measurement data on the production of light hydrocarbons are related to a limited number of individual species. The most common is that only some C_2 and C_3 hydrocarbons are measured, although hydrocarbons up to say C_5 can be found in the gas-phase. Thus, the collected data on the yield of C_xH_y can be viewed as a reasonable estimate for the yield of lumped C_2+C_3 fractions but not so good for the whole non-methane light hydrocarbons [1].

Up to around 550-600ºC, peak temperature seems of little influence on determining the yields of CO, CH_4 and H_2 (Fig.7). Bellow this temperature range these yields are typically bellow, 10%, 1% and 0.1% (mass % of daf fuel), respectively for CO, CH_4 and H_2. However, above 600ºC the gas yields become a strong function of pyrolysis peak temperature. Typically, above 800ºC gas yields become higher than 20%, 3% and 0.5% (mass % of daf fuel), respectively for CO, CH_4 and H_2. This behavior of gas yields *vs.* peak temperature resembles the two-step biomass pyrolysis, where the first step is the primary release of volatiles and the second step is its secondary conversion. Literature data show that during pyrolysis, biomass losses most of its original mass up to around 600ºC while tars are only appreciably converted above this temperature [1]. Hence, the gas yields bellow 550-600ºC (Fig. 7) are likely a result of the thermal break down of the parent fuel structures, while above 600ºC its strong dependence on temperature is an indication of the activity of the secondary reactions of volatiles (mainly tars). Accordingly, both CO and CH_4 are produced during the primary decomposition while H_2 is mostly a product of the secondary reactions of volatiles. This is in good agreement with the experimental data of Funazukuri et al. [69] who observed that: (i) up to almost a complete release of volatiles, the gas yields were well correlated with fuel mass loss but independent of peak temperature, and (ii) thereafter, peak temperature was of increasing importance on determining gas yields. Thus, there appears that bellow around 550-600ºC, CO and CH_4 yields depends mainly on the quantity of fuel already decomposed while above that temperature it is mostly driven by peak temperature.

From the collected data, temperature-dependent yields of CO, CH_4 and H_2 (denoted by $Y_{i,F}$, where i is the i^{th} pyrolytic product and F the daf fuel) are here satisfactorily fitted by Eq.5, with regression coefficients, range of validity, number of data points and R^2 given in Table II.

$$Y_{i,F} = k1 + k2 \cdot \left(1 - \exp\left(-k3 \cdot T\right)\right)^{k4} \quad i=CO,CH_4,H_2 \quad \text{Eq. 5}$$

A similar behavior for CO, CH_4 and H_2 yields *vs.* pyrolysis peak temperature suggests correlating the yields of two gases against the yield of the third gas. By using data in Fig. 7, the yields of CH_4 and H_2 were here plotted vs. the respective yields of CO (Fig.8), showing a very similar behavior. These results are also in agreement with previous reviews of literature data on this matter [28,69]. It is worth to point out that Fig. 8 is made of data from investigations where biomass has been heated up to various temperatures (within 300-1000ºC); so, in case of experiments above around 600ºC, the behavior shown combines the effect of both primary pyrolysis and secondary reactions. It has been found that heating rate, particle size, degree of parent fuel conversion and peak temperature does not affect this kind of relationships [69], although it depends slightly on the biomass being pyrolysed [28]. Despite of this, good correlation (Table III) was obtained from the collected data, which accounts for pyrolysis of diverse biomasses.

Figure 9 show the yields of CH_4+C_xH_y as a function of respective yields of CH_4. A linear relationship is also obtained. Since here C_xH_y approximates the yield of C_2+C_3 light hydrocarbons, it can be concluded that these hydrocarbon fractions behave as CH_4 on peak temperature dependence. Identical results can also be found in the literature [69]. These results suggests that similar formation/destruction pathways for both CH_4 and C_2+C_3 hydrocarbons.

In this work, the plots of specific gas yields against another gas yield (Fig. 8 and 9) were fitted by linear relationships (Eq.6 and 7), with coefficients, range of validity, number of data-pints and R^2 given in Table III.

$$Y_{i,F} = k1 + k2 \cdot Y_{CO,F} \quad i=CH_4, H_2 \quad \text{Eq. 6}$$

$$Y_{CH4,F} + Y_{CxHy,F} = k1 + k2 \cdot Y_{CH4,F} \quad \text{Eq. 7}$$

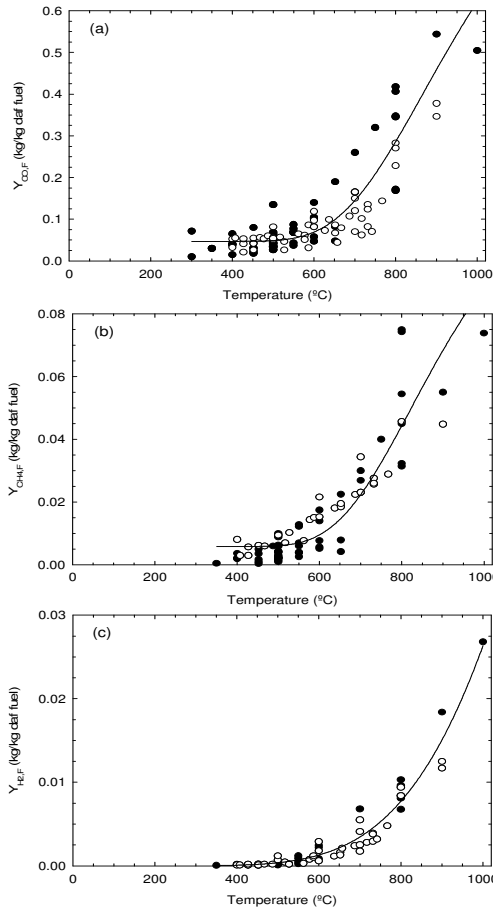

Figure 7: Yields of (a) CO, (b) CH_4 and (c) H_2 as a function of pyrolysis peak temperature. Solid lines are given by Eq.5 with coefficients according to Table II [○ - slow heating rates; ● - fast heating rates].

Table II: Coefficients of the non-linear fits to plots of CO, CH_4 and H_2 yields *vs.* pyrolysis peak temperature. [k1, k2, k3 and k4 according to Eq.5. T is temperature inºC. R^2 is the square of correlation coefficient for the result of curve fitting to n data-points].

i	Yield (kg/kg daf fuel)	k1	k2	k3	k4	T (ºC)	n	R^2
CO	$Y_{CO,F}$	0.047	0.975	$0.485 \cdot 10^{-2}$	67.48	300 to 1000	108	0.76
CH_4	$Y_{CH4,F}$	$0.58 \cdot 10^{-2}$	0.120	$0.55 \cdot 10^{-2}$	93.61	350 to 1000	78	0.82
H_2	$Y_{H2,F}$	0.0	1.145	$0.11 \cdot 10^{-2}$	9.38	350 to 1000	65	0.94

Table III: Coefficients of the linear fits to plots of CH_4 and H_2 yields *vs.* CO yields and $CH_4+C_xH_y$ yields *vs.* CH_4 yields. [k1 and k2 according to Eq. 6 and 7. R^2 is the square of correlation coefficient for the result of curve fitting to n data-points].

	i	Yield (kg/kg daf fuel)	k1	k2	$Y_{CO,F}$ (kg/kg daf fuel)	$Y_{CH4,F}$ (kg/kg daf fuel)		R^2
Eq. 6	CH_4	$Y_{CH4,F}$	$-8.95 \cdot 10^{-4}$	$14.45 \cdot 10^{-2}$	0.04 to 0.55	--	77	0.89
	H_2	$Y_{H2,F}$	$-1.55 \cdot 10^{-3}$	$3.81 \cdot 10^{-2}$	0.04 to 0.55	--	57	0.87
Eq. 7	--	$Y_{CH4,F}+ Y_{CxHy,F}$	$1.60 \cdot 10^{-3}$	1.51	--	0.001 to 0.075	58	0.94

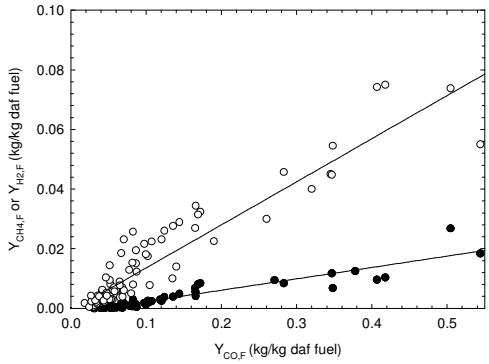

Figure 8: Yields of CH_4 ($Y_{CH4,F}$) and H_2 ($Y_{H2,F}$) as a function of the respective yield of CO ($Y_{CO,F}$). Solid lines are given by Eq.6 with coefficients according to Table III. [○ – CH_4; ● – H_2].

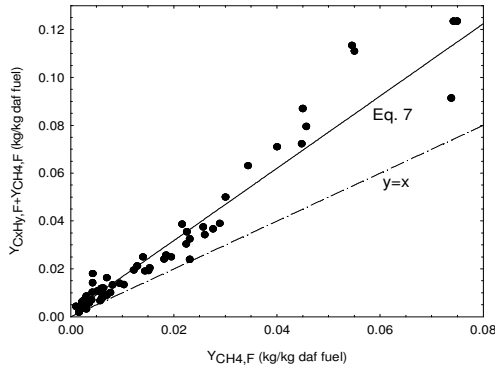

Figure 9: Yields of $C_xH_y+CH_4$ ($Y_{CxHy,F}+Y_{CH4,F}$) as a function of the respective yields of CH_4 ($Y_{CH4,F}$). Solid line is given by Eq.7 with coefficients according to Table III.

4 CONCLUSIONS

From a database of experimental results on biomass pyrolysis, empirical relationships have been developed to approximate selected properties (elemental composition and heating value) of pyrolytic products and yields of main combustible permanent gases. Despite of the variety of biomass fuels, reactors, operating conditions and methodologies among the analyzed investigations, some of these relationships can be of very general use.

There is a distinct behavior on the CHO composition of biomass derived chars and tars as a function of pyrolysis peak temperature. The carbon content of char increases rapidly with increasing temperature while the one of tar shows weak temperature dependence. At high temperatures (say, >600ºC) chars are very depleted of oxygen and hydrogen but tars are still highly oxygenated. Moreover, in opposition to chars, the hydrogen content of tars increases slightly with peak temperature. In someway the composition of tars resembles the one of parent fuels; this further suggests that biomass undergoes low temperature cleavage (i.e. primary pyrolysis) into smaller organic molecules (i.e. tars) without an extensive modification of the parent chemical structures.

The heating value of chars and total permanent gas increases with pyrolysis peak temperature. In particular, a linear fit of the LHV of gas *vs.* peak temperature is good over a wide range of temperature. However, the collected data do not permit to draw the respective trend for tars. In an attempt overcome the scarcity of data, the heating value of tars was estimated from the respective elemental composition showing also a weak dependence on peak temperature. Typically, the heating value of chars, tars and permanent gas ranges within roughly 25-35MJ/kg, 20-30MJ/kg and 2-18MJ/kg, respectively.

The yields of the main combustible gases, CO, CH_4 and H_2, show a very similar pattern of change with peak temperature. Bellow around 550-600ºC the release of these gases from solid fuel is more or less independent of peak temperature but thereafter it depends strongly of temperature. CO and CH_4 are products of both primary pyrolysis and secondary reactions while H_2 seems mainly a product of secondary reactions of volatiles. General relationships exist for the yields of CH_4 and H_2 as a function of respective CO yields. Yields of total light hydrocarbons ($CH_4+C_xH_y$) are also well correlated with yields of CH_4. These relationships are weekly dependent on the biomass under conversion and apply over a wide range of pyrolysis conditions.

5 NOMENCLATURE

T - pyrolysis (reactor) peak temperature (ºC)
$Y_{i,F}$ – yield of i^{th} pyrolytic product in a dry ash-free fuel basis (kg i/kg dry ash-free fuel)
$Y_{j,F}$ – mass fraction of j^{th} element in fuel, dry ash-free fuel basis (kg j/kg dry ash-free fuel)
$Y_{j,i}$ – mass fraction of j^{th} element in i^{th} pyrolytic product (kg j/kg i)
k1, k2, k3, k4 – regression coefficients
R^2 – square of the correlation coefficient
n – number of data-points

Subscripts
i = G, total pyrolytic permanent gas
= ch, dry ash-free char
= tar, lumped condensable compounds, liquids at ambient conditions
= C_xH_y, lumped non-methane light hydrocarbons, non-condensable at ambient conditions
= CO, carbon monoxide
= CH_4, methane
= H_2, hydrogen
j = C, carbon element
= H, hydrogen element
= O, oxygen element

Abbreviations
db – dry basis
daf – dry ash-free basis
LHV – lower heating value (MJ/kg)
HHV – higher heating value (MJ/kg)

6 REFERENCES

[1] Neves D, Thunman H, Seeman M, Ideias P, Matos A, Tarelho L, Gómez-Barea A. A database on biomass pyrolysis for gasification applications. Proceedings of the 17th European Biomass Conference & Exhibition: 1018-1028. Hamburg, Germany, 2009.

[2] Wang X, Kersten SRA, Prins W, van Swaaij WPM. Biomass pyrolysis in fluidizes bed reactor. Part 2: Experimental validation of model results. Ind. Eng. Chem. Res. 2005;44:8786-8795.

[3] Bridgwater AV, Meier D, Radlein D. An overview of fast pyrolysis of biomass. Organic Geochemistry 1999;30:1479-1493.

[4] Fagbemi L, Khezami L, Capart R. Pyrolysis products from different biomasses: application to the thermal cracking of tar. Applied Energy 2001;69:293-306.

[5] Thunman H, Niklasson F, Johnsson F, Leckner B. Composition of volatile gases and thermochemical properties of wood for modeling of fixed or fluidized beds. Energy & Fuels 2001;15:1488-1497.

[6] Onay O, Beis SH, Koçkar OM. Pyrolysis of walnut shell in a well-swept fixed-bed reactor. Energy Sources 2004;26:771-782.

[7] Nunn T, Howard JB, Longwell JP, Peters WA. Product compositions and kinetics in the rapid pyrolysis of sweet gum hardwood. Ind. Eng. Chem. Process Des. Dev. 1985;24:837-841.

[8] Agblevor FA, Besler S, Wiselogel AE. Fast pyrolysis of stored biomass feedstocks. Energy & Fuels 1995;9:635-640.

[9] Sensöz S, Can M. Pyrolysis of pine (Pinus Brutia Ten.) Chips: 1. Effect of pyrolysis temperature and heating rate on the product yields. Energy Sources 2002;24:347-355.

[10] Raveendran K, Ganesh A, Khilar KC. Pyrolysis characteristics of biomass and biomass components. Fuel 1996;75:987-998.

[11] Özbay N, Apaydin-Varol E, Uzun BB, Pütün AE. Characterization of bio-oil obtained from fruit pulp pyrolysis. Energy 2008;33:1233-1240.

[12] Beis SH, Onay O, Koçkar OM. Fixed-bed pyrolysis of safflower seed: influence of pyrolysis parameters on product yields and compositions. Renewable Energy 2002;26:21-32.

[13] Valenzuela C, Bernalte A, Gómez V, Bernate M. Influence of particle size and pyrolysis conditions on yield, density and some textural parameters of chars prepared from holm-oak wood. J. Anal. Appl. Pyrolysis 1987;12:61-70.

[14] Demirbas A, Arin G. An overview of biomass pyrolysis. Energy Sources 2002;24:471–482.

[15] Balci S, Dogu T, Yücel H. Pyrolysis kinetics of lignocellulosic materials. Ind. Chem. Res. 1993;32:2573-2579.

[16] Barooah JN, Long VD. Rates of thermal decomposition of some carbonaceous materials in a fluidized bed. Fuel 1976;55:116-120.

[17] Beaumont O, Schwob Y. Influence of physical and chemical parameters on wood pyrolysis. Ind. Eng. Chem. Process Des. Dev. 1984;23:637-641.

[18] Di Blasi C, Signorelli G, Di Russo C, Rea G. Product distribution from pyrolysis of wood and agricultural residues. Ind. Eng. Chem. Res. 1999;38:2216-2224.

[19] Di Blasi C, Branca C. Kinetics of primary product formation from wood pyrolysis. Ind. Eng. Chem. Res. 2001;40:5547-5556.

[20] Della Roca PA, Cerrella EG, Bonelli PR, Cukierman AL. Pyrolysis of hardwoods residues: on kinetics and chars characterization. Biomass and Bioenergy 1999;16:79-88.

[21] Demirbas A. Properties of charcoal derived from hazelnut shell and the production of briquettes using pyrolytic oil. Energy 1999;24:141-150.

[22] Encinar JM, González JF, González J. Fixed-bed pyrolysis of Cynara cardunculus L. Product yields and compositions. Fuel Processing Technology 2000;68:209- 222.

[23] Gray MR, Corcoran WH, Gavalas GR. Pyrolysis of a wood-derived material. Effects of moisture and ash content. Ind. Eng. Chem. Process Des. Dev. 1985;24:646-651.

[24] Horne PA, Williams T. Influence of temperature on the products from the flash pyrolysis of biomass. Fuel 1996;75:1051-1059.

[25] Islam MN, Zailani R, Ani FN. Pyrolytic oil from fluidized bed pyrolysis of oil palm shell and its characterization. Renewable Energy 1999;17:73-84.

[26] Nunn T, Howard JB, Longwell JP, Peters WA. Product compositions and kinetics in the rapid

pyrolysis of milled wood lignin. Ind. Eng. Chem. Process Des. Dev. 1985;24:844-852.
[27] Oasmaa A, Kuoppala E. Fast pyrolysis of forestry residue. 3. Storage stability of liquid fuel. Energy & Fuels 2003;17:1075-1084.
[28] Scott DS, Piskorz J, Radlein D. Liquid products from the continuous flash pyrolysis of biomass. Ind. Eng. Chem. Process Des. Dev. 1985;24:581-588.
[29] Scott DS, Piskorz J, Bergougnou MA, Graham R, Overend RP. The role of temperature in the fast pyrolysis of cellulose and wood. Ind. Chem. Res. 1988;27:8-15.
[30] Sipilä K, Kuoppala E, Fagernäs L, Oasmaa A. Characterization of biomass-based flash pyrolysis oils. Biomass and Bioenergy 1998;14:103-113.
[31] Thurner F, Mann U. Kinetic investigation of wood pyrolysis. Ind. Eng. Chem. Process Des. Dev. 1981;20:482-488.
[32] Williams PT, Besler S. The influence of temperature and heating rate on the slow pyrolysis of biomass. Renewable Energy 1996;7:233-250.
[33] Xianwen D, Chuangzhi W, Haibin L, Yong C. The fast pyrolysis of biomass in CFB reactor. Energy & Fuels 2000;14:552-557.
[34] Shihadeh A, Hochgreb S. Diesel engine combustion of biomass pyrolysis oils. Energy & Fuels 2000;14;260-274.
[35] Dupont C, Commandré JM, Gauthier P, Boissonnet G, Salvador S, Schweich D. Biomass pyrolysis experiments in an analytical entrained flow reactor between 1073K and 1273K. Fuel 2008;87:1155-1164.
[36] Shuanging X, Zhihe L, Boaming L, Weiming Y, Xueyuan B. Devolatilization characteristics of biomass at flash heating rate. Fuel 2006;85:664-670.
[37] Channiwala SA, Parikh PP. A unified correlation for estimating HHV of solid, liquid and gaseous fluels. Fuel 2002;81;1051-1063.
[38] Demirbas A. Analysis of liquid products from biomass via flash pyrolysis. Energy sources 2002;24:337-345.
[39] Özbay N, Pütün AE, Uzun BB, Pütün E. Biocrude from biomass: pyrolysis of cottonseed cake. Renewable Energy 2001;24:615-625.
[40] Pütün AE. Biomass to bio-oil via fast pyrolysis of cotton straw and stalk. Energy Sources 2002;24:275-285.
[41] Çaglar A, Dermibas A. Conversion of cotton cocoon shell to hydrogen rich gaseous products by pyrolysis. Energy Conversion Management 2002;43:489-497.
[42] Güllü D. (2003). Effect of catalyst on yield of liquid products from biomass via pyrolysis. Energy Sources, 25, 755-757.
[43] Uzun BB, Pütün AE, Pütün E. Fast pyrolysis of soybean cake: product yields and compositions. Bioresource Technology 2006;97:569-576.
[44] Sensöz S, Demiral I, Gerçel HF. Olive bagasse (Olea europea L.) pyrolysis. Bioresource Technology 2006; 97:429-436.
[45] Tuncel F, Gerçel HF. Production and characterization of pyrolysis oils from Euphorbia Macroclada. Energy Sources 2004;26:761-770.
[46] Demirbas A. Pyrolysis and steam gasification processes of black liquor. Energy Conversion Management 2002;43:877-884.
[47] Pütün AE, Özcan A, Pütün E. Pyrolysis of hazelnut shells in a fixed-bed tubular reactor: yields and structural analysis of bio-oil. J. Anal. Appl. Pyrolysis 1999;52:33-49.
[48] Sensöz S, Angin D. Pyrolysis of safflower (Chartamus tinctorius L.) seed press cake: Part 1. The effects of pyrolysis parameters on the products yields. Biosource Technology 2008;99:5492-5497.
[49] Li L, Zhang H, Zhuang X. Pyrolysis of waste paper: characterization and composition of pyrolysis oil. Energy Sources 2005;27:867-873.
[50] Zanzi R, Sjöström K, Björnbom E. Rapid pyrolysis of agricultural residues at high temperature. Biomass & Bioenergy 2002;23:357-366.
[51] Bonelli PR, Cerrella EG, Cukierman AL. Slow pyrolysis of nutshells: characterization of derived chars and of process kinetics. Energy Sources 2003;25:767-778.
[52] Apaydin-Varol E, Pütün E, Pütün AE. Slow pyrolysis of pistachio shell. Fuel 2007;86:1892-1899.
[53] Zandersons J, Gravitis J, Kokorevics A, Zhurinsh A, Bikovens O, Tardenaka A, Spince B. Studies of the Brazilian sugarcane bagasse carbonization process and products properties. Biomass and Bioenergy 1999;17:209-219.
[54] Pütün AE, Önay E, Uzun BB, Özbay N. Comparison between the 'slow' and 'fast' pyrolysis of tobacco residue. Industrial Crops and Products 2007;26, 307-314.
[55] Onay O, Beis SH, Kockar OM. Fast pyrolysis of rape seed in a well-swept fixed bed reactor. J. Anal. Appl. Pyrolysis 2001; 58-59:995-1007.
[56] Tsai WT, Lee MK, Chang YM. Fast pyrolysis of rice husks: product yields and compositions. Bioresource Technology 2007; 98:22-28.
[57] Tsai WT, Lee MK, Chang YM. Fast pyrolysis of rice straw, sugarcane bagasse and coconut shell in an induction-heating reactor. J. Anal. Appl. Pyrolysis 2006;76:230-237.
[58] Ates F, Putun E, Putun AE. Fast pyrolysis of sesame stalk: yields and structural analysis of bio-oil. J. Anal. Appl. Pyrolysis 2004; 71:779-790.
[59] Miao X, Wu Q. High yield bio-oil production from fast pyrolysis by metabolic controlling of Chorella protothecoides. Journal of Biotechnology 2004;110:85-93.
[60] Yu Q, Brage C, Chen G, Sjöström K. Temperature impact on the formation of tar from biomass pyrolysis in a free-fall reactor. J. Anal. Appl. Pyrolysis 1997;40-41:481-489.
[61] Schröder E. Experiments on the pyrolysis of large beechwood particles in fixed beds. J. Anal. Appl. Pyrolysis 2004;71:669-694.
[62] Aguado R, Olazar M, José MJS, Aguirre G, Bilbao J. Pyrolysis of sawdust in a conical spouted bed reactor. Yields and product composition. Ind. Eng. Chem. Res.2000;39:1925-1933.
[63] Figueiredo JL, Valenzuela C, Bernalte A, Encinar JM. Pyrolysis of holm-oak wood: influence of temperature and particle size. Fuel 1989; 68:1012-1016.

[64] Raveendran K, Ganesh A. Heating value of biomass and biomass pyrolysis products. Fuel 1996;75:1715-1720.
[65] Sensöz S, Can M. Pyrolysis of pine (Pinus Brutia Ten.) Chips: 2. Structural Analysis of Bio-oil. Energy Sources 2002;24:357-364.
[66] Zanzi R, Sjöström K, Björnbom E. Rapid high-temperature pyrolysis of biomass in a free-fall reactor. Fuel 1996;75:545-550.
[67] Onay Ö, Koçkar Ö. Production of bio-oil from biomass: slow pyrolysis of rapeseed (Brassica napus L.) in a fixed-bed reactor. Energy Sources 2003;25:879-892.
[68] Elliot DC. Relation of reaction time and temperature to chemical composition of pyrolysis oils. In: Pyrolysis Oils from Biomass: Producing, Analysing and Upgrading (ACS Symposium Series 376); Soltes ED, Milne TA Ed., ACS, Washington D.C., 1998.
[69] Funazukuri T, Hudgins RR, Silveston PL. Correlation of volatile products from fast cellulose pyrolysis. Ind. Eng. Chem. Process. Des. Dev. 1986;25:172-181.

7 ACKNOWLEDGEMENT

This work has been financially supported by a grant to D. Neves from the Fundação para a Ciência e a Tecnologia (FCT), Portugal (SFRH/BD/39567/2007).